QUANTITATIVE WOOD ANATOMY TO EXPLORE TREE RESPONSES TO GLOBAL CHANGE

EDITED BY: Fabio Gennaretti, Ignacio García-González, Marco Carrer, Sergio Rossi and Georg von Arx

PUBLISHED IN: Frontiers in Plant Science

frontiers Research Topics

frontiers

ISSN 1664-8714
ISBN 978-2-83250-304-1
DOI 10.3389/978-2-83250-304-1

About Frontiers

Frontiers is more than just an open-access publisher of scholarly articles: it is a pioneering approach to the world of academia, radically improving the way scholarly research is managed. The grand vision of Frontiers is a world where all people have an equal opportunity to seek, share and generate knowledge. Frontiers provides immediate and permanent online open access to all its publications, but this alone is not enough to realize our grand goals.

Frontiers Journal Series

The Frontiers Journal Series is a multi-tier and interdisciplinary set of open-access, online journals, promising a paradigm shift from the current review, selection and dissemination processes in academic publishing. All Frontiers journals are driven by researchers for researchers; therefore, they constitute a service to the scholarly community. At the same time, the Frontiers Journal Series operates on a revolutionary invention, the tiered publishing system, initially addressing specific communities of scholars, and gradually climbing up to broader public understanding, thus serving the interests of the lay society, too.

Dedication to Quality

Each Frontiers article is a landmark of the highest quality, thanks to genuinely collaborative interactions between authors and review editors, who include some of the world's best academicians. Research must be certified by peers before entering a stream of knowledge that may eventually reach the public - and shape society; therefore, Frontiers only applies the most rigorous and unbiased reviews.
Frontiers revolutionizes research publishing by freely delivering the most outstanding research, evaluated with no bias from both the academic and social point of view. By applying the most advanced information technologies, Frontiers is catapulting scholarly publishing into a new generation.

What are Frontiers Research Topics?

Frontiers Research Topics are very popular trademarks of the Frontiers Journals Series: they are collections of at least ten articles, all centered on a particular subject. With their unique mix of varied contributions from Original Research to Review Articles, Frontiers Research Topics unify the most influential researchers, the latest key findings and historical advances in a hot research area! Find out more on how to host your own Frontiers Research Topic or contribute to one as an author by contacting the Frontiers Editorial Office: frontiersin.org/about/contact

QUANTITATIVE WOOD ANATOMY TO EXPLORE TREE RESPONSES TO GLOBAL CHANGE

Topic Editors:
Fabio Gennaretti, Université du Québec en Abitibi Témiscamingue, Canada
Ignacio García-González, University of Santiago de Compostela, Spain
Marco Carrer, University of Padua, Italy
Sergio Rossi, Université du Québec à Chicoutimi, Canada
Georg von Arx, Swiss Federal Institute for Forest, Snow and Landscape Research (WSL), Switzerland

Citation: Gennaretti, F., García-González, I., Carrer, M., Rossi, S., von Arx, G., eds. (2022). Quantitative Wood Anatomy to Explore Tree Responses to Global Change. Lausanne: Frontiers Media SA. doi: 10.3389/978-2-83250-304-1

Table of Contents

frontiers | Frontiers in Plant Science

TYPE Editorial
PUBLISHED 09 September 2022
DOI 10.3389/fpls.2022.998895

OPEN ACCESS

EDITED BY
Peter Prislan,
Slovenian Forestry Institute, Slovenia

REVIEWED BY
Cristina Nabais,
University of Coimbra, Portugal

*CORRESPONDENCE
Fabio Gennaretti
fabio.gennaretti@uqat.ca

SPECIALTY SECTION
This article was submitted to Functional Plant Ecology, a section of the journal Frontiers in Plant Science

RECEIVED 20 July 2022
ACCEPTED 11 August 2022
PUBLISHED 09 September 2022

CITATION
Gennaretti F, Carrer M, García-González I, Rossi S and von Arx G (2022) Editorial: Quantitative wood anatomy to explore tree responses to global change. *Front. Plant Sci.* 13:998895. doi: 10.3389/fpls.2022.998895

Editorial: Quantitative wood anatomy to explore tree responses to global change

Fabio Gennaretti[1]*, Marco Carrer[2], Ignacio García-González[3], Sergio Rossi[4] and Georg von Arx[5,6]

[1]Forest Research Institute, Groupe de Recherche en Écologie de la MRC-Abitibi, Université du Québec en Abitibi-Témiscamingue, Amos, QC, Canada, [2]TeSAF Department, Universitá degli Studi di Padova, Padova, Italy, [3]Departamento de Botánica, Universidade de Santiago de Compostela, Lugo, Spain, [4]Laboratoire sur les écosystèmes terrestres boréaux, Département des Sciences Fondamentales, Université du Québec à Chicoutimi, Chicoutimi, QC, Canada, [5]Swiss Federal Institute for Forest, Snow and Landscape Research (WSL), Birmensdorf, Switzerland, [6]Oeschger Centre for Climate Change Research, University of Bern, Bern, Switzerland

KEYWORDS

quantitative wood anatomy (QWA), intra-annual resolution, tree functioning, trait plasticity, marginal populations, climate and environmental reconstructions, technical advancements

Editorial on the Research Topic
Quantitative wood anatomy to explore tree responses to global change

Introduction

Quantitative wood anatomy (QWA) analyzes the anatomical traits of xylem and phloem cells in trees (von Arx et al., 2016). This research field is rapidly growing because anatomical traits may give in-depth insight into plant functioning and their dynamic responses to environmental change (Fonti et al., 2010). The size and structure of woody cells and their compartments are closely linked to tree hydraulic conductivity, drought resistance, and mechanical support (Tyree and Zimmermann, 2013; Hacke et al., 2015). Furthermore, QWA may offer information at a high temporal resolution over the growing season because each cell in the tree-rings is formed over a specific time frame and its anatomical traits may be dependent on the environmental constraints acting over this time frame (Puchi et al., 2020). The main drawback of QWA is the time and expertise needed to build anatomical time series. Most of the time QWA needs appropriate sample preparation techniques, microtomy, microscopy, and image analysis (von Arx et al., 2016). All these steps are time consuming and need special care to avoid systematic errors in the analyses.

This Research Topic aimed to gather a selection of relevant articles about QWA. Contributions are included showing how QWA can be used to understand the climate and environmental responses of trees at higher temporal resolution (intra-annual) than classical dendroecological studies. Other contributions use QWA to study tree functioning and their trait plasticity according to specimen provenance and growing

site conditions, including marginal environments such as elevational treelines. Other contributions show the potential of QWA to improve climate and environmental reconstruction. Indeed, a likely future step forward in dendroclimatology will be to improve interpretations with a more in-depth understanding of tree functioning through QWA. Finally, the Research Topic includes some relevant technical advancements and standardized methods to improve the field of QWA in terms of reduction of analytic time, and improvement of reproducibility and interpretations.

Intra-annual resolution to understand plant responses to extreme events

An increase in extreme climatic events is expected under global change and QWA may give special insights into the associated tree functional responses with intra-annual temporal resolution. In this context, Buttò et al. show that broad-leaved ring-porous and diffuse-porous species may have contrasted responses to drought, in some cases reducing the formation of additional xylem vessels and in others reducing their size. These changes are also simultaneous to shifts in canopy architecture. QWA may also be used to monitor wood formation processes (i.e., xylogenesis) in real time over the growing season with repetitive samplings each week. Gao et al. used xylogenetic monitoring to highlight the link between moisture availability and intra-annual density fluctuation in tree-rings of trees growing in arid and semi-arid regions of continental Asia with seasonal monsoon changes. Their findings are important to understanding possible plant responses to climate changes in this region.

Tree functioning and their trait plasticity over environmental gradients

Another strength of QWA is that it potentially shows how trees are adapted or may acclimate (phenotypic plasticity) to different environments. Sampling European beech (*Fagus sylvatica* L.) populations differing in climatic regimes and spring leaf phenology, Arnič et al. show how mean vessel area, vessel density, and relative conductive area depend on precipitation and maximum temperature and may change over dry years. However, Miranda et al. highlight that European beech expresses limited anatomical trait plasticity and that simple interpretations may be distorted by the mixing effects of site conditions, land use changes, and ontogenetic patterns. Common garden experiments are needed to distinguish between plastic and genetic imprints on anatomical functional traits. For example, the study by Hietz et al. for the *Quercus robur* (L.) uses 10 tree provenances planted in three locations over a rainfall gradient to distinguish between the drivers of trait plasticity. Allometric dependences (ring width and tree size) accounted for stronger effects on all vessel parameters than site and provenance.

QWA for studying marginal populations

Marginal populations are often studied in ecology because they are notably sensitive to environmental changes and may be used to understand potential biogeographical shifts with climate change. A better understanding of constraints and responses of tree species at the elevational/latitudinal treeline can be achieved by combining the classical dendroecological approach with QWA. This is the case in the study of Știrbu et al. for *Pinus cembra* L. in the Carpathians where the authors combine tree-ring widths, density, and anatomical traits to assess the climatic sensitivity of those populations. The results show comparable correlations of maximum density and cell wall thickness with temperature and some negative impact of low water availability on conduit area. Similarly, Pampuch et al. sampled treeline populations of *Picea glauca* (Moench) Voss in Alaska showing that, among the anatomical traits, only cell wall thickness in the latewood is directly related to climate conditions, mainly temperature.

Enhancing climate and environmental reconstructions

The direct links between environmental variability and anatomical traits may be used to improve climate and palaeoecological reconstructions with an enhanced mechanistic understanding of tree responses. In our Research Topic, three contributions explore these potential applications that are rapidly expanding in recent years. Balanzategui et al. show that lumen diameter of *Pseudotsuga menziesii* (Mirb.) Franco has a high potential to be used for temperature and precipitation reconstructions according to the analyzed sector in the tree-rings and such traits may be related to the decadal fluctuation of regional climatic modes (namely the Southern Oscillation Index). Tardif et al. explore the hydroclimatic sensitivity of flooded and non-flooded *Fraxinus nigra* (Marshall) trees concluding that only floodplain populations have strong and stable paleoclimatic signals in vessel anatomical chronologies. Using similar material, Nolin et al. reconstructed the local relationship between a river regulation by a dam and flooding episodes using flood rings. Such rings were noticeable by an increase in earlywood vessel number simultaneous to a decrease in vessel area.

Technical advancements in QWA

New techniques and standard methods are highly sought in QWA because one of the main limiting factors of the discipline is the time and expertise needed to carry on the analyses. Thus, our Research Topic includes contributions describing new techniques that may potentially improve future analyses. A new workflow to study xylogenesis is proposed by Lehnebach et al. using high-resolution X-ray computed tomography. The most important technical advancement of this new technique is the possibility of precisely estimating biomass increments within the forming tree-rings for any tree species. This technique has the potential to provide relevant data to improve the modeling of carbon allocation and sequestration potential of forest stands (Gennaretti et al., 2017). Furthermore, Resente et al. show how an artificial intelligence algorithm may be trained to eventually save time and improve precision during the automatic detection of cell compartments. This artificial intelligence approach may be beneficial for future segmentation algorithms for QWA.

Conclusion

The contributions to this Research Topic show several applications of QWA to better understand tree responses to global change and new technical advancements that will improve the discipline. QWA is rapidly expanding and evolving because it allows making the direct link between tree growth and tree functional responses. This collection of articles contributes to increasing interest in this discipline and identifying relevant future research directions.

Author contributions

All authors acted as topic editors for this special issue in Frontiers in Plant Science entitled Quantitative Wood Anatomy to Explore Tree Responses to Global Change. All authors prepared the editorial text, sharing the tasks of writing, proofreading, and correcting the manuscript. FG initiated the idea of the special issue and organized the writing process of the editorial. All authors contributed to the article and approved the submitted version.

Funding

This Research Topic and the collaboration between editors originated by projects funded by the Fonds de recherche du Québec - Nature et technologies (FRQNT) for the programme on the contribution of forest sector in mitigating the effects of climate change (grant no. 2022-0FC-309064). FG was supported by the Discovery Grants program of the Natural Sciences and Engineering Research Council of Canada (grant no. RGPIN-2021-03553). IG-G was supported by the Xunta de Galicia (grant no. GRC GI-1809). GA was supported by the Swiss National Science Foundation (grant no. 200021_182398, XELLCLIM).

Conflict of interest

The authors declare that the research was conducted in the absence of any commercial or financial relationships that could be construed as a potential conflict of interest.

Publisher's note

All claims expressed in this article are solely those of the authors and do not necessarily represent those of their affiliated organizations, or those of the publisher, the editors and the reviewers. Any product that may be evaluated in this article, or claim that may be made by its manufacturer, is not guaranteed or endorsed by the publisher.

References

Fonti, P., von Arx, G., García-González, I., Eilmann, B., Sass-Klaassen, U., Gärtner, H., et al. (2010). Studying global change through investigation of the plastic responses of xylem anatomy in tree rings. *N. Phytol.* 185, 42–53. doi: 10.1111/j.1469-8137.2009.03030.x

Gennaretti, F., Gea-Izquierdo, G., Boucher, E., Berninger, F., Arseneault, D., and Guiot, J. (2017). Ecophysiological modeling of photosynthesis and carbon allocation to the tree stem in the boreal forest. *Biogeosciences* 14, 4851–4866. doi: 10.5194/bg-14-4851-2017

Hacke, U. G., Lachenbruch, B., Pittermann, J., Mayr, S., Domec, J.-C., and Schulte, P. J. (2015). *The Hydraulic Architecture of Conifers BT - Functional and Ecological Xylem Anatomy*. Cham: Springer International Publishing. doi: 10.1007/978-3-319-15783-2_2

Puchi, P. F., Castagneri, D., Rossi, S., and Carrer, M. (2020). Wood anatomical traits in black spruce reveal latent water constraints on the boreal forest. *Glob. Change Biol.* 26, 1767–1777. doi: 10.1111/gcb.14906

Tyree, M. T., and Zimmermann, M. H. (2013). *Xylem Structure and the Ascent of Sap*. Berlin: Springer Science and Business Media. doi: 10.1007/978-3-662-04931-0

von Arx, G., Crivellaro, A., Prendin, A. L., Cufar, K., and Carrer, M. (2016). Quantitative wood anatomy-practical guidelines. *Front. Plant Sci.* 7, 781. doi: 10.3389/fpls.2016.00781

frontiers in Plant Science

ORIGINAL RESEARCH
published: 26 July 2021
doi: 10.3389/fpls.2021.669229

Different Wood Anatomical and Growth Responses in European Beech (*Fagus sylvatica* L.) at Three Forest Sites in Slovenia

Domen Arnič[1,2], Jožica Gričar[3], Jernej Jevšenak[3], Gregor Božič[4], Georg von Arx[5] and Peter Prislan[1]*

[1]Department for Forest Technique and Economics, Slovenian Forestry Institute, Ljubljana, Slovenia, [2]Biotechnical Faculty, University of Ljubljana, Ljubljana, Slovenia, [3]Department of Forest Yield and Silviculture, Slovenian Forestry Institute, Ljubljana, Slovenia, [4]Department of Forest Physiology and Genetics, Slovenian Forestry Institute, Ljubljana, Slovenia, [5]Swiss Federal Research Institute for Forest, Snow and Landscape Research (WSL), Birmensdorf, Switzerland

OPEN ACCESS

Edited by:
Jian-Guo Huang,
South China Botanical Garden, Chinese Academy of Sciences (CAS), China

Reviewed by:
Marcin Klisz,
Forest Research Institute (IBL), Poland
Ignacio García-González,
University of Santiago de Compostela, Spain
Shaokang Zhang,
Chinese Academy of Sciences (CAS), China

***Correspondence:**
Domen Arnič
domen.arnic@gozdis.si

Specialty section:
This article was submitted to Functional Plant Ecology, a section of the journal Frontiers in Plant Science

Received: 18 February 2021
Accepted: 05 July 2021
Published: 26 July 2021

Citation:
Arnič D, Gričar J, Jevšenak J, Božič G, von Arx G and Prislan P (2021) Different Wood Anatomical and Growth Responses in European Beech (Fagus sylvatica L.) at Three Forest Sites in Slovenia. Front. Plant Sci. 12:669229. doi: 10.3389/fpls.2021.669229

European beech (*Fagus sylvatica* L.) adapts to local growing conditions to enhance its performance. In response to variations in climatic conditions, beech trees adjust leaf phenology, cambial phenology, and wood formation patterns, which result in different tree-ring widths (TRWs) and wood anatomy. Chronologies of tree ring width and vessel features [i.e., mean vessel area (MVA), vessel density (VD), and relative conductive area (RCTA)] were produced for the 1960–2016 period for three sites that differ in climatic regimes and spring leaf phenology (two early- and one late-flushing populations). These data were used to investigate long-term relationships between climatic conditions and anatomical features of four quarters of tree-rings at annual and intra-annual scales. In addition, we investigated how TRW and vessel features adjust in response to extreme weather events (i.e., summer drought). We found significant differences in TRW, VD, and RCTA among the selected sites. Precipitation and maximum temperature before and during the growing season were the most important climatic factors affecting TRW and vessel characteristics. We confirmed differences in climate-growth relationships between the selected sites, late flushing beech population at Idrija showing the least pronounced response to climate. MVA was the only vessel trait that showed no relationship with TRW or other vessel features. The relationship between MVA and climatic factors evaluated at intra-annual scale indicated that vessel area in the first quarter of tree-ring were mainly influenced by climatic conditions in the previous growing season, while vessel area in the second to fourth quarters of tree ring width was mainly influenced by maximum temperature and precipitation in the current growing season. When comparing wet and dry years, beech from all sites showed a similar response, with reduced TRW and changes in intra-annual variation in vessel area. Our findings suggest that changes in temperature and precipitation regimes as predicted by most climate change scenarios will affect tree-ring increments and wood structure in beech, yet the response between sites or populations may differ.

Keywords: *Fagus sylvatica*, wood anatomy, tracheograms, dendrochronology, intra specific plasticity

INTRODUCTION

European beech (*Fagus sylvatica* L.) is one of the dominant tree species of mixed and deciduous temperate European forests (del Río et al., 2017), with a wide distribution range and thus high intra-specific plasticity (Dieler and Pretzsch, 2013). It grows on forest sites with diverse growing conditions; from moist and cold sites in the southern part of Scandinavia to dry and hot areas in the northern part of the Iberian and Apennine peninsulas (Bolte et al., 2007). Due to the wide distribution range, beech populations adjust their growth traits, such as leaf phenology and growth and frost resistance, to their specific environmental conditions (Vitasse et al., 2011). Phenotypic plasticity of beech has been extensively studied in past decades to understand the survival and future distribution range of beech under climate change (Matyas et al., 2009). Across Europe, common garden experiments were established to understand the effect of beech provenances under different environmental conditions (Robson et al., 2018). Numerous studies performed in these experiments focused on leaf phenology. A latitudinal trend in leaf flushing was observed, with northern and southern provenances being late and early flushing, respectively, although some exceptions exist (Stojnić et al., 2015). In addition, productivity and wood structure (Eilmann et al., 2014; Jezik et al., 2016; Klisz et al., 2019) or growth strategy and survival (Vitasse et al., 2010) were investigated. Although such experiments provided important insights into differences between provenances, they were usually performed on relatively young trees, which exhibit different climate sensitivity compared to older trees (Trouillier et al., 2018). Thus, studies investigating the response to changing climate in adult beech populations differing in leaf phenology in terms of xylem wood structure are rare.

Although leaf unfolding in spring coincides with the onset of wood formation in beech (Čufar et al., 2008), no clear relationship between variation in leaf phenology and radial growth was observed (Čufar et al., 2015). The variability of climate conditions prior to and during the growing season significantly affects tree growth and thus the productivity of beech forests (Di Filippo et al., 2007). Different climatic factors influence growth throughout the European beech distribution range. In southern and western Europe, high temperatures in early spring positively affected the onset of beech xylem production, which is reflected in wider tree rings while high summer temperatures showed a negative effect on growth (Di Filippo et al., 2007; Čufar et al., 2008; Lenz et al., 2013; Martinez del Castillo et al., 2018). In northern and north-eastern parts of Europe, summer precipitation and frequent spring frosts positively and negatively influenced beech radial growth, respectively (Weigel et al., 2018; Harvey et al., 2019; Muffler et al., 2020). At the limit of the eastern distribution range, annual increments in beech were positively affected by late spring precipitation and negatively by summer temperatures (Šimůnek et al., 2019). In central and south-central Europe, tree ring width in beech was positively correlated with summer precipitation while more frequent drought-induced extreme climatic events were the main negative influencing factor on growth (Stojanović et al., 2018; Garamszegi et al., 2020). The response of trees to variations in climatic conditions also differed with elevation; in contrast to low elevation sites, higher temperatures during the growing season at high elevation sites had the opposite effect on beech growth (Di Filippo et al., 2007). Moreover, future predictions based on climate change scenarios suggest that at optimal forest sites with sufficient water availability, the duration of the growing season and, consequently, xylem increments will increase in the coming decades (Prislan et al., 2019).

While several studies have been performed on the impact of the environment on beech radial growth, little is known about how intra-annual variability of temperature and precipitation affects xylem structure. However, structural adjustments of wood to environmental cues play a decisive role in defining the hydraulic and mechanical properties of wood and, consequently, tree performance, and survival (Chave et al., 2009; Fonti et al., 2010). Stojnic et al. (2013) found similar productivity rates and wood structure in provenances from mesic sites and local provenances adapted to dry conditions at the provenance trial, suggesting that provenances form mesic conditions are able to adapt to drier conditions. Eilmann et al. (2014) confirmed that beech from southern provenances respond differently to drought conditions compared to those from northern provenances, suggesting genetic control of xylem performance in beech. Little is known about the impact of drought conditions on the anatomical features of wood. Giagli et al. (2016) found higher vessel density (VD) and water conductive area in a year characterized by drought conditions. Schume et al. (2004) observed that drought conditions were responsible for reduced vessel area in poplar. Furthermore, Hajek et al. (2016) observed that beech responds to drought by adjusting vessel number rather than vessel area. Similarly, Prislan et al. (2018) recorded differences in VD between two sites with sufficient water availability but at different altitude. Unlike short-term wood formation studies, quantifying wood cell anatomical features in tree rings provides a long-term approach to monitoring changes in growth phenology, climate sensitivity, xylem functioning, and xylem plasticity (Abrantes et al., 2012; Reyer et al., 2015; Castagneri et al., 2017). The availability of this information may be critical for evaluating the range of plasticity in tree species under different environmental conditions and, ultimately, for predicting their responses to future climate scenarios.

The aim of this study was to analyze the relationships between climatic conditions, tree ring widths, and xylem vessel features in beech in three forest stands with different climatic regimes and different leaf phenology of beech (two early and one late flushing site; Kramer et al., 2017; Robson et al., 2018) for a period between 1960 and 2016. By subdividing annual xylem increments into quarters, we evaluated intra-annual variations in the vessel characteristics to understand how beech from the selected sites adjust xylem anatomy to short-term changes in growth conditions, as previously shown by Sass and Eckstein (1995), Abrantes et al. (2012), and Castagneri et al. (2017). In addition, we analyzed the influence of extreme weather events (i.e., exceptionally hot or wet summers) on

vessel features within the tree rings. We hypothesized that (1) there is no relationship between tree-ring widths (TRWs) and vessel area because they contain different climatic information; (2) beech trees at the selected sites respond differently to local climatic conditions with respect to TRWs and vessel features suggesting adaptation to local conditions; (3) intra-annual vessel-climate relationship is not temporarily stable resulting in different trend of climatic signal in vessel area; and (4) at the site with the late flushing population, trees are more susceptible to weather variation than those characterized as early flushing, due to the shorter growing season.

MATERIALS AND METHODS

Study Species, Site Characteristics, and Climate Data

The selected forest sites represent origin forest stands for three European beech provenances in Slovenia, i.e., Idrija, Javornik, and Mašun. Seed collected at these sites was previously used in European beech provenance trials, in which differences in leaf phenology, growth trends, and survival strategies were assessed (von Wühlisch, 2004; Gömöry and Paule, 2011; Robson et al., 2011); beech at the Idrija site (IDR) is a late flushing, while beech from Mašun (MAS) and Javornik (JAV) are characterized as early flushing. All studied sites are located at a similar altitude between 904 and 958 m a.s.l. and belong to the *Abieti-Fagetum* forest association (**Table 1**).

We used the E-OBS daily climate data version 21e o 0.1 regular grid (Cornes et al., 2018) and extracted mean, minimum and maximum daily temperatures, and sum daily precipitation from the nearest grid point. All sites receive relatively large amounts of precipitation, i.e., between 1,500 and 2,100 mm annually, which are nearly equally distributed over the entire year, with a peak in October and November (**Figure 1**; **Supplementary Figure S4**). The E-OBS climate database refers to records from weather stations where daily climate data were collected from ground-based observation stations, operated by the National Meteorological Services between January 1950 and December 2019 (Cornes et al., 2018). Since the national weather stations located around the selected sites started recording climate data around 1960, we identified the 1960–2016 periods as optimal and used this for further analyses.

Sampling and Tree-Ring Width Measurements

Sampling was performed at the end of August in 2016, when the xylem ring was already fully formed (Prislan et al., 2013). At each site, 17 dominant beech trees were selected, with an average diameter at breast height (DBH) of 42 ± 6 cm (**Table 1**). Two cores were collected per tree using a 5-mm increment borer (Haglöf Sweden, Långsele). In the laboratory, the collected cores were air-dried and fixed on wooden holders. They were then sanded to obtain a clear surface for recognition of tree ring borders. ATRICS (Levanic, 2009) was used to capture high-resolution digital images, while TRW measurements were performed using CooRecorder & CDendro software (Cybis, Saltsjöbaden, Sweden). The final cross-dating was done using PAST-5 (SCIEM, Brunn, Austria) software.

Analysis of Xylem Vessel Features

Quantitative wood anatomy analysis was performed on six randomly selected cores per site. The random selection was used to ensure representative within-population variability rather than maximizing the climate signal. Since the same cores were used as for TRW measurements, they were first soaked in water before removal from the wooden holders. The samples were then prepared for observations under a light microscope according to the protocol suggested by von Arx et al. (2016); i.e., each core was split into segments of similar length (3–4 cm). A 15–20 μm thick transverse section was cut from each segment with a WSL sledge microtome using OLFA-80×9 mm spare blades (Gärtner et al., 2015). The sections were then treated with bleaching solution (5–15% chlorine content) to remove sawdust from the cell lumina and to improve the staining intensity in the subsequent staining with a water mixture of safranin and Astra-blue. Permanent slides were prepared using Euparal mounting medium. High-resolution images (0.514 pixel/1 μm) of the sections were prepared using a Leica DM 4000 B light microscope (Leica Microsystems, Wetzlar, Germany) at 50× magnification, a Leica DFC 280 digital camera (Leica Microsystems, Wetzlar, Germany), and LAS image analysis software (Leica Application Suite). Image-sequences of the xylem rings were captured with at least 25% of the overlapping area and then merged using PTGui v11.16 Pro (New House Internet Services B.V., Rotterdam, Netherlands). Panoramic pictures were then processed with image analysis software Image-Pro Plus 7.1 and ROXAS (v3.0.437) to obtain vessel features (von Arx and Carrer, 2014). Vessel lumen areas were measured within each ring for the period 1940–2016. Chronologies of the following parameters were then established; (1) mean vessel area (MVA), (2) VD as the number of vessels per squared mm, and (3) relative conductive area (RCTA) representing the percentage of cumulative vessel area within the measured area (the radial width of the measured area was represented by TRW, while the tangential width of the measured area was around 2 mm). Furthermore, to assess the intra-annual variability of vessel features, each vessel was assigned to one of four radial tree-ring sectors of equal width (henceforth "quarters") based on its center coordinate and then MVA was calculated for each quarter (Q1–Q4 MVA).

Statistical Analyses

All raw TRW series, as well as annual time series of vessel features, i.e., MVA, VD, RCTA, and Q1–Q4 MVA, were standardized using the *detrend()* function from dplR (Bunn, 2008). A cubic smoothing spline with a 50% frequency cut-off at 32 years was fitted to each individual raw series. To obtain a detrended index, the ratio between the observed and fitted values was calculated. Finally, for each parameter and site, standardized series were pre-whitened and averaged to residual chronologies by computing the robust bi-weight mean. Residual chronologies were therefore used to calculate climate-growth correlations, while raw series were compared

TABLE 1 | Characteristics of the sites JAV, MAS, and IDR; representing the local site conditions, as well as sampled tree characteristics, number of trees (N), mean diameter at breast height (DBH), and mean tree height (H).

	Site characteristics								Tree characteristics		
						Temperature (°C)					
Site	Latitude	Longitude	Bedrock	Aspect	Inclination (°)	Average	Maximal	Minimal	Precipitation (mm)	*N*	DBH (cm)	H (m)
JAV	45° 43' 59,09"	14° 20' 59,38"	Limestone	SW	10	7.9	13.0	2.8	1,514	17	43.0	30.0
MAS	45° 37' 59,87"	14° 23' 00,43"	Limestone	S	11	6.4	11.1	1.7	1,609	17	39.1	28.0
IDR	46° 00' 09,71"	13° 53' 52,94"	Limestone, Flint, and Sandstone	SE	10	8.4	13.2	4.2	2,090	17	43.7	27.5

to assess differences among sites. Please note, since we use raw and detrended chronologies, we refer to raw chronologies as TRW, MVA, VD, RCTA and Q1-Q4 MVA, while detrended chronologies are referred to by the postposition "i," i.e., TRWi, MVAi, VDi, RCTAi, and Q1–Q4 MVAi. The quality of site chronologies was described with common descriptive statistics, such as expressed population signal (EPS), mean inter-series correlation (rbar), and Gleichlaufigkeit (%GLK; Cook and Kairiukstis, 1990).

To test the hypothesis of equal means of tree-ring characteristics, i.e., TRW, MVA, VD, RCTA, and Q1–Q4 MVA among the sites, we used parametric and non-parametric statistical tests. Repeated measures (rm) ANOVA was used when assumptions for parametric tests were met, while in other cases, the nonparametric Friedman test was applied. Similarly, subsequent pairwise comparisons for rmANOVA were assessed with Tukey's test, while for the Friedman test; pairwise comparisons were done with the Wilcoxon test. Finally, linear regression models were used to assess the relationships between TRW and vessel features (MVA, VD, and RCTA).

Climate-growth correlations were analyzed using the *daily_response()* function from the dendroTools R package (Jevšenak and Levanič, 2018; Jevšenak, 2020), whereby day-wise aggregated correlations were calculated using 1,000 bootstrap samples considering all windows between 7 and 60 days from the previous June to the current October. Pearson correlation coefficients were calculated for the 1960–2016 period and only those with $p < 0.05$ were used to infer the relationship of climate and TRWi and vessel features (i.e., MVAi, VDi, and RCTAi within the tree rings, and in the case of MVAi also within the tree-ring quarters).

To assess the plasticity of tree-ring structure resulting from extreme weather conditions, we employed an additional comparison of standardized tracheograms (Schume et al., 2004) and compared these within three extreme dry and wet summers. Extreme years at each site were selected according to maximal or minimal amount of precipitation between the first of June and first of August, respectively. To ensure the selection of extreme years, the standardized precipitation evapotranspiration index (SPEI) was calculated (Vicente-Serrano et al., 2010). An ANOVA test was performed to test the differences of relationship between tree ring width characteristics (TRW, VD, and RCTA) and climatic conditions (maximum and minimum temperatures, precipitation amount, and SPEI) between dry and wet years. Furthermore, to develop the tracheograms, we divided the area of each vessel by the raw MVA in the particular year to account for the age-related trend (Carrer et al., 2015). We then smoothed each trend using the general additive model (GAM), which were then used in the Kolmogorov–Smirnov test to infer statistically significant differences in the intra-annual MVA distribution in years with extreme wet and dry conditions.

RESULTS

Tree-Ring Width and Vessel Features

The local TRW chronologies at MAS, JAV, and IDR were between 112 and 151 years long (**Table 2**). The widest mean TRW for

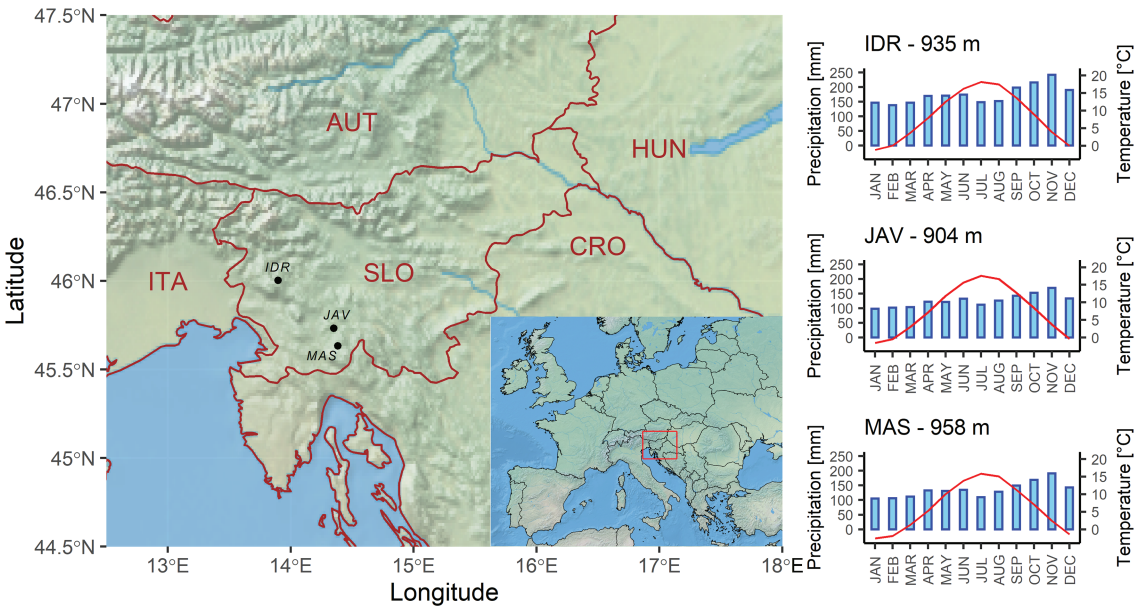

FIGURE 1 | Geographical locations and climate diagrams of selected sites, i.e., Idrija (IDR), Javornik (JAV), and Mašun (MAS). Climate diagrams are based on E-OBS daily climate datasets for the period from 1960 to 2016.

TABLE 2 | Tree ring width and wood anatomy chronologies and descriptive statistics: first-order autocorrelation (AC1), Gleichläufigkeit coefficient (%GLK), mean inter-series correlation (rbar), and expressed population signal (EPS) for the selected sites; Javornik (JAV), Masun (MAS), and Idrija (IDR).

Site		Start year	End year	AC1	%GLK	rbar	EPS
JAV	TRW	1885	2016	0.63	69	0.38	0.89
MAS		1904	2016	0.80	64	0.48	0.93
IDR		1865	2016	0.77	66	0.25	0.83
JAV	MVA	1940	2016	0.59	49	0.45	0.83
MAS		1940	2016	0.56	50	0.32	0.74
IDR		1940	2016	0.63	53	0.01	0.04
JAV	VD	1940	2016	0.63	51	0.04	0.04
MAS		1940	2016	0.73	53	0.06	0.29
IDR		1940	2016	0.61	52	0.10	0.38
JAV	RCTA	1940	2016	0.64	49	0.19	0.58
MAS		1940	2016	0.62	52	0.11	0.42
IDR		1940	2016	0.68	54	0.14	0.48
JAV	MVA-Q1	1940	2016	0.51	54	0.32	0.74
JAV	MVA-Q2	1940	2016	0.58	47	0.35	0.79
JAV	MVA-Q3	1940	2016	0.48	50	0.32	0.74
JAV	MVA-Q4	1940	2016	0.37	51	0.23	0.64
MAS	MVA-Q1	1940	2016	0.50	51	0.28	0.69
MAS	MVA-Q2	1940	2016	0.52	50	0.31	0.73
MAS	MVA-Q3	1940	2016	0.43	50	0.23	0.64
MAS	MVA-Q4	1940	2016	0.37	53	0.30	0.71
IDR	MVA-Q1	1940	2016	0.55	54	0.08	0.32
IDR	MVA-Q2	1940	2016	0.54	54	0.06	0.26
IDR	MVA-Q3	1940	2016	0.49	53	0.04	0.15
IDR	MVA-Q4	1940	2016	0.46	53	0.04	0.16

the 1960–2016 period was measured at MAS (2 ± 0.5 mm), followed by JAV (1.8 ± 0.3 mm) and IDR (1.4 ± 0.3 mm); the differences were statistically significant (**Figure 2A**). The measured vessel features VD and RCTA were significantly different between all sites (**Figures 2B–C**). MVA was similar at MAS and JAV, but significantly different at site IDR (**Figure 2D**).

The measured vessel traits generally exhibited significant relationships with TRW (**Figure 3**). At all sites, a negative relationship was observed between TRW and VD and between TRW and RCTA, indicating differences in theoretical specific conductivity and vessel densities between wider and narrower tree rings (**Figures 3A,B**; **Supplementary Tables S2** and **S3**).

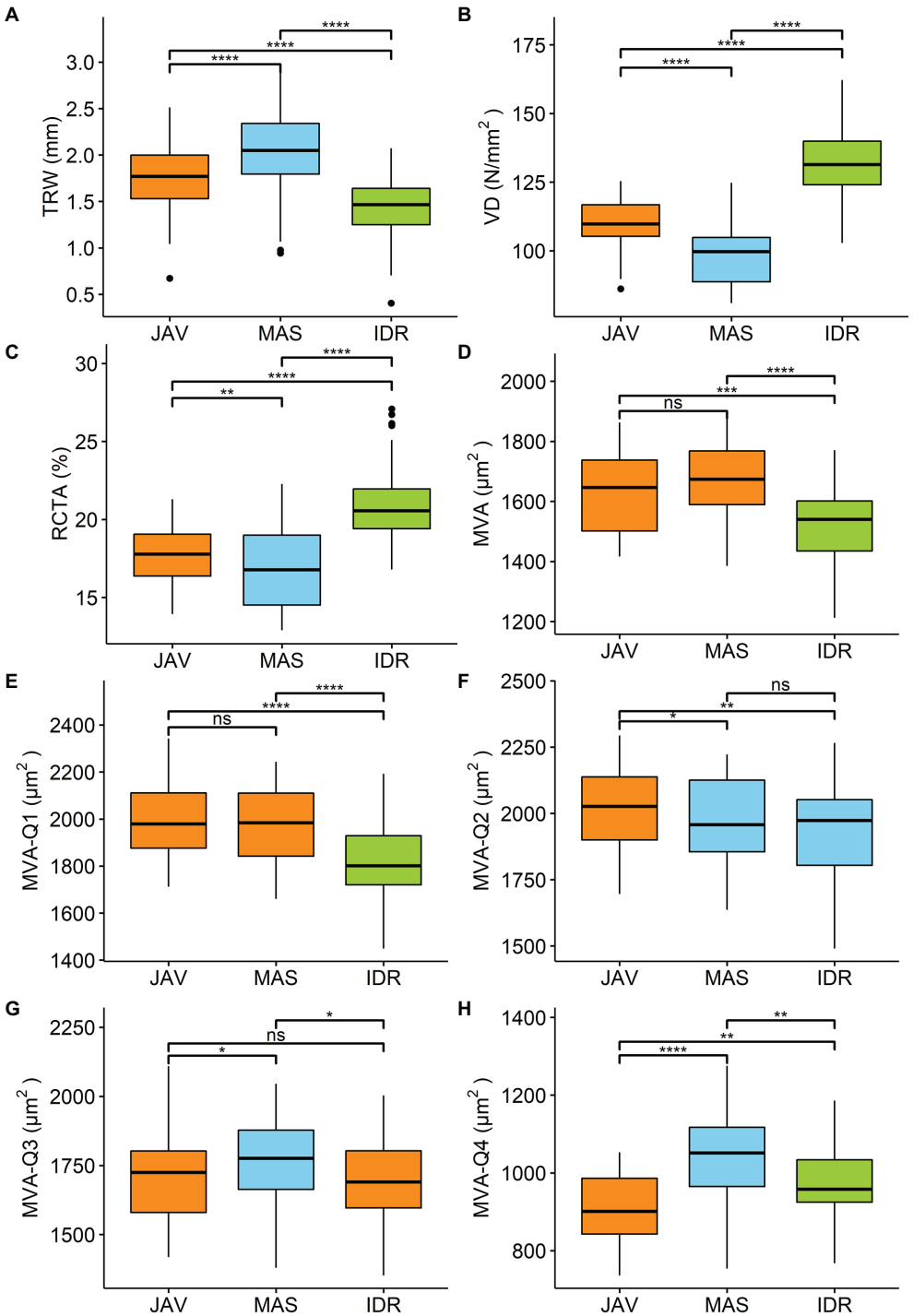

FIGURE 2 | Differences among the sites Javornik (JAV), Mašun (MAS), and Idrija (IDR) in **(A)** tree ring width (TRW), **(B)** vessel density (VD), **(C)** relative conductive area (RCTA), **(D)** mean vessel area (MVA), and **(E-H)** MVA in first to fourth quarter of tree ring (MVA-Q1–MVA-Q4) analyzed by rm-ANOVA or the Friedman test. Significance of differences in tree ring characteristic between sites are market by ns-not significant. *$p < 0.05$, **$p < 0.01$, ***$p < 0.001$, and ****$p < 0.0001$. Additional information is available in **Supplementary Table S1**.

Consequently, RCTA and VD showed a significant positive relationship at all sites (**Figure 3C**; **Supplementary Table S4**); rings with higher VD resulted in higher RCTA. As expected, neither there was no significant relationship between TRW and MVA, nor between VD and MVA (**Figures 3D,E**; **Supplementary Tables S5** and **S6**).

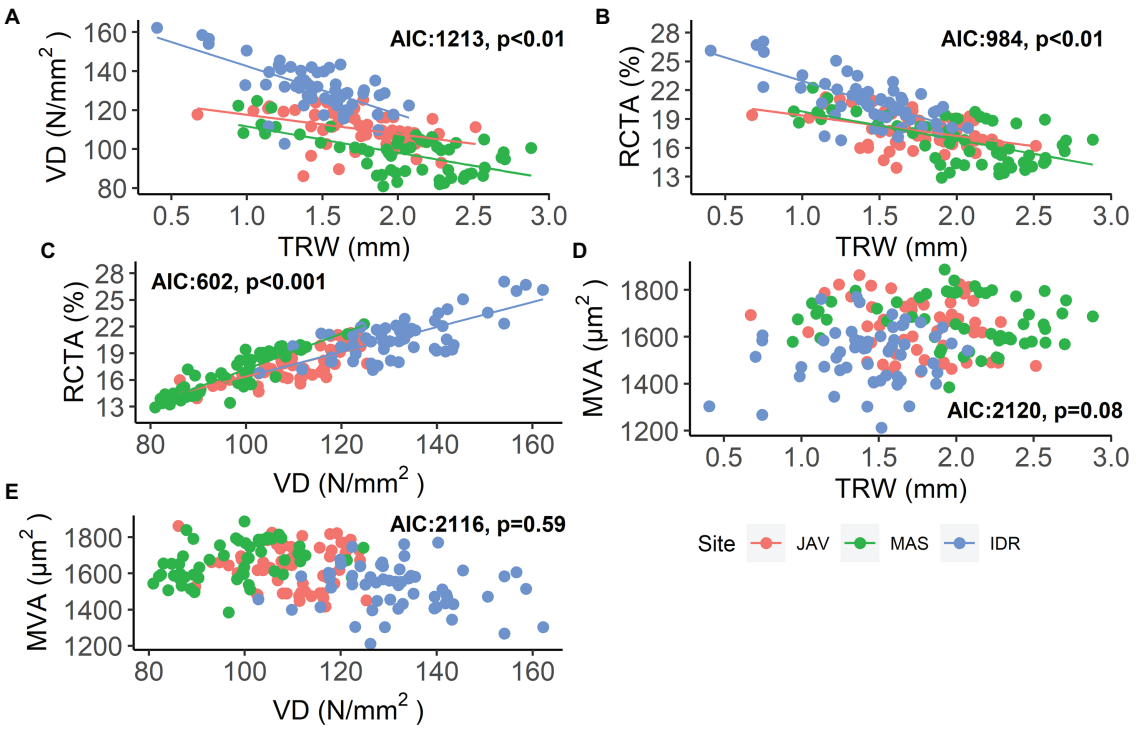

FIGURE 3 | Relationships between: **(A)** vessel density (VD) and tree-ring width (TRW), **(B)** relative conductive area (RCTA) and TRW, **(C)** RCTA and VD, **(D)** mean vessel area (MVA) and TRW, and **(E)** MVA and VD in beech at Javornik (JAV), Mašun (MAS), and Idrija (IDR) with models Akaike information criterion (AIC) and significance level. Further statistical information for the presented generalized linear models is given in **Supplementary Tables S2–S6**.

Further comparison of MVA values in the tree-ring quarters showed a consistent decrease in vessel area from the first to the last quarter (**Figure 4**). In general, MVA was similar in the first and second quarters, but was smaller in the third and fourth quarters (**Figures 2E–H, 4**). The differences in MVA between the first and second quarters were largest at IDR, while at MAS and JAV, the values were similar (**Figure 4**). MVA in the third quarter was smaller than in the first two quarters at all sites. A decrease in MVA from the second to the third quarter was between 10% at MAS and 15% at JAV. An abrupt decrease in MVA was noted for the fourth quarter, where MVA at all selected sites decreased by more than 40% compared to the third quarter (**Figures 2G,H**; **Supplementary Table S1**). Nevertheless, inter-quarter correlation analyses revealed a relatively strong positive relationship between MVA in the individual tree-ring quarters at each site. At JAV correlation values were similar between quarters, while slightly lower correlation values were found between the first and last quarters at sites MAS and IDR (**Supplementary Figure S1**).

The Effect of Climate Variables on Tree-Ring and Vessel Parameters

Correlation analysis between long-term daily climate data and the studied tree-ring parameters showed a strong and significant association with temperature and precipitation at all sites (**Figure 5**). In general, the most important climatic factors related to tree-ring characteristics were amount of precipitation and maximum temperature, while minimum temperature showed lower correlations. The time window of 7–60 days showed a relatively constant climate response with the most pronounced correlations between 25 and 35 days. In the case of the MVA, high correlations were also observed for shorter time-windows (7–20 days; **Figure 5**).

The highest correlations were observed at JAV; the inter-annual variability of TRWi was mainly related to the conditions in late winter, when maximum temperature and precipitation showed positive ($r_{tmax} > 0.40$) and negative ($r_{prec} < -0.30$) correlations, respectively. The highest negative correlation at JAV was observed between the previous autumn maximum temperature ($r_{tmax} > 0.40$) and MVAi, while the maximum temperature at the end of winter shoved a positive correlation ($r_{tmax} > 0.30$). VDi and RCTAi were negatively correlated by both maximum and minimum temperature in late winter and early spring. Correlations between climate parameters and tree-ring features were the least pronounced at IDR, where the highest positive correlations were found between MVAi and minimum and maximum temperatures at the end of the previous growing season ($r_{tmax} > 0.30$). Furthermore, the maximum temperature at the beginning of the growing season positively correlated with TRW. While at MAS, the variability in TRWi and MVAi was mainly positively correlated with early summer precipitation.

The Effect of Climate on Intra-Annual Vessel Area Characteristics

Correlation analysis revealed differences in MVAi responses to changing climatic conditions among the tree-ring quarters. In

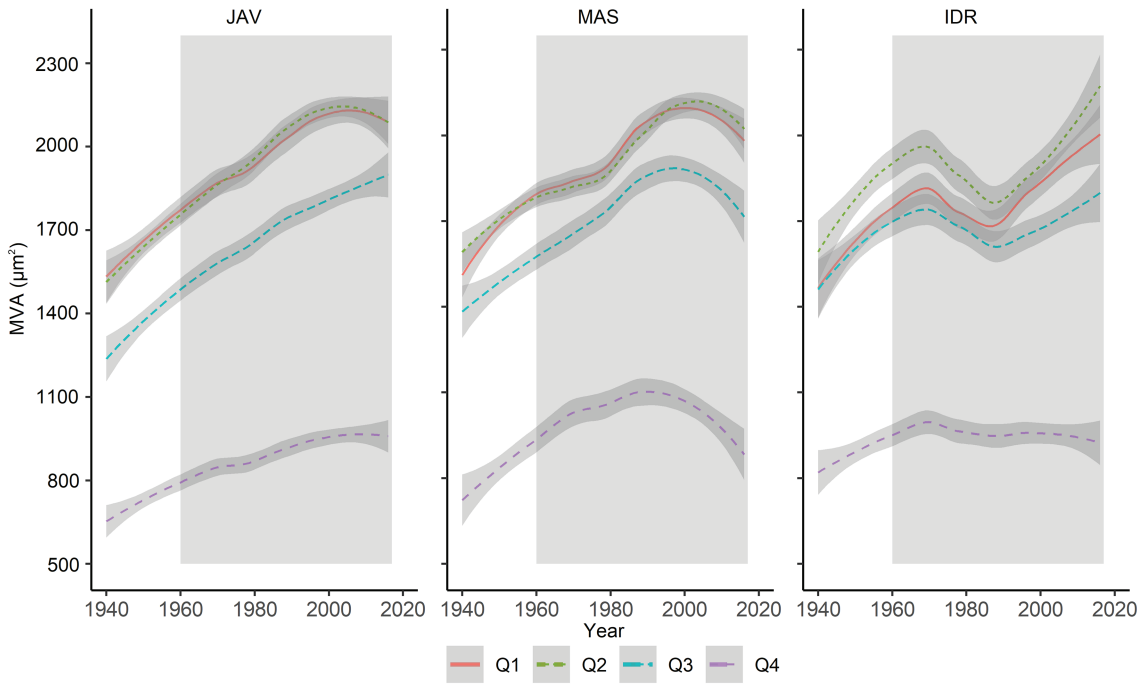

FIGURE 4 | Long-term trends in MVA in evaluated tree-ring quarters (Q1–Q4) at Javornik (JAV), Mašun (MAS) and Idrija (IDR). The gray area represents the period between 1960 and 2016, which was considered for further analysis. The relationships between sectors are presented in **Supplementary Figure S1**.

addition, differences in response to climate variations were observed among the forest sites (**Figure 6**). In general, precipitation and maximum temperature were the main climatic drivers significantly correlated with MVAi among quarters (**Figure 6**). Temporarily similar patterns of climate response among the sites were noticed for late spring temperature in the first quarter and late summer precipitation in the fourth quarter. The weakest correlation values in all quarters were observed with minimum temperature at MAS and precipitation at the site IDR, suggesting low sensitivity of MVAi to these climatic factors. Daily response functions revealed similar climate signal across 7–60 days climate window. In the case of maximum and minimum temperatures, higher signal was observed for shorter time-windows (7–20 days), while for precipitation, the highest signal was found with longer time windows, i.e., 20–35 days (**Figure 6**).

In the first quarter of the tree rings, the strongest correlations were observed with conditions at the end of the previous growing season and in the current year's spring. In general, temperature negatively affected MVAi in late spring ($r_{tmax} > 0.35$), while the positive correlations were revealed at the end of the previous growing season ($r_{tmin} > 0.30$). In the same time intervals, precipitation showed the opposite correlations on MVAi than temperature. In the second quarter, precipitation before and during the growing season showed a negative (JAV: $r_{prec} < -0.40$) and positive (JAV: $r_{prec} > 0.40$; MAS: $r_{prec} > 0.30$) correlations with MVAi, respectively. Furthermore, maximum temperature showed the highest positive correlation at the end of the previous growing season at JAV ($r_{tmax} > 0.45$), although correlations were negative during the current growing season ($r_{tmax} < -0.35$). In the third quarter, correlation values were in general lower than those of the other three quarters. The exception was maximum temperature at JAV, which showed high negative correlations in the previous autumn ($r_{tmax} < -0.50$). In the fourth quarter, the highest positive correlations were observed between MVAi and summer precipitation ($r_{prec} > 0.55$), while maximum temperature during the summer revealed negative correlations on MVAi ($r_{tmax} < -0.4$). Correlation analysis also revealed a mostly reverse climatic signal between the end of the previous and the current growing seasons. At the end of the previous growing season, MVAi of all quarters of tree ring was positively and negatively correlated with temperature and precipitation, respectively. However, in the current growing season, the relationship between MVAi of all quarters and temperature and precipitation was just the opposite.

Impact of Extreme Weather Conditions During Summer on the Studied Tree-Ring Parameters

Because late summer precipitation of the current growing season showed the highest correlation with MVA within quarters, we identified 3 years with the driest and wettest summers at the selected sites to compare intra-annual vessel area distributions between extreme wet and dry conditions. Compared to wet summers, drier summer conditions resulted in narrower TRW, higher VD, and, consequently, a higher RCTA. Differences in the studied tree-ring parameters between wet and dry summer conditions were significantly different at MAS and JAV, while beech at IDR showed smaller, insignificant differences in tree ring width parameters between extremely dry and wet years (**Table 3**).

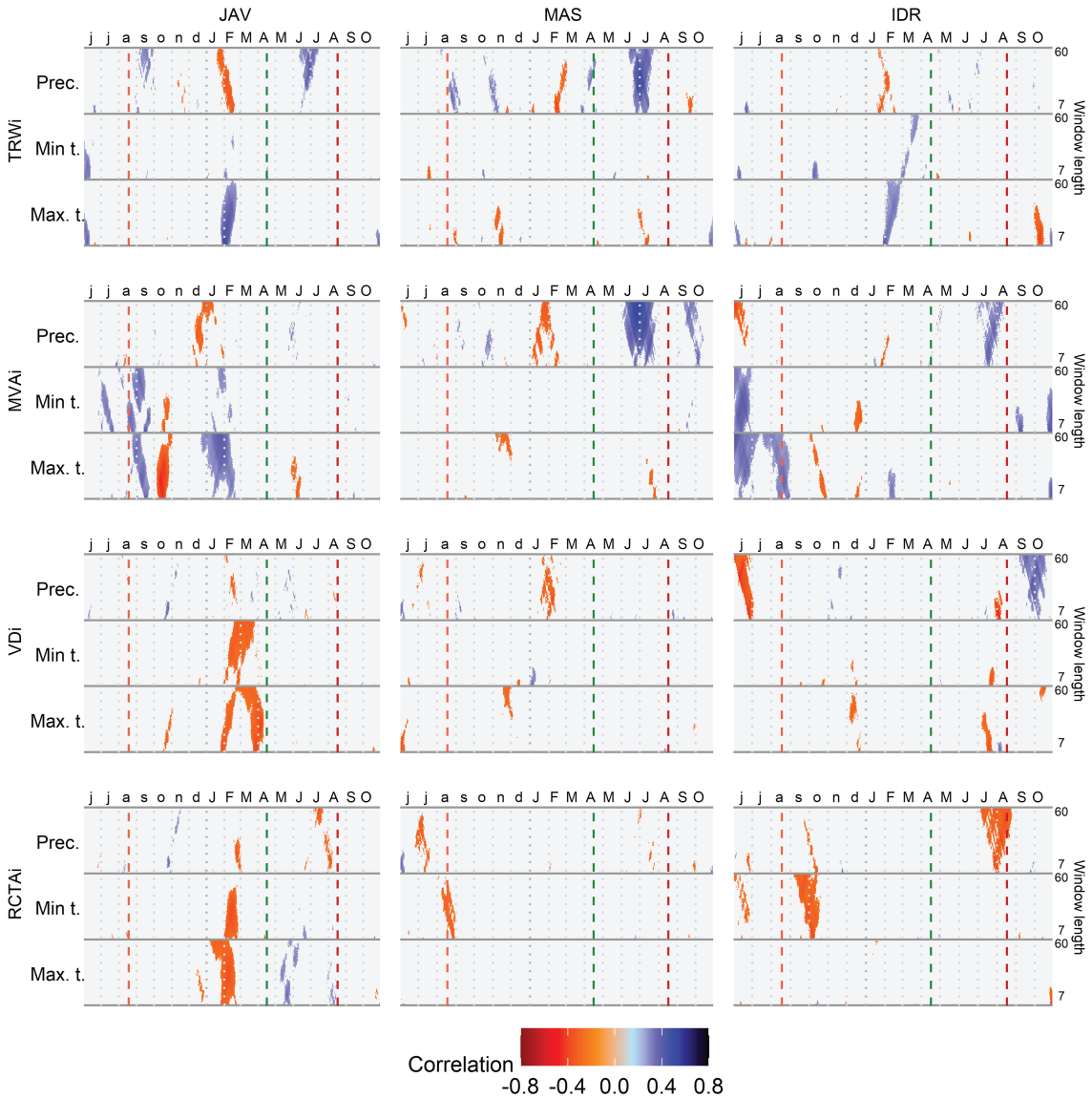

FIGURE 5 | Correlations between standardized tree-ring chronologies (tree ring width - TRWi, mean vessel area - MVAi, vessel density - VDi and relative conductive area - RCTAi) and maximum and minimum daily temperature and daily precipitation sums at Javornik (JAV), Mašun (MAS) and Idrija (IDR) using a time window spanning between 7 and 60 days. Vertical dashed lines from left to right depict the approximate timing of the growing season based on previous data (Prislan et al., 2013): end of previous growing season (light red), start (green), and end (dark red) of current growing season.

In general, vessels with the largest lumen area usually appeared between 15 and 40% of the tree ring width, whereas initial vessels were slightly smaller (**Figures 7A–C**). Furthermore, a different declining trend in MVA was observed in the second half of the tree ring width in the case of wet and dry summers. In a wet summer, MVA slowly decreased to 60–70% of tree ring width, while an abrupt decrease in MVA was observed in the last 25% of the tree ring width. In a dry summer, MVA significantly decreased after 50% of tree ring width. At all sites, the differences in intra-annual trends between dry and wet summers were significant (**Figure 7**). The most pronounced differences in decreasing MVA trend were observed at MAS (**Figure 7B**).

DISCUSSION

A comparison of TRW and vessel features, and their relationships with climate factors, revealed differences between beech trees from three sites in Slovenia differing in climate conditions and leaf phenology. At all sites, a significant relationship was found between VD, RCTA, and TRW, while MVA showed no relationship with other parameters, suggesting different response to variation in temperature and precipitation. Our first hypothesis was thus confirmed. We also confirmed our second hypothesis; the response of TRW, VD, and RCTA to local climatic conditions differed between sites at the inter-annual level. Differences were also observed between sites in

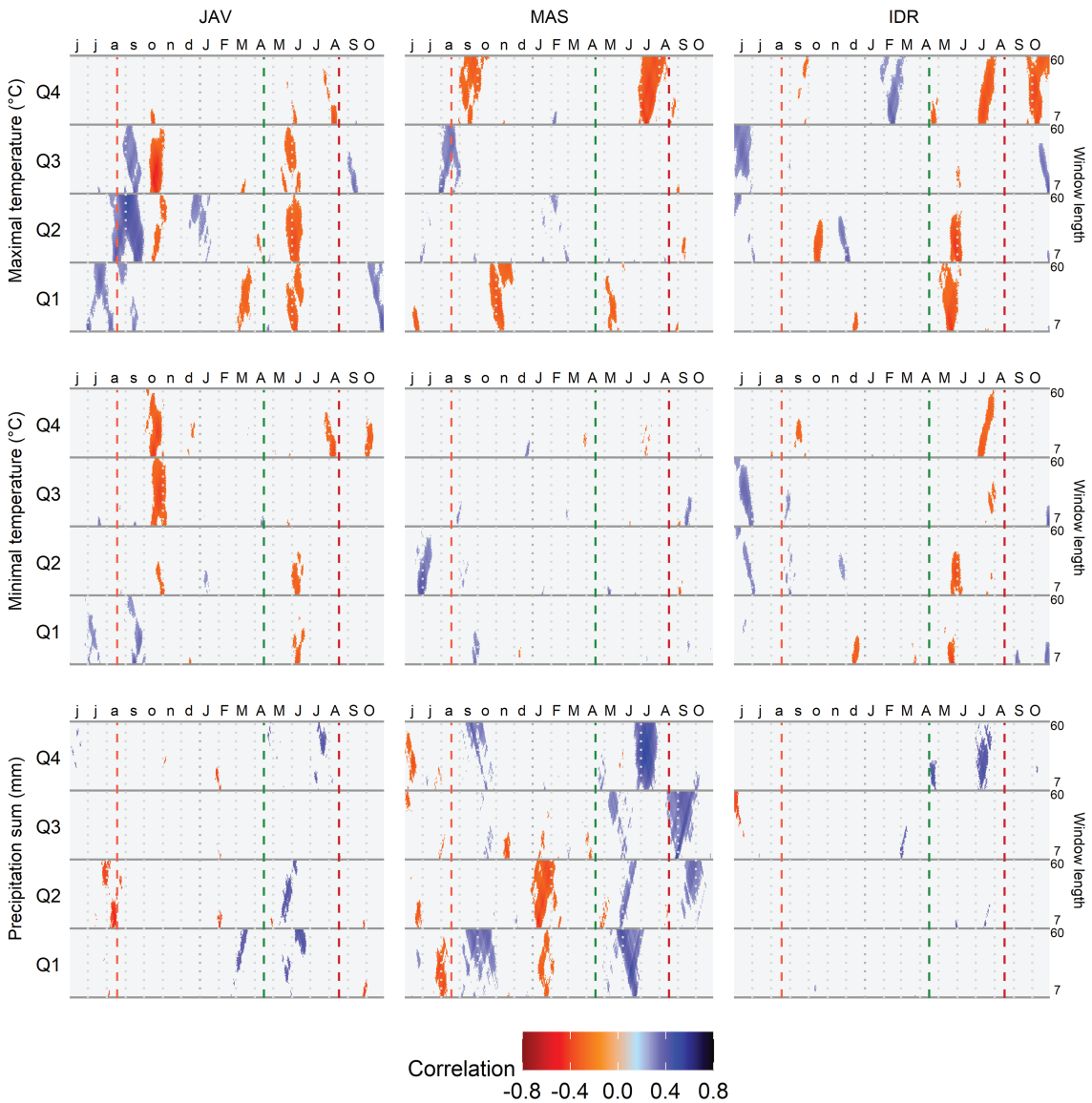

FIGURE 6 | Correlation analysis between the standardized chronologies of mean vessel area (MVA) in quarters Q1–Q4 and maximum and minimum daily temperature and daily precipitation sums at Javornik (JAV), Mašun (MAS), and Idrija (IDR) using a time window spanning between 7 and 60 days. Vertical dashed lines from left to right depict the approximate timing of the growing season based on previous data (Prislan et al., 2013): end of previous growing season (light red), start (green), and end (dark red) of current growing season.

the MVA climatic signal at the intra-annual level. In addition, the response of MVA varied temporally within the tree ring; the first quarter showed the highest correlation with the previous year's climatic conditions, while the last quarter showed the highest correlations with current summer conditions (confirming our third hypothesis). However, under extreme weather conditions (i.e., dry summer), trees at all sites responded similarly (i.e., narrower TRW, higher VD, and RCTA). Contrary to our expectations, trees at IDR (which is characterized as a late flushing site) showed the least pronounced response to climatic conditions compared to the other two sites, (characterized as early flushing), therefore the fourth hypothesis was rejected.

Relationship Between Measured Tree-Ring Parameters

We developed multi-decadal chronologies of TRW and vessel features at the three forest sites representing the original stands of three Slovenian beech provenances. The comparison showed significant differences among sites in terms of TRW, VD, and RCTA. Further correlation analysis revealed that, in wider tree rings, VD and RCTA were generally smaller, which is in agreement with previous studies (Eilmann et al., 2014; Oladi et al., 2014; Diaconu et al., 2016). Since vessels of multiple years are involved in water transport in diffuse-porous beech, the influence of a single tree ring on the total water-transport capacity is only partial (Gasson, 1985). Nevertheless, higher RTCA in narrower

TABLE 3 | Differences in mean tree-ring parameters and mean summer climatic conditions among the three wettest and driest years at sites Javornik (JAV), Mašun (MAS), and Idrija (IDR).

Site	Season	Year	TRW		RCTA		VD		Extreme June – July climate							
									Prec. (mm)		Max. temp (°C)		Min. temp (°C)		SPEI	
JAV	Dry	2006; 2012; 2013	1.2	**	21.0	**	121	ns	110	***	25.1	***	11.3	**	−2.29	***
	Wet	1965; 1961; 1989	2.1		16.4		108		402		21.1		8.9		0.81	
MAS	Dry	2006; 2013; 2016	1.1	**	20.3	***	115	**	89	***	22.5	***	9.9	**	−2.44	***
	Wet	1961; 1965; 1989	2.2		14.3		85		392		18.9		7.4		0.66	
IDR	Dry	1994; 2003; 2006	1.3	ns	21.2	ns	138	ns	174	**	26.2	***	13.7	**	−1.69	***
	Wet	1995; 1980; 1990	1.5		19.8		128		543		21.0		10.8		0.89	

*TRW, tree-ring width; RCTA, relative conductive area; VD, vessel density; Prec, precipitation amounts; Max. temp, maximum temperatures; Min. temp, minimum temperatures; and SPEI, standardized precipitation evapotranspiration index; JAV, MAS, and IDR. Significance of differences in tree ring characteristic and climate variables between dry and wet seasons (ANOVA) is market by ns, not significant; **p < 0.01 and ***p < 0.001.*

rings suggests priority being given to water transport rather than mechanical functions, since the need for additional strength becomes less important in adult trees (Rao et al., 1997).

In contrast to VD and RCTA, MVA did not show significant relationships with TRW. Similar results for beech were reported by Sass and Eckstein (1995) and Diaconu et al. (2016), who concluded that MVA is affected by different environmental signals than TRW and can therefore be used as an additional ecological indicator. Oladi et al. (2014) suggested that VD and TRW are highly dependent on environmental factors, while MVA and RCTA are more endogenously controlled and therefore show less year-to-year variation (Carrer et al., 2015). Here, we observed that MVA was similar at JAV and MAS, while it was significantly smaller at IDR, which could be linked to differences in leaf phenology. In several genetic studies (Brus, 2010; Robson et al., 2018), the beech population at IDR was considered to be late flushing, which could be an adaptation to surviving long winters during the last glacial period. The importance of the genetic predisposition of beech has been studied in recent decades with common garden experiments (Eilmann et al., 2014; Hajek et al., 2016). Eilmann et al. (2014) reported that radial increments in beech are mostly controlled by environment, while the water transport system may reflect provenance-specific adaptation and thus genetic predisposition.

Climate Influence on Tree-Ring Width

Trees at JAV showed the strongest response to variation in climatic conditions and trees at IDR the weakest. IDR was characterized by the highest amount of annual precipitation and had the highest average annual temperature among the sites (**Table 1**). Considering the findings from provenance trials (e.g., Robson et al., 2011) that IDR is a late flushing provenance, it could be assumed that radial growth at this site occurs at higher temperatures and that the trees are therefore less sensitive to fluctuations in climatic conditions (Prislan et al., 2013; Martinez del Castillo et al., 2018). Similar weak climate-growth relationships have been found for several other beech forest sites in the eastern Alps at elevations between 800 and 1,100 m a.s.l. (Dittmar et al., 2003; Di Filippo et al., 2007). This implies that precipitation is not limiting at these sites, and thus temperature mainly controls growth. Similar findings were recently shown for Norway spruce, where only temperature was found to be a limiting climatic factor at sites with more than 1,600 mm annual precipitation (Jevšenak et al., 2021).

Based on 10-year xylogenetic observations of beech from two sites in Slovenia (Prislan et al., 2019), we estimated that the growing season at the forest sites included in this study starts at the beginning of May and ends by mid-August. According to these estimates, TRW at the selected sites is mostly controlled by temperature before the growing season and current summer precipitation (**Figure 5**; Piovesan et al., 2005; Skomarkova et al., 2006). By comparing sites in southern and western Europe, Hacket-Pain et al. (2016) identified previous and current summer temperatures and summer precipitation as the main climatic signals affecting the growth of beech. While for northern and north-eastern part of beech distribution range, growth was limited by combination of spring frost and drought stress (Muffler et al., 2020). Finally, growth reduction in beech may also be associated with late spring frost, summer drought, or mast years, which are also strongly affected by temperature (Kolář et al., 2017; Hacket-Pain et al., 2018; Gazol et al., 2019; D'Andrea et al., 2020). Due to climate warming, a higher masting frequency of beech has been observed in recent decades in Central Europe (Bogdziewicz et al., 2021).

Climate Influence on Vessel Features

Variation in vessel diameter is one of the most important parameters for evaluating tree-water relations. Vessel diameter determines numerous physiological xylem traits, such as hydraulic conductivity, vulnerability to freezing-induced embolism, vulnerability to drought-induced cavitation, and probably also to pathogen spread. By adjusting vessel diameter, number and distribution within annual rings, trees regulate water transport efficiency and xylem safety (Oladi et al., 2014; Gleason et al., 2016). Hajek et al. (2016) found that beech copes with drought stress by adjusting vessel number rather than vessel area. Most recent studies, however, have shown that certain tree-level properties, such as tree size and crown size, explain vessel diameter variation much more than general climatic conditions (Rosell et al., 2017). Due to basipetal vessel widening, vessel

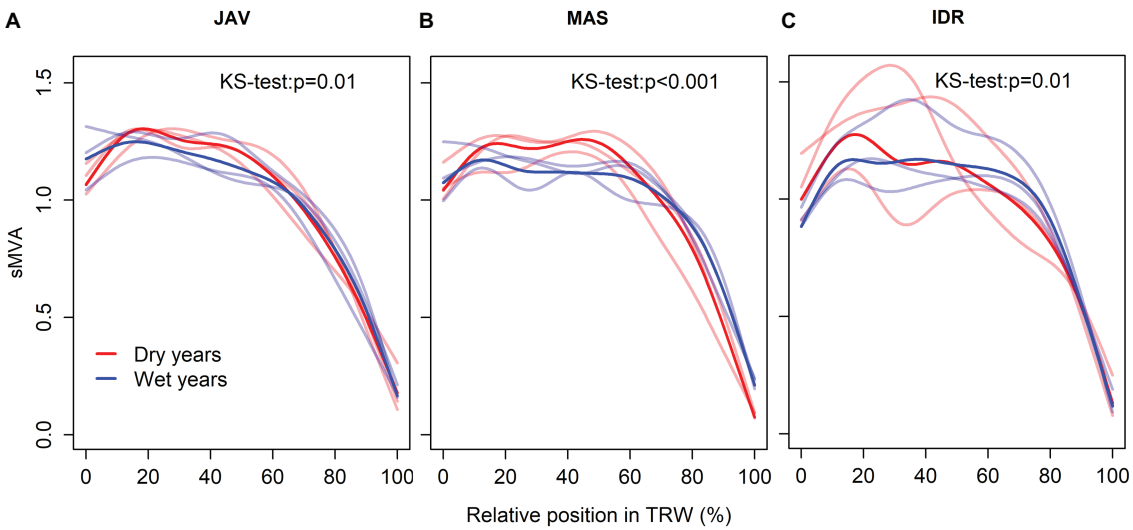

FIGURE 7 | Standardized tracheograms sMVA in common beech for the wettest and the driest summer seasons at the selected sites; **(A)** Javornik (JAV), **(B)** Mašun (MAS), and **(C)** Idrija (IDR). Red and blue lines represent extreme dry and wet years, respectively. Lines with more intensive color represent the mean while transparent lines showing the variability of the selected 3 years for each extreme climate condition. The differences between general additive model (GAM) trends were tested by the Kolmogorov–Smirnov test.

area also depends on its position in a tree (Anfodillo et al., 2012), which needs to be considered when conduit characteristics among different trees and sites are compared (Carrer et al., 2015). In our study, beech trees of comparable heights were sampled to rule out this effect on conduit properties.

The final area of vessels is influenced by endogenous (hormones and cell turgor) and environmental factors (temperature, water availability, and soil nutrients) to optimize xylem water transport from roots to leaves in terms of its safety and efficiency (Tyree and Sperry, 1989; Arend and Fromm, 2007; Hölttä et al., 2010; Hacke et al., 2017). In beech, leaf development and cambial stem reactivation in spring occur almost simultaneously (Prislan et al., 2013). Since leaf development is also environmentally controlled, this may affect the rate of photosynthetic activity and auxin production, as well as the rate of their transport within a tree. Coordination between leaf and stem vascular development therefore exists. The different timing of budburst among selected sites thus suggests that environmental conditions at the onset of radial growth differ. It can be assumed that in the case of the late flushing beech at IDR, these processes occur in the period of higher temperature compared to the early flushing beech at JAV and MAS.

There are contradicting findings in the literature regarding the dendroclimatological potential of beech vessel features (Pourtahmasi et al., 2011). Vessel features are species-specific characteristics, although external factors affect their final area to some degree. The plastic response of beech tree-ring structure in response to site conditions has been reported previously (Eilmann et al., 2014; Stojnić et al., 2015). Under favorable growing conditions, precipitation and temperature do not affect vessel characteristics (Prislan et al., 2018), while in an extremely dry year, a significant link between soil moisture and vessel area has been found (Giagli et al., 2016). Of all the measured vessel features, only MVA showed consistently high correlations with different climatic parameters at all sites, but at different time periods. While MVA at IDR and JAV showed high positive correlations with the temperature in the previous growing season, it was mainly correlated by summer precipitation at MAS. Although the annual amount of precipitation at MAS is relatively high (more than 1,600 mm), it is located in the sub-Mediterranean Karst region, on soils with low water retention capacity (Bakalowicz, 2015). Thus, trees can experience water deficit during growth, even with a relatively high amount of precipitation. The positive correlation between temperatures in summer and autumn of the previous year on vessel area at JAV and IDR could be explained by the relationship between cessation of wood formation in the previous autumn and the onset of leaf phenology in the current vegetation period, recently observed by Marchand et al. (2020). They found earlier bud-burst in the case of earlier cessation of wood formation in the previous year. Earlier bud burst and the development of leaves may be related to changes in hormone concentrations (i.e., auxin) affecting the differentiation of vessels (Aloni, 2007). The positive effect of previous autumn conditions may thus positively contribute to the amount of storage reserves, which are used for foliage development in the next spring and for maintaining winter respiration (Barbaroux et al., 2003). Furthermore, assuming sufficient water availability, we would expect more photo-assimilates in a warm summer and, consequently, greater carbohydrate reserves (and growth; Klesse et al., 2020). Greater carbohydrate reserves could affect the turgor required and thus cell size (Cabon et al., 2020). Compared to other species (e.g., pedunculate oak), the first quarter of tree ring width in beech is less dependent on stored carbohydrate reserves because its growth starts at the same time as leaf development, which quickly start to supply developing tissues with assimilates (Barbaroux and Bréda, 2002).

Although beech is a diffuse-porous species, vessel area in initial and terminal parts of the tree ring differs, being smaller in the latter part (Sass and Eckstein, 1995; Prislan et al., 2018). We found that initial vessels were smaller than the subsequent ones (**Figure 7**), which may reflect different environmental conditions at the time of their formation, especially in terms of moisture supply. On an intra-annual scale, no atypical distribution of vessel area (e.g., intra-annual density fluctuations – IADFs) was observed at any of the selected forest sites (**Supplementary Figure S2**). In the first, second, and third quarters, MVA was similar among the sites (**Figure 2**), while in the last quarter, MVA significantly differed among all sites, suggesting a strong link with local conditions (Pourtahmasi et al., 2011). By dividing tree rings into quarters, relationships between MVA and climate conditions were evaluated at the intra-annual level (**Figure 6**). To the best of our knowledge, apart from Sass and Eckstein (1995), no such analyses have been performed for beech. We found that different climatic variables generally controlled the distribution of vessel area within tree rings at the selected sites. In the first quarter, MVA negatively and positively correlated with maximum temperature and precipitation before the growing season and in spring, respectively. While, vessel area in the second quarter was negatively correlated with early summer temperatures. In addition, MVA in the last quarter was positively and negatively correlated with mid-summer precipitation and maximum temperature, respectively. A positive correlation between late summer precipitations on vessels formed at the end of the growing season was also reported by Sass and Eckstein (1995). The results suggest the intra-annual variability in vessels area could be used for reconstruction of climate conditions before and during the time they were formed (e.g., Castagneri et al., 2017). In order to better understand how short-term climate conditions during the growing season affect vessel formation, the findings should be verified with studies on intra-annual xylem formation (e.g., Prislan et al., 2018). Furthermore, the influence of intra-seasonal climate variability on other vessel features (e.g., vessel grouping or potential hydraulic conductivity) may also be evaluated (Schuldt et al., 2016).

Beech Tree Ring Features Under Climate Change (Extreme Weather Conditions)

In the past six decades, the average annual temperature has increased by 0.36°C, and the amount of precipitation has decreased by 3% per decade in central Europe (de Luis et al., 2014; Vertačnik et al., 2018). Slovenia belongs to a transitional region, which is affected by both, Mediterranean and temperate climate regimes (Koffi and Koffi, 2008). Thus, based on different future climate scenarios further increases in temperature, changes in precipitation patterns and increased frequency of extreme weather events are expected which could result in changing climate and growth conditions (Dolschak et al., 2019). Several dendroclimatological studies have suggested that increasing temperature will positively affect radial growth at typical beech forest sites (Dulamsuren et al., 2016; Martinez del Castillo et al., 2018; Vospernik and Nothdurft, 2018; Prislan et al., 2019). However, these studies did not generally take into account the overall impact of extreme weather events on tree growth and possible changes in beech spatial distribution (Saltre et al., 2015). In addition, extreme weather events may have different effects on tree growth (Weigel et al., 2018). Climate-associated severe events, such as droughts, ice storms, and heatwaves, amplify the susceptibility of beech to secondary damage by various pathogens and pests (La Porta et al., 2008). Also in this study, we observed an unusual trend in the MVA chronology at IDR, indicating a decline in MVA around 1980 (**Figure 4**). Indeed, historical records show a large-scale ice break disturbance at this site (Šifrer, 1977), which seems to have affected the growth of some trees. Recent studies showed that late spring frost essentially influenced beech foliage and TRW in the current year (D'Andrea et al., 2020; Decuyper et al., 2020; Sanguesa-Barreda et al., 2021). However, trees fully recovered in the following growing season, which indicates high resilience of beech to this stress event (D'Andrea et al., 2020). In contrast, no effect of summer drought was found on the radial growth of beech in the current year (D'Andrea et al., 2020), but it may be evident in the following year (Decuyper et al., 2020).

In addition to TRW, extreme climatic events significantly affect leaf phenology and wood anatomy (Bräuning et al., 2016; Carrer et al., 2016; Popkova et al., 2018). It was found that the effect of drought on vessel diameter is more pronounced if water shortage occurs early in the growing season rather later in the season. This suggests an increased sensitivity of earlywood cells to drought conditions (Arend and Fromm, 2007; Cabon et al., 2020). However, we found that vessel features (area and distribution) in beech at the selected sites were affected by drought conditions between June and August. In dry years, the trend of vessel area already began to decrease in the first half of tree ring width, which could affect turgor, resulting in smaller vessels (Popkova et al., 2018; Cabon et al., 2020). This was particularly evident in the exceptionally dry year 2003, when an almost semi-ring porous distribution of vessels was observed (**Supplementary Figure S3B**) in some tree rings at IDR (Bosshard, 1982; Schweingruber, 2007). In wetter and average years, on the other hand, an abrupt decrease in vessel area is observed in the fourth quarter of the annual ring (**Figure 7**; **Supplementary Figure S3A**).

CONCLUSION

This study has shown that the emerging field of quantitative wood anatomy complements both dendroecological studies and climate change research (Buttò et al., 2020; Piermattei et al., 2020). For example, vessel area and distribution, in addition to annual tree ring width, provide a better understanding of how changes in growing conditions affect not only radial growth, but also wood anatomy and its properties. Our results show differences in relationships between climate and tree ring features (e.g., TRW, VD, RCTA, and MVA) at the selected sites. We can conclude that beech trees with different leaf phenologies respond differently to changes of climatic condition, whereby early flushing beech sites are affected by similar climate drivers, while beech characterized as late flushing seems to be less sensitive to climatic changes. Although wood anatomical traits, such as vessel diameter and frequency, are easily accessible ecological or climatological

proxies for analyzing adaptation processes to environmental changes (Campelo et al., 2010; Crous et al., 2012), more detailed knowledge is needed on how much of the variability in these traits is environmentally driven (Leal et al., 2003; Fisher et al., 2007; Tixier et al., 2013). In order to better understand the response of beech with different leaf phenology and growth strategy, additional sites from elevational transect and variable soil and stand properties, as well as ecophysiological measurements should be included in future analyses.

DATA AVAILABILITY STATEMENT

The raw data supporting the conclusions of this article will be made available by the authors, without undue reservation.

AUTHOR CONTRIBUTIONS

PP, JJ, JG, and DA planned and designed the research. PP and GB performed the sampling. DA and PP contributed to the sample preparation and capturing of high resolution images with light microscope and wrote the manuscript with contributions from all co-authors. DA and GA contributed to image analyzing in Roxas and Image-Pro Plus. DA, JJ, and PP analyzed and interpreted the data. All authors contributed to the article and approved the submitted version.

FUNDING

This work was supported by the Slovenian Research Agency, the young researchers' program (DA), program P4-0107, and projects Z4-7318 and J4-2541.

ACKNOWLEDGMENTS

The authors gratefully acknowledge Robert Krajnc for his help in the field and Tatjana Rajniš and Gregor Skoberne for their help in the laboratory.

SUPPLEMENTARY MATERIAL

The Supplementary Material for this article can be found online at: https://www.frontiersin.org/articles/10.3389/fpls.2021.669229/full#supplementary-material

REFERENCES

Abrantes, J., Campelo, F., García-González, I., and Nabais, C. (2012). Environmental control of vessel traits in *Quercus ilex* under Mediterranean climate: relating xylem anatomy to function. *Trees* 27, 655–662. doi: 10.1007/s00468-012-0820-6

Aloni, R. (2007). "Phytohormonal mechanisms that control wood quality formation in young and mature trees" in *The Compromised Wood Workshop*. eds. K. Entwistle, P. Harris and J. Walker; January 29–30, 2007 (Christchurch, New Zealand: The Wood Technology Research Centre, University of Canterbury), 1–22.

Anfodillo, T., Deslauriers, A., Menardi, R., Tedoldi, L., Petit, G., and Rossi, S. (2012). Widening of xylem conduits in a conifer tree depends on the longer time of cell expansion downwards along the stem. *J. Exp. Bot.* 63, 837–845. doi: 10.1093/jxb/err309

Arend, M., and Fromm, J. (2007). Seasonal change in the drought response of wood cell development in poplar. *Tree Physiol.* 27, 985–992. doi: 10.1093/treephys/27.7.985

Bakalowicz, M. (2015). Karst and karst groundwater resources in the Mediterranean. *Environ. Earth Sci.* 74, 5–14. doi: 10.1007/s12665-015-4239-4

Barbaroux, C., and Bréda, N. (2002). Contrasting distribution and seasonal dynamics of carbohydrate reserves in stem wood of adult ring-porous sessile oak and diffuse-porous beech trees. *Tree Physiol.* 22, 1201–1210. doi: 10.1093/treephys/22.17.1201

Barbaroux, C., Bréda, N., and Dufrêne, E. (2003). Distribution of above-ground and below-ground carbohydrate reserves in adult trees of two contrasting broad-leaved species (Quercus petraea and *Fagus sylvatica*). *New Phytol.* 157, 605–615. doi: 10.1046/j.1469-8137.2003.00681.x

Bogdziewicz, M., Hacket-Pain, A., Kelly, D., Thomas, P. A., Lageard, J., and Tanentzap, A. J. (2021). Climate warming causes mast seeding to break down by reducing sensitivity to weather cues. *Glob. Chang. Biol.* 27, 1952–1961. doi: 10.1111/gcb.15560

Bolte, A., Czajkowski, T., and Kompa, T. (2007). The north-eastern distribution range of European beech: a review. *Forestry* 80, 413–429. doi: 10.1093/forestry/cpm028

Bosshard, H. H. (1982). *Holzkunde: Band 1 Mikroskopie und Makroskopie des Holzes*. Basel: Birkhäuser Basel.

Bräuning, A., De Ridder, M., Zafirov, N., García-González, I., Petrov Dimitrov, D., and Gärtner, H. (2016). Tree-ring features: indicators of extreme event impacts. *IAWA J.* 37, 206–231. doi: 10.1163/22941932-20160131

Brus, R. (2010). Growing evidence for the existence of glacial refugia of European beech (*Fagus sylvatica* L.) in the South-Eastern Alps and north-western Dinaric Alps. *Period. Biol.* 112, 239–246.

Bunn, A. G. (2008). A dendrochronology program library in R (dplR). *Dendrochronologia* 26, 115–124. doi: 10.1016/j.dendro.2008.01.002

Buttò, V., Shishov, V., Tychkov, I., Popkova, M., He, M., Rossi, S., et al. (2020). Comparing the cell dynamics of tree-ring formation observed in microcores and as predicted by the Vaganov–Shashkin model. *Front. Plant Sci.* 11:1268. doi: 10.3389/fpls.2020.01268

Cabon, A., Fernandez-de-Una, L., Gea-Izquierdo, G., Meinzer, F. C., Woodruff, D. R., Martinez-Vilalta, J., et al. (2020). Water potential control of turgor-driven tracheid enlargement in scots pine at its xeric distribution edge. *New Phytol.* 225, 209–221. doi: 10.1111/nph.16146

Campelo, F., Nabais, C., Gutiérrez, E., Freitas, H., and García-González, I. (2010). Vessel features of *Quercus ilex* L. growing under Mediterranean climate have a better climatic signal than tree-ring width. *Trees* 24, 463–470. doi: 10.1007/s00468-010-0414-0

Carrer, M., Brunetti, M., and Castagneri, D. (2016). The imprint of extreme climate events in century-long time series of wood anatomical traits in high-elevation conifers. *Front. Plant Sci.* 7:683. doi: 10.3389/fpls.2016.00683

Carrer, M., von Arx, G., Castagneri, D., and Petit, G. (2015). Distilling allometric and environmental information from time series of conduit size: the standardization issue and its relationship to tree hydraulic architecture. *Tree Physiol.* 35, 27–33. doi: 10.1093/treephys/tpu108

Castagneri, D., Fonti, P., von Arx, G., and Carrer, M. (2017). How does climate influence xylem morphogenesis over the growing season? Insights from long-term intra-ring anatomy in *Picea abies*. *Ann. Bot.* 119, 1011–1020. doi: 10.1093/aob/mcw274

Chave, J., Coomes, D., Jansen, S., Lewis, S. L., Swenson, N. G., and Zanne, A. E. (2009). Towards a worldwide wood economics spectrum. *Ecol. Lett.* 12, 351–366. doi: 10.1111/j.1461-0248.2009.01285.x

Cook, E. R., and Kairiukstis, L. A. (1990). *Methods of Dendrochronology: Applications in the Environmental Sciences*. Netherlands: Springer.

Cornes, R. C., van der Schrier, G., van den Besselaar, E. J. M., and Jones, P. D. (2018). An ensemble version of the E-OBS temperature and precipitation data sets. *J. Geophys. Res. Atmos.* 123, 9391–9409. doi: 10.1029/2017jd028200

Crous, C. J., Jacobs, S. M., and Esler, K. J. (2012). Wood anatomical traits as a measure of plant responses to water availability: invasive *Acacia mearnsii* De wild. Compared with native tree species in fynbos riparian ecotones, South Africa. *Trees* 26, 1527–1536. doi: 10.1007/s00468-012-0726-3

Čufar, K., De Luis, M., Prislan, P., Gricar, J., Crepinsek, Z., Merela, M., et al. (2015). Do variations in leaf phenology affect radial growth variations in *Fagus sylvatica*? *Int. J. Biometeorol.* 59, 1127–1132. doi: 10.1007/s00484-014-0896-3

Čufar, K., Prislan, P., de Luis, M., and Gričar, J. (2008). Tree-ring variation, wood formation and phenology of beech (*Fagus sylvatica*) from a representative site in Slovenia, SE Central Europe. *Trees* 22, 749–758. doi: 10.1007/s00468-008-0235-6

D'Andrea, E., Rezaie, N., Prislan, P., Gričar, J., Collalti, A., Muhr, J., et al. (2020). Frost and drought: effects of extreme weather events on stem carbon dynamics in a Mediterranean beech forest. *Plant Cell Environ.* 43, 2365–2379. doi: 10.1111/pce.13858

de Luis, M., Čufar, K., Saz, M. A., Longares, L. A., Ceglar, A., and Kajfež-Bogataj, L. J. R. E. C. (2014). Trends in seasonal precipitation and temperature in Slovenia during 1951–2007. *Reg. Environ. Chang.* 14, 1801–1810. doi: 10.1007/s10113-012-0365-7

Decuyper, M., Chávez, R. O., Čufar, K., Estay, S. A., Clevers, J. G. P. W., Prislan, P., et al. (2020). Spatio-temporal assessment of beech growth in relation to climate extremes in Slovenia—an integrated approach using remote sensing and tree-ring data. *Agric. For. Meteorol.* 287:107925. doi: 10.1016/j.agrformet.2020.107925

del Río, M., Pretzsch, H., Ruíz-Peinado, R., Ampoorter, E., Annighöfer, P., Barbeito, I., et al. (2017). Species interactions increase the temporal stability of community productivity in *Pinus sylvestris—Fagus sylvatica* mixtures across Europe. *J. Ecol.* 105, 1032–1043. doi: 10.1111/1365-2745.12727

Di Filippo, A., Biondi, F., Čufar, K., de Luis, M., Grabner, M., Maugeri, M., et al. (2007). Bioclimatology of beech (*Fagus sylvatica* L.) in the eastern Alps: spatial and altitudinal climatic signals identified through a tree-ring network. *J. Biogeogr.* 34, 1873–1892. doi: 10.1111/j.1365-2699.2007.01747.x

Diaconu, D., Stangler, D. F., Kahle, H. P., and Spiecker, H. (2016). Vessel plasticity of European beech in response to thinning and aspect. *Tree Physiol.* 36, 1260–1271. doi: 10.1093/treephys/tpw053

Dieler, J., and Pretzsch, H. (2013). Morphological plasticity of European beech (*Fagus sylvatica* L.) in pure and mixed-species stands. *For. Ecol. Manag.* 295, 97–108. doi: 10.1016/j.foreco.2012.12.049

Dittmar, C., Zech, W., and Elling, W. (2003). Growth variations of common beech (*Fagus sylvatica* L.) under different climatic and environmental conditions in Europe: a dendroecological study. *For. Ecol. Manag.* 173, 63–78. doi: 10.1016/S0378-1127(01)00816-7

Dolschak, K., Gartner, K., and Berger, T. W. (2019). The impact of rising temperatures on water balance and phenology of European beech (*Fagus sylvatica* L.) stands. *Model. Earth Syst. Environ.* 5, 1347–1363. doi: 10.1007/s40808-019-00602-1

Dulamsuren, C., Hauck, M., Kopp, G., Ruff, M., and Leuschner, C. (2016). European beech responds to climate change with growth decline at lower, and growth increase at higher elevations in the center of its distribution range (SW Germany). *Trees* 31, 673–686. doi: 10.1007/s00468-016-1499-x

Eilmann, B., Sterck, F., Wegner, L., de Vries, S. M., von Arx, G., Mohren, G. M., et al. (2014). Wood structural differences between northern and southern beech provenances growing at a moderate site. *Tree Physiol.* 34, 882–893. doi: 10.1093/treephys/tpu069

Fisher, J. B., Goldstein, G., Jones, T. J., and Cordell, S. (2007). Wood vessel diameter is related to elevation and genotype in the Hawaiian tree *Metrosideros polymorpha* (Myrtaceae). *Am. J. Bot.* 94, 709–715. doi: 10.3732/ajb.94.5.709

Fonti, P., von Arx, G., Garcia-Gonzalez, I., Eilmann, B., Sass-Klaassen, U., Gartner, H., et al. (2010). Studying global change through investigation of the plastic responses of xylem anatomy in tree rings. *New Phytol.* 185, 42–53. doi: 10.1111/j.1469-8137.2009.03030.x

Garamszegi, B., Kazmer, M., Kolozs, L., and Kern, Z. (2020). Changing climatic sensitivity and effects of drought frequency on the radial growth of *Fagus sylvatica* at the xeric frontiers of Central Europe. *Q. J. Hun. Meteorol. Sc.* 124, 227–251. doi: 10.28974/idojaras.2020.2.5

Gärtner, H., Lucchinetti, S., and Schweingruber, F. H. (2015). A new sledge microtome to combine wood anatomy and tree-ring ecology. *IAWA J.* 36, 452–459. doi: 10.1163/22941932-20150114

Gasson, P. (1985). Automatic measurement of vessel lumen area and diameter with particular reference to pedunculate oak and common beech. *IAWA J.* 6, 219–237. doi: 10.1163/22941932-90000941

Gazol, A., Camarero, J. J., Colangelo, M., de Luis, M., Martínez del Castillo, E., and Serra-Maluquer, X. (2019). Summer drought and spring frost, but not their interaction, constrain European beech and silver fir growth in their southern distribution limits. *Agric. For. Meteorol.* 278:107695. doi: 10.1016/j.agrformet.2019.107695

Giagli, K., Gricar, J., Vavrcík, H., Mensík, L., and Gryc, V. (2016). The effects of drought on wood formation in *Fagus sylvatica* during two contrasting years. *IAWA J.* 37, 332–348. doi: 10.1163/22941932-20160137

Gleason, S. M., Westoby, M., Jansen, S., Choat, B., Hacke, U. G., Pratt, R. B., et al. (2016). Weak tradeoff between xylem safety and xylem-specific hydraulic efficiency across the world's woody plant species. *New Phytol.* 209, 123–136. doi: 10.1111/nph.13646

Gömöry, D., and Paule, L. (2011). Trade-off between height growth and spring flushing in common beech (*Fagus sylvatica* L.). *Ann. For. Sci.* 68, 975–984. doi: 10.1007/s13595-011-0103-1

Hacke, U. G., Spicer, R., Schreiber, S. G., and Plavcova, L. (2017). An ecophysiological and developmental perspective on variation in vessel diameter. *Plant Cell Environ.* 40, 831–845. doi: 10.1111/pce.12777

Hacket-Pain, A. J., Ascoli, D., Vacchiano, G., Biondi, F., Cavin, L., Conedera, M., et al. (2018). Climatically controlled reproduction drives interannual growth variability in a temperate tree species. *Ecol. Lett.* 21, 1833–1844. doi: 10.1111/ele.13158

Hacket-Pain, A. J., Cavin, L., Friend, A. D., and Jump, A. S. (2016). Consistent limitation of growth by high temperature and low precipitation from range core to southern edge of European beech indicates widespread vulnerability to changing climate. *Eur. J. For. Res.* 135, 897–909. doi: 10.1007/s10342-016-0982-7

Hajek, P., Kurjak, D., von Wühlisch, G., Delzon, S., and Schuldt, B. (2016). Intraspecific variation in wood anatomical, hydraulic, and foliar traits in ten european beech provenances differing in growth yield. *Front. Plant Sci.* 7:791. doi: 10.3389/fpls.2016.00791

Harvey, J. E., Smiljanic, M., Scharnweber, T., Buras, A., Cedro, A., Cruz-Garcia, R., et al. (2019). Tree growth influenced by warming winter climate and summer moisture availability in northern temperate forests. *Glob. Chang. Biol.* 26, 2505–2518. doi: 10.1111/gcb.14966

Hölttä, T., Makinen, H., Nojd, P., Makela, A., and Nikinmaa, E. (2010). A physiological model of softwood cambial growth. *Tree Physiol.* 30, 1235–1252. doi: 10.1093/treephys/tpq068

Jevšenak, J. (2020). New features in the dendroTools R package: bootstrapped and partial correlation coefficients for monthly and daily climate data. *Dendrochronologia* 63:125753. doi: 10.1016/j.dendro.2020.125753

Jevšenak, J., and Levanič, T. (2018). dendroTools: R package for studying linear and nonlinear responses between tree-rings and daily environmental data. *Dendrochronologia* 48, 32–39. doi: 10.1016/j.dendro.2018.01.005

Jevšenak, J., Tychkov, I., Gricar, J., Levanic, T., Tumajer, J., Prislan, P., et al. (2021). Growth-limiting factors and climate response variability in Norway spruce (*Picea abies* L.) along an elevation and precipitation gradients in Slovenia. *Int. J. Biometeorol.* 65, 311–324. doi: 10.1007/s00484-020-02033-5

Jezik, M., Blazenec, M., Kucera, J., Strelcova, K., and Ditmarova, L. (2016). The response of intra-annual stem circumference increase of young European beech provenances to 2012-2014 weather variability. *iForest* 9, 960–969. doi: 10.3832/ifor1829-009

Klesse, S., von Arx, G., Gossner, M. M., Hug, C., Rigling, A., and Queloz, V. (2020). Amplifying feedback loop between growth and wood anatomical characteristics of *Fraxinus excelsior* explains size-related susceptibility to ash dieback. *Tree Physiol.* 41, 683–696. doi: 10.1093/treephys/tpaa091

Klisz, M., Buttò, V., Rossi, S., Morin, H., and Jastrzębowski, S. (2019). Intra-annual stem size variations converge across marginal populations of European beech. *Trees* 34, 255–265. doi: 10.1007/s00468-019-01915-5

Koffi, B., and Koffi, E. (2008). Heat waves across Europe by the end of the 21st century: multiregional climate simulations. *Clim. Res.* 36, 153–168. doi: 10.3354/cr00734

Kolář, T., Čermák, P., Trnka, M., Žid, T., and Rybníček, M. (2017). Temporal changes in the climate sensitivity of Norway spruce and European beech along an elevation gradient in Central Europe. *Agric. For. Meteorol.* 239, 24–33. doi: 10.1016/j.agrformet.2017.02.028

Kramer, K., Ducousso, A., Gömöry, D., Hansen, J. K., Ionita, L., Liesebach, M., et al. (2017). Chilling and forcing requirements for foliage bud burst of European beech (*Fagus sylvatica* L.) differ between provenances and are phenotypically plastic. *Agric. For. Meteorol.* 234-235, 172–181. doi: 10.1016/j.agrformet.2016.12.002

La Porta, N., Capretti, P., Thomsen, I. M., Kasanen, R., Hietala, A. M., and Von Weissenberg, K. (2008). Forest pathogens with higher damage potential due to climate change in Europe. *Can. J. Plant Pathol.* 30, 177–195. doi: 10.1080/07060661.2008.10540534

Leal, S., Pereira, H., Grabner, M., and Wimmer, R. (2003). Clonal and site variation of vessels in 7-year-old *Eucalyptus globulus*. *IAWA J.* 24, 185–195. doi: 10.1163/22941932-90000331

Lenz, A., Hoch, G., and Körner, C. (2013). Early season temperature controls cambial activity and total tree ring width at the alpine treeline. *Plant Ecol. Divers.* 6, 365–375. doi: 10.1080/17550874.2012.711864

Levanic, T. (2009). Atrics—a new system for image acquisition in dendrochronology. *Tree-Ring Res.* 63, 117–122. doi: 10.3959/1536-1098-63.2.117

Marchand, L. J., Dox, I., Gricar, J., Prislan, P., Leys, S., Van den Bulcke, J., et al. (2020). Inter-individual variability in spring phenology of temperate deciduous trees depends on species, tree size and previous year autumn phenology. *Agric. For. Meteorol.* 290:108031. doi: 10.1016/j.agrformet.2020.108031

Martinez del Castillo, E., Prislan, P., Gričar, J., Gryc, V., Merela, M., Giagli, K., et al. (2018). Challenges for growth of beech and co-occurring conifers in a changing climate context. *Dendrochronologia* 52, 1–10. doi: 10.1016/j.dendro.2018.09.001

Matyas, C., Bozic, G., Gomory, D., Ivankovic, M., and Rasztovits, E. (2009). Juvenile growth response of European beech (*Fagus sylvatica* L.) to sudden change of climatic environment in SE European trials. *IForest* 2, 213–220. doi: 10.3832/ifor0519-002

Muffler, L., Weigel, R., Hacket-Pain, A. J., Klisz, M., Maaten, E., Wilmking, M., et al. (2020). Lowest drought sensitivity and decreasing growth synchrony towards the dry distribution margin of European beech. *J. Biogeogr.* 47, 1910–1921. doi: 10.1111/jbi.13884

Oladi, R., Bräuning, A., and Pourtahmasi, K. (2014). "Plastic" and "static" behavior of vessel-anatomical features in oriental beech (*Fagus orientalis* Lipsky) in view of xylem hydraulic conductivity. *Trees* 28, 493–502. doi: 10.1007/s00468-013-0966-x

Piermattei, A., von Arx, G., Avanzi, C., Fonti, P., Gartner, H., Piotti, A., et al. (2020). Functional relationships of wood anatomical traits in Norway spruce. *Front. Plant Sci.* 11:683. doi: 10.3389/fpls.2020.00683

Piovesan, G., Biondi, F., Bernabei, M., Di Filippo, A., and Schirone, B. (2005). Spatial and altitudinal bioclimatic zones of the Italian peninsula identified from a beech (*Fagus sylvatica* L.) tree-ring network. *Acta Oecol.* 27, 197–210. doi: 10.1016/j.actao.2005.01.001

Popkova, M. I., Vaganov, E. A., Shishov, V. V., Babushkina, E. A., Rossi, S., Fonti, M. V., et al. (2018). Modeled tracheidograms disclose drought influence on *Pinus sylvestris* tree-rings structure from Siberian forest—steppe. *Front. Plant Sci.* 9:1144. doi: 10.3389/fpls.2018.01144

Pourtahmasi, K., Lotfiomran, N., Bräuning, A., and Parsapajouh, D. (2011). Tree-ring width and vessel characteristics of oriental beech (*Fagus Orientalis*) along an altitudinal gradient in the Caspian forests, Northern Iran. *IAWA J.* 32, 461–473. doi: 10.1163/22941932-90000071

Prislan, P., Cufar, K., De Luis, M., and Gricar, J. (2018). Precipitation is not limiting for xylem formation dynamics and vessel development in European beech from two temperate forest sites. *Tree Physiol.* 38, 186–197. doi: 10.1093/treephys/tpx167

Prislan, P., Gričar, J., Čufar, K., de Luis, M., Merela, M., and Rossi, S. (2019). Growing season and radial growth predicted for *Fagus sylvatica* under climate change. *Clim. Chang.* 153, 181–197. doi: 10.1007/s10584-019-02374-0

Prislan, P., Gričar, J., de Luis, M., Smith, K. T., and Čufar, K. (2013). Phenological variation in xylem and phloem formation in *Fagus sylvatica* from two contrasting sites. *Agric. For. Meteorol.* 180, 142–151. doi: 10.1016/j.agrformet.2013.06.001

Rao, R. V., Aebischer, D. P., and Denne, M. P. (1997). Latewood density in relation to wood fibre diameter, wall thickness, and fibre and vessel percentages in *Quercus robur* L. *IAWA J.* 18, 127–138. doi: 10.1163/22941932-90001474

Reyer, C. P. O., Brouwers, N., Rammig, A., Brook, B. W., Epila, J., Grant, R. F., et al. (2015). Forest resilience and tipping points at different spatio-temporal scales: approaches and challenges. *J. Ecol.* 103, 5–15. doi: 10.1111/1365-2745.12337

Robson, T. M., Alía, R., Božič, G., Clark, J., Forstreuter, M., Gömöry, D., et al. (2011). "The timing of leaf flush in European beech (*Fagus sylvatica* L.) saplings." in *Genetic Resources of European Beech (Fagus sylvatica L.) for Sustainable Forestry: Proceedings of the COST E52 "Evaluation of Beech Genetic Resources for Sustainable Forestry."* Final Meeting, May 4–6, 2010; Burgos, Spain (Instituto Nacional de Investigación y Tecnología Agraria y Alimentaria), 61–79.

Robson, T. M., Garzon, M. B., and BeechCOSTe52 Database Consortium (2018). Phenotypic trait variation measured on European genetic trials of *Fagus sylvatica* L. *Sci. Data* 5:180149. doi: 10.1038/sdata.2018.149

Rosell, J. A., Olson, M. E., and Anfodillo, T. (2017). Scaling of xylem vessel diameter with plant size: causes, predictions, and outstanding questions. *Curr. For. Rep.* 3, 46–59. doi: 10.1007/s40725-017-0049-0

Saltre, F., Duputie, A., Gaucherel, C., and Chuine, I. (2015). How climate, migration ability and habitat fragmentation affect the projected future distribution of European beech. *Glob. Chang. Biol.* 21, 897–910. doi: 10.1111/gcb.12771

Sanguesa-Barreda, G., Di Filippo, A., Piovesan, G., Rozas, V., Di Fiore, L., Garcia-Hidalgo, M., et al. (2021). Warmer springs have increased the frequency and extension of late-frost defoliations in southern European beech forests. *Sci. Total Environ.* 775:145860. doi: 10.1016/j.scitotenv.2021.145860

Sass, U., and Eckstein, D. (1995). The variability of vessel size in beech (*Fagus sylvatica* L.) and its ecophysiological interpretation. *Trees* 9, 247–252. doi: 10.1007/BF00202014

Schuldt, B., Knutzen, F., Delzon, S., Jansen, S., Muller-Haubold, H., Burlett, R., et al. (2016). How adaptable is the hydraulic system of European beech in the face of climate change-related precipitation reduction? *New Phytol.* 210, 443–458. doi: 10.1111/nph.13798

Schume, H., Grabner, M., and Eckmüllner, O. (2004). The influence of an altered groundwater regime on vessel properties of hybrid poplar. *Trees* 18, 184–194. doi: 10.1007/s00468-003-0294-7

Schweingruber, F. H. (2007). *Wood Structure and Environment*. Berlin Heidelberg: Springer-Verlag.

Šifrer, M. (1977). Geographic consequences of glaze in forests around Idrija and Postojna. *Acta Geogr.* 16, 195–228.

Šimůnek, V., Vacek, Z., Vacek, S., Králíček, I., and Vančura, K. (2019). Growth variability of European beech (L.) natural forests: dendroclimatic study from Krkonoše National Park. *Cent. Eur. For. J.* 65, 92–102. doi: 10.2478/forj-2019-0010

Skomarkova, M. V., Vaganov, E. A., Mund, M., Knohl, A., Linke, P., Boerner, A., et al. (2006). Inter-annual and seasonal variability of radial growth, wood density and carbon isotope ratios in tree rings of beech (*Fagus sylvatica*) growing in Germany and Italy. *Trees* 20, 571–586. doi: 10.1007/s00468-006-0072-4

Stojanović, D., Levanič, T., Matović, B., Stjepanović, S., and Orlović, S. (2018). Growth response of different tree species (oaks, beech and pine) from SE Europe to precipitation over time. *Dendrobiology* 79, 97–110. doi: 10.12657/denbio.079.009

Stojnić, S., Orlović, S., Miljković, D., Galić, Z., Kebert, M., and von Wühlisch, G. (2015). Provenance plasticity of European beech leaf traits under differing environmental conditions at two Serbian common garden sites. *Eur. J. For. Res.* 134, 1109–1125. doi: 10.1007/s10342-015-0914-y

Stojnic, S., Sass-Klaassen, U., Orlovic, S., Matovic, B., and Eilmann, B. (2013). Plastic growth response of european beech provenances to dry site conditions. *IAWA J.* 34, 475–484. doi: 10.1163/22941932-00000038

Tixier, A., Cochard, H., Badel, E., Dusotoit-Coucaud, A., Jansen, S., and Herbette, S. (2013). *Arabidopsis thaliana* as a model species for xylem hydraulics: does size matter? *J. Exp. Bot.* 64, 2295–2305. doi: 10.1093/jxb/ert087

Trouillier, M., van der Maaten-Theunissen, M., Scharnweber, T., Würth, D., Burger, A., Schnittler, M., et al. (2018). Size matters—a comparison of three methods to assess age- and size-dependent climate sensitivity of trees. *Trees* 33, 183–192. doi: 10.1007/s00468-018-1767-z

Tyree, M. T., and Sperry, J. S. (1989). Vulnerability of xylem to cavitation and ambolism. *Annu. Rev. Plant Physiol. Plant Mol. Biol.* 40, 19–36. doi: 10.1146/annurev.pp.40.060189.000315

Vertačnik, G., Bertalanič, R., Draksler, A., Dolinar, M., Vlahovič, Ž., and Fratnar, P. (2018). Podnebna spremenljivost Slovenije v obdobju 1961–2011. Ljubljana, Agencija Republike Slovenije za okolje.

Vicente-Serrano, S. M., Beguería, S., and López-Moreno, J. I. (2010). A multiscalar drought index sensitive to global warming: the standardized precipitation evapotranspiration index. *J. Clim.* 23, 1696–1718. doi: 10.1175/2009JCLI2909.1

Vitasse, Y., Bresson, C. C., Kremer, A., Michalet, R., and Delzon, S. (2010). Quantifying phenological plasticity to temperature in two temperate tree species. *Funct. Ecol.* 24, 1211–1218. doi: 10.1111/j.1365-2435.2010.01748.x

Vitasse, Y., François, C., Delpierre, N., Dufrêne, E., Kremer, A., Chuine, I., et al. (2011). Assessing the effects of climate change on the phenology of European temperate trees. *Agric. For. Meteorol.* 151, 969–980. doi: 10.1016/j.agrformet.2011.03.003

von Arx, G., and Carrer, M. (2014). ROXAS: a new tool to build centuries-long tracheid-lumen chronologies in conifers. *Dendrochronologia* 32, 290–293. doi: 10.1016/j.dendro.2013.12.001

von Arx, G., Crivellaro, A., Prendin, A. L., Cufar, K., and Carrer, M. (2016). Quantitative wood anatomy—practical guidelines. *Front. Plant Sci.* 7:781. doi: 10.3389/fpls.2016.00781

von Wühlisch, G. (2004). "Series of international provenance trials of European beech." in *Improvement and Silviculture of Beech, Proceedings from the 7th International Beech Symposium IUFRO Research Group 1.10.00*. eds. K. Sagheb-Talebi, P. Madsen and K. Terazawa; May 10-20, 2004 (Teheran, Iran: Research Insitute of Forests and Rangelands), 135–144.

Vospernik, S., and Nothdurft, A. (2018). Can trees at high elevations compensate for growth reductions at low elevations due to climate warming? *Can. J. For. Res.* 48, 650–662. doi: 10.1139/cjfr-2017-0326

Weigel, R., Muffler, L., Klisz, M., Kreyling, J., van der Maaten-Theunissen, M., Wilmking, M., et al. (2018). Winter matters: sensitivity to winter climate and cold events increases towards the cold distribution margin of European beech (*Fagus sylvatica* L.). *J. Biogeogr.* 45, 2779–2790. doi: 10.1111/jbi.13444

Conflict of Interest: The authors declare that the research was conducted in the absence of any commercial or financial relationships that could be construed as a potential conflict of interest.

The reviewer IG-G is currently organizing a Research Topic with one of the author GA. The review process met the standards of a fair and objective review.

Publisher's Note: All claims expressed in this article are solely those of the authors and do not necessarily represent those of their affiliated organizations, or those of the publisher, the editors and the reviewers. Any product that may be evaluated in this article, or claim that may be made by its manufacturer, is not guaranteed or endorsed by the publisher.

frontiers in Plant Science

ORIGINAL RESEARCH
published: 06 August 2021
doi: 10.3389/fpls.2021.698640

High-Resolution X-Ray Computed Tomography: A New Workflow for the Analysis of Xylogenesis and Intra-Seasonal Wood Biomass Production

Romain Lehnebach[1,2*], *Matteo Campioli*[3], *Jozica Gričar*[4], *Peter Prislan*[4], *Bertold Mariën*[3], *Hans Beeckman*[5] and *Jan Van den Bulcke*[1]

[1] UGCT–UGent-Woodlab, Laboratory of Wood Technology, Department of Environment, Faculty of Bioscience Engineering, Ghent University, Gent, Belgium, [2] AMAP Laboratory (botany and bio-informatics of plant architecture and vegetation), Université Montpellier, CIRAD, CNRS, INRAE, IRD, Montpellier, France, [3] Research Group PLECO (Plants and Ecosystems), Department of Biology, University of Antwerp, Antwerp, Belgium, [4] Department of Yield and Silviculture, Slovenian Forestry Institute, Ljubljana, Slovenia, [5] Royal Museum for Central Africa, Service of Wood Biology, Tervuren, Belgium

OPEN ACCESS

Edited by:
Fabio Gennaretti, Université du Québec en Abitibi Témiscamingue, Canada

Reviewed by:
Emanuele Ziaco, Uppsala University, Sweden
Valentina Buttò, Université du Québec à Chicoutimi, Canada

***Correspondence:**
Romain Lehnebach
lehnebach.romain@hotmail.fr

Specialty section:
This article was submitted to Technical Advances in Plant Science, a section of the journal Frontiers in Plant Science

Received: *21 April 2021*
Accepted: *28 June 2021*
Published: *06 August 2021*

Citation:
Lehnebach R, Campioli M, Gričar J, Prislan P, Mariën B, Beeckman H and Van den Bulcke J (2021) High-Resolution X-Ray Computed Tomography: A New Workflow for the Analysis of Xylogenesis and Intra-Seasonal Wood Biomass Production. Front. Plant Sci. 12:698640. doi: 10.3389/fpls.2021.698640

Understanding tree growth and carbon sequestration are of crucial interest to forecast the feedback of forests to climate change. To have a global understanding of the wood formation, it is necessary to develop new methodologies for xylogenesis measurements, valid across diverse wood structures and applicable to both angiosperms and gymnosperms. In this study, the authors present a new workflow to study xylogenesis using high-resolution X-ray computed tomography (HRXCT), which is generic and offers high potential for automatization. The HXRCT-based approach was benchmarked with the current classical approach (microtomy) on three tree species with contrasted wood anatomy (*Pinus nigra*, *Fagus sylvatica,* and *Quercus robur*). HRXCT proved to estimate the relevant xylogenesis parameters (timing, duration, and growth rates) across species with high accuracy. HRXCT showed to be an efficient avenue to investigate tree xylogenesis for a wide range of wood anatomies, structures, and species. HRXCT also showed its potential to provide quantification of intra-annual dynamics of biomass production through high-resolution 3D mapping of wood biomass within the forming growth ring.

Keywords: high-resolution X-ray computed tomography, microtomy, tree growth, xylogenesis, secondary growth phenology

INTRODUCTION

Forests represent the main CO_2 sink of terrestrial ecosystems. Understanding tree growth and carbon sequestration is of crucial interest to forecast the responses of forests to climate change and their climate mitigation potential. The forest carbon sink can be assessed with direct measurement of tree growth (i.e., Hubau et al., 2020) or indirectly through Dynamic Global Vegetation Models (DGVM). In DGVM, tree growth is often assumed to be limited primarily by photosynthesis (i.e., gross primary production) (Fatichi et al., 2019).

However, experimental evidence shows that tree growth does not directly depend on the photosynthesis and that tree growth is more sensitive to environmental conditions than the photosynthesis (Fatichi et al., 2014). Therefore, more attention should be devoted to determine the direct constraints on growth exerted by the environmental conditions at different temporal scales. One way to do this is by studying wood formation (i.e., xylogenesis) that defines seasonal tree growth and carbon sequestration (Friend et al., 2019).

Xylogenesis is driven by the cambium, that is, a layer of meristematic cells, forming a cylinder along the different axes of the plant body. For temperate species, when growing conditions become favorable in spring, the cambium cells start to divide and the newly formed cells undergo different structural changes (i.e., differentiation). Xylogenesis can be divided into five sequential processes: (1) cell division and (2) cell enlargement, which drive the growth in size; (3) cell-wall thickening and (4) cell-wall lignification, which are mainly responsible for the increase in mass and C sequestration (Cuny et al., 2015); and (5) programmed cell death, which allows the woody cell skeleton to be used as mechanical support and conduit for water transport. The wood formation and its dynamics are strongly influenced by environmental conditions, such as the temperature, day length, and water availability (Delpierre et al., 2016; Dox et al., 2021). Therefore, climate change is expected to affect the tree growth and carbon accumulation through the modulation of the timing and duration of xylogenesis.

An appealing method to study the phenology and the seasonal dynamics of wood formation as well as the climate-wood growth relationships consists in monitoring wood development in small cores (i.e., microcores) collected at regular time intervals during the growing season (Rossi et al., 2006). Seasonal observations of anatomical features characterizing the wood formation (e.g., cell morphology, cell developmental stage, or number of cells in a given stage) are made possible by brightfield microscopy after histological slicing and staining. Most of the xylogenesis studies and the development of the histological approach (referred hereafter as "microtomy") have been performed on conifers with a homogeneous wood structure (Rossi et al., 2009, Deslauriers et al., 2008, Camarero et al., 2010). This intensive work on conifers also permitted to refine the understanding of the asynchrony between xylem size increase and biomass production through a detailed quantification of cell development kinetic during xylogenesis (Cuny et al., 2015). This approach allowed to develop a clear view on xylogenesis in conifer species (Rathgeber, 2017), while its knowledge on angiosperm species remains limited (ref. Delpierre et al., 2016, but see Cufar et al., 2008; Gričar et al., 2018; Prislan et al., 2018; Dox et al., 2020). In fact, the structural heterogeneity of angiosperm wood challenges the acquisition of xylogenesis data from a methodological point of view. Indeed, the diversity of cell types encountered in angiosperm wood (vessels, fibers, and parenchyma) makes cell-counting and morphometrics difficult, while limiting the acquisition of information on the xylogenesis dynamics. Therefore, even if some authors have been able to quantify the proportion of growth increment attributed to the different stages of development (Prislan et al., 2018), intra-seasonal studies of secondary growth in angiosperms have been often limited to the estimation of the timing of qualitative events (e.g., earlywood vessel formation, latewood formation). From the biomass accounting point of view, bypassing cell-level information by characterizing the biomass accumulated during the season at the tissue level is a promising perspective. In this respect, the methodology of Andrianantenaina et al. (2019), based on an estimation of the apparent density of the forming wood, should allow to overcome the issue of structurally heterogeneous wood and thus to quantify the dynamics of intra-annual biomass production in angiosperms. The global predominance of angiosperms stresses the importance of further methodological development allowing straightforward xylogenesis measurements across the diversity of wood structures and species found within the angiosperm group, and across the different climates and biomes.

Investigating how tree growth interacts with environmental factors at a global scale requires the development of a high-throughput methodology for xylogenesis studies applicable also to angiosperms. Such methodology should avoid the histological preparation and analysis that are labor intensive, requiring specific expertise, and several manual steps, such as paraffin embedding, slicing, staining, mounting, and observation using bright field microscopy. So far, the labor intensity of the manual steps during sample preparation (requiring skilled technicians) and data collection (observations, requiring skilled wood anatomists) has limited the automation of the microtomic approach, pointing out the importance to develop an automated methodology to study seasonal wood formation.

High-resolution X-ray computed tomography (HXRCT) is becoming popular in the analysis and imaging of plant anatomy (Brodersen and Roddy, 2016). Different research fields related to tree growth and functioning, such as dendrochronology (De Mil et al., 2016; Van den Bulcke et al., 2019) and ecophysiology (Knipfer et al., 2015; De Baerdemaeker et al., 2019), seized the opportunity of HXRCT for substantial methodological improvements. However, HXRCT has never been used in the demanding field of xylogenesis. Producing three-dimensional gray scale images with pixel values (attenuation coefficients) directly related to the density of the material, HXRCT represents a powerful mean to study xylogenesis. More precisely, HXRCT can be used to track cell wall density change occurring during the formation and thickening of the secondary cell wall in order to differentiate the mature wood from the forming wood and to assess secondary growth phenology. In addition, HRXCT can quantify the biomass accumulated by trees throughout the course of the season.

The use of HXRCT in the framework of xylogenesis requires both high contrast and resolution to discern the forming cells and the cell wall. Obtaining a sufficient contrast between cell lumens and cell walls with HRXCT requires water removal from the sample. For mature xylem, water is generally removed by oven-drying the sample prior to scanning (De Mil et al., 2016). However, drying without collapsing and destroying the soft tissue, such as cambial and newly forming xylem cells, cannot be

achieved through oven- or air-drying (Stuppy et al., 2003; Leroux et al., 2009).

Therefore, monitoring of xylogenesis with HXRCT requires the development of an entire workflow including sample preparation, image acquisition, and an analysis protocol, alongside a methodology to follow the cell wall density change within the forming growth ring.

Here, a new methodology is presented and validated to study xylogenesis using HXRCT based on a new workflow to monitor cell wall density changes occurring during xylogenesis (**Figure 1**), applied to three tree species (black pine, common beech, and pedunculate oak) with contrasted wood anatomy growing in a temperate region. Several relevant parameters, such as the timing and duration of size growth, mature xylem production, and overall xylogenesis, as well as rates of size growth and mature xylem production, were estimated with HXRCT and validated with the classical microtomy approach. In addition, the gray scale images produced by HRXCT were used to account for seasonal biomass production dynamics. Concerning the latter aspect, the authors ask whether the intra-seasonal stem biomass production and size growth differ between conifers and angiosperms, specifically among pine, beech, and oak. While information on intra-seasonal biomass production exist for conifers (Cuny et al., 2015; Andrianantenaina et al., 2019) to the best of our knowledge, no study has investigated the intra-seasonal biomass production in angiosperms.

MATERIALS AND METHODS

Selected Species, Study Sites, and Sampling

To assess the applicability of the HXRCT method on tree species with different functional strategies, three species growing in Belgium were selected: black pine (*Pinus nigra*), common beech (*Fagus sylvatica*), and pedunculate oak (*Quercus robur*). With 778 mm.year^{-1} of precipitation and an average monthly temperature ranging from +3°C to 17°C (average annual temperature of 10.1°C), Belgium is characterized by a maritime temperate climate (Campioli et al., 2012). Beech and oak trees were sampled in the "park of Brasschaat" (51°12′ N−4°26′ E) while pine trees were sampled in the military domain "Klein Schietveld" (51°21′ N−4°37′ E) (Dox et al., 2020; Marchand et al., 2020). The sites are at a distance of 9.5 km in a lowland (18–22 m a.s.l.) region with a similar climate. The three species present contrasted xylem anatomy: beech and oak are diffuse and ring porous species respectively, whereas black pine has the typical conifer wood structure made mostly of tracheids. Four healthy and (co)dominant trees per species were selected. From the beginning of April to mid-November 2019, two microcores were collected on each tree every two weeks using a Trephor tool resulting in 18 sampling dates. The sampling was performed between 1.3 m and 2 m above the ground following an upward spiraling pattern with a distance of 4 cm between consecutive sampling points to avoid wound reactions. The microcores were immediately transferred to an Eppendorf tube filled with 70% ethanol solution.

X-Ray CT Workflow

Dehydration, Critical Point Drying, and Sample Mounting

After dehydration by increasing ethanol concentrations, the samples for HXRCT were dried to obtain a sufficient contrast between cell lumens and cell walls. Therefore, a gentle drying method was required in order to preserve the structure of the soft, newly forming wood cells. Therefore, critical point drying (CPD), a technique commonly used for the preparation of scanning electron microscopy samples (Bray, 2000), was used, but has proven its efficiency in the drying of fresh plant structures also for CT imaging (See **Supplementary Figure 1** for a comparison of an air dried and CPD processed pine microcore) (Leroux et al., 2009; Gutiérrez et al., 2018).

The samples were critically point dried with liquid CO_2 using a CPD device (Baltec CPD 030). Each drying cycle consisted of a mixing-draining procedure (repeated 10 times) allowing the gradual replacement of the dehydration media (i.e., 100% ethanol) by liquid CO_2. Then, the samples were dried by removing the CO_2 in a supercritical state ($> 31°C$, > 73 bar).

Six samples were dried at the same time. After drying, the samples were mounted on a cylindrical carbon stick (5 cm x2 mm) for scanning. The mounted samples were stabilized in the scanner room for 12 h, at 25°C and a relative humidity of 40%, to avoid sample movement during scanning.

X-Ray CT Scanning and Reconstruction

Samples were scanned with the Nanowood X-ray CT scanner, developed at the Ghent University Centre for X-ray tomography (UGCT; http://www.ugct.ugent.be) (Dierick et al., 2014). The directional X-ray tube (Microfocus, Hamamatsu) was operated at a tube voltage of 70 kV and a target current of 100 μA. A large (25 x 20 cm, 1920 x 1536 px) Varian Si flat detector was used allowing to capture the region of interest (i.e., innermost phloem layers, cambium, and forming xylem growth ring) in a single field of view. A total of 2001 projections were taken with an exposure time of 700 ms per projection, resulting in 25 min per scan.

Scanned volumes were reconstructed with the Octopus reconstruction software (Vlassenbroeck et al., 2007), including Paganin phase contrast filtering (Paganin et al., 2002). The reconstructed volume, with an approximate voxel pitch of 2.49 μm, consisted of 16-bit tangential images running from the bark to the inner side of the xylem.

Processing and Analysis of the Reconstructed Volume

Selection of the Regions of Interest and Gray-Value Extraction

When sampling, the axis of the Trephor tool can substantially deviate from both the radial direction and the transverse plane of the stem. Therefore, the reconstructed volume was reoriented to realign the cambium surface parallel to the volume edge in both transverse and longitudinal plane (**Supplementary Figure 2**) using ImageJ (Rasband, 2012). A volume of interest (VOI) containing the inner layers of the phloem, the cambium, and the

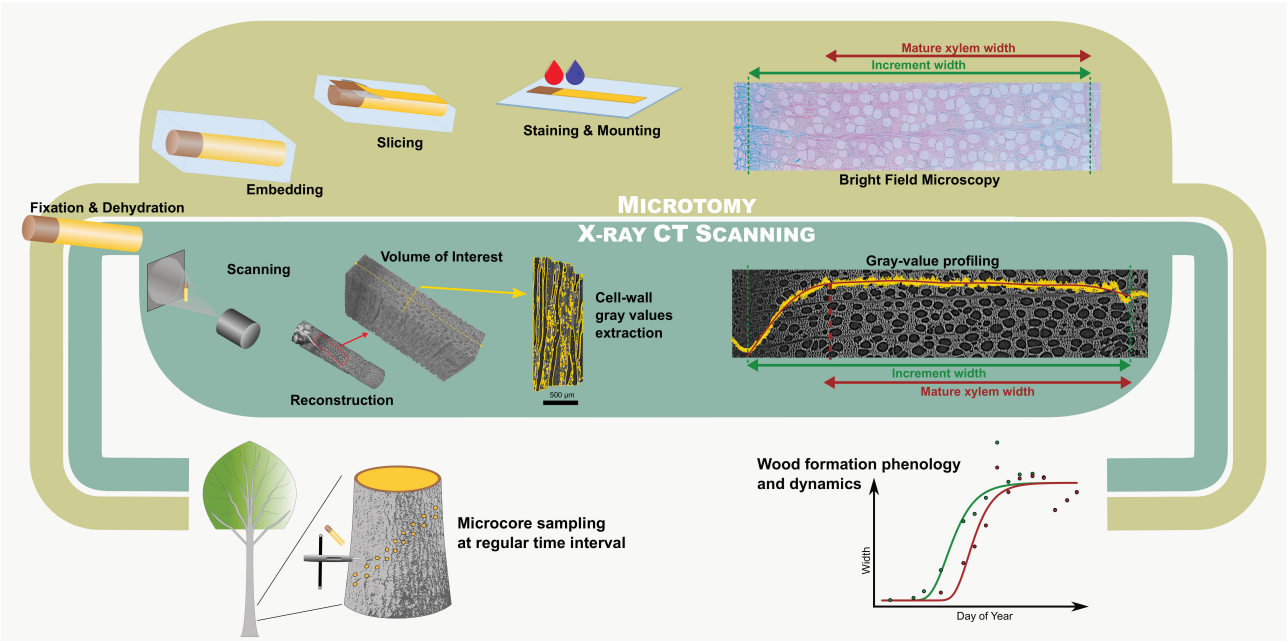

FIGURE 1 | Comparison between the microtomy and HXRCT workflow developed in the present study. The flowchart covers the different steps from field sampling to data analysis through sample preparation and data extraction.

forming xylem growth ring was selected while avoiding selection of wide rays, resin ducts, or cracks.

This VOI was then processed with Octopus analysis, formerly distributed by the UGCT spin-off company XRE (now TESCAN-XRE, part of the TESCAN ORSAY HOLDING a.s.) (Brabant et al., 2011). For each tangential slice of the VOI, a first thresholding was applied to create a mask covering the area containing the sample. The masks were used to create a first region of interest (ROI) image stack containing xylem pixels (xylem ROI stack). For each tangential slice of the xylem ROI stack, a second thresholding was applied to create a mask excluding the pixels associated to cell lumens. The masks were used to create a second region of interest image stack containing cell wall pixels exclusively (cell wall ROI stack). Both xylem and cell wall ROI stacks of each microcore were then processed with R software (R Development Core Team, 2019), using the packages "*magick*" (Ooms, 2020) and "*imager*" (Barthelme, 2019), to extract the mean gray value per ROI resulting in two radial gray-value profiles per microcore, herein after referred to as "xylem gray profile" and "cell wall gray profile," respectively.

Cell Wall Gray-Value Profiling: Rationale

The gray-value profiling methodology developed here relies on the positive and linear relationship between the gray value of HXRCT-derived images and the density of the scanned material. Therefore, cell wall density changes occurring within the forming growth ring can be assessed through cell wall gray value changes. From a structural point of view, the forming growth ring consists of a maturing xylem zone (where xylogenesis occurs), and a mature xylem zone, where xylogenesis already ended (**Figure 2**). Within the maturing xylem, the secondary cell wall is formed and lignin is deposited resulting in an increase of the cell wall density from the cambium until the boundary with the mature xylem zone.

Apart from secondary changes occurring many years later, such as heartwood formation, the structure of the fully mature cell wall does not change in time (Lehnebach et al., 2019), its density is assumed to vary both between and within species in a very narrow range (1.4–1.5 g/cm3). Cell wall density, and consequently cell wall gray value are therefore assumed to remain constant within the mature xylem zone. Consequently, the cell wall density profile along the growing ring follows a two-phased pattern with (1) an increase from cambium to the end of the maturing xylem zone followed by (2) a constant density toward the innermost layers of the mature xylem zone.

Identifying the distance from the cambium at which the phase transition occurs, allows estimating the width of both maturing and mature xylem. An analytical approach is developed in this study, aiming to quantify the width of both maturing and mature xylem.

Cell Wall Gray-Value Profiling: Implementation

For each sample, the cell wall gray profile was plotted over a transversal reference image, with each data point corresponding to the average gray value of the corresponding tangential slice (**Figure 3**). We used the smoothing property of a generalized additive model (GAM) to analyze the cell wall gray profile of each microcore. GAMs are extremely versatile in fitting non-linear and non-monotonic data series, and offer the possibility to

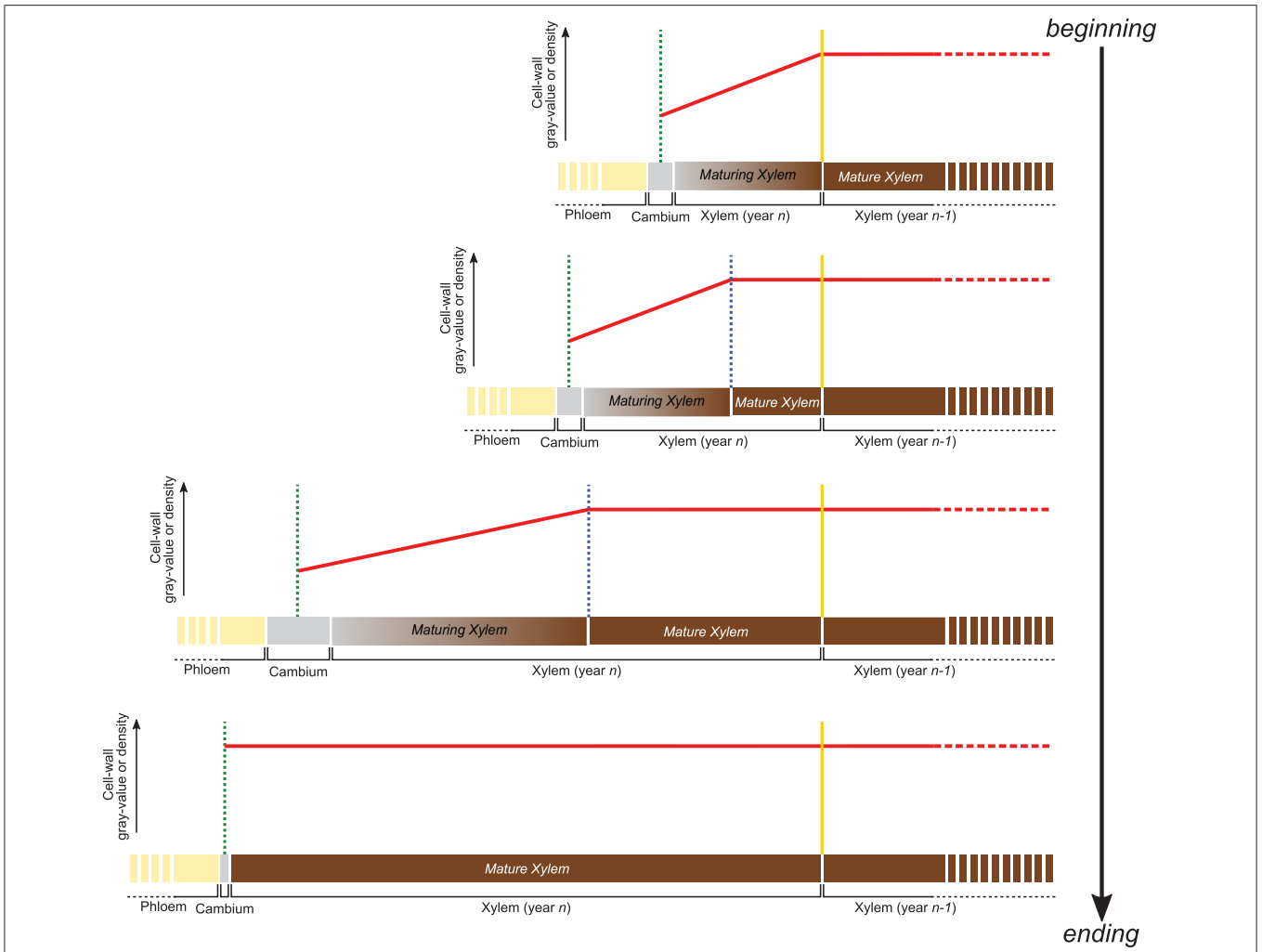

FIGURE 2 | Variation of cell wall gray value or density within the forming growth ring. Following cell wall maturation during xylogenesis, the cell wall density (red line) is expected to increase from the cambium (green dotted line) to the most recent mature xylem layer (blue dotted line). Within the mature xylem, the cell wall is fully developed and its basic density is assumed to be constant until the growth ring boundary (yellow dotted line) and beyond. The distance from the cambium at which the phase transition occurs, allows estimating the width of both mature and maturing xylem.

estimate and analyze their derivative. GAMs are therefore well-suited to analyze cell wall gray profile of diverse tree species. All GAMs were fitted with a Gaussian distribution and identity link function. The goodness of each fit was assessed visually.

Consisting of primary-walled cells, the cambium and the enlarging phloem and xylem cells have the lowest cell wall density (**Figures 2**, **3**, **4A,B**). The cell wall density increases at both sides of the cambium because of phloem and xylem cell wall differentiation (**Figures 4A,B**). We took advantage of this feature to define the cambium position semi-automatically by fitting a GAM and analyzing its derivative within a manually defined subset of the sample containing the cambium and the newly differentiating phloem and xylem cells (**Figure 4B**). Within this subset, the pointwise 95% confidence intervals of the GAM derivatives were used to detect the part where the GAM predicted values were constant (i.e., where the fitted GAM derivative values were significantly different from 0, i.e., 0 lying outside the confidence interval). The median radial position of this part was fixed as the cambium position (**Figure 4B**). The radial position of the previous growth ring boundary was indicated manually on the reference image (**Figure 4A**). It allowed to estimate the width of the increment, $w_{incr-CT}$.

The distance from the cambium for each data point was calculated and fitted another GAM over the data spanning from the cambium (i.e., distance from the cambium = 0) to the previous growth-ring boundary. As for cambium detection, the 95% confidence intervals of the GAM derivatives allowed the identification of growth ring parts where the gray values are constant. The constant part closest to the cambium was selected as the region where the transition between maturing and mature zone occurs (**Figure 4C**). The radial position of the left edge of the transition region was considered as the width of the maturing xylem, $w_{maturing-CT}$. Finally, the width of the mature zone was computed as, $w_{mat-CT} = w_{incr-CT} - w_{maturing-CT}$.

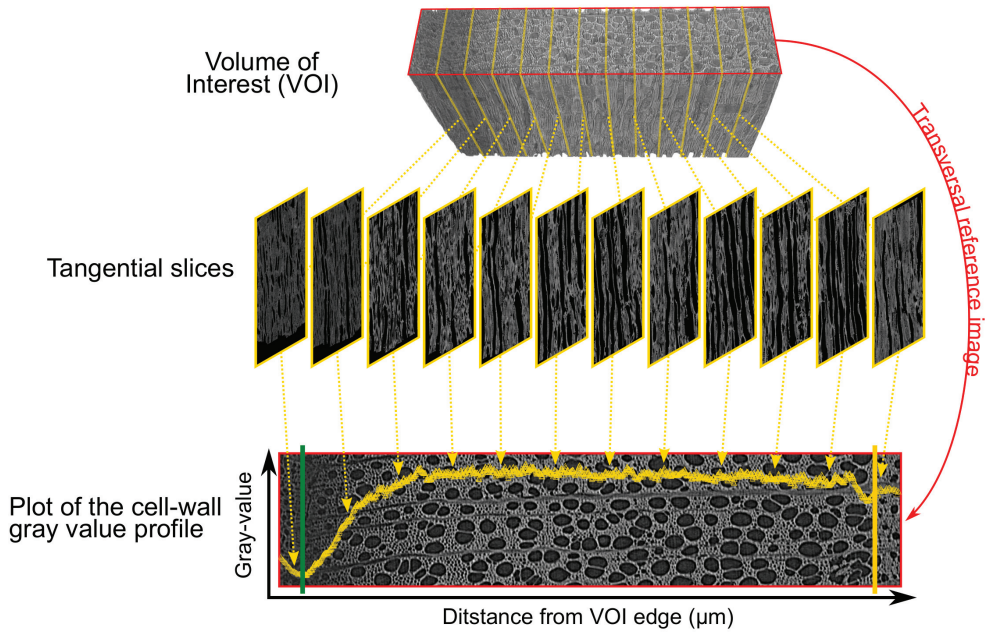

FIGURE 3 | Plot of the cell wall gray profile. The volume of interest (VOI) containing the inner layers of the phloem, the cambium, and the forming xylem growth ring (top) is sliced tangentially (middle). Averaging the cell wall gray values of each tangential slices results in a cell wall gray value profile plotted over the transversal reference image (bottom). The reference image is in the red frame (top and bottom image), the cambium and previous ring boundary are highlighted by the green and yellow lines respectively.

GAM fitting and derivative analysis were performed using the R packages "*mgcv*" (Wood, 2017) and "*gratia*" (Simpson, 2020). A step by step description of the gray-value profiling methodology is available in **Supplementary File 1**.

Microtomy Workflow

The microcores for microtomy were dehydrated in graded ethanol series, infiltrated, and embedded in paraffin blocks and finally sliced using a rotary microtome. The thin sections were stained in a water solution of safranin and astra blue, staining lignin in red and cellulose/hemicellulose in blue, respectively. Histological sections were prepared at the Slovenian Forestry Institute (Ljubljana), following the detailed protocol of Prislan et al. (2014). Observation under light microscope allowed to distinguish between maturing and mature xylem. For each microcore, the width of the cambium, and the width of the maturing and mature xylem were measured at three positions to consider potential within-sample heterogeneity. The maturing zone was measured as the ring part between the cambium and the first mature cells. Xylem cells were considered mature when the entire cell wall was stained red and the lumen was empty of any cellular content. In order to be comparable to the HXRCT methodology, the increment width was computed as the sum of both mature and maturing xylem width and the width of the cambium divided by two. When the maturing zone was absent (i.e., for samples collected at the very end of the growing season), the mature zone was set equal to the increment width.

Estimation of Xylogenesis Parameters and Statistical Analysis

Computation of Xylogenesis Critical Dates and Duration, and Growth Rate

Computation of xylogenesis phenological parameters was first performed through a "model-driven" approach, such as the fitting and derivation of the Gompertz function (e.g., Rossi et al., 2003). However, a recent methodological breakthrough suggests that a "data-driven" approach is able to capture properly the variation of xylogenesis dynamics (i.e., durations and rates) while the model-driven approach fails (Cuny et al., 2013). Preliminary analysis of the data (not shown) using a Gompertz function produced improper fitting and led us to opt for the GAM data-driven approach.

As the increase of the increment width during the growing season is monotone, a shape constrained additive model (SCAM) was used (Pya and Wood, 2015) to analyze the phenology of wood formation. SCAM was fitted using monotone increasing P-splines, Gaussian distribution, and identity link function. Circumferential growth heterogeneity was accounted for using the correction formula for cell counting data adapted to widths at the individual tree scale:

$$w_{cor,j} = w_{obs,j} * \frac{w_{prev,j}}{\frac{1}{n} \sum w_{prev,j}} \quad (1)$$

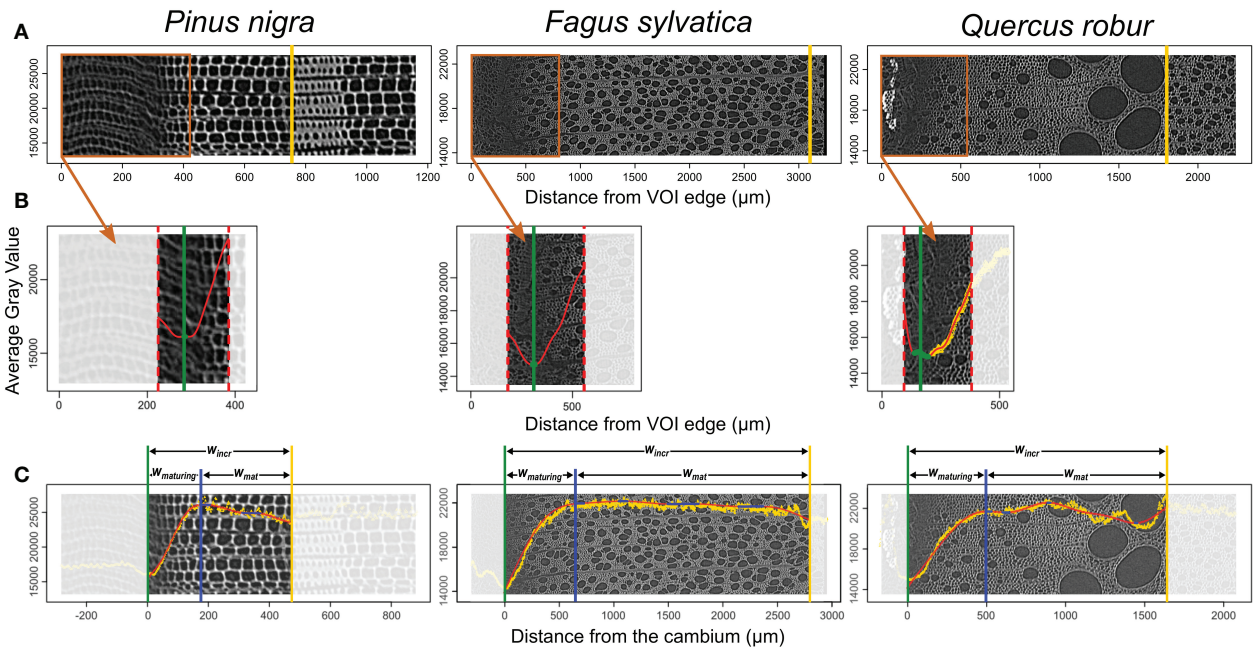

FIGURE 4 | Implementation of the gray-value profiling. **(A)** The average gray value of each tangential slice is plotted on the reference cross-section image. At this stage, the previous growth ring boundary is identified (yellow vertical line). **(B)** Within the subset containing the cambium, a GAM fit (red) and its derivative allow automatic identification of the cambium position (green vertical line). **(C)** Within the growth ring, a GAM fit (red) and its derivative allows the detection of a constant gray value (blue filled circles). The constant gray value closest to the cambium is set as the boundary between maturing and mature xylem (blue vertical line). This procedure allows to estimate maturing xylem width ($w_{maturing}$), mature xylem width (w_{mature}), and increment width (w_{incr}). The gray scale is unitless. It varies from 0 to 65,535 for 16 bits images used here.

where, n is the number of sampling dates, and for each jth sample, $w_{cor,j}$ is the corrected width; $w_{obs,j}$ is the observed width; $w_{prev,j}$ is the observed width of the previous growth year (Rossi et al., 2003; Prislan et al., 2013).

First, the constrained GAM was fitted over the width of the increment to analyze the size growth dynamics at the tree level (**Figure 5**). The final increment width was computed as the median of the increment width predicted for the last three sampling dates (i.e., the dates for which the increment width had already stabilized), in order to account for circumferential growth heterogeneity. We defined the date of beginning (tb_{incr}) and ending (te_{incr}) of size growth as the day of year for which, respectively, 5% and 95% (i.e., wb_{incr} and we_{incr}) of the increment is formed. The duration of size growth was computed as the time span between both dates:

$$d_{incr} = te_{incr} - tb_{incr} \quad (2)$$

The average daily rate of size growth was calculated as:

$$r_{incr} = (we_{incr} - wb_{incr})/(te_{incr} - tb_{incr}) \quad (3)$$

The differences between the increment width predicted by GAM on the consecutive days, spanning from tb_{incr} to te_{incr}, were calculated to assess the distribution of size growth daily rates.

The same procedure was applied for the width of the mature xylem in order to define the date of beginning (tb_{mat}) and ending (te_{mat}), the duration (d_{mat}) and the average rate (r_{mat}) of mature xylem production. Finally, the duration of the whole xylogenesis was defined as:

$$d_{xylo} = te_{incr} - tb_{incr} \quad (4)$$

These parameters were estimated for both microtomy and HXRCT datasets.

Consistency Between HXRCT and Microtomy Measurements

The consistency between increment, mature, and maturing xylem width measured with HXRCT and microtomy was assessed using major axis regression. The value of both intercept and slope and their respective 95% confidence intervals (CI) were used to detect significant differences compared to a 1:1 regression. An intercept differing from 0 (i.e., 0 lies outside the CI of the intercept) indicates a fixed bias across the entire range, that is, the HXRCT provides greater (or lower) values than microtomy. A slope differing from 1 (i.e., 1 lies outside the CI of the slope) indicates a proportional bias, that is, the HXRCT provided progressively greater (or lower) values with increasing values of the considered measurement than microtomy. Major axes were fitted with the "*lmodel2*" package in R (Legendre, 2018).

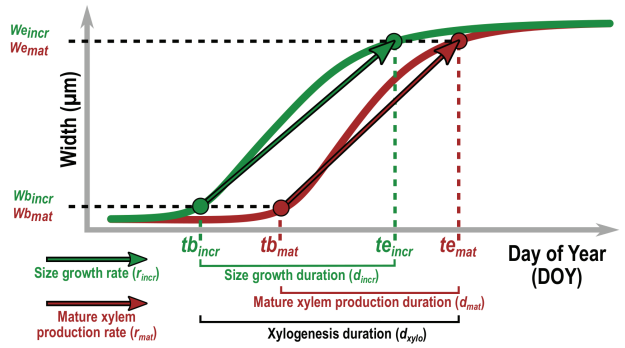

FIGURE 5 | Description of the xylogenesis parameters estimated for both HXRCT and microtomy datasets. Parameters related to size growth (green) and mature xylem production (brown) are reported. The date of beginning (tb_{incr}) and ending (te_{incr}) of size growth are defined as the day of year for which, respectively, 5% and 95% (i.e., wb_{incr} and wc_{incr}) of the increment is formed. The date of beginning (tb_{mat}) and ending (te_{mat}) of mature xylem production are defined as the day of year for which, respectively, 5% and 95% (i.e., wb_{mat} and wc_{mat}) of the mature xylem is formed. The duration of size growth (d_{incr}), mature xylem production (d_{mat}) and xylogenesis (d_{xylo}) are computed as the time span between te_{incr} and tb_{incr}, te_{mat} and tb_{mat}, and te_{mat} and tb_{incr} respectively. The average daily rate of size growth and mature xylem production are calculated as, $r_{incr} = (we_{incr} - wb_{incr}) / (te_{incr} - tb_{incr})$ and $r_{mat} = (we_{mat} - wb_{mat}) / (te_{mat} - tb_{mat})$.

Comparison of Parameters Estimated With HXRCT and Microtomy

To assess the agreement between critical dates, durations, and growth rates estimated using HXRCT and microtomy, the significant differences between the two datasets by case-based bootstrap resampling were tested. For a given species and for each parameter of interest (**Figure 5**), the difference between the median of the four trees based on HXRCT data on one hand, and microtomy data on the other hand was computed. The observed median difference was compared to the median reference distribution simulated under the null hypothesis (H_0: the parameters extracted from HXRCT do not differ from the parameters extracted from microtomy). The reference distribution resulted in 10,000 resampled median differences. A two-tailed test was performed by computing the achieved significance level (ASL) as the proportion of absolute values in the reference distribution that are equal, or greater, than the observed absolute median difference. ASL is interpreted in the same way as the p value (P).

Accounting for Biomass Production Dynamic Trough Xylem Gray Value

The ability of HRXCT to assess biomass production dynamics throughout the course of the growing season was assessed by using the gray-value information. Here, the xylem gray profile (i.e., including lumen and cell wall pixels) was preferred to the cell wall gray profile as it accounts for both the proportions of the xylem layer allocated to cell wall (biomass) and lumens (void). The sum of the gray values of each xylem gray profile was calculated. Being linearly related to the biomass accumulated in a given volume of the forming xylem ring, this variable was considered as a proxy of the biomass accumulated at the trunk base (b_{trunk}) of the tree from the beginning of the growing season up to the considered sampling date. As for xylem widths, we accounted for circumferential growth heterogeneity by correcting b_{trunk} by the observed width of the previous growth year at the individual tree scale. We fitted constrained GAM over b_{trunk} to analyze the biomass production dynamics at the species level. The biomass production and the size increase were compared by analyzing the seasonal variation of both b_{trunk} and the increment width (w_{incr}). For convenience, both variables were normalized (i.e., ranging between 0 and 1) using the median of b_{trunk} and w_{incr}, respectively, predicted for the last three sampling dates. This provided the relative completion of each process (i.e., size growth and biomass production) and allowed to compute the time lag between biomass production and size growth on the course of the growing season. For this purpose, we computed the time lag between the relative completion of a given proportion of the final b_{trunk} and the final w_{incr} (e.g., Day of year (DOY) when a given relative completion of the final b_{trunk} is produced - DOY when a given relative completion of the final w_{incr} is produced). The time lags were computed for relative completion values ranging between 0 and 1 and every 0.01. The differences between both b_{trunk} and w_{incr} predicted by GAM on the consecutive days were also calculated. This allowed to assess the seasonal variation of size growth rate and biomass production rate and estimate their seasonal maximum.

RESULTS

Seasonal Growth Pattern

The patterns of seasonal xylem growth, at the species level, derived from HXRCT and microtomy strongly overlap (**Figure 6**). For both pine and beech, increment and mature xylem width increased along the growing season following a typical sigmoidal curve (**Figure 6**). For oak, the width of the increment follows a curvilinear increase while the mature xylem width follows a bisigmoidal pattern. Major axis fits did not detect any significant bias in the estimation of increment width by HXRCT compared to microtomy (**Supplementary Figure 3**; **Supplementary Table 1**). Regarding the mature xylem width, no biases were detected for beech and oak, however, a slight slope departure from 1 for pine (**Supplementary Table 1**) is found. Microtomy and HRXCT described similarly the seasonal variation of maturing xylem width. For beech, the maturing xylem width followed a bell-shaped pattern while for oak and pine the pattern was bimodal, with a first peak in spring and a second peak in July for oak and in September for pine.

Overall, the estimated maturing xylem width by HXRCT is significantly lower than for microtomy for pine and beech (see **Supplementary Table 1**), especially during summer (**Figure 6**). These represent the only cases in our study when HXRCT and microtomy produce different estimates (see the third paragraph of the discussion section).

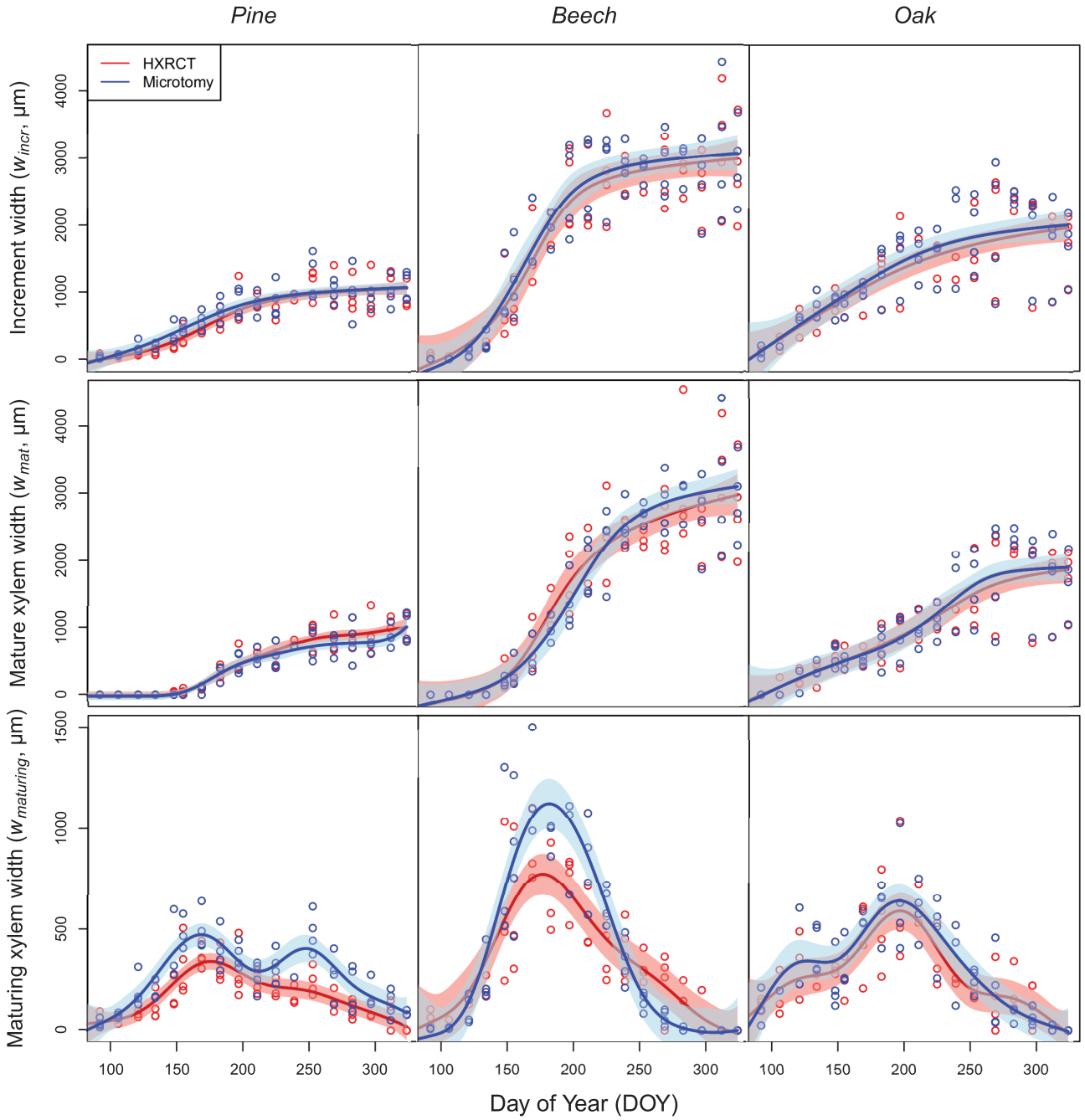

FIGURE 6 | Seasonal growth pattern assessed with HXRCT (red) and microtomy (blue). Variations of increment and mature xylem were fitted with constrained GAMs (top and middle row), while maturing xylem width was fitted with unconstrained GAMs (bottom row). The shaded band represents the standard error of the fit.

Wood Formation Calendar

Size growth, and therefore xylogenesis, began (tb_{incr}) at the end of March in oak (one week before the first sampling date, $tb_{incr-micro}$ = DOY 89, while $tb_{incr-CT}$ = DOY 88, see **Supplementary Table 2**), while it started between mid- and end of April for pine ($tb_{incr-micro}$ = DOY 100, while $tb_{incr-CT}$ = DOY 106) and beech ($tb_{incr-micro}$ = DOY 122, while $tb_{incr-CT}$ = DOY 108, the difference is not significant). Microtomy and HXRCT gave similar estimates of tb_{incr} (**Figure 7**; **Supplementary Table 2**). Size growth was completed in mid-September for beech ($te_{incr-micro}$ = DOY 256, while $te_{incr-CT}$ = DOY 251), and oak ($te_{incr-micro}$ = DOY 260, while $te_{incr-CT}$ = DOY 264) while it lasted until the beginning of October for pine ($te_{incr-micro}$ = DOY 277, while $te_{incr-CT}$ = DOY 270). Again,

microtomy and HXRCT provided similar estimate of te_{incr} and therefore the duration of size growth (d_{incr}) was highly similar for both methods ($d_{incr-micro}$ = DOY 177, $d_{incr-CT}$ = DOY 162 for pine, $d_{incr-micro}$ = DOY 134, $d_{incr-CT}$ = DOY 140 for beech and $d_{incr-micro}$ = DOY 163, $d_{incr-CT}$ = DOY 171 for oak, the differences are not significant, see **Supplementary Table 2**).

The mature xylem production began in April for oak ($tb_{mat-micro}$ = DOY 105, while tb_{mat-CT} = DOY 104), and from the end of May to beginning of June for beech ($tb_{mat-micro}$ = DOY 145, while tb_{mat-CT} = DOY 141) and pine ($tb_{mat-micro}$ = DOY 152, while tb_{mat-CT} = DOY 154). However, the end of mature xylem production, and therefore the end of xylogenesis, occurred by the end of September for beech ($te_{mat-micro}$ = DOY 265, while te_{mat-CT} = DOY 264) and oak ($te_{mat-micro}$ = DOY 262, while te_{mat-CT} = DOY 262), and by the end of October for pine ($te_{mat-micro}$ = DOY 304, while te_{mat-CT} = DOY 294, the difference is not significant). Overall the duration of mature xylem production (d_{mat}) is shorter for beech ($d_{xylo-micro}$ = 142 days, while $d_{xylo-CT}$ = 154 days, the difference is not significant) than for pine ($d_{xylo-micro}$ = 206 days, while $d_{xylo-CT}$ = 188 days, the difference is not significant) and oak ($d_{xylo-micro}$ = 166 days, while $d_{xylo-CT}$ = 169 days, the difference is not significant). Dates (tb_{mat}, te_{mat}) and durations (d_{mat}) related to mature xylem formation as well as the duration of xylogenesis (d_{xylo}) were similar across methods (**Figure 7**; **Supplementary Table 2**).

Growth Rates

The estimated size growth rate (r_{incr}) ranged from 5 to 6 μm.day^{-1} in pine to 21 to 22 μm.day^{-1} in beech. The mature xylem production rate (r_{mat}) presented similar values. Overall, estimates of size growth and mature xylem production rate by microtomy and HXRCT are highly similar (**Figure 8**; **Supplementary Table 3**). Moreover, the distributions of r_{incr} and r_{mat} estimated with HXRCT and microtomy strongly overlap (**Supplementary Figure 3**).

Seasonal Pattern of Biomass Production and Size Growth and Their Time Lag

The patterns of biomass production and size growth are very similar at the species level (**Figure 9**). For both pine and beech, the biomass increases during the growing season following a sigmoidal curve, while biomass in oak increases curvilinearly. However, biomass production lags behind size growth. The time lag observed in respect of both size and biomass completion of the xylem ring is more important for pine (mean = 9 days, maximum=15 days) than for beech (mean = 4 days, maximum = 9 days) and oak (mean = 5 days, maximum = 7 days). For pine and beech, the time lag reaches its maximum during the latewood formation (at the end of the growing season, when 80–90% of the ring width is formed). In oak, the time lag is maximum from the end of the earlywood formation up to half of the latewood formation (between 40% and 70% of the ring formation).

The time lags observed at the peak of both size growth and biomass production rate contrast with the time lag observed in respect of both size growth and biomass completion. For both pine and beech, the relative size growth rate, as well as the biomass production rate peaked at the end of June. The difference between maximum size growth (DOY = 173) and biomass production rates (DOY = 177) was four days in pine. This difference was even smaller in beech, that is, two days (DOY = 171 vs. DOY = 173). For oak, the relative size growth rate was maximal at the end of March (DOY = 89), while the biomass production rate peaked at the beginning of June (DOY = 152), resulting in a time lag of 63 days.

DISCUSSION

This is the first time that xylogenesis dynamics and intra-seasonal growth rate parameters are assessed using HRXCT The development of an entire HRXCT workflow from sample preparation, to reconstructed volume analysis, allowed the estimation of relevant xylogenesis parameters (i.e., dates, durations, and rates) and seasonal time series of increment width. Moreover, the benchmarking of HRXCT with the classical microtomy proved the HRXCT approach to produce accurate estimates of xylogenesis dynamics over species with contrasted xylem anatomies.

The ability of HRXCT to encompass diverse xylem structure relies on the gray-value profiling methodology. While 2D cell morphometric analysis is not applicable on various anatomical structure, the gray-value profiling overcomes this issue by assessing the maturation state from monitoring of density at the xylem layer scale. The HRXCT methodology also proved to produce accurate estimates of actual ring width along the whole growing season ranging from ca. 30 to 5000 μm (see **Supplementary Table 4**). Given this result and the high resolution of HRXCT (i.e., 2.5 μm/pixel), the authors assume that HRXCT will succeed in estimating xylogenesis dynamics of slow-growing trees. Therefore, the generic and data-driven HRXCT method showed to offer a very interesting perspective to fill the knowledge gap about secondary growth phenology and intra-annual wood production over a structural and taxonomical diversity.

It is important to pinpoint that the xylem dimensions estimated with microtomy and HRXCT slightly differ in their nature. HRXCT differentiates the mature xylem from the maturing xylem on the basis of cell wall density differences. Therefore, cells in the very late stages of wood formation, for which the biomass accumulation process is almost accomplished (i.e., cells at the end of secondary wall formation and lignifying cells) or terminated (i.e., fully lignified cells but still alive) might be considered as mature cells with HRXCT. On the other hand, with microtomy such cells are considered as still maturing since the mature zone consists exclusively of fully lignified dead cells. Therefore, the slight overestimation and underestimation of the mature and the maturing zone, respectively, with HRXCT may rely on the different nature of xylem dimensions estimated with HRXCT and microtomy. However, these differences are not sufficiently important to bias the estimation of xylogenesis dynamics.

As gray scale information can be directly converted into estimates of biomass, X-ray computed tomography has been successfully used in the field of dendrochronology and biomass

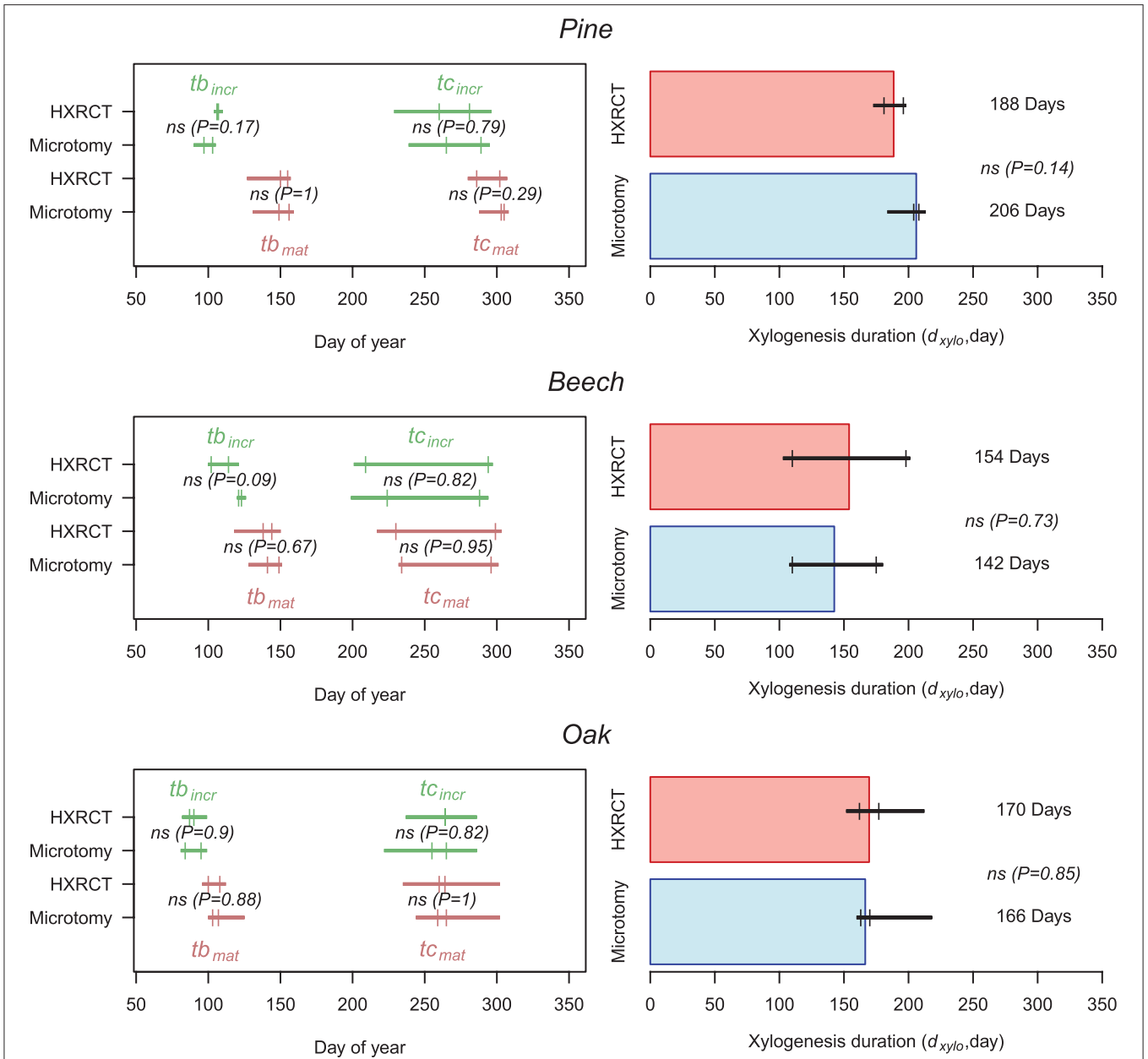

FIGURE 7 | Xylogenesis calendar and duration. Left panels: Estimates of size growth beginning (tb_{incr}) (i.e., beginning of xylogenesis) and size growth ending (te_{incr}) (green) as well as mature xylem production beginning (tb_{mat}) and ending (te_{mat}) (i.e., ending of xylogenesis) (brown) are presented for HXRCT and microtomy. Green and brown lines range from minimum to maximum estimated dates, while second and third quartile are represented by short vertical lines. Right panels: Estimates of xylogenesis duration (d_{xylo}) (median) for HXRCT (red) and microtomy (blue) are presented. Black lines range from minimum to maximum estimated duration, while second and third quartile are represented by short vertical lines. The significance of the bootstrap resampling test (P) assessing the difference between HXRCT and microtomy is reported.

estimation (Bastin et al., 2015; De Mil et al., 2016). A significant step forward in the quantification of the intra-annual dynamics of carbon sequestration, for both conifers and angiosperms, relies on the calculation of the apparent density of the forming wood (i.e., the product of cell wall density and the ratio of cell wall area to xylem area) (Andrianantenaina et al., 2019). Although the apparent density approach proved to be more direct and accurate than the cell morphometric approach (Cuny et al., 2015), it still relies on physical 2D slicing of the sample. Here, it is showed that HRXCT can also be used in the field of intra-seasonal biomass production and carbon sequestration research. In fact, the sum of the xylem gray value, which is actually directly related to density (attenuation coefficients are recorded), and therefore to the biomass accumulated at the trunk base provided a very

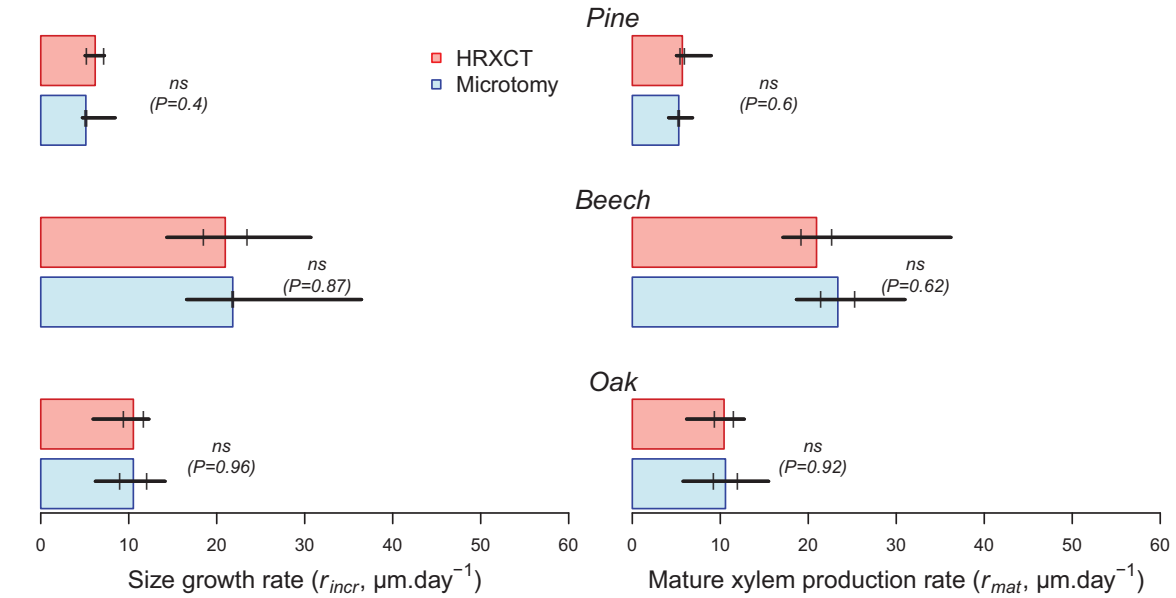

FIGURE 8 | Size growth (r_{incr}) and mature xylem (r_{mat}) production rates (median) estimated with CT (red) and microtomy (blue). Black lines range from minimum to maximum estimated duration, while second and third quartile are represented by short vertical lines. The significance of the bootstrap resampling test (P) assessing the difference between HXRCT and microtomy is reported.

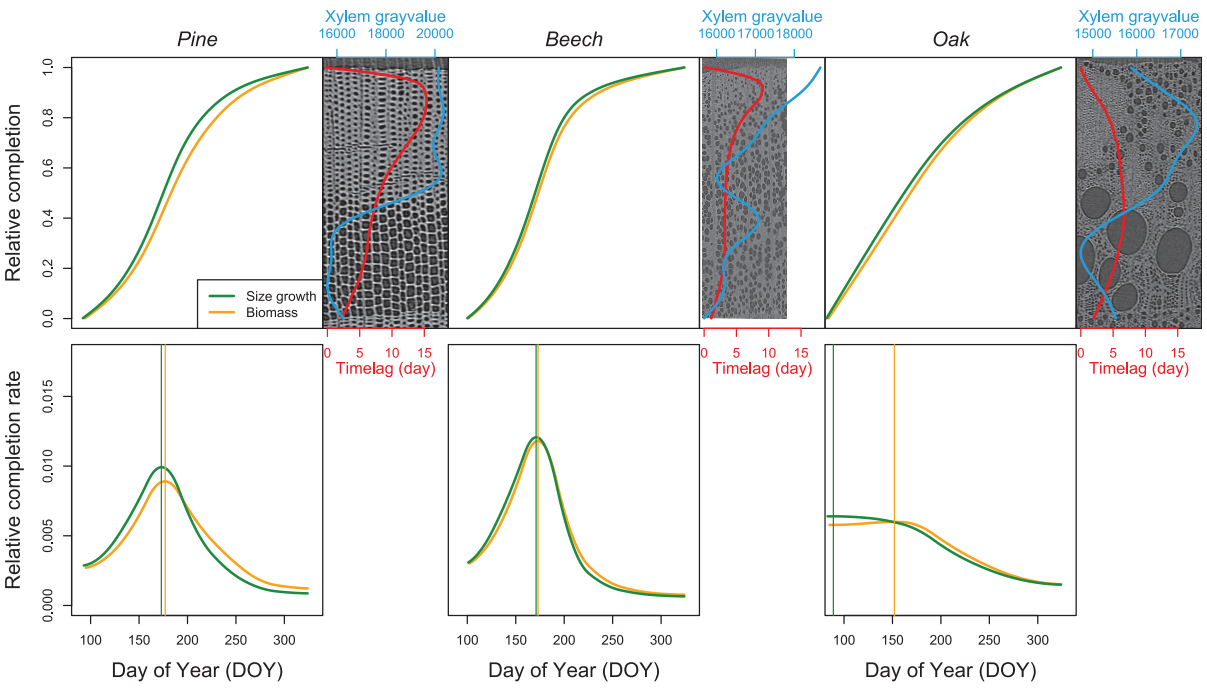

FIGURE 9 | Relative completion of size growth and biomass production. The top line presents the relative completion of size growth and biomass production during the growing season as well as the time lag between size growth and biomass production (red line). For each species, a reference image and its associated xylem gray-value profile (blue line) is shown. The bottom line presents the variation of the relative completion rate, with the vertical lines highlighting the DOY at which the maximum rate occurs.

interesting insight into the capability of HRXCT to assess biomass production dynamic throughout the course of the growing season. The observed seasonal variation of the time lag between biomass production and size growth agrees with the anatomical signature of the studied species. For both pine and beech, the time lag reaches its maximum during the latewood formation, when 80–90% of the growth ring width is already achieved and thick-walled tracheids or fibers are produced. In oak, the time lag shows the largest values from the end of earlywood formation to the half of the completion of the latewood, thus between 40% and 70% of the growing ring part consists mainly of thick-walled fibers and narrow vessels. Therefore, for all species, the time lag is largest when the denser part of the growth ring is forming and suggests that wall formation and maturation of thick-walled cells require a longer period than the formation and maturation of thin-walled cells. This pattern already observed in conifers (Cuny et al., 2014) seems therefore to apply to angiosperms.

A very short time lag was found (four days) between the maximal size growth rate and the maximal biomass production rate in pine. This result strongly contrasts with the one-month time lag generally acknowledged in conifers (Cuny et al., 2015). However, Andrianantenaina et al. (2019) reported a two weeks lag between biomass production and size growth in spruce growing in north-east France. They speculated that this reduced time lag could be accounted for by the occurrence of a long summer drought during the measurement period in 2015, resulting in the shortening of the growing season and less investment in cell production. The growing season 2019 (when the samples were collected) experienced a very intense drought in late spring-early summer. Also because of the water deficit accumulated during the very dry 2018, the soil in late spring-early summer of 2019 was dry as never observed before in Belgium (Mariën et al., 2021). Therefore, wood formation in black pine might be sensitive to drought as in other conifer species (Andrianantenaina et al., 2019).

At the same site of our sampling, Dox et al. (2021) found that the end of wood formation in oak occurs earlier under drought conditions while this parameter is rather insensitive to drought in beech. In 2019, the authors found that wood formation in oak stopped earlier (DOY = 262) than in 2018 (DOY = 282 in Dox et al., 2021). As the drought in 2019 was even more pronounced than in 2018 (see above), the results corroborate the drought sensitivity of wood formation in oak.

The time lag in beech (two days) was even lower than for pine, while it was much longer in oak (63 days). However, we note that for oak, the peaks of size growth rate and of biomass production rate are much less pronounced than for the other species. During earlywood formation, from late March till early June, both size growth rate and biomass production rate were maximal and rather constant in oak. We believe that the large time lag in oak results from the ring-porous structure of its wood, which implies a fast size growth, due to the enlargement of the vessels, at the beginning of the growing season. Given the uniqueness of such parameters computed for angiosperms, any comparison with previous studies is not possible.

We believe that further development of HRXCT will open the way for more insight into biomass production in angiosperms.

Therefore, we expect that the new HRXCT workflow presented here will be the foundation for major breakthroughs also in the field of intra-seasonal biomass production and carbon sequestration research. Together with a proper conversion of gray value into wood density and species-specific allometric relationships, HXRCT has the clear potential to provide a better quantification of intra-annual dynamics of biomass production and carbon sequestration through high-resolution 3D mapping of carbon within the forming growth ring and among different tree species.

HXRCT is a growing and wide spreading technology in the field of tree- and wood sciences. Both forthcoming technological improvements of scanning devices and protocol optimization (batch preparation and actual scanning of samples), as well as increased computer capacity, will offer potential for the further development of a high-throughput analysis of xylogenesis with HXRCT. Such development will allow to (1) cover a broad range of biomes and climates by increasing drastically the number of sampled individuals and to (2) integrate different tree components (i.e., root, stem, and branches) that may present different phenological patterns and react differently to similar climatic conditions. Thus, the HRXCT approach, developed here, offers a promising avenue to investigate seasonal plant-climate growth relationships spanning a wide range of wood structures, species, biomes, and climatic conditions, and to generate a substantial amount of data that could trigger a new generation of vegetations models fully considering the seasonal wood growth dynamics.

DATA AVAILABILITY STATEMENT

The raw data supporting the conclusions of this article will be made available by the authors on request, without undue reservation.

AUTHOR CONTRIBUTIONS

RL, JVdB, and MC designed the study. BM, MC, and RL collected the samples. JG and PP processed the sample for microtomy. RL and JG conducted the analysis of the histologic slices. RL conducted the X-ray computed tomography analysis and the analysis of the data. RL, JVdB, MC, and HB wrote the first draft of the manuscript. RL, JVdB, MC, and HB wrote the revised manuscript. BM, JG, and PP made significant contributions to the manuscript. All authors gave final approval for publication.

FUNDING

This research was funded by the BOF Special Research Fund for RL (BOF Starting Grant JVdB, BOFSTG2018000701), the UGCT Center of Expertise (BOF.EXP.2017.0007), the Research Foundation Flanders (FWO grant G009720N), and the LEAF-FALL starting ERC grant (714916).

ACKNOWLEDGMENTS

We acknowledge the institutions that gave permission to conduct research in the study areas: Agency for Nature and Forest

of the Flemish Government (ANB), the Military Defense of Belgium, and City of Brasschaat. We would like to thank Stijn Willen for the technical support and Inge Dox and Sebastien Leys for their help in collecting and processing the samples for microtomy.

SUPPLEMENTARY MATERIAL

The Supplementary Material for this article can be found online at: https://www.frontiersin.org/articles/10.3389/fpls.2021.698640/full#supplementary-material

REFERENCES

Andrianantenaina, A. N., Rathgeber, C. B. K., Pérez-de-Lis, G., Cuny, H., and Ruelle, J. (2019). Quantifying intra-annual dynamics of carbon sequestration in the forming wood: a novel histologic approach. *Ann. Forest Sci.* 76:62. doi: 10.1007/s13595-019-0846-7

Barthelme, S. (2019). *imager: Image Processing Library Based on 'CImg'. R package version 0.41.42*.

Bastin, J. F., Fayolle, A., Tarelkin, Y., et al. (2015). Wood specific gravity variations and biomass of central african tree species: the simple choice of the outer wood. *PLoS ONE* 10:e0142146. doi: 10.1371/journal.pone.0142146

Brabant, L., Vlassenbroeck, J., De Witte, Y., et al. (2011). Three-dimensional analysis of high-resolution X-ray computed tomography data with Morpho+. *Microsc. Microanal.* 17, 252–263. doi: 10.1017/S1431927610094389

Bray, D. (2000). "Critical point drying of biological specimens for scanning electron microscopy," in *Supercritical Fluid Methods and Protocols*, eds J. R. Williams, A. A. Clifford (Totowa, NJ: Humana Press), 235–243. doi: 10.1385/1-59259-030-6:235

Brodersen, C. R., and Roddy, A. B. (2016). New frontiers in the three-dimensional visualization of plant structure and function. *Am. J. Bot.* 103, 184–188. doi: 10.3732/ajb.1500532

Camarero, J. J., Olano, J. M., and Parras, A. (2010). Plastic bimodal xylogenesis in conifers from continental Mediterranean climates. *New Phytol.* 185, 471–480. doi: 10.1111/j.1469-8137.2009.03073.x

Campioli, M., Vincke, C., Jonard, M., Kint, V., Demarée, G., and Ponette, Q. (2012). Current status and predicted impact of climate change on forest production and biogeochemistry in the temperate oceanic European zone: review and prospects for Belgium as a case study. *J. For. Res.* 17, 1–18. doi: 10.1007/s10310-011-0255-8

Cufar, K., Prislan, P., de Luis, M., and Gričar, J. (2008). Tree-ring variation, wood formation and phenology of beech (Fagus sylvatica) from a representative site in Slovenia, SE Central Europe. *Trees* 22, 749–758. doi: 10.1007/s00468-008-0235-6

Cuny, H. E., Rathgeber, C. B., Kiesse, T. S., Hartmann, F. P., Barbeito, I., and Fournier, M. (2013). Generalized additive models reveal the intrinsic complexity of wood formation dynamics. *J. Exp. Bot.* 64, 1983–1994. doi: 10.1093/jxb/ert057

Cuny, H. E., Rathgeber, C. B. K., Frank, D., Fonti, P., and Fournier, M. (2014). Kinetics of tracheid development explain conifer tree-ring structure. *New Phytol.* 203, 1231–1241. doi: 10.1111/nph.12871

Cuny, H. E., Rathgeber, C. B. K., Frank, D., Fonti, P., Mäkinen, H., Prislan, P., et al. (2015). Woody biomass production lags stem-girth increase by over one month in coniferous forests. *Nat. Plants* 1:15160. doi: 10.1038/nplants.2015.160

De Baerdemaeker, N. J. F., Stock, M., Van den Bulcke, J., De Baets, B., Van Hoorebeke, L., and Steppe, K. (2019). X-ray microtomography and linear discriminant analysis enable detection of embolism-related acoustic emissions. *Plant Methods* 15:153. doi: 10.1186/s13007-019-0543-4

De Mil, T., Vannoppen, A., Beeckman, H., Van Acker, J., and Van den Bulcke, J. (2016). A field-to-desktop toolchain for X-ray CT densitometry enables tree ring analysis. *Ann. Bot.* 117, 1187–1196. doi: 10.1093/aob/mcw063

Delpierre, N., Vitasse, Y., Chuine, I., Guillemot, J., Bazot, S., Rutishauser, T., et al. (2016). Temperate and boreal forest tree phenology: from organ-scale processes to terrestrial ecosystem models. *Ann. For. Sci.* 73, 5–25. doi: 10.1007/s13595-015-0477-6

Deslauriers, A., Rossi, S., Anfodillo, T., and Saracino, A. (2008). Cambial phenology, wood formation and temperature thresholds in two contrasting years at high altitude in southern Italy. *Tree Physiol.* 28, 863–871. doi: 10.1093/treephys/28.6.863

Dierick, M., Van Loo, D., Masschaele, B., Bulcke, J., Acker, J., Cnudde, V., et al. (2014). Recent micro-CT scanner developments at UGCT. *Nucl. Instrum. Methods Phys. Res. B.* 324, 35–40. doi: 10.1016/j.nimb.2013.10.051

Dox, I., Gričar, J., Marchand, L. J., Leys, S., Zuccarini, P., Géron, C., et al. (2020). Timeline of autumn phenology in temperate deciduous trees. *Tree Physiol.* 40, 1001–1013. doi: 10.1093/treephys/tpaa058

Dox, I., Prislan, P., Gričar, J., Mariën, B., Delpierre, N., Flores, O., et al. (2021). Drought elicits contrasting responses on the autumn dynamics of wood formation in late successional deciduous tree species. *Tree Physiol.* 41, 1171–1185. doi: 10.1093/treephys/tpaa175

Fatichi, S., Leuzinger, S., and Körner, C. (2014). Moving beyond photosynthesis: from carbon source to sink-driven vegetation modeling. *New Phytol.* 201, 1086–1095. doi: 10.1111/nph.12614

Fatichi, S., Pappas, C., Zscheischler, J., and Leuzinger, S. (2019). Modelling carbon sources and sinks in terrestrial vegetation. *New Phytol* 221, 652–668. doi: 10.1111/nph.15451

Friend, A. D., Eckes-Shephard, A. H., Fonti, P., Rademacher, T. T., Rathgeber, C. B. K., Richardson, A. D., et al. (2019). On the need to consider wood formation processes in global vegetation models and a suggested approach. *Ann. For. Sci.* 76:49. doi: 10.1007/s13595-019-0819-x

Gričar, J., Zavadlav, S., Jyske, T., Lavri,č, M., Laakso, T., Hafner, P., et al. (2018). Effect of soil water availability on intra-annual xylem and phloem formation and non-structural carbohydrate pools in stem of Quercus pubescens. *Tree Physiology* 39: 222–233. doi: 10.1093/treephys/tpy101

Gutiérrez, Y., Ott, D., Töpperwien, M., Salditt, T., and Scherber, C. (2018). X-ray computed tomography and its potential in ecological research: a review of studies and optimization of specimen preparation. *Ecol. Evol.* 8, 7717–7732. doi: 10.1002/ece3.4149

Hubau, W., Lewis, S. L., Phillips, O. L., Affum-Baffoe, K.,Beeckman, H., Cuní-Sanchez, A., et al. (2020). Asynchronous carbon sink saturation in African and Amazonian tropical forests. *Nature* 579, 80–87. doi: 10.1038/s41586-020-2035-0

Knipfer, T., Eustis, A., Brodersen, C., Walker, A. M., and McElrone, A. J. (2015). Grapevine species from varied native habitats exhibit differences in embolism formation/repair associated with leaf gas exchange and root pressure. *Plant Cell Environ.* 38, 1503–1513. doi: 10.1111/pce.12497

Legendre, P. (2018). *lmodel2: Model II Regression. R Package Version 1.7–3*.

Lehnebach, R., Bossu, J., Va, S., Morel, H., Amusant, N., Nicolini, É., et al. (2019). Wood density variations of Legume trees in French Guiana along the shade tolerance continuum: heartwood effects on radial patterns and Gradients. *Forests* 10:80. doi: 10.3390/f10020080

Leroux, O., Leroux, F., Bellefroid, E., Claeys, M., Couvreur, M., Borgonie, G., et al. (2009). A new preparation method to study fresh plant structures with X-ray computed tomography. *J. Microsc.* 233, 1–4. doi: 10.1111/j.1365-2818.2008.03088.x

Marchand, L. J., Dox, I., Gricar, J., Prislan, P., Leys, S., Van den Bulcke, J., et al. (2020). Inter-individual variability in spring phenology of temperate deciduous trees depends on species, tree size and previous year autumn phenology. *Agric. For. Meteorol.* 290:108031. doi: 10.1016/j.agrformet.2020.108031

Mariën, B., Dox, I., De Boeck, H. J., Willems, P., Leys, S., Papadimitriou, D., et al. (2021). Does drought advance the onset of autumn leaf senescence in temperate deciduous forest trees? *Biogeosciences* 18, 3309–3330. doi: 10.5194/bg-18-3309-2021

Ooms, J. (2020). *magick: Advanced Graphics and Image-Processing in R. R Package Version 2.3*.

Paganin, D., Mayo, S. C., Gureyev, T. E., Miller, P. R., and Wilkins, S. W. (2002). Simultaneous phase and amplitude extraction from a

single defocused image of a homogeneous object. *J. Microsc.* 206, 33–40. doi: 10.1046/j.1365-2818.2002.01010.x

Prislan, P., Cufar, K., and De Luis, M., Gričar, J. (2018). Precipitation is not limiting for xylem formation dynamics and vessel development in European beech from two temperate forest sites. *Tree Physiol.* 38, 186–197. doi: 10.1093/treephys/tpx167

Prislan, P., Gričar, J., and Cufar, K. (2014). *Wood Sample Preparation for Microscopic Analysis - Protocol of the sTReESS COST Action FP1106*. Available online at: http://www.streess-cost.eu/images/stories/Documents/protocol_wood_sample_preparation_for_microscopic_analysis.pdf

Prislan, P., Gričar, J., de Luis, M., and Smith, K. T., Cufar, K. (2013). Phenological variation in xylem and phloem formation in *Fagus sylvatica* from two contrasting sites. *Agric. For. Meteorol.* 180, 142–151. doi: 10.1016/j.agrformet.2013.06.001

Pya, N., and Wood, S. N. (2015). Shape constrained additive models. *Stat. Comput.* 25, 543–559. doi: 10.1007/s,11222-013-9448-7

R Development Core Team (2019). *R: A Language and Environment for Statistical Computing*. Vienna, Austria: R Foundation for Statistical Computing.

Rasband, W. S. (2012). *ImageJ*. Bethesda, MD: U. S. National Institutes of Health.

Rathgeber, C. (2017). Conifer tree-ring density interannual variability—anatomical, physiological and environmental determinants. *New Phytol.* 216, 621–625. doi: 10.1111/nph.14763

Rossi, S., Anfodillo, T., and Menardi, R. (2006). Trephor: a new tool for sampling microcores from tree stems. *IAWA J.* 27:89. doi: 10.1163/22941932-90000139

Rossi, S., Deslauriers, A., and Morin, H. (2003). Application of the Gompertz equation for the study of xylem cell development. *Dendrochronologia* 21, 33–39. doi: 10.1078/1125-7865-00034

Rossi, S., Rathgeber, C. B. K., and Deslauriers, A. (2009). Comparing needle and shoot phenology with xylem development on three conifer species in Italy. *Ann. For. Sci.* 66, 206. doi: 10.1051/forest/2008088

Simpson, G. L. (2020). gratia: Graceful 'ggplot'-Based Graphics and Other Functions for GAMs Fitted Using 'mgcv'. *R Package Version* 0.3.0.

Stuppy, W. H., Maisano, J. A., Colbert, M. W., Rudall, P. J., and Rowe, T. B. (2003). Three-dimensional analysis of plant structure using high-resolution X-ray computed tomography. *Trends Plant Sci.* 8, 2–6. doi: 10.1016/S1360-1385(02)00004-3

Van den Bulcke, J., Boone, M., Dhaene, J., Loo, D., Hoorebeke, L., Wyffels, F., et al. (2019). Advanced X-ray CT scanning can boost tree-ring research for earth-system sciences. *Ann. Bot.* 124, 837–847. doi: 10.1093/aob/mcz126

Vlassenbroeck, J., Dierick, M., Masschaele, B., Cnudde, V., Van Hoorebeke, L., and Jacobs, P. (2007). Software tools for quantification of X-ray microtomography at the UGCT. *Nucl. Instrum. Methods Phys. Res. B.* 580, 442–445. doi: 10.1016/j.nima.2007.05.073

Wood, S. N. (2017). *Generalized Additive Models: An Introduction with R*. Boca Raton, FL: Chapman and Hall/CRC. doi: 10.1201/9781315370279

Conflict of Interest: The authors declare that the research was conducted in the absence of any commercial or financial relationships that could be construed as a potential conflict of interest.

Publisher's Note: All claims expressed in this article are solely those of the authors and do not necessarily represent those of their affiliated organizations, or those of the publisher, the editors and the reviewers. Any product that may be evaluated in this article, or claim that may be made by its manufacturer, is not guaranteed or endorsed by the publisher.

frontiers in Plant Science

ORIGINAL RESEARCH
published: 01 September 2021
doi: 10.3389/fpls.2021.702442

Wood Anatomy of Douglas-Fir in Eastern Arizona and Its Relationship With Pacific Basin Climate

*Daniel Balanzategui[1,2,3], Henry Nordhauß[1], Ingo Heinrich[1,2,3], Franco Biondi[4], Nicholas Miley[4], Alexander G. Hurley[1] and Emanuele Ziaco[1,5]**

[1]GFZ German Research Centre for Geosciences, Potsdam, Germany, [2]Institute of Geography, Humboldt-University, Berlin, Germany, [3]Department of Natural Sciences, DAI German Archaeological Institute, Berlin, Germany, [4]DendroLab, Department of Natural Resources & Environmental Science, University of Nevada, Reno, NV, United States, [5]Department of Ecology and Genetics, Plant Ecology and Evolution, University of Uppsala, Uppsala, Sweden

Dendroclimatic reconstructions, which are a well-known tool for extending records of climatic variability, have recently been expanded by using wood anatomical parameters. However, the relationships between wood cellular structures and large-scale climatic patterns, such as El Niño-Southern Oscillation (ENSO) and the Pacific Decadal Oscillation (PDO), are still not completely understood, hindering the potential for wood anatomy as a paleoclimatic proxy. To better understand the teleconnection between regional and local climate processes in the western United States, our main objective was to assess the value of these emerging tree-ring parameters for reconstructing climate dynamics. Using Confocal Laser Scanning Microscopy, we measured cell lumen diameter and cell wall thickness (CWT) for the period 1966 to 2015 in five Douglas-firs [*Pseudotsuga menziesii* (Mirb.) Franco] from two sites in eastern Arizona (United States). Dendroclimatic analysis was performed using chronologies developed for 10 equally distributed sectors of the ring and daily climatic records to identify the strongest climatic signal for each sector. We found that lumen diameter in the first ring sector was sensitive to previous fall–winter temperature (September 25th to January 23rd), while a precipitation signal (October 27th to February 13th) persisted for the entire first half of the ring. The lack of synchronous patterns between trees for CWT prevented conducting meaningful climate-response analysis for that anatomical parameter. Time series of lumen diameter showed an anti-phase relationship with the Southern Oscillation Index (a proxy for ENSO) at 10 to 14 year periodicity and particularly in 1980–2005, suggesting that chronologies of wood anatomical parameters respond to multidecadal variability of regional climatic modes. Our findings demonstrate the potential of cell structural characteristics of southwestern United States conifers for reconstructing past climatic variability, while also improving our understanding of how large-scale ocean–atmosphere interactions impact local hydroclimatic patterns.

Keywords: quantitative wood anatomy, *Pseudotsuga menziesii*, El Niño/Southern Oscillation, Pacific Decadal Oscillation, paleoclimate, western United States

OPEN ACCESS

Edited by:
Marco Carrer, University of Padua, Italy

Reviewed by:
Daniele Castagneri, University of Padua, Italy
Bao Yang, Cold and Arid Regions Environmental and Engineering Research Institute, Chinese Academy of Sciences, China

***Correspondence:**
Emanuele Ziaco
emanuele.ziaco@ebc.uu.se

Specialty section:
This article was submitted to Functional Plant Ecology, a section of the journal Frontiers in Plant Science

Received: *29 April 2021*
Accepted: *02 August 2021*
Published: *01 September 2021*

Citation:
Balanzategui D, Nordhauß H, Heinrich I, Biondi F, Miley N, Hurley AG and Ziaco E (2021) Wood Anatomy of Douglas-Fir in Eastern Arizona and Its Relationship With Pacific Basin Climate. Front. Plant Sci. 12:702442. doi: 10.3389/fpls.2021.702442

INTRODUCTION

The climate of the North American West is closely connected with ocean–atmosphere variability in the Pacific Basin, which is often defined through indices, such as the El Niño-Southern Oscillation (ENSO) index (Barnett et al., 1991) and the Pacific Decadal Oscillation (PDO) index (Mantua and Hare, 2002). Both climatic modes play a fundamental role in determining interannual variability of ecohydrological conditions, affecting water resources, particularly in the moisture-limited environments of the western United States (Corringham and Cayan, 2019; White et al., 2019), and long-term vegetation dynamics (Viglizzo et al., 2015). Over the western United States, the southward shift of convective air masses that occurs over the ocean during an El Niño (La Niña) event often results in above (below) average winter rainfall over the southwest (Sheppard et al., 2002). Similarly, warm (cold) PDO phases are positively (negatively) correlated with winter precipitation along the coast of southern California, Arizona, and New Mexico (Mantua et al., 1997). Recently, model predictions based on large-scale atmospheric circulation patterns have been shown to unsatisfactorily reproduce observed precipitation dynamics (Jong et al., 2018). This is because linking ENSO- and PDO-driven regional climatic conditions with local hydroclimatic variability requires properly accounting for additional site-specific factors. For example, wind direction and local topography can cause abnormally high rainfalls to occur, contrary to expectation, during La Niña events in the southwest United States (Feldl and Roe, 2010).

Since instrumental records of ENSO and PDO begin in the late 19th century, the range of local climate variability that can be expected during different modes of ENSO and PDO can be better estimated by extending instrumental observations using proxy records, such as climate-sensitive tree-ring chronologies (Biondi et al., 2001; Stahle et al., 2009; Woodhouse et al., 2013; Ziaco et al., 2020). The inclusion of cellular-level wood anatomical traits in dendroclimatological studies has the potential to improve the spatiotemporal coverage of hydroclimatic reconstructions (González-Cásares et al., 2019; Seftigen et al., 2020). Quantitative wood anatomy (QWA) in dendroclimatology, namely, the response between woody cell structures and climatic variability (von Arx et al. 2016), has been applied to angiosperm (García-González and Eckstein, 2003; Tardif and Conciatori, 2006; Fonti and García-Gonzalez, 2008; Campelo et al., 2010) and conifer species (Wang et al., 2002; Panyushkina et al., 2003; DeSoto et al., 2011; Liang et al., 2013b), but cellular-level dendroclimatology in the western United States is still relatively new (Ziaco et al., 2016; Edwards et al., 2020). Intra-annual variability of xylem structures depends on resource allocation and trade-offs between plant growth and reproduction that are driven by local hydroclimatic variability (Lauder et al., 2019) at short (sub-seasonal) time scales (Bouriaud et al., 2005). Hence, annually resolved time series of cellular parameters often present stronger or different relationships with seasonal climate compared to their ring-width counterpart (Castagneri et al., 2017), offering studies with limited wood material the potential to overcome some of the restrictions of tree-ring-based paleoclimatic reconstructions, such as the minimum sample size (Pearl et al., 2020). For instance, multi-centennial reconstructions of summer (Panyushkina et al., 2003) and winter temperature (Pritzkow et al., 2016) have been produced using wood anatomical parameters extracted from a limited number of samples otherwise deemed insufficient for standard ring-width analysis. Furthermore, the partitioning of tree rings into sub-sections (herein referred to as "sectors") is a rapidly growing technique with the potential to improve the temporal resolution of the climatic signal encoded in intra-annual xylem cellular structures (Carrer et al., 2017). Tree-ring partitioning, either in equal parts (Castagneri et al., 2017) or between earlywood and latewood (Fonti and García-González, 2004; Torbenson et al., 2016), better characterizes intra-seasonal changes in wood anatomical features along the tree ring and is expected to enhance the temporal resolution of climate-anatomy relationships while also clarifying and expanding the amount and quality of environmental information obtainable from trees (Ziaco and Liang, 2019).

Douglas-fir [*Pseudotsuga menziesii* (Mirb.) Franco] is one of the most widely used species for dendroclimatic research in the western United States. It is widely distributed along the coast of the American northwest and western Canada, and from Mexico to the Rocky Mountains (Li and Adams, 1989), it can reach ages greater than 1,000 years (Contributors of the International Tree-Ring Data Bank, 2020) and its ring-width chronologies are typically sensitive to climate. It is therefore an ideal target for testing the potential of cellular-level dendroclimatology. The main goal of this explorative study was to assess the utility of wood anatomy of *P. menziesii* for dendroclimatic reconstructions with particular focus on Pacific Basin climate, and specifically, 1) to test the temporal and spatial climate relationships of intra-annual xylem anatomical parameters in *P. menziesii* and 2) to evaluate the potential contribution of these proxies for bridging the gap between large-scale atmospheric circulation modes (such as ENSO and PDO) and local hydroclimatic variability. To achieve these goals, we developed ring-sector chronologies and assessed the strength of the climatic signal encoded in their wood anatomical structures.

MATERIALS AND METHODS

Study Area

The study site, located in the White Mountains of eastern Arizona on the southern edge of the Colorado Plateau (**Figure 1A**), was preselected based on a preliminary analysis of the site characteristics performed with the web-based tool Dendrobox (Zang, 2015). Despite falling within the core region of the North American Monsoon (NAM), where precipitation is mostly concentrated in the summer months (Griffin et al., 2013), mountain areas in this part of the southwestern United States are also sensitive to cool-season conditions linked to ENSO, and the Dendrobox tool allowed us to search the International Tree-Ring Data Bank (Grissino-Mayer and Fritts, 1997) for existing sites with ring-width chronologies

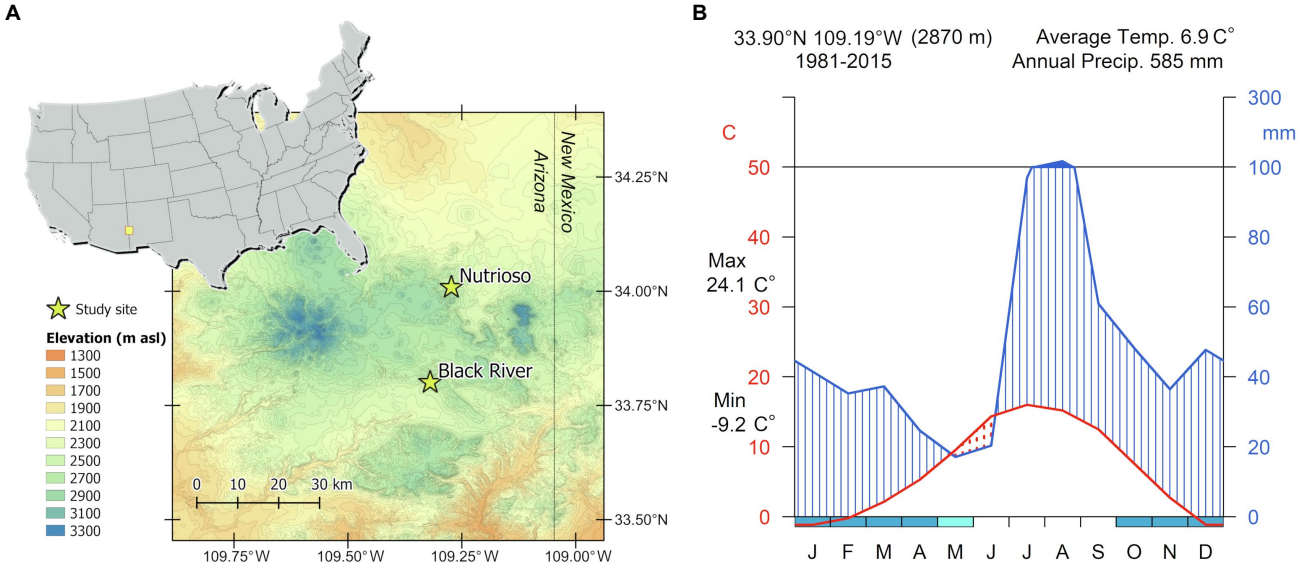

FIGURE 1 | **(A)** Geographical location of the two study sites. **(B)** Walter-Lieth climatic diagram for the period 1981–2015 based on PRISM data.

sensitive to winter precipitation. Tree samples were collected in forest stands dominated by *P. menziesii* near the village of Alpine, Arizona. Trees were located at altitudes between 2,500 and 2,900 m a.s.l. on south- to southeast-facing slopes with 25–52% steepness.

The topographically complex landscape of the White Mountains is influenced by multiple climatic patterns linked to the Pacific Ocean, including the Gulf of California, and the Atlantic Ocean, including the Gulf of Mexico (Jana et al., 2018). The precipitation regime reflects the typical bimodal pattern found in the southwestern United States (**Figure 1B**), with a peak in late winter derived from large-scale frontal storms originating over the eastern Pacific, followed by summer rainfall carried inland by the NAM (Sheppard et al., 2002). Daily time series of maximum temperature (Tmax) and total precipitation for the years 1981–2015 were obtained from the PRISM (Parameter-elevation Relationships on Independent Slopes Model) 4 km dataset (Daly et al., 2008) at the grid point 33.90° N 109.19°W. The climate during this period was characterized by a mean annual temperature of 6.9 ± 3.2°C, with January and July being the coldest (−1.2 ± 3.8°C) and warmest months (16.0 ± 1.8°C), respectively. Total annual precipitation was 585 ± 113 mm, with a substantial amount falling from July to August (37% of the annual total), and snowpack lasting on average from November to March (**Figure 1B**).

Tree-Ring Chronologies and Anatomical Measurements

In April 2016, a total of 31 increment cores were collected from two sites (Nutrioso and Black River; **Figure 1A**) from healthy *P. menziesii* trees with diameters at breast height (~1.3 m from the ground) ranging from 45 cm to 93 cm, and an average height of 35 m. Increment cores were taken with a 4 mm increment borer in a direction parallel to topographic contours to avoid compression wood produced by gymnosperms on the downhill side of the stem (Speer, 2010). Increment cores were mounted with wood tracheids oriented vertically, sanded with progressively finer sandpaper, and finally hand polished until individual cells were visible under 10-50x magnification. Individual series were cross-dated and measured on a Velmex sliding-scale micrometer table interfaced with a video camera with the Measure J2X software (VoorTech Consulting), and finally averaged to develop a ring-width chronology (**Supplementary Figure S1a**). Trees from Nutrioso were on average 118 ± 35 years old with minimum and maximum ages of 92 and 250 years, respectively, while trees sampled at Black River were 142 ± 35 years old on average and ranging from 83 to 174 years. The mean ring width was 1.47 ± 0.37 mm at Nutrioso and 1.62 ± 0.41 mm at Black River. Raw ring-width series were standardized using a 50-year smoothing spline with 0.5 frequency cutoff and pre-whitened to remove first-order autocorrelation. As a preliminary step, we tested climate-growth relationships for the period 1950–2015 using monthly data of Tmax and precipitation. Response functions showed that *P. menziesii* radial growth at these sites is positively influenced by previous December to current January precipitation, while also negatively affected by July temperature (**Supplementary Figure S1b**).

The wood anatomical analysis was conducted on a subset of five trees (three from Nutrioso and two from Black River) by selecting cores with high-quality intra-annual xylem structures, and absence of surface cracks or other alteration of the woody tissue. For the extraction of resinous compounds, samples were separated from their mounts, divided into 5-cm long pieces, and submerged in glass vessels filled with 99.9% isopropanol for 48 h in a 70° C ultrasonic water bath operating at a frequency of 37 kHz. Samples were then air dried, remounted, and stabilized using non-Newtonian fluid to avoid cell wall breakage during

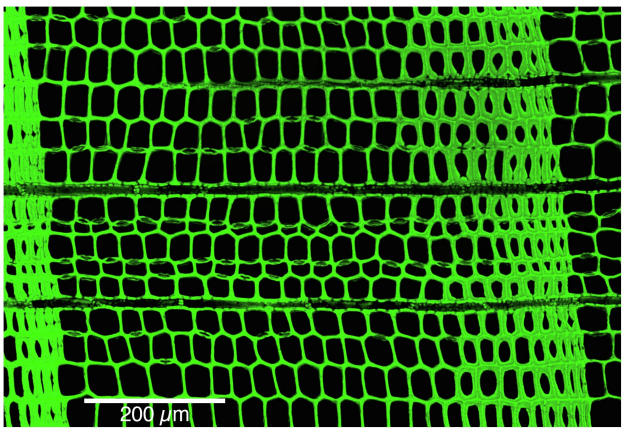

FIGURE 2 | Microscopic composite (merged) image of *Pseudotsuga menziesii* at 300x magnification with brightness correction.

the cutting procedure (Schneider and Gartner, 2013). Micro sections (~20 µm) were cut from the transversal surface with an advanced core-microtome (Gartner and Nievergelt, 2010). Thin sections were then stained with 1% safranin diluted in distilled water, dehydrated with alcohol, and temporarily fixed in glycerol between two glass microscope slides (Gärtner and Schweingruber, 2013). Sequential micro-images were taken at 100x magnification following the procedures and settings described by Liang et al. (2013a) using an Olympus FluoView FV300 Confocal Laser Scanning Microscope (CLSM) that displays cell wall (green) and lumen (black) in strong contrast (**Figure 2**). Large, single frame images derived from composite CLSM micrographs (25 to 30 images) were processed with the quantitative wood anatomical program, ROXAS 3.0.1 (von Arx and Carrer, 2014 and supporting software Image-Pro Plus v6.1 Media Cybernetics, Silver Spring, MA, United States), to identify, date, edit, and measure all cell structures. Although CLSM allows to acquire images directly on the wood surface, in our set of samples we found the wood properties of the inner part of the tree, where the rings are darker, to be more suitable for direct surface scanning, whereas the lighter sap wood rings were not, requiring additional steps of staining and thin sectioning to allow CLSM imaging to enhance the contrast between cell structures. As in this study we focused on the outermost, light-colored sapwood rings, we preferred to use thin sections, which provided better results although more time-consuming.

From the QWA data produced by ROXAS, our analysis focused on the intra- and inter-annual variability in radial diameter of cell lumen (LD) and tangential cell wall thickness (CWT). The QWA specific search algorithms of the R package, RAPTOR 1.0.1 (Row and Position Tracheid Organizer in R), were used to locate cell rows and assign each cell (tracheid) and corresponding QWA measurements to the correct position within its respective radial file (Peters et al., 2018). Depending on the quality of the scanned material and the number of resin ducts within each tree ring, between 10 to 25 cell rows were identified, exceeding the number usually recommended (Seo et al., 2014). While the distance across each ring was mostly homogenous the number of cells within each cell row showed some variation, therefore standardized profiles (tracheidograms) for each cell file were produced to better illustrate intra-seasonal and year-to-year site-wide growth patterns along the tree ring (Vaganov, 1990; Ziaco, 2020). Tracheidograms for each radial file, year, and tree were divided into 10 equal sized sectors (from I to X). While tree-ring partitioning is generally performed by visually dividing the ring into 10 equally spaced portions based on ring width, in our approach the location of each sector boundary was determined for each analyzed row in relation to the total number of cells found in that row – an analytical step made possible with the inclusion of the RAPTOR algorithms. With this approach, the cells of each radial file could be precisely assigned to their respective sectors. The simple average of LD or CWT measurements for all cells falling within a specific sector within the row and ring was then calculated to produce 10 sectorial chronologies for each anatomical parameter. Finally, the 10 sector chronologies of each tree were normalized (zero mean and unit standard deviation) across the common period 1966–2015, and the average taken across all trees to obtain sector chronologies revealing site-wide, intra-seasonal anatomical variability. Due to lack of a long-term trend, which usually occurs in ring-width series because of inherent non-climatic trends interfering with the climatic signal, no detrending procedure was applied (Carrer et al., 2017). Chronology descriptive statistics commonly employed in tree-ring studies were used to gage the quality of the common variance (i.e., climatic signal) shared among trees (Hughes et al., 2011). These included mean inter-series correlation (rbar), expressed population signal (EPS), and signal-to-noise ratio (SNR). Descriptive statistics were calculated using the R package *dplR* (Bunn et al., 2014).

Dendroclimatic Analysis

Each sector chronology was compared with daily Tmax and total precipitation (PPT) from 1981 to 2015 using the Climate Impact on Tree Growth (CLIMTREG) program (Beck et al., 2013). CLIMTREG initially calculates correlations between climate and anatomical parameters for a 21-day-long period, then iteratively adds one day to the correlation window until a maximum interval length of 121 days is reached. The moving correlation procedure starts on July first of the previous year and stops on October 31st of the current year, resulting in 42,218 correlations calculated per run. Hence, the starting and ending date of climate-anatomy correlations could be identified with daily resolution, summarized for each climatic parameter (temperature and precipitation), and visualized for each tree-ring sector. Since our interest was in evaluating the potential of wood anatomy for dendroclimatic reconstructions, whenever multiple significant correlations with climate emerged we identified and retained only the period most strongly correlated with a given parameter and used only that respective window for further analyses and visualization.

The sectors that showed acceptable chronology statistics (Wigley et al., 1984) and relationships with daily climate

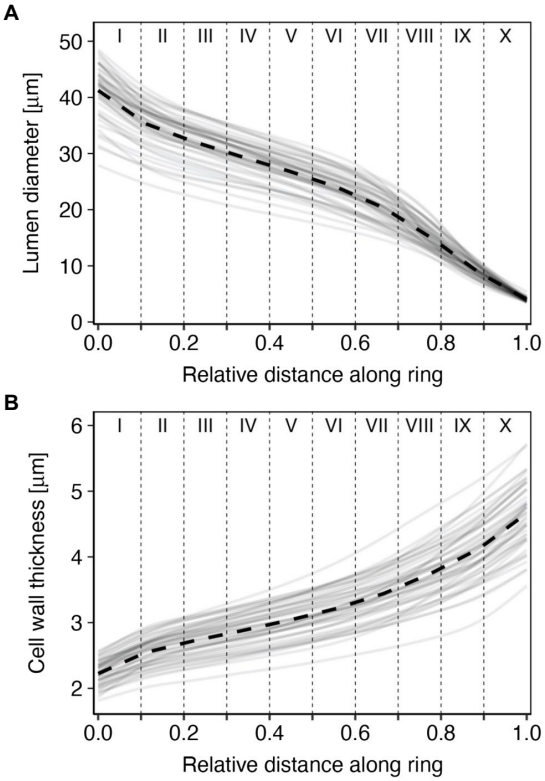

FIGURE 3 | Annual (gray solid lines) and mean (black dashed lines) standardized tracheidograms of **(A)** lumen diameter and **(B)** cell wall thickness (CWT) for the five sampled trees at Nutrioso and Black River for the years 1966–2015. Roman numerals indicate tree-ring sectors, from the beginning (sector I) to the end of the ring (sector X).

parameters were chosen to assess spatial field correlations. The spatial signature of the growth response to climate was investigated using the web-based KNMI Climate Explorer tool[1] (Trouet and Van Oldenborgh, 2013) to generate correlation fields over the United States and Mexico, as well as the Pacific, Gulf of Mexico, and Atlantic regions. Because daily data are not available for spatial field correlation in KNMI Climate Explorer, this analysis was done using monthly climate data. Temperature and precipitation were taken from the CRU TS4.03 dataset with 50 km x 50-km grid cells (Mitchell and Jones, 2005). Sector chronologies were also correlated against 1-month Standardized Precipitation and Evaporation Index (SPEI-1; CSIC 2.6; Beguería et al., 2014) and sea surface temperature (SST; NOAA/NCEP Reynolds OI.v2; Reynolds et al., 2002) to investigate the influence of interdecadal or decadal climatic oscillations patterns derived from ENSO and PDO.

Finally, the relationship between wood anatomy in *P. menziesii* and supra-regional climatic modes was quantified by applying a cross-wavelet transform (Grinsted et al., 2004) to annually resolved time series of anatomical parameters for selected sectors against the Southern Oscillation Index (SOI; Ropelewski and Jones, 1987) and PDO (Mantua et al., 1997) indices over the period 1966–2015. The SOI is a measure of fluctuations in air pressure occurring between the western and eastern tropical Pacific and is one of the most commonly used proxy indicators to describe anomalies in ENSO behavior (Ropelewski and Jones, 1987). Negative (positive) phases of the SOI are associated with El Niño (La Niña) conditions that often result in above (below) average precipitation in the southwestern United States. Cross-wavelet analysis highlights common time frequency phase variations, phase cyclicity, and links between different bio-geophysical proxies (Wang et al., 2011; Land et al., 2020). Explanatory monthly variables of SOI and PDO series were pre-determined based on the outcomes of the dendroclimatic calibration. Cross-wavelet analysis was performed using the package *WaveletComp* (Roesch and Schmidbauer, 2018) for the R statistical environment (R Core Team, 2021).

[1]https://climexp.knmi.nl/

RESULTS

Cell Structure and Sector Chronologies

From the start to the end of the tree ring, lumen diameter (LD) decreased from 41.3 ± 4.7 µm in the first part of the ring (sector I) to 4.0 ± 0.4 µm in the last part (sector X; **Figure 3A**; **Table 1**). CWT instead increased from about 2.2 ± 0.2 µm in the first sector (I) to 4.7 ± 0.5 µm in the last sector (X; **Figure 3B**; **Table 1**). Site-averaged sector chronologies of LD had negligible first-order autocorrelation ranging from 0.07 to 0.32, whereas first-order autocorrelation was higher for CWT chronologies, ranging between 0.62 and 0.73 (**Table 1**). Inter-annual variability of LD between the five trees generally showed stronger synchronization in the earlier sectors compared to the later ones (**Table 1, Figure 4A**). These common growth patterns from the first to the fifth sector were shown by rbar values from 0.438 to 0.658, EPS from 0.796 to 0.906, and SNR from 3.496 to 6.368. On the other hand, CWT series were noisy along the entire ring (rbar from 0.004 to 0.166, EPS from 0.026 to 0.501, and SNR from 0.012 to 1.314) and generally lacked common variability between trees (**Table 1, Figure 4B**). For this reason, CWT chronologies were excluded from further analysis.

Correlations Between Anatomical Chronologies and Daily Climate

Several significant ($p < 0.05$) climate-anatomy relationships were found between all LD sectors and daily Tmax and precipitation. The strongest correlations for the first five sectors were with previous mid-September to current mid-February, and generally decreased in strength toward the transition zone between earlywood and latewood cells. Temperature was negatively correlated with LD, with Pearson's correlation coefficient r between −0.56 and −0.72 (**Figure 5A**), whereas precipitation had a positive correlation, ranging between 0.7 and 0.75 (**Figure 5B**). For sectors six to 10, the relationship between LD and temperature remained negative, but the temporal window of maximum correlation progressively

TABLE 1 | Summary statistics of cell lumen diameter and cell wall thickness chronologies.

	Lumen diameter (LD)					Cell wall thickness (CWT)				
Sector	**Mean ± SD**	**AC1**	**rbar**	**EPS**	**SNR**	**Mean ± SD**	**AC1**	**rbar**	**EPS**	**SNR**
I	41.3 ± 4.7	0.07	0.658	0.906	6.368	2.2 ± 0.2	0.73	0.004	0.026	0.012
II	35.3 ± 3.8	0.04	0.623	0.893	5.755	2.5 ± 0.2	0.76	0.108	0.379	0.634
III	32.1 ± 3.5	0.05	0.504	0.836	4.193	2.7 ± 0.2	0.72	0.166	0.501	1.314
IV	29.5 ± 3.3	0.10	0.447	0.802	4.051	2.9 ± 0.3	0.67	0.137	0.444	0.837
V	26.9 ± 3.1	0.14	0.438	0.796	3.496	3.0 ± 0.3	0.65	0.115	0.397	0.962
VI	24.0 ± 3.0	0.16	0.243	0.616	1.697	3.2 ± 0.3	0.62	0.089	0.332	0.829
VII	20.3 ± 2.7	0.16	0.119	0.402	0.632	3.4 ± 0.3	0.62	0.066	0.263	0.698
VIII	15.0 ± 2.0	0.17	0.093	0.338	0.531	3.8 ± 0.4	0.63	0.045	0.194	0.508
IX	8.8 ± 1.0	0.32	0.108	0.375	0.602	4.1 ± 0.4	0.62	0.015	0.076	0.158
X	4.0 ± 0.4	0.22	0.159	0.486	0.893	4.7 ± 0.5	0.62	0.011	0.062	0.172

Mean and standard deviation (SD = ± one standard deviation, both shown in μm), one-year lag autocorrelation (AC1), series inter-correlation (rbar), expressed population signal (EPS), and signal-to-noise ratio (SNR) were calculated for the period 1966 to 2015, moving from the start of the earlywood (sector I) to the end of the latewood (sector X).

shifted toward the spring and summer of the current growing season as sector number increased. In the second half of the tree ring, LD maintained a positive linkage with previous-September to current-February precipitation. Maximum dendroclimatic correlations in the latter half of the tree ring were usually weaker than those in the first half. However, sector IX, despite showing poor signal quality (rbar = 0.108, EPS = 0.375, SNR = 0.602), had a strong negative correlation with mid-July to mid-August temperature ($r = -0.72$). Overall, the first sector (I) carried the strongest signal, responding to Tmax from previous September 25th to current January 23rd (**Supplementary Figure S2**). The average of sectors I-V showed high correlation ($r = 0.75$) with rainfall between previous October 27th and current February 13th (**Figure 6** and **Supplementary Figure S3**). Based on these results, sector I and the mean of sectors I-V were chosen for further calibration analysis.

Spatial Field Correlations and Cross-Wavelet Analysis

Spatial field correlations were performed between lumen diameter chronologies for sector I and for the average of sectors I-V against October–January average Tmax, SPEI-1, SST, and November–January total PPT. The negative correlation between Tmax and LD in sector I was spatially consistent and significant throughout the entire southwestern United States and northern Mexico, with correlations ranging from $r = -0.34$ to $r = -0.71$ (**Figure 7A**). A similar geographical pattern, but positive and with an extension reaching into the American mid-west, was found between sector I-V LD and PPT during previous November to current January (**Figure 7B**) with correlations ranging between $r = 0.34$ and $r = 0.70$. Spatial correlations between sector I-V LD and SPEI-1 were almost identical in terms of geographical distribution to those with PPT (r from 0.34 to 0.75) but were slightly higher and more homogeneously distributed over the southwestern United States, especially Arizona, New Mexico, and southern Colorado (**Figure 7C**). The sector I-V LD chronology showed widespread significant relationships with October to January SSTs in the Pacific Ocean, resembling the typical pattern of SST anomalies associated with ENSO events (**Figure 7D**). Correlations between LD in the first half of the ring and SST were positive in the eastern Pacific (r from 0.34 to 0.57), and negative in the western and southern Pacific (r from −0.34 to −0.69).

The October–January SOI index and LD were correlated between 1966 and 2015 (**Figure 8A**). This relationship was higher during the period 1980–2005, when the cross-wavelet power showed a significant anti-phase relationship on the 10-14-year band (**Figure 8B**). Since El Niño episodes, characterized by above average precipitation and cooler temperatures in the southwestern United States, are associated with negative SOI phases, the emergence of such anti-phase relationships highlighted the potential of wood anatomical structures to record large-scale climatic variability, confirming at the same time the outcomes of the dendroclimatic analysis performed with local temperature and precipitation data. On the other hand, no clear connections were observed between PDO and LD series (**Supplementary Figures S4a,b**).

DISCUSSION

Intra-annual Wood Cellular Dendroclimatic Relationships

Xylem cellular features of *P. menziesii* were not equally suitable as paleoclimatic proxies. In this study, lumen diameter and CWT differed at both the inter- and intra-annual level in terms of common signal among trees and sensitivity to climate. In contrast to LD, CWT time series lacked common variability (low rbar, EPS, and SNR) and showed high serial autocorrelation (AC1). The high values of AC1 in the chronologies of CWT, particularly in the first sectors (i.e., I and II), might be due to complex dynamics of carbon assimilation and allocation, whose description is beyond the scope of this work, that can be further complicated by external factors, such as disturbance events like drought (Peltier and Ogle, 2020). The low agreement between CWT series observed here and in previous studies (Ziaco et al., 2016), suggests that in drought-prone locations of the Southwest, sub-seasonal internal processes responsible

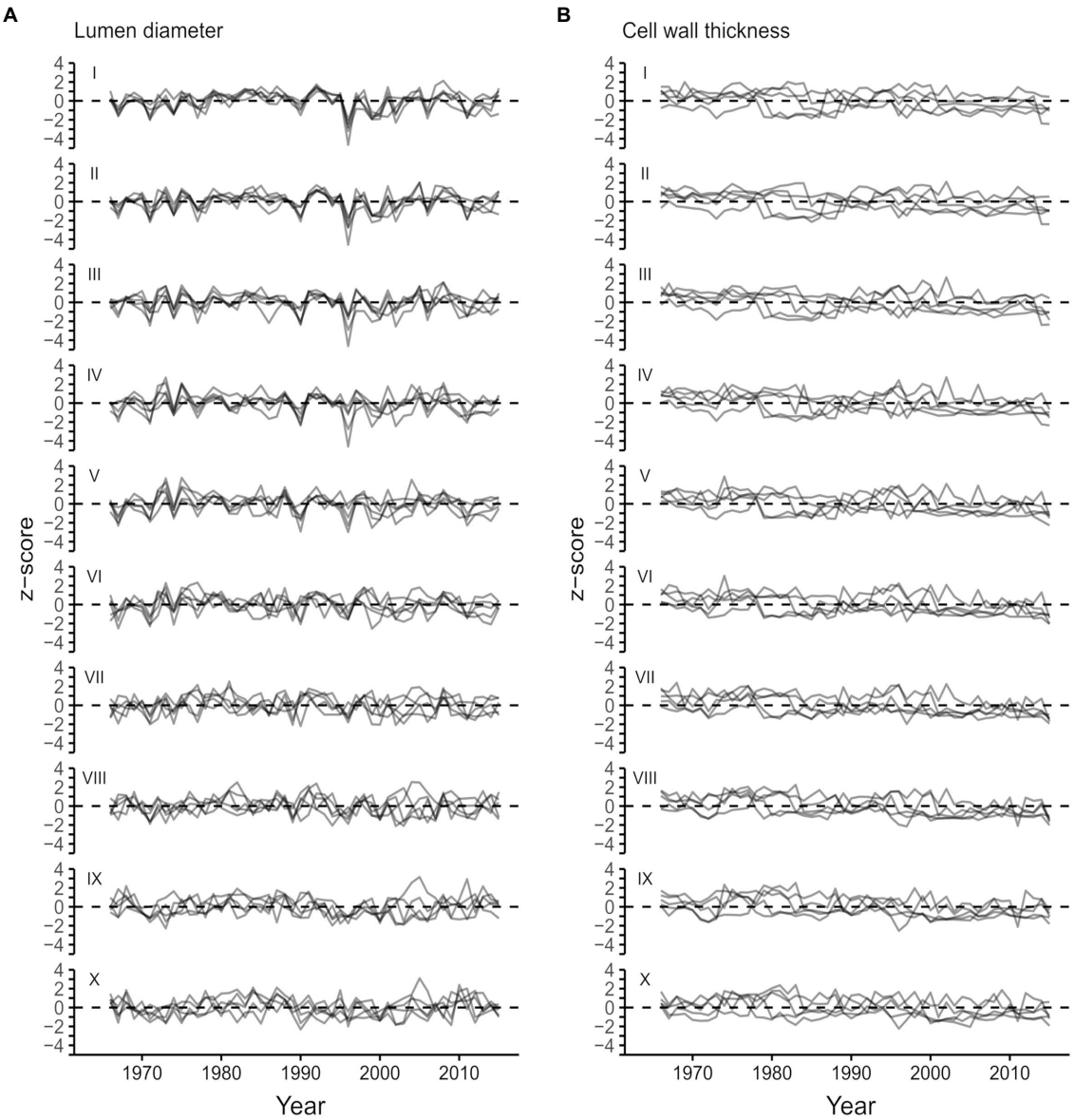

FIGURE 4 | Standardized sector chronologies for the period 1966–-2015 for lumen radial diameter **(A)** and CWT **(B)** moving from the beginning (sector I) to the end (sector X) of the ring.

for partitioning of carbohydrates between structural and non-structural sinks (i.e., primary and secondary productivity, storage; Carbone et al., 2013) remains highly variable between trees (Herrera-Ramirez, 2020). On the other hand, the effect of climatic conditions on growth and carbon dynamics in *P. menziesii* (Peltier et al., 2018), as well as in other western United States conifers (Szejner et al., 2018), is known to last for several years. Plant-dependent controls acting on the timing, rate, and duration of cell wall thickening generally reflect a conservative strategy adapted to aridity for maintaining hydraulic integrity (Cuny et al., 2015; Cuny and Rathgeber, 2016). However, under water-limited conditions, *P. menziesii* seems to respond to climatic variability primarily by adjusting lumen size to maintain hydraulic integrity as observed for other conifer species (Carvalho et al., 2015), which makes lumen diameter a valuable paleoclimatic proxy.

Tree-ring sectoring allowed us to enhance the overall quality of dendroclimatic relationships with lumen diameter in *P. menziesii* by targeting the most signal-rich sectors of the ring. This was possible because sampled trees had wide rings and enough cells to make numerous meaningful subdivisions. Intra-annual variability characterized each anatomical parameter at all positions along the ring, especially in the first sectors (i.e., I to V), roughly corresponding to the earlywood. Intra-annual patterns of LD and CWT, as illustrated by 1966–2015 standardized tracheidograms, were characterized by a constant

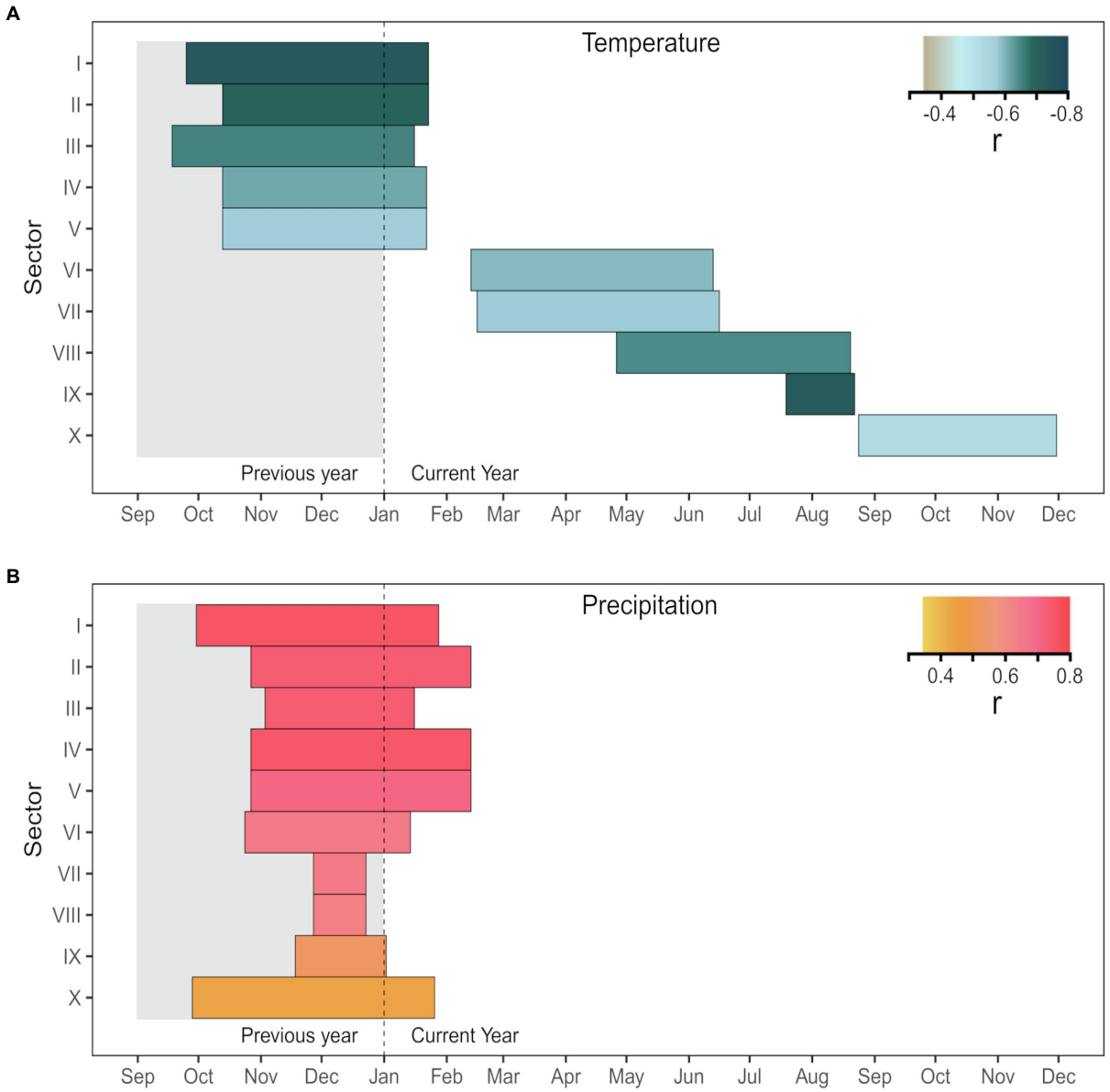

FIGURE 5 | Correlations of sector chronologies of lumen diameter with daily **(A)** maximum temperature (Tmax) and **(B)** precipitation for the period 1981 to 2015. The horizontal length of each bar corresponds to the strongest optimal period identified by the moving window correlation analysis. All correlations, whose value is given by the color, are significant at $p < 0.05$.

decrease of lumen diameter and gradual thickening of cell walls, without any major, stand-wide intra-annual density fluctuations. LD chronologies showed a consistent inter-annual pattern of synchronous variability among trees in the earlywood, but the common signal gradually decreased approaching the earlywood/latewood transition zone approximately around sector V or VI and disappeared in the later sectors.

Climate-anatomy correlations established for lumen diameter of *P. menziesii* showed the predominant cold-season signal in the first half of the ring, while the contribution of spring climate, although present (see **Supplementary Figures S2, S3**), was lower. The strongest correlation between daily temperature and lumen diameter found for sectors I to V was with a period ranging from October to January, while it transitioned to a spring–summer signal starting with sector VI (**Figure 5**). In the southwestern United States, winter temperature may affect snowpack dynamics by favoring snow sublimation, reducing the amount of water penetrating the ground at the time of snow melting (Sheppard et al., 2002). Furthermore, air temperature is tightly related to cloudiness and inversely related to snowy precipitation during the cold season. Hence, previous winter temperature influences the morphogenesis of the first ring cells of each ring (Wang et al., 2002; Martin-Benito et al., 2013; Novak et al., 2013), while summer

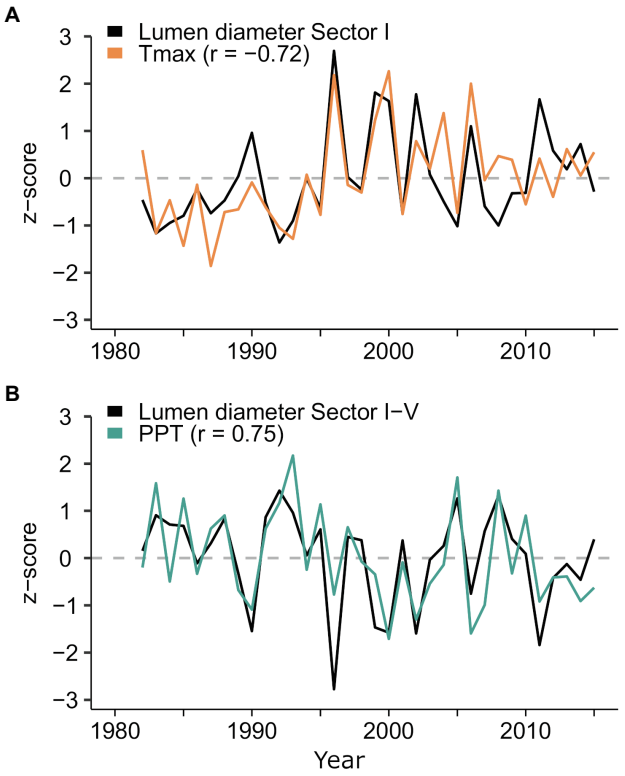

FIGURE 6 | Normalized time series of radial lumen diameter chronologies for sector I and for the average between sectors I-V plotted against **(A)** temperature and **(B)** precipitation. Climate data are the average daily Tmax from September 25th to January 23rd, and the sum of daily precipitation from previous October 27th to current February 13th. The sector I chronology of lumen diameter is shown with opposite sign for easier comparison with the temperature time series.

temperature conditions, and their control on evaporative demand and drought stress in particular, become more important later in the growing season especially around sectors VIII and IX (Cuny and Rathgeber, 2016; Cuny et al., 2019). The similar temporal response to temperature across LD sectors in the first half of the ring suggests that these trees experience fast rates of xylem production in the spring, aimed at maximizing radial growth when evapotranspiration is less demanding, and to avoid the negative effects of spring temperature (**Supplementary Figures S2, S3**). The previous cold-season precipitation signal persisted, although decreasing in strength, throughout the entire ring. This consistent pattern of correlation across the tree ring confirms the importance of winter precipitation for western conifers (Kerhoulas et al., 2013) and its footprint on wood anatomy even in the core area of the NAM (Ziaco et al., 2018), whereas under non-monsoonal climatic regimes other species tend to show a predominant response to current year precipitation (Ziaco et al., 2016). In line with this, we also found that positive effects of precipitation on lumen diameter persisted until May in sectors I, and within the average of sectors I-V. However, in a short temporal window of 23 days (from June 28th to July 20th), we observed a temporary inversion in the sign of correlation between precipitation and lumen size (**Supplementary Figures S2, S3**). However, these two temporal windows showed an overall weaker correlation strength and were not considered useful for further dendroclimatic investigation. In addition to site-specific differences, particularly in seasonal dynamics of moisture availability, it should be noted that discrepancies in the temporal window of climatic responses between our study and previous ones could also be a consequence of parameter selection, i.e., tree-ring partitioning *versus* a whole ring approach, that in this case allowed us to focus on the climatic signal recorded in specific, signal-rich portions of the ring.

Under limiting conditions, the cellular response of tree species to changing moisture conditions is expected to act on lumen size rather than their quantity (Olano et al., 2012). Furthermore, tracheid dimensions are directly dependent on the hydration status of the tree stem during the time of cell formation when water is needed to maintain adequate turgor during the cell enlargement phase (Arzac et al., 2018; Cabon et al., 2020). We observed sensitivity to drought in *P. menziesii*, although the strongest relationship was with previous cold-season climate, which is far from contemporaneous with the timing of the cell enlargement phase, and got weaker with spring conditions. It should be noted that in the mountain ranges of the western United States, winter October–April precipitation falls mainly as snow, contributing to the formation of the snowpack, which in turn determines soil moisture at the beginning of the growing season and the amount of water available for the resumption of cambial processes (Maurer and Bowling, 2014). Hence, snowpack dynamics can affect inter-annual variability of cellular structures and explain a large proportion of the observed variance in earlywood tracheids (Ziaco, 2020). A drought signal in xylem anatomy of *P. menziesii* was demonstrated by the correlation between LD in the earlywood and the SPEI-1 for the months October to January. This correlation is particularly relevant, as the SPEI-1 includes potential evapotranspiration, possibly capturing the effect of water deficit/surplus on tree growth and xylem features (Vicente-Serrano et al., 2010).

Correlations With Supra-Regional Climatic Patterns

We have shown that annually resolved time series of lumen diameter (LD) hold great potential for linking local temperature and precipitation patterns with large-scale climatic modes in the southwestern United States. This was possible due to the strong climatic signal encoded in cellular structures, and the possibility to enhance the temporal resolution of dendroclimatic correlations using tree-ring partitioning and daily climatic records. Regional correlation fields suggested that the climatic signal encoded in *P. menziesii* tracheids accurately reproduced the same hydroclimatic pattern over the entire American southwest typically shaped by large-scale winter climatic modes (St. George et al., 2010). Weather conditions along western North America are associated with ocean–atmosphere variability over the Pacific Basin, which is responsible for regulating

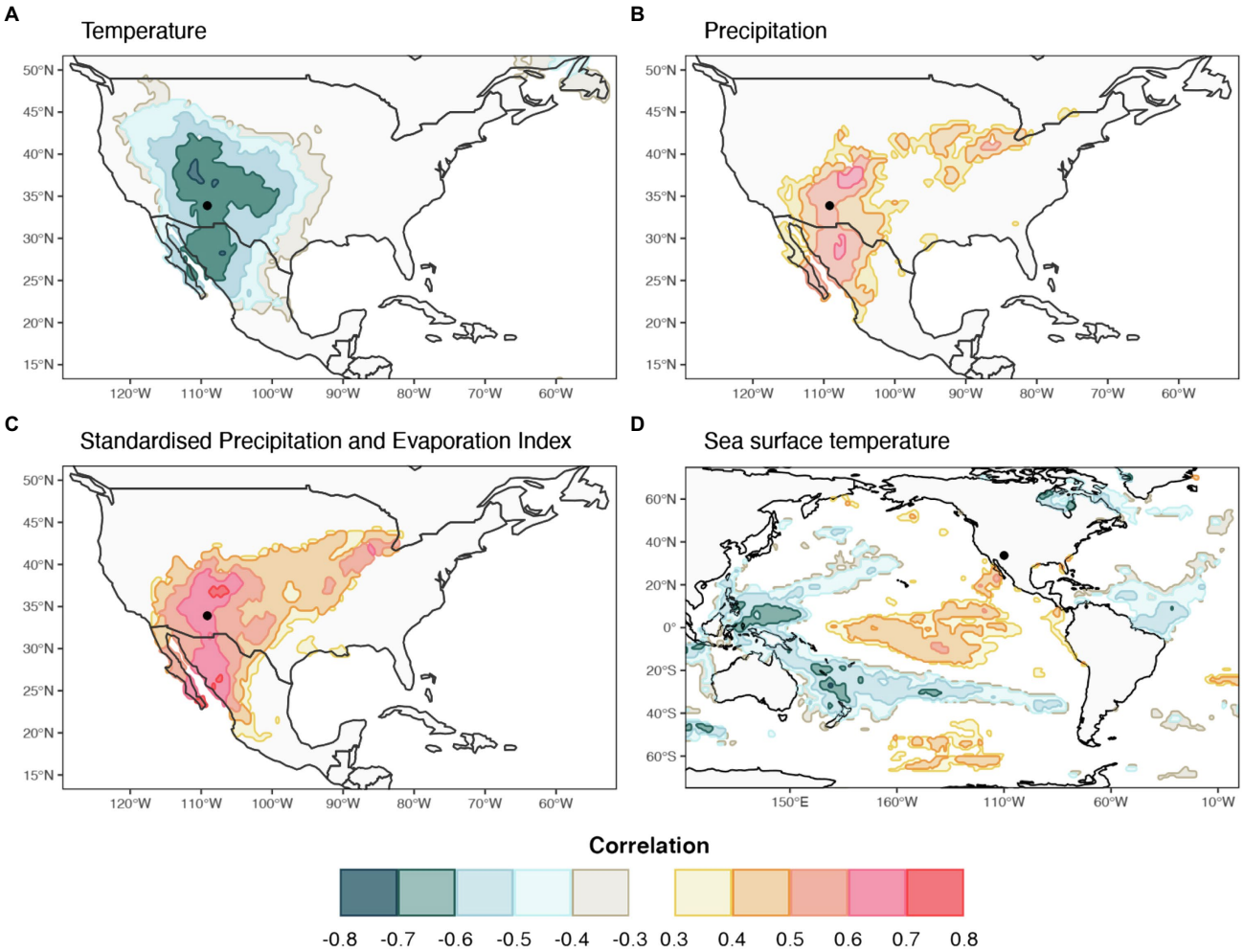

FIGURE 7 | Spatial field correlation maps between selected radial lumen diameter sector chronologies and climate parameters for the period 1981–2015. Sector I chronology was correlated against **(A)** mean October to January temperature (**C**) October to January one-month Standardized Precipitation and Evaporation Index, and **(D)** October to January sea surface temperature. Mean chronology for sectors I-V was correlated against **(B)** November to January precipitation. The location of the study site is identified by a black dot. Colored areas show correlations significant at $p < 0.05$.

moisture transport at intra-annual to multidecadal time scales (Cook et al., 2004; Potito and MacDonald, 2008; Li et al., 2014). LD in the first half of the tree ring showed positive correlations with winter SST over the central-eastern Pacific, and negative ones over the western and southern Pacific. This correlation pattern reflects the typical conditions leading to El Niño episodes in the United States southwest (Feldl and Roe, 2010). This kind of signal is found in earlywood ring-width chronologies of several conifer species of the southwestern United States, including *P. menziesii* (Stahle et al., 1998), but it has not been observed in time series of wood anatomical parameters.

Teleconnections between different modes of atmospheric circulation over the Pacific Ocean are responsible for a well pronounced NW/SW dipole of precipitation patterns (Brown and Comrie, 2004). Hence, when the PDO is in its constructive (warm) phase, it can strengthen the influence of ENSO and lead to stronger El Niño events, which can amplify the effect on winter precipitation in the southwest (Gershunov and Barnett, 1998). Instrumental records (Mantua et al., 1997) indicate the beginning of a warm phase of the PDO in 1977 with several ENSO events starting right after that period and typically peaking in activity during the northern hemisphere winter. This warm PDO phase leads to wetter than normal conditions over the American southwest, including southern California, Arizona, and New Mexico (Sheppard et al., 2002). By applying a cross-wavelet transform, we found a significant inverse relationship between time series of LD in sector I and I-V with SOI for the period 1980–2005, which corresponds with the last warm PDO phase.

We found no significant LD correlations with climatic parameters that would suggest an influence of the NAM on tracheid size. This was an unexpected result because the NAM is extremely important for relieving summer drought in the southwestern United States, and previous tree-ring network studies indicated a direct NAM effect on the annual variability of *P. menziesii*

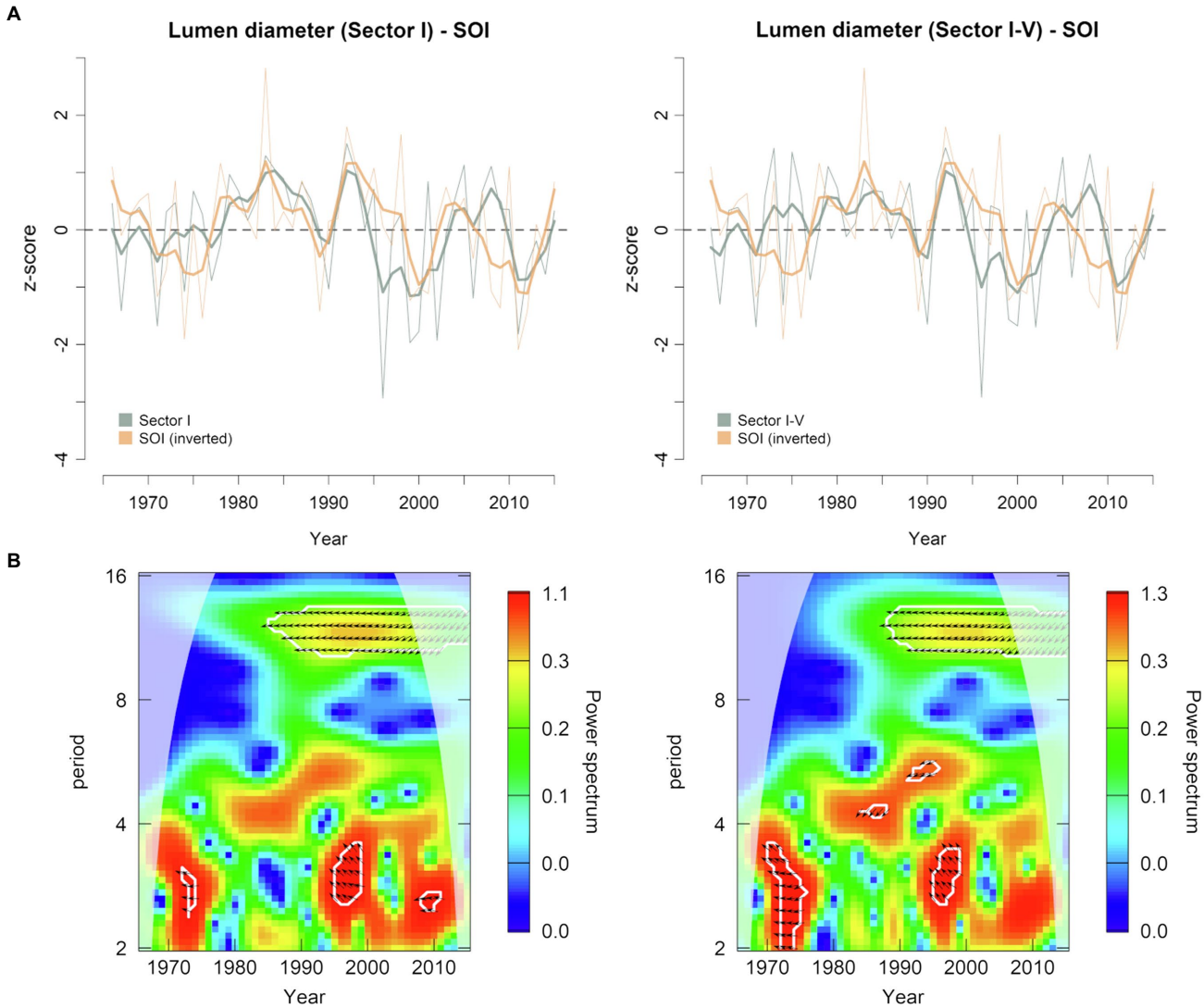

FIGURE 8 | (A) Normalized time series of earlywood lumen diameter (sectors I and I-V) plotted against previous October-current January Southern Oscillation Index (SOI) for the period 1966 to 2015 (bold lines are 5-year cubic smoothing splines). The sign of SOI has been inverted for easier interpretation. **(B)** Cross-wavelet transform of lumen diameter (sectors I and I-V) and SOI index. White contours represent 95% significance level. The relative phase relationship is shown as arrows (in-phase pointing right, anti-phase pointing left, and SOI leading lumen diameter by 90° pointing down). Results falling outside the cone of influence (white shaded area) might be distorted by edge effect.

latewood width (Griffin et al., 2013). The short, intense, and localized nature of NAM thunderstorms mitigates evapotranspiration demands of trees exposed to summer drought, reduces tree water deficit, and by increasing cell turgor potentially promotes the temporal reactivation of cambial activity (Vieira et al., 2014), resulting in cell division and wider latewood bands (Griffin et al., 2013). However, it is likely that on the sloping terrain that dominates the topography of our sites, large volumes of monsoonal rainwater might be lost as runoff instead of recharging soil water storage, limiting the beneficial effects of summer precipitation on tree hydration status (i.e., on cell turgor), and thus reducing its footprint on xylem anatomy, in particular on the radial diameter of newly formed cells, compared to the observed winter-dominant correlation. Furthermore, it should be noted that these sites were selected for their cold-season signal (see **Supplementary Figure S1**), therefore it is possible that winter, and to a lesser extent early spring precipitation, is generally enough to support growth in this species, making it insensitive to summer precipitation; in fact, decreased sensitivity to monsoonal precipitation after a wet winter has been documented in other western conifers (Ziaco et al., 2018). A recent dendroclimatic reconstruction of seasonal hydroclimate based on earlywood and latewood chronologies has demonstrated that ENSO-driven winter climate is the main driver of precipitation anomalies in this region, also highlighting the weaker signal recorded in latewood chronologies of *Pinus ponderosa* at our study sites (Ziaco et al., 2020). Finally, it should be noted that latewood chronologies of *P. menziesii* from the four corners region show

a high correlation with previous earlywood width (Torbenson et al., 2016). In our study, we noticed the absence of first-order autocorrelation for both earlywood and latewood time series of lumen diameter, which may therefore augment precipitation reconstructions based on earlywood and latewood widths without the need to deal with autocorrelation of anatomical parameters (Carrillo et al., 2016).

CONCLUSION

Wood anatomical analysis of Douglas-fir growing at high elevations in eastern Arizona showed the dendroclimatic potential of lumen radial diameter. Correlation analyses between intra-annual cell features and climatic conditions suggested that intra-annual cell morphogenesis is driven by climatic conditions during the winter. Cold-season temperature and precipitation were related to radial lumen diameter, while precipitation during the current growing season did not have a significant effect on tracheid dimensions. Snowpack formation during the dormant period and cool-season temperature, affecting the amount of water available at the beginning of the growing season, appeared to be a more relevant limiting factor for intra-annual xylem adjustment than summertime precipitation events and their relieving effect on evapotranspiration demands.

Our findings are species specific and further investigation into the timing and kinetics of cell formation in this species at a similar topographically extreme site would help to refine the strong link observed between lumen size and winter climate and also assist in explaining the missing summer precipitation signal. Spatial field correlations indicated a significant influence of ENSO and, to a lesser extent, PDO patterns on the precipitation regime, particularly when in their "constructive" (warm) phases. By combining high-resolution climatic data and new analytical techniques, we uncovered the potential of cell structural characteristics for reconstructing climatic conditions in mountainous environments with the intention to improve our understanding of teleconnections between climate dynamics in the Pacific region and local hydroclimatic variability in the southwestern United States.

DATA AVAILABILITY STATEMENT

The raw data supporting the conclusions of this article will be made available by the authors, without undue reservation. All codes for the analyses presented in this document will be made available upon request.

AUTHORS CONTRIBUTIONS

DB, IH, FB, and EZ conceived the research design and the sampling procedures. NM and EZ conducted the sample collection. NM developed the ring-width chronologies. DB, HN, and AH performed the wood anatomical sample preparation, measurements, and elaboration of raw data. DB, HN, IH, FB, and EZ performed the dendroclimatic analysis, developed the hypotheses, and wrote the initial draft of the manuscript. All authors contributed to the final version.

FUNDING

This research was funded, in part, by the US National Science Foundation under grants AGS-P2C2-1502379 to FB and EZ. FB was also supported, in part, by NSF grant AGS-P2C2-1903561. The views and conclusions contained in this document are those of the authors and should not be interpreted as representing the opinions or policies of the funding agencies and supporting institutions.

SUPPLEMENTARY MATERIAL

The Supplementary Material for this article can be found online at: https://www.frontiersin.org/articles/10.3389/fpls.2021.702442/full#supplementary-material

REFERENCES

Arzac, A., Babushkina, E. A., Fonti, P., Slobodchikova, V., Sviderskaya, I. V., and Vaganov, E. A. (2018). Evidences of wider latewood in Pinus sylvestris from a forest-steppe of southern Siberia. *Dendrochronologia* 49, 1–8. doi: 10.1016/j.dendro.2018.02.007

Barnett, T. P., Latif, M., Kirk, E., and Roeckner, E. (1991). On ENSO physics. *J. Clim.* 4, 487–515. doi: 10.1175/1520-0442(1991)004<0487:OEP>2.0.CO;2

Beck, W., Sanders, T. G. M., and Pofahl, U. (2013). CLIMTREG: detecting temporal changes in climate-growth reactions - a computer program using intra-annual daily and yearly moving time intervals of variable width. *Dendrochronologia* 31, 232–241. doi: 10.1016/j.dendro.2013.02.003

Beguería, S., Vicente-Serrano, S. M., Reig, F., and Latorre, B. (2014). Standardized precipitation evapotranspiration index (SPEI) revisited: parameter fitting, evapotranspiration models, tools, datasets and drought monitoring. *Int. J. Climatol.* 34, 3001–3023. doi: 10.1002/joc.3887

Biondi, F., Gershunov, A., and Cayan, D. R. (2001). North Pacific decadal climate variability since 1661. *J. Clim.* 14, 5–10. doi: 10.1175/1520-0442(2001)014<0005:NPDCVS>2.0.CO;2

Bouriaud, O., Leban, J. M., Bert, D., and Deleuze, C. (2005). Intra-annual variations in climate influence growth and wood density of Norway spruce. *Tree Physiol.* 25, 651–660. doi: 10.1093/treephys/25.6.651

Brown, D. P., and Comrie, A. C. (2004). A winter precipitation 'dipole' in the western United States associated with multidecadal ENSO variability. *Geophys. Res. Lett.* 31, L09203. doi: 10.1029/2003GL018726

Bunn, A.G., Korpela, M., Biondi, F., Campelo, F., Mérian, P., Mudelsee, M., et al. (2014). "dplR: Dendrochronology Program Library in R." R package version 1.5.9 ed: http://CRAN.R-project.org/package=dplR.

Cabon, A., Peters, R. L., Fonti, P., Martínez-Vilalta, J., and De Cáceres, M. (2020). Temperature and water potential co-limit stem cambial activity along a steep elevational gradient. *New Phytol.* 226, 1325–1340. doi: 10.1111/nph.16456

Campelo, F., Nabais, C., Gutiérrez, E., Freitas, H., and García-González, I. (2010). Vessel features of quercus ilex L. growing under Mediterranean climate have a better climatic signal than tree-ring width. *Trees* 24, 463–470. doi: 10.1007/s00468-010-0414-0

Carbone, M. S., Czimczik, C. I., Keenan, T. F., Murakami, P. F., Pederson, N., Schaberg, P. G., et al. (2013). Age, allocation and availability of nonstructural

carbon in mature red maple trees. *New Phytol.* 200, 1145–1155. doi: 10.1111/nph.12448

Carrer, M., Castagneri, D., Prendin, A. L., Petit, G., and von Arx, G. (2017). Retrospective analysis of wood anatomical traits reveals a recent extension in tree cambial activity in two high-elevation conifers. *Front. Plant Sci.* 8:737. doi: 10.3389/fpls.2017.00737

Carrillo, C. M., Castro, C. L., Woodhouse, C. A., and Griffin, D. (2016). Low-frequency variability of precipitation in the North American monsoon region as diagnosed through earlywood and latewood tree-ring chronologies in the southwestern US. *Int. J. Climatol.* 36, 2254–2272. doi: 10.1002/joc.4493

Carvalho, A., Nabais, C., Vieira, J., Rossi, S., and Campelo, F. (2015). Plastic response of tracheids in *Pinus pinaster* in a water-limited environment: adjusting lumen size instead of wall thickness. *PLoS One* 10:e0136305. doi:10.1371/journal.pone.0136305, PMID: 26305893.

Castagneri, D., Fonti, P., von Arx, G., and Carrer, M. (2017). How does climate influence xylem morphogenesis over the growing season? Insights from long-term intra-ring anatomy in Picea abies. *Ann. Bot.* 119, 1011–1020. doi: 10.1093/aob/mcw274

Contributors of the International Tree-Ring Data Bank (2020). *International Tree-Ring Data Bank (ITRDB)* [Online]. Available at: https://www.ncei.noaa.gov/products/paleoclimatology/tree-ring. (Accessed March 2021).

Cook, E. R., Woodhouse, C. A., Eakin, C. M., Meko, D. M., and Stahle, D. W. (2004). Long-term aridity changes in the Western United States. *Science* 306, 1015–1018. doi: 10.1126/science.1102586

Core Team, R (2021). *R: A Language and Environment for Statistical Computing*. Vienna, Austria: R Foundation for Statistical Computing.

Corringham, T. W., and Cayan, D. R. (2019). The effect of El Niño on flood damages in the Western United States. *Weather. Clim. Soc.* 11, 489–504. doi: 10.1175/WCAS-D-18-0071.1

Cuny, H. E., Fonti, P., Rathgeber, C. B. K., von Arx, G., Peters, R. L., and Frank, D. C. (2019). Couplings in cell differentiation kinetics mitigate air temperature influence on conifer wood anatomy. *Plant Cell Env* 42, 1222–1232. doi: 10.1111/pce.13464

Cuny, H. E., and Rathgeber, C. B. K. (2016). Xylogenesis: coniferous trees of temperate forests are listening to the climate tale during the growing season But only remember the last words! *Plant Phys* 171, 306–317. doi: 10.1104/pp.16.00037

Cuny, H. E., Rathgeber, C. B. K., Frank, D., Fonti, P., Mäkinen, H., Prislan, P., et al. (2015). Woody biomass production lags stem-girth increase by over one month in coniferous forests. *Nat. Plants.* 1:15160. doi: 10.1038/nplants.2015.160

Daly, C., Halbleib, M., Smith, J. I., Gibson, W. P., Doggett, M. K., Taylor, G. H., et al. (2008). Physiographically sensitive mapping of climatological temperature and precipitation across the conterminous United States. *Int. J. Climatol.* 28, 2031–2064. doi: 10.1002/joc.1688

DeSoto, L., De la Cruz, M., and Fonti, P. (2011). Intra-annual patterns of tracheid size in the Mediterranean tree *Juniperus thurifera* as an indicator of seasonal water stress. *Can. J. For. Res.* 41, 1280–1294. doi: 10.1139/x11-045

Edwards, J., Anchukaitis, K. J., Zambri, B., Andreu-Hayles, L., Oelkers, R., D'Arrigo, R., et al. (2020). Intra-annual climate anomalies in northwestern North America following the 1783-1784 CE Laki eruption. *J. Geophys. Res. Atmo.* 126:e2020JD033544. doi: 10.1029/2020JD033544

Feldl, N., and Roe, G. H. (2010). Synoptic weather patterns associated with intense ENSO rainfall in the Southwest United States. *Geophys. Res. Lett.* 37, L23803. doi: 10.1029/2010GL045439

Fonti, P., and García-González, I. (2004). Suitability of chestnut earlywood vessel chronologies for ecological studies. *New Phytol.* 163, 77–86. doi: 10.1111/j.1469-8137.2004.01089.x

Fonti, P., and García-Gonzalez, I. (2008). Earlywood vessel size of oak as a potential proxy for spring precipitation in mesic sites. *J. Biogeogr.* 35, 2249–2257. doi: 10.1111/j.1365-2699.2008.01961.x

García-González, I., and Eckstein, D. (2003). Climatic signal of earlywood vessels of oak on a maritime site. *Tree Phys* 23, 497–504. doi: 10.1093/treephys/23.7.497

Gartner, H., and Nievergelt, D. (2010). The core-microtome: a new tool for surface preparation on cores and time series analysis of varying cell parameters. *Dendrochronologia* 28, 85–92. doi: 10.1016/j.dendro.2009.09.002

Gärtner, H., and Schweingruber, F. (2013). *Microscopic Preparation Techniques for Plant Stem Analysis*. Remagen, Germany: Verlag Kessel.

Gershunov, A., and Barnett, T. P. (1998). Interdecadal modulation of ENSO teleconnections. *Bull. Am. Meteorol. Soc.* 79, 2715–2726. doi: 10.1175/1520-0477(1998)079<2715:imoet>2.0.co;2

González-Cásares, M., Camarero, J. J., Colangelo, M., Rita, A., and Pompa-García, M. (2019). High responsiveness of wood anatomy to water availability and drought near the equatorial rear edge of Douglas-fir. *Can. J. For. Res.* 49, 1114–1123. doi: 10.1139/cjfr-2019-0120

Griffin, D., Woodhouse, C. A., Meko, D. M., Stahle, D. W., Faulstich, H. L., Carrillo, C., et al. (2013). North American monsoon precipitation reconstructed from tree-ring latewood. *Geophys. Res. Lett.* 40, 954–958. doi: 10.1002/grl.50184

Grinsted, A., Moore, J. C., and Jevrejeva, S. (2004). Application of the cross wavelet transform and wavelet coherence to geophysical time series. *Nonlin. Processes. Geophys.* 11, 561–566. doi: 10.5194/npg-11-561-2004

Grissino-Mayer, H. D., and Fritts, H. C. (1997). The international tree-ring data bank: an enhanced global database serving the global scientific community. *The Holocene* 7, 235–238. doi: 10.1177/095968369700700212

Herrera-Ramirez, D., Muhr, J., Hartmann, H., Roemermann, C., Trumbore, S., and Sierra, C. A. (2020). Probability distributions of nonstructural carbon ages and transit times provide insights into carbon allocation dynamics of mature trees. *New Phytol.* 226, 1299–1311. doi: 10.1111/nph.16461

Hughes, M.K., Swetnam, T.W., and Diaz, H.F. (2011). *Dendroclimatology*. Springer Netherlands: Progress and Prospects.

Jana, S., Rajagopalan, B., Alexander, M. A., and Ray, A. J. (2018). Understanding the dominant sources and tracks of moisture for summer rainfall in the Southwest United States. *J Geophys Res Atmo* 123, 4850–4870. doi: 10.1029/2017JD027652

Jong, B.-T., Ting, M., Seager, R., Henderson, N., and Lee, D. E. (2018). Role of equatorial Pacific SST forecast error in the late winter California precipitation forecast for the 2015/16 El Niño. *J. Clim.* 31, 839–852. doi: 10.1175/JCLI-D-17-0145.1

Kerhoulas, L. P., Kolb, T. E., and Koch, G. W. (2013). Tree size, stand density, and the source of water used across seasons by ponderosa pine in northern Arizona. *For. Ecol. Manag.* 289(Supplement C), 425–433. doi: 10.1016/j.foreco.2012.10.036

Land, A., Kromer, B., Remmele, S., Brehm, N., and Wacker, L. (2020). Complex imprint of solar variability on tree rings. *Env Res Comm* 2:101003. doi: 10.1088/2515-7620/abc063

Lauder, J. D., Moran, E. V., and Hart, S. C. (2019). Fight or flight? Potential tradeoffs between drought defense and reproduction in conifers. *Tree Phys* 39, 1071–1085. doi: 10.1093/treephys/tpz031

Li, P., and Adams, W. T. (1989). Range-wide patterns of allozyme variation in Douglas-fir (Pseudotsuga menziesii). *Can. J. For. Res.* 19, 149–161. doi: 10.1139/x89-022

Li, J., Xie, S.-P., and Cook, E. R. (2014). El Niño phases embedded in Asian and North American drought reconstructions. *Quat Sci Rew* 85, 20–34. doi: 10.1016/j.quascirev.2013.11.014

Liang, W., Heinrich, I., Helle, G., Liñán, I. D., and Heinken, T. (2013a). Applying CLSM to increment core surfaces for histometric analyses: a novel advance in quantitative wood anatomy. *Dendrochronologia* 31, 140–145. doi: 10.1016/j.dendro.2012.09.002

Liang, W., Heinrich, I., Simard, S., Helle, G., Linan, I. D., and Heinken, T. (2013b). Climate signals derived from cell anatomy of scots pine in NE Germany. *Tree Phys* 33, 833–844. doi: 10.1093/treephys/tpt059

Mantua, N. J., and Hare, S. R. (2002). The Pacific decadal oscillation. *J Ocean* 58, 35–44. doi: 10.1023/A:1015820616384

Mantua, N. J., Hare, S. R., Zhang, Y., Wallace, J. M., and Francis, R. C. (1997). A Pacific interdecadal climate oscillation with impacts on Salmon production*. *Bull. Am. Meteorol. Soc.* 78, 1069–1080. doi: 10.1175/1520-0477(1997)078<1069:apicow>2.0.co;2

Martin-Benito, D., Beeckman, H., and Canellas, I. (2013). Influence of drought on tree rings and tracheid features of *Pinus nigra* and *Pinus sylvestris* in a Mesic Mediterranean forest. *Eur. J. For. Res.* 132, 33–45. doi: 10.1007/s10342-012-0652-3

Maurer, G. E., and Bowling, D. R. (2014). Seasonal snowpack characteristics influence soil temperature and water content at multiple scales in interior western U.S. mountain ecosystems. *Water Resour. Res.* 50, 5216–5234. doi: 10.1002/2013WR014452

Mitchell, T. D., and Jones, P. D. (2005). An improved method of constructing a database of monthly climate observations and associated high-resolution grids. *Int. J. Climatol.* 25, 693–712. doi: 10.1002/joc.1181

Novak, K., de Luis, M., Raventos, J., and Cufar, K. (2013). Climatic signals in tree-ring widths and wood structure of *Pinus halepensis* in contrasted environmental conditions. *Trees* 27, 927–936. doi: 10.1007/s00468-013-0845-5

Olano, J. M., Eugenio, M., Garcia-Cervigon, A. I., Folch, M., and Rozas, V. (2012). Quantitative tracheid anatomy reveals a complex environmental control of wood structure in continental mediterranean climate. *Intl J Plant Sci* 173, 137–149. doi: 10.1086/663165

Panyushkina, I. P., Hughes, M. K., Vaganov, E. A., and Munro, M. A. R. (2003). Summer temperature in northeastern Siberia since 1642 reconstructed from tracheid dimensions and cell numbers of Larix cajanderi. *Can. J. For. Res.* 33, 1905–1914. doi: 10.1139/x03-109

Pearl, J. K., Keck, J. R., Tintor, W., Siekacz, L., Herrick, H. M., Meko, M. D., et al. (2020). New frontiers in tree-ring research. *Holocene* 30, 923–941. doi: 10.1177/0959683620902230

Peltier, D. M. P., Barber, J. J., and Ogle, K. (2018). Quantifying antecedent climatic drivers of tree growth in the southwestern US. *J. Ecol.* 106, 613–624. doi: 10.1111/1365-2745.12878

Peltier, D. M. P., and Ogle, K. (2020). Tree growth sensitivity to climate is temporally variable. *Ecol. Lett.* 23, 1561–1572. doi: 10.1111/ele.13575

Peters, R. L., Balanzategui, D., Hurley, A. G., von Arx, G., Prendin, A. L., Cuny, H. E., et al. (2018). RAPTOR: row and position tracheid organizer in R. *Dendrochronologia* 47, 10–16. doi: 10.1016/j.dendro.2017.10.003

Potito, A. P., and MacDonald, G. M. (2008). The effects of aridity on conifer radial growth, recruitment, and mortality patterns in the eastern Sierra Nevada, California. *Arct. Antarct. Alp. Res.* 40, 129–139. doi: 10.1657/1523-0430(05-080)[POTITO]2.0.CO;2

Pritzkow, C., Wazny, T., Heußner, K. U., Słowiński, M., Bieber, A., Dorado Liñán, I., et al. (2016). Minimum winter temperature reconstruction from average earlywood vessel area of European oak (Quercus robur) in N-Poland. *Paleo Paleo Paleo* 449, 520–530. doi: 10.1016/j.palaeo.2016.02.046

Reynolds, R. W., Rayner, N. A., Smith, T. M., Stokes, D. C., and Wang, W. (2002). An improved In situ and satellite SST analysis for climate. *J. Clim.* 15, 1609–1625. doi: 10.1175/1520-0442(2002)015<1609:aiisas>2.0.co;2

Roesch, A., and Schmidbauer, H. (2018). WaveletComp: A guided tour through the R-package. Available at: http://www.hs-stat.com/projects/WaveletComp/WaveletComp_guided_tour.pdf (Accessed March 29, 2021).

Ropelewski, C. F., and Jones, P. D. (1987). An extension of the Tahiti–Darwin southern oscillation index. *Mon. Weather Rev.* 115, 2161–2165. doi: 10.1175/1520-0493(1987)115<2161:AEOTTS>2.0.CO;2

Schneider, L., and Gartner, H. (2013). The advantage of using a starch based non-Newtonian fluid to prepare micro sections. *Dendrochronologia* 31, 175–178. doi: 10.1016/j.dendro.2013.04.002

Seftigen, K., Fuentes, M., Ljungqvist, F. C., and Björklund, J. (2020). Using blue intensity from drought-sensitive *Pinus sylvestris* in Fennoscandia to improve reconstruction of past hydroclimate variability. *Clim. Dyn.* 55, 579–594. doi: 10.1007/s00382-020-05287-2

Seo, J.-W., Smiljanić, M., and Wilmking, M. (2014). Optimizing cell-anatomical chronologies of scots pine by stepwise increasing the number of radial tracheid rows included-case study based on three Scandinavian sites. *Dendrochronologia* 32, 205–209. doi: 10.1016/j.dendro.2014.02.002

Sheppard, P. R., Comrie, A. C., Packin, G. D., Angersbach, K., and Hughes, M. K. (2002). The climate of the US southwest. *Clim. Res.* 21, 219–238. doi: 10.3354/cr021219

Speer, J.H. (2010). *Fundamentals of Tree-Ring Research*. Tuscon, Arizona, USA: University of Arizona Press.

St. George, S., Meko, D. M., and Cook, E. R. (2010). The seasonality of precipitation signals embedded within the north American drought atlas. *The Holocene* 20, 983–988. doi: 10.1177/0959683610365937

Stahle, D. W., Cleaveland, M. K., Grissino-Mayer, H. D., Griffin, R. D., Fye, F. K., Therrell, M. D., et al. (2009). Cool- and warm-season precipitation reconstructions over western New Mexico. *J. Clim.* 22, 3729–3750. doi: 10.1175/2008JCLI2752.1

Stahle, D. W., D'Arrigo, R. D., Krusic, P. J., Cleaveland, M. K., Cook, E. R., Allan, R. J., et al. (1998). Experimental dendroclimatic reconstruction of the southern oscillation. *Bull. Am. Meteorol. Soc.* 79, 2137–2152.

Szejner, P., Wright, W. E., Belmecheri, S., Meko, D., Leavitt, S. W., Ehleringer, J. R., et al. (2018). Disentangling seasonal and interannual legacies from inferred patterns of forest water and carbon cycling using tree-ring stable isotopes. *Glob. Chang. Biol.* 24, 5332–5347. doi: 10.1111/gcb.14395

Tardif, J. C., and Conciatori, F. (2006). Influence of climate on tree rings and vessel features in red oak and white oak growing near their northern distribution limit, southwestern Quebec, Canada. *Can. J. For. Res.* 36, 2317–2330. doi: 10.1139/x06-133

Torbenson, M. C. A., Stahle, D. W., Villanueva-Díaz, J., Cook, E. R., and Griffin, D. (2016). The relationship between earlywood and latewood ring-growth across North America. *Tree-Ring. Res* 72, 53–66. doi: 10.3959/1536-1098-72.02.53

Trouet, V., and Van Oldenborgh, G. J. (2013). KNMI climate explorer: A web-based research tool for high-resolution paleoclimatology. *Tree-Ring. Res* 69, 3–13. doi: 10.3959/1536-1098-69.1.3

Vaganov, E. A. (1990). "The tracheidogram method in tree-ring analysis and its application," in *Methods of Dendrochronology*. eds. E. R. Cook and L. A. Kairiukstis (Dordrecht, The Netherlands: Kluver), 63–76.

Vicente-Serrano, S. M., Beguería, S., and López-Moreno, J. I. (2010). A Multiscalar Drought Index Sensitive to Global Warming: The Standardized Precipitation Evapotranspiration Index. *J. Clim.* 23, 1696–1718. doi: 10.1175/2009JCLI2909.1

Vieira, J., Rossi, S., Campelo, F., Freitas, H., and Nabais, C. (2014). Xylogenesis of *Pinus pinaster* under a Mediterranean climate. *Ann. For. Sci.* 71, 71–80. doi: 10.1007/s13595-013-0341-5

Viglizzo, E. F., Nosetto, M. D., Jobbágy, E. G., Ricard, M. F., and Frank, F. C. (2015). The ecohydrology of ecosystem transitions: a meta-analysis. *Ecohydrology* 8, 911–921. doi: 10.1002/eco.1540

von Arx, G., and Carrer, M. (2014). ROXAS – A new tool to build centuries-long tracheid-lumen chronologies in conifers. *Dendrochronologia* 32, 290–293. doi: 10.1016/j.dendro.2013.12.001

Wang, X., Brown, P. M., Zhang, Y., and Song, L. (2011). Imprint of the Atlantic multidecadal oscillation on tree-ring widths in northeastern Asia since 1568. *PLoS One* 6:e22740. doi: 10.1371/journal.pone.0022740

Wang, L., Payette, S., and Begin, Y. (2002). Relationships between anatomical and densitometric characteristics of black spruce and summer temperature at tree line in northern Quebec. *Can. J. For. Res.* 32, 477–486. doi: 10.1139/x01-208

White, A. B., Moore, B. J., Gottas, D. J., and Neiman, P. J. (2019). Winter storm conditions leading to excessive runoff above California's Oroville dam during January and February 2017. *Bull. Am. Meteorol. Soc.* 100, 55–70. doi: 10.1175/bams-d-18-0091.1

Wigley, T. M. L., Briffa, K. R., and Jones, P. D. (1984). On the average value of correlated time series, with applications in dendroclimatology and hydrometeorology. *J. Appl. Meteorol. Climatol.* 23, 201–213. doi: 10.1175/1520-0450(1984)023<0201:otavoc>2.0.co;2

Woodhouse, C. A., Meko, D. M., Griffin, D., and Castro, C. L. (2013). Tree rings and multiseason drought variability in the lower Rio Grande Basin, USA. *Water Resour. Res.* 49, 844–850. doi: 10.1002/wrcr.20098

Zang, C. (2015). Dendrobox – An interactive exploration tool for the international tree ring data Bank. *Dendrochronologia* 33, 31–33. doi: 10.1016/j.dendro.2014.10.002

Ziaco, E. (2020). A phenology-based approach to the analysis of conifers intra-annual xylem anatomy in water-limited environments. *Dendrochronologia* 59:125662. doi: 10.1016/j.dendro.2019.125662

Ziaco, E., Biondi, F., and Heinrich, I. (2016). Wood cellular dendroclimatology: testing new proxies in Great Basin bristlecone pine. *Front. Plant Sci.* 7:1602. doi: 10.3389/fpls.2016.01602

Ziaco, E., and Liang, E. (2019). New perspectives on sub-seasonal xylem anatomical responses to climatic variability. *Trees* 33, 973–975. doi: 10.1007/s00468-018-1786-9

Ziaco, E., Miley, N., and Biondi, F. (2020). Reconstruction of seasonal and water-year precipitation anomalies from tree-ring records of the southwestern United States. *Paleo Paleo Paleo* 547:109689. doi: 10.1016/j.palaeo.2020.109689

Ziaco, E., Truettner, C., Biondi, F., and Bullock, S. (2018). Moisture-driven xylogenesis in Pinus ponderosa from a Mojave Desert mountain reveals high phenological plasticity. *Plant Cell Env* 41, 823–836. doi: 10.1111/pce.13152

Conflict of Interest: The authors declare that the research was conducted in the absence of any commercial or financial relationships that could be construed as a potential conflict of interest.

Publisher's Note: All claims expressed in this article are solely those of the authors and do not necessarily represent those of their affiliated organizations, or those of the publisher, the editors and the reviewers. Any product that may be evaluated in this article, or claim that may be made by its manufacturer, is not guaranteed or endorsed by the publisher.

frontiers in Plant Science

ORIGINAL RESEARCH
published: 14 October 2021
doi: 10.3389/fpls.2021.754596

Earlywood Vessels in Black Ash (*Fraxinus nigra* Marsh.) Trees Show Contrasting Sensitivity to Hydroclimate Variables According to Flood Exposure

Jacques Clément Tardif[1,2,3]*, *Susanne Kames*[1,4], *Alexandre Florent Nolin*[2,3] and *Yves Bergeron*[2,3]

[1] Centre for Forest Interdisciplinary Research (C-FIR), Department of Biology/Environmental Studies and Sciences, University of Winnipeg, Winnipeg, MB, Canada, [2] Institut de Recherche sur les Forêts, Université du Québec en Abitibi-Témiscamingue (UQAT), Rouyn-Noranda, QC, Canada, [3] Centre d'Étude de la Forêt, Université du Québec à Montréal (UQAM), Montréal, QC, Canada, [4] Department of Botany, University of Manitoba, Winnipeg, MB, Canada

OPEN ACCESS

Edited by:
Ignacio García-González, University of Santiago de Compostela, Spain

Reviewed by:
Patrick Fonti, Swiss Federal Institute for Forest, Snow and Landscape Research (WSL), Switzerland
Radoslaw Puchalka, Nicolaus Copernicus University in Toruń, Poland

***Correspondence:**
Jacques Clément Tardif
j.tardif@uwinnipeg.ca

Specialty section:
This article was submitted to Functional Plant Ecology, a section of the journal Frontiers in Plant Science

Received: *06 August 2021*
Accepted: *10 September 2021*
Published: *14 October 2021*

Citation:
Tardif JC, Kames S, Nolin AF and Bergeron Y (2021) Earlywood Vessels in Black Ash (Fraxinus nigra Marsh.) Trees Show Contrasting Sensitivity to Hydroclimate Variables According to Flood Exposure. Front. Plant Sci. 12:754596. doi: 10.3389/fpls.2021.754596

In recent years, the utility of earlywood vessels anatomical characteristics in identifying and reconstructing hydrological conditions has been fully recognized. In riparian ring-porous species, flood rings have been used to identify discrete flood events, and chronologies developed from cross-sectional lumen areas of earlywood vessels have been used to successfully reconstruct seasonal discharge. In contrast, the utility of the earlywood vessel chronologies in non-riparian habitats has been less compelling. No studies have contrasted within species their earlywood vessel anatomical characteristics, specifically from trees that are inversely exposed to flooding. In this study, earlywood vessel and ring-width chronologies were compared between flooded and non-flooded control *Fraxinus nigra* trees. The association between chronologies and hydroclimate variables was also assessed. *Fraxinus nigra* trees from both settings shared similar mean tree-ring width but floodplain trees did produce, on average, thicker earlywood. Vessel chronologies from the floodplain trees generally recorded higher mean sensitivity (standard deviation) and lower autocorrelation than corresponding control chronologies indicating higher year-to-year variations. Principal components analysis (PCA) revealed that control and floodplain chronologies shared little variance indicating habitat-specific signals. At the habitat level, the PCA indicated that vessel characteristics were strongly associated with tree-ring width descriptors in control trees whereas, in floodplain trees, they were decoupled from the width. The most striking difference found between flood exposures related to the chronologies' associations with hydroclimatic variables. Floodplain vessel chronologies were strongly associated with climate variables modulating spring-flood conditions as well as with spring discharge whereas control ones showed weaker and few consistent correlations. Our results illustrated how spring flood conditions modulate earlywood vessel plasticity. In floodplain *F. nigra* trees, the use of earlywood vessel characteristics could potentially be extended to assess and/or mitigate anthropogenic modifications of hydrological regimes. In absence of major

recurring environmental stressors like spring flooding, our results support the idea that the production of continuous earlywood vessel chronologies may be of limited utility in dendroclimatology.

Keywords: ring-porous wood, earlywood vessels, spring floods, flooded and non-flooded habitats, eastern boreal Canada, dendrohydrology, dendroclimatology

INTRODUCTION

In recent decades, developments in tree-ring research have facilitated the quantification of the anatomical traits of tree-ring and contributed to the promotion of wood anatomical research. The recent assembly of microtomes adapted for tree-ring research (Gärtner and Nievergelt, 2010; Gärtner et al., 2014, 2015a) and the concomitant publications on the art of making wood thin sections (Gärtner and Schweingruber, 2013; Gärtner et al., 2015b; Tardif and Conciatori, 2015; von Arx et al., 2015, 2016) added to this trend. High-definition digital cameras and scanners have made it easier and faster to acquire images of tree rings at both macroscopic and microscopic scales. Image analysis procedures and software, e.g., Canny edge algorithm—Canny, 1986, ImageJ2—Rueden et al., 2017, WinCell—Régent Instruments Inc, 2005, ROXAS—von Arx et al., 2013 and von Arx and Carrer, 2014, and CATS—Land et al., 2017, have all eased measuring and analyzing wood cell dimensions. Methodological reviews and recipe-type publications have also contributed to systematize many procedures (García-González and Fonti, 2006, 2008; Fonti et al., 2009a, 2010; Scholz et al., 2013; Gärtner et al., 2015b; García-González et al., 2016; von Arx et al., 2016).

Tree rings and their intra-annual anatomical variations form important environmental archives. Older and recent reviews have emphasized the utility of many anatomical features in both coniferous and broadleaf species as they relate, among others, to extreme climate events (Wimmer, 2002; Ballesteros-Cánovas et al., 2015; Bräuning et al., 2016; De Micco et al., 2016; Tardif et al., 2020, 2021). Many tree-ring features like frost rings, false rings [or intra-annual density fluctuation (IADF) in Europe], and flood rings are easily identified macroscopically. However, as the visual cues used to identify these anomalies often weaken alongside the intensity of the stressor, e.g., climate signal, microscopic identification with detailed anatomical analyses may often remain the only detection pathway. For example, Waito et al. (2013) reported that many weakly developed frost rings could not be observed macroscopically but only microscopically after thin sections preparation. The current discussion surrounding light rings (macroscopic) and blue rings (microscopic) [see Crivellaro et al. (2018) and Tardif et al. (2020)] also echoes the recent developments and applications of detailed wood anatomical research in dendrochronology.

Earlywood Vessels and Riparian Ring-Porous Tree Species

In dendrohydrology, the utility of vessel anatomical traits in riparian ring-porous species has long been recognized (Ballesteros-Cánovas et al., 2015; Tardif et al., 2021). In response to spring flood events, many ring-porous tree species produce well-developed flood rings in the submerged portion of their stem, i.e., when inundation coincides with active earlywood vessel formation (St. George et al., 2002; Copini et al., 2016). Flood rings are not to be confounded with the anatomical response of ring-porous species to mechanical injuries associated with flooding (Tardif et al., 2021). Flood rings can easily be distinguished macroscopically (visually) due to their distinct vessel characteristics compared with typical tree rings. Novice dendrochronologists after receiving proper training can reliably identify them (Tardif et al., 2021). Flood rings were characterized through earlywood vessels with the abnormally small lumen in both white and green ash (*Fraxinus americana* L. and *Fraxinus pennsylvanica* Marsh; Yanosky, 1983), in pedunculate oak (*Quercus robur* L.; Astrade and Bégin, 1997; Sass-Klaassen, 2009; Sass-Klaassen et al., 2010; Copini et al., 2016), in bur oak (*Quercus macrocarpa* Michx, St. George and Nielsen, 2000, 2002, 2003; Wertz et al., 2013; Therrell and Bialecki, 2015), in overcup oak (*Quercus lyrata* Walt, Therrell and Bialecki, 2015; Meko and Therrell, 2020), and black ash (*Fraxinus nigra* Marsh., Tardif et al., 2010, 2021; Kames et al., 2016; Nolin et al., 2021a,b, accepted).

The majority of the aforementioned studies used macroscopically identified flood rings and their annual frequency as pointer years to detect exceptional flood events. In some studies (Astrade and Bégin, 1997; St. George and Nielsen, 2002; St. George et al., 2002), short time series derived from earlywood vessel cross-sectional lumen area were made to quantitatively define these flood-signature rings. The study of Meko and Therrell (2020), in addition to visual identification of flood rings, measured the width of the first row of earlywood vessels in *Q. lyrata*. Both proxies were strongly related to spring river flooding. In contrast, the study of Astrade and Bégin (1997) observed in *Q. robur* that vessels in the first row were of normal size during the flood of 1983 but that they were followed by several rows of abnormally narrow vessels. In these two studies, the location of abnormal vessels (first row or subsequent rows) may be attributable to different flood dynamics (timing and duration) and these differences remind us of the need to make thoughtful choices when developing research protocols. Some studies using floodplain ring-porous species did not report the presence of flood rings nor decisive associations between earlywood vessel dimensions and current year floods (Gričar et al., 2013; Tumajer and Treml, 2016; Koprowski et al., 2018). Results from these studies may relate to specific flood regimes but also to sampling at 1.3 m above ground level and/or neglecting small vessel measurements. At last, recent work has focused on developing long annually resolved measurement series of

earlywood vessel attributes (Tardif et al., 2010; Kames et al., 2016) leading to a multi-century spring discharge reconstruction for northeastern boreal Canada (Nolin et al., 2021a).

Earlywood Vessels and Non-riparian Ring-Porous Tree Species

In non-riparian ring-porous tree species, no earlywood vessel abnormalities have to our knowledge been utilized to the extent of flood rings in riparian species. No comparable features to flood rings have been macroscopically used to identify extreme events despite studies indicating that abnormally small cross-sectional earlywood vessel lumen areas may result from insect defoliation (Huber, 1993; Asshoff et al., 1999; Thomas et al., 2006), severe drought (García-González and Eckstein, 2003), and forest fires (Kames et al., 2011). The study of Fletcher (1975) mentioned using abnormally small earlywood vessels to cross-date oak panels. Nonetheless, the hydroclimatic signal in ring-porous species growing in mesic and xeric habitats have often been said to belong essentially in the largest earlywood vessels (García-González and Fonti, 2006; Fonti et al., 2009a; García-González et al., 2016), while small earlywood vessels constitute noise (García-González and Fonti, 2006; González-González et al., 2015). This is largely contrasting with riparian species in which the hydroclimatic signal resides particularly in small earlywood vessels (St. George et al., 2002; Kames et al., 2016; Nolin et al., 2021a). Studies [for example, refer to García-González and Fonti (2006), Fonti et al. (2009a), and González-González et al. (2014)] recommending that small earlywood vessels, e.g., <6,000 or <10,000 μm^2, be omitted to speed-up the development of ring-porous earlywood vessel chronologies "without any signal lost" have had an undetermined impact on knowledge acquisition in the field and especially when the environmental signal lies in small vessels.

Nonetheless, earlywood vessel cross-sectional lumen area in non-riparian trees have been shown to be affected by temperature and water availability during the previous growing season, the dormant period and/or the current growing season, wherein the prevalence of any factor being dependent on the requirements of species, climate regions, and microsite conditions (for examples, see Villar-Salvador et al., 1997; García-González and Eckstein, 2003; Corcuera et al., 2004, 2006; Fonti and García-González, 2004, 2008; Tardif and Conciatori, 2006; Fonti et al., 2009b; Alla and Camarero, 2012; González-González et al., 2015; Pritzkow et al., 2016; García-González and Souto-Herrero, 2017; Pérez-de-Lis et al., 2018; Zhu et al., 2020). The study of García-González et al. (2016) provided an informed review on the topic. Many studies that analyzed vessel attributes and ring width showed that earlywood vessel cross-sectional lumen area contained unique climate information but that this variable was not very sensitive (Fonti and García-González, 2004, 2008; Tardif and Conciatori, 2006; Alla and Camarero, 2012; García-González et al., 2016; Pritzkow et al., 2016), or was deemed to be too weak compared with tree-ring width features to be used in dendroclimatological reconstruction (Tardif and Conciatori, 2006; Alla and Camarero, 2012). Current climate reconstructions using vessel traits from *Q. robur* report fairly low *r*-square values ranging from 0.22 (period 1961–2011; Davis and Loader, 2020) to 0.31 (period 1951–2010; Pritzkow et al., 2016). These values largely contrast with those reported for floodplain environments. The study of Nolin et al. (2021a) explained more than 69% of the variance in instrumental discharge using *F. nigra* earlywood vessel chronologies over the period 1916–2016.

Objectives and Hypotheses

The general objective of this study was to provide a thorough comparison of earlywood vessel major anatomical traits in *F. nigra* trees growing under the same general climate but with contrasting exposure to spring floods. Tree-ring widths and earlywood vessel chronologies were developed from wood samples collected from *F. nigra* trees growing in flooded and non-flooded sites. In addition to the traditional measurements of earlywood, latewood, and total ring width, the number of vessels and their cross-sectional lumen area above 800 μm^2 was measured. It was hypothesized that chronologies developed from the non-flooded site are independent of those developed from the flooded site, thus, confirming the uniqueness of the flood signal to floodplain trees. Given that water availability differs in the two study areas and throughout the growing season, it was further hypothesized that earlywood vessels in each situation will provide different hydroclimatic signals due to their distinct exposure to water and drought stresses. Finally, it was hypothesized that earlywood vessel chronologies developed from non-flooded trees would bear little potential for hydroclimate reconstruction compared with their floodplain equivalents.

MATERIALS AND METHODS

Study Area

The study area is located in the Lake Duparquet region of north-western Quebec (**Figure 1**). The region is part of the Northern Clay Belt of Ontario and Quebec where rocky hills surrounding Lake Duparquet contain glacial till and lacustrine clay deposits (Daubois et al., 2015). The study area is situated in the mixed-wood boreal forest in the balsam fir-white birch domain (Bergeron et al., 1983). The nearest active weather station to the study area is located at Mont Brun (station 7085106), 41 km southeast of Lake Duparquet (https://climate.weather.gc.ca/). Between 1981 and 2010, the mean annual temperature was 1°C. The total annual precipitation was 985.2 mm with snowfall accounting for 28.5%. At Lake Duparquet, spring ice-breakup and subsequent flooding generally begin between mid-April and mid-May (Tardif and Bergeron, 1997a; Mongrain, 2014; Nolin et al., 2021a).

In the Lake Duparquet region, two sampling areas characterized by contrasting exposure to spring flooding were sampled. First, *F. nigra* stands were sampled along the floodplain of Lake Duparquet (48°28'N, 79°17'W; at an approximate elevation of 260 m above sea level; **Figure 1**). These stands were described in numerous studies (Tardif and Bergeron, 1992, 1999; Kames et al., 2016; Nolin et al., 2021a; Tardif et al., 2021). During extreme spring flood years like 1989 and 2019, *F. nigra* trees in the lower floodplain may have the lower portion of their stem remaining underwater into early July (Tardif,

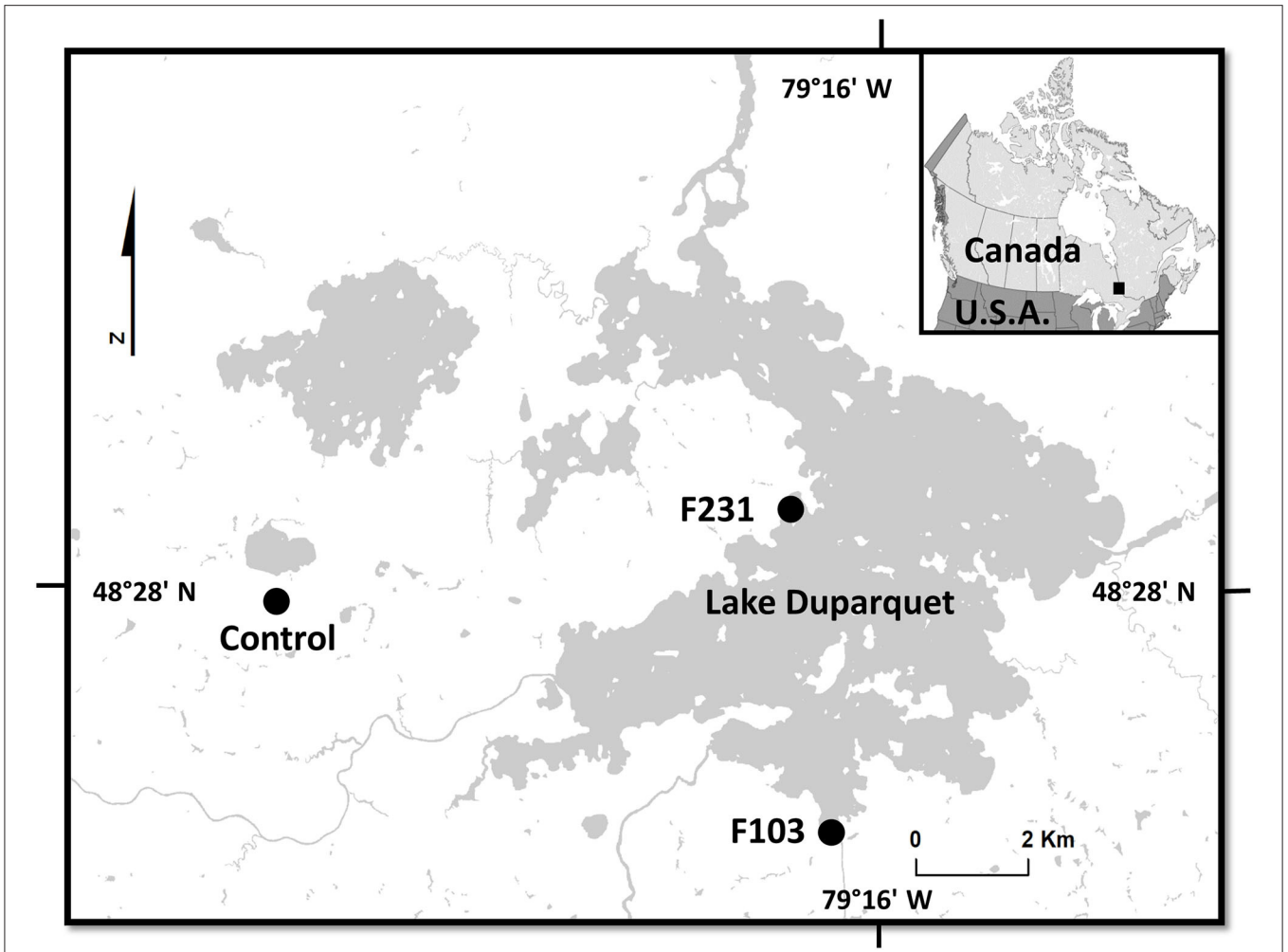

FIGURE 1 | Map of Lake Duparquet showing the location of the sampled floodplain sites (F103 and F231) and the upland non-flooded control site (Control).

personal observation; Tardif et al., 2021). Second, a non-flooded *F. nigra* stand was sampled south of Lake Monsabrais and about 6 km east of Lake Duparquet (48°27'N, 79°25'W, approximate elevation 300 m above sea level, **Figure 1**). In this upland mesic site, *F. nigra* trees were not exposed to flood events and served as a control (hereafter referred to as control). Upland *F. nigra* stands in the study area have also previously been described (Bergeron et al., 1983; Tardif and Bergeron, 1997b; Kames et al., 2011). It should be noted that *F. nigra* prefers shallow or deep organic soils but also grows well on sandy soils underlain by clay that impedes drainage of water. The species is intolerant to severe drought due to its shallow root system and is adapted to mesic and hydric sites along streams, rivers, and lakes (Sims et al., 1990; Wright and Rauscher, 1990).

Sample Collection and Preparation

In this study, we used *F. nigra* trees sampled by Kames (2009) and subsequently used in Kames et al. (2011, 2016). Detailed sampling and chronology development procedures can be found in the aforementioned publications. In each sampling area, wood samples were extracted as close to the tree base as possible using 5-mm diameter increment borers. Two cores were collected from each tree. At the laboratory, all cores were carefully mounted and glued on wooden supports. After drying, all cores were carefully sanded. After eliminating samples that were partly rotten and not suitable for image analysis, a total of 20 floodplain trees from two floodplain sites (**Figure 1**) and 21 trees from the control site (**Figure 1**) were retained for image analysis.

Crossdating, Ring-Width Measurements, and Image Analysis

The date of tree-ring formation was determined by visual crossdating and matching tree-ring patterns based on the listing of unusually narrow and large rings (Phipps, 1985). Pointer years identified and chronologies developed for *F. nigra* in the Lake Duparquet region (Tardif and Bergeron, 1993, 1997b) were also used. After cross-dating, annual tree-ring widths in each core were measured with a VELMEX UniSlide measuring system (Velmex, Inc., Bloomfield, New York) and to a precision of

0.001 mm. The program COFECHA was used to validate cross-dating and measurement (Holmes, 1983).

Following initial ring-width measurement, samples were prepared for image analysis as described in the study of Tardif and Conciatori (2006). All cores were cleaned with pressurized air and rubbed with white chalk to increase the contrast between vessel elements and other cells. The surfaces were scanned with a Polaroid, USA, DMC digital camera connected to a Nikon Japan, SMZ stereo microscope to generate color images at a 25× magnification and a resolution of 1,600 × 1,200 pixels. Color images were analyzed with the program WinCell Pro (v. 2004a, Régent Instruments Inc., Quebec City, Canada, 2005) and the minimum cross-sectional lumen vessel area was set to 800 μm^2 to capture all earlywood vessels. On each tree-ring image, the ring area was delimited, and the earlywood/latewood boundary was determined from the bimodal vessel size distribution in which larger-sized earlywood vessels can be distinguished from smaller-sized latewood ones (Panshin and de Zeeuw, 1980). The earlywood and latewood widths were also measured on each tree-ring image along with two radial files (lower and upper image portion) and averaged to obtain earlywood and latewood mean width which when summed provided mean annual ring width. These new ring-width measurements were validated with those obtained from direct measurements using the VELMEX (Velmex, Inc., Bloomfield, New York) system to control for potential mistakes. In this study, tree rings of very young cambial age, i.e., up to 10 years from the pith, were omitted from the analysis given their rather diffuse-porous vessel pattern.

Chronology Developments

After data quality control, ring-width and vessel measurements were averaged by the tree (two cores) prior to deriving tree-ring anatomical traits. For each of the control and floodplain trees, nine variables were generated, namely, (1) earlywood width (EW), (2) latewood width (LW), (3) total ring width (RW), (4) earlywood total vessel cross-sectional lumen area (T), (5) earlywood number of vessels (N), (6) earlywood mean vessel cross-sectional lumen area (M), (7) earlywood mean cross-sectional area of the 25% largest vessels (25), (8) earlywood vessel density (d), and (9) earlywood porosity (p). Given that both the earlywood vessel fraction and lumen fraction are highly correlated to wood porosity (Ding et al., 2008), earlywood porosity was defined as the earlywood total vessel cross-sectional lumen area divided by the earlywood area. Density was defined as the number of vessels divided by the earlywood area. For each tree ring, the earlywood area was calculated by multiplying the ring area by the earlywood width and dividing the obtained value by ring width. Note that for chronologies generated for the control site, the capital letter C will be used whereas the capital letter F will be used for those originating from floodplain trees. In this study, the two flooded sites (**Figure 1**) were pooled to provide a single flood chronology given the excellent cross-dating (narrow, large, and flood ring) between sites (see also chronology statistics in **Table 1**). The study of Nolin et al. (2021b) also recently showed that the spring flood signal contained in earlywood vessels from floodplain *F. nigra* trees was coherent across four hydrological basins covering about 20,000 km^2 in northeastern Canada.

To produce flood and control chronologies, time series pertaining to each of the 18 tree-ring variables were standardized using a cubic spline function with a 50% frequency response of 60 years. This procedure largely removed low-frequency variations associated with age-related trends or stands dynamics (Cook and Peters, 1981) while retaining high-frequency variability. Autoregressive modeling was only performed when autocorrelation was significant so all analyses were conducted using either standard or residual chronologies, i.e., with no significant serial autocorrelation. Each chronology was also developed using a biweight robust mean (Cook et al., 1990). To evaluate the statistical quality of each chronology, the mean sensitivity expressed population signal (EPS), percent variance of the first principal component, and between tree correlations were calculated. For all the above procedures, the program ARSTAN Windows (v. 4.0a; Cook, 1985) was used.

Correlation Structure and Associations With Hydroclimatic Data

Prior to establishing correlations with hydroclimate data, principal components analysis (PCA) was performed on the 18 chronologies to explore their correlation structure and as a variable reduction procedure. All chronologies were equally weighted by using a correlation input matrix (Legendre and Legendre, 1998). All PCA was carried out using the period 1930–2005 which corresponded to a minimum of 10 trees being included in the chronologies.

In this study, the association between chronologies and hydroclimate variables was analyzed using two approaches. First, a PCA of the covariance matrix of solely significant correlation coefficients calculated between chronologies and hydroclimate variables was computed. For these correlation analyses, gridded monthly mean temperatures and total precipitation were obtained from the Climate Research Unit (CRU TS4.04; Harris et al., 2020; http://climexp.knmi.nl) for the 0.5° × 0.5° grid corresponding to Lake Duparquet (48.00°N, −79.50° E; 48.50N°, −79.00°E). The 3-month standardized precipitation evapotranspiration index (SPEI) derived from the CRU dataset was also used to assess drought impacts (Vicente-Serrano et al., 2010). The monthly record of snow cover extent from the Rutgers University Global Snow Lab (Estilow et al., 2015; https://climate.rutgers.edu/snowcover/) for the 1° × 1° grid corresponding to Lake Duparquet was also extracted. The monthly mean of the naturally flowing Harricana River daily discharge (station 04NA001-2; 48.57°N, −78.12° E) was also downloaded from the Reference Hydrometric Basin Network of Water Survey Canada (Water Survey of Canada, 2021; https://wateroffice.ec.gc.ca). We also made use of the global gridded runoff dataset (GRUN) providing monthly runoff time series on a 5° grid (Ghiggi et al., 2019). Second, the Climate Explorer engine (http://www.knmi.nl; Trouet and Oldenborgh, 2013) of the Royal Netherlands Meteorological Institute (KNMI) was used to calculate spatial field correlations between the first principal components obtained for each flood exposure (floodplain and

TABLE 1 | General statistics characterizing the standard (S) or residual (R) tree-ring widths and earlywood vessel chronologies generated from 21 and 20 trees from the control (C) and floodplain sites (F) respectively.

Chronology	Mean[a]		Mean sensitivity		Standard deviation		Auto-correlation[b]		Variance in PC-1 (%)[c]		EPS[c]		Intertree correlation		Type[d]	
	C	F	C	F	C	F	C	F	C	F	C	F	C	F	C	F
EW (mm)	0.39	0.52	0.13	0.08	0.13	0.07	0.44	0.48	28	28	0.85	0.84	0.21	0.21	R	R
LW (mm)	0.65	0.56	0.44	0.39	0.37	0.36	0.27	0.12	59	45	0.96	0.92	0.56	0.36	R	S
RW (mm)	1.0	1.1	0.27	0.21	0.25	0.19	0.30	0.17	60	48	0.96	0.94	0.56	0.44	R	R
N	31	38	0.11	0.13	0.11	0.14	0.34	0.12	40	57	0.92	0.96	0.35	0.53	R	S
T (10^4 µm^2)	55	62	0.12	0.14	0.12	0.12	0.42	0.19	38	53	0.91	0.95	0.32	0.49	R	R
M (10^4 µm^2)	1.8	1.7	0.08	0.20	0.08	0.17	0.41	−0.05	29	67	0.87	0.97	0.24	0.64	R	S
25 (10^4 µm^2)	2.9	2.6	0.08	0.18	0.07	0.15	0.35	−0.05	26	67	0.84	0.97	0.20	0.63	R	S
d (10^{-13} mm^{-2})	1.8	1.6	0.09	0.10	0.08	0.12	0.16	−0.01	18	42	0.73	0.92	0.11	0.35	R	S
p	0.31	0.26	0.07	0.12	0.07	0.10	0.19	−0.06	15	52	0.56	0.95	0.06	0.47	R	S

The chronologies for control and floodplain site trees cover the periods 1857–2006 and 1890–2006, respectively. All statistics, except when indicated, were calculated for these respective periods.

PC-1, first principal component; EPS, expressed population signal; EW, earlywood width; LW, latewood width; RW, ring-width; N, number of earlywood vessels; T, total cross-sectional vessel area of earlywood; M, mean cross-sectional vessel area of earlywood; 25, mean cross-sectional vessel area of the 25% largest earlywood vessels; d, vessel density in the earlywood and p, porosity in the earlywood.

[a] *Calculated from measurement series.*

[b] *Calculated from standard chronologies.*

[c] *Calculated from the common period 1957–1998.*

[d] *Type of chronology used: Standard (S) or Residual (R). Note that standard chronologies were used when autocorrelation was not significant.*

control) and the individual surrounding grids. Unless specified, Spearman Rank Order correlations were calculated in all analyses and for the period 1930-2005, and all PCA were calculated using the program CANOCO v.5.12 (ter Braak and Šmilauer, 2018).

RESULTS

Chronology Descriptive Statistics

Trees growing on control and floodplain had overall similar mean measurement values (**Table 1**). In floodplain trees, earlywood width however tended to be larger with earlywood vessels being slightly more numerous and smaller than in control trees. Width variables (EW, LW, and RW) had higher mean sensitivity and standard deviation values in control chronologies compared with the floodplain (**Table 1**). The inverse was however observed for each vessel chronology indicating higher year-to-year variations in floodplain trees. Comparing standard chronologies, each floodplain chronology except EW showed lower autocorrelation than control ones (**Table 1**). Statistics over the common period revealed that the floodplain vessel chronologies tended to share more common variance than the control ones and the inverse was true for width chronologies in control trees. For example, LW and RW in control trees recorded the highest values for variance accounted for by the first principal component (PC-1), the expressed population signal (EPS), and the mean inter-tree correlation. In contrast to the control, vessel chronologies from the floodplain shared the most variance. The floodplain vessel chronologies FM and F25 showed higher values for percent variance in PC-1, EPS, and Intertree correlation than did LW and RW of the control trees (**Table 1**). Overall all chronologies derived for control trees had a high common signal except earlywood vessel density and earlywood porosity (**Table 1**).

Ring-Width, Vessel Chronologies, and Correlation Structure

Control and floodplain chronologies were generally dissimilar (**Figure 2**). The highest correlation observed between any two chronologies was for their respective latewood width (rho = 0.539, $p < 0.001$, $n = 76$). In both control and floodplain chronologies, LW and RW displayed the highest year-to-year variability (**Table 1**; **Figure 2**). In contrast to the control, all floodplain earlywood vessel chronologies presented much higher year-to-year variability with highly pronounced peaks and/or troughs observed over the period 1930–2005 (**Figure 2**). Years in which the floodplain mean vessel area chronology departed negatively from the mean by 1.28 standard deviations were 1947, 1950, 1960, 1967, 1979, 1989, and 1996. None of these years stood out in the corresponding control chronology. In the control, years that deviated negatively by at least 1.28 standard deviations from the mean vessel area chronology were 1930, 1932, 1961, 1966, 1972, and 1981 (**Figure 2**). Common years in which the respective control and floodplain mean vessel area chronology departed positively from the mean by 1.28 standard deviations were 1943, 1959, 1962, and 1968.

The PCA of the 18 chronologies (**Figure 3**) confirmed the weak common variance between floodplain and control chronologies and especially of their vessel chronologies

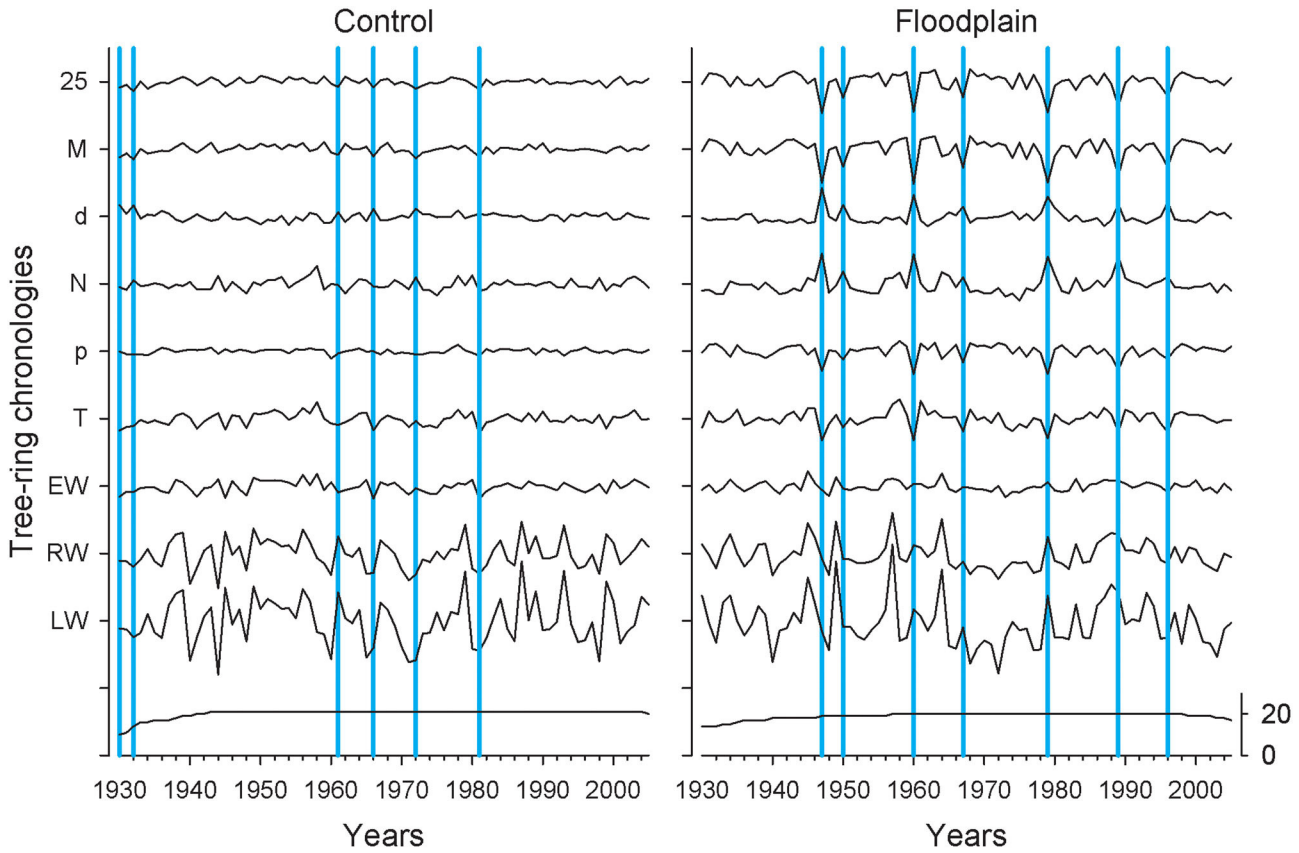

FIGURE 2 | The 9 tree-ring chronologies for *Fraxinus nigra* growing on the control (left panel) and floodplain sites (right panel) with the number of samples indicated at the bottom (black line). The year 1930 corresponds to *F. nigra* chronologies in each flood exposure having a minimum of 10 trees. Years in which the earlywood mean vessel area (M) chronology deviated by −1.28 standard deviations are highlighted in blue. Chronologies are abbreviated as in **Table 1**.

(**Figure 3A**). The first two components totalized 53.8% of the variance with PC-1 and PC-2 representing respectively 30.6 and 23.2% of the total variance. The first PC was strongly associated with floodplain earlywood vessel chronologies (**Figure 3A**). Floodplain vessel number (FN) displayed a strong negative correlation with PC-1 with vessel dimensions (FM, F25, and Fp) being positively correlated with it. The acute angle between vectors pertaining to floodplain earlywood vessel chronologies indicates strong positive correlations and both FN and Fd chronologies were negatively associated with FM, F25, FT, and Fp. Major flood years, e.g., 1960 and 1979, also had negative loadings on PC-1. In these years, floodplain trees recorded a high number of earlywood vessels (density) of small size (**Figures 3A**, **4A,B**). In contrast, the control trees recorded larger vessels in both 1960 and 1979, with 1960 being a year with thin latewood (**Figures 4C,D**). The second PC was positively associated with both control and floodplain width chronologies and, with control vessel dimension (**Figure 3A**). Floodplain earlywood total vessel cross-sectional lumen area had the highest loading on PC-2. It should be noted that a robust-PCA calculated from a Spearman's correlation matrix, and another calculated after eliminating the years for which the floodplain mean vessel area chronology departed negatively from the mean by at least 1.28 standard deviations, revealed essentially the same structure (not presented) indicating that the differences observed between flood exposures were not driven by a few extreme values.

Given the distinct signal originating from floodplain and control chronologies, a PCA was recalculated for each hydrological context (floodplain and control) to get a finer view of the intricate linkages among earlywood attributes. For the floodplain, the first two PCs explained 88.5% of the total variance with PC-1 and PC-2 capturing, respectively, 56.1 and 32.4% of the variance (**Figure 3B**). Again, PC-1 evidently reflected its strong association with earlywood vessel chronologies and PC-2 with ring-width chronologies (EW, LW, and RW). The total vessel area chronology from the floodplain also loaded high on PC-2 as did the large tree rings of 1945, 1949, 1957, and 1964. While vessel size attributes were strongly correlated with one another as shown by their acute and/or obtuse angles, they were decoupled from width attributes as shown by the nearly right (90°) angle between respective vectors (**Figure 3B**). Flood years were generally characterized by numerous and small earlywood vessels in floodplain trees (**Figures 4A,B**). For the control PCA, the first two PCs explained, respectively,

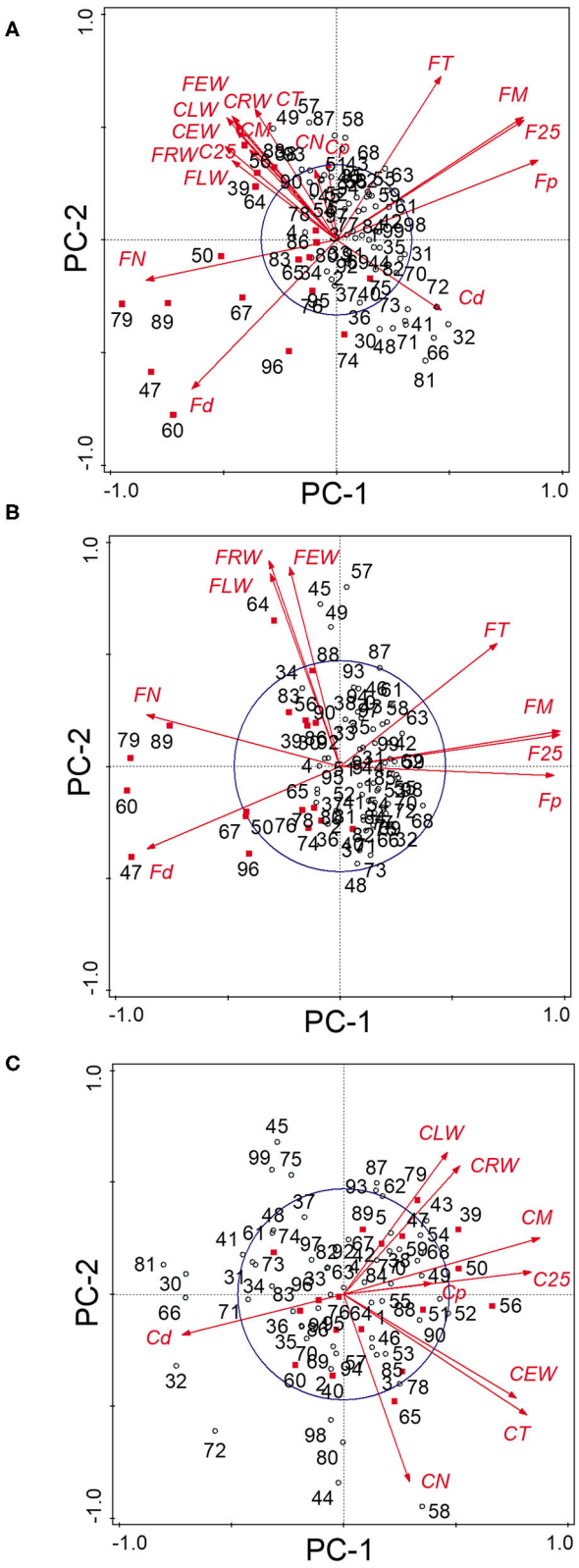

FIGURE 3 | Principal components analysis of the **(A)** 18 tree-ring chronologies for the control and floodplain sites, **(B)** for the floodplain site, and **(C)** for the control site. The first two principal components axes are shown. The capital *(Continued)*

FIGURE 3 | letter preceding each chronology abbreviation indicates their origin: control (C) or floodplain (F). Chronologies are abbreviated as in **Table 1**. The reference period is 1930–2005 with years marked in red indicating major flood-ring years (Tardif et al., 2021). The circle of equilibrium is indicated on each sub-figure.

44.2 and 22.8% of the total variance (**Figure 3C**). The third PC (not presented) expressed 17.1% of the variance and was mainly related to latewood and total ring width. Similar to the floodplain site, PC-1 of the control site was negatively associated with vessel density (Cd) and positively with earlywood vessel dimensions (CM, C25, and CT; **Figure 3C**). However, in the control site, width attributes had a positive loading on PC-1 as well as the number of earlywood vessels. Earlywood width and total vessel area were also strongly correlated as indicated by the acute angle between their respective vectors (**Figure 3C**). Years with thicker earlywood were characterized by a greater total vessel area (CT); a trait not observed on the floodplain site (**Figure 3B**). On the control site, earlywood width was most strongly correlated with earlywood total vessel area (*rho* = 0.826, $p < 0.001$, $n = 76$); this correlation dropped in the flooded site (*rho* = 0.252, $p = 0.028$, $n = 76$). Interestingly, some flood-ring years, e.g., 1950; 1956, also corresponded to years with thick earlywood and high mean vessel area. The spread of the identified flood-ring years in the ordination plane however strongly differs from that of the floodplain (**Figures 3B,C**). The flood year 1960 and 1979, respectively, led to narrow and thick rings in the control site (**Figures 3C**, **4C,D**). The respective PC-1 calculated from the nine control and the nine floodplain chronologies (**Figures 3B,C**) were not significantly associated (*rho* = −0.102, $p = 0.381$, $n = 76$) despite each representing variance contained in their respective earlywood vessel chronologies. A significant but small correlation was however observed between control PC-1 and floodplain PC-2 (*rho* = 0.255, $p = 0.026$, $n = 76$), wherein both axes accounting for variance, among others, related to ring-width attributes (EW, LW, and RW).

Associations Between Chronologies and Climate Data

In continuity with the previous analyses, the floodplain and control chronologies showed distinct patterns in their correlations with selected hydroclimate variables. First, the control chronologies were significantly ($p < 0.05$) associated with 26 variables out of 93 candidate ones whereas the floodplain ones were significantly associated with 40 candidate variables. Second, the control chronologies had 51 significant ($p < 0.05$) correlation coefficients compared with 124 for the floodplain chronologies. Third, the significant correlation coefficients from the control chronologies had a smaller range [from −0.414 to 0.392] compared with floodplain ones [from −0.696 to 0.458]. The PCA calculated from the significant correlation coefficients indicated a distinctive response between flood exposures (**Figure 5**).

For the floodplain site, the first three PCs explained, respectively, 73.0, 9.9, and 5.5% of the total variance

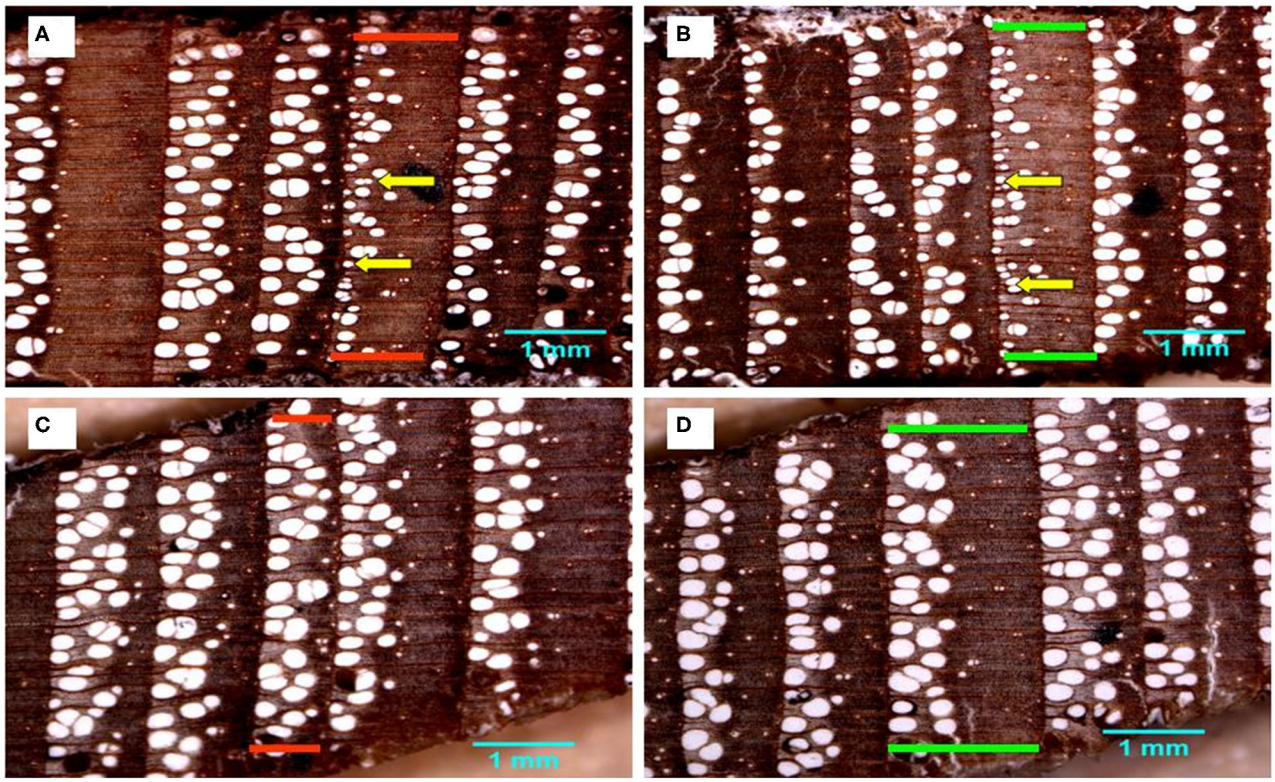

FIGURE 4 | *Fraxinus nigra* tree rings from floodplain **(A,B)** and control **(C,D)** trees showing rings of the years 1960 and 1979 delineated in red and green, respectively. Yellow arrows point to examples of earlywood vessels with largely reduced lumen area and characteristic of macroscopically defined flood rings.

(**Figures 5A,B**). The ordination plan (**Figure 5A**) was very similar to that obtained from the chronologies (**Figure 3B**). The acute angle between earlywood vessel chronologies, e.g., FM, Fp, and F25, indicated that they shared similar correlations with hydroclimate variables. The near 90° angles between vessels and width variables (exception of the number of vessels) also illustrated the aforementioned decoupling between ring-width and earlywood vessel dimensions in floodplain trees (**Figure 5A**). The first PC was associated with vessel dimension, e.g., total and mean vessel area, and these attributes were associated with the May and June Harricana discharge (negative association) and March and April temperature (positive association). These associations were inverted with vessel density. The highest correlation coefficient (-0.696, $p < 0.01$, $n = 76$) was obtained between the mean vessel area and the May Harricana discharge. The may GRUN runoff was also negatively associated with vessel dimensions. The high April-May-June SPEI-3 (especially May), indicating wetness, was also negatively associated with earlywood vessel dimensions (**Figure 5A**). The negative influence of hydric conditions was further emphasized by the negative association between the April and May snow cover and earlywood vessel dimensions, e.g., mean vessel area: -0.426 and -0.384, respectively; vessel density: 0.458 and 0.403, respectively, $p < 0.05$, $n = 36$. For the floodplain site, PC-2 was mainly associated with earlywood width and vessel number, and to a lesser extent, with latewood and total ring width (**Figure 5A**). These variables were positively associated with the June GRUN runoff and both June-July SPEI-3. The may temperatures of the previous year were also positively associated with the variables. The June GRUN runoff of the previous year as well as the March-April SPEI-3 of the current year was also negatively associated with PC-2. Little variance (5.5%) was associated with PC-3 with earlywood and total ring width being mainly associated positively with the May temperature of the previous year and negatively with the June GRUN runoff of the previous year (**Figure 5B**).

Similar to floodplain chronologies (**Figure 3B**) approximating that of the correlation coefficient with hydroclimate variables (**Figure 5A**), both PCAs of the control site (**Figures 3C**, **5C**) were similar with all vectors (except vessel density) having a positive loading on PC-1. The first three PC explained respectively 35.8, 27.2, and 19.2% of the total variance indicating that tree-ring attributes were less severely modulated by a single set of hydroclimate variables. No significant negative correlations with the May-June GRUN runoff or Harricana discharge of the current year were observed. In contrast, the June and July GRUN runoff were positively associated with PC-1. The first PC largely reflected the common variance in latewood (total ring) width, and to a lesser extent, with earlywood vessel attributes. PC-2 separated earlywood characteristics (width and vessels) from latewood (total ring) width. The April Harricana discharge of the previous year was positively associated with PC-1 and

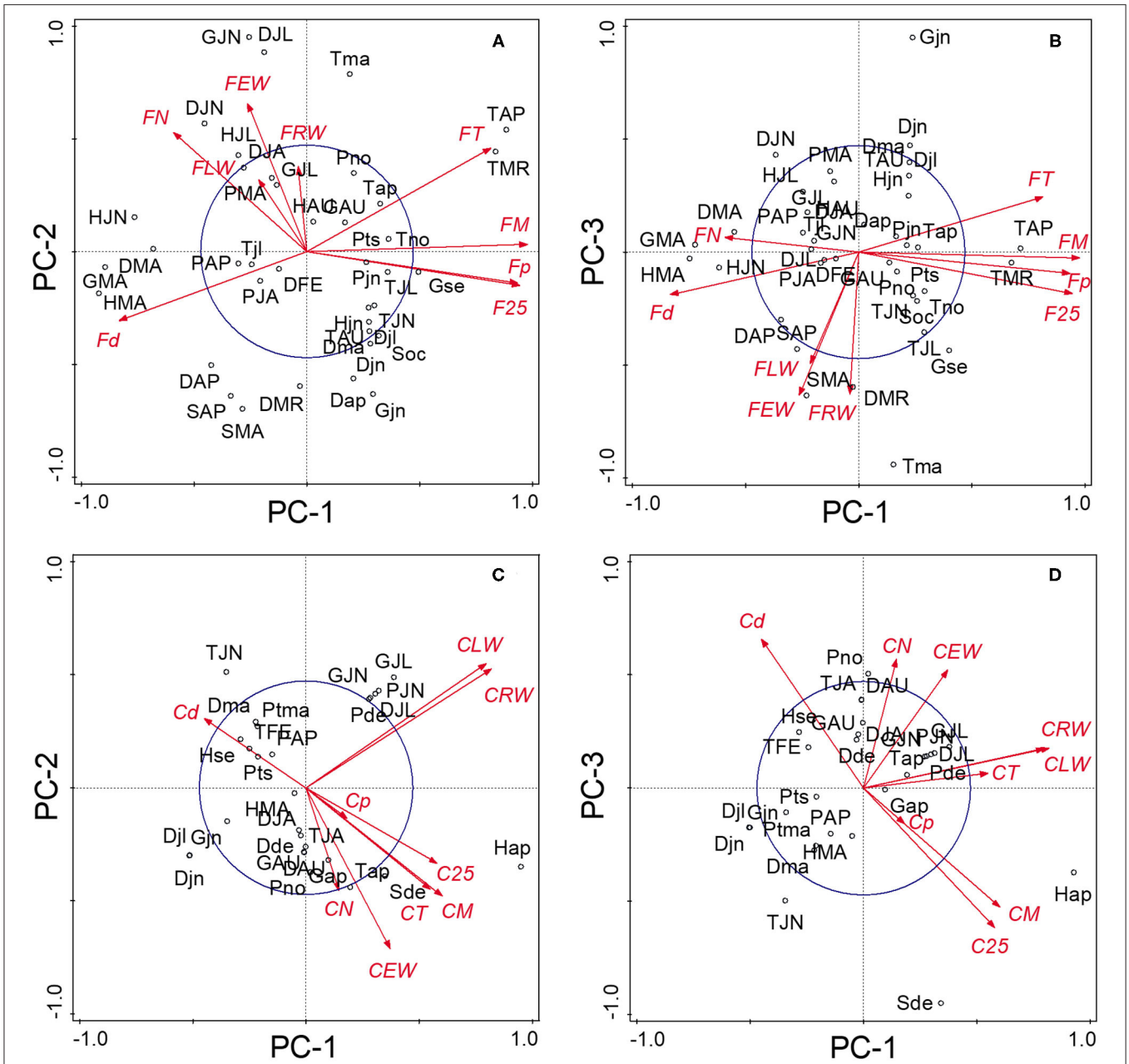

FIGURE 5 | Principal components analysis calculated from significant ($p < 0.05$) Spearman's rho correlation coefficients between chronologies and hydroclimatic variables. The first two principal components for the floodplain site are shown in **(A)** and components 1 and 3 are shown in **(B)**. The first two principal components for the control site are shown in **(C)** and **(D)** represents the first and third components. T, temperature; P, precipitation; S, snow cover; D, SPEI-3; H, Harricana River discharge; G, GRUN runoff. Months are identified by their first two letters with capital letters indicating the current growing season. Chronologies are abbreviated as in **Table 1**. The circle of equilibrium is indicated on each sub-figure.

to the production of thick tree rings and large earlywood vessels (**Figure 5C**). More specifically, large rings were positively associated with precipitation in December and June, with the June-July GRUN runoff, and July SPEI-3. The June-July SPEI-3 of the previous year was negatively associated with latewood (total ring) width. Earlywood width and vessel dimensions were negatively associated with the June temperature and positively with the December snow cover extent (**Figure 5B**). The third PC mainly separated earlywood width (and the number of vessels) from mean vessel area (and largest vessels), wherein the latter being positively associated with December snow cover extent [$rho = 0.381$ (and.392), $p < 0.05$, $n = 36$]. The number of

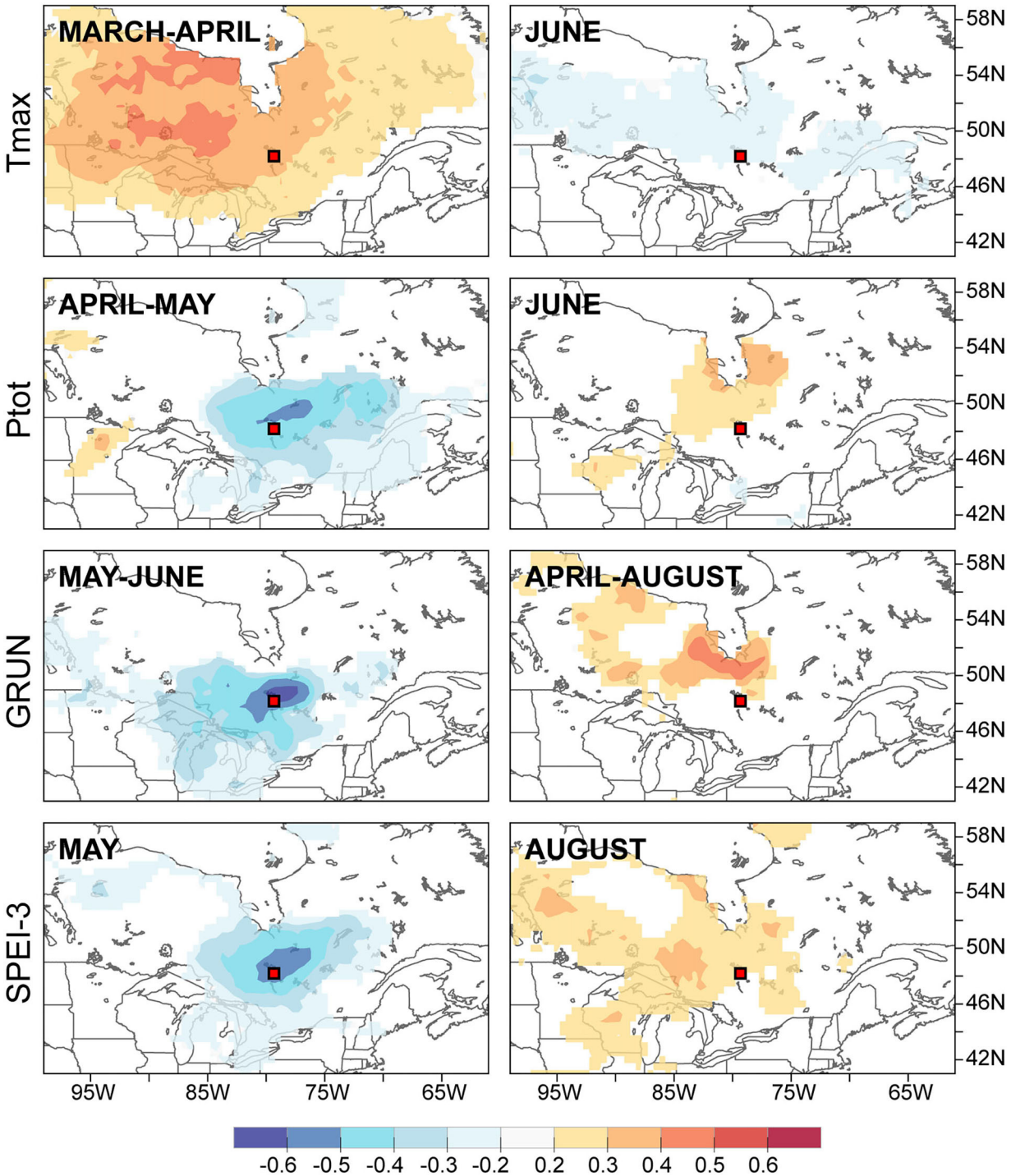

FIGURE 6 | Spatial field correlation between the first principal components extracted from the floodplain chronologies (left column) and the control chronologies (right column) and selected hydroclimate variables.

earlywood vessels was negatively associated with the current June temperature ($rho = -0.298$, $p < 0.05$, $n = 76$).

The spatial field correlations calculated between the PC-1 yearly loadings of the chronologies (**Figures 3B,C**) and selected hydroclimatic variables further highlighted the distinct but spatially coherent signal in trees from both flood exposures (**Figure 6**). Floodplain trees with tree rings with large earlywood vessel dimensions (FM, F25, and Fp) were positively associated

with the warm March-April temperatures, low April-May precipitation, low May-June runoff, and low May SPEI-3 values. In other words, flood rings were favored by cold and wet springs with high runoff and high (wet) SPEI-3 values (**Figure 6**). This signal was spatially coherent over a large portion of northeastern Ontario and northwestern Quebec. In contrast, few and weak spatially coherent associations were found with PC-1 of the control site. Among them, the June maximum temperature was negatively associated with PC-1 (inverse with June precipitation). In contrast to the floodplain, the control site displayed a positive correlation with the April-August average GRUN runoff north of the study area (**Figure 6**). The August SPEI-3 was also positively associated with PC-1. In other words, thick tree rings with large vessels were mainly associated with abundant runoff and a lack of drought during the growing season in the control site.

DISCUSSION

The differences between flooded and non-flooded control *F. nigra* trees could be systematically observed from their chronology statistics, cross-correlation structure, and distinct associations with hydroclimate variables. Some tree-ring traits transcended flood exposure like the lower year-to-year variability in EW compared with LW and RW which has been reported in numerous ring-porous species growing in various habitats (Tardif, 1996; Corcuera et al., 2004; Fonti and García-González, 2004, 2008; Tardif and Conciatori, 2006; Davis and Loader, 2020). The low EW year-to-year variability in ring-porous species may reflect strong developmental controls. Similarly, the lower common signal strength and mean sensitivity of earlywood vessel vs. width chronologies (observed more strongly in control trees) were also reported in numerous ring-porous species (Woodcock, 1989; Fonti and García-González, 2004; Tardif and Conciatori, 2006; Alla and Camarero, 2012; García-González et al., 2016; Pritzkow et al., 2016). However, compared with the control, the floodplain earlywood vessel chronologies generally showed greater common signal strength including higher mean sensitivity and a stronger response to hydroclimate factors.

Another noticeable difference between control and floodplain trees was related to the thicker EW observed in the latter and its greater contribution to RW. Floodplain trees may experience a lengthened leaf development period compared with control trees making earlywood production last longer than in the control site. Studies indicated that in ring-porous species earlywood may cease to be produced 1–2 weeks after shoot extension and complete leaf expansion (Chalk, 1930; Zasada and Zahner, 1969). Recent studies have also shown that the relation between vessel formation and leaf phenology may vary within and between ring-porous species (Sass-Klaassen et al., 2011; Puchałka et al., 2017). In the 5-year study Ahlgren (1957) reported that *F. nigra* trees growing in northeastern Minnesota started radial growth between the first to the third week of May and that the first leaves in recognizable form were observed between the 3rd week of May and the 1st week of June. In southeastern Ontario, the wood formation was also initiated in *F. nigra* at the beginning of May (Fraser, 1958). In major flood years, leaf development in floodplain *F. nigra* trees is delayed and/or slower than in non-flood years (Tardif pers. observation). Xylogenesis and phenological monitoring of flooded and non-flooded trees along a timeframe including years with low and high flood magnitude may help to better clarify these habitat-specific differences (Sass-Klaassen, 2009; Sass-Klaassen et al., 2010).

Differences Among Control and Floodplain Chronologies

Another striking difference between control and flooded chronologies was the decoupling of vessel attributes from earlywood width in the latter. In the control site, the strong positive associations of EW with vessel number and total vessel area have been reported in numerous ring-porous species growing in various non-riparian habitats (Fonti and García-González, 2004; Tardif and Conciatori, 2006; González-González et al., 2015; Zhu et al., 2020). Environmental conditions that favored large EW at the control site also promote the production of numerous somewhat larger-sized vessels resulting in a high total vessel area with low earlywood vessel density. In contrast, environmental conditions inducing large EW on the floodplain also brought an increase in vessel number but not in vessel dimension (M, T). On the floodplain, earlywood characterized by a high number of vessels tended to contain small-sized vessels culminating in a low total vessel area. These rather "diffuse-porous" earlywood vessel patterns were unique to floodplain trees, most pronounced in years of high magnitude spring flood and not observed in control trees. These results further confirm that in the floodplain trees, the production of a higher number of vessels of smaller areas is associated with spring flood duration. As hypothesized, vessel chronologies from non-flooded trees were independent from those developed from flooded trees confirming the uniqueness of the flood signal to floodplain trees.

In contrast to earlywood vessels, ring-width attributes showed to be positively correlated between flood exposures indicating some shared variance. Tardif and Bergeron (1997b) which used different sites also reported as in this study a lack of clear cross-dating between the floodplain and upland *F. nigra* trees with their total ring width chronologies showing a low correlation ($r = 0.32$, $p < 0.01$). It is speculated that more similar growth conditions may occur in years of low flood magnitude (relaxing of flood influence) with tree-ring development (EW and LW) being more similarly affected by the prevalent climate conditions than during major flood years. Again, xylogenesis and phenological monitoring of flooded and non-flooded trees over a range of flood years may help clarify why ring-width attributes show more between habitats similarities than vessel ones. In a recent study comparing upper- and lower-floodplain trees, Tardif et al. (2021) observed that flood rings almost disappeared in upper-floodplain trees compared with lower-floodplain trees. While the authors did not report on ring width, total ring width chronologies developed for the upper and lower floodplain sites showed to be significantly and positively correlated (result not presented). In a similar way, the study of Nolin et al. (this issue) reported that flood rings became less frequent and harder to distinguish in riparian *F. nigra* trees after hydrological regulation with little

impact noticeable in total ring width among sites. These results suggest that earlywood vessels attributes (number and mean area), in contrast to tree-ring width, could be used to assess the impact of hydrological regulation and/or to maintain (restore) spring flood conditions within their historical range of variability in managed systems.

In this study, flooding occurring during the active growing season was presumably the most important factor influencing the number, density, and especially the mean and total area of the earlywood vessels in floodplain trees. Of all the vessel attributes measured, earlywood mean vessel area and vessel number were the most strongly associated with discharge (Kames et al., 2016; Nolin et al., 2021a). The lack of negative correlation between the control earlywood vessel chronologies and spring river discharge further reinforces the hypothesis that flooding exerts a strong influence on earlywood vessel formation. The large decrease in earlywood mean vessel area in high magnitude flood years observed in this study was consistent with observations made for *F. americana*, *F. pennsylvanica* (Yanosky, 1983), *Q. macrocarpa* (St. George and Nielsen, 2000, 2003), and *Q. robur* (Astrade and Bégin, 1997; Sass-Klaassen, 2009, Copini et al., 2016). Compared with these studies, a unique feature in the response of *F. nigra* to flooding was the increase in the number of earlywood vessels. It is possible that the specific response of *F. nigra* may be associated with its strong tolerance to flooding (Sims et al., 1990). Comparisons with other species are further complicated by the fact that the study of Yanosky (1983) did not develop continuous vessel chronologies, while the study of Astrade and Bégin (1997) developed only a short time series in which the number of vessels was not assessed.

As previously proposed, the decrease in mean vessel area and the increase in the number of vessels in response to spring flooding may be related to alterations in growth regulator dynamics including both ethylene and auxin which act on xylem development (Yamamoto and Kozlowski, 1987; Yamamoto et al., 1987; Aloni, 2015). An interplay of both, auxin and ethylene on vessel size is supported through studies with hybrid poplars (*Populus tremula* L. × *Populus tremuloides* Michx. and *Populus tremula* L. *x Populus alba* L.), white poplar (*Populus alba* L.), as in these species large increases in the concentrations of auxin and ethylene led to reductions in vessel area (Tuominen et al., 1995; Junghans et al., 2004). A decreased vessel area was also observed following the application of the ethylene releasing compound ethrel in American elm (*Ulmus americana* L.) (Yamamoto et al., 1987) and Norway maple (*Acer platanoides* L.) (Yamamoto and Kozlowski, 1987). In *U. americana,* ethrel application also caused an increase in the number of vessels (Yamamoto et al., 1987). Further, ethylene was reported to decrease the vessel diameter in Manitoba maple (*Acer negundo* L.; Savidge, 1988).

While not studied, preliminary observations indicate that vessel grouping [see von Arx et al. (2013)] may be altered during years with high magnitude spring flood. Tardif et al. (2021) noted that flooded *F. nigra* trees often produced vessel chains instead of solitary vessels during flood years. This response may however not be systematic (see **Figure 2**) and it raises the question whether alterations in vessel connectivity could be traced back to either core sampling height and/or to the duration of stem submersion. Answering this question may provide added value to flood rings as a hydrological proxy. Detailed analysis of specific flood years (accompanied by thin sectioning) may provide further insights on the impact of flooding on *F. nigra* growth. In this study, the impact of flooding on latewood characteristics was not investigated. The study of Yamamoto et al. (1995) observed a reduction in the cell wall thickness of wood fibers following a flood treatment of Manchurian ash (*Fraxinus mandshurica* Rupr. var. *japonica* Maxim.) seedlings. In floodplain habitat, neglecting small vessels ($< 6{,}000$ or $< 10{,}000$ μm^2) as often recommended in numerous studies (García-González and Fonti, 2006; for examples, see García-González and Fonti, 2006; Fonti et al., 2009a; González-González et al., 2014; García-González et al., 2016) may prove prejudicial and thresholds smaller than 800 μm^2 may be needed to better quantify the impact of flooding on latewood characteristics in species like *F. nigra*.

Different Responses to Hydroclimatic Factors

The correlations between chronologies and hydroclimate variables displayed by the floodplain and control *F. nigra* trees were as contrasted as their chronologies. The results of this study supported the hypothesis that earlywood vessel chronologies from non-flooded trees show lesser potential for hydroclimate reconstruction compared with their floodplain counterparts. Vessel attributes in floodplain trees strongly responded to hydrological signal of Lake Duparquet. Years with increasing May and June mean Harricana River discharge (also May and June GRUN runoff) were strongly associated with tree rings with more numerous but reduced sized earlywood vessels. Vessel chronologies were also essentially correlated with climate factors leading to high magnitude spring floods, i.e., cool March and April temperatures leading to a persistent snow cover in the spring. These findings are in line with previous *F. nigra* studies (Tardif et al., 2010, 2021; Kames et al., 2016; Nolin et al., 2021a,b). The results from these studies all converged, revealing the major role played by flood magnitude (timing and duration) on tree-ring development in floodplain trees.

These results evidently contrast with those obtained from the control site in which vessel chronologies and spring discharge were not significantly correlated. Control *F. nigra* trees displayed a different signal than floodplain trees with surprisingly no strong drought signal observed. Significant correlations with hydroclimate variables were few and generally weak. In the control site, the mean earlywood vessel area solely showed a weak correlation with the December snow cover (positive) and mean February temperatures (negative), suggesting that a sufficient amount of water may be supplied by snowmelt during the earlywood vessel production period. The June and July GRUN runoff were positively associated with large tree rings as well as the June precipitation and July and August SPEI-3, indicating the importance of water availability during the growing season. Despite *F. nigra* trees exhibiting determinate growth (Lechowicz, 1984) with winter buds containing all leaf primordia that will develop in the next growing season (Pallardy, 2008), previous year conditions did not show to be strongly associated with

the current year growth. In both flood exposures, conditions in the prior growing season including warm spring (April for control and May for floodplain) and the reduced June GRUN runoff could indicate that early breakage of dormancy and a long growing season may allow for greater carbohydrates production to be used in the following year earlywood production.

In both flood exposures, ring-width attributes were correlated to a different set of hydroclimatic variables compared with vessel attributes. In floodplain trees, width attributes contrary to vessels showed little correlation to spring discharge data and revealed to be lower quality hydrological proxies. Using *F. nigra* ring-width chronology only, the study of Tardif and Bergeron (1997b) had also stressed major differences between upland and floodplain regarding their climate associations. In this study, the absence of a significant association between the floodplain EW and May (t) discharge was unexpected. The study of Tardif (1996) has found a weak but significant negative relationship between the EW of floodplain *F. nigra* growing on the floodplain of the Lake Duparquet. *Fraxinus nigra* trees analyzed by Tardif (1996) were however growing at a very low elevation and more exposed to flooding than trees analyzed in the present study (Tardif and Bergeron, 1992, 1999). In floodplain habitats, small differences in elevation (also coring height) may affect tree-ring attributes and their association with hydrological (Tardif and Bergeron, 1993; Nolin et al., this issue; Tardif et al., 2021). In this context, extracting cores at 1.3 m and/or excluding small earlywood vessels in floodplain ring-porous species may not be desirable when maximizing flood signal is the objective.

CONCLUSION

The objectives of this study were (i) to describe and compare ring-width and earlywood vessel chronologies in *F. nigra* trees growing in two contrasting exposure to spring floods and (ii) to determine their degree of association to hydroclimatic variables. The clear distinctions between flooded and non-flooded chronologies were maintained from their descriptive statistics to their associations with hydroclimate variables. In control trees, the linkage between earlywood width and vessel characteristics was much more pronounced than in floodplain trees. In control of *F. nigra* trees, conditions leading to large EW promote the production of numerous and large-sized vessels, thus resulting in a higher mean and total vessel area. In floodplain trees, this linkage between earlywood width and vessel size was weak and the most important factor influencing vessel number and especially mean and total vessel area was spring flood magnitude. Control trees, compared with floodplain ones, displayed no negative associations with spring river discharge. The weak and rare correlations displayed by control trees support the idea that vessel chronologies from trees growing in sites that are not highly "stressed" may not be worth developing for dendroclimatological purposes.

Given the unambiguous influence of spring floods on floodplain *F. nigra* trees, future work may focus more actively on them. In floodplain habitat, a threshold smaller than 800 μm^2 (accompanied by thin sectioning) may be needed to further quantify the impact of spring floods on latewood characteristics. Detailed tree-ring analyses of specific flood years would allow measuring alterations in both vessels and fibers. Looking at changes in vessel connectivity may also be of interest. Detailed studies may also help elucidate why mean vessel area chronology over- and/or underestimate flood magnitude in some years. Given that flood rings appear to be essentially restricted below the flood-water line during vessel formation; stem analysis may prove useful to determine if *in-situ* spring water levels can be reconstructed. Finally, the observed earlywood vessel plasticity in floodplain *F. nigra* trees suggests that it could be used to (i) evaluate flood regime alterations following regulation and/or (ii) restore/maintain flooding within its historical range assuming reference trees are available. Further studies are also required that investigate vessel chronologies in other floodplain (ring- and diffuse-porous) species and under various hydrological contexts.

DATA AVAILABILITY STATEMENT

The raw data supporting the conclusions of this article will be made available by the authors, without undue reservation.

AUTHOR CONTRIBUTIONS

JT, SK, and YB contributed to conception and design of the study. SK and JT performed sampling. SK performed measurements and organized the database. JT, SK, and AN performed formal analyses and data interpretation. JT and YB supervised and provided funding for the project. JT and SK wrote the first draft of the manuscript. All authors provided critical feedback, contributed to manuscript revision, read, and approved the submitted version.

FUNDING

This research was funded by a NSERC-Discovery grant to YB and a NSERC-Discovery grant to JT.

ACKNOWLEDGMENTS

We thank F. Conciatori and M. Hoffer for assistance during laboratory work and D. Charron for assistance with fieldwork logistics. This research was undertaken, in part, thanks to funding from the Canada Research Chairs Program. The University of Winnipeg also supported this research project. Partial funding for S. Kames came from NSERC grants to Dr. Tardif and Dr. Bergeron and the Faculty of Graduate Science Studentship from the University of Manitoba. We also thank the two reviewers and the guest associate editor, Dr. I. García-González, for their constructive comments on an earlier draft of the manuscript.

REFERENCES

Ahlgren, C. E. (1957). Phenological observations of nineteen native tree species in northeastern Minnesota. *Ecology* 38, 622–628. doi: 10.2307/1943128

Alla, A. Q., and Camarero, J. J. (2012). Contrasting responses of radial growth and wood anatomy to climate in a Mediterranean ring-porous oak: implications for its future persistence or why the variance matters more than the mean. *Eur. J. Forest Res.* 131, 1537–1550. doi: 10.1007/s10342-012-0621-x

Aloni, R. (2015). Ecophysiological implications of vascular differentiation and plant evolution. *Trees* 29, 1–16. doi: 10.1007/s00468-014-1070-6

Asshoff, R., Schweingruber, F. H., and Wermelinger, B. (1999). Influence of a gypsy moth (*Lymantria dispar* L.) outbreak on radial growth and wood-anatomy of Spanish chestnut (*Castanea sativa* Mill.) in Ticino (Switzerland). *Dendrochronologia* 16–17, 133–145.

Astrade, L., and Bégin, Y. (1997). Tree-ring response of *Populus tremula* L. and *Quercus robur* L. to recent spring floods of the Saone River, France. *Écoscience* 4, 232–239. doi: 10.1080/11956860.1997.11682400

Ballesteros-Cánovas, J. A., Stoffel, M., St. George, S., and Hirschboeck, K. (2015). A review of flood records from tree rings. *Prog. Phys. Geogr.* 39, 794–816. doi: 10.1177/0309133315608758

Bergeron, Y., Bouchard, A., Gangloff, P., and Camiré, C. (1983). *La classification écologique des milieux forestiers de la partie ouest des cantons d'Hébécourt et de Roquemaure, Abitibi, Québec Études écologiques no.9, Université Laval, Ste-Foy, Québec.*

Bräuning, A., De Ridder, M., Zafirov, N., García-González, I., Dimitrov, D., and Gärtner, H. (2016). Macroscopic tree-ring features: indicators of extreme event impacts. *IAWA J.* 37, 206–231. doi: 10.1163/22941932-20160131

Canny, J. (1986). A computational approach to edge detection. IEEE Transactions on Pattern Analysis and Machine Intelligence. *PAMI-8* 6, 679–698. doi: 10.1109/TPAMI.1986.4767851

Chalk, L. (1930). *The Formation of Spring and Summer Wood in Ash and Douglas Fir. Oxford Forestry Memoires No. 10*. Oxford: Oxford University Press, 48.

Cook, E. R. (1985). *A Time Series Analysis Approach to Tree Ring Standardization*. (Ph.D. dissertation), Faculty of the School of Renewable Natural Resources, Graduate College of the University of Arizona, Tucson, AZ, United States, 171.

Cook, E. R., and Peters, K. (1981). The smoothing spline: a new approach to standardizing forest interior tree-ring width series for dendroclimatic studies. *Tree-Ring Bull.* 41, 45–53.

Cook, E. R., Shiyatov, S., and Mazepa, V. (1990). "Estimation of the mean chronology," in *Methods of Dendrochronology: Applications in the Environmental Sciences*, eds E. R. Cook and L. A. Kairiukštis (Boston: Kluwer Academic Publishers), 123–132.

Copini, P., Ouden, J., Robert, E. M. R., Tardif, J. C., Loesberg, W. A., Goudzwaard, L., et al. (2016). Flood-ring formation and root development in response to experimental flooding of young *Quercus robur* trees. *Front. Plant Sci.* 7, 1–14. doi: 10.3389/fpls.2016.00775

Corcuera, L., Camareo, J. J., and Gil-Pelegrin, E. (2004). Effects of a severe drought on growth and wood anatomical properties of *Quercus faginea*. *IAWA J.* 25, 185–204. doi: 10.1163/22941932-90000360

Corcuera, L., Camareo, J. J., Siso, S., and Gil-Pelegrin, E. (2006). Radial-growth and wood-anatomical changes in overaged *Quercus pyrenaica* coppice stands: functional responses in a new Mediterranean landscape. *Trees* 20, 91–98. doi: 10.1007/s00468-005-0016-4

Crivellaro, A., Reverenna, M., Ruffinatto, F., Urbinati, C., and Piermattei, A. (2018). The anatomy of "blue ring" in the wood of *Pinus nigra*. *Les/Wood* 67, 21–28. doi: 10.26614/les-wood.2018.v67n02a02

Daubois, V., Roy, M., Veillette, J. J., and Ménard, M. (2015). The drainage of Lake Ojibway in glaciolacustrine sediments of northern Ontario and Quebec, Canada. *Boreas* 44, 305–318. doi: 10.1111/bor.12101

Davis, D., and Loader, N. J. (2020). An evaluation of english oak earlywood vessel area as a climate proxy in the UK. *Dendrochronologia* 64:125777. doi: 10.1016/j.dendro.2020.125777

De Micco, V., Campelo, F., de Luis, M., Bräuning, A., Grabner, M., Battipaglia, G., et al. (2016). Formation of intra-annual-density-fluctuations in tree rings: how, when, where and why? *IAWA J.* 37, 232–259. doi: 10.1163/22941932-20160132

Ding, W.-D., Koubaa, A., Chaala, A., Belem, T., and Krause, C. (2008). Relationship between wood porosity, wood density and methyl methacrylate impregnation rate. *Wood Mat. Sci. Eng.* 1–2, 62–70. doi: 10.1080/17480270802607947

Estilow, T., Young, A., and Robinson, D. (2015). A long-term northern hemisphere snow cover extent data record for climate studies and monitoring. *Earth Syst. Sci. Data* 7, 137–142. doi: 10.5194/essd-7-137-2015

Fletcher, J. M. (1975). Relation of abnormal earlywood in oaks to dendrochronology and climatology. *Nature* 254, 506–507. doi: 10.1038/254506a0

Fonti, P., Eilmann, B., García-González, I., and von Arx, G. (2009a). Expeditious building of ring porous earlywood vessel chronologies without losing signal information. *Trees* 23, 665–671. doi: 10.1007/s00468-008-0310-z

Fonti, P., Treydte, K., Osenstetter, S., Frank, D., and Esper, J. (2009b). Frequency-dependent signals in multi-centennial oak vessel data. *Palaeogeogr. Palaeoclimatol. Palaeoecol.* 275, 92–99. doi: 10.1016/j.palaeo.2009.02.021

Fonti, P., and García-González, I. (2004). Suitability of chestnut earlywood vessel chronologies for ecological studies. *New Phytol.* 163, 77–86. doi: 10.1111/j.1469-8137.2004.01089.x

Fonti, P., and García-González, I. (2008). Earlywood vessel size of oak as a potential proxy for spring precipitation in mesic sites. *J. Biogeogr.* 35, 2249–2257. doi: 10.1111/j.1365-2699.2008.01961.x

Fonti, P., von Arx, G., Garcia-Gonzalez, I., Eilmann, B., Sass-Klaassen, U., Gartner, H., et al. (2010). Studying global change through investigation of the plastic responses of xylem anatomy in tree rings. *New Phytol.* 185, 42–53. doi: 10.1111/j.1469-8137.2009.03030.x

Fraser, D. A. (1958). Growth mechanisms in hardwoods. *Pulp Paper Mag.* 1958, 202–209.

García-González, I., and Eckstein, D. (2003). Climatic signal of earlywood vessels of oak on a maritime site. *Tree Physiol.* 23, 497–504. doi: 10.1093/treephys/23.7.497

García-González, I., and Fonti, P. (2006). Selecting earlywood vessels to maximize their environmental signal. *Tree Physiol.* 26, 1289–1296. doi: 10.1093/treephys/26.10.1289

García-González, I., and Fonti, P. (2008). Ensuring a representatives sample of earlywood vessels for dendroecological studies: an example from two ring-porous species. *Trees* 22, 237–244. doi: 10.1007/s00468-007-0180-9

García-González, I., and Souto-Herrero, M. (2017). Earlywood vessel area of Quercus pyrenaica Willd. is a powerful indicator of soil water excess at growth resumption. *Eur. J. For. Res.* 136, 329–344. doi: 10.1007/s10342-017-1035-6

García-González, I., Souto-Herrero, M., and Campelo, F. (2016). Ring porosity and earlywood vessels: a review on extracting environmental information through time. *IAWA J.* 37, 295–314. doi: 10.1163/22941932-20160135

Gärtner, H., Lucchinetti, S., and Schweingruber, F. H. (2014). New perspectives for wood anatomical analysis in Dendrosciences: the GSL1-microtome. *Dendrochronologia* 32, 47–51. doi: 10.1016/j.dendro.2013.07.002

Gärtner, H., Lucchinetti, S., and Schweingruber, F. H. (2015a). A new sledge microtome to combine wood anatomy and tree-ring ecology. *IAWA J.* 36, 452–459. doi: 10.1163/22941932-20150114

Gärtner, H., Cherubini, P., Fonti, P., Von Arx, G., Schneider, L., Nievergelt, D., et al. (2015b). A technical perspective in modern tree-ring research - how to overcome dendroecological and wood anatomical challenges. *J. Vis. Exp.* 97:e52337. doi: 10.3791/52337

Gärtner, H., and Nievergelt, D. (2010). The core-microtome: a new tool for surface preparation on cores and time series analysis of varying cell parameters. *Dendrochronologia* 28, 85–92. doi: 10.1016/j.dendro.2009.09.002

Gärtner, H., and Schweingruber, F. H. (2013). *Microscopic Preparation Techniques for Plant Stem Analysis*. Verlag Dr. Kessel, Remagen.

Ghiggi, G., Humphrey, V., Seneviratne, S. I., and Gudmundsson, L. (2019). GRUN: an observation-based global gridded runoff dataset from 1902 to 2014, Earth Syst. *Sci. Data* 11, 1655–1674. doi: 10.5194/essd-11-1655-2019

González-González, B .D., Vázquez-Ruiz, R. A., and García-González, I. (2015). Effects of climate on earlywood vessel formation of *Quercus robur* and *Q. pyrenaica* at a site in the northwestern Iberian Peninsula. *Can. J. For. Res.* 45, 698–709. doi: 10.1139/cjfr-2014-0436

González-González, B. D., Rozas, V., García-González, I. (2014). Earlywood vessels of the sub-Mediterranean oak *Quercus pyrenaica* have greater plasticity and sensitivity than those of the temperate *Q. petraea* at the Atlantic-Mediterranean boundary. *Trees*. 28, 237–252. doi: 10.1007/s00468-013-0945-2

Gričar, J., de Luis, M., Hafner, P., and Levanič, T. (2013). Anatomical characteristics and hydrologic signals in tree-rings of oaks (*Quercus robur* L.). *Trees* 27, 1669–1680. doi: 10.1007/s00468-013-0914-9

Harris, I., Osborn, T., Jones, P., and Lister, D. (2020). Version 4 of the CRUTS monthly high-resolution gridded multivariate climate dataset. *Sci. Data* 7, 1–18. doi: 10.1038/s41597-020-0453-3

Holmes, R. L. (1983). Computer-assisted quality control in tree-ring dating and measuring. *Tree-Ring Bull.* 43, 69–78.

Huber, F. (1993). Déterminisme de la surface des vaisseaux du bois des chênes indigènes (*Quercus robur* L., *Quercus petraea* Liebl.). Effet individuel, effet de l'appareil foliaire, des conditions climatiques et de l'âge de l'arbre. *Ann. For. Sci.* 50, 509–524. doi: 10.1051/forest:19930507

Junghans, U., Langenfeld-Heyser, R., Polle, A., and Teichmann, T. (2004). Effect of auxin transport inhibitors and ethylene on the wood anatomy of poplar. *Plant Biol.* 6, 22–29. doi: 10.1055/s-2003-44712

Kames, S. (2009). *Sensitivity of Vessels in Black Ash (Fraxinus nigra Marsh.) Tree Rings to Fire and Hydro-Climatic Variables*. (M.Sc. Thesis), Department of Botany, University of Manitoba, Winnipeg, MB, Canada.

Kames, S., Tardif, J. C., and Bergeron, Y. (2011). Anomalous earlywood vessel lumen area in black ash (*Fraxinus nigra* Marsh.) tree rings as a potential indicator of forest fires. *Dendrochronologia* 29, 109–114. doi: 10.1016/j.dendro.2009.10.004

Kames, S., Tardif, J. C., and Bergeron, Y. (2016). Continuous earlywood vessels chronologies in floodplain ring-porous species can improve dendrohydrological reconstructions of spring high flows and flood levels. *J. Hydrol.* 534, 377–389. doi: 10.1016/j.jhydrol.2016.01.002

Koprowski, M., Okoński, B., Gričar, J., and Puchałka, R. (2018). Streamflow as an ecological factor influencing radial growth of European ash [*Fraxinus excelsior* (L.)]. *Ecol. Indic.* 85, 390–399. doi: 10.1016/j.ecolind.2017.09.051

Land, A., Wehr, M., Roelfs, K. U., Epkes, S., Reichle, D., and Kauer, G. (2017). A novel computer-aided tree-ring analysis software (CATS): oak earlywood vessel size reveals a clear spring heat sum response. *Trees* 31, 1683–1695. doi: 10.1007/s00468-017-1578-7

Lechowicz, M. J. (1984). Why do deciduous trees leaf out at different times? Adaptation and ecology of forest communities. *Am. Nat.* 124, 821–842. doi: 10.1086/284319

Legendre, P., and Legendre, L. (1998). *Numerical Ecology, 2nd Edn*. New York, NY: Elsevier Scientific Publishing Co., 853.

Meko, M. D., and Therrell, M. D. (2020). A record of flooding on the White River, Arkansas derived from tree-ring anatomical variability and vessel width. *Phys. Geogr.* 41, 83–98. doi: 10.1080/02723646.2019.1677411

Mongrain, S. (2014). Dates de dégel du lac Duparquet. *Le Grand Héron Le Journal de Duparquet*. 19:6.

Nolin, A. F., Tardif, J. C., Conciatori, F., and Bergeron, Y., (accepted). Flood-ring production modulated by river regulation in eastern boreal Canada. *Front. Plant Sci.*

Nolin, A. F., Tardif, J. C., Kames, S., Conciatori, F., Meko, D., and Bergeron, Y. (2021a). Multi-century tree-ring anatomical evidence reveals increasing frequency and magnitude of spring discharge and floods in eastern boreal Canada. *Glob. Planet. Change* 199:103444. doi: 10.1016/j.gloplacha.2021.103444

Nolin, A., Tardif, J. C., Conciatori, F., and Bergeron, Y. (2021b). Spatial coherency of the spring flood signal among major river basins of eastern boreal Canada inferred from flood rings. *J. Hydrol.* 596:126084. doi: 10.1016/j.jhydrol.2021.126084

Pallardy, S. G. (2008). *Physiology of Woody Plants, 3rd Edn.* Burlington, San Diego, London: Academic Press, 454.

Panshin, A. J., and de Zeeuw, C. (1980). *In Textbook of Wood Technology: Structure, Identification, Properties, and Uses of the Commercial Woods of the United States and Canada*. New York, NY: McGraw-Hill Publishing Company, 722.

Pérez-de-Lis, G., Rozas, V., Vázquez-Ruiz, R. A., and García-González, I. (2018). Do ring-porous oaks prioritize earlywood vessel efficiency over safety? Environmental effects on vessel diameter and tyloses formation. *Agric. For. Meteorol.* 248, 205–214. doi: 10.1016/j.agrformet.2017.09.022

Phipps, R. L. (1985). "Collecting, preparing, crossdating, and measuring tree increment cores," in *USGS Water-Resources Investigations Report 85-4148* (Virginia: U.S. Geological Survey). doi: 10.3133/wri854148

Pritzkow, C., Wazny, T., Heußner, K. U., Słowiński, M., Bieber, A., Dorado Liñán, I., et al. (2016). Minimum winter temperature reconstruction from average earlywood vessel area of European oak (*Quercus robur*) in N-Poland. *Palaeo.* 449, 520–530. doi: 10.1016/j.palaeo.2016.02.046

Puchałka, R., Koprowski, M., Gričar, J., and Przybylak, R. (2017). Does tree-ring formation follow leaf phenology in Pedunculate oak (*Quercus robur* L.)? *Eur. J. For. Res.* 136, 259–268. doi: 10.1007/s10342-017-1026-7

Régent Instruments Inc. (2005). *WinCell Pro Version 2004a User Manual*. Quebec.

Rueden, C. T., Schindelin, J., Hiner, M. C., DeZonia, B. E., Walter, A. E., Arena, E. T., et al. (2017). ImageJ2: ImageJ for the next generation of scientific image data. *BMC Bioinform.* 18:529. doi: 10.1186/s12859-017-1934-z

Sass-Klaassen, U. (2009). "Combining phenology, cambial analysis and vessel-size analysis to understand the effect of flooding on oak and ash," in *Workshop Monitoring Seasonal Dynamic of Wood Formation. Otocec, Slovenia, April 20–22nd*.

Sass-Klaassen, U., Sabajo, C., Belien, E., and den Ouden, J. (2010). "Effect of experimental flooding on vessel area of pedunculate oak and common ash—a matter of timing," in *WorldDendro 2010: The 8th International Conference on Dendrochronology*, eds K. Mielikäinen, H. Mäkinen, and M. Timonen (Rovaniemi: Finnish Forest Research Institute (Metla)), 155. Available online at: http://www.metla.fi/tapahtumat/2010/WD2010/abstraktikirja.pdf

Sass-Klaassen, U., Sabajo, C. R., and den Ouden, J. (2011). Vessel formation in relation to leaf phenology in Pedunculate oak and European ash. *Dendrochronologia* 29, 171–175. doi: 10.1016/j.dendro.2011.01.002

Savidge, R. A. (1988). Auxin and ethylene regulation of diameter growth in trees. *Tree Physiol.* 4, 401–414. doi: 10.1093/treephys/4.4.401

Scholz, A., Klepsch, M., Karimi, Z., and Jansen, S. (2013). How to quantify conduits in wood? *Front. Plant Sci.* 4, 1–11. doi: 10.3389/fpls.2013.00056

Sims, R. A., Kershaw, H. M., and Wickware, G. M. (1990). *The Autecology of Major Tree Species in the North Central Region of Ontario. COFRDA Report 3302. NWOFTU Tech. Rep. 48, Ottawa*, 95–99.

St. George, S., and Nielsen, E. (2000). Signatures of high-magnitude 19th-century floods in *Quercus macrocarpa* tree rings along the Red River, Manitoba, Canada. *Geology* 28, 899–902. doi: 10.1130/0091-7613(2000)28<899:SOHTFI>2.0.CO;2

St. George, S., and Nielsen, E. (2002). Flood ring evidence and its application to paleoflood hydrology of the Red River and Assiniboine River in Manitoba. *Geogr. Phys. Quatern.* 56, 181–190. doi: 10.7202/009104ar

St. George, S., and Nielsen, E. (2003). Paleoflood records for the Red River, Manitoba, Canada, derived from tree-ring signatures. *Holocene* 13, 547–555. doi: 10.1191/0959683603hl645rp

St. George, S., Nielsen, E., Conciatori, F., and Tardif, J. (2002). Trends in *Quercus macrocarpa* vessel areas and their implications for tree-ring paleofloods studies. *Tree-Ring Res.* 58, 3–10. Available online at: https://repository.arizona.edu/handle/10150/262561

Tardif, J., and Bergeron, Y. (1992). Analyse écologique des peuplements de frêne noir (*Fraxinus nigra* Marsh.) des rives du lac Duparquet, nord-ouest du Québec. *Can. J. Bot.* 70, 2294–2302. doi: 10.1139/b92-285

Tardif, J., and Bergeron, Y. (1993). Radial growth of *Fraxinus nigra* in a Canadian boreal floodplain in response to climatic and hydrologic fluctuations. *J. Veg. Sci.* 4, 751–758. doi: 10.2307/3235611

Tardif, J., and Bergeron, Y. (1997a). Ice-flood history reconstructed with tree rings from the southern boreal forest limit, western Québec. *Holocene* 3, 291–300. doi: 10.1177/095968369700700305

Tardif, J., and Bergeron, Y. (1997b). Comparative dendroclimatological analysis of two black ash and two white cedar populations from contrasting sites in the lake Duparquet region, northwestern Québec. *Can. J. For. Res.* 27, 108–116. doi: 10.1139/x96-150

Tardif, J., and Bergeron, Y. (1999). Population dynamics and radial growth of black ash (*Fraxinus nigra* Marsh.) in response to flood-level variations in a boreal floodplain, northwestern Québec. *Ecol. Monogr.* 69, 107–125. doi: 10.1890/0012-9615(1999)0690107:PDOFNI2.0.CO;2

Tardif, J. C. (1996). "Earlywood, latewood and total ring width of a ring-porous species (*Fraxinus nigra* Marsh.) in relation to climate and hydrologic factors," in *Tree Rings, Environment and Humanities*, eds J. S. Dean, D. M. Meko, and T. W. Swetnam (Tucson, AZ: Radiocarbon University of Arizona), 315–324.

Tardif, J. C., and Conciatori, F. (2006). Influence of climate on tree rings and vessel features in red oak and white oak growing near their northern distribution limit, southwestern Québec, Canada. *Can. J. For. Res.* 36, 2317–2330. doi: 10.1139/x06-133

Tardif, J. C., and Conciatori, F. (2015). "Microscopic examination of wood: sample preparation and techniques for light microscopy," in *Plant Microtechniques and Protocols*, eds E. C. T. Yeung, C. Stasolla, M. J. Sumner, and B. Q. Huang (Cham: Springer), 373–415. doi: 10.1007/978-3-319-19944-3_22

Tardif, J. C., Dickson, H., Conciatori, F., Nolin, A. F., and Bergeron Y. (2021). Are periodic (intra-annual) tangential bands of vessels in diffuse-porous tree species the equivalent of flood rings in ring-porous species: reproducibility and cause? *Dendrochronologia.* doi: 10.1016/j.dendro.2021.125889

Tardif, J. C., Kames, S., and Bergeron, Y. (2010). "Spring water levels reconstructed from ice-scarred trees and cross-sectional area of the earlywood vessels in tree rings from eastern boreal Canada," in *Tree Rings and Natural Hazards: A State-of-the-Art*, eds M. Stoffel, M. Bollschweiler, D. Butler, B. Luckman (Netherlands: Springer), 257–261. doi: 10.1007/978-90-481-8736-2

Tardif, J. C., Salzer, M. W., Conciatori, F., Bunn, A. G., and Hughes, M. K. (2020). Formation, structure and climatic significance of blue rings and frost rings in high elevation bristlecone pine (*Pinus longaeva* D.K. Bailey). *Quat. Sci. Rev.* 244:106516. doi: 10.1016/j.quascirev.2020.106516

ter Braak, C. J. F., and Šmilauer, P. (2018). *Canoco Reference Manual and User's Guide: Software for Ordination, Version 5.10*. Wageningen: Biometris, Wageningen University & Research.

Therrell, M. D., and Bialecki, M. B. (2015). A multi-century tree-ring record of spring flooding on the Mississippi River. *J. Hydrol.* 529, 490–498. doi: 10.1016/j.jhydrol.2014.11.005

Thomas, F. M., Bartels, C., and Gieger, T. (2006). Alterations in vessel size in twigs of *Quercus robur* and *Q. petraea* upon defoliation and consequences for water transport under drought. *IAWA J.* 27, 395–407. doi: 10.1163/22941932-90000162

Trouet, V., and Oldenborgh, G. (2013). KNMI climate explorer: a web-based research tool for high-resolution paleoclimatology. *Tree-Ring Res.* 69, 3–13. doi: 10.3959/1536-1098-69.1.3

Tumajer, J., and Treml, V. (2016). Response of floodplain pedunculate oak (*Quercus robur* L.) tree-ring width and vessel anatomy to climatic trends and extreme hydroclimatic events. *For. Ecol. Manag.* 379, 185–194. doi: 10.1016/j.foreco.2016.08.013

Tuominen, H., Sitbon, F., Jacobsson, C., Sandberg, G., Olsson, O., and Sundberg, B. (1995). Altered growth and wood characteristics in transgenic hybrid aspen expressing *Agrobacterium tumefaciens* T-DNA indoleacetic acid-biosynthetic genes. *Plant Physiol.* 109, 1179–1189. doi: 10.1104/pp.109.4.1179

Vicente-Serrano, S. M., Beguería, S., and López-Moreno, J. I. (2010). A multiscalar drought index sensitive to global warming: the standardized precipitation evapotranspiration index. *J. Clim.* 23, 1696–1718. doi: 10.1175/2009JCLI2909.1

Villar-Salvador, P., Castro-Díez, P., Pérez-Rontomé, C., *and* Montserrat-Martí, G. (1997). Stem xylem features in three Quercus (Fagaceae) species along a climatic gradient in NE Spain. *Trees* 12, 90–96. doi: 10.1007/PL00009701

von Arx, G., and Carrer, M. (2014). ROXAS - a new tool to build centuries-long tracheid-lumen chronologies in conifers. *Dendrochronologia* 32, 290–293. doi: 10.1016/j.dendro.2013.12.001

von Arx, G., Crivellaro, A., Prendin, A. L., Cufar, K., and Carrer, M. (2016). Quantitative wood anatomy - practical guidelines. *Front. Plant Sci.* 7:781. doi: 10.3389/fpls.2016.00781

von Arx, G., Kueffer, C., and Fonti, P. (2013). Quantifying plasticity in vessel grouping - added value from the image analysis tool ROXAS. *IAWA J.* 34, 433–445. doi: 10.1163/22941932-00000035

von Arx, G., Stritih, A., Cufar, K., Crivellaro, A., and Carrer, M. (2015). *Quantitative Wood Anatomy: From Sample to Data for Environmental Research*.

Waito, J., Conciatori, F., and Tardif, J. C. (2013). Frost rings and white earlywood rings in *Picea mariana* trees from the boreal plains, Central Canada. *IAWA J.* 34, 71–87. doi: 10.1163/22941932-00000007

Wertz, E., St. George, S., and Zeleznik, J. (2013). Vessel anomalies in *Quercus macrocarpa* tree rings associated with recent flood s along the Red River of the North, United States. *Water Resour. Res.* 49, 630–634. doi: 10.1029/2012WR012900

Wimmer, R. (2002). Wood anatomical features in tree-rings as indicators of environmental change. *Dendrochronologia* 20, 21–36. doi: 10.1078/1125-7865-00005

Woodcock, D. W. (1989). Climate sensitivity of wood-anatomical features in a ring-porous oak (*Quercus macrocarpa*). *Can. J. For. Res.* 19, 639–644. doi: 10.1139/x89-100

Wright, J. W., and Rauscher, H. M. R. (1990). "Black ash," in *Silvics of North America. Volume 2, Hardwoods. Agricultural Handbook 654*, eds R. M. Burns and B. H. Honkala (Washington, DC: USDA), 344–347.

Yamamoto, F., Angeles, G., and Kozlowski, T. T. (1987). Effect of ethrel on stem anatomy of *Ulmus americana* seedlings. *IAWA Bull.* 8, 3–9. doi: 10.1163/22941932-90001018

Yamamoto, F., and Kozlowski, T. T. (1987). Effects of flooding, tilting of stems, and ethrel application on growth, stem anatomy, and ethylene production of *Acer platanoides* seedlings. *Scand. J. For. Res.* 2, 141–156. doi: 10.1080/02827588709382453

Yamamoto, F., Sakata, T., and Terazawa, K. (1995). Physiological, morphological and anatomical responses of *Fraxinus mandshurica* seedlings to flooding. *Tree Physiol.* 15, 713–719. doi: 10.1093/treephys/15.11.713

Yanosky, T. M. (1983). Evidence of floods on the Potomac River from anatomical anomalies in the wood of flood-plain trees. *U.S. Geol. Surv. Prof. Pap.* 1296:42. doi: 10.3133/pp1296

Zasada, J. C., and Zahner, R. (1969). Vessel element development in the earlywood of red oak (*Quercus rubra*). *Can. J. Bot.* 47, 1965–1971. doi: 10.1139/b69-288

Zhu, L., Cooper, D. J., Yuan, D., Li, Z., Zhang, Y., Liang, H., et al. (2020). Regional scale weather than precipitation determines vessel features in earlywood of Manchurian ash in temperate forests. *J. Geophys. Res. Biogeosci.* 125:e05955. doi: 10.1029/2020JG005955

Conflict of Interest: The authors declare that the research was conducted in the absence of any commercial or financial relationships that could be construed as a potential conflict of interest.

Publisher's Note: All claims expressed in this article are solely those of the authors and do not necessarily represent those of their affiliated organizations, or those of the publisher, the editors and the reviewers. Any product that may be evaluated in this article, or claim that may be made by its manufacturer, is not guaranteed or endorsed by the publisher.

frontiers in Plant Science

ORIGINAL RESEARCH
published: 25 October 2021
doi: 10.3389/fpls.2021.748055

Direct and Indirect Effects of Environmental Limitations on White Spruce Xylem Anatomy at Treeline

Timo Pampuch[1], Alba Anadon-Rosell[1,2], Mario Trouillier[1], Jelena Lange[1,3] and Martin Wilmking[1]*

[1] Institute of Botany and Landscape Ecology, University Greifswald, Greifswald, Germany, [2] CREAF – Centre for Research on Ecology and Forestry Applications, Barcelona, Spain, [3] Department of Physical Geography and Geoecology, Charles University in Prague, Prague, Czechia

Treeline ecosystems are of great scientific interest to study the effects of limiting environmental conditions on tree growth. However, tree growth is multidimensional, with complex interactions between height and radial growth. In this study, we aimed to disentangle effects of height and climate on xylem anatomy of white spruce [*Picea glauca* (Moench) Voss] at three treeline sites in Alaska; i.e., one warm and drought-limited, and two cold, temperature-limited. To analyze general growth differences between trees from different sites, we used data on annual ring width, diameter at breast height (DBH), and tree height. A representative subset of the samples was used to investigate xylem anatomical traits. We then used linear mixed-effects models to estimate the effects of height and climatic variables on our study traits. Our study showed that xylem anatomical traits in white spruce can be directly and indirectly controlled by environmental conditions: hydraulic-related traits seem to be mainly influenced by tree height, especially in the earlywood. Thus, they are indirectly driven by environmental conditions, through the environment's effects on tree height. Traits related to mechanical support show a direct response to environmental conditions, mainly temperature, especially in the latewood. These results highlight the importance of assessing tree growth in a multidimensional way by considering both direct and indirect effects of environmental forcing to better understand the complexity of tree growth responses to the environment.

Keywords: boreal forest, conduit reinforcement, drought limitation, hydraulic stability, *Picea glauca*, temperature limitation, tree allometry, tree height

OPEN ACCESS

Edited by:
Marco Carrer, University of Padua, Italy

Reviewed by:
Anna Lintunen, University of Helsinki, Finland
Tim Rademacher, Harvard University, United States

****Correspondence:***
Timo Pampuch
timo.pampuch@uni-greifswald.de

Specialty section:
This article was submitted to Functional Plant Ecology, a section of the journal Frontiers in Plant Science

Received: *27 July 2021*
Accepted: *04 October 2021*
Published: *25 October 2021*

Citation:
Pampuch T, Anadon-Rosell A, Trouillier M, Lange J and Wilmking M (2021) Direct and Indirect Effects of Environmental Limitations on White Spruce Xylem Anatomy at Treeline. Front. Plant Sci. 12:748055. doi: 10.3389/fpls.2021.748055

INTRODUCTION

Boreal forests play a crucial role for the global carbon cycle, are an important source for timber and non-timber products and provide several ecosystem services (Arneth et al., 2010; Gauthier et al., 2015; Tagesson et al., 2020). Yet they are particularly challenged by global warming. The effects of global warming are assumed to be more severe in areas of high latitude (Soja et al., 2007; Charney et al., 2016; IPCC, 2021), such as parts of Canada and Alaska, and will certainly have a lasting impact on boreal forest ecosystems. Especially trees that are growing under marginal conditions, i.e., at treelines, will be influenced by climate change. Treelines are characterized as the edge of the habitat at which trees are able to grow. This edge is caused by environmental limitations

like low temperatures or drought (Brockmann-Jerosch, 1919; Däniker, 1932). With climate change, the conditions at treelines are expected to shift, with drastic consequences for tree growth, spatial distribution and dynamics of treeline populations (Grace et al., 2002; Wieser, 2020). In order to evaluate how trees at treelines respond to these rapid shifts, we need to understand the impacts of changing environmental conditions on tree growth.

White spruce is one of the most important and widespread tree species of the North American boreal forest (Little and Viereck, 1971). It grows under a variety of environmental conditions, making it a model organism for investigating the influence of climate on tree growth (Lloyd and Fastie, 2002; Wilmking and Juday, 2005; Sherriff et al., 2017). Most previous studies on white spruce have focused on the growth performance and total annual growth using tree ring-based analyses. However, to understand the complexity of growth and how environmental conditions influence trees in multiple ways, more holistic approaches at intra-annual resolution are needed, e.g., by including investigations on phenology, xylogenesis or xylem anatomy. While collecting data on phenology and xylogenesis is labor intensive and requires regular monitoring, xylem anatomical analyses can be performed retrospectively using typical increment cores. Xylem is multifunctional as it is responsible for conducting water from the roots, through the stem to the leaves and to provide the structural support of a tree (Domec and Gartner, 2002; Hacke et al., 2015). The benefit of studying the structure of this multifunctional tissue is that it can provide deeper insights into inter- and intra-annual variation of growth and how different parts of a tree ring are influenced by environmental conditions and by biotic factors at different times (Fonti et al., 2010; von Arx et al., 2016). On the one hand, it is well known that xylem anatomical traits that are linked to water transport, like lumen area, are influenced by tree height, especially in earlywood (Callaham, 1962; Anfodillo et al., 2006; Carrer et al., 2015). With up to 90% of the total water flow, water transport is mainly occurring through the earlywood tracheids (Domec and Gartner, 2002), making the structure of the earlywood tracheids potentially sensitive to changes in the water availability. Tracheids with smaller lumen are known to occur as an adjustment toward dry conditions to avoid drought induced cavitation (Cochard, 2006; Eldhuset et al., 2013) and thus drought-induced damage to the tree. Yet to secure a safe water transport in the earlywood, also the so-called conduit widening is an important driver that influences the tracheid structure. Conduit widening means that with increasing vertical path length (i.e., tree height) the lumen area widens from the apex to the base to maintain a constant hydraulic resistance along the path (Sanio, 1872; Mencuccini et al., 2007; Anfodillo et al., 2013; Kašpar et al., 2019). On the other hand, traits related to structural integrity (i.e., the ability of a structure to support a certain weight and/or force without being damaged) like xylem cell wall thickness (CWT) are largely driven by climatic conditions, especially in latewood (Antonova and Stasova, 1993; Yasue et al., 2000; Fonti et al., 2013; Cuny and Rathgeber, 2016). In the latewood structure of conifers, water transport is less important and cell wall deposition take place to a greater extent. Cell wall deposition and thus the resulting thickness of the cell wall is a temperature sensitive process. With higher temperatures, the processes can occur faster and thicker cell walls might be build and vice versa, making the latewood potentially more sensible toward climatic changes (Yasue et al., 2000; Fonti et al., 2013; Björklund et al., 2020). However, different xylem anatomical traits are also linked to each other and function in multiple dimensions. For example, although lumen area is mainly influenced by tree height and CWT is mainly influenced by climatic conditions, CWT is also linked to lumen area, due to physiological limitations. I.e., if a certain amount of resources is available for cell wall deposition, the maximum functional cell-size (i.e., functional in way that the cell is capable to efficiently transport water and provide structural support) is limited by this amount. Building smaller cells using the exact same amount of resources would result in cells with thicker walls, due to a surplus of available material (Cuny et al., 2014). This relation inevitably influences traits that are derived both from cell wall and lumen measurements, such as wood density and the conduit reinforcement index (Hacke and Sperry, 2001; Hacke et al., 2001; Pittermann et al., 2006). This complexity makes the analysis of these traits challenging and requires careful interpretation. A comprehensive study approach that combines xylem anatomical investigations with modeling helps to disentangle and better understand the underlying patterns.

Here, we investigate the multifunctionality (i.e., water transport and structural integrity) and multidimensionality of xylem anatomy in white spruce by studying the effects of tree height (i.e., vertical dimension), precipitation, and temperature on four xylem anatomical traits (lumen area, conduit reinforcement index, anatomical wood density, and CWT) separated into earlywood and latewood (i.e., temporal dimension) of 18 individuals from three treeline sites (two temperature-limited and one drought-limited) in Alaska. We expected to find that (1) earlywood traits related to water transport would be strongly influenced by tree height due to the importance of earlywood for water transport, while (2) latewood traits related to structural integrity would be mainly influenced by climatic conditions, since climate-sensitive processes like cell wall deposition have a larger effect during latewood formation. We additionally assumed that trees from the drought-limited treeline would have (3) smaller lumen areas compared to trees from the temperature-limited sites as a strategy to lower the risk of cavitation (Cochard, 2006; Eldhuset et al., 2013) and (4) thicker cell walls due to the higher temperatures during the vegetation period, as well as longer vegetation periods at the drought-limited treeline, which would lead to an increased level of cell wall deposition (Fonti et al., 2013; Björklund et al., 2020).

MATERIALS AND METHODS

Study Species and Study Sites

White spruce [*Picea glauca* (Moench) Voss] is a widely distributed tree species in the boreal forests of North America. It is of large economic importance (Attree et al., 1991) and its distributional range covers most of the boreal area in Canada and Alaska, and parts of the northernmost US mainland (Little and Viereck, 1971; **Supplementary Figure 1**). White spruce

is the dominant tree species at the elevational and latitudinal treeline in the north-western parts of its distributional range (Nienstaedt and Zasada, 1990; Abrahamson, 2015). We sampled white spruce trees at three study sites (**Supplementary Figure 1**), one treeline site where tree growth is mainly limited by drought and two treeline sites where tree growth is mainly limited by low temperatures. The presumably drought-limited treeline is located in Interior Alaska at a steep (12–34°) bluff of the Tanana River near Fairbanks—Warm—Dry Treeline (W-D; 64°42′ N, 148°18′ W). W-D is characterized by a very low precipitation but relatively high temperatures during the vegetation period (**Figure 1**), causing a potential water limitation (Barber et al., 2000; Juday et al., 2003; Lloyd et al., 2013). The first temperature-limited study site is a latitudinal treeline located on a slope of Nutirwik Creek valley in the central Brooks Range—Cold—Dry Treeline (C-D; 67°56′N, 149°44′W). At C-D, tree growth is mainly limited by low temperatures (Wilmking et al., 2017), yet the mean annual precipitation is comparably low as well, which could lead to occasional drought stress (**Figure 1**; Trouillier et al., 2019). The second temperature-limited site is in Denali National Park—Cold—Moist Treeline (C-M, 63°43′N, 149°00′W). At C-M, growth is mainly limited by low temperatures as it is a typical elevational treeline (Körner, 2007), while the precipitation is relatively high in comparison to the other study sites (**Figure 1**). All three study sites are located on south-facing slopes. For more details on the characteristics of the study sites see also Trouillier et al. (2018) and Zacharias et al. (2021).

Climate Data

Modeled historical monthly climate data (i.e., mean temperature and total precipitation sums) for the period of 1901–2015 were obtained from the Scenarios Network for Alaska and Arctic Planning at 1 × 1 km spatial resolution (SNAP, 2019; **Figure 1**). The climate data is based on a General Circulation Model (GCM) data set that was downscaled to 2 × 2 km gridded climate data using a Weather Research and Forecasting Model (WRF; Bieniek et al., 2016). The downscaled 2 × 2 km data was then resampled to a 1 × 1 km spatial resolution using bilinear interpolation (SNAP, 2019). To reduce the number of parameters in the models we averaged the mean temperature and total precipitation for each of the four seasons of the year. Tree growth at our study sites typically starts in May/June and presumably ceases toward the end of August (Ueyama et al., 2013), thus the seasons used in the analysis were defined as follows: previous fall (i.e., previous year September to previous year November), previous winter (i.e., previous year December to current year February), spring (March to May) and summer (June to August).

Sampling and Data Acquisition

Increment cores were originally collected in 2012 (Eusemann et al., 2016), 2015 and 2016 (Wilmking et al., 2017) from 1254 trees (W-D: 309 trees, C-D: 474 trees, C-M: 471 trees). We documented the diameter at breast height (DBH) and the total height of each individual once at the moment it was sampled. These samples were used for the general diameter-height analysis. All cores were taken with a 4.3 mm Haglöf increment borer (Haglöf, Sweden). Cores were air dried and glued onto wooden sample holders. The surfaces were either polished with progressively finer sandpaper (up to 800 grit) or cut with a core-microtome (Gärtner and Nievergelt, 2010), before they were digitized with a flatbed scanner (Epson Perfection V700 Photo; Seiko Epson Corporation, Japan) with 3,200 dpi. Tree-ring widths (TRW) were subsequently measured using CooRecorder (version 9.3.1; Cybis Elektronik and Data AB, Sweden) and all radii were cross-dated using CDendro (version 9.3.1; Cybis Elektronik and Data AB, Sweden).

To explore how tree growth differs between sites, we explored the relationship between tree's age, DBH and height: First, we fitted a modified Weibull function for each site to describe the relationship between DBH and tree height (Huang et al., 1992):

$$\text{Equation1} \qquad h_t = h_{max} * e^{(a * DBH_t{}^b)},$$

where h_t is the current tree height, h_{max} is the maximum height (asymptote) that a tree approaches, while the parameters a and b modulate how this asymptote is approached. The parameters were estimated in R v4.0.2 (R Core Team, 2020) with the nls2 R-package (Grothendieck, 2013). Next, we used the rcs function from the dplR package (Bunn, 2008) to estimate the relationship between ring width and tree age. Because the cumulative ring width is (half) the stem diameter, this function can also describe the stem diameter-age relationship. Thus, combined these functions describe the relationship between age, diameter and height for each site, which is the tree's ontological development over time. We used this relationship for the visualization of site differences and to guide the interpretation of the results.

For xylem anatomical analysis, six samples were selected each from the samples collected in 2012 at W-D and in 2015 at C-D. Six additional samples were collected in 2018 at C-M. All trees used for xylem anatomical analysis were selected from the available samples based on their height, being approximately similar (**Supplementary Table 1**). The samples were handled the same as the aforementioned samples of the entire set. Afterward we cut 12 μm-thin cross-sections from one radius of each tree using a rotary microtome (Leica RM 2245; Leica Camera AG, Germany). The cross-sections were stained with 1:1 safranin and astrablue solution, rinsed with ethanol solutions of increasing concentration (50, 70, 96%), mounted on microscope slides with Euparal and dried at 60°C for 48 h (Gärtner and Schweingruber, 2013). The slides were digitized with a Leica DFC450C camera installed on a Leica DM2500 microscope with a 10 × magnification objective (Leica 506505). We used the digitized images to quantify TRW and the xylem anatomical traits lumen area (LA), lumen diameter (LD), cell wall area (CWA), radial, tangential, mean CWT and conduit reinforcement index (TB^2) with the image analysis tool ROXAS v3.0.326 (von Arx and Carrer, 2014; Prendin et al., 2017).

TB^2 was calculated in ROXAS based on Hacke et al. (2001):

$$\text{Equation2} \qquad TB^2 = \left(\frac{T}{B}\right)^2,$$

where *T* is double CWT and *B* the length of the same cell wall. For each cell, the smaller of radial and tangential CWT measurements was selected (Hacke et al., 2001; von Arx and Carrer, 2014;

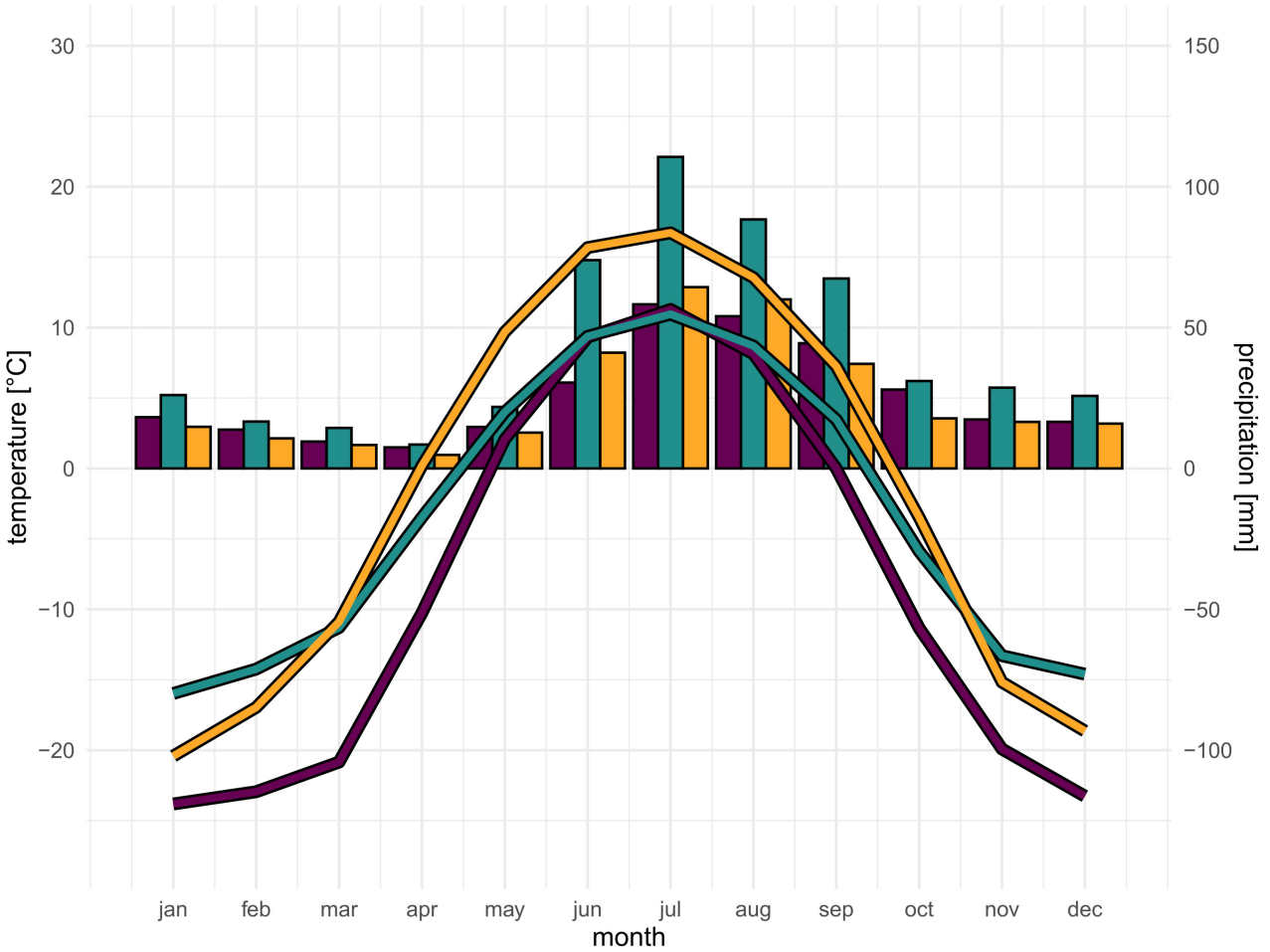

FIGURE 1 | Site-specific climatic conditions (SNAP, 2019). Bars showing precipitation sum per month, curve showing average temperature per month for the period 1970–2016. Purple = Brooks Range (C-D), Green = Denali National Park (C-M), Orange = Bluff (W-D).

Prendin et al., 2017). We approximated wood density (DEN) as the proportion of the estimated CWA to the total cell area (only including tracheid cells; i.e., the sum of CWA and LA; Eq. 3) according to Björklund et al. (2017):

$$\text{Equation3} \qquad \text{DEN} = \frac{\text{CWA}}{\text{CWA} + \text{LA}}$$

From all xylem anatomical traits, we selected two traits related to water transport (LA and TB^2) and two traits related to structural integrity (DEN and CWT) for further analysis. LA and CWT represent the two main functions of xylem tissue in conifers and their use has been reported in several previous studies (Prendin et al., 2017; Cuny et al., 2019; Puchi et al., 2020). TB^2 and DEN were chosen to represent those functions as well, while also including the link between LA and CWT to incorporate the multifunctionality of xylem tissue (Hacke et al., 2001; Myburg et al., 2013; von Arx and Carrer, 2014; Björklund et al., 2017). We used the measurements of lumen diameter and CWT to distinguish between early and latewood using Mork's index (Denne, 1989) and calculated annual means separately for earlywood and latewood for LA, TB^2, DEN and CWT using R v4.0.2 (R Core Team, 2020).

For the analysis on the selected xylem anatomical traits, we calculated individual tree height for each year (h_i) for each of the 18 trees that were used for anatomical investigations. In contrast to the calculations for the entire dataset, h_i for the xylem anatomy analysis was estimated based on a linear function of DBH. We used this linear approach to achieve a potentially more precise calculation of the approximate height for each tree and each year (and thus potentially more precise models), as we accounted for missing rings and the distance to pith from the first measured ring. The method was only valid because tree height of the trees sampled for xylem anatomical analysis was relatively low at the time of sampling and still in the rising leg of the asymptote characteristic for each stand (**Supplementary Table 1** and **Figure 2**). Annual DBH was calculated by subtracting double ring width cumulatively for each year until the first measured year. Missing rings were estimated by averaging the ring width

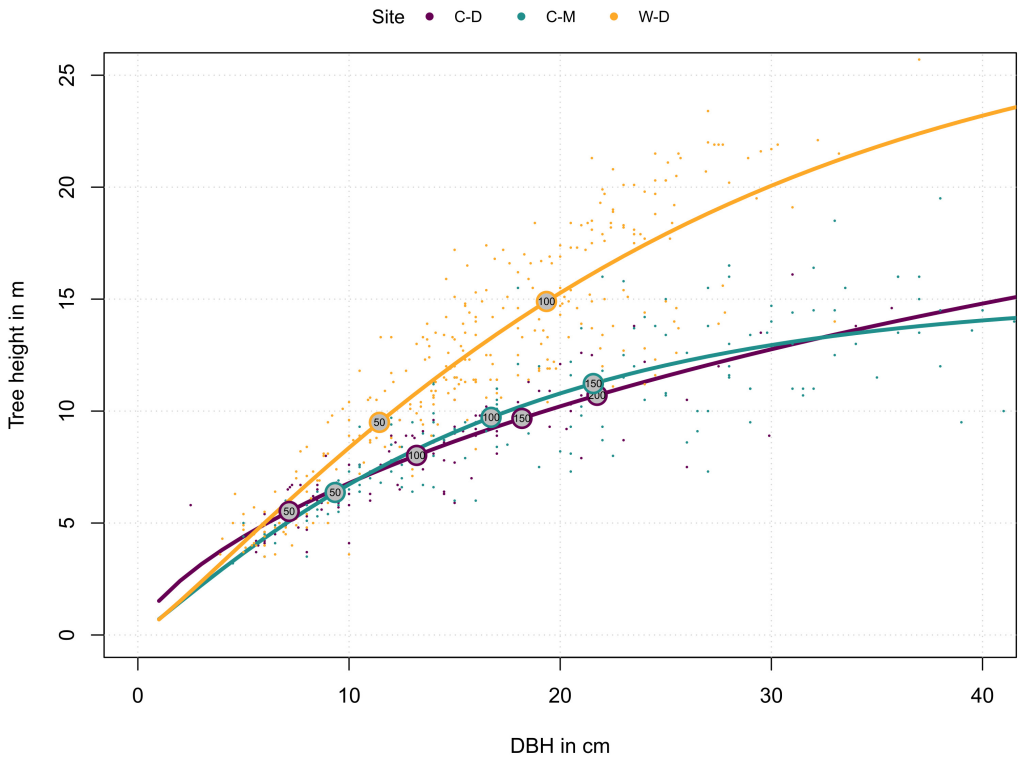

FIGURE 2 | Relationship of site-specific diameter at breast height (DBH) and tree height. Dots represent individual trees. Lines represent the site-specific means as described by the functions in the methods (Eqs. 1 and 2). Numbers in the circles indicate tree age. Purple = Brooks Range (C-D), Green = Denali National Park (C-M), Orange = Bluff (W-D).

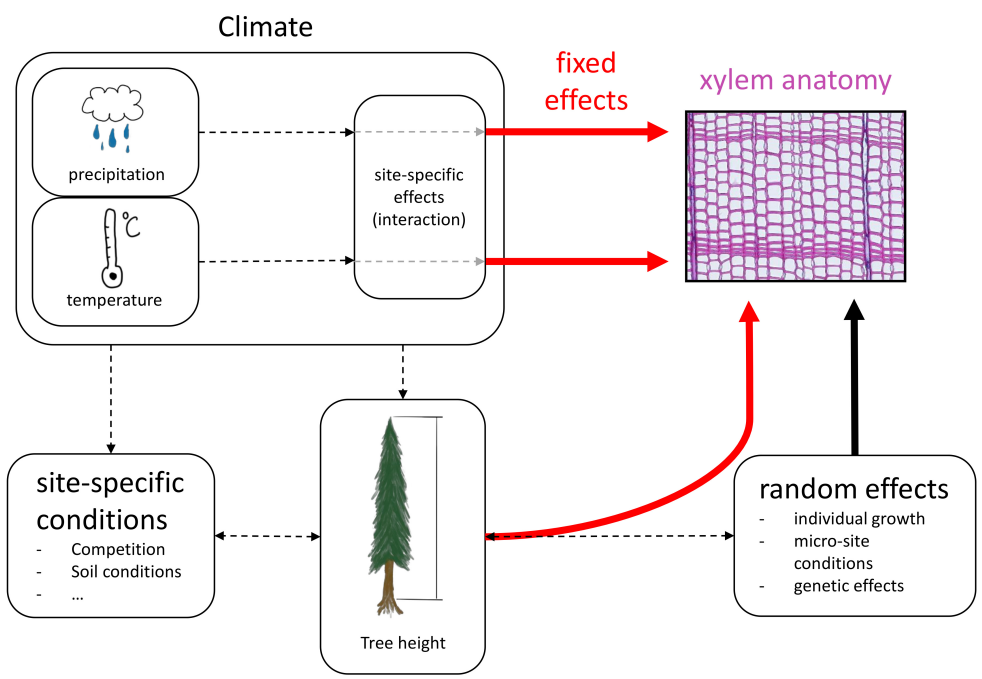

FIGURE 3 | Conceptual design of the linear mixed-effects model. Red arrows indicate fixed effects, the black arrow indicates random effects and black dashed arrows show interactions and effects that are not quantified in the models.

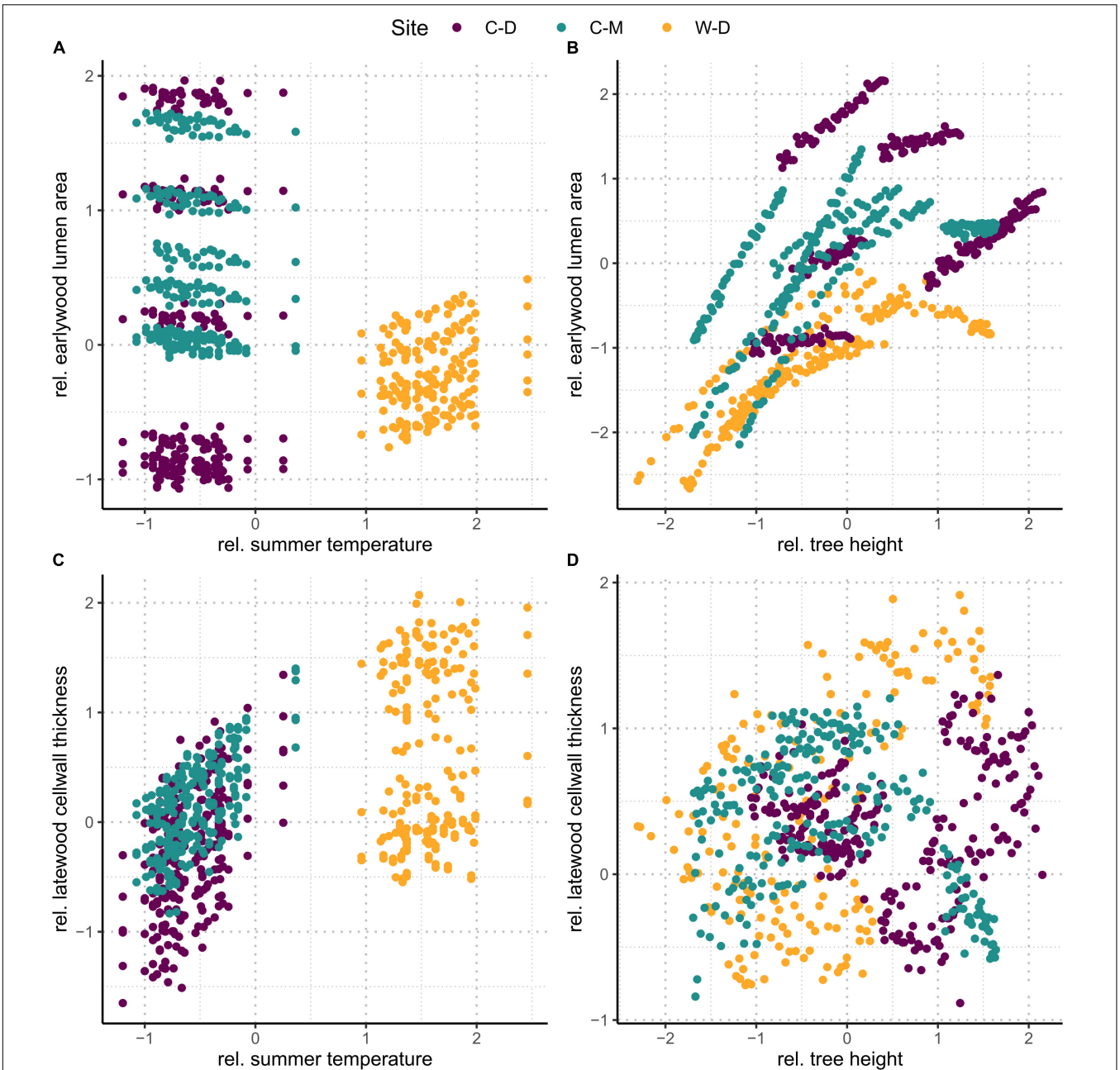

FIGURE 4 | Upper row **(A,B)**: predicted relative earlywood lumen area. Lower row **(C,D)**: predicted relative latewood cell wall thickness. Left column **(A,C)**: values predicted on a dataset where height was set to the mean (i.e., 0). The figures show the effect of summer temperature without the effect of height. Right column **(B,D)**: values predicted on a dataset where summer temperature was set to the mean (i.e., 0). The figures show the effect of height without the effect of summer temperature.

10 years before and 10 years after the missing ring. For height estimations we then used the coring height as the initial height of the tree with a hypothetical DBH of zero (i.e., the intercept) and tree height measured in the year of sampling as height of the youngest measured ring. We then interpolated h_i for each year based on a linear function of DBH (Eq. 4).

$$\text{Equation4} \qquad h_{it} = h_{i0} + a_i * DBH_{it}, \tag{4}$$

where h_{it} is the height of tree i at time t, h_{i0} is the interecept (i.e., the initial height = coring height), a_i the slope for tree i and DBH_{it} the previously estimated DBH of tree i at time t (**Supplementary Figure 2**).

Statistics

For all statistical analyses we used R v4.0.2 (R Core Team, 2020). We calculated linear mixed-effects models to estimate the effects

of tree height and site-specific climatic conditions on the four selected xylem anatomical traits, separated into earlywood and latewood. Xylem anatomical traits were used as response variable (i.e., LA, TB^2, CWT, DEN). h_i, squared h_i (h_i^2), site and the climate variables mean temperature and total precipitation of previous fall, previous winter, spring, and summer were set as fixed effects including interactions between site and each climate variable to account for potential differences in site-specific responses to climatic conditions (**Figure 3**). h_i^2 was included in the fixed effects to allow for potential non-linear effects of h_i on xylem anatomical traits (e.g., LA; Anfodillo et al., 2006). TB^2 and CWT were log-transformed before the analysis to better meet the assumptions of normality and homoscedasticity of residuals. All investigated numeric response and explanatory variables were standardized to a mean of 0 with a standard deviation of 1 to keep effects comparable across traits. All linear mixed-effects models were fitted using the lme function of the nlme package (Pinheiro et al., 2020) with the restricted maximum likelihood (REML) approach. Random effects were defined for each tree ID with random intercepts and random slopes for h_i and h_i^2 to account for individual growth patterns. The random effects structure was constructed with the pdDiag function from the nlme R-package. We accounted for first order autocorrelation in each tree using the corAR1 constructor from the nlme package. Weightings to correct for non-homogeneous variance between individuals were included with the varIdent function from the nlme package.

For pairwise comparison of site effects we used the lsmeans function of the lsmeans package with a Tukey-adjustment to account for non-homogeneous variances among the groups (Lenth, 2016).

To further visualize the effects of summer temperature and cumulative tree height increment, we used the linear mixed-effects model to predict trait values under two hypothetical conditions, i.e., (1) no change in tree height and (2) no change in summer temperature. First, we predicted trait values on a dataset, where tree height was set to the mean value (i.e., 0), while all other traits remained the same as in our original dataset to explore the effects of summer temperature (**Figures 4A,C**). Then we did the same on a second dataset, but instead of tree height, summer temperature was set to the mean value (i.e., 0) to explore the effects of tree height (**Figures 4B,D**).

RESULTS

Tree height reconstructions showed that trees from W-D on average grew faster in height and had a different allometry: they tended to grow taller when compared to trees from C-D or C-M of the same diameter (**Figure 2**). Trees from C-M grew faster than trees from C-D but they were similar in terms of allometry (**Figure 2**).

The linear mixed-effects models showed that the water transport-related traits LA and TB^2 were mostly driven by tree height (**Table 1** and **Supplementary Table 2**), especially in the earlywood. Specifically, LA was positively influenced by tree height in both earlywood and latewood with a particularly strong effect in earlywood (**Table 1** and **Figure 4B**). Estimated climate effects on LA were only found for the reference site W-D (**Table 1** and **Figure 4A**). Summer temperature showed a notable significant effect on earlywood lumen area at the W-D site (**Table 1**). Previous winter and spring precipitation had a positive effect on latewood LA at the W-D site (**Table 1**). TB^2 was negatively influenced by tree height, both in earlywood and latewood, with stronger effects in the earlywood as well (**Table 1**). The most notable estimated climatic effects on TB^2 were the negative effect of summer precipitation at the W-D site as well as the positive effect of summer temperature at the C-D and C-M sites (**Table 1**).

In contrast, DEN and CWT, which are related to structural integrity, were mainly influenced by climatic conditions, especially in the latewood. Summer temperature had a positive influence on DEN at the sites C-D and C-M, which was especially strong in the latewood. At W-D, latewood DEN was positively influenced by spring temperature (**Table 1**) and earlywood DEN was negatively influenced by summer temperature. Precipitation had only a weak influence on this trait (**Table 1**). DEN was only slightly negatively influenced by tree height in the latewood. CWT was most strongly impacted by summer temperature in the latewood at the sites C-D and C-M (**Table 1** and **Figure 4C**). At W-D, latewood CWT was positively influenced by spring temperature and latewood CWT was negatively influenced by summer precipitation (**Table 1**). CWT was positively influenced by tree height in the earlywood.

The trait-values predicted by the linear mixed-effects models showed significant pairwise differences between C-M and W-D in predicted earlywood LA with W-D showing lower values, and between C-D and W-D in predicted earlywood density with W-D showing higher values (**Figure 5** and **Supplementary Table 3**).

DISCUSSION

We used linear mixed-effects models to disentangle the effects of climatic conditions and tree height on four characteristic xylem anatomical traits. Our results can help to understand complex direct and indirect relationships between the investigated multifunctional xylem anatomical traits on the one hand and climatic conditions and physiological limitations on the other hand. We found that in earlywood, traits related to water transport (LA and TB^2) were mainly driven by height at all sites, seemingly independent of the different climatic growth limitations (**Figure 4**). In the latewood, traits related to structural integrity (CWT and DEN) were mainly affected by climatic variables. We found a strong impact of summer temperature on latewood CWT (**Table 1** and **Figure 4C**) especially in trees from the temperature-limited treeline sites C-D and C-M.

As expected, h_i had a strong effect, especially on traits related to water transport (LA and TB^2), supporting our first hypothesis that earlywood traits related to water transport would be under a strong influence of tree height due to the importance of earlywood for water transport. Height influenced LA positively (i.e., larger lumen in taller trees) and TB^2 negatively [i.e., taller trees have thinner cell walls relative to the cell wall length due to enlarged lumen with equal amounts of cell-wall material (Eq. 3)].

TABLE 1 | Results of trait specific linear mixed-effects models for the investigated traits (LA, lumen area; TB^2, conduit reinforcement index; DEN, density; CWT, cell wall thickness) divided into earlywood (ew) and latewood (lw).

		Intercept		Site C-D		Site C-M		Height (h_i)		Height (h_i^2)	
		Value	Std.error	Value	Std.error	Value	Std.error	Value	Std.error	Value	Std.error
LA	ew	–0.714	0.371	0.875	0.529	**1.346***	**0.511**	**0.688*****	**0.1510**	**–0.244****	**0.085**
	lw	0.233	0.386	–0.294	0.500	0.773	0.481	**0.401****	**0.134**	**–0.342****	**0.103**
TB^2	ew	0.452	0.396	–0.765	0.530	–0.491	0.498	**–0.339***	**0.142**	0.212	0.112
	lw	0.230	0.388	–0.302	0.520	0.167	0.478	**–0.247***	**0.113**	0.084	0.083
DEN	ew	0.846	0.355	**–1.363***	**0.475**	–0.838	0.445	–0.253	0.158	0.169	0.116
	lw	–0.003	0.417	0.107	0.514	0.072	0.476	**–0.201***	**0.100**	**0.1489***	**0.075**
CWT	ew	0.196	0.447	–0.533	0.598	0.323	0.576	**0.435*****	**0.103**	–0.052	0.077
	lw	0.452	0.435	–0.300	0.549	0.257	0.515	0.108	0.107	–0.086	0.079
Precipitation		**previous fall precipitation**		**previous winter precipitation**		**spring precipitation**		**summer precipitation**			
Reference site W-D		**Value**	**Std.error**	**Value**	**Std.error**	**Value**	**Std.error**	**Value**	**Std.error**		
LA	ew	0.002	0.028	0.034	0.028	0.041	0.028	0.028	0.041		
	lw	–0.017	0.064	**0.180****	**0.058**	**0.179****	**0.061**	0.004	0.089		
TB^2	ew	0.073	0.052	–0.003	0.052	–0.058	0.051	**–0.170***	**0.078**		
	lw	0.073	0.061	0.023	0.051	–0.108	0.056	**–0.202***	**0.082**		
DEN	ew	0.035	0.046	–0.027	0.046	–0.069	0.045	–0.111	0.068		
	lw	0.128	0.081	–0.102	0.072	–0.083	0.075	–0.127	0.111		
CWT	ew	0.037	0.050	–0.011	0.050	–0.048	0.048	–0.081	0.072		
	lw	0.122	0.075	0.059	0.069	0.032	0.071	**–0.221***	**0.105**		
Interaction		**C-D:fall.prec.**		**C-D:winter.prec.**		**C-D:spring.prec.**		**C-D:summer.prec.**			
C-D * precipitation		**Value**	**Std.error**	**Value**	**Std.error**	**Value**	**Std.error**	**Value**	**Std.error**		
LA	ew	–0.016	0.040	–0.009	0.040	–0.028	0.035	–0.081	0.059		
	lw	–0.007	0.082	–0.091	0.077	–0.104	0.070	–0.045	0.116		
TB^2	ew	**–0.166***	**0.068**	0.067	0.069	**0.150***	**0.060**	0.129	0.102		
	lw	**–0.199***	**0.082**	**–0.162***	**0.075**	**0.165***	**0.069**	0.058	0.116		
DEN	ew	–0.101	0.059	0.079	0.060	**0.134***	**0.052**	0.113	0.088		
	lw	**–0.209***	**0.099**	–0.025	0.091	0.139	0.085	0.026	0.140		
CWT	ew	**–0.182****	**0.063**	**0.131***	**0.064**	**0.168****	**0.055**	–0.007	0.093		
	lw	**–0.259***	**0.092**	**–0.171***	**0.087**	0.080	0.080	0.052	0.132		

(Continued)

TABLE 1 | (Continued)

Interaction		C-M:fall.prec.		C-M:winter.prec.		C-M:spring.prec.		C-M:summer.prec.	
C-M * precipitation		**Value**	**Std.error**	**Value**	**Std.error**	**Value**	**Std.error**	**Value**	**Std.error**
LA	ew	–0.024	0.031	–0.021	0.032	–0.024	0.032	–0.043	0.047
	lw	–0.027	0.077	–0.126	0.073	**–0.172***	**0.077**	0.034	0.113
TB²	ew	**–0.126***	**0.056**	0.015	0.057	0.053	0.057	0.163	0.086
	lw	–0.097	0.065	–0.049	0.057	0.116	0.062	0.158	0.091
DEN	ew	–0.085	0.050	0.026	0.052	0.049	0.051	0.088	0.076
	lw	–0.147	0.087	0.049	0.079	0.067	0.083	0.028	0.122
CWT	ew	**–0.133***	**0.054**	0.043	0.056	0.027	0.054	0.027	0.081
	lw	**–0.193***	**0.082**	–0.103	0.077	–0.060	0.080	0.164	0.118
Temperature		**previous fall temp.**		**previous winter temp.**		**spring temperature**		**summer temperature**	
Reference site W-D		**Value**	**Std.error**	**Value**	**Std.error**	**Value**	**Std.error**	**Value**	**Std.error**
LA	ew	0.040	0.040	0.030	0.038	0.021	0.050	**0.291*** **	**0.075**
	lw	0.047	0.088	0.090	0.078	–0.147	0.108	–0.063	0.160
TB²	ew	–0.054	0.076	0.060	0.067	0.134	0.091	**–0.329***	**0.139**
	lw	–0.139	0.077	0.005	0.067	0.141	0.096	0.226	0.149
DEN	ew	–0.080	0.067	–0.001	0.059	0.106	0.080	**–0.444*** **	**0.123**
	lw	–0.182	0.107	0.037	0.093	**0.330***	**0.133**	0.205	0.195
CWT	ew	–0.151	0.072	0.043	0.064	**0.263****	**0.087**	–0.212	0.131
	lw	–0.155	0.101	0.039	0.089	0.196	0.124	0.096	0.186
Interaction		**C-D:fall.temp**		**C-D:winter.temp**		**C-D:spring.temp**		**C-D:summer.temp**	
C-D * temperature		**Value**	**Std.error**	**Value**	**Std.error**	**Value**	**Std.error**	**Value**	**Std.error**
LA	ew	0.031	0.057	0.030	0.058	–0.040	0.073	**–0.311****	**0.110**
	lw	0.032	0.112	–0.012	0.109	0.084	0.142	–0.021	0.210
TB²	ew	0.008	0.099	–0.040	0.096	–0.093	0.123	**0.499****	**0.186**
	lw	0.104	0.108	–0.040	0.107	–0.093	0.139	**0.746*****	**0.209**
DEN	ew	0.061	0.086	–0.025	0.083	–0.087	0.106	**0.504****	**0.162**
	lw	0.057	0.133	–0.043	0.126	–0.209	0.169	**0.736****	**0.246**
CWT	ew	**0.222***	**0.090**	–0.039	0.088	**–0.290***	**0.113**	0.302	0.170
	lw	0.113	0.125	–0.059	0.120	–0.131	0.158	**0.934*****	**0.234**

(Continued)

TABLE 1 | (Continued)

Interaction		C-M:fall.temp		C-M:winter.temp		C-M:spring.temp		C-M:summer.temp	
C-M * temperature		Value	Std.error	Value	Std.error	Value	Std.error	Value	Std.error
LA	ew	–0.026	0.052	–0.077	0.047	–0.036	0.064	**–0.397*****	**0.095**
	lw	0.052	0.131	–0.127	0.112	–0.028	0.162	0.052	0.240
TB^2	ew	0.023	0.092	0.022	0.080	–0.035	0.111	**0.540****	**0.168**
	lw	0.115	0.094	0.001	0.081	0.084	0.118	**0.645*****	**0.180**
DEN	ew	0.096	0.082	0.073	0.072	–0.001	0.099	**0.528*****	**0.151**
	lw	0.142	0.130	–0.024	0.112	0.095	0.162	**0.493***	**0.235**
CWT	ew	0.158	0.089	0.024	0.079	–0.123	0.109	0.194	0.163
	lw	0.183	0.126	–0.068	0.110	0.106	0.156	**0.767*****	**0.231**

*Fixed effects: Intercept, site (C-D = Brooks Range, C-M = Denali NP) relative to Bluff (W-D), height, squared height, precipitation and temperature per season, interaction between seasonal precipitation/temperature and site, relative to Bluff (W-D), which was set as the reference point for the categorical variable "site." Choosing another site as reference would not have changed the outcome of the models in a way that it would alter the interpretation of the results. Bold text shows significant values ($p < 0.05$ *$p < 0.01$ **$p < 0.001$ ***, exact p-values are mentioned in **Supplementary Table 2**). Red text marks significant negative and blue marks significant positive effects.*

Similar results were found by Kašpar et al. (2019) for different conifer species at various elevational treelines. The strong positive effect of tree height on earlywood LA highlights the importance of "conduit widening" in conifers. Conduit widening describes the increase of LA from the apex toward the base of a tree. It is argued to occur due to the effects defined by the Hagen-Poiseuille law, which predicts a linearly increasing resistance with increasing conduit length for Newtonian fluids flowing in cylindrical conduits (Pfitzner, 1976; Gooch, 2011). This hydraulic resistance is maintained constant throughout the tree by conduit widening to ensure a cost-effective water transport (West et al., 1999; Becker et al., 2000; Enquist, 2002; Anfodillo et al., 2006). Consequently, when measuring LA from pith to bark at a particular height of the tree, it increases from year to year due to an increase of absolute tree height (Carrer et al., 2015). This effect also explains the influence of tree height on TB^2. TB^2 is the relation between CWT and cell wall length, and it increases with tree height because of the enlargement of cells while cell wall deposition stays similar. The usage of a constant amount of resources as mentioned in Cuny et al. (2014) leads to relatively thinner cell walls on bigger cells and thus a negative effect of tree height on TB^2 (Hacke et al., 2001). As tree height itself is influenced by various environmental conditions, especially competition, temperature, and water availability (Lines et al., 2012; Fransson et al., 2021), it can be assumed that a large part of the height effects that we found correspond to indirect effects of environmental conditions on xylem anatomical traits related to water transport.

Regarding direct environmental effects, more complex patterns were found. LA did not seem to be strongly influenced by climatic conditions. Considering the rather weak effects of precipitation, that were only found in the latewood, the strong effects of tree height in earlywood and latewood (**Table 1** and **Figure 4**) and the modest evidence for differences between sites in the earlywood lumen area (**Figure 5**), we can only assume that the potential impact of drought on LA was overruled by the height effect. Our third hypothesis, assuming smaller lumen area at the drought-limited W-D site as an adjustment for lowering the risk of cavitation, cannot be resolved, as evidence is deficient. The most noticeable climatic effect on LA was the positive effect of summer temperature on earlywood LA at W-D. Growth in general is positively correlated with temperature, thus warmer conditions could mean a greater increment in height and therefore bigger increase in lumen (Gillooly et al., 2001; Petit et al., 2011; Anfodillo et al., 2016). The height parameter used in the models is cumulative and might not fully reflect the effect of increased growth rates in warm years. Yet, the effect only occurred at W-D and cannot be explained with certainty.

Considering all sites together, the largest direct environmental effects on xylem anatomy were found in traits that are related to the structural integrity of the tree—DEN and CWT. With both latewood DEN and CWT being largely driven by temperature, our results support our second hypothesis stating that latewood traits related to structural integrity would be mainly influenced by climatic conditions. CWT was positively influenced by spring and summer temperature, yet this influence differed between sites. At the drought-limited site W-D only spring temperature showed a

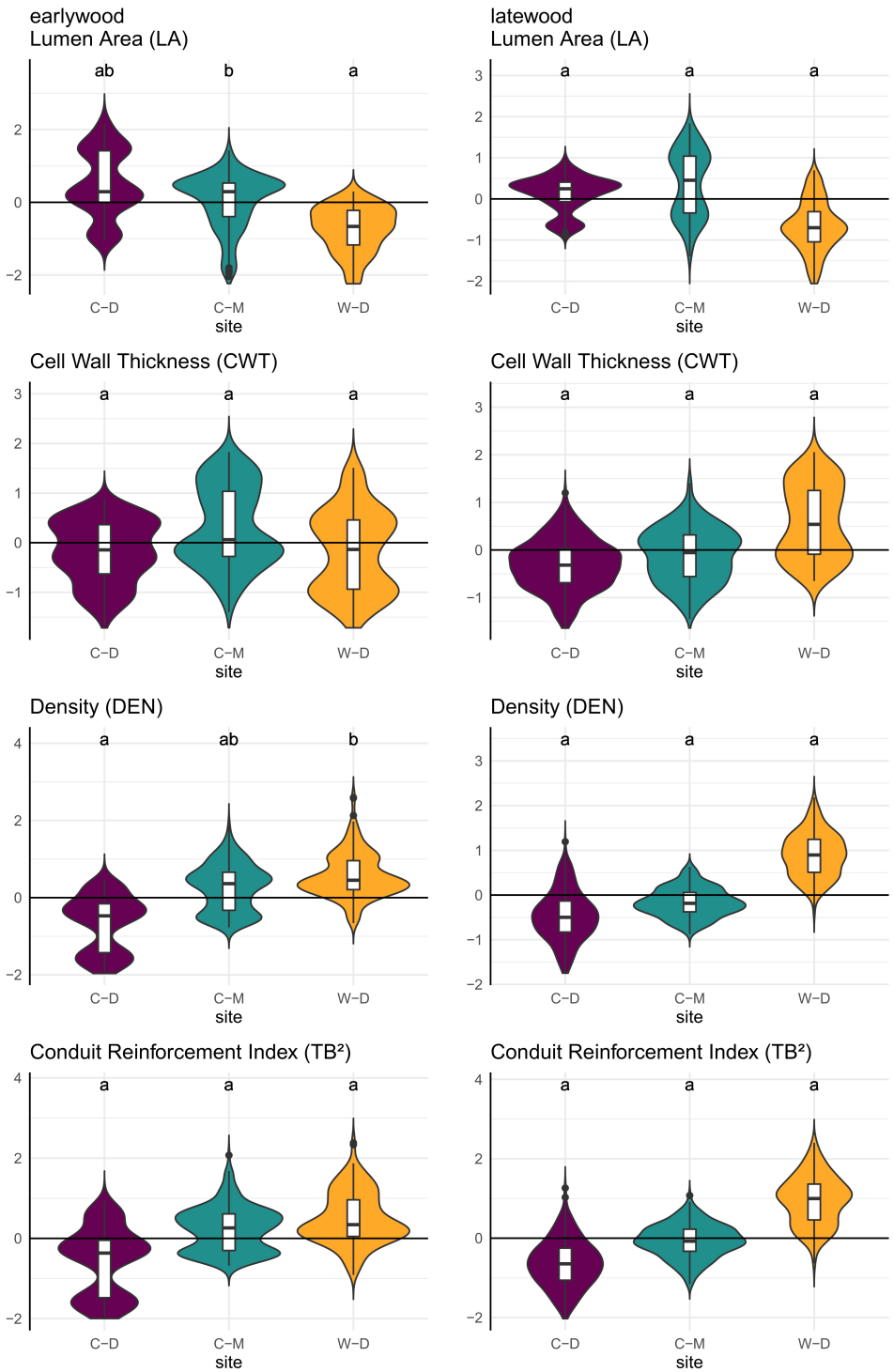

FIGURE 5 | Violin plots combined with boxplots of predicted relative trait values (*y*-axis), based on linear mixed-effects models as described in the methods. Small letters indicate significance groups based on pairwise comparison with a significance threshold of $p = 0.05$. Purple = Brooks Range (C-D), Green = Denali National Park (C-M), Orange = Bluff (W-D).

significantly positive but rather weak effect on earlywood CWT. However, as expected, we found a strong effect of summer temperature on latewood CWT for the sites C-D and C-M (**Table 1** and **Figure 4C**). The increase of latewood CWT with increasing summer supports our fourth hypothesis stating that due to longer vegetation periods and higher temperatures

CWT would be higher at W-D. Higher temperatures generally lead to faster biochemical processes and therefore a potentially faster cell wall deposition in trees, causing thicker cell walls (Yasue et al., 2000; Gillooly et al., 2001; Fonti et al., 2013; Rossi et al., 2014; Castagneri et al., 2017). Tree growth at the sites C-D and C-M is limited mainly by low temperatures, consequently leading to a high sensitivity to temperature. This effect is particularly apparent in latewood, toward the end of the vegetation period, since at the time of latewood formation it is more important for the tree to grow a stable wood structure with thick cell walls than to produce larger or more tracheids (Zobel and van Buijtenen, 1989; Fonti et al., 2013; Cuny and Rathgeber, 2016; Björklund et al., 2017). Additionally, we found a negative effect of summer precipitation on latewood CWT at the W-D and C-D sites. The increase in water availability could have induced an increase in the total lumen area while not influencing the total amount of cell wall material, leading to relatively thinner cell walls on larger or more tracheids (Cuny et al., 2014; Lange et al., 2020). Since in our study we did not find any noticeable effect of summer precipitation on LA, it is possible that higher water availability decreased CWT by increasing the number of cells instead of increasing their lumen area (Fonti et al., 2010; Jyske et al., 2010; Cuny and Rathgeber, 2016). We were not able to estimate the total number of cells per year, because it would have required a disproportionate amount of work to improve the sample quality further to a point where we would have been able to estimate a reliable result.

The effects found in DEN are in line with the effects found in CWT and LA. DEN is correlating with both CWT and LA due to the way it is calculated (Eq. 4). It must also be mentioned that according to the methodology of estimating density separately for earlywood and latewood it did not reflect the typical negative correlation to increased secondary growth induced by higher temperatures as found in other studies (Cortini et al., 2016; Hassegawa et al., 2019). DEN showed similar but overall relatively weaker reactions to climate conditions than CWT. This pattern might be explained by a stronger genetic control on DEN than on CWT, as found in previous studies (Lenz et al., 2011; Hassegawa et al., 2019; Pampuch et al., 2020). Therefore, it seems possible that especially the relation between total cell area and CWA (i.e., the anatomical allometry) is under a strong genetic control. Since TB^2 is also derived from LA and CWT, climatic effects were found in TB^2 as well. Again, these effects are in line with the effects we found in CWT. In contrast to DEN, earlywood TB^2 expressed a slightly stronger response to summer precipitation and summer temperature than CWT. TB^2 reflects the hydraulic safety, which is increased by building relatively thicker cell walls in relation to cell wall length (Hacke et al., 2001). This explains why latewood TB^2 was negatively related to precipitation at the drought-limited site W-D (i.e., high precipitation leads to relatively bigger cell lumen).

Model predictions showed significant differences between the sites for earlywood LA and earlywood DEN (**Figure 5**). These differences must be interpreted carefully, as in both cases we had a high standard error and high *p*-values, indicating a weak confidence (**Supplementary Table 2**). Still, they showed that differences might also occur on yet another aspect that was not investigated in this study (e.g., adaptation; Lenz et al., 2011; Pampuch et al., 2020). Stronger differences between the sites regarding LA might have been mitigated by the beneficial effect of smaller lumen, which can also potentially reduce the risk of freeze-thaw embolisms (Pittermann and Sperry, 2006). However, a more reliable evidence for differences between the sites was expressed by the differences in allometry and growth speed (**Figure 2**), as well as by the significance and strength at which climatic drivers influenced the anatomy of trees (**Table 1** and **Figure 4**). The differences in growth speed between the cold- and drought-limited sites were potentially caused by the differences in average temperatures and the length of the vegetation period (**Figure 1**). The higher temperatures and presumably longer vegetation period at W-D potentially led to longer and faster growth (Nienstaedt and Zasada, 1990; Gillooly et al., 2001) than at the other sites. The differences between the sites regarding the ratio between DBH and height, with relatively taller trees growing at W-D, was somewhat unexpected. Considering that W-D was classified as a drought-limited treeline and tree height influences the traits related to water transport, we expected trees to be rather short at W-D as a result of local phenotypic adjustment (Lines et al., 2012; Hacke et al., 2015; Stovall et al., 2019). It's possible that in the sampled trees drought effects are not very pronounced due to their relatively short height, i.e., the trees might have not reached a critical size at which they would suffer severely from the dry conditions (Bennett et al., 2015). This could also explain why precipitation is not influencing LA. Yet, various other potential factors like competition for light (Grams and Andersen, 2007), differences in microsite-conditions (Li and Yang, 2004; Marquis et al., 2021; Zacharias et al., 2021), soil conditions (Urban et al., 2013) but also fire events (Johnstone et al., 2016; Whitman et al., 2019), or a combination of these factors could have had consequences for the forest dynamics and thus altered height growth and the allometry of white spruce at the W-D site. However, no detailed information on competition in the past, microsite or soil conditions was available to us to explain the found patterns with certainty.

CONCLUSION

We found that, due to the multifunctionality of xylem tissue, anatomical traits are tied into complex multidimensional interactions between each other, direct and indirect climatic effects, and tree height.

Traits related to water transport, particularly earlywood lumen area, are indirectly influenced by the environmental conditions that affected tree height. Future studies aiming at examining xylem anatomical features of trees should be well aware of these effects, as they can heavily affect traits like LA when measured across an increment core. It is especially important to observe the correlation of tracheid dimensions with tree height when working on natural populations and on trees growing under varying environmental conditions.

Traits related to the structural integrity, particularly latewood CWT are under a strong direct influence of temperature. While not entirely new, this influence highlights the trait potential

for dendroclimatological studies. With advancing technology, measuring xylem anatomical traits becomes less and less labor intensive. Latewood CWT could thus be used more widely for conducting studies on climate-growth correlations or to create climate reconstructions.

In general an increasing number of studies are taking advantage of investigating xylem anatomical traits. Yet, a proper interpretation of results requires a good level of understanding the function of xylem anatomical traits, how they are linked with each other, and to what extent they are influenced by environmental conditions. The complexity of xylem anatomy must be carefully considered, especially in studies that are conducted under natural conditions, and along gradients or in contrasting environments. Our study helps to better understand this complexity, and could be a useful inspiration for future studies to work on a more holistic approach to study xylem anatomy.

DATA AVAILABILITY STATEMENT

The raw data supporting the conclusions of this article will be made available by the authors, without undue reservation.

AUTHOR CONTRIBUTIONS

TP, MW, MT, and JL designed the study and conducted field work and sampling. TP, JL, and MT prepared the samples and performed xylem anatomical measurements. MT performed the statistical analysis for estimating site-specific tree height and stem diameter relationships. TP performed all further statistical analyses with help from AA-R. TP wrote the manuscript with contributions from all authors. All authors contributed to the article and approved the submitted version.

FUNDING

This project was funded by the German Research Foundation (DFG) within the Research Training Group RESPONSE (DFG RTG 2010). AA-R was funded by a Research Fellowship from the Alexander von Humboldt Foundation.

ACKNOWLEDGMENTS

We thank Andreas Burger for his help in organizing and executing parts of the field work and Sanju Shrestha for her help in preparing parts of the xylem anatomical samples. We are also thankful to the reviewers and the editor Marco Carrer for their constructive comments.

SUPPLEMENTARY MATERIAL

The Supplementary Material for this article can be found online at: https://www.frontiersin.org/articles/10.3389/fpls.2021.748055/full#supplementary-material

REFERENCES

Abrahamson, I. (2015). *Fire Effects Information System. Picea glauca*. Available online at: https://www.feis-crs.org/feis/ (accessed January 31, 2020)

Anfodillo, T., Carraro, V., Carrer, M., Fior, C., and Rossi, S. (2006). Convergent tapering of xylem conduits in different woody species. *New Phytol.* 169, 279–290. doi: 10.1111/j.1469-8137.2005.01587.x

Anfodillo, T., Petit, G., and Crivellaro, A. (2013). Axial conduit widening in woody species: a still neglected anatomical pattern. *IAWA J.* 34, 352–364. doi: 10.1163/22941932-00000030

Anfodillo, T., Petit, G., Sterck, F., Lechthaler, S., and Olson, M. E. (2016). Allometric trajectories and "stress": A quantitative approach. *Front. Plant Sci.* 7:1681. doi: 10.3389/fpls.2016.01681

Antonova, G. F., and Stasova, V. V. (1993). Effects of environmental factors on wood formation in Scots pine stems. *Trees* 7, 214–219. doi: 10.1007/BF00202076

Arneth, A., Harrison, S. P., Zaehle, S., Tsigaridis, K., Menon, S., Bartlein, P. J., et al. (2010). Terrestrial biogeochemical feedbacks in the climate system. *Nat. Geosci.* 3, 525–532. doi: 10.1038/ngeo905

Attree, S. M., Dunstan, D. I., and Fowke, L. C. (1991). *Trees III*. (Berlin: Springer)

Barber, V., Juday, G., and Finney, B. (2000). Reduced growth of Alaska white spruce in the twentieth century from temperature-induced drought stress. *Nature* 405, 668–672.

Becker, P., Gribben, R. J., and Lim, C. M. (2000). Tapered conduits can buffer hydraulic conductance from path-length effects. *Tree Physiol.* 20, 965–967. doi: 10.1093/treephys/20.14.965

Bennett, A. C., Mcdowell, N. G., Allen, C. D., and Anderson-Teixeira, K. J. (2015). Larger trees suffer most during drought in forests worldwide. *Nat. Plants* 1:139. doi: 10.1038/nplants.2015.139

Bieniek, P. A., Bhatt, U. S., Walsh, J. E., Rupp, T. S., Zhang, J., Krieger, J. R., et al. (2016). Full access dynamical downscaling of ERA-interim temperature and precipitation for Alaska. *J. Appl. Meteorol. Climatol.* 55, 635–654. doi: 10.1175/JAMC-D-15-0153.1

Björklund, J., Seftigen, K., Fonti, P., Nievergelt, D., and von Arx, G. (2020). Dendroclimatic potential of dendroanatomy in temperature-sensitive Pinus sylvestris. *Dendrochronologia* 60:125673. doi: 10.1016/j.dendro.2020.125673

Björklund, J., Seftigen, K., Schweingruber, F., Fonti, P., von Arx, G., Bryukhanova, M. V., et al. (2017). Cell size and wall dimensions drive distinct variability of earlywood and latewood density in Northern Hemisphere conifers. *New Phytol.* 216, 728–740. doi: 10.1111/nph.14639

Brockmann-Jerosch, H. (1919). *Baumgrenze und Klimacharakter. Pflanzengeographische Kommission der Schweizerischen Naturforschenden Gesellschaft. Beiträge zur geobotanischen Landesaufnahme, Bd. 6*. Zürich: Rascher & Cie.

Bunn, A. G. (2008). A dendrochronology program library in R (dplR). *Dendrochronologia* 26, 115–124. doi: 10.1016/j.dendro.2008.01.002

Callaham, R. Z. (1962). Geographic variability in growth of forest trees. *Tree Growth* 1962, 311–325.

Carrer, M., von Arx, G., Castagneri, D., and Petit, G. (2015). Distilling allometric and environmental information from time series of conduit size: the standardization issue and its relationship to tree hydraulic architecture. *Tree Physiol.* 35, 27–33. doi: 10.1093/treephys/tpu108

Castagneri, D., Fonti, P., Von Arx, G., and Carrer, M. (2017). How does climate influence xylem morphogenesis over the growing season? Insights from long-Term intra-ring anatomy in Picea abies. *Anna. Bot.* 119, 1011–1020. doi: 10.1093/aob/mcw274

Charney, N. D., Babst, F., Poulter, B., Record, S., Trouet, V. M., Frank, D., et al. (2016). Observed forest sensitivity to climate implies large changes in 21st century North American forest growth. *Ecol. Lett.* 19, 1119–1128. doi: 10.1111/ele.12650

Cochard, H. (2006). Cavitation in trees. *Comptes Rendus Physique* 7, 1018–1026. doi: 10.1016/j.crhy.2006.10.012

Cortini, F., MacIsaac, D., and Comeau, P. (2016). White spruce growth and wood properties over multiple time periods in relation to current tree and stand attributes. *Forests* 7:49. doi: 10.3390/f7030049

Cuny, H. E., Fonti, P., Rathgeber, C. B. K., von Arx, G., Peters, R. L., and Frank, D. C. (2019). Couplings in cell differentiation kinetics mitigate air temperature influence on conifer wood anatomy. *Plant Cell Environ.* 42, 1222–1232. doi: 10.1111/pce.13464

Cuny, H. E., and Rathgeber, C. B. K. (2016). Xylogenesis: Coniferous trees of temperate forests are listening to the climate tale during the growing season but only remember the last words! Plant Physiology. 171, 306–317. doi: 10.1104/pp.16.00037

Cuny, H. E., Rathgeber, C. B. K., Frank, D., Fonti, P., and Fournier, M. (2014). Kinetics of tracheid development explain conifer tree-ring structure. *New Phytol.* 203, 1231–1241. doi: 10.1111/nph.12871

Däniker, A. (1932). *Biologische Studien über Baum- und Waldgrenze, insbesondere über die klimatischen Ursachen und deren Zusammenhänge*. Zürich: Vierteljahrsschrift d. Naturf. Ges.

Denne, M. P. (1989). Definition of Latewood According to Mork (1928). *IAWA J.* 10, 59–62. doi: 10.1163/22941932-90001112

Domec, J.-C., and Gartner, B. L. (2002). How do water transport and water storage differ in coniferous earlywood and latewood? *J. Experimen. Bot.* 53, 2369–2379. doi: 10.1093/jxb/erf100

Eldhuset, T. D., Nagy, N. E., Volařík, D., Børja, I., Gebauer, R., Yakovlev, I. A., et al. (2013). Drought affects tracheid structure, dehydrin expression, and above- and belowground growth in 5-year-old Norway spruce. *Plant Soil* 366, 305–320. doi: 10.1007/s11104-012-1432-z

Enquist, B. J. (2002). Universal scaling in tree and vascular plant allometry: Toward a general quantitative theory linking plant form and function from cells to ecosystems. *Tree Physiol.* 22, 1045–1064. doi: 10.1093/treephys/22.15-16.1045

Eusemann, P., Schnittler, M., Nilsson, R. H., Jumpponen, A., Dahl, M. B., Würth, D. G., et al. (2016). Habitat conditions and phenological tree traits overrule the influence of tree genotype in the needle mycobiome–Picea glauca system at an arctic treeline ecotone. *New Phytol.* 211, 1221–1231. doi: 10.1111/nph.13988

Fonti, P., Bryukhanova, M. V., Myglan, V. S., Kirdyanov, A. V., Naumova, O. V., and Vaganov, E. A. (2013). Temperature-induced responses of xylem structure of Larix sibirica (pinaceae) from the Russian Altay. *Am. J. Bot.* 100, 1332–1343. doi: 10.3732/ajb.1200484

Fonti, P., von Arx, G., García-González, I., Eilmann, B., Sass-Klaassen, U., Gärtner, H., et al. (2010). Studying global change through investigation of the plastic responses of xylem anatomy in tree rings. *New Phytol.* 185, 42–53. doi: 10.1111/j.1469-8137.2009.03030.x

Fransson, P., Brännström, A., and Franklin, O. (2021). A tree's quest for light-optimal height and diameter growth under a shading canopy. *Tree Physiol.* 41, 1–11. doi: 10.1093/treephys/tpaa110

Gärtner, H., and Nievergelt, D. (2010). The core-microtome: A new tool for surface preparation on cores and time series analysis of varying cell parameters. *Dendrochronologia* 28, 85–92. doi: 10.1016/j.dendro.2009.09.002

Gärtner, H., and Schweingruber, F. H. (2013). *Microscopic preparation techniques for plant stem analysis*. Remagen: Verlag Dr. Kessel.

Gauthier, S., Bernier, P., Kuuluvainen, T., Shvidenko, A. Z., and Schepaschenko, D. G. (2015). Boreal forest health and global change. *Science* 349, 819–822. doi: 10.1126/science.aaa9092

Gillooly, J. F., Brown, J. H., West, G. B., Savage, V. M., and Charnov, E. L. (2001). Effects of size and temperature on metabolic rate. *Science* 293, 2248–2251. doi: 10.1126/science.1061967

Gooch, J. W. (2011). "Hagen-Poiseuille Equation," in *Encyclopedic Dictionary of Polymers*, ed. J. W. Gooch (New York, NY: Springer).

Grace, J., Berninger, F., and Nagy, L. (2002). Impacts of climate change on the tree line. *Anna. Bot.* 90, 537–544. doi: 10.1093/aob/mcf222

Grams, T. E. E., and Andersen, C. P. (2007). *Competition for resources in trees: physiological versus morphological plasticity in progress in botany*. Berlin: Springer. 356–381. doi: 10.1007/978-3-540-36832-8_16

Grothendieck, G. (2013). nls2: Non-linear regression with brute force. Available online at: https://cran.r-project.org/package=nls2 (accessed March 08, 2013)

Hacke, U. G., Lachenbruch, B., Pittermann, J., Mayr, S., Domec, J.-C., and Schulte, P. J. (2015). *Functional and Ecological Xylem Anatomy*. (Berlin: Springer International Publishing), doi: 10.1007/978-3-319-15783-2

Hacke, U. G., and Sperry, J. S. (2001). Functional and ecological xylem anatomy. *Pers. Plant Ecol. Evol. Syst.* 4, 97–115. doi: 10.1078/1433-8319-00017

Hacke, U. G., Sperry, J. S., Pockman, W. T., Davis, S. D., and McCulloh, K. A. (2001). Trends in wood density and structure are linked to prevention of xylem implosion by negative pressure. *Oecologia* 126, 457–461. doi: 10.1007/s004420100628

Hassegawa, M., Savard, M., Lenz, P. R. N., Duchateau, E., Gélinas, N., Bousquet, J., et al. (2019). White spruce wood quality for lumber products: priority traits and their enhancement through tree improvement. *Forestry* 93, 1–22. doi: 10.1093/forestry/cpz050

Huang, S., Titus, S. J., and Wiens, D. P. (1992). Comparison of nonlinear height–diameter functions for major Alberta tree species. *Can. J. Forest Res.* 22, 1297–1304. doi: 10.1139/x92-172

IPCC. (2021). "Climate Change 2021: The Physical Science Basis". in *Contribution of Working Group I to the Sixth Assessment Report of the Intergovernmental Panel on Climate Change*, eds V. MassonDelmotte, P. Zhai, A. Pirani, S. L. Connors, C. Pean, S. Berger, et al. (Cambridge: Cambridge University Press).

Johnstone, J. F., Allen, C. D., Franklin, J. F., Frelich, L. E., Harvey, B. J., Higuera, P. E., et al. (2016). Changing disturbance regimes, ecological memory, and forest resilience. *Front. Ecol. Environ.* 14:369–378. doi: 10.1002/fee.1311

Juday, G. P., Barber, V., Rupp, S., Zasada, J., and Wilmking, M. (2003). *A 200-Year perspective of climate variability and the response of white spruce in interior alaska. in Climate Variability and Ecosystem Response at Long-Term Ecological Research Sites*. Oxford: Oxford University Press.226–250.

Jyske, T., Holtta, T., Makinen, H., Nojd, P., Lumme, I., and Spiecker, H. (2010). The effect of artificially induced drought on radial increment and wood properties of Norway spruce. *Tree Physiol.* 30, 103–115. doi: 10.1093/treephys/tpp099

Kašpar, J., Anfodillo, T., and Treml, V. (2019). Tree size mostly drives the variation of xylem traits at the treeline ecotone. *Trees Struct. Funct.* 33, 1657–1665. doi: 10.1007/s00468-019-01887-6

Körner, C. (2007). Climatic Treelines: Conventions. Global Patterns, Causes (Klimatische Baumgrenzen: Konventionen, globale Muster, Ursachen). *Erdkunde* 4, 316–324.

Lange, J., Carrer, M., Pisaric, M. F. J., Porter, T. J., Seo, J., Trouillier, M., et al. (2020). Moisture−driven shift in the climate sensitivity of white spruce xylem anatomical traits is coupled to large−scale oscillation patterns across northern treeline in northwest North America. *Glob. Change Biol.* 26, 1842–1856. doi: 10.1111/gcb.14947

Lenth, R. V. (2016). Least-Squares Means: The R Package lsmeans. *J. Statist. Softw.* 69, 1–33. doi: 10.18637/jss.v069.i01

Lenz, P., MacKay, J., Rainville, A., Cloutier, A., and Beaulieu, J. (2011). The influence of cambial age on breeding for wood properties in Picea glauca. *Tree Genet. Genomes* 7, 641–653. doi: 10.1007/s11295-011-0364-8

Li, M.-H., and Yang, J. (2004). Effects of microsite on growth of Pinus cembra in the subalpine zone of the Austrian Alps. *Anna. Forest Sci.* 61, 319–325. doi: 10.1051/forest:2004025

Lines, E. R., Zavala, M. A., Purves, D. W., and Coomes, D. A. (2012). Predictable changes in aboveground allometry of trees along gradients of temperature, aridity and competition. *Glob. Ecol Biogeography* 21, 1017–1028. doi: 10.1111/j.1466-8238.2011.00746.x

Little, E. L., and Viereck, L. A. (1971). *Atlas of United States trees*. Washington, DC: U.S. Dept. of Agriculture, Forest Service

Lloyd, A. H., Duffy, P. A., and Mann, D. H. (2013). Nonlinear responses of white spruce growth to climate variability in interior Alaska. *Can. J. Forest Res.* 43, 331–343. doi: 10.1139/cjfr-2012-0372

Lloyd, A. H., and Fastie, C. L. (2002). Spatial and temporal variability in the growth and climate response of treeline trees in Alaska. *Clim. change* 52, 481–509. doi: 10.1023/a:1014278819094

Marquis, B., Duval, P., Bergeron, Y., Simard, M., Thiffault, N., and Tremblay, F. (2021). Height growth stagnation of planted spruce in boreal mixedwoods: Importance of landscape, microsite, and growing-season frosts. *Forest Ecol. Manag.* 479:118533. doi: 10.1016/j.foreco.2020.118533

Mencuccini, M., Hölttä, T., Petit, G., and Magnani, F. (2007). Sanio's laws revisited. Size-dependent changes in the xylem architecture of trees. *Ecol. Lett.* 10, 1084–1093. doi: 10.1111/j.1461-0248.2007.01104.x

Myburg, A. A., Lev-Yadun, S., and Sederoff, R. R. (2013). Xylem Structure and Function. *eLS* 2013, 1–19. doi: 10.1002/9780470015902.a0001302.pub2

Nienstaedt, H., and Zasada, J. C. (1990). Picea glauca (Moench) Voss white spruce. *Silvics North Am.* 1, 204–226.

Pampuch, T., Anadon-Rosell, A., Zacharias, M., von Arx, G., and Wilmking, M. (2020). Xylem anatomical variability in white spruce at treeline is largely driven by spatial clustering. *Front. Plant Sci.* 11:1–10. doi: 10.3389/fpls.2020.581378

Petit, G., Anfodillo, T., Carraro, V., Grani, F., and Carrer, M. (2011). Hydraulic constraints limit height growth in trees at high altitude. *New Phytol.* 189, 241–252. doi: 10.1111/j.1469-8137.2010.03455.x

Pfitzner, J. (1976). Poiseuille and his law. *Anaesthesia* 31, 273–275. doi: 10.1111/j.1365-2044.1976.tb11804.x

Pinheiro, J., Bates, D., DebRoy, S., Sarkar, D., and R Core Team. (2020). *{nlme}: Linear and Nonlinear Mixed Effects Models*. Available online at: https://cran.r-project.org/package=nlme (accessed September 7, 2021)

Pittermann, J., and Sperry, J. S. (2006). Analysis of freeze-thaw embolism in conifers. The interaction between cavitation pressure and tracheid size. *Plant Physiol.* 140, 374–382. doi: 10.1104/pp.105.067900

Pittermann, J., Sperry, J. S., Wheeler, J. K., Hacke, U. G., and Sikkema, E. H. (2006). Mechanical reinforcement of tracheids compromises the hydraulic efficiency of conifer xylem. *Plant Cell Environ.* 29, 1618–1628. doi: 10.1111/j.1365-3040.2006.01539.x

Prendin, A. L., Petit, G., Carrer, M., Fonti, P., Björklund, J., and Von Arx, G. (2017). New research perspectives from a novel approach to quantify tracheid wall thickness. *Tree Physiol.* 37, 1–8. doi: 10.1093/treephys/tpx037

Puchi, P. F., Castagneri, D., Rossi, S., and Carrer, M. (2020). Wood anatomical traits in black spruce reveal latent water constraints on the boreal forest. *Glob. Change Biol.* 26, 1767–1777. doi: 10.1111/gcb.14906

R Core Team (2020). *R: A language and environment for statistical computing*. Vienna: R Core Team.

Rossi, S., Girard, M. J., and Morin, H. (2014). Lengthening of the duration of xylogenesis engenders disproportionate increases in xylem production. *Glob. Change Biol.* 20, 2261–2271. doi: 10.1111/gcb.12470

Sanio, K. (1872). Ueber die Grösse der Holzzellen bei der gemeinen Kiefer (Pinus silvestris). *Jahrbücher für wissenschaftliche Botanik.* 8, 401–420.

Sherriff, R. L., Miller, A. E., Muth, K., Schriver, M., and Batzel, R. (2017). Spruce growth responses to warming vary by ecoregion and ecosystem type near the forest-tundra boundary in south-west Alaska. *J. Biogeogra.* 44, 1457–1468. doi: 10.1111/jbi.12968

SNAP. (2019). *Scenarios network for Alaska and arctic planning*. Available online at: http://ckan.snap.uaf.edu/dataset. (accessed June 23, 2019)

Soja, A. J., Tchebakova, N. M., French, N. H. F., Flannigan, M. D., Shugart, H. H., Stocks, B. J., et al. (2007). Climate-induced boreal forest change: Predictions versus current observations. *Glob. Planet. Change* 56, 274–296. doi: 10.1016/j.gloplacha.2006.07.028

Stovall, A. E. L., Shugart, H., and Yang, X. (2019). Tree height explains mortality risk during an intense drought. *Nat. Commun.* 10:4385. doi: 10.1038/s41467-019-12380-6

Tagesson, T., Schurgers, G., Horion, S., Ciais, P., Tian, F., Brandt, M., et al. (2020). Recent divergence in the contributions of tropical and boreal forests to the terrestrial carbon sink. *Nat. Ecol. Evol.* 4, 202–209. doi: 10.1038/s41559-019-1090-0

Trouillier, M., van der Maaten-Theunissen, M., Harvey, J., Würth, D., Schnittler, M., and Wilmking, M. (2018). Visualizing individual tree differences in tree-ring studies. *Forests* 9:216. doi: 10.3390/f9040216

Trouillier, M., van der Maaten-Theunissen, M., Scharnweber, T., Würth, D., Burger, A., Schnittler, M., et al. (2019). Size matters—a comparison of three methods to assess age- and size-dependent climate sensitivity of trees. *Trees Struct. Funct.* 33, 183–192. doi: 10.1007/s00468-018-1767-z

Ueyama, M., Iwata, H., Harazono, Y., Euskirchen, E. S., Oechel, W. C., and Zona, D. (2013). Growing season and spatial variations of carbon fluxes of Arctic and boreal ecosystems in Alaska (USA). *Ecol. Appl.* 23, 1798–1816. doi: 10.1890/11-0875.1

Urban, J., Holušová, K., Menšík, L., Čermák, J., and Kantor, P. (2013). Tree allometry of Douglas fir and Norway spruce on a nutrient-poor and a nutrient-rich site. *Trees Struct. Funct.* 27, 97–110. doi: 10.1007/s00468-012-0771-y

von Arx, G., and Carrer, M. (2014). Roxas -A new tool to build centuries-long tracheid-lumen chronologies in conifers. *Dendrochronologia* 32, 290–293. doi: 10.1016/j.dendro.2013.12.001

von Arx, G., Crivellaro, A., Prendin, A. L., Čufar, K., and Carrer, M. (2016). Quantitative Wood Anatomy—Practical Guidelines. *Front. Plant Sci.* 7:1–13. doi: 10.3389/fpls.2016.00781

West, G. B., Brown, J. H., and Enquist, B. J. (1999). A general model for the structure and allometry of plant vascular systems. *Nature* 400, 664–667. doi: 10.1038/23251

Whitman, E., Parisien, M. A., Thompson, D. K., and Flannigan, M. D. (2019). Short-interval wildfire and drought overwhelm boreal forest resilience. *Sci. Rep.* 9, 1–12. doi: 10.1038/s41598-019-55036-7

Wieser, G. (2020). Alpine and polar treelines in a changing environment. *Forests* 11:254. doi: 10.3390/f11030254

Wilmking, M., Buras, A., Eusemann, P., Schnittler, M., Trouillier, M., Würth, D., et al. (2017). High frequency growth variability of White spruce clones does not differ from non-clonal trees at Alaskan treelines. *Dendrochronologia* 44, 187–192. doi: 10.1016/j.dendro.2017.05.005

Wilmking, M., and Juday, G. P. (2005). Longitudinal variation of radial growth at Alaska's northern treeline - Recent changes and possible scenarios for the 21st century. *Glob. Planet. Change* 47, 282–300. doi: 10.1016/j.gloplacha.2004.10.017

Yasue, K., Funada, R., Kobayashi, O., and Ohtani, J. (2000). The effects of tracheid dimensions on variations in maximum density of Picea glehnii and relationships to climatic factors. *Trees Struct. Funct.* 14, 223–229. doi: 10.1007/PL00009766

Zacharias, M., Pampuch, T., Heer, K., Avanzi, C., Würth, D. G., Trouillier, M., et al. (2021). Population structure and the influence of microenvironment and genetic similarity on individual growth at Alaskan white spruce treelines. *Sci. Total Environ.* 798:149267. doi: 10.1016/j.scitotenv.2021.149267

Zobel, B. J., and van Buijtenen, J. P. (1989). *Wood Variation and Wood Properties*. Berlin: Springer. doi: 10.1007/978-3-642-74069-5_1

Conflict of Interest: The authors declare that the research was conducted in the absence of any commercial or financial relationships that could be construed as a potential conflict of interest.

Publisher's Note: All claims expressed in this article are solely those of the authors and do not necessarily represent those of their affiliated organizations, or those of the publisher, the editors and the reviewers. Any product that may be evaluated in this article, or claim that may be made by its manufacturer, is not guaranteed or endorsed by the publisher.

frontiers in Plant Science

ORIGINAL RESEARCH
published: 28 October 2021
doi: 10.3389/fpls.2021.757280

Flood-Rings Production Modulated by River Regulation in Eastern Boreal Canada

Alexandre F. Nolin[1,2,3†], Jacques C. Tardif[2,3†], France Conciatori[2] and Yves Bergeron[1,3†]*

[1] Institut de Recherche sur les Forêts, Université du Québec en Abitibi-Témiscamingue (UQAT), Rouyn-Noranda, QC, Canada, [2] Centre for Forest Interdisciplinary Research (C-FIR), Department of Biology/Environmental Studies and Sciences, The University of Winnipeg, Winnipeg, MB, Canada, [3] Centre d'Étude de la Forêt, Université du Québec à Montréal (UQAM), Montréal, QC, Canada

OPEN ACCESS

Edited by:
Ignacio García-González, University of Santiago de Compostela, Spain

Reviewed by:
Michael J. Clifford, The Nature Conservancy (United States), United States
Radoslaw Puchalka, Nicolaus Copernicus University in Toruń, Poland

***Correspondence:**
Alexandre F. Nolin
alexandreflorent.nolin@uqat.ca

†ORCID:
Alexandre F. Nolin
orcid.org/0000-0003-1033-9123
Jacques C. Tardif
orcid.org/0000-0002-0145-9898
Yves Bergeron
orcid.org/0000-0003-3707-3687

Specialty section:
This article was submitted to Functional Plant Ecology, a section of the journal Frontiers in Plant Science

Received: *11 August 2021*
Accepted: *04 October 2021*
Published: *28 October 2021*

Citation:
Nolin AF, Tardif JC, Conciatori F and Bergeron Y (2021) Flood-Rings Production Modulated by River Regulation in Eastern Boreal Canada. Front. Plant Sci. 12:757280. doi: 10.3389/fpls.2021.757280

In northeastern boreal Canada, the long-term perspective on spring flooding is hampered by the absence of long gage records. Changes in the tree-ring anatomy of periodically flooded trees have allowed the reconstruction of historical floods in unregulated hydrological systems. In regulated rivers, the study of flood rings could recover past flood history, assuming that the effects of hydrological regulation on their production can be understood. This study analyzes the effect of regulation on the flood-ring occurrence (visual intensity and relative frequency) and on ring widths in *Fraxinus nigra* trees growing at five sites distributed along the Driftwood River floodplain. Driftwood River was regulated by a dam in 1917 that was replaced at the same location in 1953. Ring width revealed little, to no evidence, of the impact of river regulation, in contrast to the flood rings. Prior to 1917, high relative frequencies of well-defined flood rings were recorded during known flood years, as indicated by significant correlations with reconstructed spring discharge of the nearby Harricana River. After the construction and the replacement of the dam, relative frequencies of flood rings and their intensities gradually decreased. Flood-ring relative frequencies after 1917, and particularly after 1953, were mostly composed of weakly defined (less distinct) flood rings with some corresponding to known flood years and others likely reflecting dam management. The strength of the correlations with the instrumental Harricana River discharge also gradually decrease starting after 1917. Compared with upper floodplain trees, shoreline trees at each site recorded flood rings less frequently following the construction of the first but especially of the second dam, indicating that water level regulation limited flooding in the floodplains. Compared with the downstream site to the dam, the upstream ones recorded significantly more flood rings in the postdam period, reemphasizing the importance of considering the position of the site along with the river continuum and site conditions in relation to flood exposure. The results demonstrated that sampling trees in multiple riparian stands and along with various hydrological contexts at a far distance of the dams could help disentangle the flooding signal from the dam management signal.

Keywords: dendrohydrology, *Fraxinus nigra* Marsh., earlywood vessels, Ontario (Canada), black ash

INTRODUCTION

Over the last decades, extreme floods and droughts have become more recurrent and severe in boreal eastern Canada (Buttle et al., 2016; Bush and Lemmen, 2019; Aygün et al., 2020). Understanding if these recent trends are part of the natural hydrological variability is critical and studies remain complicated due to the lack of long instrumental hydrological series (Mortsch et al., 2015; Bush and Lemmen, 2019; Pellerin, 2019). Most gage stations in remote northern rivers were installed in the 1920s following the construction of water regulation systems or hydroelectric facilities, which reduced the availability of natural records (Pellerin, 2019; Nolin et al., 2021b). Therefore, biological proxies such as tree rings have provided hydrological time series in areas that lack instrumental records and have allowed dendrohydrologists to extend existing instrumental records when available.

Tree-ring proxies, among others, have been used to successfully reconstruct monthly, seasonal, and annual discharge (Boucher et al., 2011; Nolin et al., 2021a), lake-level fluctuations (Lemay and Bégin, 2008), droughts (Girardin et al., 2006), and floods (Tardif et al., 1997b; Boucher et al., 2011). Recent studies of anatomical changes in tree rings of periodically flooded trees (i.e., flood rings) have demonstrated their effectiveness in detecting major historical floods and comparing their magnitude (St. George et al., 2002; St. George and Nielsen, 2003; Tardif et al., 2010; Therrell and Bialecki, 2015; Kames et al., 2016; Meko and Therrell, 2020; Nolin et al., 2021a; Tardif et al., 2021a). In riparian ring-porous genus (e.g., *Quercus, Fraxinus*), flooding of tree stems at the time of earlywood formation resulted in decreased earlywood vessel cross-sectional areas (i.e., flood ring; St. George et al., 2002; Copini et al., 2016). Flood rings induced under experimental flooding conditions for amplitudes ranging from 3, 6, or 8 weeks in 4-years-old *Quercus robur* trees indicated that their occurrence was independent of the sapling age and of flooding duration (Copini et al., 2016). Developing quantitative earlywood vessel chronologies led to a significant reconstruction of high spring river discharge compared to the sole use of ring-width chronologies (Nolin et al., 2021a). Indeed, the ring width of riparian trees showed little, and often contrasting, association with flooding (Kames et al., 2016; Tardif et al., 2021b). For example, in Lake Duparquet, the radial growth of black ash (*Fraxinus nigra* Marsh.) in lowland floodplains (Tardif and Bergeron, 1993, Tardif et al., 1997a; Kames et al., 2016; Nolin et al., 2021a; Tardif et al., 2021b) and tamarack (*Larix laricina* K. Koch) in alluvial bogs (Girardin et al., 2001) showed a negative impact of spring flooding, while radial growth of eastern white cedar (*Thuja occidentalis* L.) in upper floodplains showed a positive impact of spring flooding (Denneler et al., 2010). Few consistent responses have been found between tree-ring width and discharge in riparian bur oak (*Quercus macrocarpa* Michx.) along the Red River (Manitoba, Canada; St. George and Nielsen, 2003), but tree-ring widths of riparian European ash, sampled along the Warta River in Poland, demonstrated a positive and significant correlation with previous fall (September to January) and current July and September maximum river flow (Koprowski et al., 2018). The presence and/or absence of flood rings in tree rings of ring-porous trees depends, however, on their exposure to spring flooding. Depending on the hydrological context, flood rings varied in relative frequency and intensity (Nolin et al., 2021b; Tardif et al., 2021b). For instance, Tardif et al. (2021a) and Tardif et al. (2021b) demonstrated that flood rings were formed mainly in *F. nigra* trees located in the lower floodplain but not in trees exposed to the same hydrological regime, but growing at a higher elevation. Fewer trees recorded flood rings in floodplains of regulated rivers compared with those of natural rivers, and flood rings in regulated rivers were also less distinct (intense) than those in natural rivers (Nolin et al., 2021b). Compared to the hydrological records from natural rivers, the natural discharge variability is masked by dam regulation and management maneuvers in regulated-river hydrological records (Déry et al., 2016) with a particular reduction in maximum daily and annual peak discharge downstream of dams (Williams and Wolman, 1984; Magilligan and Nislow, 2005; Graf, 2006). After water-level regulation, floodplain trees would be inundated less frequently due to flood attenuation by the dam. The tree rings would therefore be less likely to record all the same years of flooding as in nearby natural rivers. The impact of dam regulation on riparian forests could thus alter their ability to provide proxy (natural) hydrological data when trees have coped with altered hydrological regimes.

River regulation and dam management alter water availability for both upstream and downstream riparian forests in space and time and are further influenced by an interplay of factors such as plasticity of species, soil moisture, microtopography, etc. (Nilsson and Berggren, 2000; Magilligan and Nislow, 2005; Stella and Bendix, 2019). Downstream of a dam, the water table may be lowered, and the flood peaks attenuated with the frequency and magnitude of flooding reduced, suppressed, or shifted in time depending on reservoir management (Ashmore and Church, 2001; Nilsson and Berggren, 2000; Magilligan and Nislow, 2005; Graf, 2006). The composition of floodplain forests downstream of a dam often shifts to more drought-tolerant species than in the predam period with a loss of old-growth trees (DeWine and Cooper, 2007; Stallins et al., 2010; Schook et al., 2016). The response time of riparian forests varies widely across hydrological contexts. For example, Smith et al. (2013) found that the regulation of the Apalachicola River, initiated in the 1970s, reduced flood disturbance that positively affected tree age, and negatively affected radial growth and recruitment.

Hydrological effects upstream of dams have been less commonly studied (Petts, 1980; Evans et al., 2007; Baena-Escudero et al., 2021). In the short term, water regulation raises the water level for riparian forests upstream of a dam in the portion of the river under the influence of the dam (reservoir) resulting in forest mortality or composition change (Nilsson and Berggren, 2000), or in the loss of trees/species presenting flood rings. In the longer term, a dam can also cause progressive siltation reducing the river cross-section upstream of the dam. For example, Baena-Escudero et al. (2021) demonstrated that the siltation induced by dams on the Guadalquivir River in Spain, laden with silty sand sediments, resulted in a reduction in the discharge capacity of the river during floods less than 100 years after the dams were built. As a result, higher water levels

were reached after siltation, for an equivalent discharge before siltation, increasing the frequency and duration of flooding of the floodplains along the reservoir (Baena-Escudero et al., 2021). Slater and Villarini (2016) also noted that trends in flood frequencies among American rivers were different for some river basins that had undergone regulation or reduction in the capacity of the main river channel (urbanization). However, the length of the dam reservoir varies depending on the characteristics of the river and of the dam (Nilsson and Berggren, 2000). Further upstream of this reservoir, riparian forests, and flood dynamics are not affected and retain their natural attributes.

The impact of river regulation on radial tree growth has been little studied, but dendrochronological studies suggest that river damming generally has an adverse effect on the radial growth of riparian trees. Downstream of dams, regulation increases the sensitivity of riparian tree growth to drought and low water levels (Reily and Johnson, 1982; Salzer et al., 1996; Coble and Kolb, 2012). As a result, tree growth is more highly correlated to discharge during the predam period and to drought (low discharge) and precipitation during the postdam period (Reily and Johnson, 1982; Stromberg and Patten, 1990; Salzer et al., 1996; Coble and Kolb, 2012; Netsvetov et al., 2019). The damming also tends to reduce the ring-width variability in the postdam period (Salzer et al., 1996). Reily and Johnson (1982) compared regulation effects on radial tree growth of several riparian species along elevation gradients in the Missouri River and demonstrated that tree growth downstream of an altered hydrological regime responds in variable ways depending on, among others, tree species and elevation to water levels.

The aim of this study was to determine how discharge regulation by dams affects both ring width and the production of flood rings along with various regulated hydrological contexts. More precisely, we asked how are radial growth and flood-ring production of riparian *F. nigra* trees are impacted by the construction of hydrological dams, and if the ability of trees to record high-magnitude flood rings differ according to distance to the shoreline and among different sites located upstream and downstream of the dam. It was hypothesized (i) that flood rings would present no differences between sites prior to dam construction whereas (ii) after dam construction, flood rings would be recorded more abundantly and be of higher intensity upstream. It was also hypothesized that dam construction would reduce ring width and its variability, as well as alter the correlation structure with discharge and precipitation. In addition to enhancing our understanding of the impact of dam regulation on the ability of riparian *F. nigra* trees to record hydrological events, this study addresses sampling strategies that maximize the success of generating flood records of riparian trees in a context of hydrological regulation.

MATERIALS AND METHODS

Study Area

The study area is located on the Driftwood River, meandering in the clayey and peatland plains of northeastern Ontario at the southern fringe of the boreal forest (**Figure 1**). The source of Driftwood River is located near Lipsett Lake (48°19′49″ N; 80°42′46″ W). After flowing north to reach Moose Lake, the river ends in the Abitibi River (**Figure 1**). Because the head of the Driftwood River basin is not easily accessible, the sampling started on the shores of Moose Lake (11 km^2) to the confluence with the Abitibi River (**Figure 1**). The Driftwood River was flowing naturally until the construction of a log dam in 1917–1918 at Monteith (Ontario Ministry of Natural Resources and Forestry [OMNRF], 2019; **Figures 1**, **2**). The height of the log dam is not known but the structure was built with two spillways to store the water in a reservoir and to supply electricity (60-cycle power) to a Demonstration Farm for the Ontario Government. In 1941, the generator was downsized to a 25-cycle electric power to light a prisoners-of-war camp. The reservoir and spillways were maintained but apparently abandoned. From 1952 to April 1953, the old log dam was replaced at the same location by a 5.9-meter-high and 52-meter-long concrete gravity structure to supply water for an industrial farm (The old and the new on Driftwood River, 1953). It is possible that the dam was built on an existing rapid or on a natural constriction of the riverbed as is the case for other rivers in the region. Monteith dam is owned and operated by the Ontario Ministry of Natural Resources to control the Driftwood River as far upstream as Moose Lake. Most of the year, the dam is maintained at a fixed operating level of 260.36 m (**Figure 3**; Ontario Ministry of Natural Resources [OMNR], 2004). The dam is operated solely at spring for flood mitigation with manually operated stop logs to maintain Moose Lake level at, or below, 260.66 m (**Figure 3**; Ontario Ministry of Natural Resources [OMNR], 2004).

Upstream of the Monteith dam, a gage station (04MB002; Water Survey of Canada, 2021; **Figures 1**, **3**) has been in service since 2006 to record water levels about 10 m upstream of the dam. While of short duration, the daily hydrographs indicate that the Driftwood River follows a boreal regime with a peak response to ice and snowmelt in spring lasting for several weeks. Relatively high water levels are maintained through the summer, probably because of the dam, and with a late recession in winter a few months before the freshet (**Figure 3**). There is no record of the Driftwood River hydrological regime prior to the dam, making it impossible to assess the exact impact of the dam on flood magnitude or mean water levels upstream and/or downstream. The nearest unregulated hydrological record is for the Porcupine River (04MD004), located about 50 km to the west with data from 2007 to 2019. The drainage areas of the gage stations on the Driftwood and Porcupine Rivers are similar (537 km^2 compared to 408 km^2) allowing a direct comparison. The nearest, longest unregulated records are for the Harricana River (04NA001 and 04NA002), located about 200 km to the East, with data from 1915 to 2021, over a larger gross drainage area (3, 680 km^2).

Tree-Ring Data

Tree-ring data were collected in the summer of 2017 to investigate the spatial coherency of spring floods in eastern boreal Canada (Nolin et al., 2021b). A total of 43 living *F. nigra* trees were sampled in five sites representing different hydrological contexts with site Rapid River (RPR) 1 located 1 km downstream of Monteith dam; site Driftwood River (DFR) 1, located 10 km

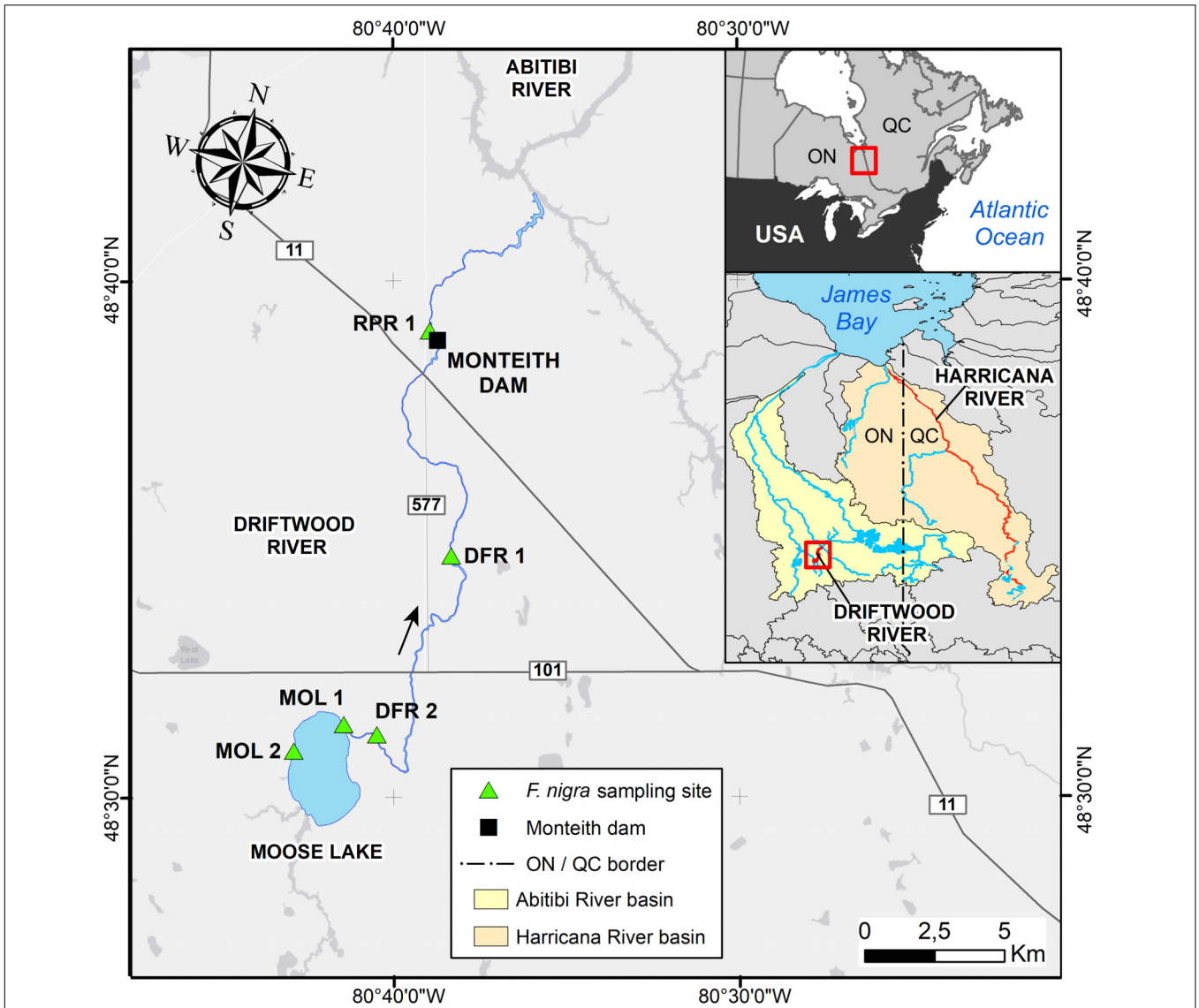

FIGURE 1 | Map of the study area. The geographic location of the Driftwood River at the border between Ontario and Québec in Canada (upper right inset) and within the Abitibi River basin (lower right inset). Locations of the *Fraxinus nigra* sampling sites along the Driftwood River are coded as follows: MOL - Moose Lake; DFR - Driftwood River; RPR - Rapid River.

upstream of the dam; site DFR 2 located 25 km upstream on the tip of a meander and 1 km downstream of the estuary of Moose Lake (MOL); site MOL 1 located 27 km upstream at the estuary of Moose Lake; and site MOL 2 located 31 km upstream on the opposite shore of Moose Lake estuary (**Figure 1** and **Table 1**). *Fraxinus nigra* trees growing on the shoreline of the Driftwood River are situated close to their northern distribution limit. The species grows on fine waterlogged clay soils and occurs in pure or mixed stands in association with eastern white cedar and balsam poplar (*Populus balsamifera* L.; Tardif and Bergeron, 1992; Tardif and Bergeron, 1999; Denneler et al., 2008). The species is tolerant to water-level fluctuations (Sims et al., 1990) and was sampled in the lower floodplains where sensitive fern (*Onoclea sensibilis* L.) is indicative of long-lasting floods (Tardif and Bergeron, 1992). Dominant trees were selected, and two cores were collected on trees with the largest diameter with the aim to produce long chronologies. Coring was done with a 5 mm increment borer in two opposite directions to reach the tree center and as close to the tree base as possible. Diameter at breast height was recorded as well as the distance of each tree to the shoreline. Each core sample was prepared according to standard dendrochronological procedures (Phipps, 1985) and sanded with a progressively finer grit. Prior to cross-dating, each sample was inspected for the presence of flood rings by two observers, each processing half of the samples. In *F. nigra*, flood rings are characterized by a noticeable increase in earlywood vessel number which is accompanied by a noticeable decrease of earlywood vessels area (Tardif et al., 2010; Kames et al., 2016;

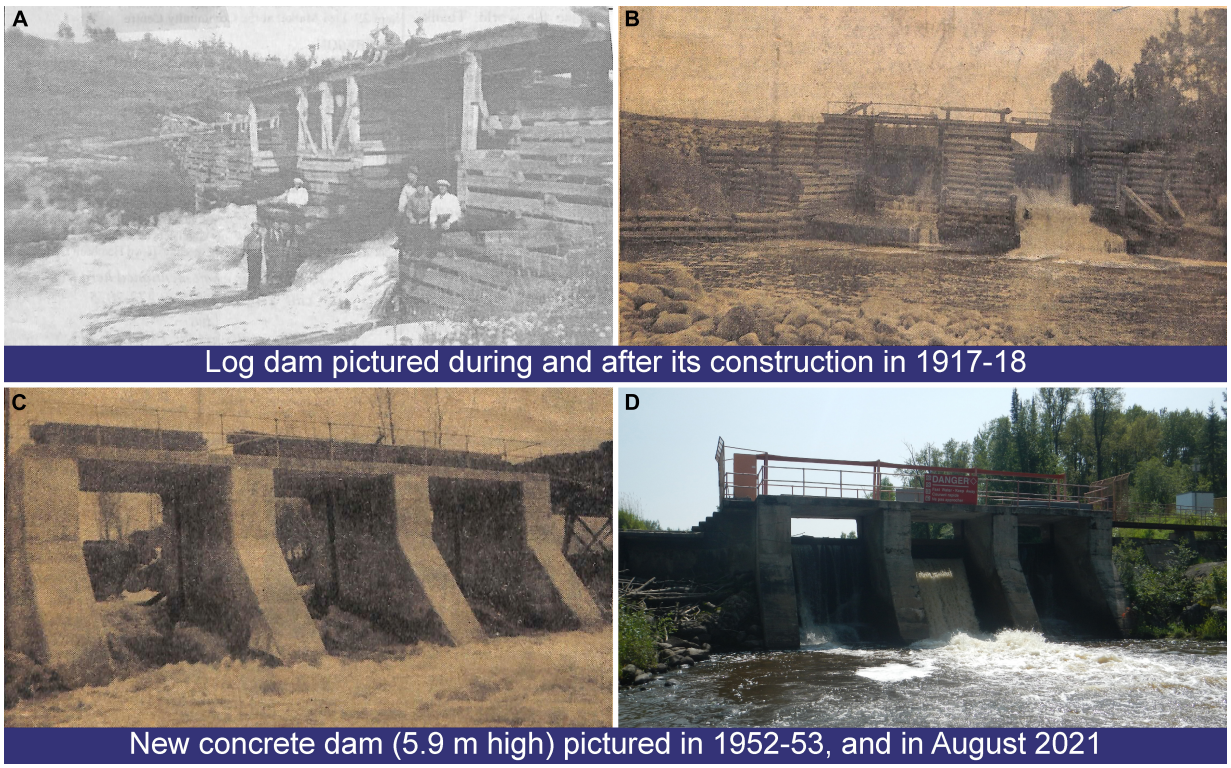

FIGURE 2 | The old and the new on Driftwood River at Monteith. First log dam **(A,B)** and second concrete dam **(C)** in the years of their construction as compared to today structure **(D)**. Historical photos **(B,C)** by Mrs. C. Clifford were published in an unknown local newspaper on May 6, 1953. All historical photos retrieved from the digitalized archives of the Monteith Women Institute Tweedsmuir Community History, a courtesy of the Federated Women's Institutes of Ontario (FWIO; https://collections.fwio.on.ca). Photo in August 2021 by AFN.

Nolin et al., 2021a,b; Tardif et al., 2021a). A dual numerical code was used to record the level of distinctiveness of flood rings with an F1 code indicating a weakly defined flood ring and an F2 code indicating a well-defined flood ring (Nolin et al., 2021b; Tardif et al., 2021a). Cross-dating was then performed using the previously defined regional *F. nigra* pointers years (Tardif et al., 1997a; Kames et al., 2016; Nolin et al., 2021b). The age of each tree was determined from the oldest core sample and was either the age of the pith or the age of the last visible tree ring when the pith was not present on the core. Ring widths were measured with CooRecorder (v9.0.1; Larsson, 2003a) on 2400 dpi scanned images and were validated with CDendro (v9.0.1; Larsson, 2003b) and COFECHA (Holmes, 1983).

Statistical Analysis and Independent Data

Both, flood-ring relative frequencies and ring-width chronologies, were generated. Flood-ring series were produced from visual identification of flood rings and of their intensity (F1 and F2) by two expert observers. Tardif et al. (2021a) demonstrated that both flood rings and their intensity could be identified with high consistency by novice and expert observers and that visual identification of flood rings could provide accurate and reproducible semiquantitative data. Flood-ring series were pooled by the tree, keeping the code with the maximum intensity for each year ($0 < F1 < F2$; Nolin et al., 2021b). Flood-ring categories have been shown to respond to the same hydroclimatic variables and to be complementary with F1 observed in most years, F2 observed in known high-flood years, and both F1 and F2 being almost absent from unflooded control sites (Nolin et al., 2021b; Tardif et al., 2021a). The relative frequencies of F1 and F2 by sites were then calculated by dividing their respective sum by the number of trees per year. Both F1 and F2 relative frequencies were also summed (F12). Ring-width measurement series were averaged by the tree (n = 2 cores) and the old non-overlapping portion was kept (n = 1 core) to maximize temporal coverage. Ring-width series were standardized by dividing each tree series by its mean to conserve the integrity of the low-frequency variations (Cook and Kairiukstis, 1990). Standardized ring-width series and F1, F2, and F12 relative frequencies were then averaged by sites. To assess a possible effect of distance from the shoreline, each of those series was grouped into two distance classes representing shoreline trees [0–10 m] and floodplain trees [10–100 m].

Non-parametric change point analysis was performed on mean site ring-width chronologies using the "ecp" package (v3.1.3; James and Matteson, 2014). A univariate change point analysis was performed for each site, and multivariate analysis was performed using all mean site chronologies at

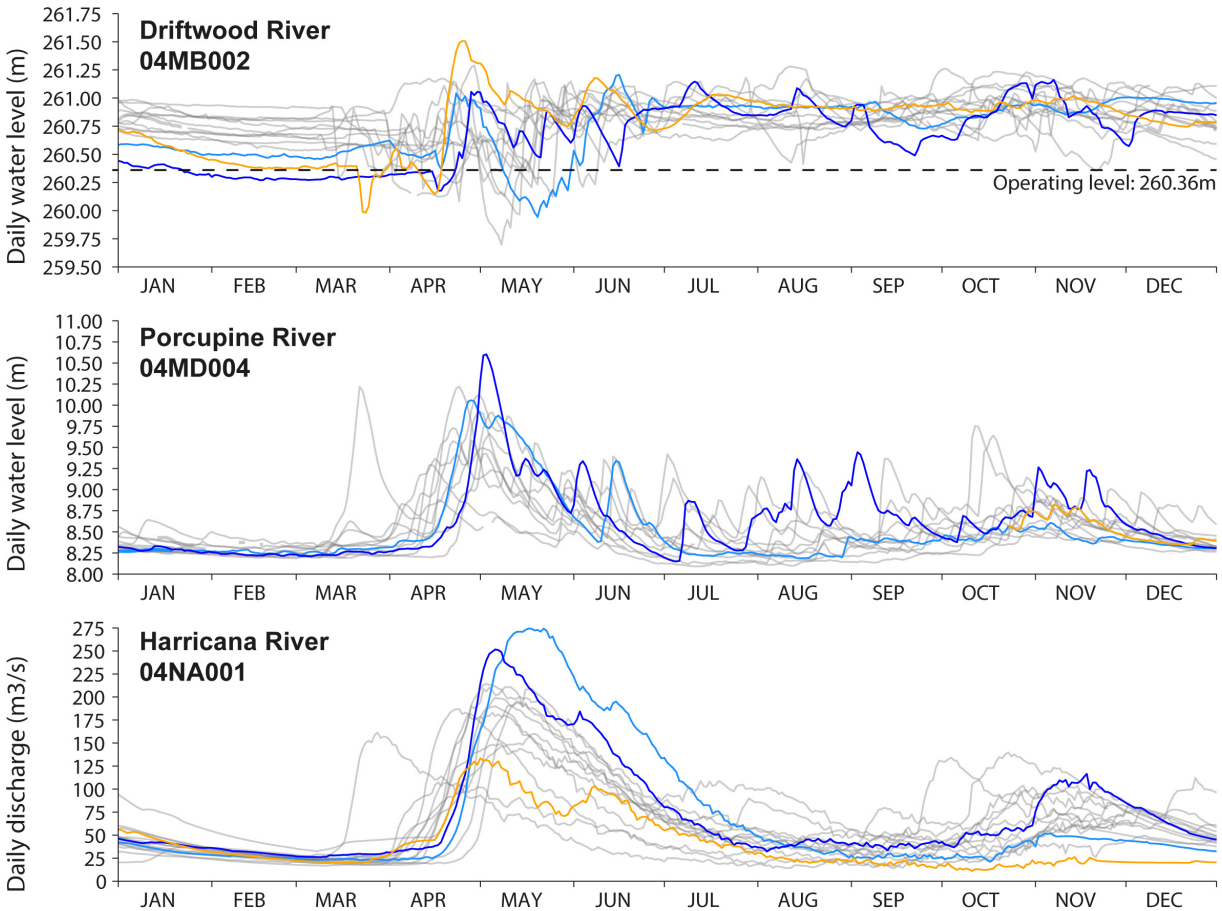

FIGURE 3 | Comparison of the daily water level of the Driftwood River downstream of the Monteith dam (2006–2020) with the daily water levels of the unregulated Porcupine River at Hoyle (~50 km west; 2007–2019) and the daily discharge of the unregulated Harricana River at Amos (~200 km east; 2006–2020). Daily data for the year 2007 are incomplete at the Porcupine River gage station. Data were extracted from the historical hydrological station data of the Water Survey Canada. The years of maximum discharge or water level found during the 2006–2020 period and in the three rivers are highlighted in color. The light blue line represents the year 2019 (maximum discharge in the Harricana River), the dark blue line represents the year 2013 (maximum water level found in the Porcupine River), and the orange line represents the year 2007 (maximum level found in the Driftwood River). The dashed line in the upper panel depict the operating level (260.36 m) of the Monteith dam.

once. Multivariate analysis of change points was performed by successive common periods, removing the youngest chronology each time until there were only two chronologies left. Change points were estimated by iterative hierarchical segmentation of chronologies and tested for significance using 1,000 Monte Carlo permutation tests (Matteson and James, 2014).

Flood-ring relative frequencies and ring-width chronologies were finally compared to four independent instrumental and proxy series. First, daily discharge data from the unregulated Harricana River (1915–2021; Water Survey of Canada, 2021) were used (**Figure 1**). Second, both a reconstruction of the spring (April 15-June 30) discharge and a chronology of flood-ring relative frequency for the Harricana River were available for the period 1771–2016 (Nolin et al., 2021a,b). The reconstructed Harricana River discharge data are highly correlated with the instrumental data ($r = 0.819$, $p < 0.001$, 1915–2016) and can be used as a proxy for the period before 1915 (Nolin et al., 2021a). At last, precipitation data were also retrieved from gridded CRU TS4.04 (Harris et al., 2020) using the KNMI Climate Explorer[1] (Trouet and Van Oldenborgh, 2013). Spring (March-April-May) precipitation data were averaged over the 0.5° × 0.5° grid cells corresponding to the spatial extent of the sampling sites (48°N; −80°E to 48.5°N; −80.5°E; **Figure 1**) and covering 1901–2019.

The flood-ring relative frequencies (F1, F2, F12) were compared among sites using bootstrapped Spearman correlation coefficients (Legendre and Legendre, 2012). Each correlation was calculated on 10,000 random samplings of the chronologies to approximate the sampling distribution of the Spearman correlation coefficient and to return its mean (Efron, 1992), using the "boot" package (Canty and Ripley, 2021). Ring-width chronologies were compared among sites and with the aforementioned hydroclimatic data using 40-year moving windows of bootstrapped Pearson correlation coefficients lagged backward by 5 years (Legendre and Legendre, 2012) using

[1]https://climexp.knmi.nl

TABLE 1 | Location of sampling sites.

Site	No. trees	Position to dam	Latitude/Longitude	Period
RPR 1	8	1 km downstream	48°38′53″N; 80°40′42″W	1930–2017
DFR 1	6	10 km upstream	48°34′31″N; 80°40′05″W	1917–2017
DFR 2	10	25 km upstream	48°31′03″N; 80°42′15″W	1879–2017
MOL 1	8	27 km upstream	48°31′15″N; 80°43′13″W	1898–2017
MOL 2	11	31 km upstream	48°30′44″N; 80°44′39″W	1852–2017

Data are ordered by increasing the distance to the dam from top to bottom. A period is the length of flood-ring records.

TABLE 2 | Characteristics of *Fraxinus nigra* stands.

Site	Diameter	Age	Distance to shore
RPR 1	27.5 ± 6.3	68.9 ± 15.3	13.4 ± 11.8
DFR 1	26.7 ± 5.8	89.3 ± 10.2	6.8 ± 6.4
DFR 2	35.4 ± 10.9	85.0 ± 31.2	35.9 ± 18.0
MOL 1	33.9 ± 7.1	98.4 ± 14.9	8.8 ± 5.5
MOL 2	48.5 ± 9.9	122.1 ± 31.3	29.5 ± 25.6

Mean values and standard deviation by site indicating (1) stem diameters at breast height, (2) maximum tree age, and (3) their position in the floodplain relative to the shoreline.
Data are ordered by increasing distance to the dam from top to bottom.

the "treeclim" package (Zang and Biondi, 2015). All statistical analyses were conducted in the R statistical environment (R Core Team, 2021).

RESULTS AND DISCUSSION

Impact of Regulation on Stand Structure

The comparison of daily hydrographs of regulated and unregulated rivers illustrates the reduction of spring flood peaks and the maintenance of high-water levels throughout the year in the Driftwood River compared to a natural regime (**Figure 3**). Comparing the years of the highest water levels and discharge in the Driftwood, Porcupine, and Harricana Rivers also shows that years of high-water levels in the regulated Driftwood River do not necessarily correspond to years of high-water levels or high discharge in the two other natural rivers (2007 orange line in **Figure 3**). In the natural Porcupine and Harricana Rivers, the years 2013 and 2019 are known as major flood years and show comparable high-water levels and discharge (blue lines in **Figure 3**).

The ages of the trees sampled on the Driftwood River ranged from 32 to 166 years with differences observed from upstream to downstream (**Table 2**). The oldest and largest *F. nigra* trees were located at the greatest distance upstream of Monteith dam (MOL 2) while the youngest and smallest trees were found at the site right downstream of the dam (RPR 1) and at the closest site upstream of the dam (DFR 1; **Table 2** and **Figure 4**). Site DFR 2 presented the most dispersed age class compared with others with tree ages ranging from 38 to 138 years (**Table 2** and **Figure 4**). The difference in age between upstream and downstream sites was consistent, although the maximum age of a few trees was underestimated because of rotten parts (14 of 43 trees) and could therefore be assumed to be older. The maximum ages of the trees suggest that sites DFR1, DFR2, MOL1, and MOL2 were present prior to the construction of the log dam in 1917–1918 and that RPR1 was established prior to the construction of the second dam in 1952–1953 (**Table 2** and **Figure 4**). On the shores of Moose Lake (MOL 1, MOL 2), *F. nigra* trees formed dense and thick fringe forests from the shoreline to a maximum of 100 m in the floodplain. Further downstream on the Driftwood River (DFR 2, DFR 1, RPR 1), *F. nigra* trees were organized in narrow linear stands along the river and extended to a maximum of 30 m in the floodplain. The old age and extent of the stands suggest that *F. nigra* trees at Moose Lake have survived the dam constructions. In the nearby Lake Abitibi, the first damming of the lake in 1915 raised the water level of ca. 1.2 m and caused the mortality of the riparian fringe forest (Denneler et al., 2008). Investigating the spatial coherency of flood rings, Nolin et al. (2021b) found significatively shorter flood-ring records in regulated rivers compared with natural rivers, which suggested that regulation may have permanently eliminated old-growth floodplain forests. Several studies also reported a negative effect of peak flow regulation recruitment and establishment of riparian trees downstream of a dam (DeWine and Cooper, 2007; Smith et al., 2013; Schook et al., 2016). In this study, no additional stands of *F. nigra* were found downstream of RPR 1. Besides an effect of regulation, other factors could also explain the age difference between sites (oldest upstream, youngest downstream) such as land-use changes, timber harvest, or natural dynamic of seeds propagation. However, no evidence of land-use changes and lowland forest harvesting was found in the archives consulted (Geography of Monteith, n.d.; The old and the new on Driftwood River, 1953). Seeds of *Fraxinus* trees (samaras) are morphologically adapted to be dispersed by wind, and dispersal by water current in periodically flooded riverine lowlands has also been reported (Merritt and Wohl, 2002; Schmiedel and Tackenberg, 2013). *F. nigra* sexual regeneration at Lake Duparquet was also positively influenced by high water levels during spring and early summer, while the species also regenerate by vegetative reproduction (Tardif et al., 1994). In the Saône River in France, flooding favored *Populus* regeneration by eliminating seedlings of other flood-intolerant species (Astrade and Bégin, 1997). It can thus be hypothesized that river regulation may result in a regeneration deficit of riparian *F. nigra* downstream of the dam and upstream at the reservoir. Since only old trees were sampled in this study, the data do not provide evidence of an effect of Monteith dams on *F. nigra* recruitment in the Driftwood River floodplains. A future research avenue should thus investigate age classes and seedling perennity among floodplain forests and between hydrological contexts.

Flood-Ring Relative Frequencies (Predam Period)

The flood-ring chronologies covered 1852–2017 with a common overlap period between 1930 and 2017 (**Table 1**). Little flood-ring data were available prior to the construction of the first log dam (1917–1918; **Figure 4**). The most consistent flood-ring

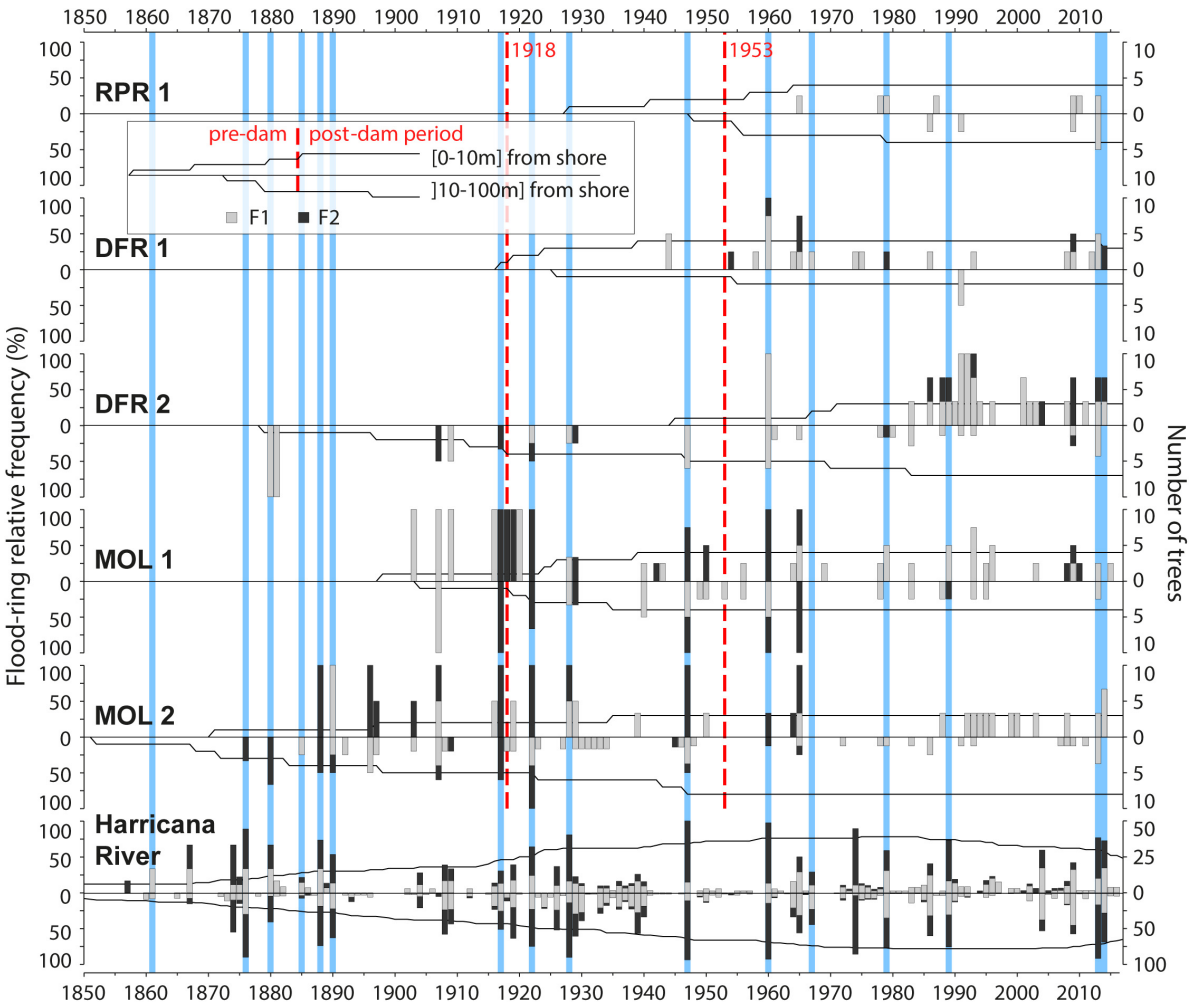

FIGURE 4 | Flood-ring chronologies for each of the five sites and organized by distance classes to the shoreline (0–10 and 10–100 m) and for the naturally flowing Harricana River. Trees close to the shoreline (0–10 m) are shown with positive bars and trees from the floodplain (10–100 m) with negative bars. Gray and black histograms are, respectively, F1 and F2 flood-ring relative frequencies, and the black solid line in the background indicates temporal replication among the trees sampled per year. Vertical red dashed lines indicate dates of construction of the first and second Monteith dam. Blue vertical bars indicate the years with the highest reconstructed spring discharge for the Harricana River (threshold value = 151.3 m^3/s; Nolin et al., 2021a,b).

record for the predam period was found at the most ancient and upstream site MOL 2 (**Figure 4**). The high spring discharge years evidenced in the F12 relative frequencies from the Harricana River were identified by the years 1880, 1888, 1890, and 1917 recorded by 33 to 100% of the trees growing on the shoreline and in the floodplain of Moose Lake with mainly F2 flood rings (**Figure 4**). F12 relative frequencies from MOL 2, MOL 1, and DFR 2 also correlated positively (r = 0.25–0.50) and significantly ($p < 0.05$) with the reconstructed Harricana River spring discharge (**Table 3**). Few years exhibited high F1 and F2 relative frequencies while not being equaled in the Harricana River records and supported the regional contrasts evidenced in years 1896 and 1907 by Nolin et al. (2021a,b). Those 2 years were similarly characterized by high spring discharge and mid to high frequency of flood rings at Lake Duparquet (20 and 81%, respectively) and in the Little Abitibi River (38 and 76%, respectively; Nolin et al., 2021a,b). Other years with high F12 relative frequencies for this period in the Driftwood River (DFR1, DFR2) demonstrated a good agreement with MOL 2 and with the reconstructed Harricana River spring discharge (**Figure 4** and **Table 3**). Of importance is that the relative frequencies of F1 and F2 were higher in trees growing on the shoreline than in the floodplain, where more abundant F1 with lower relative frequencies were found (**Figure 4**). Not all years with F2 values in shoreline trees were matched by comparable F2 values in floodplain trees, as is the case for the Harricana River flood-ring record (**Figure 4**). Tardif et al. (2021, 2021b) showed that flood rings gradually disappeared from low to high elevation floodplains to non-flooded upland stands and that microtopography led to differences in exposure of trees to flooding. This result suggests that natural historical floods may have flooded for short distances to the shoreline, which would

TABLE 3 | Comparison of F12 flood-ring relative frequencies with instrumental and reconstructed mean spring (April 15–June 30) discharge of the naturally flowing Harricana River and by distance to the shoreline (0–10 and 10–100 m).

	Pre-dam period (*)				After the first dam: 1918–2016				In-between the two dams: 1918–1952				After the second dam: 1953–2016			
	[0–10 m]		[10–100 m]		[0–10 m]		[10–100 m]		[0–10 m]		[10–100 m]		[0–10 m]		[10–100 m]	
	rho	*p*	*rho*	*p*	*rho*	*p*	*rho*	*p*	*rho*	*p*	*rho*	*p*	*rho*	*p*	*rho*	*p*
RPR 1	ND	ND	ND	ND	ND	ND	ND	ND	ND	ND	ND	ND	0.04	0.742	0.23	0.075
DFR 1	ND	ND	ND	ND	**0.23**	0.024	ND	ND	−0.23	0.204	ND	ND	**0.41**	0.001	−0.05	0.674
DFR 2	ND	ND	**0.35**	0.005	ND	ND	**0.27**	0.008	ND	ND	**0.49**	0.006	**0.28**	0.034	0.18	0.16–0
MOL 1	**0.31**	0.013	**0.25**	0.051	**0.27**	0.007	**0.32**	0.002	0.26	0.172	**0.48**	0.008	**0.27**	0.041	0.20	0.120
MOL 2	**0.38**	0.003	**0.50**	0.000	**0.28**	0.007	0.15	0.152	**0.60**	0.000	0.05	0.721	0.11	0.427	0.20	0.131

Spearman correlation coefficients (rho) are given after calculating 10,000 bootstrap iterations.
Bold characters denote significant rho coefficients at $p < 0.05$.
Spearman coefficients were calculated for four periods (1) The predam period before the first log dam (1850–1917), (2) After the first log dam (1918–2016); (3) In between the first log dam and the second concrete dam (1918–1952); and (4) After the second concrete dam (1953–2016).
*(*) Note that for the predam period, the number of years varies among sites and distance classes with DFR 2 (1879–1917), MOL 1 (1898–1917), MOL 2 (1852–1917; **Figure 4** and **Table 1**). The predam period has been calculated with the reconstructed Harricana River discharge, the other periods with the instrumental Harricana River discharge.*
ND: no data.

further increase the sensitivity of the *F. nigra* forests to a change in flood regime or water levels by dams. Overall, the results from the predam period compared well with the findings from other regulated rivers in the area that showed a high spatial coherency with most flood rings recorded in natural rivers prior to the period of dam implementations in the region (1920–1930s; Nolin et al., 2021b).

Flood-Ring Relative Frequencies (Postdam Period)

In contrast to the flood-rings chronology from the unregulated Harricana River, those from the Driftwood River tracked the hydrological changes that occurred after the implementation (1917) and the replacement (1953) of the Monteith dam. The most striking features were the decrease in the flood-ring relative frequencies and the decrease in the number of F2 in the postdam period (**Figure 4**). This response was also seen in the decrease in the number of sites with a significant correlation of F12 relative frequencies with the mean Harricana River instrumental spring discharge (**Table 3**).

During the period between the first and the second dam (1918–1952), high F12 relative frequencies with high values of F2 were still recorded during the known high spring discharge years of 1922, 1928, and 1947 at upstream sites MOL 2, MOL 1, and DFR 2 (**Figure 4**). The F12 relative frequencies from those sites still correlated positively and significantly with the instrumental Harricana River mean spring discharge. However, the correlations from shoreline trees at MOL 1 presented a non-significant ($p < 0.05$) correlation while in a range of the correlation strength found in the other periods (**Table 3**). Few high values of F12 relative frequencies were observed in floodplain trees growing on the MOL 2 site compared to the predam period. Abundant F1 flood rings of low relative frequency (<20%) were also observed in floodplain trees at the MOL 2 site during the 1917–1952 period, but not in shoreline trees, which contrasts with the other flood-ring records from the other four sites (**Figure 4**). Like the predam period, higher F12 relative frequencies, and mostly F2 flood rings, were found for trees close to the shoreline compared to floodplain trees (**Figure 4**).

After the replacement of the dam in 1953, values of F12 relative frequencies decreased at all sites compared with the previous two periods, with mainly F1 being recorded. The lowest F12 relative frequencies were found near the dam (RPR 1 and DFR 1) and the highest values were found upstream and at a far distance from the dam (MOL 2, MOL 1, DFR 2). Site RPR 1 showed almost no flood rings (37.5% at maximum in three of eight trees) although the age of the stand does not allow comparison with a predam period. Experimentally induced flood rings, however, have been shown to form in 4-year-old pedunculate oak (*Q. robur* L.) trees suggesting that young riparian forests should be able to record flood history (Copini et al., 2016). The absence of flood rings at RPR 1 might thus reflect the river regulation.

At the other sites, flood rings were primarily F1, with high F2 relative frequencies found in both known regional flood years and in random years. High spring discharge years 1960, 1967, 1979, 1989, 2013, and 2014 were evidenced in the Harricana

River record (**Figure 4**). The 1960 flood was reconstructed as the highest discharge of the last 250 years in the Harricana River (Nolin et al., 2021a) and showed very high F12 relative frequencies (approaching 100%) in multiple natural regional rivers (Nolin et al., 2021b). In the Driftwood River, high flood-ring relative frequencies of F1 and F2 types were still found in 1960 after the dam was replaced (**Figure 3**). Other years with high F12 relative frequencies such as 1965 or 2007 may result from the dam management in the Driftwood River, or from regional contrasts in spring flooding (**Figure 4**). For instance, the year 1965 was characterized by high ice-scar frequency in Lake Duparquet (Tardif et al., 1997b) and by mid to high F12 flood-ring relative frequencies in Lake Duparquet (69%) and regional natural rivers (44%; Nolin et al., 2021b). The year 2007 was the highest spring water level recorded in the Driftwood River upstream of the Monteith dam and over the period 2006–2020, which was not the case in the natural Harricana River (**Figure 3**). The mean spring discharge of the Harricana River for the year 2007 (91.5 m^3/s) was well below the discharge threshold used to define high spring discharge years in this river (151.3 m^3/s, Nolin et al., 2021a,b).

Floodplain trees recorded very low F12 relative frequencies compared with the shoreline trees at all sites (**Figure 4**). No significant correlation with instrumental mean Harricana River spring discharge was either found for F12 from floodplains trees at all sites (**Table 3**). Trees of site MOL 2 almost stopped recording flood rings after 1960 and it can be assumed that the decrease in the flood peak regime induced by the dam has ended the flooding of this site while maintaining the old-growth forest. The F12 records from shoreline trees at other sites upstream of the dam (MOL 1, DFR 2, DFR 1) still correlated positively and significantly with the instrumental Harricana River mean spring discharge (**Table 3**). Higher F12 relative frequencies were found after ∼1980 in the shoreline trees at site DFR 2, which may indicate an intensification of spring water storage by the dam over this period compared to the other sites over the same period, and to the period before 1980 at site DFR 2 (**Figure 4**).

Throughout the flood-ring records in the postdam period, no extremely high relative frequencies were found during the known date of town settlement, or road and bridge construction. The small village of Driftwood city established on the east side of the Driftwood River was destroyed in the 1916 fire. The first buildings of the actual Monteith were built in 1916, after the fire, and on the opposite side of the river (Geography of Monteith, n.d.). No particularly high flood-ring relative frequencies were neither found for the years of the construction or modification of roads and bridges. The Ontario Highway 11 and Secondary Highway 577 (**Figure 1**) were built in 1920 and 1956, respectively, and were modified in 1953, 1958, and 1959 (Highway 11) and in 1978 (Highway 577) sometimes associated with muskeg excavations.[2] While the number of samples used in this study is a limiting factor, the overall findings agree with those from regional regulated rivers where trees recorded few flood rings and of low intensity (F1) after the period of dam constructions in the region (1920–1930s; Nolin et al., 2021b).

[2]http://www.thekingshighway.ca/list.htm

The exclusion of low F12 frequencies or partitioning of F12 frequencies between F1 and F2 flood rings may allow separating years of a major flood from years of high-water stage induced by dam management or other anthropogenic alterations (e.g., bridge construction, muskeg excavations). This may become important in a context where it is not possible to compare flood-ring relative frequencies to regional hydrologic records (instrumental or reconstructed). The high F12 relative frequencies that are present in both, shoreline trees (F12 > 75%) and floodplain trees (F12 > 50%), indicate that the spring discharge from 1960 to 1965 flooded the shoreline and the floodplain trees after the Monteith dam construction. The years for which F2 have been recorded in both, shoreline and floodplain trees, also indicated that the years 1960, 1965, and the year 2009 inundated the distant floodplain. Different flood-ring responses to those flood years at sites MOL 1 (high relative frequencies) and MOL 2 (low relative frequencies; **Figure 4**) emphasized that sampling sites with different elevation and flood exposure gradients might help in disentangling major flood years from water-level management events. Moreover, in this study, cores were taken at varying heights due to varying wood quality (i.e., rot, frost scars). It would be interesting to include sampling height in future analyses since flood rings have been shown to solely occur below water level (Copini et al., 2016) and/or to weaken along with stem height and with increasing distance to the ground (St. George et al., 2002). Studying the flood-ring distribution in relation to stem height could provide a proxy for flood height and it would add to the information that can be provided by flood-ring intensity. For instance, Tardif et al. (2021a) noted that flooded *F. nigra* trees in close proximity could record flood rings of different intensity (F1, F2) supporting the idea that sampling height and tree elevation might affect the distinctiveness of flood-ring signature. The authors also noted that the identification error between two observers was greater for weakly defined flood rings (F1) than for well-defined flood rings (F2).

Ring-Width Chronologies

Over the 1930–2017 common period, the mean correlation between the five site chronologies was generally high (r = 0.49 ± 0.24 sd) except for the site RPR1, which was weakly correlated with the other sites (r = 0.19 ± 0.28 sd). The highest significant correlation among ring-width chronologies was found between the most upstream sites MOL 1 and MOL 2 (r = 0.69, $p < 0.001$). The univariate change point analysis identified no change in mean and/or variance in each mean site ring-width chronologies that could be related to the first or second dam construction (**Figure 5** and **Supplementary Table 1**). Significant change points were detected with low consistency in multivariate analysis in years 1909, 1914, 1917, 1941, 1945, 1974, and 1975 ($p < 0.05$) over most of the common periods used for the multivariate change point analysis (**Supplementary Table 1**). The most significant change point was the year 1974, identified in three different combinations of mean site chronologies (**Supplementary Table 1**). This year does not correspond to any of the years of the village (1916), road, bridge (1920, 1953, 1956, 1958, 1959, 1978), or dam (1917, 1953) constructions that may have possibly affected the hydrology

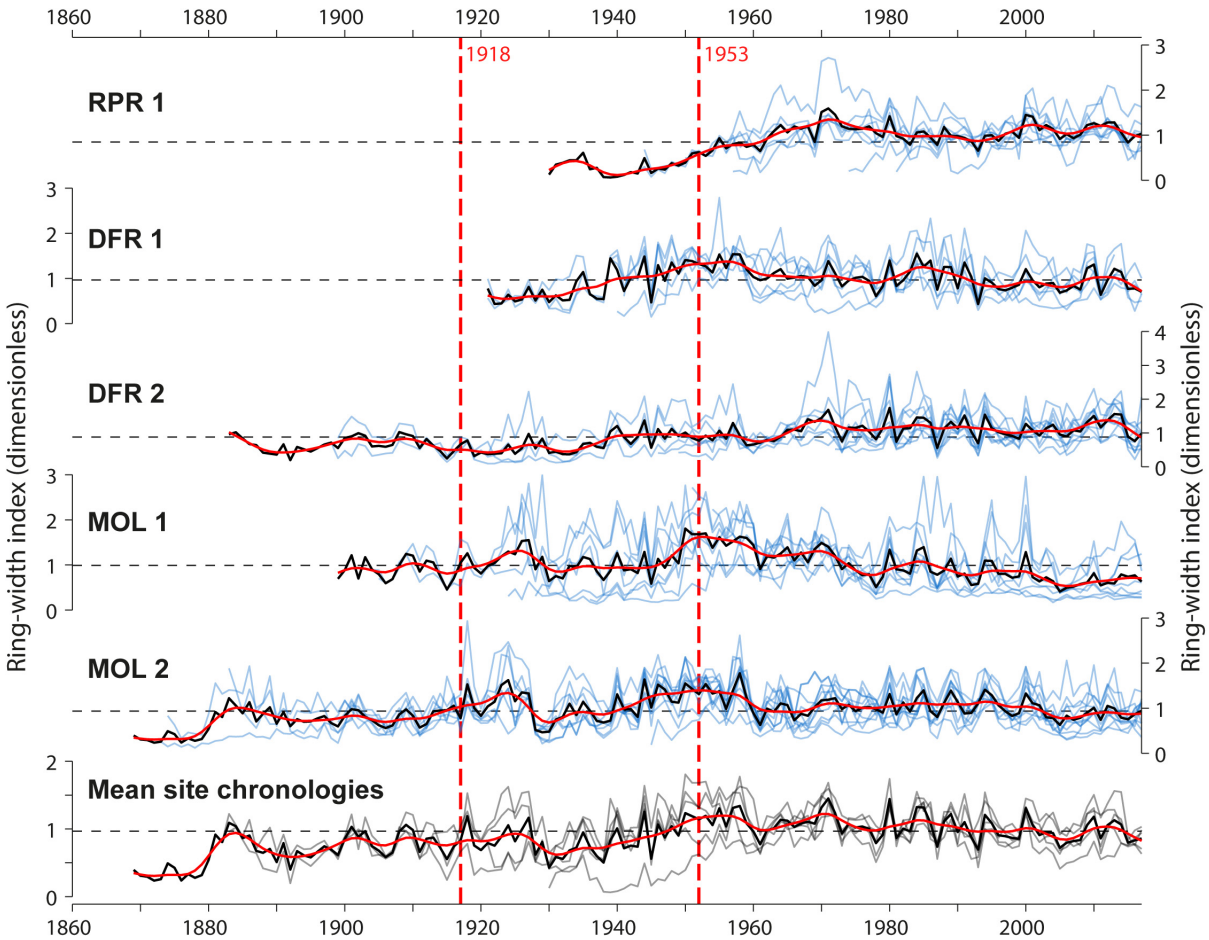

FIGURE 5 | Standardized tree-ring width series (pale blue line) and mean site chronologies (dark black lines), and comparison of mean site chronologies among the five sites. Vertical red dashed lines indicate dates of construction of the first and second Monteith dam. The red curves are 10-year spline functions and depict decadal variations in the mean radial tree growth at each site.

of the Driftwood River. Grouping the mean site chronologies into distance classes (shoreline and floodplain trees) resulted in no improvement of the results (results not shown). At each site, ring-width chronologies showed little association with instrumental Harricana River mean spring discharge or average spring precipitation for all periods considered (before and after 1953, common period 1930–2016). For example, considering the common period 1930–2016, correlations between ring-width chronologies and, respectively, river mean spring discharge or average spring precipitation were close to zero (mean $r = -0.02 \pm 0.07$; mean $r = -0.07 \pm 0.07$; $n = 5$).

Investigation of the temporal stability of these associations also suggested that radial growth at none of the sites was significantly and consistently correlated with mean spring discharge or precipitation (**Figure 6**). After the 1970s, each mean site chronology, however, demonstrated a change from negative to positive correlations ($p > 0.05$) between the radial growth and mean spring discharge (**Figure 6**). The correlation between radial growth and average spring precipitation was mostly negative, with a trend toward positive correlations since about the 1990s at three of five sites (**Figure 6**). Overall, this weak evidence of a dam effect on riparian tree growth demonstrated the advantages of flood-rings over ring-width records in flood history studies when ring-porous species are available. It is also possible that the change created by the Monteith Dam was not strong enough to affect radial tree growth but still affected the earlywood vessels. In this case, further study on a larger number of rivers and hydrological contexts is needed to determine if ring widths can be used to supplement flood rings. However, little to no consistent responses between total and sub-annual tree-ring width and spring flood discharge has neither been found in riparian *Q. macrocarpa* (St. George et al., 2002; St. George and Nielsen, 2003) nor in *F. nigra* (Tardif and Bergeron, 1993; Tardif et al., 1997b; Kames et al., 2016; Nolin et al., 2021a; Tardif et al., 2021b). The inversion of correlation sign found between ring width and discharge after damming is consistent with previous studies of North American rivers (Reily and Johnson, 1982; Stromberg and Patten, 1990; Salzer et al., 1996; Coble and Kolb, 2012; Netsvetov et al., 2019). Although in our study, the change in the sign was the opposite, from a negative correlation before

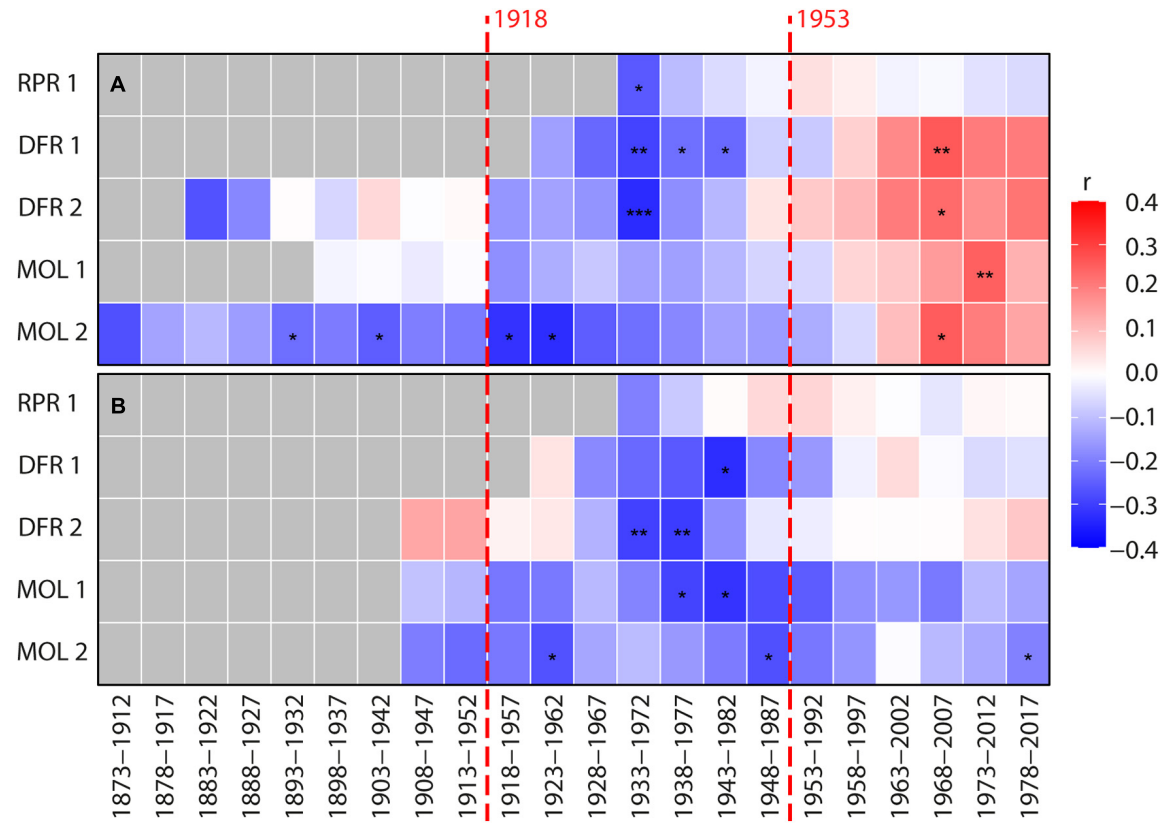

FIGURE 6 | Bootstrapped moving Pearson correlations between individual site ring-width chronologies **(A)** Harricana River spring (April 15–June 30; 1869–2017) discharge, and **(B)** the CRU TS 4.04 mean spring precipitation (MAR-APR-MAY-JUN; 1901–2017). The mean spring discharge of the Harricana River used in this analysis is constructed from the reconstructed (1869–1914) and instrumental (1915–2017) series. Pearson correlation coefficients were calculated by 40-year moving windows lagged backward by 5 years and range from red (positive correlation) to blue (negative correlation). Gray color indicates no data. Asterisks in **(A,B)** panels indicate *p*-value <0.1 (*), <0.05 (*), and <0.01 (***). Vertical red dashed lines indicate dates of construction of the first and second Monteith dam.

1970 to a positive correlation after 1970. The weak and poorly significant correlations in the case of the Driftwood River also contrast with the strong and significant changes found in these studies. Most of these studies have, however, been conducted in arid to semiarid environments where water (precipitation and/or discharge) constitutes a limiting factor to growth, which is rarely the case near boreal rivers. Since the first dam was built about 100 years ago, it is also possible that the riparian forests of the Driftwood River are surviving forests within which the trees whose ring widths were severely affected may have died already and thus not appear in the data.

In conclusion, this study demonstrated the feasibility of extracting hydrological information from regulated rivers and in particular in the predam period. The flood rings successfully recorded the spring floods in the predam period, as indicated by comparison with instrumental and reconstructed records from nearby unregulated rivers. The number of trees recording flood rings, as well as their intensity within tree rings (F1, F2 types), decreased after the construction of the first dam in 1917–1918, and particularly after its replacement in 1952–1953. Compared to flood-ring chronologies, ring-width chronologies in the sampled trees were weakly correlated to the instrumental and reconstructed discharge of the Harricana River and did not record river regulation and at any distance to the shore. On the contrary, trees within 10 m from the shoreline recorded more well-defined flood rings and of higher intensity (F2) than those further away, thus presenting a better association with known regional flood years. Comparing to the downstream site to the dam, the upstream ones recorded significantly more flood rings in the postdam period, reemphasizing the importance of considering the position of the site along with the river continuum and site conditions in relation to flood exposure. Our results suggest that a sampling strategy taking advantage of tree sampling at a far distance upstream from the dam and along various hydrologic contexts may maximize the flood signal recorded by riparian ring-porous trees in regulated rivers. A good strategy might be to sample upstream of any natural or rapid restrictions in a river, as these restrictions back up some of the water to the riparian zone during flood events. Given the importance of hydropower in northern Canada and the need for hydrological proxies in the context of climate change, it remains critical to continue developing dendrohydrological research using riparian trees and to better understand the interaction between hydrological proxies and water-level regulation.

DATA AVAILABILITY STATEMENT

Relevant data for this study are available at Mendeley Data, v1. (http://dx.doi.org/10.17632/6pgc25nk27.1). All other data are available upon request to the corresponding author (alexandreflorent.nolin@uqat.ca or alexandreflorent.nolin@gmail.com).

AUTHOR CONTRIBUTIONS

AN: conceptualization, methodology, investigation, formal analysis, writing - original draft, writing - review and editing, and visualization. JT: conceptualization, methodology, investigation, writing - review and editing, supervision, project administration, and funding acquisition. FC: methodology, investigation, resources, data curation, and writing - review and editing. YB: conceptualization, writing - review and editing, supervision, project administration, and funding acquisition. All authors contributed to the article and approved the submitted version.

FUNDING

This research is a contribution of the Canada Research Chairs (NSERC-CRC) held by YB and JT and was funded by a Natural Sciences and Engineering Research Council of Canada Collaborative research program including Ouranos, Hydro-Québec, Ontario Power Generation (OPG), and The University of Winnipeg. This work was also supported by a scholarship from RIISQ – Intersectorial Flood Network of Québec (2nd Program 2020–2021) awarded to AN.

ACKNOWLEDGMENTS

We acknowledge Martin Girardin (CFL), Lars Hildebrandt, and Gordon Kayahara (Ontario Forest Service) for their precious help in locating habitats of *Fraxinus nigra* tree. We also thank the Forêt d'enseignement et de recherche du Lac Duparquet team, and especially Danielle Charron and Raynald Julien, for their continuous support during the field campaigns, as well as field assistants Stéphane Hébert, Cyrielle Ducrot, and Chloé Lavelle. The earlier version of the manuscript benefited from constructive discussions and comments by David Huard (Ouranos), Susanne Kames (University of Winnipeg), and Kurt C. Kornelsen (OPG). We also acknowledge the contribution of the Editor, IG-G and two reviewers who provided constructive comments and suggestions to improve the earlier draft of the manuscript.

SUPPLEMENTARY MATERIAL

The Supplementary Material for this article can be found online at: https://www.frontiersin.org/articles/10.3389/fpls.2021.757280/full#supplementary-material

REFERENCES

Ashmore, P., and Church, M. (2001). *The Impact of Climate Change on Rivers and River Processes in Canada. Geological Survey of Canada, Bulletin 555. Natural Resources Canada*. (Ottawa: Geological Survey of Canada), 69. doi: 10.4095/211891

Astrade, L., and Bégin, Y. (1997). Tree-ring response of *Populus tremula* L. and *Quercus robur* L. to recent spring floods of the Saône River, France. *Écoscience* 4, 232–239. doi: 10.1080/11956860.1997.11682400

Aygün, O., Kinnard, C., and Campeau, S. (2020). Impacts of climate change on the hydrology of northern midlatitude cold regions. *Prog. Phys. Geogr. Earth Environ.* 44, 338–375. doi: 10.1177/0309133319878123

Baena-Escudero, R., Guerrero-Amador, I. C., Rinaldi, M., and González-Sayago, A. (2021). Hydrological and geomorphic effects upstream of the Cantillana Dam along the Guadalquivir River (southern Spain). *Geomorphology* 388:107786. doi: 10.1016/j.geomorph.2021.107786

Boucher, É, Ouarda, T. B., Bégin, Y., and Nicault, A. (2011). Spring flood reconstruction from continuous and discrete tree ring series. *Water Resour. Res.* 47:W07516. doi: 10.1029/2010WR010131

Bush, E., and Lemmen, D. S. (eds) (2019). *Canada's Changing Climate Report*. (Ottawa, ON: Government of Canada), 444.

Buttle, J. M., Allen, D. M., Caissie, D., Davison, B., Hayashi, M., Peters, D. L., et al. (2016). Flood processes in Canada: regional and special aspects. *Can. Water Resour. J.* 41, 7–30. doi: 10.1080/07011784.2015.1131629

Canty, A., and Ripley, B. (2021). Boot: Functions and Datasets for Bootstrapping from the book "Bootstrap Methods and their Application"' by A.C. Davison and D.V. Hinkley (1997, CUP). R Package version 1.3-28. Available online at: https://cran.r-project.org/web/packages/boot/index.html (accessed July 26, 2021).

Coble, A. P., and Kolb, T. E. (2012). Riparian tree growth response to drought and altered streamflow along the Dolores River, Colorado. *West. J. Appl. For.* 27, 205–211. doi: 10.5849/wjaf.12-001

Cook, E. R., and Kairiukstis, L. A. (1990). *Methods of Dendrochronology - Applications in the Environmental Sciences*. Dordrecht: Springer. doi: 10.1007/978-94-015-7879-0

Copini, P., den Ouden, J., Robert, E. M., Tardif, J. C., Loesberg, W. A., Goudzwaard, L., et al. (2016). Flood-ring formation and root development in response to experimental flooding of young *Quercus robur* trees. *Front. Plant Sci.* 7:775. doi: 10.3389/fpls.2016.00775

Denneler, B., Bergeron, Y., and Bégin, Y. (2010). Flooding effects on tree-ring formation of riparian eastern white-cedar (*Thuja occidentalis* L.), Northwestern Quebec, Canada. *Tree Ring Res.* 66, 3–17. doi: 10.3959/2008-11.1

Denneler, B., Bergeron, Y., Begin, Y., and Asselin, H. (2008). Growth responses of riparian Thuja occidentalis to the damming of a large boreal lake. *Botany* 86, 53–62. doi: 10.1139/B07-116

Déry, S. J., Stadnyk, T. A., MacDonald, M. K., and Gauli-Sharma, B. (2016). Recent trends and variability in river discharge across northern Canada. *Hydrol. Earth Syst. Sci.* 20, 4801–4818. doi: 10.5194/hess-20-4801-2016

DeWine, J. M., and Cooper, D. J. (2007). Effects of river regulation on riparian box elder (*Acer negundo*) forests in canyons of the Upper Colorado River Basin, USA. *Wetlands* 27, 278–289.

Efron, B. (1992). "Bootstrap methods: another look at the jackknife," in *Breakthroughs in Statistics*, eds S. Kotz and N. L. Johnson (New York, NY: Springer), 569–593. doi: 10.1007/978-1-4612-4380-9_41

Evans, J. E., Huxley, J. M., and Vincent, R. K. (2007). Upstream channel changes following dam construction and removal using a GIS/Remote Sensing Approach 1. *JAWRA J. Am. Water Resour. Assoc.* 43, 683–697. doi: 10.1111/j.1752-1688.2007.00055.x

Geography of Monteith (n.d.). *"Geography of Monteith" in Handwritten Journal Entitled "History of Monteith". Monteith Women Institute Tweedsmuir*

Community History, Volume 1:. 1912-81, 1989, p. 4. Available online at: https://collections.fwio.on.ca/3505132/page/6?n (accessed July 26, 2021).

Girardin, M. P., Tardif, J., and Bergeron, Y. (2001). Radial growth analysis of Larix laricina from the Lake Duparquet area, Quebec, in relation to climate and larch sawfly outbreaks. *Ecoscience* 8, 127–138. doi: 10.1080/11956860.2001.11682638

Girardin, M. P., Tardif, J. C., Flannigan, M. D., and Bergeron, Y. (2006). Synoptic-scale atmospheric circulation and boreal Canada summer drought variability of the past three centuries. *J. Clim.* 19, 1922–1947. doi: 10.1175/JCLI3716.1

Graf, W. L. (2006). Downstream hydrologic and geomorphic effects of large dams on American rivers. *Geomorphology* 79, 336–360. doi: 10.1016/j.geomorph.2006.06.022

Harris, I., Osborn, T. J., Jones, P., and Lister, D. (2020). Version 4 of the CRU TS monthly high-resolution gridded multivariate climate dataset. *Sci. Data* 7:109. doi: 10.1038/s41597-020-0453-3

Holmes, R. L. (1983). Computer-assisted quality control in tree-ring dating and measurement - COFECHA. *Tree Ring Bull.* 43, 69–78.

James, N. A., and Matteson, D. S. (2014). ecp: an R package for nonparametric multiple change point analysis of multivariate data. *J. Stat. Softw.* 62, 1–25. doi: 10.18637/jss.v062.i07

Kames, S., Tardif, J. C., and Bergeron, Y. (2016). Continuous earlywood vessels chronologies in floodplain ring-porous species can improve dendrohydrological reconstructions of spring high flows and flood levels. *J. Hydrol.* 534, 377–389. doi: 10.1016/j.jhydrol.2016.01.002

Koprowski, M., Okoński, B., Gričar, J., and Puchałka, R. (2018). Streamflow as an ecological factor influencing radial growth of European ash (*Fraxinus excelsior* (L.)). *Ecol. Indic.* 85, 390–399. doi: 10.1016/j.ecolind.2017.09.051

Larsson, L. A. (2003a). *CooRecorder: Image Co-Ordinate Recording Program*. Available online at: http://www.cybis.se (accessed July 26, 2021).

Larsson, L. A. (2003b). *CDendro: Cybis Dendro Dating Program*. Available online at: http://www.cybis.se (accessed July 26, 2021).

Legendre, P., and Legendre, L. (2012). *Numerical Ecology (Development)*, 3rd Edn. (Amsterdam: Elsevier), 1006.

Lemay, M., and Bégin, Y. (2008). Hydroclimatic analysis of an ice-scar tree-ring chronology of a high-boreal lake in Northern Québec, Canada. *Hydrol. Res.* 39, 451–464. doi: 10.2166/nh.2008.003

Magilligan, F. J., and Nislow, K. H. (2005). Changes in hydrologic regime by dams. *Geomorphology* 71, 61–78. doi: 10.1016/j.geomorph.2004.08.017

Matteson, D. S., and James, N. A. (2014). A nonparametric approach for multiple change point analysis of multivariate data. *J. Am. Stat. Assoc.* 109, 334–345. doi: 10.1080/01621459.2013.849605

Meko, M. D., and Therrell, M. D. (2020). A record of flooding on the White River, Arkansas derived from tree-ring anatomical variability and vessel width. *Phys. Geogr.* 41, 83–98. doi: 10.1080/02723646.2019.1677411

Merritt, D. M., and Wohl, E. E. (2002). Processes governing hydrochory along rivers: hydraulics, hydrology, and dispersal phenology. *Ecol. Appl.* 12, 1071–1087.

Mortsch, L., Cohen, S., and Koshida, G. (2015). Climate and water availability indicators in Canada: challenges and a way forward. Part II–Historic trends. *Can. Water Resour. J.* 40, 146–159. doi: 10.1080/07011784.2015.1006024

Netsvetov, M., Prokopuk, Y., Puchałka, R., Koprowski, M., Klisz, M., and Romenskyy, M. (2019). River regulation causes rapid changes in relationships between floodplain oak growth and environmental variables. *Front. Plant Sci.* 10:96. doi: 10.3389/fpls.2019.00096

Nilsson, C., and Berggren, K. (2000). Alterations of riparian ecosystems caused by river regulation: dam operations have caused global-scale ecological changes in riparian ecosystems. How to protect river environments and human needs of rivers remains one of the most important questions of our time. *BioScience* 50, 783–792.

Nolin, A. F., Tardif, J. C., Conciatori, F., and Bergeron, Y. (2021b). Spatial coherency of the spring flood signal among major river basins of eastern boreal Canada inferred from flood rings. *J. Hydrol.* 596:126084. doi: 10.1016/j.jhydrol.2021.126084

Nolin, A. F., Tardif, J. C., Conciatori, F., Kames, S., Meko, D. M., and Bergeron, Y. (2021a). Multi-century tree-ring anatomical evidence reveals increasing frequency and magnitude of spring discharge and floods in eastern boreal Canada. *Glob. Planet. Change* 199:103444. doi: 10.1016/j.gloplacha.2021.103444

Ontario Ministry of Natural Resources and Forestry [OMNRF] (2019). *Ontario Dam Inventory, Provincial Mapping Unit*. Toronto: Government of Ontario.

Ontario Ministry of Natural Resources [OMNR] (2004). *Abitibi River Management Plan*. (Toronto: Government of Ontario), 709.

Pellerin, J. (2019). *Updating the Canadian Reference Hydrometric Basin Network to detect Climate-Related Trends in Streamflow*. Master's thesis. Waterloo: University of Waterloo.

Petts, G. E. (1980). Long-term consequences of upstream impoundment. *Environ. Conserv.* 7, 325–332. doi: 10.1017/S0376892900008183

Phipps, R. L. (1985). *Collecting, Preparing, crossdating, and Measuring tree Increment Cores (No. 85-4148)*. Washington, DC: US Department of the Interior, Geological Survey.

R Core Team (2021). *R: A Language and Environment for Statistical Computing*. Vienna: R Foundation for Statistical Computing.

Reily, P. W., and Johnson, W. C. (1982). The effects of altered hydrologic regime on tree growth along the Missouri River in North Dakota. *Can. J. Bot.* 60, 2410–2423. doi: 10.1139/b82-294

Salzer, M. W., McCord, V. A. S., Stevens, L. E., and Webb, R. H. (1996). "The dendrochronology of *Celtis reticulata* in the grand canyon: assessing the impact of regulated river flow on tree growth," in *Tree Rings, Environment, and Humanity*, eds J. S. Dean, D. M. Meko and T. W. Swetnam (Tucson, AZ: University of Arizona), 273–281.

Schmiedel, D., and Tackenberg, O. (2013). Hydrochory and water induced germination enhance invasion of *Fraxinus pennsylvanica*. *For. Ecol. Manage.* 304, 437–443. doi: 10.1016/j.foreco.2013.04.027

Schook, D. M., Carlson, E. A., Sholtes, J. S., and Cooper, D. J. (2016). Effects of moderate and extreme flow regulation on Populus growth along the Green and Yampa Rivers, Colorado, and Utah. *River Res. Appl.* 32, 1698–1708. doi: 10.1002/rra.3020

Sims, R. A., Kershaw, H. M., and Wickware, G. M. (1990). *The Autecology of Major Tree Species in the North Central Region of Ontario. Forestry Canada, Ontario Region, Sault Ste. Marie, Ontario. COFRDA Report 3302 – NWOFTDU Technical Report 48*. Available online at: https://cfs.nrcan.gc.ca/publications/download-pdf/22213 (accessed July 26, 2021).

Slater, L. J., and Villarini, G. (2016). Recent trends in US flood risk. *Geophys. Res. Lett.* 43, 12–428. doi: 10.1002/2016GL071199

Smith, M. C., Anthony Stallins, J., Maxwell, J. T., and Van Dyke, C. (2013). Hydrological shifts and tree growth responses to river modification along the Apalachicola River, Florida. *Phys. Geogr.* 34, 491–511. doi: 10.1080/02723646.2013.853019

St. George, S., and Nielsen, E. (2003). Palaeoflood records for the Red River, Manitoba, Canada, derived from anatomical tree-ring signatures. *Holocene* 13, 547–555. doi: 10.1191/0959683603hl645rp

St. George, S., Nielsen, E., Conciatori, F., and Tardif, J. C. (2002). Trends in Quercus macrocarpa vessel areas and their implications for tree-ring paleoflood studies. *Tree Ring Res.* 58, 3–10.

Stallins, J. A., Nesius, M., Smith, M., and Watson, K. (2010). Biogeomorphic characterization of floodplain forest change in response to reduced flows along the Apalachicola River, Florida. *River Res. Appl.* 26, 242–260. doi: 10.1002/rra.1251

Stella, J. C., and Bendix, J. (2019). "Chapter 5 - Multiple stressors in riparian ecosystems," in *Multiple Stressors in River Ecosystems*, eds S. Sabater, A. Elosegi, and R. Ludwig (Amsterdam: Elsevier), 81–110. doi: 10.1016/B978-0-12-811713-2.00005-4

Stromberg, J. C., and Patten, D. T. (1990). Riparian vegetation instream flow requirements: a case study from a diverted stream in the Eastern Sierra Nevada, California, USA. *Environ. Manage.* 14, 185–194. doi: 10.1007/BF02394035

Tardif, J., and Bergeron, Y. (1993). Radial growth of Fraxinus nigra in a Canadian boreal floodplain in response to climatic and hydrological fluctuations. *J. Veg. Sci.* 4, 751–758. doi: 10.2307/3235611

Tardif, J. C., and Bergeron, Y. (1992). Analyse écologique des peuplements de frêne noir (*Fraxinus nigra*) des rives du lac Duparquet, nord-ouest du Québec. *Can. J. Bot.* 70, 2294–2302. doi: 10.1139/b92-285

Tardif, J. C., and Bergeron, Y. (1997b). Ice-flood history reconstructed with tree-rings from the southern boreal forest limit, western Québec. *Holocene* 7, 291–300. doi: 10.1177/095968369700700305

Tardif, J. C., and Bergeron, Y. (1997a). Comparative dendroclimatological analysis of two black ash and two white cedar populations from contrasting sites in the Lake Duparquet region, northwestern Quebec. *Can. J. For. Res.* 27, 108–116. doi: 10.1139/x96-150

Tardif, J. C., and Bergeron, Y. (1999). Population dynamics of *Fraxinus nigra* in response to flood-level variations, in northwestern Quebec. *Ecol. Monogr.* 69, 107–125.

Tardif, J. C., Dery, S., and Bergeron, Y. (1994). Sexual regeneration of black ash (*Fraxinus nigra* Marsh.) in a boreal floodplain. *Am. Midl. Nat.* 132, 124–135. doi: 10.2307/2426207

Tardif, J. C., Dickson, H., Conciatori, F., Nolin, A. F., and Bergeron, Y. (2021a). Are periodical (intra-annual) tangential bands of vessels in diffuse-porous tree species the equivalent of flood rings in ring-porous species: reproducibility and cause? *Dendrochronologia* 70:125889. doi: 10.1016/j.dendro.2021.125889

Tardif, J. C., Kames, S., Nolin, A., and Bergeron, Y. (2021b). Earlywood vessels in black ash (*Fraxinus nigra* Marsh.) trees show contrasting sensitivity to hydroclimate variables according to flood exposure. *Front. Plant Sci.* 12:754596. doi: 10.3389/fpls.2021.754596

Tardif, J. C., Kames, S., and Bergeron, Y. (2010). "Spring water levels reconstructed from ice-scarred trees and cross-sectional area of the earlywood vessels in tree rings from eastern boreal Canada," in *Tree Rings and NATURAL Hazards*, eds M. Stoffel, M. Bollschweiler, D. R. Butler, and B. H. Luckman (Dordrecht: Springer), 257–261.

The old and the new on Driftwood River (1953). *Unknown Newspaper Archive. Monteith Women Institute Tweedsmuir Community History*. Available online at: https://collections.fwio.on.ca/3505133/page/111?q=dam&docid=OOI.3505133 (accessed July 26, 2021).

Therrell, M. D., and Bialecki, M. B. (2015). A multi-century tree-ring record of spring flooding on the Mississippi River. *J. Hydrol.* 529, 490–498. doi: 10.1016/j.jhydrol.2014.11.005

Trouet, V., and Van Oldenborgh, G. J. (2013). KNMI Climate Explorer: a web-based research tool for high-resolution paleoclimatology. *Tree Ring Res.* 69, 3–13. doi: 10.3959/1536-1098-69.1.3

Water Survey of Canada (2021). *Daily water levels at Driftwood River at Monteith (04MB002), Ontario – Online Hydrometric Report*. Available online at: https://wateroffice.ec.gc.ca/report/historical_e.html?stn=04MB002 (accessed May 12, 2021).

Williams, G. P., and Wolman, M. G. (1984). *Downstream Effects of Dams on Alluvial Rivers. US Geological Survey Professional Paper Vol.* 1286. (Washington, DC: United States Government Printing Office), 83.

Zang, C., and Biondi, F. (2015). treeclim: an R package for the numerical calibration of proxy-climate relationships. *Ecography* 38, 431–436. doi: 10.1111/ecog.01335

Conflict of Interest: The authors declare that the research was conducted in the absence of any commercial or financial relationships that could be construed as a potential conflict of interest.

Publisher's Note: All claims expressed in this article are solely those of the authors and do not necessarily represent those of their affiliated organizations, or those of the publisher, the editors and the reviewers. Any product that may be evaluated in this article, or claim that may be made by its manufacturer, is not guaranteed or endorsed by the publisher.

frontiers in Plant Science

METHODS
published: 04 November 2021
doi: 10.3389/fpls.2021.767400

Mask, Train, Repeat! Artificial Intelligence for Quantitative Wood Anatomy

Giulia Resente[1], Alexander Gillert[2], Mario Trouillier[1], Alba Anadon-Rosell[1,3], Richard L. Peters[4,5], Georg von Arx[5,6], Uwe von Lukas[2,7] and Martin Wilmking[1]*

[1] Institute of Botany and Landscape Ecology, Ernst Moritz Arndt University Greifswald, Greifswald, Germany, [2] Fraunhofer-Institut für Graphische Datenverarbeitung IGD, Rostock, Germany, [3] CREAF, Campus de Bellaterra (UAB), Cerdanyola del Vallès, Spain, [4] Department of Environment, Faculty of Bioscience Engineering, Ghent, Belgium, [5] Swiss Federal Institute for Forest, Snow and Landscape Research, Birmensdorf, Switzerland, [6] Oeschger Centre for Climate Change Research, University of Bern, Bern, Switzerland, [7] Institute for Visual and Analytic Computing, University of Rostock, Rostock, Germany

The recent developments in artificial intelligence have the potential to facilitate new research methods in ecology. Especially Deep Convolutional Neural Networks (DCNNs) have been shown to outperform other approaches in automatic image analyses. Here we apply a DCNN to facilitate quantitative wood anatomical (QWA) analyses, where the main challenges reside in the detection of a high number of cells, in the intrinsic variability of wood anatomical features, and in the sample quality. To properly classify and interpret features within the images, DCNNs need to undergo a training stage. We performed the training with images from transversal wood anatomical sections, together with manually created optimal outputs of the target cell areas. The target species included an example for the most common wood anatomical structures: four conifer species; a diffuse-porous species, black alder (*Alnus glutinosa* L.); a diffuse to semi-diffuse-porous species, European beech (*Fagus sylvatica* L.); and a ring-porous species, sessile oak (*Quercus petraea* Liebl.). The DCNN was created in Python with Pytorch, and relies on a Mask-RCNN architecture. The developed algorithm detects and segments cells, and provides information on the measurement accuracy. To evaluate the performance of this tool we compared our Mask-RCNN outputs with U-Net, a model architecture employed in a similar study, and with ROXAS, a program based on traditional image analysis techniques. First, we evaluated how many target cells were correctly recognized. Next, we assessed the cell measurement accuracy by evaluating the number of pixels that were correctly assigned to each target cell. Overall, the "learning process" defining artificial intelligence plays a key role in overcoming the issues that are usually manually solved in QWA analyses. Mask-RCNN is the model that better detects which are the features characterizing a target cell when these issues occur. In general, U-Net did not attain the other algorithms' performance, while ROXAS performed best for conifers, and Mask-RCNN showed the highest accuracy in detecting target cells and segmenting lumen areas of angiosperms. Our research demonstrates that future software tools for QWA analyses would greatly benefit from using DCNNs, saving time during the analysis phase, and providing a flexible approach that allows model retraining.

Keywords: artificial intelligence, wood anatomy, deep learning, lumen area, F1 score, ROXAS

OPEN ACCESS

Edited by:
Miha Humar,
University of Ljubljana, Slovenia

Reviewed by:
Angela Balzano,
University of Ljubljana, Slovenia
Jozica Gricar,
Slovenian Forestry Institute, Slovenia

****Correspondence:***
Giulia Resente
giulia.resente@uni-greifswald.de

Specialty section:
This article was submitted to Technical Advances in Plant Science, a section of the journal Frontiers in Plant Science

Received: *30 August 2021*
Accepted: *15 October 2021*
Published: *04 November 2021*

Citation:
Resente G, Gillert A, Trouillier M, Anadon-Rosell A, Peters RL, von Arx G, von Lukas U and Wilmking M (2021) Mask, Train, Repeat! Artificial Intelligence for Quantitative Wood Anatomy. Front. Plant Sci. 12:767400. doi: 10.3389/fpls.2021.767400

INTRODUCTION

In recent years, deep learning, as a subset of artificial intelligence, has proven to be the new key tool to investigate ecological research questions (Christin et al., 2019). Hierarchically, deep learning is a sub-field of machine learning, a modeling approach able to detect common patterns in datasets (Olden et al., 2008). The reason of deep learning suitability to ecological investigations lies in its intrinsic characteristics: deep learning can automate the pattern interpolation processes from the provided data (LeCun et al., 2015). The step forward lies in the particular algorithm architecture, which de-structures data features through different evaluation layers. This allows the machine to automatically change internal parameters and fit the computational process according to the required task (Zhang et al., 2016).

Overall, ecological investigations are enhanced by the flexibility of deep learning tools, especially when dealing with large and complex datasets (Christin et al., 2019). This is the case for image analysis tasks, where Deep Convolutional Neural Networks (DCNNs) stand out by performance (Krizhevsky et al., 2017). In this specialized architecture, the different layers are composed by artificial neurons (Zhang et al., 2016) and each layer has a specific task, such as feature extraction, mathematical computation-based training, or dimensional adjustment, that makes DCNNs particularly suitable for image interpretation (James and Bradshaw, 2020).

Wood anatomical research is a field where DCNNs find an ideal application (Garcia-Pedrero et al., 2019). In the past, machine learning methods have mainly been used for wood species identification (Luis et al., 2009; Mallik et al., 2011; Ravindran et al., 2018; He et al., 2020; Wu et al., 2021). In contrast, quantitative wood anatomy (QWA), that refers to the broad set of analyses quantifying and interpreting the variation of xylem features in trees, shrubs, and herbaceous plants (von Arx et al., 2016), has just started being investigated with such tools. Investigations are performed on wood anatomical images at a microscopic level, to study number, distribution, and properties of the main cell types: conduits, parenchyma cells, and fibers (von Arx and Carrer, 2014). Wood anatomical analyses can provide a higher temporal resolution than annual tree-ring width measurements, and the wood anatomical structure is more directly linked to biological processes and tree functioning. This allows to link tree growth to the study of phenology, tree allometry, species physiological performance, and ecosystem dynamics, among others (Fonti et al., 2010; Carrer et al., 2015; De Micco et al., 2019; Castagneri et al., 2020).

To obtain wood anatomical images, the wooden sample has to undergo several steps. Standard procedures start with cutting thin sections from the sample and mounting them on a glass slide, whereas, in case of damaged or particularly fragile material, the wood sample can be embedded in paraffin to stabilize the tissues before the cutting. This stage is followed by the image acquisition process, where images of the slides are taken with a camera installed on a microscope, or *via* specialized scanners. The images are then analyzed with image analysis tools to perform quantitative wood anatomical investigations (Gärtner et al., 2015; Yeung et al., 2015; von Arx et al., 2016; Prendin et al., 2017; Peters et al., 2018). Despite the great advances in the procedures for wood sectioning and image acquisition, the actual feature recognition phase still requires human supervision (Hwang and Sugiyama, 2021). In fact, traditional image analysis is often not able to overcome the artifacts generated by the sample processing: the great number of cells occurring in the sections, combined with a non-optimal image quality, is the reason why automated image analysis is often followed by a manual editing phase. However, the effort taken to fix these issues by hand can be very time-consuming. This is exactly where DCNNs show their strength, as many of these issues can benefit from a DCNN approach. Images showing excessive darkness, brightness or blurred areas, for example, can be easily processed after a proper neural network training. Moreover, DCNNs have the ability to encode specific wood features, which is the key to accelerate data production: fibers are less likely to be mistaken for conduits, for example, or pit chambers will be recognized as such and automatically excluded from the lumen area.

In this study, we aimed to overcome these general QWA challenges in transversal images using DCNNs. Specifically, we created a practical graphical user interface relying on a Mask-RCNN algorithm architecture (He et al., 2017), that detects cells and quantifies the lumen area on four conifers and three angiosperms. We also present the comparison on the accuracy of cell instance (cell identification as an object) and lumen area detection with another neural network architecture (U-Net; Garcia-Pedrero et al., 2019), and ROXAS, one of the most widely used programs for wood anatomical image analyses (von Arx and Dietz, 2005; von Arx and Carrer, 2014; Garcia-Pedrero et al., 2019).

MATERIALS

To perform classification analyses on wood anatomical parameters, such as cell instance recognition (i.e., the identification of the cell as an individual structure) and lumen area detection (cell segmentation), the neural network has to undergo a training stage. During this training, the neural network architecture is provided with wood anatomical images as well as the desired output, the ground truth – a map of the original image where all the target cells have been manually marked (segmented). Given the original and the segmented images, the algorithm can learn to generalize the features that are characteristic for a target cell. For this purpose, we chose four conifers: Norway spruce (*Picea abies* L. Karst), Scots pine (*Pinus sylvestris* L.), White spruce (*Picea glauca* Moench), and European larch (*Larix decidua* Mill); and three angiosperms: Black alder (*Alnus glutinosa* L.), European beech (*Fagus sylvatica* L.), and Sessile oak (*Quercus petraea* Liebl.). We will refer to these groups as: conifers, alder, beech, and oak. Each of them represents a typical wood anatomical structure: softwood for gymnosperms and the three typologies of hardwood for angiosperms, a diffuse-porous species, a diffuse to semi-diffuse-porous species and a ring-porous species.

Conifers, beech, and oak are some of the most used species for tree ring studies in general (Scharnweber et al., 2013;

Príncipe et al., 2017; Lange et al., 2018; Janecka et al., 2020) and specifically for wood anatomical analyses (Björklund et al., 2020; Pampuch et al., 2020; Peters et al., 2020). Images were collected from several sources, to ensure variability in the image quality and within the sample processing (**Supplementary Table 1**). Conifer species were grouped due to the high similarity in wood anatomical structure, therefore it was possible to train one single neural network for this group; whereas the angiosperms remained separated per species, due to their less uniform structural properties. Moreover, because it is more common to perform QWA analyses on gymnosperms due to their homogeneous wood structure, having a broadly trained algorithm is of high value. Concerning gymnosperms images, the provenance is more restricted and the quality is generally very high. While for conifer images we managed to collect examples of a wide quality range, the image acquisition process of all the angiosperms slides was carried out by the high-end Zeiss Axio Scan.Z1 slide scanner (Carl Zeiss AG, Germany), except part of the alder samples.

METHODS

Neural Network Architecture

Our goal was to perform cell instance and lumen area detection together in a single algorithm architecture to maximize the utility for QWA analyses. We treated lumen area detection as an instance segmentation problem rather than a semantic segmentation task as we see in Garcia-Pedrero et al. (2019) with the U-Net neural network architecture. The difference between these two is that with the U-Net algorithm every pixel is classified (as "cell" or "not-cell") independently from each other, whereas in instance segmentation the objects (cells) are first identified and located as a whole, and then segmented to their estimated real dimension in a following stage. In practice, this has the benefit of fewer spurious false detections because a larger field of view can be used for the object detection stage, allowing to put distance between the image and the "observer" in order to focus better the objects themselves.

Specifically, we used the Mask-RCNN (He et al., 2017) neural network architecture for this task. This model employs a feature pyramid network (FPN) (Lin et al., 2017) to extract visual features from the input image at different levels of detail. These features are then forwarded to the next stages: first, a region proposal network (RPN) which identifies regions in the image that might be objects of interest, and second, a classification head, which filters out undesired regions. In our case this can include ray cells, pits, or air bubbles. Finally, if the region is classified as a target object, the third step performs a per-pixel segmentation. We refer to He et al. (2017) for a more detailed description of the used Mask-RCNN.

Neural Network Training

We used the version implemented in the PyTorch v1.6 library (Paszke et al., 2019) with a ResNet50 backbone. Weights (model parameters) were obtained from pre-training on the COCO dataset (Lin et al., 2014). They were used as a starting point and then fine-tuned on image patches of anatomical wood thin sections of size 1000 × 1000 pixels for all species except oak, for which images of 2000 × 3000 pixels were used to safely include the larger vessels in the tiles. Although COCO contains natural images that have little in common with wood anatomical thin sections, this process is still beneficial as part of transfer learning. As we started algorithm development with alder, our training set consisted of 89 patches for this species, while only 31 patches were employed for conifers, 20 for beech and 20 for oak.

The images were annotated in the form of a semantic segmentation map, the ground truth, which is an image file (in png format) created for every training image, containing the information related to the correct identification of the lumen area. This map was created using Gimp (Spencer et al., 2021) a free and open-source raster graphics editor, used to draw the lumen areas on an additional layer with transparent background.

We converted this annotation into boxes by taking the minimum and maximum X and Y pixel coordinates of the connected components. During training we used data augmentation in the form of random horizontal and vertical flipping as well as 90° rotations to artificially enlarge the data set. The stochastic gradient descent (SGD) optimizer was used as the training algorithm, with a learning rate of 0.005, momentum 0.9 and weight decay of 0.0005 for overall 20 epochs and a batch size of 1.

For each wood type a separate neural network was trained. At the training stage, some modifications were required for the different species. Particularly for oak, we trained two networks that specialize in either the small or the large vessels. However, the networks belong to the same model in the graphical user interface, therefore the analyses are run in parallel, providing a single output per picture. For the large vessel network, we used patches of half the resolution (but same patch size), thus doubling the field of view.

Neural Network Evaluation

The testing phase was performed on patches cropped from wood anatomical images of the same dimensions as the ones included in the training dataset and completely new to the algorithm (i.e., not present in the training dataset), 15 for each group. The patches were extrapolated from images of seven different trees for conifer, eight trees for alder, seven for beech, and six for oak. The aim of using this dataset was to cover all the problematic issues that might hamper a smooth workflow and require large correction efforts during the post-analysis editing phase.

Sample processing is the most delicate step in QWA analyses. When the tissue is sectioned, the fragile structure of the wooden sample can be compromised, often resulting in broken vessel or tracheid walls, and cell wall protrusion into the lumen area. The microslide preparation step is also critical as sections are very thin and can overlap with themselves, if they are not positioned carefully. Moreover, depending on the accuracy used in the following section processing, stains from coloring solutions, drops of paraffin or air bubbles can occur on the slide. If these artifacts cannot be avoided in the image acquisition step with a tailored cropping, they have to be solved manually after the automated image analysis. Acquiring high quality images

can be difficult as well, since artifacts from wrongly stitched images, blurred areas due to uneven surfaces, dust spots, or inhomogeneous lighting can hamper a smooth analysis of the image and consequently, of the whole the dataset. Moreover, even the species-specific structure can hamper a traditional image analysis approach. In general, pits, fibers, apotracheal parenchyma, bark cells, vessels with scalariform perforation plates, resin canals and the related parenchyma cells constitute an issue. The testing dataset we created included at least one image for every feature mentioned above, in detail:

- Overlaying pollution particles (dirt or dust);
- Overlapping/folded tissue;
- Stains from coloring solutions of variable intensity;
- Drops of paraffin from embedding;
- Broken cell walls;
- Reduced lumen area in the latewood hampering a proper cell recognition;
- Cells that are not conduits (resin canals, bark cells, fibers, and parenchyma cells);
- Pit chambers connecting conifer tracheids;
- Pith fleck in alder;
- Scalariform perforation plate for alder and beech.

The evaluation procedure has been implemented in a web browser-based software *via* a graphical user interface, and is automated. Within the graphical user interface, four different models can be selected and applied to new images. One model corresponds to gymnosperms and one for each angiosperm. Furthermore, we implemented the possibility to upload ground truth references and previously computed prediction files. This facilitates testing and evaluating the algorithm, and also comparing its accuracy to the output of other specialized software such as the traditional image-analysis tool ROXAS (von Arx and Carrer, 2014) running on Image-Pro Plus (Media Cybernetics, 2021, Rockville, MD, United States).

For the cell instance metrics (cell detected: yes/no), the procedure first matches the connected components (cells) of the outputs with the corresponding ground truth maps. Two cells are matched if they have a high similarity (overlap) to each other and thus count as a true positive instance (TP). Unmatched cells from the output are counted as false positive instances (FP), that is when the algorithm detected a cell that is not present in the ground truth. On the other hand, unmatched cells of the ground truth are counted as false negative instances (FN), in this case cells are not present in the output and therefore they are counted as missed cells (**Table 1**).

Matched target cells are then compared in terms of lumen area accuracy by directly comparing individual pixels. Pixels that are positive in both predicted and ground truth cell count as true positive lumen area. Pixels that are positive only in the predicted cell are counted as FP lumen area and those that are positive only in the ground truth cell are FN lumen area. These lumen area metrics, along with the F1 score, an index to evaluate the algorithm performance, are computed for each cell individually and results are provided as Excel files.

Along with the computational data, an error map is given to visually interpret the graphical user interface results on every image of the dataset (**Figure 1**). These image files report all the categories used to classify cell instance recognition and lumen area detection, and three other specific cases: disconnected positive, a single cell that was detected as two or more (thus counts as FP); merged negative, two or more cells that were detected as a single one (thus counts as FN); and incomplete cells, which are cut at the borders and ignored since they are irrelevant for the analysis.

The testing dataset was analyzed with ROXAS, with the Mask-RCNN algorithm, and with the U-Net algorithm. ROXAS program was run without any additional manual editing, but employing a configuration file per group species, tailored to the specific sub-datasets. Configurations are batches of settings adjusted to specific image characteristics, with the purpose of improving the performance in the cell and lumen area recognition. Subsequently, the output provided by the three approaches was compared to the ground truth, since it represents an unbiased reference (**Figure 2**). Results from the Mask-RCNN segmentation approach have been compared to the other two algorithms in terms of cell instance detection and lumen area detection accuracy (how accurately the cell area has been detected). Training and evaluation code can be found in the online repository: https://github.com/alexander-g/Cell-Detection-for-Wood-Anatomy.

TABLE 1 | Confusion matrix approach applied to cell instance detection.

Prediction / Ground truth	**Positive**	**Negative**	
Positive	True positive (TP)	False negative (FN)	Recall
	It is a target cell, it was detected	It is a target cell, it was not detected	How many of the target cells are detected?
Negative	False positive (FP)	True negative (TN)	
	It is not a target cell, it was detected	It is not a target cell, it was not detected	
	Precision		
	How many of the detected cells are target cells?		

Both recall and precision parameters are a benchmark of accuracy, respectively, they assess how many cells were missed (FN) and how many redundant cells were segmented (FP), considering the total amount of correctly detected cells (TP). See Equation 1 for reference.

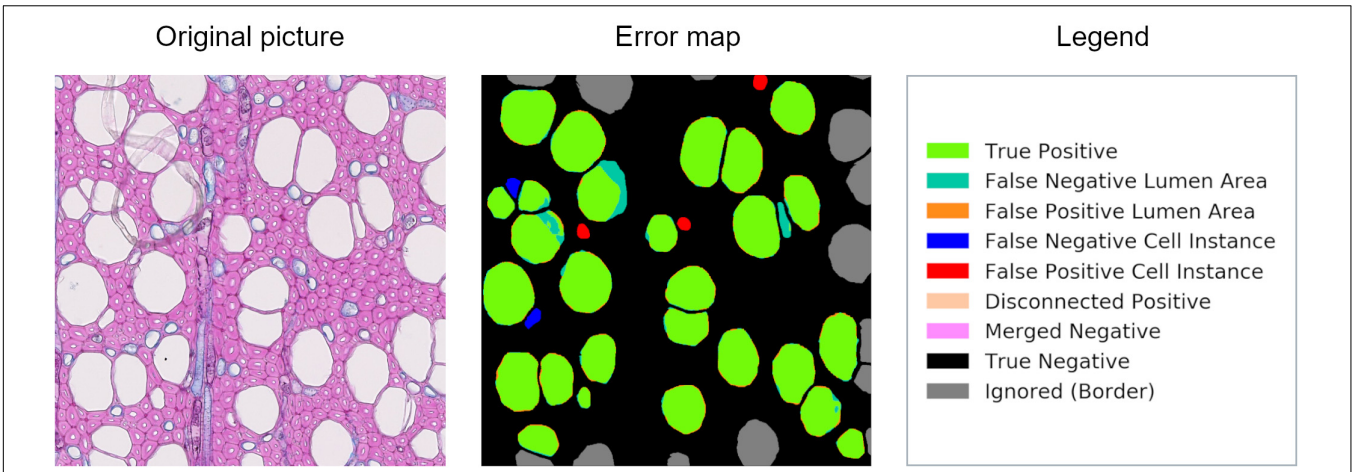

FIGURE 1 | Patch from an original beech thin section, error map, and related legend. The error map is the visual comparison between the algorithm computation and the ground truth, and it helps in the visual assessment of the algorithms' performance.

Cell Instance Detection and Lumen Area Detection

We defined the cells masked in the ground truth as target cells because they represent the optimal image analysis output, in this case, they are represented by vessels for angiosperms and tracheids for gymnosperms. As a first step, we evaluated how many target cells were correctly identified; furthermore, we analyzed and compared the results with the other two algorithms: ROXAS and U-Net. The latter is the same architecture used in Garcia-Pedrero et al. (2019). In this study, U-Net was employed with the same purpose but trained on ROXAS output as ground truth, while in our research the ground truth was manually created, allowing first, a consistent training of the neural network models, and second an unbiased reference for comparing the algorithms. For the same purpose, in our study, the U-Net neural network architecture was trained on the same training dataset as the Mask-RCNN version. Comparing U-Net performance with Mask-RCNN should allow us to provide a more complete overview on the topic and to highlight the improvements in this research field.

Cell instance accuracy was assessed with the help of a confusion matrix (**Table 1**). The confusion matrix helps to bring together and compare the results from the two sides: the algorithm (Mask-RCNN, ROXAS, or U-Net) and the ideal output (ground truth).

False positive and false negative values were used to analyze recall, which estimates the missed cells numbers (FN) considering the total TP detected; and precision, which gives an estimation of the redundant cells (FP) weighting the value with TP (Equation 1, 2).

$$Recall = \frac{TP}{TP + FN} \tag{1}$$

$$Precision = \frac{TP}{TP + FP} \tag{2}$$

A general overview of the performance of the algorithm in cell instance detection is provided by the F1 score. This index is the harmonic mean between precision and recall (Equation 3), for this reason it reflects both when the cell instance count is overestimated and/or when it is underestimated.

$$F_1 = 2 * \frac{Precision * Recall}{Precision + Recall} \tag{3}$$

Computing TN for the cell instance analysis, does not apply in this case, since there is no reference on the number of total cells of all the typologies (vessels/tracheids, fibers, rays, and axial parenchyma) present in the images. The definite and important value is the number of target cells shown by the patches, obtained *via* the ground truth mask. Overall, we calculated the confusion matrix for all the species and for all the segmenting approaches (**Supplementary Table 2**).

After assessing how many cells were correctly identified, we analogously (i.e., with the same recall, precision, and F1 score scheme) evaluated the accuracy of the cell lumen area detection, in the following referred to as lumen area. In fact, parameters belonging to the cell instance classification can be applied to the pixel dimension as well: pixels correctly assigned to the cell area are TP and those which are misclassified belong to the FP or FN categories. We used the F1 score to provide an overall assessment of the algorithms' performance, and subsequently analyzed precision and recall to understand when the lumen area is overestimated and/or when it is underestimated.

Moreover, an additional sub-dataset was created to increase variability of the original testing dataset, and to test the ability of the Mask-RCNN algorithm to handle the most insidious issues faced in QWA analyses (see list in section "Neural Network Evaluation"). This dataset consisted of five images per group (conifer, alder, beech, and oak) that were not analyzed with ROXAS, since they would have required a tailor-made configuration, which requires expert knowledge.

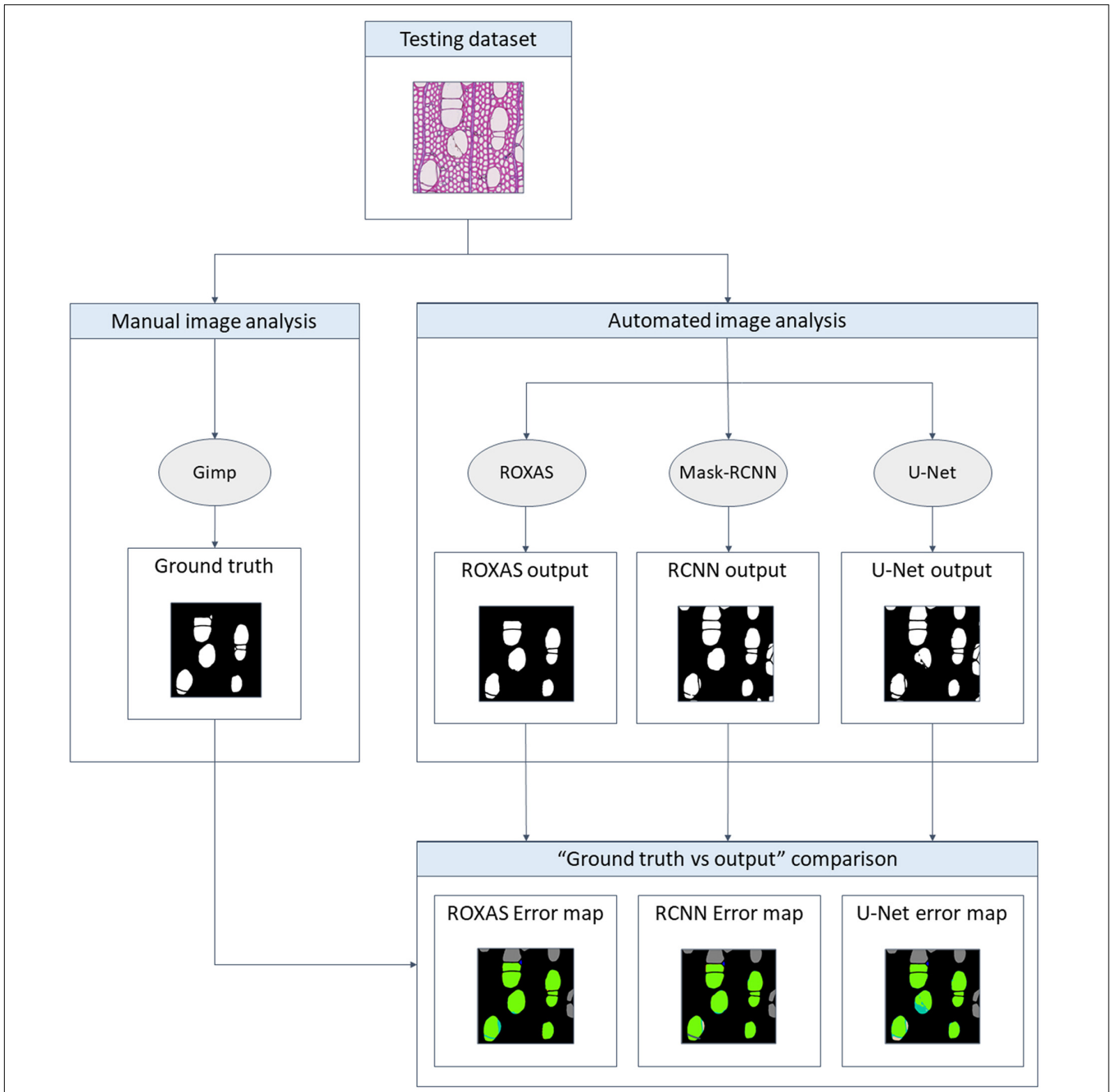

FIGURE 2 | Flowchart of the comparison process. To obtain a meaningful result, the output from the algorithms has to be compared to the ground truth, a manually segmented image for every image of the groups investigated. Mask-RCNN output was then compared to the one of U-Net and ROXAS in terms of cell instance (cell detected: yes/no) and lumen area accuracy (how accurately the lumen area was detected).

RESULTS AND DISCUSSION

Result Structure

The relatively complex analysis structure used to highlight different aspects of algorithm performance as described in section "Methods" is summarized in **Figure 3** for convenience.

Cell Instance Detection

First, performances on cell instance detection have been calculated using the F1 score (**Table 2**). Since the values provide an overall assessment of the accuracy reached by the algorithms, we could already infer that in general Mask-RCNN and ROXAS records were very high and that these two approaches performed

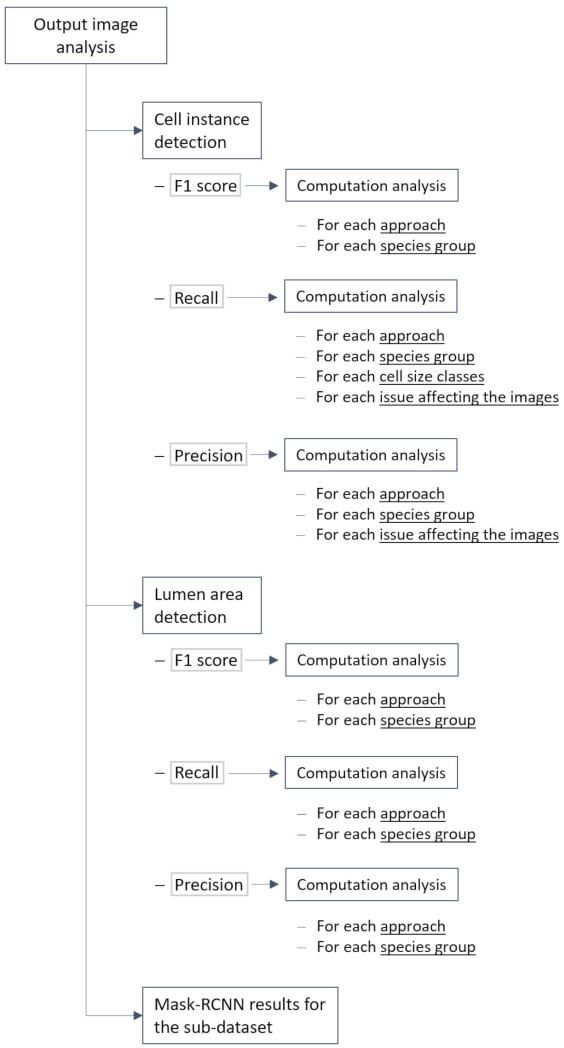

FIGURE 3 | Flowchart summarizing how performance of the considered approaches was assessed.

very similarly for all the groups, while U-Net consistently showed lower values.

As the F1 score is the harmonic mean between precision and recall, it raised interest in the investigation of the algorithms' trend about underestimation and overestimation of the cell instance detection. The recall parameter was generally higher for the U-Net algorithm, followed by Mask-RCNN and ROXAS (**Table 2**). High recall values indicate that, overall, fewer cells are missed compared to the total amount of cells correctly recognized. Although this might seem in contrast to the F1 score results, the U-Net approach of recognizing cells – pixel per pixel – seems to lose the perspective on the cell instance identification, generating many spurious cells detection, therefore rising the probability of segmenting the right ones. Conifer was the group showing the best result for all algorithms (0.99 for U-Net, 0.97 for Mask-RCNN, and ROXAS); while alder, beech, and oak vessels segmentation showed very similar results for the artificial intelligence algorithms (0.96, 0.91, and 0.93 for Mask RCNN, and 0.96, 0.95, and 0.92 for U-Net, respectively). Slightly lower values were shown for ROXAS, where oak was the species with the lowest recall value (0.85).

Furthermore, we investigated the characteristics of the FN instance within the cell size classes, to determine where the lack of cell detection was more pronounced (**Figure 4**). This assessment is useful for the future training of the DCNN, in order to fine-tune the cell instance detection process. Generally, the most affected size classes are the smaller ones, but wood anatomical type plays a consistent role in this evaluation. Oak as a ring-porous species shows great differences in size between the earlywood the latewood vessels. This size difference exists also in conifers, where latewood cells are distinctively smaller than the earlywood cells. However, in conifers the difference is smaller and the transition occurs less abruptly. In these two categories, the most affected size classes were the smallest, supporting the predictable trend that the smallest cells are more difficult to identify. In contrast, alder and beech, diffuse and semi-diffuse porous species, respectively, show the bias shifted to medium-small cells and more evenly distributed across size classes. This analysis demonstrates that, when the wood structure is more homogeneous, cell size has less effect on cell instance recognition.

Since the testing dataset was built to include artifacts generated by sample preparation, we analyzed how the detection process is affected when an artifact occurs, comparing the Mask-RCNN segmentation approach with ROXAS. As a result, we observed that tackling FN issues from the segmentation methodology perspective highlights the benefit of using artificial intelligence for the feature recognition step. A visual comparison between Mask-RCNN output and the ROXAS output, involving the issues that might generate FN instances, is shown in **Figure 5**: blurred areas caused by various artifacts such as overlapping object (**Figure 5A**), paraffin drops (**Figure 5B**), and stains of coloring solutions (**Figure 5C**).

To estimate how many non-target (redundant) cells got recognized, we used the precision parameter: the closer to 1 the value, the lower is the overestimation in cell instance detection.

As we expected, U-Net architecture provided the lowest values, therefore the worst performance. Mask-RCNN and ROXAS results showed the same general pattern: from the worst to the best precision rate we found alder (0.82, 0.84), conifers (0.89, 0.91), oak (0.94 for both), and beech (0.94, 0.96). Overall, results on the precision values were very high and close for both approaches, although ROXAS demonstrated to be slightly more efficient in the task (**Table 2**).

Precision values interpretation was performed on a visual level, comparing the error maps provided by the different algorithms, to identify in which situations errors occurred more frequently and which cells were most susceptible. Since the U-Net architecture proved not to be particularly meaningful in filtering target cells from non-target cells, we focused on the comparison between ROXAS and Mask-RCNN outputs (**Supplementary Table 3**).

The wood anatomical feature that produced the most FP instances was the bark, with similar results for both approaches. In this respect, ROXAS provides the possibility to define an area

TABLE 2 | Average values of F1 score, recall, and precision for cell instance detection using different segmenting approaches (Mask-RCNN, U-Net, and ROXAS) calculated for all anatomical groups.

	Conifer			Alder			Beech			Oak		
	Mask-RCNN	**U-Net**	**ROXAS**	**Mask-RCNN**	**U-Net**	**ROXAS**	**Mask-RCNN**	**U-Net**	**ROXAS**	**Mask-RCNN**	**U-Net**	**ROXAS**
F1	0.93	0.91	0.94	0.88	0.83	0.88	0.92	0.80	0.92	0.93	0.85	0.89
Recall	0.97	0.99	0.97	0.96	0.96	0.92	0.91	0.95	0.89	0.93	0.92	0.85
Precision	0.89	0.84	0.91	0.82	0.73	0.84	0.94	0.69	0.96	0.94	0.79	0.94

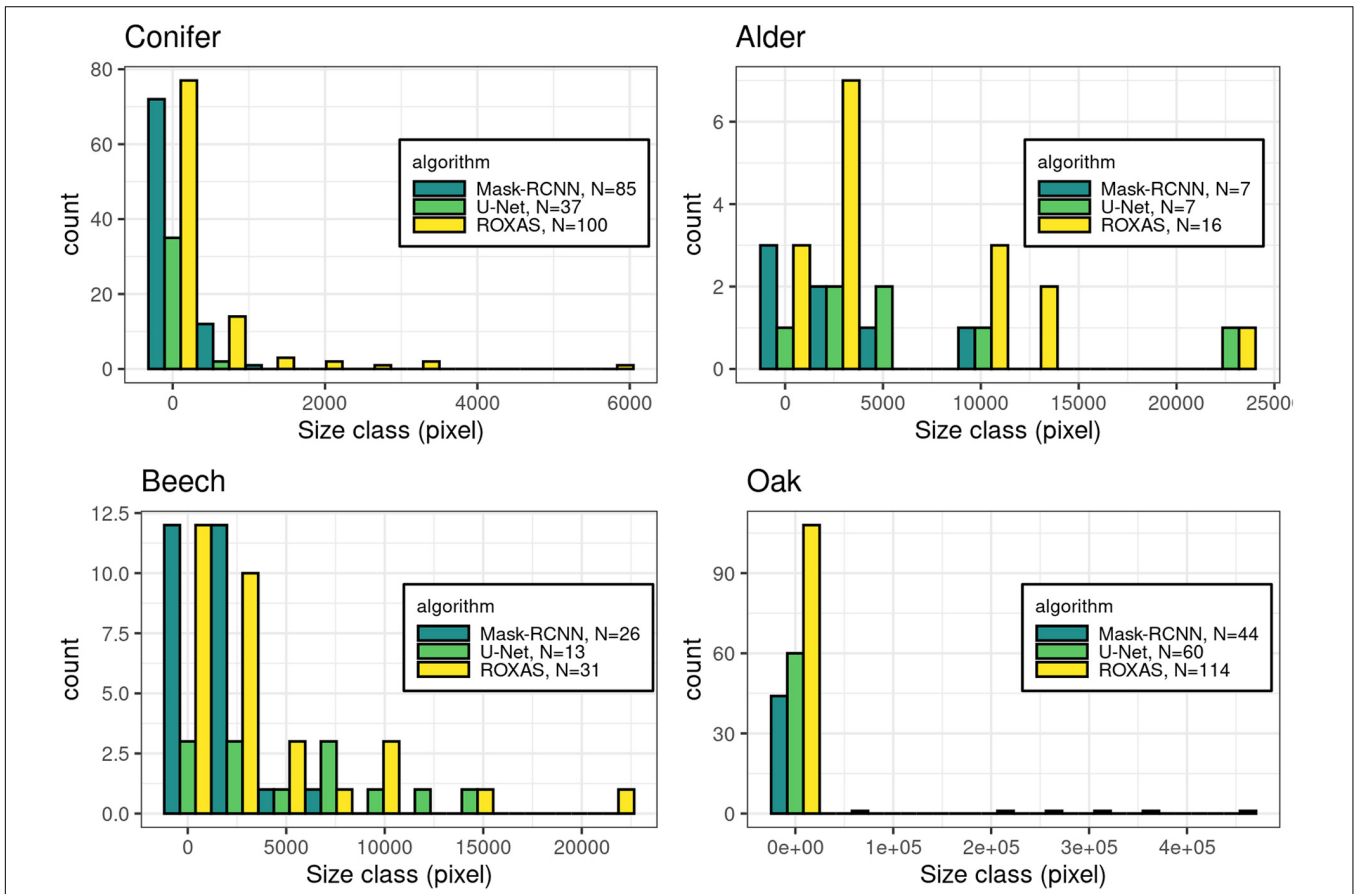

FIGURE 4 | Histograms of the missed cells (FN value) per groups: conifer, alder, beech, and oak. The count in the legend refers to the FN instances that were recorded in total per algorithm for each species, while the histograms show the respective size-frequency distributions.

of interest and thus to manually exclude the bark. Nevertheless, the comparison was done on images analyzed without any manual editing (no tailored area of interest defined), and it was performed with the same methodology than with the Mask-RCNN algorithm. The process could be further streamlined if the algorithm training focused on bark/non-bark area recognition, since the manual editing step of creating the area of interest could be skipped.

Overall, the cell categories presenting FP issues coincide for the Mask-RCNN algorithm and ROXAS on conifers. However, one advantage of the Mask-RCNN seems to be pit recognition. The high amount of target cells per unit area allowed the algorithm to perfectly recognize this feature, and no pit was included in the lumen area nor mistaken for a cell itself for every image of the dataset analyzed.

For the angiosperms, Mask-RCNN FPs included all those small cells that could resemble a small vessel (our target), or a big fiber or apotracheal parenchyma; while ROXAS automatically filtered them out by their size thanks to the tailored configuration files. Nonetheless, we believe that this challenging category cannot be clarified unambiguously without a closer look at the longitudinal sections of a sample. This highlights how the learning process of the DCNN approach really took place, and clearly had an effect on the image segmentation. Another example of FP included the scalariform perforation plates (**Figure 6**), a feature abundantly present in alder and occasionally in

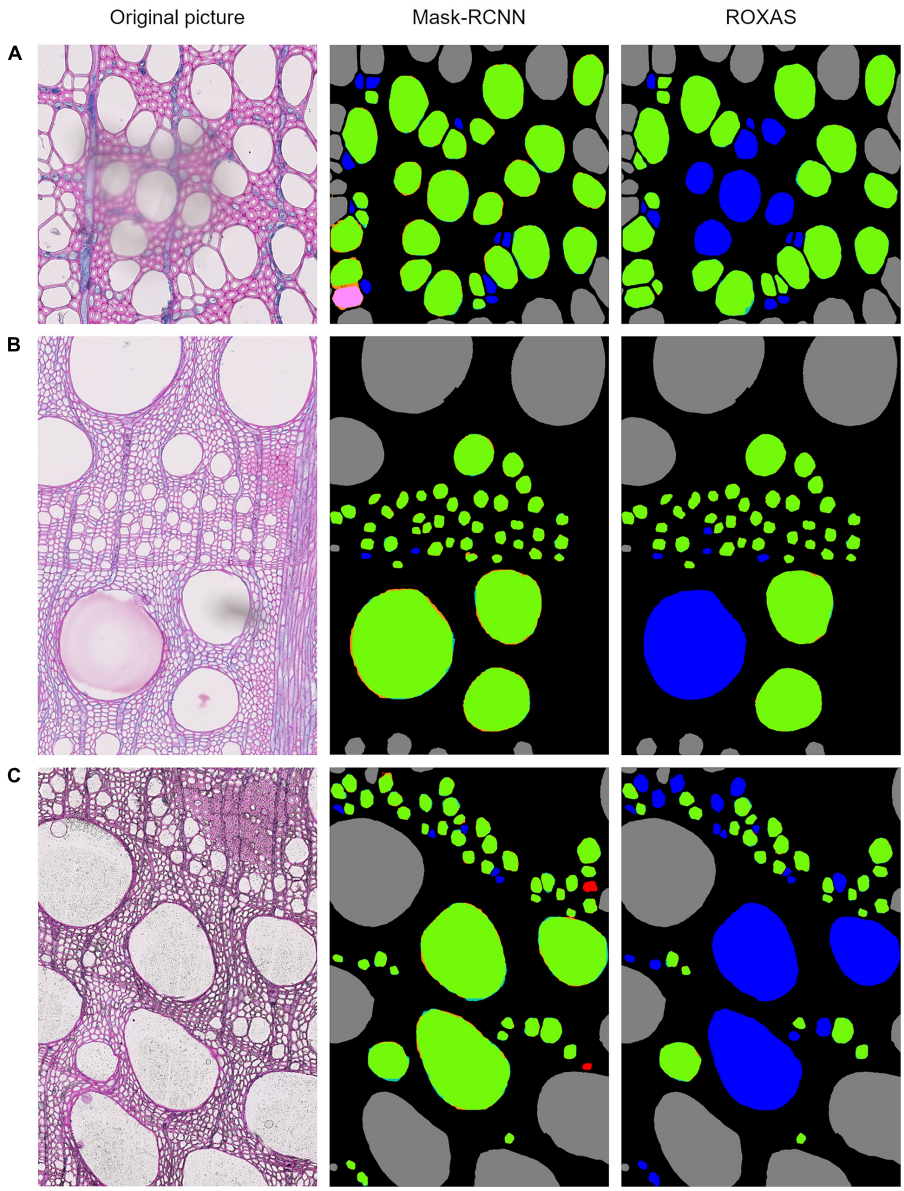

FIGURE 5 | Output comparison between Mask-RCNN and ROXAS on examples of overlaying dust particle **(A)**, paraffin drops **(B),** and stains of coloring solutions **(C)**. Error legend can be found in **Figure 1**. The FN cell instance are marked in blue, and in ROXAS outputs they exactly correspond to the area interested by the **(A–C)** issue.

beech. Here the algorithm, within certain limits, successfully distinguished between adjacent vessels and individual vessels sectioned at a scalariform perforation plate with thin bars, which could be wrongly interpreted as two adjacent vessels. The interpretation as one or two separate conduits influences the calculation of theoretical hydraulic conductivity of the specimen and therefore matters for studies dealing with water transport.

The Mask-RCNN output presented some FP instances related to damaged cells. This happened because the algorithm training aimed to consider every cell whose shape can be accurately predicted, as long as it fulfills the requirements for a reliable measurement. What is usually a matter of exclusion when the whole dataset is of average quality, sometimes has to be reconsidered as usable if this happens to be the only material available, therefore as many cells as possible should be measured. In this testing dataset, the slide quality was very high and quite homogeneous, which explains why many high-quality cells were available and thus damaged and dubious cells were not segmented in the ground truth. This sheds light on how FP evaluation is very case-specific regarding this issue. However, applied to QWA analyses and specifically to ROXAS use, the FP error can be considered less time-consuming to handle, since eventually requires deleting redundant cells, rather than drawing new ones from scratch, as it happens in the case of FNs.

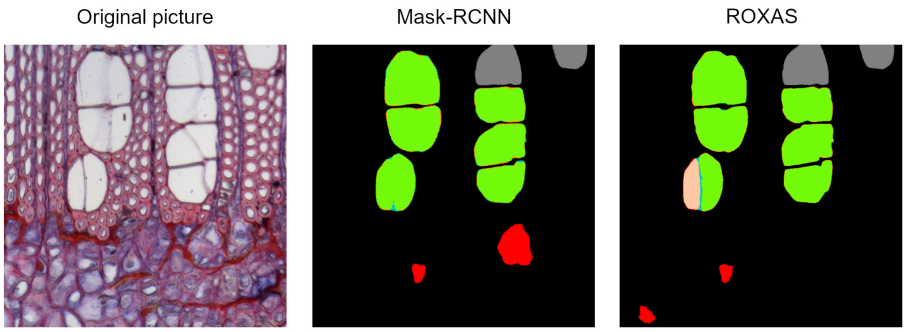

FIGURE 6 | Output comparison on vessel identification. Original alder image from the testing dataset, Mask-RCNN error map, and ROXAS error map. When the perforation plate is strongly visible, there is a high chance that one single vessel is wrongly recognized as two separate ones.

TABLE 3 | Average values of F1 score, recall, and precision for lumen area detection using different segmenting approaches (Mask-RCNN, U-Net, and ROXAS) calculated for all the groups.

	Conifer			Alder			Beech			Oak		
	Mask-RCNN	**U-Net**	**ROXAS**	**Mask-RCNN**	**U-Net**	**ROXAS**	**Mask-RCNN**	**U-Net**	**ROXAS**	**Mask-RCNN**	**U-Net**	**ROXAS**
F1	0.95	0.96	0.98	0.97	0.95	0.96	0.97	0.93	0.97	0.97	0.91	0.97
Recall	0.97	0.94	0.97	0.98	0.94	0.94	0.97	0.92	0.96	0.97	0.90	0.97
Precision	0.93	0.98	0.98	0.96	0.98	0.97	0.97	0.97	0.99	0.97	0.96	0.98

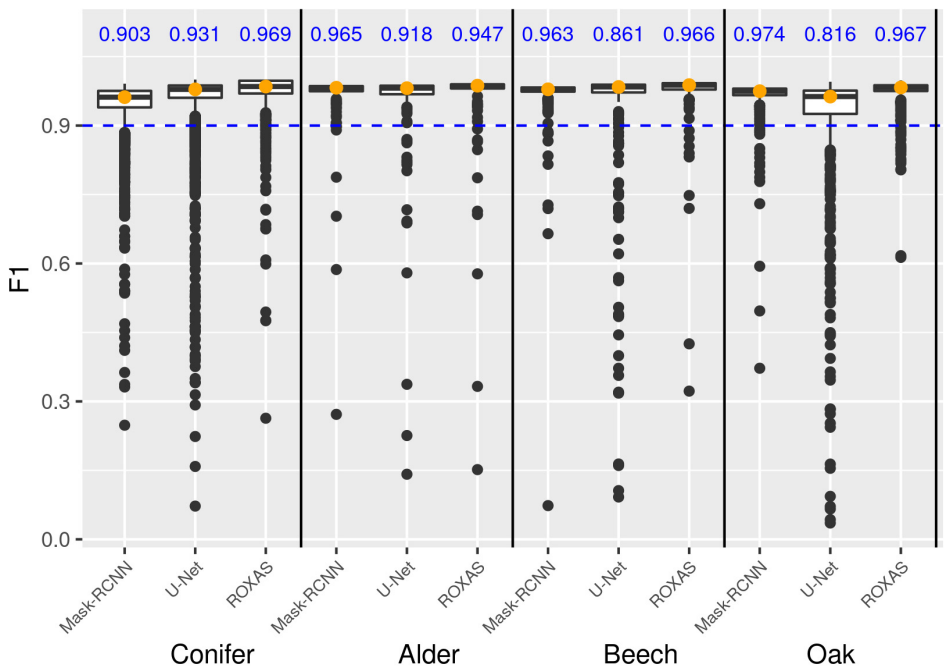

FIGURE 7 | Box plot showing the frequency distribution of the F1 score for lumen area, which allows a comparison of the three algorithms (Mask-RCNN, U-Net, and ROXAS) for each tree-species group. The blue values represent the fraction of cells reaching and surpassing the F1 score threshold of 0.9.

Lumen Area Detection

Overall, all segmentation approaches showed very high F1 scores for lumen area (**Table 3**). For conifers, values varied between 0.98 (ROXAS) to 0.95 (Mask-RCNN algorithm). A different trend characterized the angiosperms. The Mask-RCNN algorithm results for alder, beech, and, oak, all reported an F1 score of 0.97. This value was the same for ROXAS with beech and oak, but it was slightly lower (0.96) for the ROXAS segmentation results on alder. U-Net algorithm did not cope as well as the other approaches, and while the value was

TABLE 4 | Example of parameters calculated for an underestimated lumen area and an overestimated lumen area.

	Area	Prediction	TP	FP	FN	Precision	Recall	F1
Underestimated lumen area	1715	482	482	0	1233	1	0.28	0.44
Overestimated lumen area	85	600	85	515	0	0.14	1	0.25

When high precision is associated to low recall, then the area is underestimated. When the values are low for precision and high for recall, then the area is overestimated.

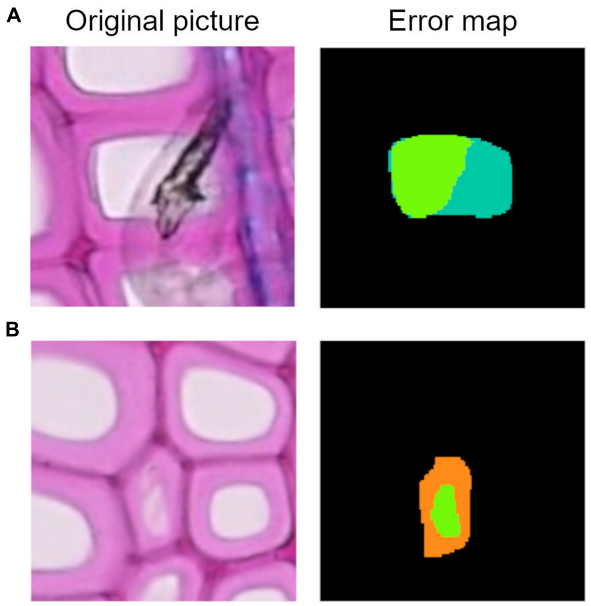

FIGURE 8 | (A) Example of lumen area underestimation, the dark green area represents the FN pixels. **(B)** Example of lumen area overestimation, the orange area represents the FP pixels.

still very similar for alder (0.95), it dropped for beech (0.93), and oak (0.91).

Overall, F1 scores were very high and results were close for all the segmenting approaches, but generally ROXAS performed slightly better. Nonetheless, since with artificial intelligence we aimed at very high accuracy levels to avoid manual editing as much as possible, we additionally analyzed the percentage of cells belonging to the highest accuracy class, that is when F1 $\geq$ 0.9 (**Figure 7**, blue number). U-Net underperforms for beech and oak and to a lesser extent for alder. The Mask-RCNN algorithm and ROXAS perform generally similarly well for the angiosperms, but Mask-RCNN performs lower in the conifer category.

The F1 score gives an overall idea of how well lumen area is detected. To understand if the algorithms are generally underestimating or overestimating the areas, we need to closely analyze precision and recall parameters. In **Table 4** we show two cell records from the conifer dataset generated by the Mask-RCNN algorithm. Both show very low F1 scores, meaning that the segmentation process failed in accuracy for both cells. In the first row, it is shown how precision, which ranges from 0 to 1, reaches its maximum, while recall is very low. In practice, what happened is that all the pixels that were recognized as belonging to the cell were indeed target pixels, but not all the target pixels were recognized, leading to an underestimation of the area (**Figure 8A**). The second row in **Table 4** reports the opposite situation, recall reaches the maximum value, but precision is low. **Figure 8B** visually explains this case: all the pixels belonging to the cell were recognized, but redundant pixels around the area were included in the segmentation, resulting in an overestimated lumen area.

TABLE 5 | Summary result on the comparison of the algorithms' performances.

		Cell instance detection			Lumen area detection		
Best performing algorithm (F1 score)	Conifer			*			*
	Alder	*		*	*		
	Beech	*		*	*		*
	Oak	*			*		*
Detection accuracy trend (precision and recall)	Conifer	+	+	+	−	+	+
	Alder	+	+	+	+	−	−
	Beech	−	+	−	=	−	−
	Oak	−	+	−	=	−	−
		Mask-RCNN	U-Net	ROXAS	Mask-RCNN	U-Net	ROXAS

The best performing algorithm was signaled with an asterisk (*). If the F1 score of a group type reported the same number for more than one approach, the star is represented twice. With respect to the detection accuracy trend, the overestimation both of the cell instance and the lumen area was reported with a plus sign (+), underestimation with a minus (−), and if there was no evident trend an equal symbol was noted (=).

Results for all the three approaches demonstrated a very high performance, even in terms of precision and recall of lumen area segmentation (**Table 3**). In the conifer group, we found that ROXAS had the highest F1, precision, and recall values (0.98, 0.98, 0.97, respectively). This resulted in very few redundant pixels and even less missed ones. Regarding the deep learning approaches, cells were more likely to be underestimated with U-Net (0.94 for recall and 0.98 for precision), while the opposite held for Mask-RCNN (0.97 for recall and 0.93 for precision). Analyses of alder samples were most precise when performed by the Mask-RCNN algorithm. The advantage of this approach consists of a lower percentage of lumen area underestimated (0.98 for recall), and still a very good result on the overestimation issue (0.96 for precision). ROXAS and U-Net, in contrast, tend to underestimate cell areas (0.94 for both approaches on recall) more than overestimating them (0.97 for ROXAS and 0.98 for U-Net on precision). Beech and oak segmentation behaved very similarly in the three approaches. Mask-RCNN was the most stable of the three, where 0.97 was the value for both species and for both parameters, meaning that there was no evident tendency in under- or over-estimating. ROXAS, which performs better than U-Net, showed a strong precision both on beech (0.99) and oak (0.98), but generally underestimated lumen area. The same trend was confirmed for U-Net, with a stronger tendency in underestimating lumen area (0.92 for beech and 0.90 for oak).

Since many aspects contribute to the evaluation process of the algorithms' performances, we include a general overview of the results to summarize the main outcomes of this analysis (**Table 5**).

Mask-RCNN Results for the Sub-Dataset

The Mask-RCNN approach worked properly for all the species and accurately segmented cells (**Supplementary Figure 1**). The visual assessment revealed that conifers remain the main weakness of the Mask-RCNN. The most occurring issue is represented by missed cells, especially small cells in the latewood. Regarding the lumen area detection, underestimation was more likely to happen, but the algorithm coped particularly well with problematic regions where the cell wall protrudes in the lumen area or where stains occurred. Alder is one of the species the model worked best with: error maps showed few redundant vessels and some broken ones wrongly segmented. This great performance is partially explained by the fact that the neural network could rely on a larger training dataset, but most likely by the fact that vessels have a distinctive shape and size compared to the surrounding fibers, and the diffuse porous organization of the vessels make them quite consistent in shape along the ring. If the larger training dataset would have had a major impact, we would have also noticed a difference within the groups in the F1 scores calculated for the main dataset. In general, for alder images, a very small portion of target cells were missed, in contrast to beech. Beech presented very accurately segmented lumen areas but some of them, especially when affected by very dark stains, were not identified. The large oak earlywood vessels were almost perfectly recognized, with only a minor percentage of missing cells and some redundant fibers which were segmented in the latewood.

In this smaller sample we also tested the running time of the Mask-RCNN model, using a 15-10210U CPU. By monitoring the process with a timer, we found out that the time needed for analyzing cells per single image varied from a minimum of 7.76 s to a maximum of 1.37 min depending on the species and the complexity of the image. Running time is also dependent on the task; when the comparison between other outputs is performed along with the cell detection, time can slightly increase. On average, oak is the species that employs more time because of the two models running on the same image.

CONCLUSION

Our results show that Mask-RCNN is highly suitable for the analysis of wood anatomical images. In all four wood-type groups, cells could be detected and segmented with high accuracy (i.e., high F1 score, precision, and recall).

While ROXAS always performed better for conifers in all the different parameters analyzed, the Mask-RCNN was better suited for angiosperms. We can thus infer that the wood anatomical variability of the angiosperms does not hamper a proper segmentation process with the Mask-RCNN algorithm. This is explained by the methodology employed by the Mask-RCNN approach: the instance segmentation operated by the algorithm first evaluates the context of a target cell and then proceeds in the segmentation. Therefore, the more stable the features of the target cells in the images, the more likely the Mask-RCNN is to succeed in the detection process, despite the diversity of the surrounding structures. Oak vessels, for example required two different algorithms, due to the difference in shape and size. Analogously, the homogeneous pattern of conifers is not facilitating a proper detection and segmentation of the tracheids, due to the small lumen of the latewood cells.

Another important aspect is the perspective we take to look at the data. A strict evaluation of numeric results would suggest that Mask-RCNN accomplishes the best performance for the F1 score with three species categories out of four; U-Net performed best for the recall parameter, very close to the Mask-RCNN results; and ROXAS recorded the best values for the precision parameter, still very close to Mask-RCNN results (**Table 2**). However, the visual interpretation of the error maps allowed us to draw additional conclusions. Looking at the recall value on cell instances (i.e., missed cells) from the cell characteristic perspective, highlighted how the detection process benefits from the neural network methodology. Many of the issues we selected, that hamper a smooth workflow with a traditional image analysis approach (i.e., ROXAS), were better handled with the DCNNs. Both U-Net and Mask-RCNN showed not only the best results, but also a similar trend. At the same time, visual interpretation of the error maps was also important for the analysis of redundant cell instances (i.e., precision). If on a first look, ROXAS and Mask-RCNN seemed to behave similarly, a further analysis demonstrated the Mask-RCNN ability to encode species-specific features, thus avoiding certain undesirable cell categories that we previously classified as issues. Moving the focus to the precision of the lumen area detection and the fraction of target cells reaching and surpassing a 0.9 threshold for the F1 score, we obtained the highest values for Mask-RCNN in all the angiosperm groups. Although Mask-RCNN was not always the best performing, it demonstrated to be the most stable concerning the underestimation and overestimation of lumen area parameter. Overall, the most frequent issue hampering the lumen area segmentation was the underestimation of lumen areas.

As expected, the Mask-RCNN is best suited for the detection of a high numbers of objects in a single image. As previously stated, the algorithm first detects all the possible target cells, therefore a consistent number of redundant predictions are avoided. Because segmenting a higher number of cells makes it more likely to identify all the target cell instances, recall values showed the highest results for U-Net model.

Overall, ROXAS performed very well, despite the traditional image analysis methodology. This is partially explained by the characteristics of the testing dataset. The selected images already belonged to a very high-quality standard, i.e., they were quite homogeneous and tissue identification was generally very clear. Moreover, ROXAS configuration files used to analyze the images were specifically created for each dataset, to obtain the best performance from the program. In contrast, we demonstrated how the Mask-RCNN model can deal with bad quality samples reaching an acceptable result, even with a rather small training dataset (at least 30 images per group), consisting of cropped images from original sections. The development of a very flexible and user-friendly tool is particularly beneficial for future studies on various species. For this reason, our next aim is to implement

the current version with the ability of retraining the models as a permanent feature. Generally, the advantage of the Mask-RCNN approach does not rely in a high-speed processing of the images, but if the performance in detecting and segmenting target cell is high, then the manual editing phase afterward can be avoided or significantly reduced.

In summary, this study shows that future QWA analyses could greatly benefit from Mask-RCNN approaches, such as the one presented here, due to their high accuracy, stability, and ability to deal with artifacts, coupled with high usability. Moreover, a highly automatized approach, like Mask-RCNN, will allow the processing of larger quantities of wood anatomical measurements in a shorter time, opening the way for higher replicated studies on variability in wood anatomical features.

DATA AVAILABILITY STATEMENT

The raw data supporting the conclusions of this article will be made available by the authors, without undue reservation.

AUTHOR CONTRIBUTIONS

GR, MT, and MW designed the study with the contribution of AA-R. AG and UL provided the user interface and the models for the algorithm. GR, GA, AA-R, RP, and MT contributed with data. GR and MT performed the measurements and statistic assessment. GR wrote the manuscript with the contribution of all the co-authors. All authors contributed to the article and approved the submitted version.

FUNDING

GR, AG, MT, UL, and MW have been supported by the European Social Fund (ESF) and the Ministry of Education, Science and Culture of Mecklenburg-Vorpommern, Germany under the project "DigIT!" (ESF/14-BM-A55-0012/19 and ESF/14-BM-A55-0015/19). AA-R was funded by a Postdoctoral Research Fellowship by the Alexander von Humboldt Foundation. RP acknowledges the support of the Swiss National Science Foundation (SNSF), Grant P2BSP3_184475. GA was supported by the Swiss National Science Foundation SNSF (Grant No. 200021_182398, XELLCLIM).

ACKNOWLEDGMENTS

We are grateful to all the researchers providing data for the algorithm training and testing steps. Namely: Angela Luisa Prendin, Timo Pampuch, and Jelena Lange. We also thank Alan Crivellaro for his contribution to the wood anatomical knowledge, and all the students that helped in the creation of the training and testing datasets.

SUPPLEMENTARY MATERIAL

The Supplementary Material for this article can be found online at: https://www.frontiersin.org/articles/10.3389/fpls.2021.767400/full#supplementary-material

REFERENCES

Björklund, J., Seftigen, K., Fonti, P., Nievergelt, D., and von Arx, G. (2020). Dendroclimatic potential of dendroanatomy in temperature-sensitive Pinus sylvestris. *Dendrochronologia* 60:125673. doi: 10.1016/j.dendro.2020.125673

Carrer, M., von Arx, G., Castagneri, D., and Petit, G. (2015). Distilling allometric and environmental information from time series of conduit size: the standardization issue and its relationship to tree hydraulic architecture. *Tree Physiol.* 35, 27–33. doi: 10.1093/treephys/tpu108

Castagneri, D., Prendin, A. L., Peters, R. L., Carrer, M., von Arx, G., and Fonti, P. (2020). Long-term impacts of defoliator outbreaks on larch xylem structure and tree-ring biomass. *Front. Plant Sci.* 11:1078. doi: 10.3389/fpls.2020.01078

Christin, S., Hervet, É, and Lecomte, N. (2019). Applications for deep learning in ecology. *Methods Ecol. Evol.* 10, 1632–1644. doi: 10.1111/2041-210X.13256

De Micco, V., Carrer, M., Rathgeber, C. B., Julio Camarero, J., Voltas, J., Cherubini, P., et al. (2019). From xylogenesis to tree rings: wood traits to investigate tree response to environmental changes. *IAWA J.* 40, 155–182. doi: 10.1163/22941932-40190246

Fonti, P., von Arx, G., García-González, I., Eilmann, B., Sass-Klaassen, U., Gärtner, H., et al. (2010). Studying global change through investigation of the plastic responses of xylem anatomy in tree rings. *New Phytol.* 185, 42–53. doi: 10.1111/j.1469-8137.2009.03030.x

Garcia-Pedrero, A., García-Cervigón, A. I., Olano, J. M., García-Hidalgo, M., Lillo-Saavedra, M., Gonzalo-Martín, C., et al. (2019). Convolutional neural networks for segmenting xylem vessels in stained cross-sectional images. *Neural Comput. Appl.* 32, 17927–17939. doi: 10.1007/s00521-019-04546-6

Gärtner, H., Cherubini, P., Fonti, P., von Arx, G., Schneider, L., Nievergelt, D., et al. (2015). A technical perspective in modern tree-ring research–how to overcome dendroecological and wood anatomical challenges. *J. Vis. Exp.* 97:52337. doi: 10.3791/52337

He, K., Gkioxari, G., Dollár, P., and Girshick, R. (2017). *Mask R-CNN*. Dubai: ICCV.

He, T., Marco, J., Soares, R., Yin, Y., and Wiedenhoeft, A. (2020). Machine learning models with quantitative wood anatomy data can discriminate between *Swietenia macrophylla* and *Swietenia mahagoni*. *Forests* 11:36. doi: 10.3390/f11010036

Hwang, S.-W., and Sugiyama, J. (2021). Computer vision-based wood identification and its expansion and contribution potentials in wood science: a review. *Plant Methods* 17:47. doi: 10.1186/s13007-021-00746-1

James, K., and Bradshaw, K. (2020). Detecting plant species in the field with deep learning and drone technology. *Methods Ecol. Evol.* 11, 1509–1519. doi: 10.1111/2041-210X.13473

Janecka, K., Harvey, J. E., Trouillier, M., Kaczka, R. J., Metslaid, S., Metslaid, M., et al. (2020). Higher winter-spring temperature and winter-spring/summer moisture availability increase scots pine growth on coastal dune microsites around the South Baltic Sea. *Front. For. Glob. Change* 3:578912. doi: 10.3389/ffgc.2020.578912

Krizhevsky, A., Sutskever, I., and Hinton, G. E. (2017). ImageNet classification with deep convolutional neural networks. *Commun. ACM* 60, 84–90. doi: 10.1145/3065386

Lange, J., Buras, A., Cruz-García, R., Gurskaya, M., Jalkanen, R., Kukarskih, V., et al. (2018). Climate regimes override micro-site effects on the summer temperature signal of scots pine at its northern distribution limits. *Front. Plant Sci.* 9:1597. doi: 10.3389/fpls.2018.01597

LeCun, Y., Bengio, Y., and Hinton, G. (2015). Deep learning. *Nature* 521, 436–444. doi: 10.1038/nature14539

Lin, T.-Y., Dollár, P., Girshick, R., He, K., Hariharan, B., and Belongie, S. (2017). Feature pyramid networks for object detection. *arXiv* [Preprint]. arXiv:1612.03144

Lin, T.-Y., Maire, M., Belongie, S., Hays, J., Perona, P., Ramanan, D., et al. (2014). "Microsoft COCO: common objects in context," in *Computer Vision – ECCV 2014*, eds D. Fleet, T. Pajdla, B. Schiele, and T. Tuytelaars (Cham: Springer International Publishing), 740–755.

Luis, G. E., Francisco, G. F., de Palacios de Palacios, P., Ruth, M. R., and Nieves, N. C. (2009). Artificial neural network in wood identification the case of two *Juniperus* species from the Canary Islands. *IAWA J.* 30, 87–94. doi: 10.1163/22941932-90000206

Mallik, A., Tarrío-Saavedra, J., Francisco-Fernández, M., and Naya, S. (2011). Classification of wood micrographs by image segmentation. *Chemometr. Intell. Lab. Syst.* 107, 351–362. doi: 10.1016/j.chemolab.2011.05.005

Media Cybernetics. (2021). *Image-Pro Plus*. Rockville, MD: Media Cybernetics, Inc.

Olden, J. D., Lawler, J. J., and Poff, N. L. (2008). Machine learning methods without tears: a primer for ecologists. *Q. Rev. Biol.* 83, 171–193. doi: 10.1086/587826

Pampuch, T., Anadon-Rosell, A., Zacharias, M., von Arx, G., and Wilmking, M. (2020). Xylem anatomical variability in white spruce at treeline is largely driven by spatial clustering. *Front. Plant Sci.* 11:581378. doi: 10.3389/fpls.2020.581378

Paszke, A., Gross, S., Massa, F., Lerer, A., Bradbury, J., Chanan, G., et al. (2019). *PyTorch: An Imperative Style, High-Performance Deep Learning Library*. Vancouver, BC: NeurIPS 2019.

Peters, R. L., Balanzategui, D., Hurley, A. G., von Arx, G., Prendin, A. L., Cuny, H. E., et al. (2018). RAPTOR: row and position tracheid organizer in R. *Dendrochronologia* 47, 10–16. doi: 10.1016/j.dendro.2017.10.003

Peters, R. L., von Arx, G., Nievergelt, D., Ibrom, A., Stillhard, J., Trotsiuk, V., et al. (2020). Axial changes in wood functional traits have limited net effects on stem biomass increment in European beech (*Fagus sylvatica*). *Tree Physiol.* 40, 498–510. doi: 10.1093/treephys/tpaa002

Prendin, A. L., Petit, G., Carrer, M., Fonti, P., Björklund, J., and von Arx, G. (2017). New research perspectives from a novel approach to quantify tracheid wall thickness. *Tree Physiol.* 37, 976–983. doi: 10.1093/treephys/tpx037

Príncipe, A., van der Maaten, E., van der Maaten-Theunissen, M., Struwe, T., Wilmking, M., and Kreyling, J. (2017). Low resistance but high resilience in growth of a major deciduous forest tree (*Fagus sylvatica* L.) in response to late spring frost in southern Germany. *Trees* 31, 743–751. doi: 10.1007/s00468-016-1505-3

Ravindran, P., Costa, A., Soares, R., and Wiedenhoeft, A. C. (2018). Classification of CITES-listed and other neotropical Meliaceae wood images using convolutional neural networks. *Plant Methods* 14:25. doi: 10.1186/s13007-018-0292-9

Scharnweber, T., Manthey, M., and Wilmking, M. (2013). Differential radial growth patterns between beech (*Fagus sylvatica* L.) and oak (*Quercus robur* L.) on periodically waterlogged soils. *Tree Physiol.* 33, 425–437. doi: 10.1093/treephys/tpt020

Spencer, K., Peter, M., and The GIMP Development Team (2021). *GNU Image Manipulation Program (GIMP)*. Berkeley: GIMP.

von Arx, G., and Carrer, M. (2014). ROXAS – a new tool to build centuries-long tracheid-lumen chronologies in conifers. *Dendrochronologia* 32, 290–293. doi: 10.1016/j.dendro.2013.12.001

von Arx, G., Crivellaro, A., Prendin, A. L., Čufar, K., and Carrer, M. (2016). Quantitative wood anatomy-practical guidelines. *Front. Plant Sci.* 7:781. doi: 10.3389/fpls.2016.00781

von Arx, G., and Dietz, H. (2005). Automated image analysis of annual rings in the roots of perennial forbs. *Int. J. Plant Sci.* 166, 723–732. doi: 10.1086/431230

Wu, F., Gazo, R., Haviarova, E., and Benes, B. (2021). Wood identification based on longitudinal section images by using deep learning. *Wood Sci. Technol.* 55, 553–563. doi: 10.1007/s00226-021-01261-1

Yeung, E. C. T., Stasolla, C., Sumner, M. J., and Huang, B. Q. (2015). *Plant Microtechniques and Protocols*. Cham: Springer International Publishing.

Zhang, L., Zhang, L., and Du, B. (2016). Deep learning for remote sensing data: a technical tutorial on the state of the art. *IEEE Geosci. Remote Sens. Mag.* 4, 22–40. doi: 10.1109/MGRS.2016.2540798

Conflict of Interest: The authors declare that the research was conducted in the absence of any commercial or financial relationships that could be construed as a potential conflict of interest.

The reviewer AB declared a past collaboration with one of the authors MW to the handling editor.

frontiers in Plant Science

ORIGINAL RESEARCH
published: 22 November 2021
doi: 10.3389/fpls.2021.777753

Origin of Intra-annual Density Fluctuations in a Semi-arid Area of Northwestern China

Jiani Gao[1,2,3], *Sergio Rossi*[3,4] *and Bao Yang*[1,5,6]*

[1]*Key Laboratory of Desert and Desertification, Northwest Institute of Eco-Environment and Resources, Chinese Academy of Sciences, Lanzhou, China,* [2]*College of Resources and Environment, University of Chinese Academy of Sciences, Beijing, China,* [3]*Département des Sciences Fondamentales, Université du Quebec à Chicoutimi, Chicoutimi, QC, Canada,* [4]*Key Laboratory of Vegetation Restoration and Management of Degraded Ecosystems, Guangdong Provincial Key Laboratory of Applied Botany, South China Botanical Garden, Chinese Academy of Sciences, Guangzhou, China,* [5]*Center for Excellence in Tibetan Plateau Earth Sciences, Chinese Academy of Sciences, Beijing, China,* [6]*Qinghai Research Center of Qilian Mountain National Park, Academy of Plateau Science and Sustainability and Qinghai Normal University, Xining, China*

Intra-annual density fluctuation (IADF) is a structural modification of the tree ring in response to fluctuations in the weather. The expected changes in monsoon flow would lead to heterogeneous moisture conditions during the growing season and increase the occurrence of IADF in trees of the arid ecosystems of continental Asia. To reveal the timings and physiological mechanisms behind IADF formation, we monitored cambial activity and wood formation in Chinese pine (*Pinus tabuliformis*) during 2017–2019 at three sites in semi-arid China. We compared the dynamics of xylem formation under a drought event, testing the hypothesis that drought affects the process of cell enlargement and thus induces the production of IADF. Wood microcores collected weekly from April to October were used for anatomical analyses to estimate the timings of cambial activity, and the phases of enlargement, wall thickening, and lignification of the xylem. The first cells started enlargement from late April to early May. The last latewood cells completed differentiation in mid-September. Trees produced IADF in 2018. During that year, a drought in June limited cell production in the cambium, only 36% of the xylem cells being formed in IADF trees, compared to 68% in normal tree rings. IADF cells enlarged under drought in early July and started wall thickening during the rainfall events of late July. The drought restricted cell enlargement and affected wall thickening, resulting in narrow cells with wide walls. Cambium and cell enlargement recovered from the abundant rainfall, producing a new layer with large earlywood tracheids. IADF is a specific adaptation of trees to cope with water deficit events occurring during xylem formation. Our findings confirmed the hypothesis that the June-July drought induces latewood-like IADFs by limiting the process of cell enlargement in the xylem. Our finding suggests a higher occurrence of IADF in trees of arid and semi-arid climates of continental Asia if the changes to monsoon flows result in more frequent drought events during the earlywood formation in June.

Keywords: water availability, IADF, xylogenesis, cambial activity, Chinese pine, cell enlargement

OPEN ACCESS

Edited by:
Ze-Xin Fan,
Xishuangbanna Tropical Botanical Garden (CAS), China

Reviewed by:
Angela Balzano,
University of Ljubljana, Slovenia
Xin Song,
Shenzhen University, China

***Correspondence:**
Bao Yang
yangbao@lzb.ac.cn

Specialty section:
This article was submitted to Functional Plant Ecology, a section of the journal Frontiers in Plant Science

Received: *15 September 2021*
Accepted: *26 October 2021*
Published: *22 November 2021*

Citation:
Gao J, Rossi S and Yang B (2021) Origin of Intra-annual Density Fluctuations in a Semi-arid Area of Northwestern China. Front. Plant Sci. 12:777753. doi: 10.3389/fpls.2021.777753

INTRODUCTION

Intra-annual density fluctuation (IADF) is a structural modification of the tree ring involving an abrupt change in wood density (Battipaglia et al., 2016), producing a cell layer similar to the boundary of a true tree ring. IADF exhibit either latewood-like cells with thicker cell wall and narrower lumen area in earlywood intra-annual density fluctuations (*E*-IADFs), or earlywood-like cells with larger lumina and thinner walls in latewood intra-annual density fluctuation (*L*-IADFs; Campelo et al., 2007). Large tracheids are the key for efficient water conduction but are more vulnerable to cavitation and embolism. Thick cell walls contribute to the increase of wood density (Beeckman, 2016). IADF represents the ability of a species to adapt to the substantial changes in the growing conditions according to changes in xylogenesis, i.e., cambial activity or cell differentiation or both (Eilmann et al., 2011; Deslauriers et al., 2016; De Micco et al., 2016a). The morphology of IADF cells affects the hydraulic properties of wood and tree survival. In addition, an abrupt modification of the tree-ring structure due to IADF affects the physical or mechanical properties of the xylem and reduces wood quality and its potential use (Olivar et al., 2015).

Intra-annual density fluctuations have been studied mainly in Mediterranean ecosystems, characterized by a long growing season with a hot and dry summer, inducing bimodal growth patterns in most conifers. Trees in Mediterranean ecosystems generally exhibit *L*-IADFs occurring after the summer drought, at the beginning of the autumnal rainfall (Battipaglia et al., 2010; De Micco et al., 2016b; Balzano et al., 2018). *E*-IADFs are observed in temperate forests, as a result of latewood cells developed within earlywood or at the transition between earlywood and latewood (Edmondson, 2010; Rozas et al., 2011; Gao et al., 2021). *E*-IADF is linked to drought conditions during the summer. IADFs occur in other environments such as tropical and boreal forests (Marchand and Filion, 2012; Palakit et al., 2015; Venegas-González et al., 2015). Despite the wide literature on *L*-IADF, knowledge on the mechanisms of the formation on *E*-IADF remains unclear in ecosystems outside the Mediterranean area, especially in arid inland areas. Based on the available literature, IADF is less investigated in China (Zhang et al., 2020; Gao et al., 2021).

Precipitation and temperature are the climatic factors most frequently considered in relation to IADF, although late frosts and defoliation may be involved in its formation (De Micco et al., 2016b). The study indicated that 72% of the years showing IADF in the tree ring of black pine had low precipitations in May (Wimmer et al., 2000). The frequency of IADFs varies greatly among trees with different species, ages, and tree ring widths. Different species show a different aptitude to form IADFs (Balzano et al., 2019). It is also suggested that younger trees with wider tree rings are more prone to form IADF than older trees with narrower rings (Schweingruber, 1996). Knowledge on the occurrence, frequency, and mechanisms of the production on IADF remains scarce and deserve more attention. Detailed analyses of xylem phenology at high time resolution can be a tool to characterize IADF phenology and its environment drivers.

The rise in temperature worldwide, associated with local reduction in precipitation, is expected to increase frequency and severity of warming-induced drought (IPCC. Climate Change, 2014; Wu et al., 2018). Vegetation and fertility of Eastern Asia benefits from the wet spring and summer resulting from precipitation due to the periodic monsoons (Ding et al., 2018). The asymmetric changes in land and ocean temperatures are expected to weaken the monsoon flows, resulting in a drier climate, with serious consequences for the arid Asian regions (Huang et al., 2017). The fluctuations of monsoon intensity would lead to diversified water vapor patterns and frequent extreme climate events, making trees growing in this area experience a more complicated hydrothermal environment. Severe drought events and fluctuations in moisture conditions affect stem growth and increase the production of abnormal tree ring structures and IADFs (Cuny and Rathgeber, 2016). This region is therefore an ideal location to investigate the responses of xylogenesis to drought.

In this study, we collected samples in Chinese pine (*Pinus tabuliformis*) in three sites located in the semi-arid region lying between the East Asian monsoon zone and the arid region of Northwestern China and investigated the dynamics of xylogenesis and IADF formation. The objective of this study was to (i) assess the phenology of IADF and (ii) investigate the climatic drivers of IADF production. We tested the hypothesis that summer drought affects the process of cell enlargement and thus induces IADF.

MATERIALS AND METHODS

Study Site and Tree Selection

We selected three sites in a semi-arid forest in Northwestern China (**Figure 1A**). Two sites (named as Helan1 and Helan2) were located at two altitudes (2010 m a.s.l. and 2,330 m a.s.l.) at the Helan Mountain national forest park in Ningxia (38°44′ N, 105°54′ E). The third site (named as Hasi) was located 400 km away, on Hasi Mountain (37°03′ N, 104°31′ E, 2410 m a.s.l.). This study area forms the boundary between the arid region in the Northwest and the East Asian monsoon zone. Chinese pine (*Pinus tabuliformis*) is one of the dominant tree species growing at the northwestern boundary of its distribution. The long-term climate recorded by the national weather stations during 1951–2019 showed similar mean annual temperature between the two regions, with 9.7 and 10°C in Helan and Hasi, respectively (**Figures 1B,C**). Total precipitation was 195 and 234 mm, with 65 and 55% of the rain falling in June–August, at Helan and Hasi, respectively. The climate is dry in winter and generally wet from spring to autumn. Hasi receives more precipitation in late spring and summer compared with Helan.

Sixteen dominant and healthy Chinese pines were chosen (eight trees per site at Helan1 and Helan2, 10 trees at Hasi). Trees at Hasi were bigger, i.e., larger and taller, and older than those at the other two sites (**Table 1**). The younger trees (70 years old) were located at Helan2.

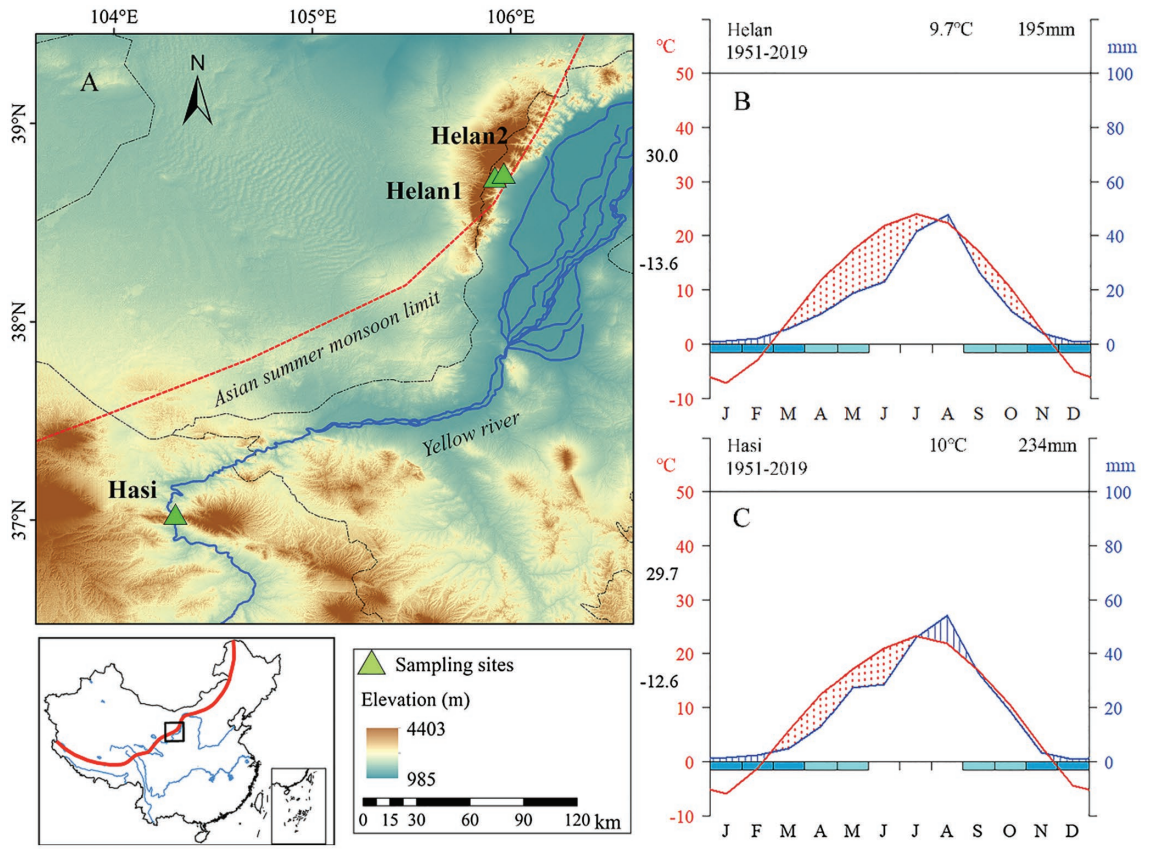

FIGURE 1 | (A) Map of sampling sites, and **(B,C)** Walter and Lieth climatic diagram at Helan and Hasi during 1951–2019. Red line and blue line represent the monthly mean temperature and precipitation. Values on the left axis are the average maximum temperature of the warmest month and average minimum temperature of the coldest month. The upper right of the diagram shows an annual mean temperature and annual total precipitation.

TABLE 1 | Characteristics of the trees sampled in three sites in a semi-arid region of Northwestern China.

	DBH (cm)	Height (m)	Age (years)
Helan1	72 ± 9	7.6 ± 1.8	103 ± 7
Helan2	72 ± 12	10.5 ± 1.5	70 ± 10
Hasi	105 ± 23	12 ± 4	93 ± 25

Meteorological Data

Three automated weather stations were installed at each site to measure air temperature and precipitation every 30 min, and daily means were calculated from the half-an-hour time series. To quantify drought severity, the standardized precipitation evapotranspiration index (SPEI) was calculated according to the Hargreaves equation, as a monthly difference between precipitation and potential evapotranspiration, using "SPEI" package (Beguería et al., 2017) in R environment (R Core Team, 2017).

Xylem Collection and Observation

Wood samples were collected in 2017–2019 weekly, at breast height (1.3 m above ground), from April to September, the main growing season of Chinese pine (Zeng et al., 2018) using a Trephor (Rossi et al., 2006a), and stored in 50% ethanol solution. Microcores were dehydrated through successive immersions in ethanol solutions and dewaxing agent, embedded in paraffin, cut in sections (8–12 μm thickness) using a rotary microtome, and then stained with a water solution of safranin and astral blue. Sections were examined under visible and polarized light at 200–400 × magnifications to discriminate cells in different stages of xylem differentiation. The number of cells in the cambial zone, enlargement, secondary wall thickening, and mature xylem cells were counted along three radial files. Cambial cells were flat with thin primary walls. Enlarging cells were at least twice the radial length of cambial cells, with thin cell walls. In spring, xylogenesis was considered to have started when at least one horizontal row of enlarging cells was observed (Rossi et al., 2006b). Cell wall thickening and mature cells were blue or light red and dark red, respectively, with thick walls and showed birefringence under polarized light. We consider that xylem formation was complete when all cells of the tree ring were mature.

IADFs Identification and Statistics

We recorded the proportion of trees with IADFs in all sampling trees in each site and year; we compared difference in monthly

air temperature, precipitation, and SPEI using mixed models to assess which factor affected IADFs occurrence. Year and site were considered as random effects in the model. To identify the timings of IADFs formation, the number of cells in earlywood, IADFs, and latewood were counted and reported in the form of proportion. Tracheids were classified as earlywood or latewood according to the Mork's formula, which classifies all cells with lumen areas of less than twice the thickness of a double cell wall as latewood (Denne, 1988). The cumulative proportion of (i) mature cells, (ii) mature cell and wall thickening cells, and (iii) total xylem cells (mature, wall thickening, and enlarging cells) in the tree ring for each day in 2018 were estimated using the Gompertz function. The function is defined as:

$$Y(t) = A\mathrm{e}^{-\mathrm{e}^{\beta - kt}}$$

where $Y(t)$ is the cumulative proportion of cells at time t; A is the upper asymptote parameter; β is the x-axis placement parameter; and k is the rate of change parameter. The cumulative proportion of mature cells, mature cell and wall thickening cells, and total xylem cells represented the timings when the cells produced by the cambium underwent enlargement and wall thickening (Rossi et al., 2003).

RESULTS

IADF Occurrence

The sections of all sampled trees during 3 years were identified to investigate the occurrence of IADFs. No IADFs were observed at three sites in 2017 and 2019 (**Table 2**). A normal tree ring structure exhibits large, thin-walled earlywood cells, followed by small, heavy-walled latewood cells (**Figure 2**). E-IADFs were observed in earlywood of all trees from Helan1 and Helan2 sampled in 2018. E-IADF appeared in the form of narrow cells with thick walls within the earlywood zone. No IADF was observed at Hasi.

In 2018, 35% of xylem cells were classified as earlywood at Helan1 and Helan2 (**Figure 3**). IADFs accounted for about 12 and 16% of tree ring at Helan1 and Helan2, and 50% of the tree ring was latewood at the two sites. At Hasi, 68% of the tree ring was earlywood, and 32% was latewood.

Comparing Climate Between Years

The years 2017 and 2019 were warmer than 2018. A lower precipitation was recorded in 2019 compared to the other 2 years (**Figure 4**). The mean air temperature was 6.3°C in March and April 2018, which was 4°C and 1.6°C higher than that in 2017 and 2019, respectively. Precipitation of June was lower in 2018 (27 mm) compared to 2017 (100 mm) and 2019 (102 mm). However, rain was more abundant in July and August in 2018 compared to the same period in 2017 and 2019. As a consequence, the climate in June was dry in 2018, with SPEI being <−1. In June 2017 and 2019, SPEI indicated wet conditions. July and August were wetter in 2018 compared to 2017 and 2019. Overall, SPEI of April and May 2018 was higher at Hasi (1.3 and 0.19) compared to Helan1 (−0.25 and −0.58) and Helan2 (−0.23 and −0.78).

May temperature was significantly higher at the sites where IADF occurred (**Figure 5**). Lower winter temperature was recorded at sites where IADF occurred. IADF was associated to lower precipitations in June and October, and higher precipitations in July and August. No significant difference in precipitation was observed in the other months. The monthly drought condition between the presence of and absence of IADF was contrary. The climate was dry from March to June and humid from July to September in the IADF group, while it was humid from March to June and July to September in the absence of IADF group.

TABLE 2 | Occurrence of Intra-annual density fluctuations (IADFs) of the trees sampled in three sites in a semi-arid region of Northwestern China. Values are reported as trees showing IADFs on total sampled trees.

	2017	2018	2019
Helan1	0/8	8/8	0/8
Helan2	0/8	8/8	0/8
Hasi	0/10	0/10	0/10

Xylem Formation in 2018

To test our hypothesis, we focused on the xylogenesis in 2018, the year with IADF formation. The first enlarging cells, corresponding to the onset of xylem cell differentiation, were observed from late April to early May in 2018 (**Figure 6**). The process of cell enlargement lasted until late August at Hasi, and until mid-September at the two sites in Helan. Compared to Hasi, the number of enlarging cells increased more slowly at Helan1 and Helan2 at the beginning of the growing season. Cell wall thickening began in late May to early June and was completed in mid-September. The first mature xylem cells were observed in mid-June. Xylem differentiation, including cell enlargement and secondary wall formation, lasted for 112, 127 and 130 days at Helan1, Helan2 and Hasi, respectively. The total number of xylem cells increased slowly before DOY 200, with only 40% of the xylem cells being produced at the two sites in Helan.

IADF Phenology

At the beginning of the growing season, xylem formation progressed slowly under low or absent precipitations at Helan1 and Helan2 (**Figure 7**), and only 35–37% of xylem cells were formed before DOY 190. IADF cells enlarged between DOY 190 and 210 at the Helan sites. In this period, Helan was warm, and precipitation was absent during the first half of the period when IADF cells enlarged. After DOY 200, the temperature decreased and precipitation recovered. IADF cells underwent wall thickening during DOY 200–220, under abundant rainfall. During IADF formation, the proportion of enlarging cells in the tree ring decreased, and only 12–16% of the tree ring belonging to IADF was formed. After DOY 220, cell number increased again, and more than 50% of the total amount of annual xylem cells was produced within 50 days.

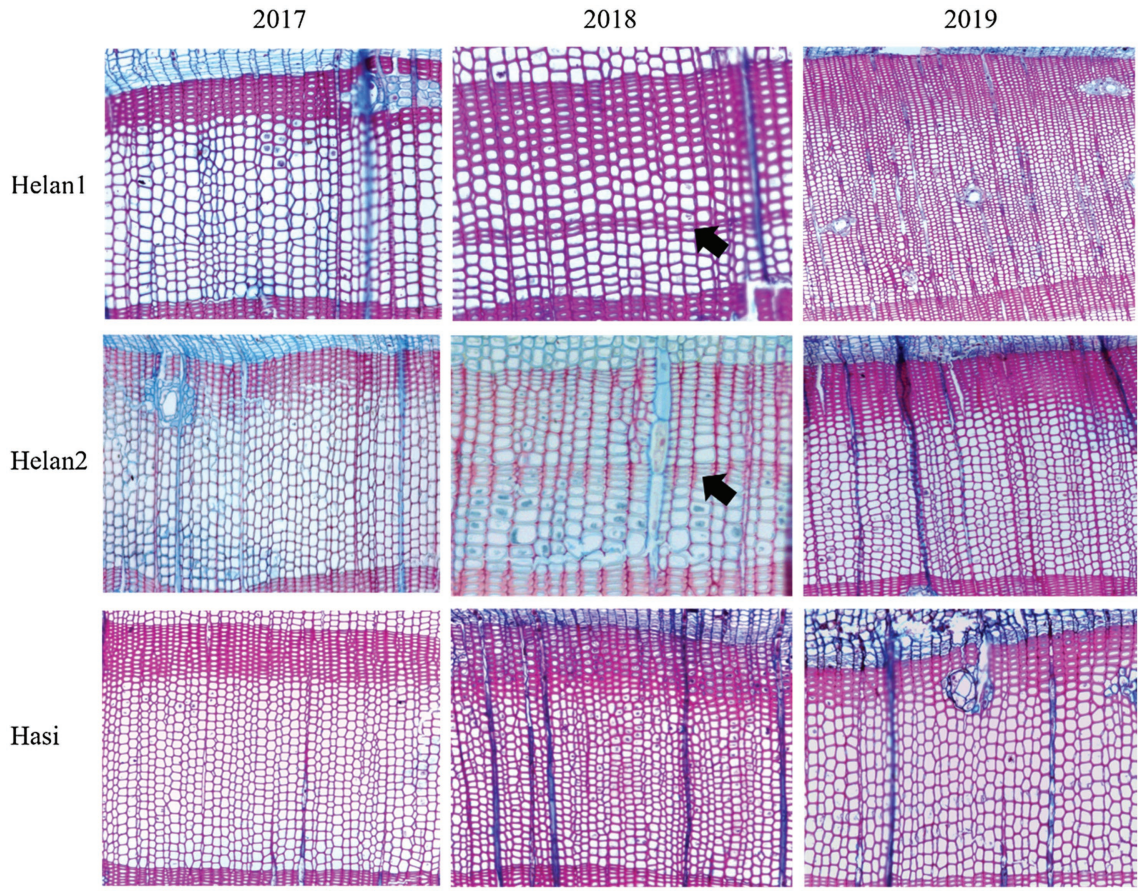

FIGURE 2 | Wood anatomy in tree-rings sampled at three sites during 2017–2019 in a semi-arid region of Northwestern China. Arrows indicate the IADF.

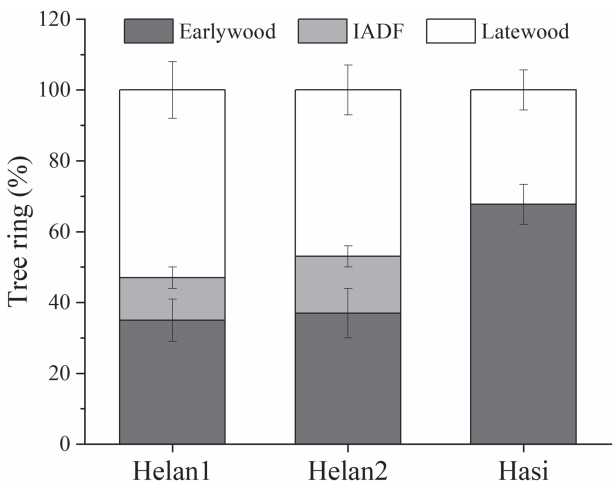

FIGURE 3 | Proportion of earlywood, IADF, and latewood in tree ring in 2018 at three sites in a semi-arid region of Northwestern China.

Regarding at Hasi site, precipitation during DOY 100–150 was three times higher compared to Helan, and 68% of the tree ring was produced before DOY 190. At that date, all the earlywood cells had completed cell enlargement at Hasi, which indicated a faster progression of xylem formation compared to Helan. No IADF cells were observed at Hasi, where cell enlargement of latewood cells progressed after DOY 190.

DISCUSSION

Earlywood intra-annual density fluctuation is a response to a drought event occurring during the growing season, mainly in the summer (Campelo et al., 2007, 2015). In this study, we investigated the dynamics of xylogenesis and IADF formation in Chinese pine (*Pinus tabuliformis*) in a semi-arid region of northwest China and found that IADF cells were produced under a prolonged summer drought and differentiate during the precipitation deficit in June and abundant rainfall in July and August. These findings suggest that summer drought triggers cell enlargement and affects IADF formation, which allowed us to accept our initial hypothesis.

IADF Formation and Its Environmental Control

Latewood-like IADF cells enlarged during the drought event, although some of them completed enlargement at the beginning

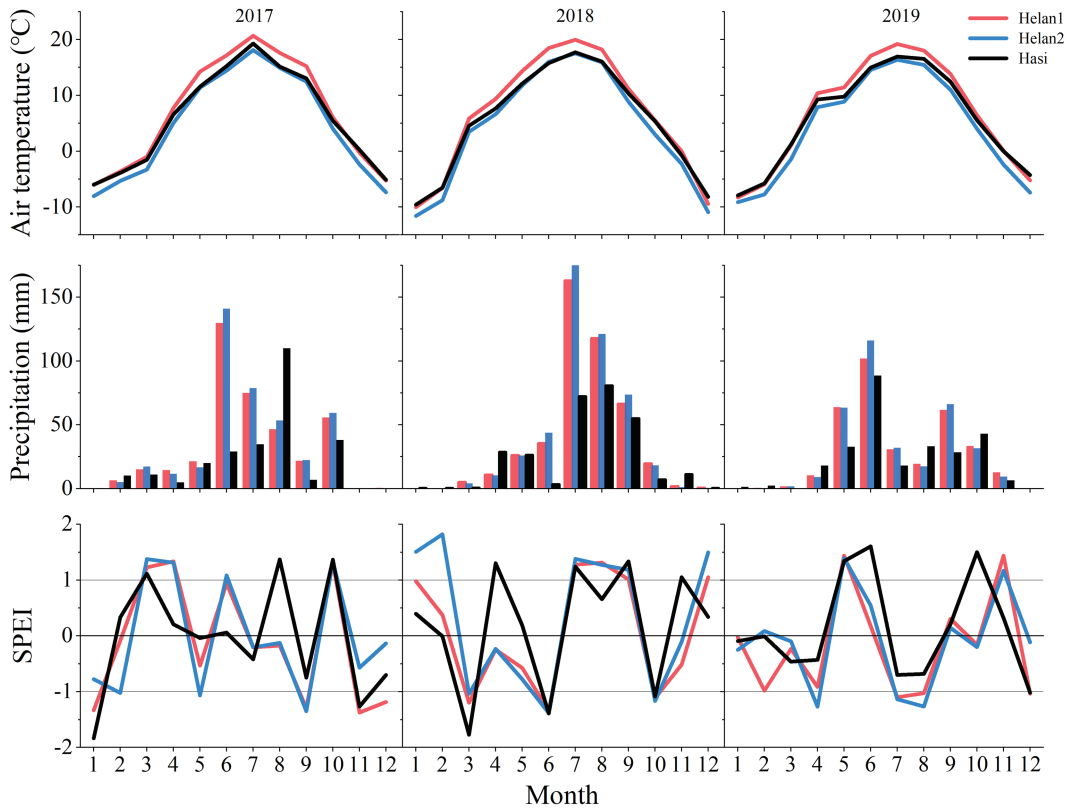

FIGURE 4 | Monthly mean air temperature, precipitation and SPEI at three sites during 2017–2019.

of the abundant rainfall (DOY 190–210). IADF cells started wall thickening when the precipitations had started again (DOY 200) and matured before mid-August. A significant decrease in the number of cambial and enlarging cells at the end of the drought was also observed, suggesting that drought inhibited cambial division and thus limited cell differentiation. Water availability is the primary climatic factor limiting stem growth in dry and warm regions (Rossi et al., 2014). Prolonged and severe summer droughts or high transpiration rates can disrupt the steady-state of water transfer in xylem cells and cause declines in water potential of the xylem (Bogeat-Triboulot et al., 2007). A low turgor pressure during enlargement prevents differentiating tracheids to increase in diameter, resulting in narrow, latewood-like cells (Steppe et al., 2015). Our finding is consistent with other studies, demonstrating that narrower cells are formed under water deficit occurring during formation (Rossi et al., 2009; Battipaglia et al., 2010). According to our findings, some IADF cells completed enlargement during the rainfall period. This unexpected result may represent the time lag between rainfall and the increase of water potential in xylem cells, or be related to a statistical error due to the weekly sampling used in this study.

IADF cells started secondary wall formation during the rainfall period, producing thick cell walls. It is suggested that wall thickness is encoded during the previous phase of cell enlargement (Cuny et al., 2014; Buttò et al., 2019). It is widely documented that carbohydrate in the stem, including structural C, such as cellulose and lignin, often accumulates under drought (Muller et al., 2011), suggesting that more carbon is available for the wall thickening process. Furthermore, the amount of materials of wall deposition stays almost constant in most of the cells in a tree ring (Cuny et al., 2014). The reduction in size of IADF cells would lead to more wall materials allocated to wall thickening, producing thicker walls in IADF cells. The availability of soluble sugars regulates the wall deposition process (Cartenì et al., 2018). Our results indicate that climate drivers are uniform for cell enlarging and wall thickening of IADF cells: large IADF cells with thick walls were mainly induced by summer drought. Stangler et al. (2021) demonstrated that the transition from a dry June to a wet July initiated IADF formation in Norway spruce at lower elevations in Germany. Accordingly, we detected the specific IADF phenology under water deficit and showed evidence of the climate driver of enlargement and wall thickening during IADF formation.

The Functional Explanation of the IADF Formation

IADF formation is a specific adaptation under summer drought. This modification in the xylem structure protects the trees from irreversible damage by xylem cavitation and vessel embolism at the cost of the reduction of water transfer efficiency

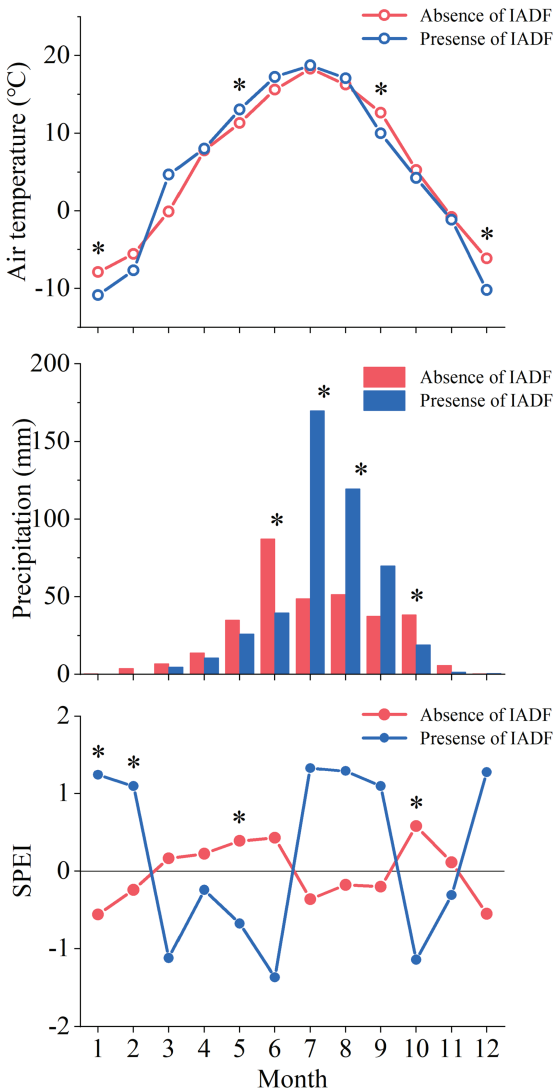

FIGURE 5 | Monthly air temperature, precipitation, and SPEI between absence and presence of IADF during 2017–2019 at three sites. Asterisks represent significant differences ($p < 0.05$) between the two categories.

(Martin-Benito et al., 2013; Puchi et al., 2019). The physiological response to water limitation is to protect trees against irreversible damage when stress becomes severe and long (Claeys and Inzé, 2013). In other words, trees ensure their survival when a water stress is prolonged or becomes more severe.

The rainfall of mid-July improved growing conditions and reactivated cambial activity and cell enlargement. In other words, once water availability is sufficient, xylogenesis recovers the expected activities of cell division and differentiation. During cell enlargement, the vacuoles loaded with sugars increase the turgor pressure and attract water inside the cells, then producing the large earlywood tracheids (Vieira et al., 2020). This mechanism failed under a Mediterranean climate, where a small amount of irrigation in September was unable to trigger a second period of cambial activity (Vieira et al., 2020). The observed flexible xylogenesis reflects the plasticity of our species, which allows trees to survive under water deficit and concentrate growth during favorable water supply conditions. Our study demonstrates the mechanism of IADF formation under summer drought and highlights the plasticity of xylogenesis to the varied water conditions.

Water Availability and Cell Production

Drought affected both wood anatomy and xylem cell production. Growth dropped once water deficit began. Enlargement of the first earlywood cells occurred during the high precipitation of April-May at Hasi, resulting in 30% of the tree ring. In the same period, only 10% of xylem cells started enlargement at Helan, because of a lack of rain and despite the water provided by the snowmelt in spring. The rainfall in the early growing season at Hasi provided sufficient water availability, thus trees could maintain high photosynthetic rates for sustaining cambium division and xylem growth, processes that are large carbon sinks (Bréda et al., 2006; Zhang et al., 2020). Moreover, the precipitation in April and May might have helped trees to maintain a higher water potential and protect the xylem cells from the negative influence of drought. As a result, xylem cells at Hasi were able to differentiate and mature their secondary walls under dry conditions, thus producing tree rings lacking IADF. Conversely, dry conditions during March–June may limit stem growth and, in case of prolonged lack of rain, accelerate leaf senescence to maintain the water balance. This defense mechanism led to growth losses, as observed by the lower amount of xylem cells produced at Helan, compared to Hasi, before the July precipitations. Our weekly monitoring of xylem formation provides evidence of the limiting effect of drought on cambial activity and xylogenesis at Helan. Dendrochronological studies also demonstrated that water availability of March–July affected stem growth (Li et al., 2007; Cai, 2009). Moreover, the precipitation from late spring to early summer (May–June) played a role in stem growth of *Sabina przewalskii* in semi-arid northwestern China (Gou et al., 2015; Yang et al., 2019, 2021).

CONCLUSION

As a structural anomaly of the tree ring, IADF is a suitable indicator of weather fluctuations occurring during the growing season. However, the physiological processes behind IADF formation and the impacts of the climate drivers remain partially unknown. To our knowledge, this is the first time that timings and dynamics of IADF formation have been assessed at high temporal resolutions. We investigated the weekly xylogenesis of Chinese pine at three sites in semi-arid continental China by describing the development of an *E*-IADF. Prolonged and severe drought in June and early July affected the processes of xylem production and differentiation and induced IADF. Specifically, drought limited enlargement and affected wall thickening, resulting in IADF cells with narrow tracheids and wide walls. Rainfall on April–May provided sufficient water availability for xylogenesis, protecting trees against summer drought. Warming-induced droughts may become more frequent and severe during the summer in the drier regions of the

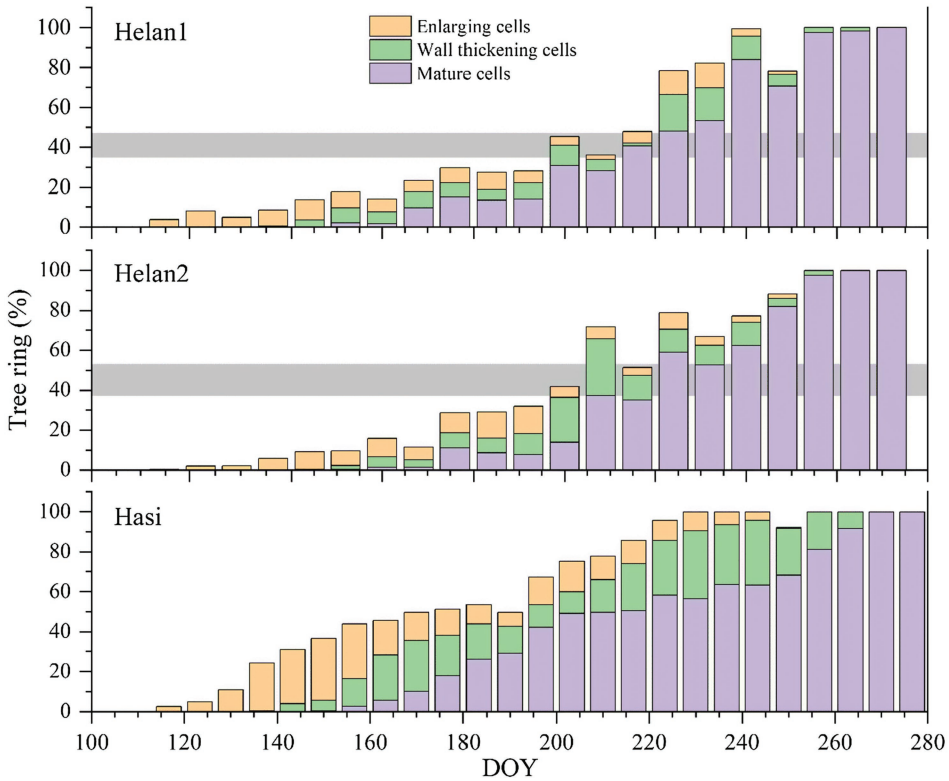

FIGURE 6 | Proportion of tree ring of cells during different phases of xylem formation at three sites in 2018 in a semi-arid region of Northwestern China. Horizontal bars represent IADFs at Helan1 and Helan2.

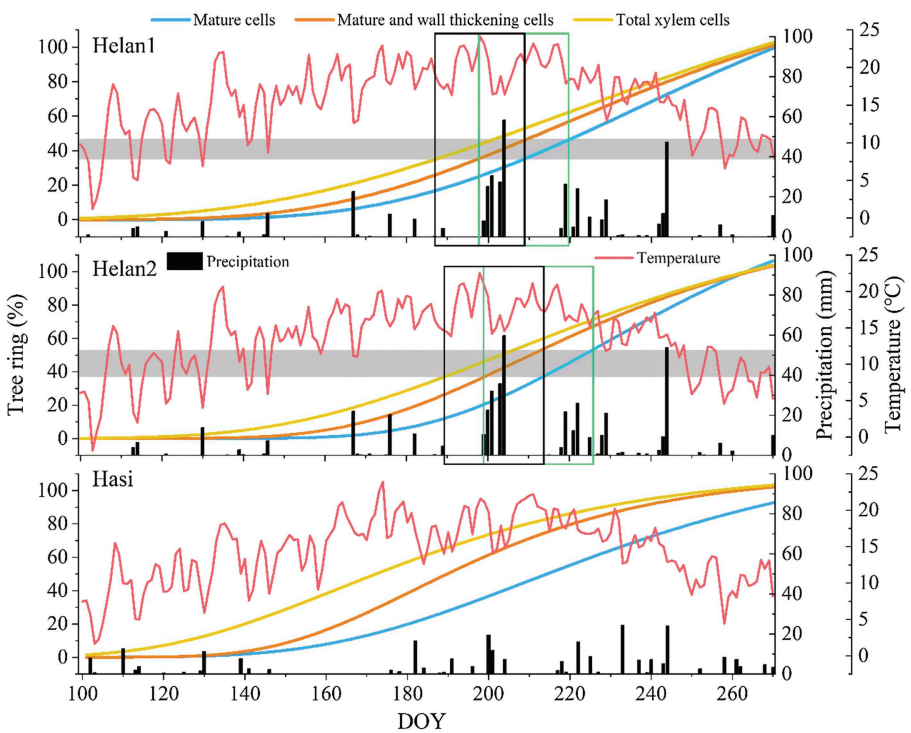

FIGURE 7 | Xylem formation described by Gompertz functions and weather at three sites in 2018 in a semi-arid region of Northwestern China. Horizontal bars represent IADFs at Helan1 and Helan2. Black and green rectangles correspond to the time windows of enlargement and cell-wall thickening of IADF cells.

northern hemisphere, enhancing the occurrence of IADF in trees. The formation of IADF appears to be a defense mechanism of trees against unfavorable environmental conditions, which ensures plasticity to the conducting system of trees and the capacity to tolerate and resist to water deficits.

DATA AVAILABILITY STATEMENT

The original contributions presented in the study are included in the article/supplementary material, and further inquiries can be directed to the corresponding author.

AUTHOR CONTRIBUTIONS

JG, SR, and BY designed the study and revised the manuscript. JG and SR performed the statistical analysis. JG wrote the first version of the manuscript. All authors contributed to the article and approved the submitted version.

FUNDING

This work was jointly supported by the National Natural Science Foundation of China (grant no. 42130511 and 41520104005), and a State Scholarship Fund provided by the China Scholarship Council (202004910757).

ACKNOWLEDGMENTS

We are grateful to the two reviewers for their helpful and constructive comments. We thank Linzhou Xia for the help of samples collection. We thank Alison Garside for English correction of the text.

REFERENCES

Balzano, A., Battipaglia, G., and De Micco, V. (2019). Wood-trait analysis to understand climatic factors triggering intra-annual density-fluctuations in co-occurring Mediterranean trees. *IAWA J.* 40, 241–258. doi: 10.1163/22941932-40190220

Balzano, A., Čufar, K., Battipaglia, G., Merela, M., Prislan, P., Aronne, G., et al. (2018). Xylogenesis reveals the genesis and ecological signal of IADFs in *Pinus pinea* L. and Arbutus unedo L. *Ann. Bot.* 121, 1231–1242. doi: 10.1093/aob/mcy008

Battipaglia, G., Campelo, F., Vieira, J., Grabner, M., De Micco, V., Nabais, C., et al. (2016). Structure and function of intra–annual density fluctuations: mind the gaps. *Front. Plant Sci.* 7:595. doi: 10.3389/fpls.2016.00595

Battipaglia, G., De Micco, V., Brand, W. A., Linke, P., Aronne, G., Saurer, M., et al. (2010). Variations of vessel diameter and $\delta^{13}C$ in false rings of *Arbutus unedo* L. reflect different environmental conditions. *New Phytol.* 188, 1099–1112. doi: 10.1111/j.1469-8137.2010.03443.x

Beeckman, H. (2016). Wood anatomy and trait-based ecology. *IAWA J.* 37, 127–151. doi: 10.1163/22941932-20160127

Beguería, S., Vicente-Serrano, S.M., and Beguería, M.S. (2017). SPEI: Calculation of the Standardised Precipitation-Evapotranspiration Index. Available at: https://CRAN.R-project.org/package=SPEI (Accessed July 7, 2021).

Bogeat-Triboulot, M. B., Brosché, M., Renaut, J., Jouve, L., Thiec, D. L., Fayyaz, P., et al. (2007). Gradual soil water depletion results in reversible changes of gene expression, protein profiles, ecophysiology, and growth performance in *Populus euphratica*, a poplar growing in arid regions. *Plant Physiol.* 143, 876–892. doi: 10.1104/pp.106.088708

Bréda, N., Huc, R., Granier, A., and Dreye, E. (2006). Temperate forest trees and stands under severe drought: a review of ecophysiological responses, adaptation processes and long-term consequences. *Ann. Forest Sci.* 63, 625–644. doi: 10.1051/forest:2006042

Buttò, V., Rossi, S., Deslauriers, A., and Morin, H. (2019). Is size an issue of time? Relationship between the duration of xylem development and cell traits. *Ann. Bot.* 123, 1257–1265. doi: 10.1093/aob/mcz032

Cai, Q. (2009). Response of *Pinus tabuliformis* tree-ring growth to three moisture indices and January to July Walter index reconstruction in Helan Mountain. *Marine Ecol. Quaternary. Geol.* 29, 131–136. doi: 10.3724/SP.J.1140.2009.06131

Campelo, F., Nabais, C., Freitas, H., and Gutiérrez, E. (2007). Climatic significance of tree-ring width and intra-annual density fluctuations in *Pinus pinea* from a dry Mediterranean area in Portugal. *Ann. For. Sci.* 64, 229–238. doi: 10.1051/forest:2006107

Campelo, F., Vieira, J., Battipaglia, G., De Luis, M., Nabais, C., Freitas, H., et al. (2015). Which matters most for the formation of intra-annual density fluctuations in *Pinus pinaster*: age or size? *Trees Struct. Funct.* 29, 237–245. doi: 10.1007/s00468-014-1108-9

Cartenì, F., Deslauriers, A., Rossi, S., Morin, H., De Micco, V., Mazzoleni, S., et al. (2018). The physiological mechanisms behind the earlywood-to-latewood transition: a process-based modeling approach. *Front. Plant Sci.* 9:1053. doi: 10.3389/fpls.2018.01053

Claeys, H., and Inzé, D. (2013). The agony of choice: how plants balance growth and survival under water-limiting conditions. *Plant Physiol.* 162, 1768–1779. doi: 10.1104/pp.113.220921

Cuny, H. E., and Rathgeber, C. B. K. (2016). Xylogenesis: coniferous trees of temperate forests are listening to the climate tale during the growing season but only remember the last words! *Plant Physiol.* 171, 306–317. doi: 10.1104/pp.16.00037

Cuny, H. E., Rathgeber, C. B. K., Frank, D., Fonti, P., and Fournier, M. (2014). Kinetics of tracheid development explain conifer tree-ring structure. *New Phytol.* 203, 1231–1241. doi: 10.1111/nph.12871

De Micco, V., Balzano, A., Čufar, K., Aronne, G., Gričar, J., Merela, M., et al. (2016a). Timing of false ring formation in *Pinus halepensis* and *Aruburus unedo* in southern Italy: outlook from an analysis of xylogenesis and tree-ring chronologies. *Front. Plant Sci.* 7:705. doi: 10.3389/fpls.2016.00705

De Micco, V., Campelo, F., De Luis, M., Bräuning, A., Grabner, M., Battipaglia, G., et al. (2016b). Intra-annual density fluctuations in tree rings: how, when, where, and why? *IAWA J.* 37, 232–259. doi: 10.1163/22941932-20160132

Denne, M. P. (1988). Definition of latewood according to Mork. *IAWA J.* 10, 59–62. doi: 10.1163/22941932-90001112

Deslauriers, A., Huang, J., Balducci, L., Beaulieu, M., and Rossi, S. (2016). The contribution of carbon and water in modulating wood formation in black spruce saplings. *Plant Physiol.* 170, 2072–2084. doi: 10.1104/pp.15.01525

Ding, Y., Si, D., Liu, Y., Wang, Z., Li, Y., Zhao, L., et al. (2018). On the characteristics, driving forces and inter-decadal variability of the east Asian summer monsoon. *Chin. J. Atmos. Sci.* 42, 533–558. doi: 10.3878/j.issn.1006-9895.1712.17261

Edmondson, J. R. (2010). The meteorological significance of false rings in eastern redcedar (*Juniperus virginiana* L.) from the southern Great Plains, USA. *Tree Ring Res.* 66, 19–33. doi: 10.3959/2008-13.1

Eilmann, B., Zweifel, R., Buchmann, N., Pannatier, E. G., and Rigling, A. (2011). Drought alters timing, quantity, and quality of wood formation in scots pine. *J. Exp. Bot.* 62, 2763–2771. doi: 10.1093/jxb/erq443

Gao, J., Yang, B., Peng, X., and Rossi, S. (2021). Tracheid development under a drought event producing intra-annual density fluctuations in the semi-arid China. *Agric. For. Meteorol.* 308-309:108572. doi: 10.1016/j.agrformet.2021.108572

Gou, X., Deng, Y., Gao, L., Chen, F., Cook, E., Yang, M., et al. (2015). Millennium tree-ring reconstruction of drought variability in the eastern Qilian Mountains, Northwest China. *Clim. Dyn.* 45, 1761–1770. doi: 10.1007/s00382-014-2431-y

Huang, J., Li, Y., Fu, C., Chen, F., Fu, Q., Dai, A., et al. (2017). Dryland climate change: recent progress and challenges. *Rev. Geophys.* 55, 719–778. doi: 10.1002/2016RG000550

IPCC. Climate Change 2014: *Mitigation of Climate Change: Working Group III Contribution to the IPCC Fifth Assessment Report*. Cambridge, UK: Cambridge University Press.

Li, J., Chen, F., Cook, E. R., Gou, X., and Zhang, Y. (2007). Drought reconstruction for North China from tree rings: the value of the palmer drought severity index. *Int. J. Climatol.* 27, 903–909. doi: 10.1002/joc.1450

Marchand, N., and Filion, L. (2012). False rings in the white pine (*Pinus strobus*) of the Outaouais Hills, Québec (Canada), as indicators of water stress. *Can. J. For. Res.* 42, 12–22. doi: 10.1139/x11-151

Martin-Benito, D., Beeckman, H., and Canellas, I. (2013). Influence of drought on tree rings and tracheid features of *Pinus nigra* and *Pinus sylvestris* in a Mesic Mediterranean forest. *Eur. J. For. Res.* 132, 33–45. doi: 10.1007/s10342-012-0652-3

Muller, B., Pantin, F., Génard, M., Turc, O., Freixes, S., Piques, M., et al. (2011). Water deficits uncouple growth from photosynthesis, increase C content, and modify the relationships between C and growth in sink organs. *J. Exp. Bot.* 62, 1715–1729. doi: 10.1093/jxb/erq438

Olivar, J., Rathgeber, C., and Bravo, F. (2015). Climate change, tree-ring width and wood density of pines in Mediterranean environments. *IAWA J.* 36, 257–269. doi: 10.1163/22941932-20150098

Palakit, K., Duangsathaporn, K., and Siripatanadilok, S. (2015). Climatic fluctuations trigger false ring occurrence and radial-growth variation in teak (*Tectona grandis* L.f.). *iForest* 9, 286–293. doi: 10.3832/ifor1100-008

Puchi, P. F., Castagneri, D., Rossi, S., and Carrer, M. (2019). Wood anatomical traits in black spruce reveal latent water constraints on the boreal forest. *Glob. Chang. Biol.* 26, 1767–1777. doi: 10.1111/gcb.14906

R Core Team (2017). *R: A Language and Environment for Statistical Computing*. Vienna, Austria: R Foundation for Statistical Computing.

Rossi, S., Anfodillo, T., and Menardi, R. (2006a). Trephor: a new tool for sampling microcores from tree stems. *IAWA J.* 27, 89–97. doi: 10.1163/22941932-90000139

Rossi, S., Deslauriers, A., and Anfodillo, T. (2006b). Assessment of cambial activity and xylogenesis by microsampling tree species: an example at the alpine timberline. *IAWA J.* 27, 383–394. doi: 10.1163/22941932-90000161

Rossi, S., Deslauriers, A., and Morin, H. (2003). Application of the Gompertz equation for the study of xylem cell development. *Dendrochronologia* 21, 33–39. doi: 10.1078/1125-7865-00034

Rossi, S., Girard, M. J., and Morin, H. (2014). Lengthening of the duration of xylogenesis engenders disproportionate increases in xylem production. *Glob. Chang. Biol.* 20, 2261–2271. doi: 10.1111/gcb.12470

Rossi, S., Simard, S., Rathgeber, C. B. K., Deslauriers, A., and De Zan, C. (2009). Effects of a 20-day-long dry period on cambial and apical meristem growth in *Abies balsamea* seedlings. *Trees Struct. Funct.* 23, 85–93. doi: 10.1007/s00468-008-0257-0

Rozas, V., García-González, I., and Zas, R. (2011). Climatic control of intra-annual wood density fluctuations of *Pinus pinaster* in NW Spain. *Trees Struct. Funct.* 25, 443–453. doi: 10.1007/s00468-010-0519-5

Schweingruber, F.H. (1996). *Tree Rings and Environment: Dendroecology*. Berne: Paul Haupt AG Bern.

Stangler, D. F., Kahle, H.-P., Raden, M., Larysch, E., Seifert, T., and Spiecker, H. (2021). Effects of intra-seasonal drought on kinetics of tracheid differentiation and seasonal growth dynamics of Norway spruce along an elevational gradient. *Forests* 12:274. doi: 10.3390/f12030274

Steppe, K., Sterck, F., and Deslauriers, A. (2015). Diel growth dynamics in tree stems: linking anatomy and ecophysiology. *Trends Plant Sci.* 20, 335–343. doi: 10.1016/j.tplants.2015.03.015

Venegas-González, A., von Arx, G., Chagas, M. P., and Tomazello Filho, M. (2015). Plasticity in xylem anatomical traits of two tropical species in response to intra-seasonal climate variability. *Trees Struct. Funct.* 29, 423–435. doi: 10.1007/s00468-014-1121-z

Vieira, J., Carvalho, A., and Campelo, F. (2020). Tree growth under climate change: evidence from xylogenesis timings and kinetics. *Front. Plant Sci.* 11:90. doi: 10.3389/fpls.2020.00090

Wimmer, R., Strumia, G., and Holawe, F. (2000). Use of false rings in Austrian pine to reconstruct early growing season precipitation. *Can. J. For. Res.* 30, 1691–1697. doi: 10.1139/x00-095

Wu, X., Liu, H., Li, X., Ciais, P., Babst, F., Guo, W., et al. (2018). Differentiating drought legacy effects on vegetation growth over the temperate northern hemisphere. *Glob. Chang. Biol.* 24, 504–516. doi: 10.1111/gcb.13920

Yang, B., Qin, C., Bräuning, A., Osborn, T. J., Trouet, V., Ljungqvist, F. C., et al. (2021). Long-term decrease in Asian monsoon rainfall and abrupt climate change events over the past 6,700 years. *Proc. Natl. Acad. Sci. U. S. A.* 118:e2102007118. doi: 10.1073/pnas.2102007118

Yang, B., Wang, J. L., and Liu, J. J. (2019). A 1556 year-long early summer moisture reconstruction for the Hexi corridor, northwestern China. *Sci. China Earth Sci.* 62, 953–963. doi: 10.1007/s11430-018-9327-1

Zeng, Q., Rossi, S., and Yang, B. (2018). Effects of age and size on xylem phenology in two conifers of northwestern China. *Front. Plant Sci.* 8:2264. doi: 10.3389/fpls.2017.02264

Zhang, J., Alexander, M. R., Gou, X., Deslauriers, A., Fonti, P., Zhang, F., et al. (2020). Extended xylogenesis and stem biomass production in *Juniperus przewalskii* Kom. During extreme late-season climatic events. *Ann. For. Sci.* 77:99. doi: 10.1007/s13595-020-01008-1

Conflict of Interest: The authors declare that the research was conducted in the absence of any commercial or financial relationships that could be construed as a potential conflict of interest.

frontiers in Plant Science

ORIGINAL RESEARCH
published: 16 December 2021
doi: 10.3389/fpls.2021.760859

Contrasting Carbon Allocation Strategies of Ring-Porous and Diffuse-Porous Species Converge Toward Similar Growth Responses to Drought

Valentina Buttó[1,2], Mathilde Millan[1], Sergio Rossi[2,3] and Sylvain Delagrange[1]*

[1] Département des Sciences Naturelles, Institut des Sciences de la Forêt Tempérée, Université du Québec en Outaouais, Ripon, QC, Canada, [2] Département des Sciences Fondamentales, Université du Québec à Chicoutimi, Chicoutimi, QC, Canada, [3] Key Laboratory of Vegetation Restoration and Management of Degraded Ecosystems, South China Botanical Garden, Chinese Academy of Sciences, Guangzhou, China

OPEN ACCESS

Edited by:
Sebastian Leuzinger, Auckland University of Technology, New Zealand

Reviewed by:
Claudia Cocozza, University of Florence, Italy
Juan Pedro Ferrio, Fundacion Agencia Aragonesa para la Investigacion y el Desarrollo, Spain
Martin Karl-Friedrich Bader, Linnaeus University, Sweden

***Correspondence:**
Valentina Buttó
valentina.butto1@uqac.ca
orcid.org/0000-0003-1595-6745

Specialty section:
This article was submitted to Functional Plant Ecology, a section of the journal Frontiers in Plant Science

Received: *18 August 2021*
Accepted: *24 November 2021*
Published: *16 December 2021*

Citation:
Buttó V, Millan M, Rossi S and Delagrange S (2021) Contrasting Carbon Allocation Strategies of Ring-Porous and Diffuse-Porous Species Converge Toward Similar Growth Responses to Drought. Front. Plant Sci. 12:760859. doi: 10.3389/fpls.2021.760859

Extreme climatic events that are expected under global warming expose forest ecosystems to drought stress, which may affect the growth and productivity. We assessed intra-annual growth responses of trees to soil water content in species belonging to different functional groups of tree-ring porosity. We pose the hypothesis that species with contrasting carbon allocation strategies, which emerge from different relationships between wood traits and canopy architecture, display divergent growth responses to drought. We selected two diffuse-porous species (*Acer saccharum* and *Betula alleghaniensis*) and two ring-porous species (*Quercus rubra* and *Fraxinus americana*) from the mixed forest of Quebec (Canada). We measured anatomical wood traits and canopy architecture in eight individuals per species and assessed tree growth sensitivity to water balance during 2008–2017 using the standardized precipitation evapotranspiration index (SPEI). Stem elongation in diffuse-porous species mainly depended upon the total number of ramifications and hydraulic diameter of the tree-ring vessels. In ring-porous species, stem elongation mainly depended upon the productivity of the current year, i.e., number of vessels and basal area increment. Diffuse-porous and ring-porous species had similar responses to soil water balance. The effect of soil water balance on tree growth changed during the growing season. In April, decreasing soil temperature linked to wet conditions could explain the negative relationship between SPEI and tree growth. In late spring, greater water availability affected carbon partitioning, by promoting the formation of larger xylem vessels in both functional groups. Results suggest that timings and duration of drought events affect meristem growth and carbon allocation in both functional groups. Drought induces the formation of fewer xylem vessels in ring-porous species, and smaller xylem vessels in diffuse-porous species, the latter being also prone to a decline in stem elongation due to a reduced number of ramifications. Indeed, stem elongation of diffuse-porous species

is influenced by environmental conditions of the previous year, which determine the total number of ramifications during the current year. Drought responses in different functional groups are thus characterized by different drivers, express contrasting levels of resistance or resilience, but finally result in an overall similar loss of productivity.

Keywords: functional group, SPEI, primary growth, secondary growth, ramifications, stem elongation, hydraulic diameter, vessels

INTRODUCTION

A reliable understanding of tree growth responses to environmental conditions is important in confronting the changes caused by the global warming. Strategies of carbon allocation in trees can be identified through the study of functional traits, i.e., morpho-physio-phenological features that affect all aspects of the life histories of living organisms (Violle et al., 2007). Plant physiological traits provide the basis for a conversation that is aimed at creating a harmonious modeling framework, integrating descriptive and experimental results into more advanced digital vegetation models (Yang et al., 2015).

Allometric scaling among the different plant organs drives primary and secondary growth toward convergent patterns to changing environmental conditions, leading to adjustments in biomass allocation and sapwood area (Petit et al., 2018). Yet, within the angiosperms, the presence of diverging wood types, e.g., ring-porous and diffuse-porous species, entails differing sensitivity to the environment, concurrently implying different degrees of dependency among functional traits in different organs (Palacio et al., 2011; García-González et al., 2016). Ring-porous and diffuse-porous species are thus expected to undergo contrasting growth responses to seasonal stresses, such as drought events. Given that these groups demonstrate divergent seasonal patterns in their developmental phases (Barbaroux and Bréda, 2002; Delpierre et al., 2016), they could manifest contrasting consequences in terms of resource partitioning between radial growth and stem elongation.

Bud break of ring-porous species is preceded by an earlier resumption of cambial growth, which enables the formation of large earlywood vessels in spring (von Allmen et al., 2015). These large vessels are efficient in conducting water, but prone to freeze–thaw embolisms and cavitation during drought events (Sperry et al., 2012; Kitin and Funada, 2016). Compared with ring-porous species, diffuse-porous species produce smaller vessels, but demonstrate a greater conductivity per stem area. They are also characterized by a lower vulnerability to cavitation (Taneda and Sperry, 2008). Nevertheless, during a drought event, diffuse-porous species of temperate biomes are demonstrably less efficient in controlling stomatal transpiration than are ring-porous species, resulting in declining water potentials and subsequent water transport (Bush et al., 2008). This response pattern is ascribable to an anisohydric behavior, which is achieved by maintaining both open stomata and high carbon assimilation rates, despite the risk of hydraulic failure (Martínez-Vilalta et al., 2014). According to their growth responses to drought events, plant survival can indeed be associated with isohydric or anisohydric regulation of water status, whereby these strategies depend upon the capacity to avoid hydraulic failure by closing the stomata or by tracking environmental variation by adjusting their leaf water potentials (McDowell et al., 2008). Compartmentalizing view of the anisohydric and isohydric spectrum does not explain sufficiently hydraulic strategies of trees, which implies mortality to drought happening through multiple mediated trait responses, not always directly linked to non-structural carbohydrate responses (Klein, 2014; Adams et al., 2017). Traits linked to non-structural carbohydrate responses, such as wood porosity, might thus not resolve by themselves the complexity of trees' drought responses, which should be studied through multiple traits and physiological responses (Yi et al., 2017).

Like radial growth, the tree architecture is largely affected by wood type. Architecture is mainly defined by the number of ramifications and the number and degree of elongation of internodes, which results in sensitivity of response to environmental factors. Ring-porous species have the largest C pools, which are achieved through a greater capacity for storing carbon from the previous growing seasons (Barbaroux and Bréda, 2002; Palacio et al., 2011). This carbon pool, represented by the starch accumulated in form of reserves, is consumed to support earlywood growth, allowing for high growth rates independent of new photosynthates, and generating strong non-structural carbohydrate response fluctuations during the growing season (Michelot et al., 2012). In contrast to diffuse-porous species, ring-porous species do not change carbon allocation to growth over the lifespan of the trees. This response entails more stable lifetime allocation to shoot growth, which results in high water-use efficiency and a lowered amplitude of response to environmental variation compared to diffuse-porous species (Genet et al., 2009). Plant architecture can be affected by drought events, which inhibit the cell elongation and expansion, ultimately resulting in shorter internodes and smaller leaves (Song et al., 2021). Manipulation experiments confirm that water deficits involve an overall reduction in biomass accumulation by affecting plant carbon gain, which is linked to changes in stomatal conductance and light-capture efficiency (Valladares and Pugnaire, 1999; Rasheed and Delagrange, 2016). Studies demonstrate that canopy architecture is influenced by irrigation, which enhances biomass accumulation by increasing trunk volume and the number of branches (Devakumar et al., 1999).

To explore the response of species with divergent wood types, we must assess intra-annual processes that are involved in primary and secondary growth in an integrated manner. Indeed, a mutual correlation exists between primary and secondary growth. On the one hand, secondary growth depends upon non-structural carbon that results from the products of primary

growth (Buttó et al., 2021). On the other hand, primary growth depends upon water conduction area, which in turn depends on secondary growth (Deslauriers et al., 2016). The functional traits of primary and secondary meristems, therefore, must be studied together to obtain a comprehensive framework of tree growth. In this study, we (i) investigated the relationship between primary and secondary growth in different wood-type species and (ii) assessed the sensitivity of their growth responses to interannual soil water content variation. We posit that wood type mirrors different carbon allocation strategies, resulting in contrasting growth responses to soil water content. We predicted that ring-porous species are more sensitive to short, but intense drought events because of their isohydric behavior, while diffuse-porous species are more sensitive to moderate, but long drought events because of their anisohydric behavior (Klein, 2014). We tested the hypothesis by analyzing primary and secondary growth during 2008–2017 on four sympatric species with contrasting wood types: American ash (*Fraxinus americana* L.) and red oak (*Quercus rubra* L.), which were ring-porous, and sugar maple (*Acer saccharum* Marsh.) and yellow birch (*Betula alleghaniensis* Britt.), which were diffuse-porous.

MATERIALS AND METHODS

Study Area and Tree Selection

The study area is located within the Kenauk Nature Reserve, a large private property covering over 262 km^2 in the region of Outaouais (QC), Canada. The study area has a mean elevation of 226 m asl and lies within the northern temperate zone, in the sugar maple–basswood western bioclimate domain where sugar maple grows alongside American basswood (*Tilia americana* L.), American ash, American hophornbeam (*Ostrya virginiana* [Mill.] K. Koch), and butternut (*Juglans cinerea* L.). This study involves four tree species: sugar maple, American ash, red oak, and yellow birch. Eight trees per species were selected and sampled in May 2018 among the dominant individuals that resulted from natural regeneration in a stand that was subjected to two strips of a clearcut in 1990 and three strips of a partial cut in 2005.

Meteorological Data

Temperature and precipitation for 2008–2017 were extracted for the sampling area from the ERA5 monthly aggregate dataset of Google Earth Engine (Copernicus Climate Change Service [C3S], 2017; Gorelick et al., 2017), while standardized precipitation evapotranspiration index (SPEI) was extracted by the global SPEI dataset SPEI base v.2.6 (Beguería et al., 2014). Forests in cold and humid areas display drought responses over short time scales (3–5 months) (Vicente-Serrano et al., 2014). Accordingly, we selected $SPEI_3$, which is calculated from the cumulative precipitation for periods of 3 months. Drought episodes were identified as the month with $SPEI_3 < -1$ (Vanhellemont et al., 2019).

Primary Growth Data

Stem elongation was measured for 2008–2017 as the interannual extensions of the annual shoot by detecting the cataphylls, i.e., scale leaves on the growth units of the main tree-axis (Barthélémy and Caraglio, 2007). The number of lateral ramifications was counted and characterized on each growing period, which were cross-validated for the attribution of the correct age and polycyclic-growth unit (Barthélémy and Caraglio, 2007). Lateral ramifications were classified as long, medium, and short, based on their length, number of internodes, and leaves (Gregory, 1980).

Secondary Growth Data

A disk was cut from the stem of each tree at 1.30 m from the root-collar, and a radial section of 20 mm height × 5 mm width, which corresponded to stem disk half-diameter, was obtained from the most visible ray. From these rectangular samples, cross-sections of 51 tree cores were cut to about 10–15 μm thickness using a rotatory microtome (Leica, Heidelberg, Germany). The sections were stained with a solution of safranin (1% in distilled water), permanently fixed with BioMount mounting medium (Gärtner and Schweingruber, 2013), and photographed using a digital camera at 5× magnification. The digital images were analyzed using WinCELL^{TM} (Regent Instruments Inc., Quebec, QC, Canada) for measuring ring-width (RW), vessel diameter, and vessel area. Hydraulic diameter of vessel (HDV) was computed, based up the study by Sperry et al. (1994):

$$HDV = \frac{\sum_{i=1}^{n} d^5}{\sum_{i=1}^{n} d^4}$$

where d is the diameter of the vessels from 1 to n, estimated from the measured area.

The annual basal area increment (BAI) was computed as:

$$BAI = \pi (RW_t^2 - RW_{t-1}^2)$$

where πRW^2represents the basal area of the current (t) and previous (t-1) year.

Only individuals that were synchronized with the average tree-ring chronology for each species were retained for the following analyses. Tree-ring chronologies were considered well synchronized when Pearson's correlation coefficients were >0.5.

Relationship Between Growth and Environment in the Two Functional Groups

The most important predictors of stem elongation were obtained with random forest regressions, which were performed separately on the two functional groups of tree-ring porosity (i.e., diffuse-porous and ring-porous species). For this purpose, we tested $SPEI_3$ and growth variables as predictors. A random forest is composed of a large number of decision trees that are obtained by random bootstrap sampling of the data. The random selection of a subset of predictors allows testing the capacity of each predictor to predict the variable with accuracy (Liaw and Wiener, 2002). Random forest and permutation feature importance computed to estimate the relative contribution of predictors in prediction accuracy were performed using the *RandomForest* package in R (Liaw and Wiener, 2002). Regression performance was evaluated by the root-mean-square error (RMSE) and by regressing observations against their predicted values with linear models.

General linear mixed models (GLMMs) were used to study the effects of tree-ring porosity, $SPEI_3$ computed for each month (i.e., previous August–September and current April–July), and their interaction on growth. Growth variables were centered and normalized using the function *bestNormalize* of the *bestNormalize* package in R, which evaluates and applies the best normalization based upon the most efficient transformation (Peterson and Cavanaugh, 2019). GLMM was performed with the function *lmer* of the *lm4* package (Bates et al., 2015). Species and individual trees were retained as random effects; collinearity between variables was assessed through the calculation of variance inflation factors (VIFs) with the customized function *vif-func.r* (Beck, 2017). Only variables having VIF < 10 have been retained (Zuur et al., 2010). Normality and homoscedasticity of residuals were visually assessed. For each model, we computed the marginal and conditional R^2 representing the contribution of variance explained by the fixed effects and by the sum of the fixed and random effects, respectively, with the *MuMIn* package in R (Barton, 2020). For the significant terms, the fixed effects with their interactions have been plotted by using predictions that were computed by means of the *ggeffects* package (Lüdecke, 2018).

We retained the drought events ($SPEI_3 < 1$) between April and August to assess the effect of drought on tree growth, and we computed tree resilience to drought by identifying three characteristic periods that were defined as pre-drought, drought, and post-drought periods (Vanhellemont et al., 2019). A higher risk of mortality is associated with trees that have low resilience to drought (DeSoto et al., 2020). Due to its prolonged severity, we focused our attention on the drought event of 2012. We then considered 2009–2011 as the pre-drought period, 2012–2013 as the drought period, and 2014–2016 as the post-drought period. Following DeSoto et al.'s (2020) approach, we computed pre-drought and post-drought tree growth by averaging tree growth during 3 years prior to and following the drought period, respectively; growth patterns have been visually compared and discussed.

RESULTS

Weather Conditions and Drought Events

The mean temperature of the study area was 5.1°C, with an annual precipitation of 1,189 mm, while the absolute maximum and minimum temperatures for 2008–2017 were 29.0 and -28.9°C, respectively (**Supplementary Figure 1**). Frost occurred mainly from October to May, although frost events were also likely in September (**Supplementary Figure 1**). During 2008–2017, the mean monthly maximum temperature was 20 °C, which was reached in July, while the mean monthly minimum temperature was -12°C, which was measured in January (**Figure 1**).

The mean maximum $SPEI_3$ was 1.31, with peaks observed in April during 2011 ($SPEI_3 = 1.7$) and 2016 ($SPEI_3 = 1.8$), in February of 2008 ($SPEI_3 = 2.1$) and 2013 ($SPEI_3 = 0.9$), and in October during 2010 ($SPEI_3 = 1.8$) and 2012 ($SPEI_3 = 0.5$). Occasionally, the maximum SPEI was observed in June (2014, $SPEI_3 = 1.0$), July (2009, $SPEI_3 = 1.3$), and August (2015, $SPEI_3 = 0.6$). The mean minimum $SPEI_3$ was −1.46, with minima recorded in November for the years 2008 ($SPEI_3 = -0.4$), 2009 (SPEI3 = −0.9), and 2014 (SPEI3 = −1.5); April of 2013 ($SPEI_3 = -1.2$); June of 2016 ($SPEI_3 = -1.4$); and July of 2012 ($SPEI_3 = -1.9$). During the spring–summer period, we detected three events of severe drought ($SPEI_3 < -1$) occurring in May 2010, April and May 2012, and March 2015.

Primary and Secondary Growth

Except for the last 3 years of observation, diffuse-porous species, i.e., birch and maple, displayed synchronized stem elongation patterns (**Figure 2**). Compared with the other years, we observed that in 2012 and 2013, birch and maple experienced similar declines in stem elongation, losing, respectively, 21 and 34% of growth in 2012 and 30 and 20% of growth in 2013. Maple experienced two drops in stem elongation in 2010 (52%) and 2017 (53%). Birch showed a stem decline in 2016 (29%).

Ring-porous species, i.e., ash and oak, exhibited an average stem elongation of 60 and 80 cm, respectively, with slightly different temporal patterns (**Figure 2**). Ash stem elongation averaged 80 cm for the time period 2009–2012; oak stem elongation averaged 61 cm during 2009–2013, decreasing to 54.5 cm in 2014 and dropping to 34.5 during the last 3 years of observation (**Figure 2**). Ash exhibited the strongest decline in stem elongation in 2013 (28%). Oak displayed the strongest reduction in stem elongation in 2015, where growth reduced by 33%. In 2017, stem elongation in both ash and oak decreased by 18 and 15%, respectively.

Diffuse-porous species showed synchronized patterns in the number of total ramifications, except for the last 3 years (**Figure 2**). In both species, the minimum number of total ramifications was observed in 2013, when ramification decreased by 33% in maple and by 20% in birch (**Figure 2**). Within ring-porous species, oak displayed a larger interindividual variability in the total number of ramifications that were produced; when compared to ash, oak generally produced more ramifications starting from 2011, and the number of total ramifications averaged 8 over the observed period. More variability has been detected in the number of total ramifications that were produced by ash, which dropped by 48% in 2016 compared with the previous year.

For birch, BAI was exceptionally high in 2008 (22.1 mm^2), progressively decreasing to a local minimum in 2012, where BAI decreased by 52% compared with the previous year. BAI slightly increased to 6.6 mm^2 in 2016, but dropped to 5 mm^2 in 2017 (**Figure 2**). For sugar maple, BAI averaged 5.5 mm^2 during 2008–2010, dramatically decreasing by 48% in 2011 and by 34% in 2017. Within ring-porous species, ash had a greater basal area index, but the two time series were synchronized, showing constant growth until 2013, where the two curves declined together, displaying a growth reduction of 33% in oak and 48% in ash. Indeed, during 2008–2012, the average growth for ash and oak was, respectively, 15.5 and 11.8 mm^2, dropping to 8.3 and 8.9 mm^2 in 2013. Both species then experienced a growth decrease to reach a second local minimum in 2017, where growth declined by 77% in ash and 61% in oak (**Figure 2**).

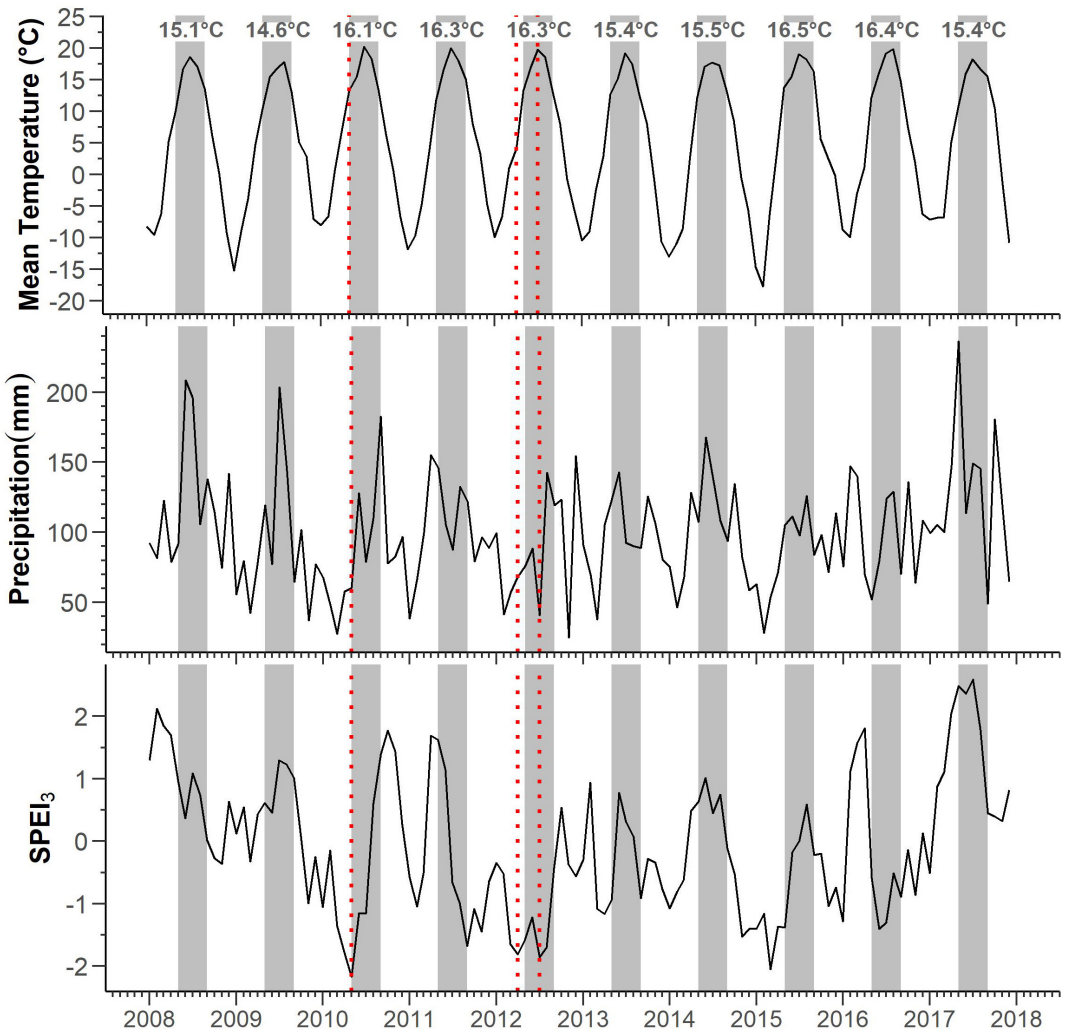

FIGURE 1 | Patterns of monthly mean temperature, total precipitation, and $SPEI_3$ 3-month windows. Red-dotted bars identify periods of severe drought ($SPEI_3 < -1$) occurring during May 2010, April and July 2012. Gray bars and annotations mark the May–September periods and their respective mean temperatures.

The number of vessels for birch and maple averaged 142 and 105, respectively, slightly decreasing to a local minimum in 2012 for birch, when only 63 vessels had been produced. Vessel production progressively increased in birch reaching a local peak in 2016 (with 82 vessels) to decrease again in 2017 (62 vessels). In contrast, maple vessel production experienced a constant decline in number of vessels that were produced, which reached an absolute minimum in 2017, with a decline in vessel production by 40% when compared to the previous year. In 2012, both maple and birch experienced a decline in vessel production by 35 and 23% compared with the previous year. For ring-porous species, vessel production averaged 46 in ash and 35 in red oak during the period 2008–2011; in 2012, both species decreased by 12 and 17%, when 40 vessels and 26 vessels were observed. After 2012, the number of vessels in ash decreased until reaching a minimum of 17 vessels in 2017, while red oak vessels increased for two years (2013 and 2014), only to decrease again in 2016 and 2017 (**Figure 2**).

Hydraulic diameter of vessels showed a variation during the observed periods. Diffuse-porous species experienced a growth decline ranging by 6 and 1%, while growth release ranged between 1 and 8% when comparing the years of our time series. For ring-porous species, the hydraulic diameter growth decline ranged within 0.5 and 4%, while the growth release was between 2 and 8%. Between the diffuse-porous species, birch produced the largest vessels, with a hydraulic diameter of 83.4 μm during 2007–2011, which decreased by 6% in 2012 and progressively increased again to 92.6 μm in 2017. Maple displayed little variation in hydraulic diameter, which ranged from 53.3 μm (2011) to 60.5 μm (2017). On average, ash produced larger vessels than oak, displaying a hydraulic diameter of 163.5 μm during 2008–2011. Ash vessels' hydraulic diameter increased to 174 μm in 2012, only to decrease again to 169 μm in 2014 and peak at 190 μm in 2017, displaying an increase by 6%. Oak produced vessels with a hydraulic diameter of 159.2 μm during 2008–2011, which became larger in 2012, where they measured 179 μm, and then

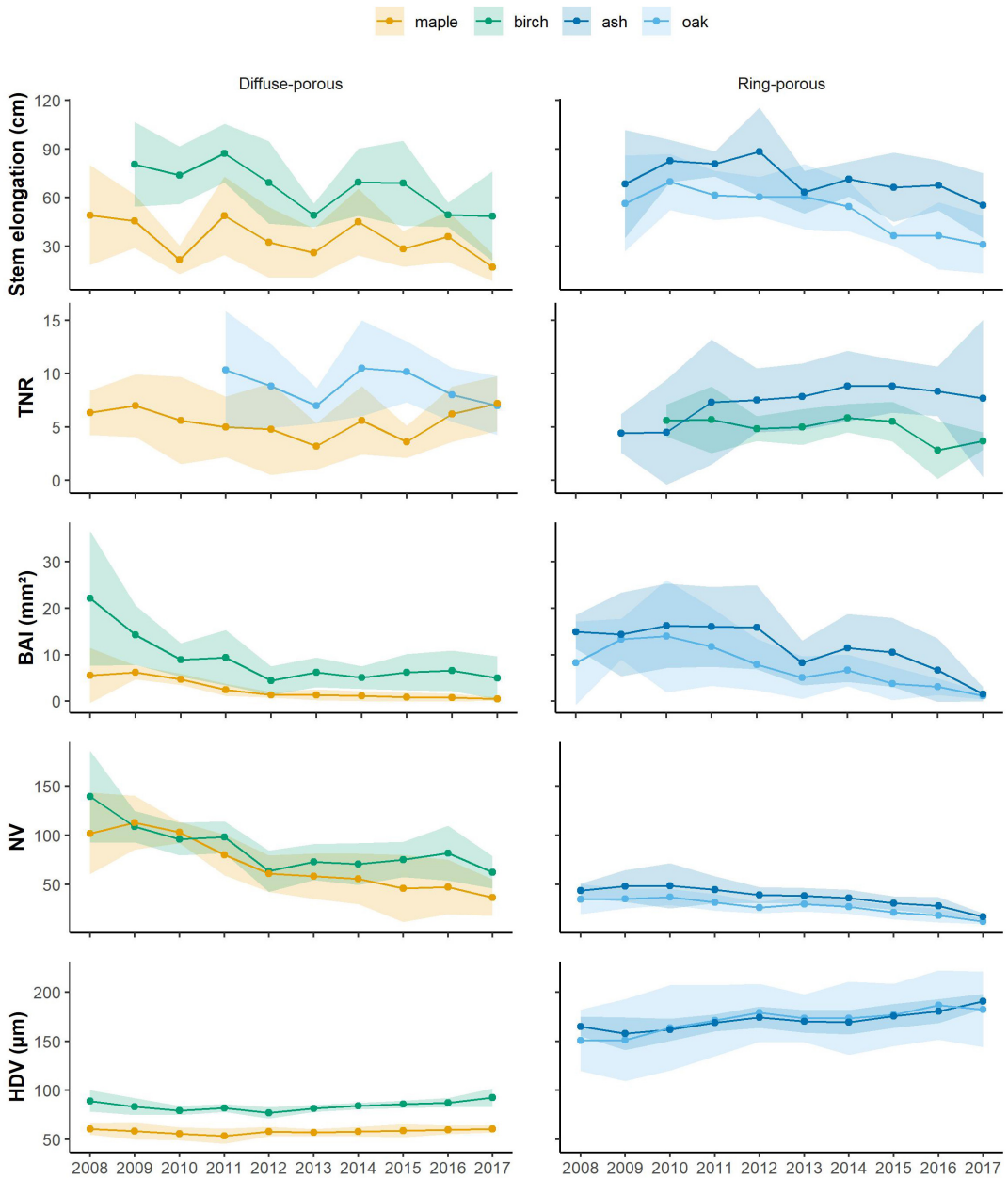

FIGURE 2 | Average time series for the primary and secondary variables that were measured and computed, with light-colored bands representing standard deviations. Blue is ash and cyan is oak, while orange is birch and green is maple. TNR, total number of ramifications; BAI, basal area increment; NV, number of vessels; HDV, hydraulic diameter of vessels.

decreased again in size until 2015. They peaked again in 2017, when diameters measured 182 µm (**Figure 2**).

Relationship Between Apical, Radial Growth, and Weather Conditions

For diffuse-porous species, the random forest regression explained 38.79% of the variance, with an RMSE of 9.17. Predicted versus observed values were closely related (R^2 = 0.86) (**Figure 3**). According to the permutation procedure, the most useful predictive variables for stem elongation were the total number of ramifications (36%), HDVs (26%), the number of vessels (9%), $SPEI_3$ for August and BAI (6%), and $SPEI_3$ of July (5%) The other anatomical and meteorological variables were not as important, ≤5% (**Figure 3**).

For ring-porous species, the random forest explained 15.83% of the variance. Predicted versus observed values were strongly related (R^2 = 0.8), with an RMSE of 9.37. Under permutation, the number of vessels was revealed as the most useful predictive factor for stem elongation (36%), followed by BAI (25%), $SPEI_3$

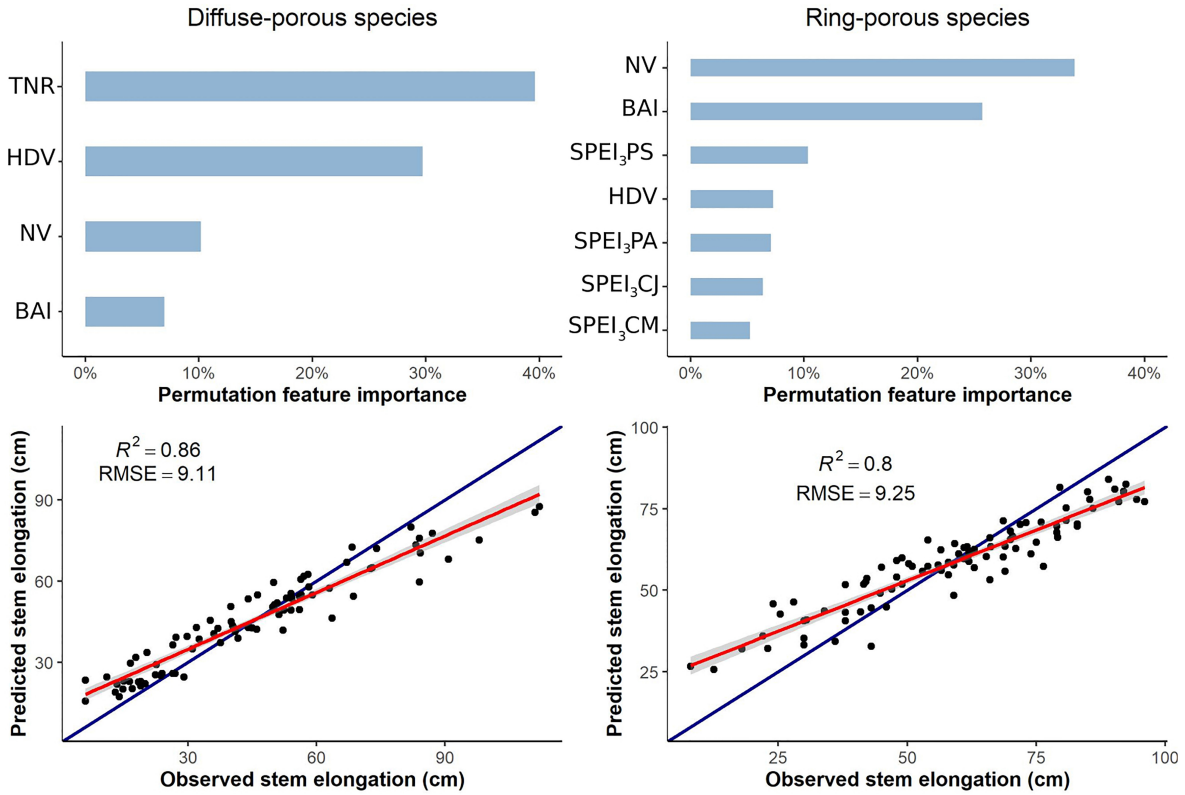

FIGURE 3 | Random forest regressions for stem elongation, including secondary and primary growth variables. Only variables with a contribution ≥5% to variance explained are shown in the permutation feature importance plot. TNR, total number of ramifications; BAI, basal area increment; NV, number of vessels; HDV, hydraulic diameter of vessels; $SPEI_3$ PA, $SPEI_3$ of the previous August; $SPEI_3$ PS, $SPEI_3$ of the previous September; $SPEI_3$ CM, $SPEI_3$ of the current May; $SPEI_3$ CJ, $SPEI_3$ of the current July.

of May (8%), $SPEI_3$ of July (7%), and $SPEI_3$ of April and August (6%) (**Figure 3**). All other variables accounted for <5% of the variance.

To circumvent the multicollinearity between $SPEI_3$ of June and that of July, only the latter was integrated into the models. GLMM between the $SPEI_3$ estimates for August and September of the previous year and March-to-August of the current year had a marginal R^2 (R^2_m) that spanned a range from 0.08 when modeling the total number of ramifications to 0.6 when modeling the hydraulic diameter. Conditional R^2 spanned (R^2_c) a range from 0.32 for the total number of ramifications to 0.88 for HDV (**Table 1**). Normalized stem elongation (R^2_m = 0.16, R^2_c = 0.60) was significantly affected by porosity, $SPEI_3$ of April and their interaction, $SPEI_3$ of August and September of the previous year, and $SPEI_3$ in July. For the number of total ramifications, only the $SPEI_3$ August × porosity and $SPEI_3$ April × porosity interactions were significant, indicating an effect that was dependent on $SPEI_3$ variation (**Table 1**). Under wet conditions, diffuse-porous species indeed display more ramifications than do ring-porous species (**Figure 4**). Normalized number of vessels (R^2_m = 0.50; R^2_c = 0.65) was significantly linked to the conditions of the previous August and September, and to $SPEI_3$ of April, and its interaction with porosity (**Table 1**). In both functional groups, HDV (R^2_m = 0.60; R^2_c = 0.88) was significantly related to the variation in $SPEI_3$ of the previous August and September, and to the variation in $SPEI_3$ in the current April and May, without contribution of the interaction terms. Normalized BAI (R^2_m = 0.20; R^2_c = 0.65) mainly depended upon the $SPEI_3$ variation in August and September of the previous year and $SPEI_3$ variation from April to July of the current year (**Table 1**).

Interannual Growth Trends

During stem elongation in the pre-drought period, diffuse-porous species exhibited an average stem elongation of 58.8 cm, which decreased to 45.5 cm during drought period and rebounded to 54 cm during the post-drought period (**Figure 5**). Diffuse-porous species produced, on average, 6 ramifications during pre-drought and drought periods and 10 ramifications during the post-drought period. The number of vessels was 100 during the pre-drought period and decreased to 64 for the drought period and the post-drought period. The HDVs were similar across the three periods, exhibiting values between 70 and 73 μm (**Figure 5**). On the one hand, ring-porous species showed a constant decline in stem elongation over the three time periods, with values ranging between 71 and 55 cm in the pre- and post-drought periods. On the other hand, the total number of branches constantly increased from 5 to 7 over the

TABLE 1 | Type I sums-of-squares (SS), *F*-statistics, and significance for the source of variation of the GLMM.

Source of variation	Stem elongation (cm) R^2_m = 0.16; R^2_c = 0.60		TNR R^2_m = 0.08; R^2_c = 0.32		NV R^2_m = 0.50; R^2_c = 0.65		HDV (μm) R^2_m = 0.60; R^2_c = 0.88		BAI (mm^2) R^2_m = 0.20; R^2_c = 0.65	
	Type I SS	*F*-value (*P*)	Type I SS	*F*-value (*P*)	Type I SS	*F*-value (*P*)	Type I SS	*F*-value (*P*)	Type I SS	*F*-value (*P*)
POR	0.23	0.42	0.28	0.35	5.71	15.35	1.53	11.51	0.3504	0.76
$SPEI_3$ P Aug	3.74	6.77 (*)	0.0196	0.02	8.51	22.87 (***)	0.54	4.10 (*)	13.48	29.18 (***)
$SPEI_3$ P Sep	2.99	5.41 (*)	0.71	0.88	7.89	21.21 (***)	1.15	8.61 (**)	5.56	12.03 (***)
$SPEI_3$ C Apr	2.43	4.40 (*)	0.20	0.25	3.97	10.68 (**)	1.21	9.13 (**)	4.34	9.40 (**)
$SPEI_3$ C May	1.06	1.92	0.04	0.05	0.42	1.12	0.53	4.00 (*)	1.94	4.21 (*)
$SPEI_3$ C Jul	10.65	19.27 (***)	0.26	0.33	0.24	0.65	0.09	0.66	0.77	1.67
$SPEI_3$ P Aug × POR	1.53	2.76	4.56	5.69 (*)	1.40	3.77	0.20	1.52	0.12	0.27
$SPEI_3$ P Sep × POR	0.48	0.87	0.05	0.06	0.02	0.05	0.01	0.10	0.00	0.01
$SPEI_3$ C Apr × POR	2.68	4.85 (*)	5.13	6.41 (*)	1.93	5.20 (***)	0.00	0.02	3.69	7.99 (*)
$SPEI_3$ C May × POR	0.65	1.18	0.07	0.09	0.03	0.07	0.13	1.00	0.01	0.03
$SPEI_3$ C Jul × POR	0.001	0.001	2.14	2.67	0.49	1.31	0.49	3.71	6.08	13.15 (***)

R^2_m, marginal R^2 (fixed effect); R^2_c, conditional R-squared (random + fixed effect).
Species and individuals are the random effects
$SPEI_3$ of June has been excluded by VIF selection.
TNR, total number of ramifications; NV, number of vessels; HDV, hydraulic diameter of vessels; BAI, basal area increment.
C denotes the current year, while P denotes the previous year and POR stands for the factor ring porosity.
*Asterisks represent the significance level: * $P < 0.05$; ** $P < 0.01$; *** $P < 0.0001$.*

three periods (**Figure 5**). BAI was 11 mm^2 during the pre-drought period, 8 mm^2 during the drought period, and 7 mm^2 during the post-drought period. The number of vessels showed a similar trend: 41 during the pre-drought period, 33 during the drought period, and 27 during the post-drought period (**Figure 5**). The decline in the number of vessels was associated with an increase in hydraulic diameter, which ranged from 162 μm during the pre-drought period to 177 μm during the post-drought period (**Figure 5**).

DISCUSSION

Diffuse- and Ring-Porous Trees Display Different Carbon Allocation Strategies

Species with contrasting wood anatomy are characterized by different carbon allocations during the growing season because of their different requirements (Palacio et al., 2011). Despite different carbon allocation strategies, stem elongation of both functional groups is linked to xylem hydraulic traits. We observed that among xylem hydraulic traits, stem elongation is related to hydraulic diameter for diffuse-porous species and to the number of vessels for the ring-porous species. In ring-porous species, early conductivity can be performed by the small latewood vessels of the previous year, which can recover from winter embolism (Kitin and Funada, 2016). Nevertheless, the contribution of latewood vessels to overall intra-ring hydraulic conductivity is marginal (Dai et al., 2020). Indeed, most conduction of the xylem relies upon the larger earlywood vessels (Hacke and Sauter, 1996; Niu et al., 2017; Dai et al., 2020), which in turn rely upon the mobilization of the reserves that were accumulated during the previous growing season (Barbaroux and Bréda, 2002; Palacio et al., 2011). Consistent with our results, soil water balance at the end of the previous growing season is important in defining primary growth and earlywood vessel development in spring. The stronger influence of soil water balance of the previous year is likely related to the environmental conditions that are required for C accumulation before leaf senescence (Hartmann and Trumbore, 2016). While hydraulic diameter, which is mostly driven by allometric relationships (Carrer et al., 2014), remains relatively constant, the number of vessels displays greater variability. For ring-porous species, BAI, and consequently, xylem hydraulic efficiency, is more related to the number of vessels than to their diameter. A greater BAI is linked to an increase in the production of both wide and narrow vessels, with the first providing greater hydraulic efficiency during the periods of intensive growth, while the second is characterized by high hydraulic safety to cope with adverse climatic conditions (Kitin and Funada, 2016).

Diffuse-porous species can rely upon previous year tree-rings to conduct water upward in spring. As a consequence, they display larger sapwood area, which enables earlier bud break compared to ring-porous species (Gebauer et al., 2008). Indeed, the structure of their sapwood allows them to rapidly reverse winter embolism by refilling the xylem of previous tree-rings (Niu et al., 2017; Dai et al., 2020). Nevertheless, diffuse-porous species are limited by fewer and smaller vessels, which may explain their lower degree of stem elongation than ring-porous species. In diffuse-porous species, the total number of ramifications is the trait that is strongly predictive of stem elongation, suggesting that adequate environmental conditions during spring stimulate the initiation of lateral shoots; once established, the latter may contribute to the growth of the main stem. Evidence based upon observations made on maple and birch would suggest that short lateral shoots are specialized for light exploitation (i.e., carbon gain through

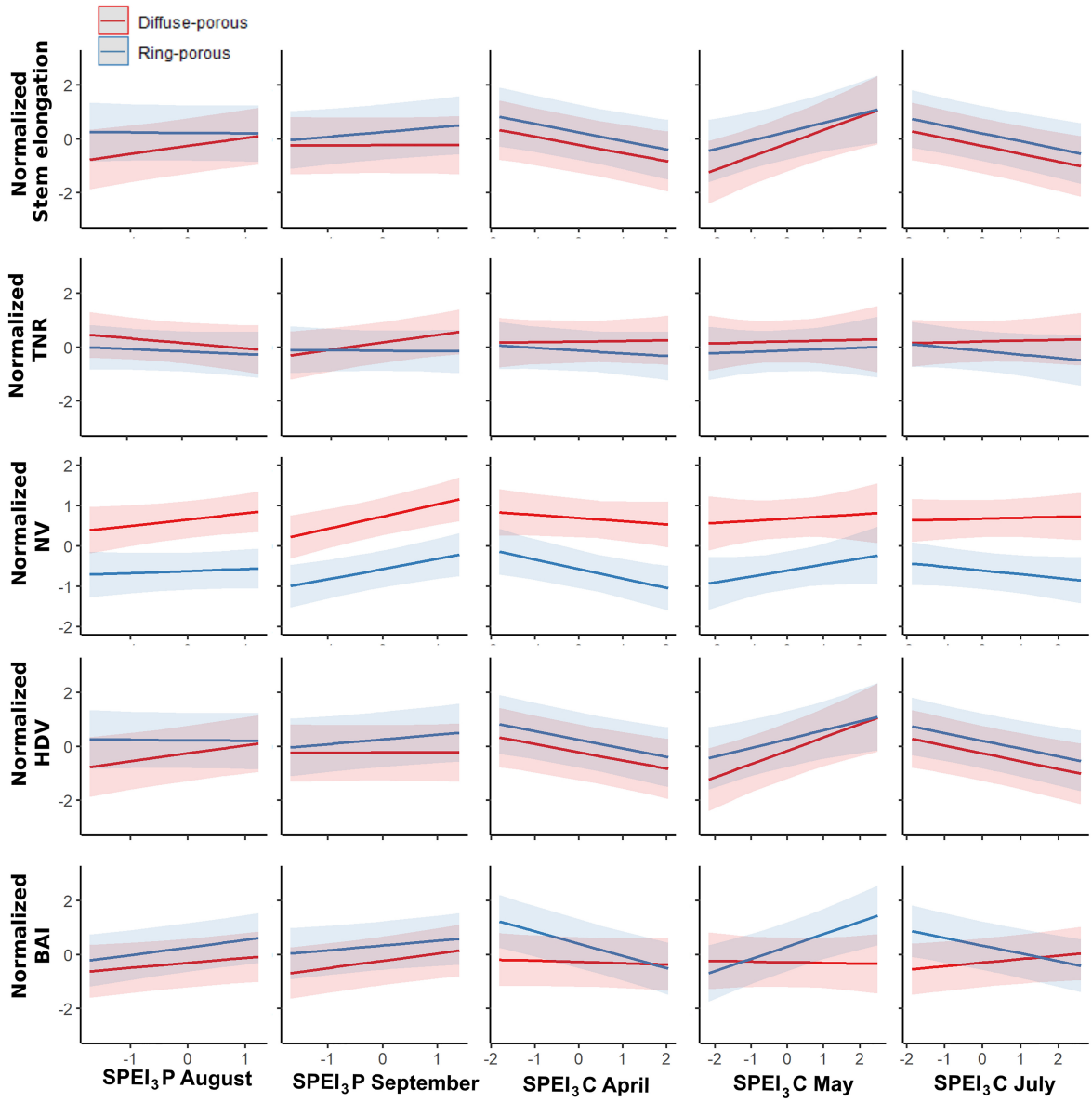

FIGURE 4 | GLMM results for the two functional groups, red = Diffuse-porous, blue = Ring-porous. TNR, total number of ramifications; NV, number of vessels; HDV, hydraulic diameter of vessels; BAI, basal area increment; P, Previous year; C, Current year.

photosynthesis), while long shoots are specialized for space exploration (Jarčuška and Milla, 2012; Taugourdeau et al., 2019). Similarly, by affecting sink strength for new growth, clipping treatments reduce tree-ring growth in diffuse-porous species, due to the loss of light exploitation shoot types (Palacio et al., 2011). Important C provisioning by lateral ramifications in diffuse-porous species may also explain the relative independence of their stem elongation in relation to environmental conditions that were experienced in the previous growing season and, thus, on carbon that was stored relative to ring-porous species (Barbaroux and Bréda, 2002; von Allmen et al., 2015). Moreover, C dating evidence demonstrates that stored C used for spring growth in sugar maple is not solely related to reserves that were accumulated in the previous year, but for longer periods. Indeed, these may span 3–5 years, thereby buffering the effects of low and high C storage years (Muhr et al., 2016).

Intra-Annual Tree Growth Responses to Soil Water Balance

Our results point to a time and process dependency of growth responses to a variation in soil water balance, which might underlie differing seasonal sensitivity of the two functional groups to drought events. On the one hand, April (reactivation of xylem growth) and July (maturation of vessels) of the

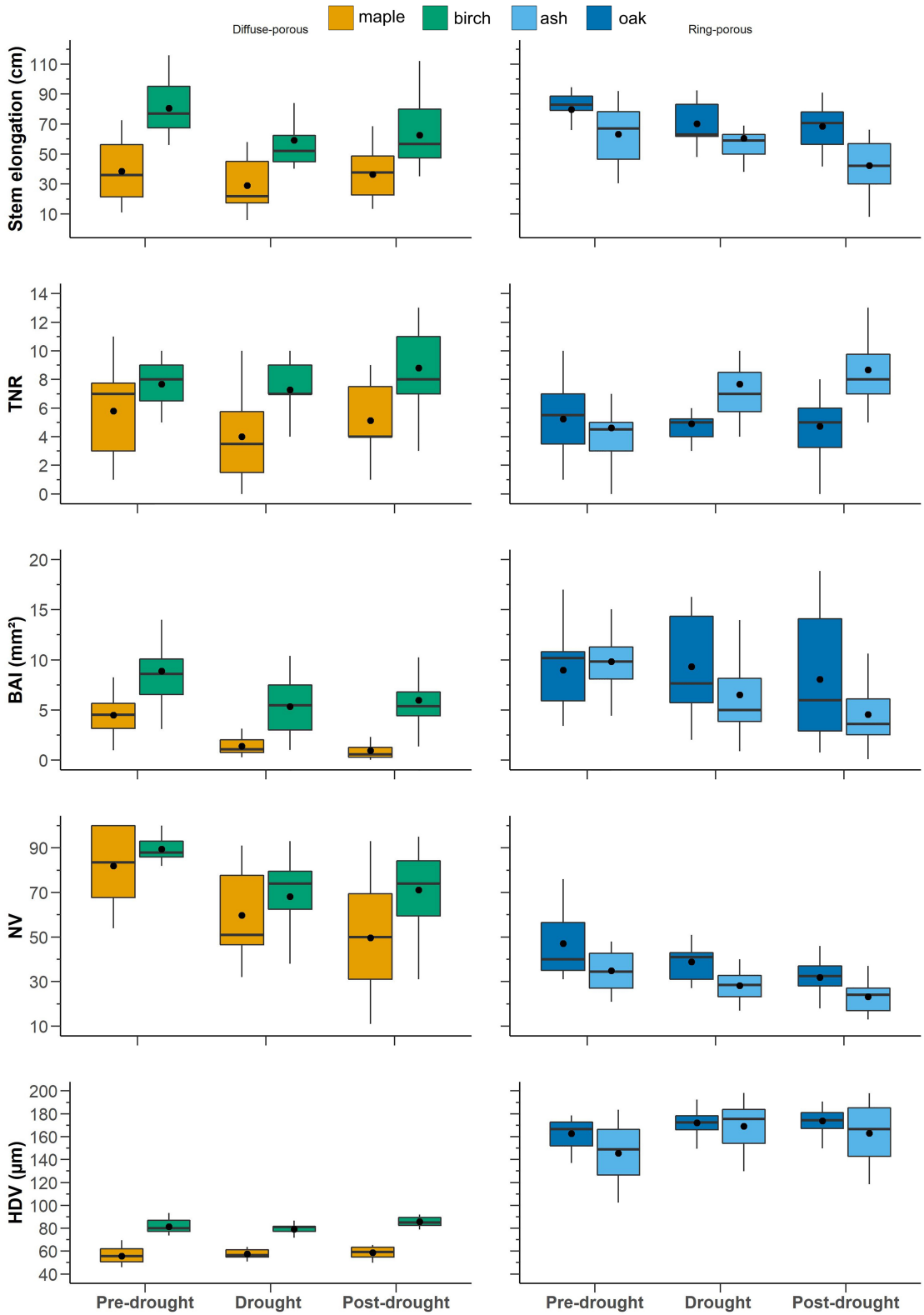

FIGURE 5 | Trait responses to pre-drought period (2009–2010–2011), drought period (2012–2013), and post-drought period (2014–2015–2016). Black dots represent the average, continuous bars represent the median (50% quartile), lower and upper box limits represent the first and third quartiles, and vertical bars represent 1.5× the interquartile range. Blue is ash and cyan is red oak, while orange is birch and green is maple.

growing season seem to be important for basal increment of ring-porous species. On the other hand, August of the previous growing season, together with current April conditions, would seem to be critical in the establishment of lateral shoots. Since bud formation occurs late in the growing season (Barthélémy and Caraglio, 2007), the importance of soil water balance during August is surely related to these critical phases of ontogenesis (Buissart et al., 2018), while in April soil conditions are related to dormancy or the initiation of buds. In both functional groups, these intra-annual differences clearly confirm contrasting developmental phenologies, which still remain to be explored in depth. Nevertheless, these different specific processes occur during the same period of time, making the conditions of both previous and current year important for the two functional groups, although for contrasting reasons.

According to von Allmen et al. (2015), we observed that species belonging to different functional groups converge toward similar water usage, by taking advantage of different situations. Diffuse-porous species have a higher water transport capacity, but require more water for their growth. Ring-porous species are able to limit water consumption due to their efficiency in terms of water use (von Allmen et al., 2015). However, calibration issues with the heat-dissipation method might result in an underestimation of total sap flow in ring-porous species, while single-point sap flow measurements could neglect the contribution of the radial sap flow profiles within the inner xylem (Poyatos et al., 2007; Bush et al., 2010; Yi et al., 2017). Taken together, these methodological issues might artificially increase the observed gap in sap flow variation between diffuse-porous and ring-porous species during periods of high transpiration demand, even though the heat ratio method sensors are widespread tools that have been continuously improved since their establishment (Poyatos et al., 2007; Bush et al., 2010).

Diffuse-porous and ring-porous species cope with hydraulic recovery after winter embolism mainly by either refilling of existing rings *vs.* new ring formation from reserves, but eventually converge on a similar level of hydraulic efficiency during the growing season (Niu et al., 2017). In our study, despite belonging to different functional groups, seasonal trajectories of functional traits converge on similar responses to soil water balance. Dry conditions at the end of the previous growing season generally result in lower primary and secondary growth during the current growing season for both functional groups. The number of vessels and HDVs are the most sensitive traits for diffuse-porous and ring-porous species, respectively. Similar patterns of carbon allocation in response to drought have also been detected in Mediterranean evergreen (diffuse-porous) and deciduous (ring-porous) oaks. Corcuera et al. (2004a,b) observed that deciduous oaks responded to drought by decreasing RW, i.e., cell production, while evergreen oaks had narrow vessels. However, compared with evergreen oaks, deciduous oaks might be more affected by drought stress, since it resulted in the lack of latewood, where vessels display greater water-use efficiencies than earlywood vessels (Corcuera et al., 2004a). Under severe and repeated drought, the higher production of narrow rings featuring wide earlywood vessels and a low or lacking proportion of latewood expose Mediterranean ring-porous oaks to cavitation risks, potentially leading to an extensive dieback (Corcuera et al., 2004a). These pieces of evidence of shared strategies between the same functional groups growing in temperate and Mediterranean environments suggest that the hydraulic adjustments in response to water stress might be closely associated with their carbon allocation strategies, enabling these relationships to be generalized to other environments.

Lower plant water potential negatively affects carbohydrate mobilization and transport, ultimately resulting in reduced resource availability (Sala et al., 2010). Similarly, wet spring conditions (generally associated with cloudier sky and colder temperatures) could negatively affect soil thermal properties and meristem activity, which may explain the negative relationship between growth and soil water content in April. We raise the hypothesis that during spring, abundant winter snowfall can maintain the cold soil, thereby preventing growth reactivation of the roots (Rossi et al., 2011) and reducing the duration of the shoot elongation phase, eventually resulting in unfavorable conditions for tree growth. During late spring and summer, soil water content affects tree growth responses by modulating carbon partitioning (Deslauriers et al., 2016). Within plant organs, regardless of functional group, cell enlargement and cell division are both hydraulic-controlled processes that occur in parallel, but respond to water deficit in rather independent ways, while still affecting one another (Tardieu et al., 2011; Körner, 2015). Water absorption for tissue expansion may decrease soil water potential, which in turn may reduce stomatal conductance and carbon assimilation (Tardieu et al., 2011). This system of loose feedbacks between cell division and cell expansion might be the basis for delay between vessel number and hydraulic diameter variation in response to soil water content. Among conspecific individuals, nutrient, carbon, and water uptake is enhanced by root grafts, the development of which is triggered by trees' proximity, thus constituting an element to be considered by managers (Gaspard and DesRochers, 2020). As a consequence of natural root grafting, close individuals display coupled responses to soil water content variation, adding further complexity to our understanding of drought responses in tree communities (Bader and Leuzinger, 2019).

Tree Growth Responses to Identified Drought

During the study period, we detected three drought events: The first occurred during May 2010, while the others occurred in spring and summer 2012. In our chronologies, the effect of the drought events of May 2010 is barely noticeable, while the long-lasting drought events in 2012 were manifested in synchronous responses between functional groups, resulting in an overall loss of growth for both years 2012 and 2013. In diffuse-porous species, BAI and the number of vessels decreased in 2012, while stem elongation and the number of total ramifications decreased slightly in 2012 and more strongly in the following year, i.e., 2013.

The number of shoots and lateral branches is predetermined and depends upon carbon storage of the previous year (Fournier et al., 2020). We observed that the number of total ramifications strongly depends upon $SPEI_3$ variation during the previous year, especially in diffuse-porous species. In July, less carbon to sustain shoot growth results in a decreasing number of shoots, decreasing carbon assimilation for the following year. Apart from 2013, diffuse-porous species experienced partial recovery of tree growth, while ring-porous species experienced a general decline in BAI, but they maintained the similar hydraulic diameter among years. Such a result is consistent with measurements that are aimed at discriminating carbon-use strategies of ring-porous and diffuse-porous species (Barbaroux and Bréda, 2002; Palacio et al., 2011). By relying upon carbon stored during the previous growing seasons, ring-porous species could be more sensitive to repeated and long-lasting summer drought, despite their higher water-use efficiency, and by closing their stomata, being more prone to carbon limitation than diffuse-porous species (Levanič et al., 2011; von Allmen et al., 2015). In our study, droughts that occurred locally over the last decade did not allow us to test the importance of repeated seasonal (spring or summer) droughts, which in turn may highlight contrasting long-term responses between functional groups because of their contrasting phenologies.

By analyzing the effect of drought on different functional groups, Vanhellemont et al. (2019) had indeed demonstrated that ring-porous species were affected by recurring dry springs, while diffuse-porous species were more strongly affected by recurring summer droughts. The fitness of ring-porous or diffuse-porous species in a specific study area would then depend upon the future timing, duration, severity, and frequency of drought events. At ecosystem scale, disclosing the drivers of drought responses vis-à-vis climate change is compulsive and extremely dependent on our understanding of the plant physiological functioning, which demand for holistic studies encompassing both the belowground and the aboveground compartments of a tree (Abrams and Nowacki, 2016; Rodriguez-Dominguez and Brodribb, 2020). Emerging pieces of evidence point indeed to the dominant role of the rhizosphere in driving the hydraulic redistribution at individual level (Johnson et al., 2018; Rodriguez-Dominguez and Brodribb, 2020). Belowground conductance patterns have recently demonstrated to be good predictors of drought responses, pointing to losses in roots' hydraulic conductivity and occurrence of shallow roots as the main drivers of species mortality (Johnson et al., 2018). It has been observed that root anatomy also plays a key role in setting hydraulic conductivity, which, in thin roots, is inversely related to the root length and the width of the root cortex (Rieger and Litvin, 1999).

CONCLUSION

In this study, we investigated how the relationships between primary and secondary growth change among four sympatric species and with soil water content. We observed similar responses between ring-porous and diffuse-porous species to variations in soil water content. Results showed differences in carbon allocation strategies among the different functional groups, implying different trade-offs between primary and secondary growth. A strong connection links plant water status and carbon balance, especially in those species with a strong capacity for controlling stomatal closure (McDowell et al., 2008; Hartmann and Trumbore, 2016). Consequently, a drought event will trigger cascading negative feedback loops between primary and secondary growth. The two functional groups seem to show similar overall growth responses to drought, although these are based on different seasonal and physiological mechanisms. Studies integrating multiple plant traits are needed to unravel the fine-tuning of the mechanisms involved in drought responses at the individual level. Ring-porous and diffuse-porous species manifested common patterns that might enable management strategies to deal with the impacts of climate change while preserving their economic and ecologic values.

DATA AVAILABILITY STATEMENT

The raw data supporting the conclusions of this article will be made available by the authors, without undue reservation.

AUTHOR CONTRIBUTIONS

SD conceived and planned the experimental design. SD and MM carried out the sampling activities and performed the data collection. VB analyzed the data and wrote the first draft of the manuscript. SD and SR provided critical feedback to the manuscript. All authors commented and approved the final version of the manuscript.

FUNDING

This project was funded by a grant from the Ministry of Forests, Wildlife and Parks of Quebec (MFFP-UQO 3329-2017-142332154) awarded to SD.

ACKNOWLEDGMENTS

We thank Liane Nowell from The Kenauk Institute for access to the Kenauk territory. We also acknowledge the invaluable help of Marie-Ève Roy in the selection of sites based on the historical disturbance in the territory, and Michel Vennetier and Olivier Taugourdeau for their input regarding the design of the study. We would also like to thank William F. J. Parsons for verifying the English.

SUPPLEMENTARY MATERIAL

The Supplementary Material for this article can be found online at: https://www.frontiersin.org/articles/10.3389/fpls.2021.760859/full#supplementary-material

REFERENCES

Abrams, M. D., and Nowacki, G. J. (2016). An interdisciplinary approach to better assess global change impacts and drought vulnerability on forest dynamics. *Tree Physiol.* 36, 421–427. doi: 10.1093/treephys/tpw005

Adams, H. D., Zeppel, M. J. B., Anderegg, W. R. L., Hartmann, H., Landhäusser, S. M., Tissue, D. T., et al. (2017). A multi-species synthesis of physiological mechanisms in drought-induced tree mortality. *Nat. Ecol. Evol.* 1, 1285–1291. doi: 10.1038/s41559-017-0248-x

Bader, M. K. F., and Leuzinger, S. (2019). Hydraulic coupling of a leafless kauri tree remnant to conspecific hosts. *iScience* 19, 1238–1247. doi: 10.1016/j.isci.2019.05.009

Barbaroux, C., and Bréda, N. (2002). Contrasting distribution and seasonal dynamics of carbohydrate reserves in stem wood of adult ring-porous sessile oak and diffuse-porous beech trees. *Tree Physiol.* 22, 1201–1210. doi: 10.1093/treephys/22.17.1201

Barthélémy, D., and Caraglio, Y. (2007). Plant architecture: a dynamic, multilevel and comprehensive approach to plant form, structure and ontogeny. *Ann. Bot.* 99, 375–407.

Barton, K. (2020). *MuMIn: Multi-Model Inference. R Packag. Version 1.43.17*. Available online at: https://cran.r-project.org/web/packages/MuMIn/index.html (accessed April 6, 2021).

Bates, D., Mächler, M., Bolker, B., and Walker, S. (2015). Fitting linear mixed-effects models using lme4. *J. Stat. Softw.* 67, 1–48. doi: 10.18637/JSS.V067.I01

Beck, M. W. (2017). *Vif_Fun.r GitHub*. Available online at: https://gist.github.com/fawda123/4717702 (accessed June 8, 2021).

Beguería, S., Vicente-Serrano, S. M., Reig, F., and Latorre, B. (2014). Standardized precipitation evapotranspiration index (SPEI) revisited: parameter fitting, evapotranspiration models, tools, datasets and drought monitoring. *Int. J. Climatol.* 34, 3001–3023. doi: 10.1002/joc.3887

Buissart, F., Vennetier, M., Delagrange, S., Girard, F., Caraglio, Y., Sabatier, S. A., et al. (2018). The relative weight of ontogeny, topology and climate in the architectural development of three North American conifers. *AoB Plants* 10:ly045. doi: 10.1093/aobpla/ply045

Bush, S. E., Hultine, K. R., Sperry, J. S., Ehleringer, J. R., and Phillips, N. (2010). Calibration of thermal dissipation sap flow probes for ring- and diffuse-porous trees. *Tree Physiol.* 30, 1545–1554. doi: 10.1093/treephys/tpq096

Bush, S. E., Pataki, D. E., Hultine, K. R., West, A. G., Sperry, J. S., and Ehleringer, J. R. (2008). Wood anatomy constrains stomatal responses to atmospheric vapor pressure deficit in irrigated, urban trees. *Oecologia* 156, 13–20. doi: 10.1007/s00442-008-0966-5

Buttó, V., Khare, S., Drolet, G., Sylvain, J.-D., Gennaretti, F., Deslaruiers, A., et al. (2021). Regionwide temporal gradients of carbon allocation allow for shoot growth and latewood formation in boreal black spruce. *Glob. Ecol. Biogeogr.* 30, 1657–1670. doi: 10.1111/geb.13340

Carrer, M., Von Arx, G., Castagneri, D., and Petit, G. (2014). Distilling allometric and environmental information from time series of conduit size: the standardization issue and its relationship to tree hydraulic architecture. *Tree Physiol.* 35, 27–33. doi: 10.1093/treephys/tpu108

Copernicus Climate Change Service [C3S] (2017). ERA5: fifth generation of ECMWF atmospheric reanalyses of the global climate. *Copernicus Clim. Chang. Serv. Clim. Data Store* Available online at: https://cds.climate.copernicus.eu/cdsapp#!/home (accessed March 31, 2021).

Corcuera, L., Camarero, J. J., and Gil-Pelegrín, E. (2004a). Effects of a severe drought on growth and wood anatomical properties of *Quercus faginea*. *IAWA J.* 25, 185–204. doi: 10.1163/22941932-90000360

Corcuera, L., Camarero, J. J., and Gil-Pelegrín, E. (2004b). Effects of a severe drought on *Quercus ilex* radial growth and xylem anatomy. *Trees Struct. Funct.* 18, 83–92. doi: 10.1007/s00468-003-0284-9

Dai, Y., Wang, L., and Wan, X. (2020). Frost fatigue and its spring recovery of xylem conduits in ring-porous, diffuse-porous, and coniferous species in situ. *Plant Physiol. Biochem.* 146, 177–186. doi: 10.1016/j.plaphy.2019.11.014

Delpierre, N., Berveiller, D., Granda, E., and Dufrêne, E. (2016). Wood phenology, not carbon input, controls the interannual variability of wood growth in a temperate oak forest. *New Phytol.* 210, 459–470. doi: 10.1111/nph.13771

Deslauriers, A., Huang, J.-G., Balducci, L., Beaulieu, M., Rossi, S., Fonti, P., et al. (2016). The contribution of carbon and water in modulating wood formation in black spruce saplings. *Plant Physiol.* 170, 2072–2084. doi: 10.1007/978-3-319-61669-8_2

DeSoto, L., Cailleret, M., Sterck, F., Jansen, S., Kramer, K., Robert, E. M. R., et al. (2020). Low growth resilience to drought is related to future mortality risk in trees. *Nat. Commun.* 11:545. doi: 10.1038/s41467-020-14300-5

Devakumar, A. S., Gawai Prakash, P., Sathik, M. B. M., and Jacob, J. (1999). Drought alters the canopy architecture and micro-climate of *Hevea brasiliensis* trees. *Trees* 13, 161–167. doi: 10.1007/pl00009747

Fournier, M.-P., Paré, M. C., Buttò, V., Delagrange, S., Lafond, J., and Deslauriers, A. (2020). How plant allometry influences bud phenology and fruit yield in two vaccinium species. *Ann. Bot.* 126, 825–835. doi: 10.1093/aob/mcaa083

García-González, I., Souto-Herrero, M., and Campelo, F. (2016). Ring porosity and earlywood vessels: a review on extracting environmental information through time. *IAWA J.* 37, 295–314. doi: 10.1163/22941932-20160135

Gärtner, H., Schweingruber, H. F. (2013). *Microscopic Preparation Techniques for Plant Stem Analysis*. Zürich: Swiss Federal Research Institute WSL, 78.

Gaspard, D. T., and DesRochers, A. (2020). Natural root grafting in hybrid poplar clones. *Trees Struct. Funct.* 34, 881–890. doi: 10.1007/s00468-020-01966-z

Gebauer, T., Horna, V., and Leuschner, C. (2008). Variability in radial sap flux density patterns and sapwood area among seven co-occurring temperate broad-leaved tree species. *Tree Physiol.* 28, 1821–1830. doi: 10.1093/treephys/28.12.1821

Genet, H., Bréda, N., and Dufrêne, E. (2009). Age-related variation in carbon allocation at tree and stand scales in beech (*Fagus sylvatica L.*) and sessile oak (*Quercus petraea* (Matt.) Liebl.) using a chronosequence approach. *Tree Physiol.* 30, 177–192. doi: 10.1093/treephys/tpp105

Gorelick, N., Hancher, M., Dixon, M., Ilyushchenko, S., Thau, D., and Moore, R. (2017). Google earth engine: planetary-scale geospatial analysis for everyone. *Remote Sens. Environ.* 202, 18–27. doi: 10.1016/j.rse.2017.06.031

Gregory, R. A. (1980). Annual cycle of shoot development in sugar maple. *Can. J. For. Res.* 10, 316–326. doi: 10.1139/x80-055

Hacke, U., and Sauter, J. J. (1996). Xylem dysfunction during winter and recovery of hydraulic conductivity in diffuse-porous and ring-porous trees. *Oecologia* 105, 435–439. doi: 10.1007/BF00330005

Hartmann, H., and Trumbore, S. (2016). Understanding the roles of nonstructural carbohydrates in forest trees - from what we can measure to what we want to know. *New Phytol.* 211, 386–403. doi: 10.1111/nph.13955

Jarčuška, B., and Milla, R. (2012). Shoot-level biomass allocation is affected by shoot type in *Fagus sylvatica*. *J. Plant Ecol.* 5, 422–428. doi: 10.1093/jpe/rts004

Johnson, D. M., Domec, J. C., Carter Berry, Z., Schwantes, A. M., McCulloh, K. A., Woodruff, D. R., et al. (2018). Co-occurring woody species have diverse hydraulic strategies and mortality rates during an extreme drought. *Plant Cell Environ.* 41, 576–588. doi: 10.1111/pce.13121

Kitin, P., and Funada, R. (2016). Earlywood vessels in ring-porous trees become functional for water transport after bud burst and before the maturation of the current-year leaves. *IAWA J.* 37, 315–331. doi: 10.1163/22941932-20160136

Klein, T. (2014). The variability of stomatal sensitivity to leaf water potential across tree species indicates a continuum between isohydric and anisohydric behaviours. *Funct. Ecol.* 28, 1313–1320. doi: 10.1111/1365-2435.12289

Körner, C. (2015). Paradigm shift in plant growth control. *Curr. Opin. Plant Biol.* 25, 107–114. doi: 10.1016/j.pbi.2015.05.003

Levanič, T., Čater, M., and McDowell, N. G. (2011). Associations between growth, wood anatomy, carbon isotope discrimination and mortality in a Quercus robur forest. *Tree Physiol.* 31, 298–308. doi: 10.1093/treephys/tpq111

Liaw, A., and Wiener, M. (2002). Classification and regression by randomForest. *R News* 2, 18–22.

Lüdecke, D. (2018). ggeffects: tidy data frames of marginal effects from regression models. *J. Open Source Softw.* 3:772. doi: 10.21105/joss.00772

Martínez-Vilalta, J., Poyatos, R., Aguadé, D., Retana, J., and Mencuccini, M. (2014). A new look at water transport regulation in plants. *New Phytol.* 204, 105–115. doi: 10.1111/nph.12912

McDowell, N., Pockman, W. T., Allen, C. D., Breshears, D. D., Cobb, N., Kolb, T., et al. (2008). Mechanisms of plant survival and mortality during drought: why do some plants survive while others succumb to drought? *New Phytol.* 178, 719–739. doi: 10.1111/j.1469-8137.2008.02436.x

Michelot, A., Simard, S., Rathgeber, C., Dufrêne, E., and Damesin, C. (2012). Comparing the intra-annual wood formation of three European species (*Fagus sylvatica*, *Quercus petraea* and *Pinus sylvestris*) as related to leaf phenology

and non-structural carbohydrate dynamics. *Tree Physiol.* 32, 1033–1045. doi: 10.1093/treephys/tps052

Muhr, J., Messier, C., Delagrange, S., Trumbore, S., Xu, X., and Hartmann, H. (2016). How fresh is maple syrup? Sugar maple trees mobilize carbon stored several years previously during early springtime sap-ascent. *New Phytol.* 209, 1410–1416. doi: 10.1111/nph.13782

Niu, C. Y., Meinzer, F. C., and Hao, G. Y. (2017). Divergence in strategies for coping with winter embolism among co-occurring temperate tree species: the role of positive xylem pressure, wood type and tree stature. *Funct. Ecol.* 31, 1550–1560. doi: 10.1111/1365-2435.12868

Palacio, S., Paterson, E., Sim, A., Hester, A. J., and Millard, P. (2011). Browsing affects intra-ring carbon allocation in species with contrasting wood anatomy. *Tree Physiol.* 31, 150–159. doi: 10.1093/treephys/tpq110

Peterson, R. A., and Cavanaugh, J. E. (2019). Ordered quantile normalization: a semiparametric transformation built for the cross-validation era. *J. Appl. Stat.* 47, 2312–2327. doi: 10.1080/02664763.2019.1630372

Petit, G., von Arx, G., Kiorapostolou, N., Lechthaler, S., Prendin, A. L., Anfodillo, T., et al. (2018). Tree differences in primary and secondary growth drive convergent scaling in leaf area to sapwood area across Europe. *New Phytol.* 218, 1383–1392. doi: 10.1111/nph.15118

Poyatos, R., Čermák, J., and Llorens, P. (2007). Variation in the radial patterns of sap flux density in pubescent oak (*Quercus pubescens*) and its implications for tree and stand transpiration measurements. *Tree Physiol.* 27, 537–548. doi: 10.1093/treephys/27.4.537

Rasheed, F., and Delagrange, S. (2016). Acclimation of *Betula alleghaniensis* Britton to moderate soil water deficit: small morphological changes make for important consequences in crown display. *Tree Physiol.* 36, 1320–1329. doi: 10.1093/treephys/tpw064

Rieger, M., and Litvin, P. (1999). Root system hydraulic conductivity in species with contrasting root anatomy. *J. Exp. Bot.* 50, 201–209. doi: 10.1093/jxb/50.331.201

Rodriguez-Dominguez, C. M., and Brodribb, T. J. (2020). Declining root water transport drives stomatal closure in olive under moderate water stress. *New Phytol.* 225, 126–134. doi: 10.1111/nph.16177

Rossi, S., Morin, H., and Deslauriers, A. (2011). Multi-scale influence of snowmelt on xylogenesis of black spruce. *Arct. Antarct. Alp. Res.* 43, 457–464. doi: 10.1657/1938-4246-43.3.457

Sala, A., Piper, F., and Hoch, G. (2010). Physiological mechanisms of drought-induced tree mortality are far from being resolved. *New Phytol.* 186, 274–281. doi: 10.1111/j.1469-8137.2009.03167.x

Song, X., Zhao, Y., Wang, J., and Lu, M.-Z. (2021). The transcription factor KNAT2/6b mediates changes in plant architecture in response to drought via down-regulating GA20ox1 in Populus alba × P. glandulosa. *J. Exp. Bot.* 72, 5625–5637. doi: 10.1093/jxb/erab201

Sperry, J. S., Christman, M. A., Torres-Ruiz, J. M., Taneda, H., and Smith, D. D. (2012). Vulnerability curves by centrifugation: is there an open vessel artefact, and are "r" shaped curves necessarily invalid? *Plant Cell Environ.* 35, 601–610. doi: 10.1111/j.1365-3040.2011.02439.x

Sperry, J. S., Nichols, K. L., Sullivan, J. E. M., and Eastlack, S. E. (1994). Xylem embolism in ring-porous, diffuse-porous, and coniferous trees of northern Utah and interior Alaska. *Ecology* 75, 1736–1752. doi: 10.2307/1939633

Taneda, H., and Sperry, J. S. (2008). A case-study of water transport in co-occurring ring- versus diffuse-porous trees: contrasts in water-status, conducting capacity, cavitation and vessel refilling. *Tree Physiol.* 28, 1641–1651. doi: 10.1093/treephys/28.11.1641

Tardieu, F., Granier, C., and Muller, B. (2011). Water deficit and growth. Co-ordinating processes without an orchestrator? *Curr. Opin. Plant Biol.* 14, 283–289. doi: 10.1016/j.pbi.2011.02.002

Taugourdeau, O., Delagrange, S., Lecigne, B., Sousa-Silva, R., and Messier, C. (2019). Sugar maple (*Acer saccharum* Marsh.) shoot architecture reveals coordinated ontogenetic changes between shoot specialization and branching pattern. *Trees Struct. Funct.* 33, 1615–1625. doi: 10.1007/s00468-019-01884-9

Valladares, F., and Pugnaire, F. I. (1999). Tradeoffs between irradiance capture and avoidance in semi-arid environments assessed with a crown architecture model. *Ann. Bot.* 83, 459–469. doi: 10.1006/anbo.1998.0843

Vanhellemont, M., Sousa-Silva, R., Maes, S. L., Van den Bulcke, J., Hertzog, L., De Groote, S. R. E., et al. (2019). Distinct growth responses to drought for oak and beech in temperate mixed forests. *Sci. Total Environ.* 650, 3017–3026.

Vicente-Serrano, S. M., Camarero, J. J., and Azorin-Molina, C. (2014). Diverse responses of forest growth to drought time-scales in the Northern hemisphere. *Glob. Ecol. Biogeogr.* 23, 1019–1030. doi: 10.1111/geb.12183

Violle, C., Navas, M.-L., Vile, D., Kazakou, E., Fortunel, C., Hummel, I., et al. (2007). Let the concept of trait be functional! *Oikos* 116, 882–892. doi: 10.1111/j.2007.0030-1299.15559.x

von Allmen, E. I., Sperry, J. S., and Bush, S. E. (2015). Contrasting whole-tree water use, hydraulics, and growth in a co-dominant diffuse-porous vs. ring-porous species pair. *Trees Struct. Funct.* 29, 717–728. doi: 10.1007/s00468-014-1149-0

Yang, Y., Zhu, Q., Peng, C., Wang, H., and Chen, H. (2015). From plant functional types to plant functional traits: a new paradigm in modelling global vegetation dynamics. *Prog. Phys. Geogr.* 39, 514–535. doi: 10.1177/0309133315582018

Yi, K., Dragoni, D., Phillips, R. P., Roman, D. T., and Novick, K. A. (2017). Dynamics of stem water uptake among isohydric and anisohydric species experiencing a severe drought. *Tree Physiol.* 37, 1379–1392. doi: 10.1093/treephys/tpw126

Zuur, A. F., Ieno, E. N., and Elphick, C. S. (2010). A protocol for data exploration to avoid common statistical problems. *Methods Ecol. Evol.* 1, 3–14. doi: 10.1111/j.2041-210X.2009.00001.x

Conflict of Interest: The authors declare that the research was conducted in the absence of any commercial or financial relationships that could be construed as a potential conflict of interest.

Publisher's Note: All claims expressed in this article are solely those of the authors and do not necessarily represent those of their affiliated organizations, or those of the publisher, the editors and the reviewers. Any product that may be evaluated in this article, or claim that may be made by its manufacturer, is not guaranteed or endorsed by the publisher.

frontiers in Plant Science

ORIGINAL RESEARCH
published: 23 March 2022
doi: 10.3389/fpls.2022.855741

Wood Anatomical Responses of European Beech to Elevation, Land Use Change, and Climate Variability in the Central Apennines, Italy

Jose Carlos Miranda[1], Chiara Calderaro[2], Claudia Cocozza[3], Bruno Lasserre[2], Roberto Tognetti[4] and Georg von Arx[1,5]*

[1] Swiss Federal Institute for Forest, Snow and Landscape Research WSL, Birmensdorf, Switzerland, [2] Dipartimento di Bioscienze e Territorio, Università degli Studi del Molise, Pesche, Italy, [3] Dipartimento di Scienze e Tecnologie Agrarie, Alimentari Ambientali e Forestali, Università di Firenze, Firenze, Italy, [4] Dipartimento di Agricoltura, Ambiente e Alimenti, Università degli Studi del Molise, Campobasso, Italy, [5] Oeschger Centre for Climate Change Research, University of Bern, Bern, Switzerland

OPEN ACCESS

Edited by:
Peter Prislan, Slovenian Forestry Institute, Slovenia

Reviewed by:
Peter Hajek, University of Freiburg, Germany
Kyriaki Giagli, Mendel University in Brno, Czechia

***Correspondence:**
Jose Carlos Miranda
jc.miranda@upm.es

Specialty section:
This article was submitted to Functional Plant Ecology, a section of the journal Frontiers in Plant Science

Received: *15 January 2022*
Accepted: *21 February 2022*
Published: *23 March 2022*

Citation:
Miranda JC, Calderaro C, Cocozza C, Lasserre B, Tognetti R and von Arx G (2022) Wood Anatomical Responses of European Beech to Elevation, Land Use Change, and Climate Variability in the Central Apennines, Italy. Front. Plant Sci. 13:855741. doi: 10.3389/fpls.2022.855741

European beech (*Fagus sylvatica* L.) is a widespread and economically important temperate tree species in Europe. The warmer temperatures and severe drought events expected in the future, especially in Mediterranean areas, could affect the vitality and productivity of beech stands that have been intensively used in these areas in the past. Here, we aim to assess the wood anatomical responses of beech to environmental variability and silvicultural practices by investigating three beech stands along an elevational gradient (1,200 to 1,950 m a.s.l.) in the Apennines (Italy). Therefore, we quantified several anatomical traits of the xylem vessels related to tree hydraulics from five trees per stand and investigated variability between and within tree rings. Our results suggest generally limited trait plasticity, with higher plasticity of mean vessel lumen area and theoretical hydraulic conductivity, while maximum vessel size and mean hydraulic diameter were less plastic, likely because of the stronger determination by tree height. High-elevation trees were hydraulically more limited than trees at a mid and lower elevation as indicated by the more conservative anatomical configuration, i.e., comparatively smaller vessels and a 50% tighter trait coordination. Cessation of coppicing resulted in a hydraulically safer anatomy with comparatively smaller vessels at the most intensively used site (1,200 m), triggered by increased water demand due to an increase in canopy density, and thus, an increase in stand transpiration. Furthermore, maximum vessel size at the beginning showed different climate sensitivity compared to the rest of the tree ring, while intra-ring anatomical profiles showed little difference between normal and the 5 years with the highest and lowest mean temperature and precipitation. Overall, this study highlights the challenges to separate the externally induced medium- to longer-term responses from ontogenetically determined patterns.

We, therefore, call for more comprehensive studies to further explore and verify the plasticity of wood anatomical traits in European beech in response to short- to long-term environmental fluctuations to gain a mechanistic understanding useful for sustainable forest ecosystems.

Keywords: elevational (altitudinal) gradient, *Fagus sylvatica* (European beech), hydraulic architecture, silvicultural practices, quantitative wood anatomy (QWA), xylem anatomy

INTRODUCTION

European beech (*Fagus sylvatica* L.) is one of the most important forest species in Europe, in terms of nature conservation as well as exploitation (Ellenberg and Leuschner, 2010). However, climate change scenarios project that forest areas suitable for beech will decrease across Europe over the next century (Sabate et al., 2002; Gessler et al., 2007; Zimmermann et al., 2015). Physiological performance and growth of beech are thought to be adversely affected by the changing environmental conditions because of its higher sensitivity toward low water availability and longer drought periods than other temperature broad-leaved species (Ellenberg, 1996; Fotelli et al., 2002; Peuke et al., 2002; Walthert et al., 2021). Specifically, the current warming trend may accelerate the cambial growth of beech at its latitudinal and elevational limits. High summer temperatures promote the radial growth of beech, suggesting a positive effect of increasing mean summer temperature at higher latitudes or elevations on the cambial activity of beech (Bosela et al., 2018). Conversely, southern European beech populations are increasingly suffering from summer drought (Piovesan et al., 2008; Linares and Camarero, 2012), which may trigger episodes of increased tree mortality (Bolte et al., 2016; Cocozza et al., 2016). However, also in central areas of beech distribution extremely warm summers have recently been shown to damage beech trees (Schuldt et al., 2020; Walthert et al., 2021).

Beech can adjust stem hydraulic performance mainly by changing xylem vessel number, vessel diameter, vessel density, vessel connectivity, and tree growth rate (Carlquist, 2012; Giagli et al., 2016; Hacke et al., 2017). Although vessel traits are largely determined by genetics and biophysical constraints (Carlquist, 2003; Wortemann et al., 2011; Eilmann et al., 2014; Olson et al., 2014), xylem formation varies between sites and years and is closely related to changes in weather conditions, particularly water availability and air temperature (Arnic et al., 2021). In Alpine environments, secondary growth (e.g., cambium differentiation and xylem formation) of beech has been found to vary with temperature (Prislan et al., 2013) and specifically to depend mainly on June–July temperature and precipitation (Di Filippo et al., 2007). Besides, in the context of precipitation regime variation, wood anatomical trade-offs between water transport capacity and relative drought resistance may shape the performance of beech populations, as has been observed in other species (Hoeber et al., 2014; Chenlemuge et al., 2015; Kotowska et al., 2015). This trade-off occurs as hydraulic efficiency increases with vessel lumen diameter to the fourth power (Tyree and Ewers, 1991), while in contrast, the wider the vessels, the lower their hydraulic safety against frost- and drought-induced embolism (Hacke and Sperry, 2001). However, trees could also vary spatial vessel arrangement in addition to vessel dimensions to adjust overall hydraulic efficiency and safety as derived from the xylem structure. Nevertheless, the large trait plasticity of beech trees after disturbance could allow this species to withstand decreasing water availability to a certain degree (Kahle, 2006; van der Werf et al., 2007).

The Italian mountain systems provide an excellent framework in which wood anatomical differences at inter- and intra-annual levels can be expected in response to changing climatic conditions, specifically soil water supply and atmospheric evaporative demand (Tognetti et al., 2019). In the Apennines, beech usually grows above 900–1,000 m a.s.l. and is widespread on northern slopes and where precipitation and fog maintain moister air conditions (Nocentini, 2009). This lower distribution limit is shifted upward on the sunnier and warmer southern slopes. Besides, tree-ring analyses have shown distinct growth responses of beech to bioclimatical and elevational gradients (Di Filippo et al., 2012; Chiesi et al., 2013; Tognetti et al., 2014).

Forest management practices have significantly modified the distribution, composition, and structure of beech forests in the Apennines (Nocentini, 2009), where it is the most widespread forest species (Scarascia-Mugnozza et al., 2000). However, after World War II, the progressive depopulation of mountain areas due to socioeconomic changes led to the abandonment of coppice-with-standards used for the production of firewood and charcoal (Hahn and Fanta, 2001; Brunet et al., 2010). Transition or conversion from management with frequent harvesting that promotes shoot regrowth from stumps (coppice) to a naturalized forest with long-harvest intervals or even cessation of active management that promotes tree regeneration from seeds (high forest) can be performed in different ways (Salomon et al., 2017; Unrau et al., 2018). Conversion of beech coppice to high forest affects different competition-related stand traits such as stand density, stand basal area, and canopy cover, which leads to changes in stand structure and local environmental conditions, in particular soil moisture and temperature (Aussenac, 2000; Salomon et al., 2016; Zellweger et al., 2020). The impact of these changes on the underlying wood anatomical structure, and the implications for tree growth and functioning in light of the increasing climate variability is largely unknown.

The aim of this study was to investigate the intra- and inter-annual variability of wood anatomical traits of beech stands in response to an elevational gradient, the cessation of the silvicultural practices (coppicing), and years of extreme climate in the Majella National Park (Central Italy). We hypothesized to observe (i) higher plasticity in intra-annual anatomical trait responses at lower elevations compared with the higher

elevations because of the expected wetter and warmer conditions (Martínez del Castillo et al., 2016) and a hydraulically more efficient anatomical structure; (ii) an increase of theoretical hydraulic safety against embolism after coppice cessation due to increased stand evapotranspiration and competition for water; and (iii) an increase in the theoretical hydraulic safety against embolism in years of extreme climate to cope with severe droughts.

MATERIALS AND METHODS

Study Area and Land Use Changes

This study was conducted in the Majella National Park on European beech (*Fagus sylvatica* L.) trees. The Majella massif is a north-south ridge at 32.5 km from the Adriatic Sea, in Abruzzo (Central Italy). Three sites were selected along an elevational gradient at the north-facing slope of Mount Ugni: U1 at 1,200 m a.s.l. (42° 8′ 27″ N, 14° 10′ 24″ E), U2 at 1,600 m a.s.l. (42° 7′ 53″ N, 14° 9′ 40″ E), and U3 at 1,950 m a.s.l. (42° 7′ 38″ N, 14° 9′ 35″ E). The two lower sites, U1 and U2, are characterized by essentially pure beech stands, whereas the highest site, U3, represents the elevational limit for beech in the study region (**Table 1**). U3 is characterized by a transition between beech and mountain pine (*Pinus mugo* Turra spp. *mugo*), with the latter species accounting for less than 14% of all the trees and less than 10% of basal area. All the three studied sites represent stands with different age structures. The whole study area has a typical Mediterranean climate, with a mean annual temperature of 13.3°C and an annual precipitation sum of 742.4 mm during the study period (1968–2004, Harris et al., 2014). Precipitation is unevenly distributed throughout the year, with a drought period during the summer months (**Figure 1**). During the study period (1968–2004), the use of the forest was changed from coppicing with standards to the cessation of all the harvesting activities when Mount Ugni was declared a Natural State Reserve in 1981. It was expected that the impact of this changed forest use would decrease in the order U1 > U2 > U3, as lower elevation sites would be subject to greater harvesting pressure due to greater accessibility. This is reflected in the higher stem/stump ratio of site U1 compared with U2 and U3 (**Table 1**) which indirectly reflects the intensity of past land use at each site. In fact, orthophotos of U3 showed relatively constant land cover between 1954 and 2017 compared with other similar elevations in the region (Calderaro et al., 2020).

TABLE 1 | Stand structural traits at each study site, U1–1,200 m a.s.l., U2–1,600 m a.s.l., U3–1,950 m a.s.l. BA–basal area, DBH–diameter at breast height. Where applicable, values are means ± SD.

	U1	U2	U3
No. stems	221	126	150
No. stumps	81	93	144
No. stems·ha^{-1}	1758.7	1002.7	1193.7
No. stumps·ha^{-1}	644.6	740.1	1145.9
No. stems·stump^{-1}	2.8	1.4	1.0
BA (m^2·ha^{-1})	31.9	28.4	27.3
DBH (cm)	12.4 ± 9.2	18.8 ± 9.5	16.5 ± 5.7
Mean tree height (m)	NA	22.8	14.7
TRW (μm)	1072.5 ± 512.5	1488.5 ± 497.6	1310.5 ± 382.7
Age of cored stems (years)	92.5 ± 21.9	85.3 ± 24.6	84.3 ± 11.7
Period with sample size n = 5 (years)	1950–2004	1968–2012	1946–2012

Tree Sample Collection and Processing

From May 2013 to September 2014, two increment cores were taken at 120° from 5 dominant trees per site with a 5-mm increment borer (Haglöf, Mora, Sweden). Tree cores were taken at breast height avoiding eccentricity and tension wood because of the slope. Subsequent vessel anatomical measurements were conducted following the procedure detailed in von Arx et al. (2016). Core samples were split into 4–5 cm long pieces and heartwood was boiled in a water-glycerin solution. Microsections of 15–20 μm thickness were cut with a rotary microtome (Leica, Heidelberg, Germany), stained with safranin (1% in distilled water), Astra blue (0.5% in distilled water and acetic acid), and fixed on permanent slides with EUKITT (BiOptica, Milan, Italy). Overlapping high-resolution digital images (0.945 pixels·μm^{-1}) were captured with a digital camera (Canon EOS 650D, Canon Incorporation, Tokyo, Japan) connected to an Olympus BX41 microscope (Olympus Corporation, Tokyo, Japan). The images from the same microsection were stitched together with PTGui (New House Internet Services BV, Rotterdam, Netherlands). Then, images were analyzed with ROXAS version 3.0.578 (von Arx and Carrer, 2014), which depends on Image-Pro Plus version 6.1 or higher (Media Cybernetics, Silver Spring, MD, United States). Image analysis covered a common period from 1968 to 2004 that was represented by n = 5 trees at all the sites and produced the following individual vessel data (**Figure 2**): vessel lumen area (VA), vessel grouping index (VG; von Arx et al., 2013), and theoretical hydraulic conductivity (KH) according to the Hagen–Poiseuille law (Tyree and Zimmermann, 2002). Further vessel traits were calculated at intra-ring sector or full ring level: number of vessels and analyzed xylem area, 95th percentile of vessel lumen area (VA95), vessel density as the number of vessels per analyzed xylem area (VD), proportion of accumulated vessel lumen to xylem area or relative vessel area (RVA), and mean hydraulic diameter (DH; Tyree and Zimmermann (2002). VA, VA95, DH, and KH features are all related different aspects of theoretical hydraulic efficiency with the first three showing mean properties while KH reflects accumulative water transport capacity. We distinguish between VA95 and VA because the widest vessels reflect maximum transport efficiency but are putatively most vulnerable to embolism (Tyree and Ewers, 1991; von Arx et al., 2012), although variation in vessel size is primarily a function of tree height (Carrer et al., 2015; Rosell et al., 2017). VG, VD, and RVA characterize the spatial vessel arrangement and integration, which affects hydraulic efficiency and safety (Carlquist, 2003; Nardini et al., 2012). These traits reflect different components of the theoretical hydraulic safety and efficiency of xylem vessels, but also of the entire xylem including mostly mechanically and physiologically important

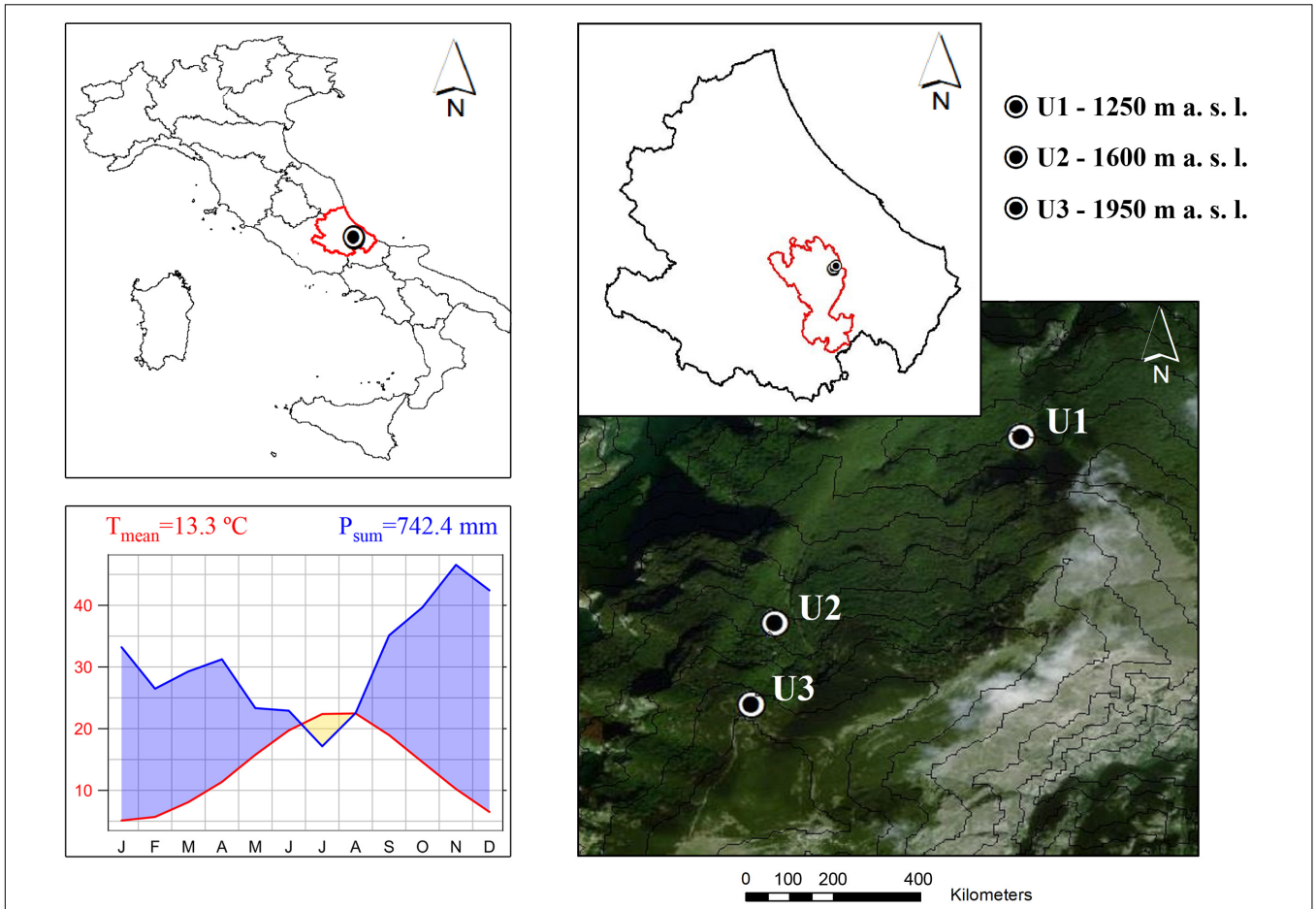

FIGURE 1 | Location of the study sites and climate diagram of the study area. T_{mean}—mean annual temperature, P_{sum}—mean annual precipitation (CRU TS4.04 Dataset, Harris et al., 2014).

fiber and parenchyma cells (Bittencourt et al., 2016; Lourenço et al., 2022).

Climate Data and Selection of Extreme Years

Monthly mean temperature and precipitation sums of the area were derived from the CRU TS 4.04 gridded dataset with 0.5° spatial resolution (Harris et al., 2014). These data were used to identify significant correlations with anatomical traits of the ring sectors. They were used as well to identify years with extreme climate. For this purpose, we selected the 5 years with the highest and lowest mean temperature and precipitation values of the June to August period of the series as "extreme years" (Jetschke et al., 2019). The period of June, July, and August was selected because seasonal drought occurs during this period and to allow comparison with previous studies in the same area and in the Mediterranean Basin (Di Filippo et al., 2007; Calderaro et al., 2020) that showed correlations between anatomical traits and/or tree ring widths and climate conditions during these months. The selected extreme years with high and low temperatures and precipitations were above and below the 85th and 15th percentile of the study period and also of all the available climate series (1901–2016), respectively.

Data Standardization and Statistical Analysis

In order to evaluate the modification of wood anatomical responses to different elevation, climate variability, and land uses, we examined vessel traits at the intra-ring level. To that end, vessels were assigned to one of 5 or 10 tangential sectors of equal width based on their position in the ring (**Figure 2**; Sass and Eckstein, 1995). The higher sectorization (10) was performed in order to obtain a semicontinuous intra-ring profile of anatomical traits with most of the sectors fulfilling the following criteria: sample depth consisting of five trees per site (study period 1968–2004), sectors containing a minimum of five vessels (0.66% of the total number of sectors did not meet this criterion and were discarded), and sectors being wider than the maximum vessel radius of the sector itself (0.5% of the rings did not fulfill this criterion). To compare wood formed early and late in the season, we refer to the early formed wood (E_fW) as the wood that is at the relative position of 0–50% in the ring, and to the late-formed

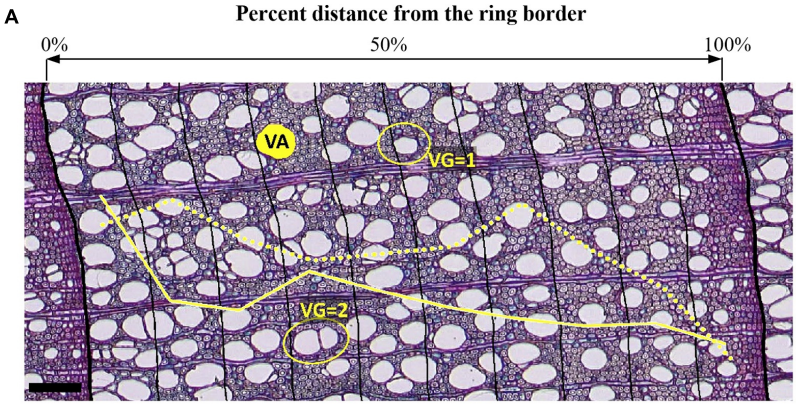

B

Acronym	Units	Definition	Formula
VA	μm^2	*Vessel lumen area*	
VG	-	*Vessel grouping*	Number of vessels per group
VA95	μm^2	*95th percentile VA*	
VD	$vessels \cdot mm^{-2}$	*vessel density*	no. vessels/xylem area
RVA	%	*Percentage of conductive area*	$\frac{\Sigma VA}{\text{xylem area}} \cdot 100$
DH	μm	*Mean hydraulic diameter*	$\left[\frac{\Sigma (\text{vessel hydraulic diameter}^4)}{\text{no. vessels}}\right]^{1/4}$
KH	$m^4 \cdot s^{-1} \cdot MPa^{-1}$	*Theoretical hydraulic conductivity*	

FIGURE 2 | Illustration of **(A)** anatomical measurements and **(B)** anatomical traits with acronyms and formulas. Thick black lines in **(A)** denote ring borders and thin lines denote intra-ring sector limits. The solid yellow curve in **(A)** shows the relative intra-ring changes in vessel grouping (VG), the dotted yellow curve shows the relative intra-ring changes in mean vessel area (VA). Scale bar = 100 μm.

wood (L_fW) as the wood that is at the relative position 50–100% in the ring. The lower sectorization (5) was performed to get robust sector estimates based on the aforementioned criteria, the number of which additionally roughly corresponded to the estimated number of months of wood formation.

As vessel dimensions have an increasing trend during ontogeny driven by distance from the distal tree parts (**Supplementary Figure 1**; Carrer et al., 2015), two standardizations methods were performed:

(i) indexed values (X_{ind}) were used to assess the correlations in anatomical traits among each other at the ring and intra-ring level and with monthly climate data. Therefore, for each core and anatomical trait, a time series was built per intra-ring sector, representing inter-annual variations of the respective trait at the intra-ring level. Then, we fitted a cubic smoothing spline with 50% frequency cutoff at 30 years to each anatomical series to remove low-frequency trends introduced by tree height growth, land use changes, and other disturbances [using dplR package in R; Bunn (2008)]. The detrended index was calculated as the ratio between the observed and the fitted values for each ring (Cook and Kairiukstis, 1990). Monthly climate data were detrended in the same way, to avoid biased correlations with anatomical features because of possible trends in climatic data (Klesse, 2021).

(ii) Standardized values (X_{std}) were used to compare the differences between intra-annual patterns at the different sites, land use regimes, and climatic extreme conditions. Standardization consisted of dividing individual intra-annual sector values by the mean annual value of the corresponding ring in each tree. With this method, we standardized using only same year data in the different sectors, thus, avoiding bias through trends and range shifts among years.

To test for anatomical differences among sites, land use intensities, and annual climate extremes, a permutation test of independence was applied as data did not meet normality assumptions. This test allows comparing the distribution of the values, which is of central interest in the case of anatomical values at the ring and sector level. Further pairwise permutation *t*-tests (*post-hoc* tests) were performed to compare between sites, periods, and extreme vs. normal climate years.

The general statistical robustness of each anatomical chronology was assessed by the average correlation between series (Rbar) and the expressed population signal (EPS). The first statistics is an estimate of the percent common variance between series, while the second statistics provides an estimate of how well the selected series reflect the entire population (Wigley et al., 1984). In general, anatomical chronologies showed weak

robustness (**Table 2**) except for VA95 and TRW (Rbar = 0.32 to 0.61, and EPS = 0.68 to 0.89). Consequently, monthly climate correlation analyses were only performed for these traits to reduce the likelihood of spurious correlations. Spearman's correlation coefficients were calculated between indexed monthly temperature and precipitation data and each sector chronology. Correlations were performed with indexed monthly climatic values for the previous and current growing seasons to allow for lagged and immediate associations.

P-values were corrected in all analyses following the Benjamini-Hochberg method to avoid inflation of the type I error. A significance level $\alpha = 5\%$ was considered for all the performed analyses. The study period covered from 1968 to 2004, with additional focus on the periods before the land use change (1968–1981) and the period 10 years after the harvesting was ceased (1990–2004). Statistical analyses were performed using R version 4.0.3 (R Core Team, 2019) and the packages coin (Hothorn et al., 2008), rcompanion (Mangiafico, 2020), nlme (Pinheiro et al., 2020), and dplR (Bunn, 2008). Figures were produced using the package ggplot2 (Wickham, 2009).

TABLE 2 | Descriptive statistics of the different wood anatomical chronologies at each site. Rbar–mean inter-series correlation; EPS–expressed population signal. Period 1968–2004 (*n* = 5). For anatomical trait abbreviations, see **Figure 2**.

Trait	Site	Rbar	EPS
VA	U1	0.12	0.38
	U2	0.27	0.65
	U3	0.10	0.36
VA95	U1	0.32	0.68
	U2	0.45	0.80
	U3	0.41	0.78
DH	U1	0.32	0.68
	U2	0.31	0.69
	U3	0.33	0.71
KH	U1	0.05	0.20
	U2	0.23	0.60
	U3	0.12	0.41
VD	U1	0.16	0.46
	U2	0.14	0.44
	U3	0.22	0.59
RVA	U1	0.08	0.28
	U2	0.41	0.78
	U3	0.20	0.56
VG	U1	0.35	0.71
	U2	0.15	0.46
	U3	0.14	0.46
TRW	U1	0.47	0.81
	U2	0.61	0.89
	U3	0.38	0.76
TRW*	U1	0.48	0.88
	U2	0.44	0.91
	U3	0.49	0.92

**Data derived from a more comprehensive dendrochronological analysis with 15 individuals including the study trees.*

RESULTS

Absolute and Intra-Annual Differences Related to the Site and Land Use Change

Overall, absolute mean anatomical traits and standardized intra-ring profiles proved to be remarkably similar among sites (**Figure 3A**). On average, vessel area consisted of about one-fourth of the total area of each sector ranging from 0.4 to 89.1%. Within the observed differences in distributions of the absolute values (**Figure 3A**), U2 showed the highest median of VA, VA95, and DH, compared with the other sites, whereas U3 showed the highest median in VD and VG. VA95, KH, RVA, and VG showed lower medians at U1 compared with the other sites. Absolute TRW values showed no significant differences among sites during the study period. The standardized values of all the anatomical traits, except for VD_{std}, showed the following general intra-ring pattern: stable to slightly decreasing values between the beginning and the relative position 50% in the ring and a clear decreasing trend from there to the end of the ring (**Figure 3B**). In contrast, VD_{std} peaked at the relative position of 90% in the ring independent from the site. Despite the generally similar intra-ring profiles, anatomical traits showed significant fine-scale differences among sites (**Figure 3B**). Particularly, intra-ring profiles of $VA95_{std}$ and DH_{std} differed significantly among sites in almost all sectors, where U1, U2, and U3 presented the highest values in the first (0–30%), second (40–60%), and third (70–100%) relative positions of the ring, respectively.

There were also differences in anatomical traits between the periods before (1968–1981) and after (1990–2004) the land use change, when Ugni was declared a Natural State Reserve and competition increased generally, with the largest impact at the lowest site (U1) and the smallest impact at the highest site (U3) (**Figure 4** and **Supplementary Figures 2, 3**). Absolute trait values were generally higher in the period after the forest land use change, but there were inversed relationships for VD, TRW (both at all sites), and VG (at U1) and no significant differences for VA95 (all the sites) and DH (at U3). Conspicuous differences between sites in intra-annual patterns were visible in $VA95_{std}$ (U2 and U3) and DH (at U2) with significantly higher values in the first part of the ring (relative position 10 and 20%) in the period after the land use change and lower almost at the end of the growing season (relative positions 70, 80, and 90%).

Correlation Among Anatomical Traits at the Ring and Intra-Ring Level

The correlation analyses between standardized ring-level values revealed many associations among anatomical traits and ring width, particularly at U3 (**Figure 5A**). The triplet formed by VA_{ind}, KH_{ind}, and RVA_{ind}, strongly correlated with each other at all sites as it was also the case between DH_{ind} and $VA95_{ind}$. Site U1 showed the lowest number of correlations between anatomical traits and TRW_{ind} (only VD_{ind} and VG_{ind}). At all the sites, significant correlations were generally positive aside from the ones of VD_{ind} that were all negative except for its positive correlation with VG_{ind}, and the generally negative correlations of TRW_{ind} with all the other traits except $VA95_{ind}$ and DH_{ind}.

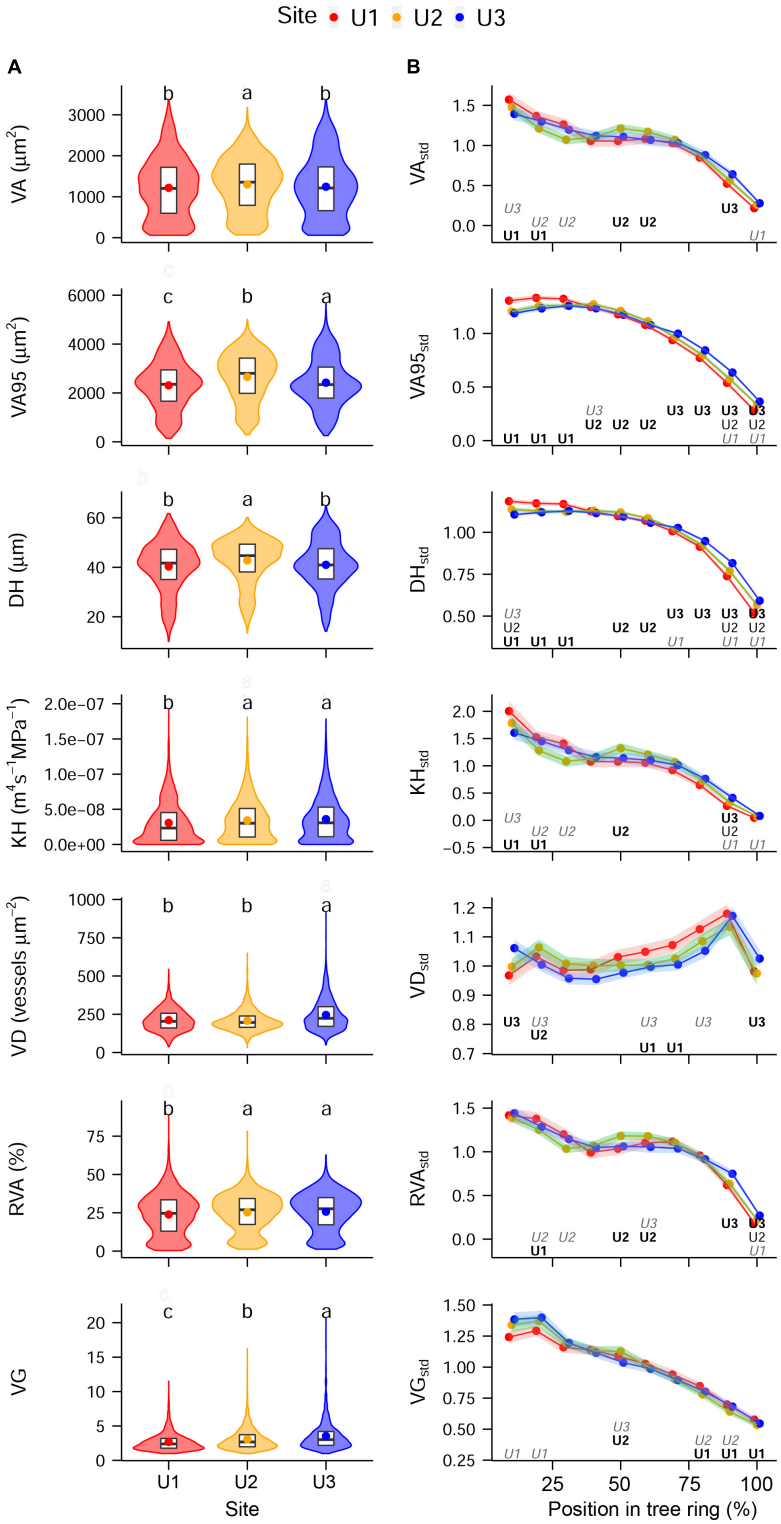

FIGURE 3 | (A) Absolute inter-annual and **(B)** standardized intra-annual values of each of the anatomical traits studied at the different study sites: U1—1,200 m a.s.l., U2—1,600 m a.s.l., and U3—1,950 m a.s.l. Panel **(A)** shows violin plots, with boxplots (1st, 2nd, and 3rd quartiles) and mean values (dots); letters indicate significant differences between sites (permutation test of independence, P-value < 0.05). Panel **(B)** shows mean values (dots) and 95% CI (shaded area); letters indicate if values are significantly higher (**bold**), lower (*italics gray*), or if they are significantly different at all sites (regular format indicates the middle value). If both **bold** and *italics gray* are shown, this means that the mid-value was the only one that did not differ significantly. Permutation test of independence, P-value < 0.05. For the anatomical trait abbreviations, see **Figure 2**.

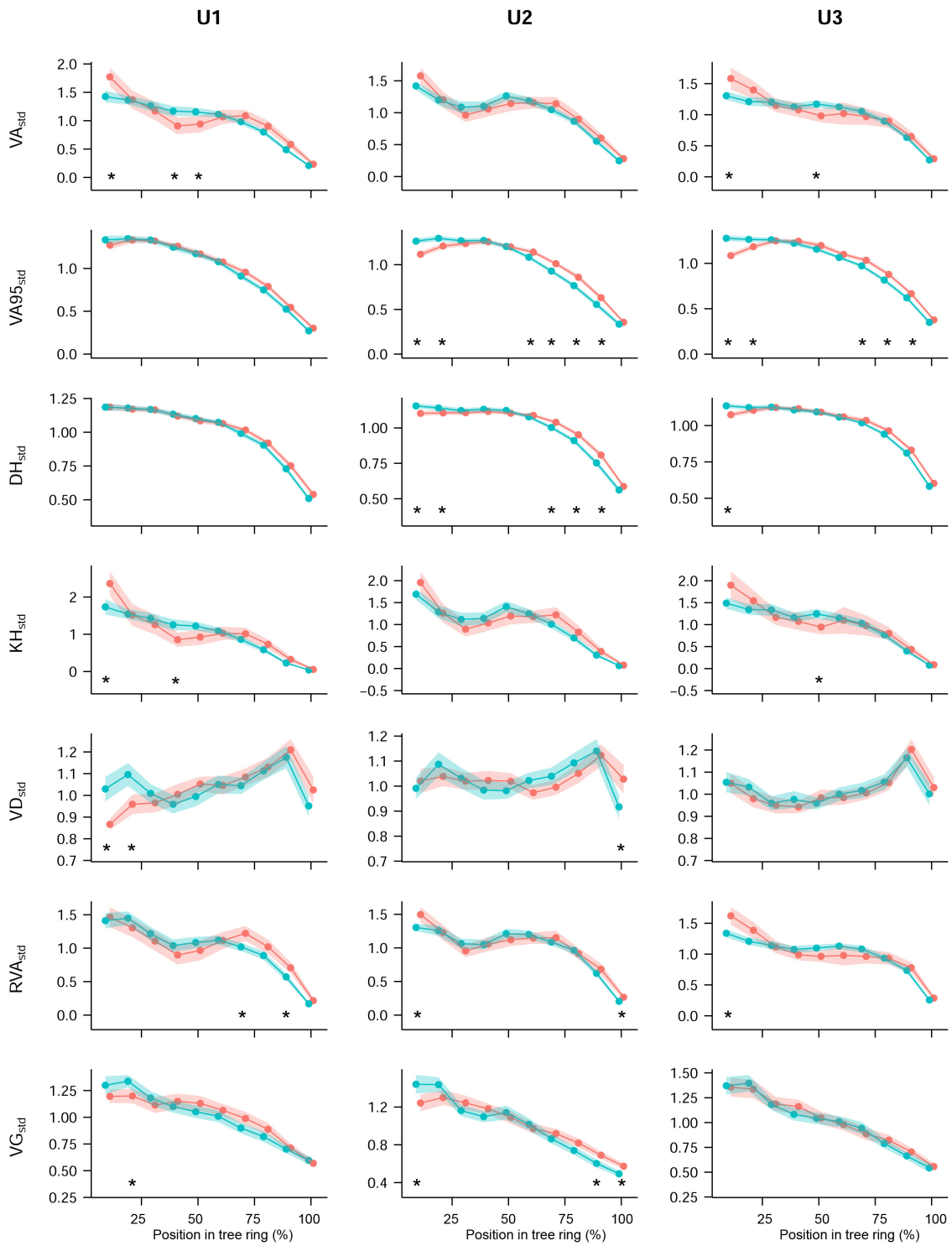

FIGURE 4 | Standardized intra-annual values of each land use period. Land use periods refer to the periods before (1968–1981) and after (1990–2004) the declaration of Ugni as Natural State Reserve in 1981 at the different study sites, which coincided with the cessation of coppicing: U1—1,200 m a.s.l.; U2—1,600 m a.s.l.; U3—1,950 m a.s.l. Mean values (dots) and 95% CI (shaded area); asterisks indicate significant differences in sector values. Permutation test of independence, *P*-value < 0.05. For the anatomical trait abbreviations, see **Figure 2**.

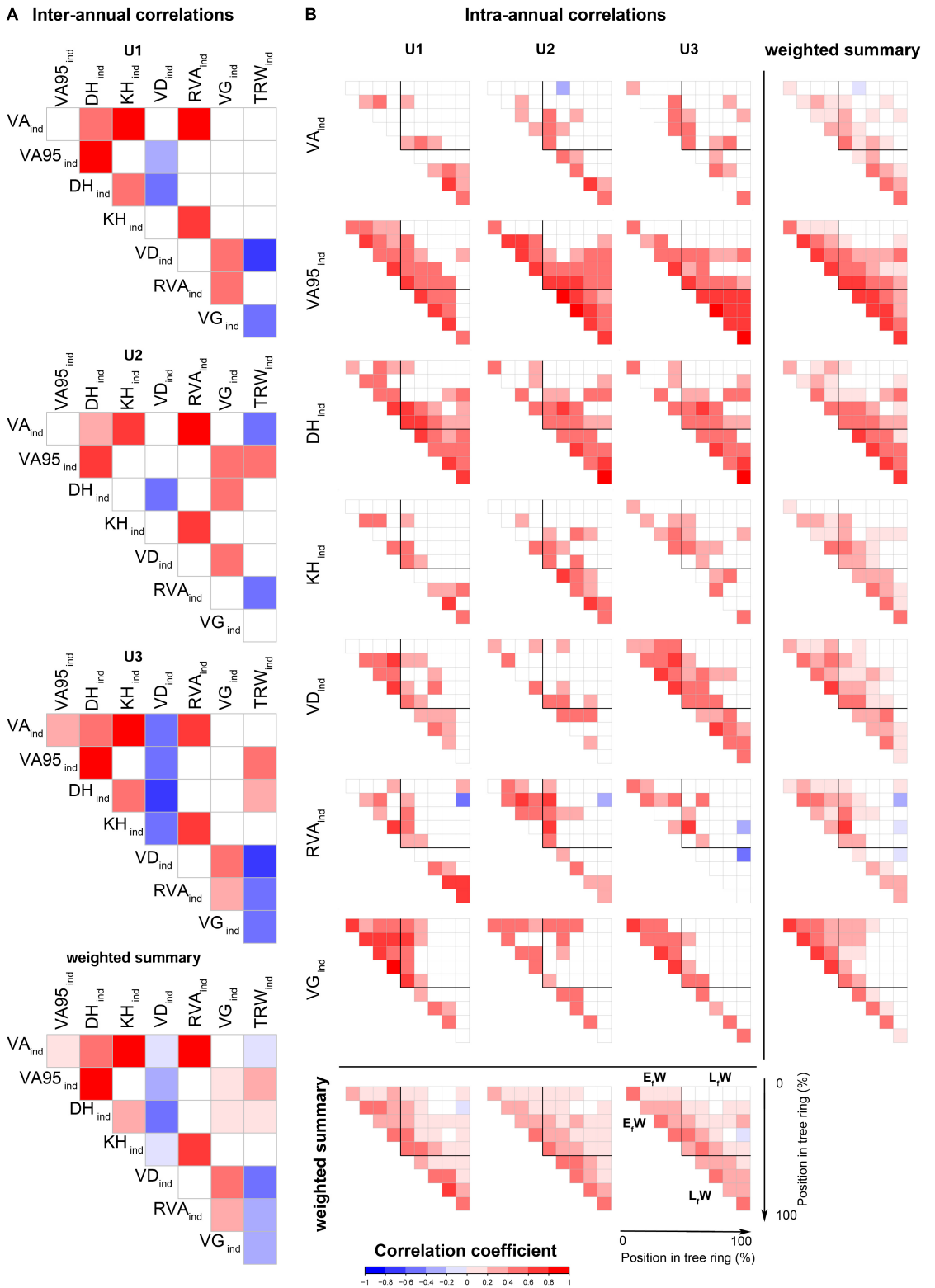

FIGURE 5 | (A) Inter-annual Spearman's correlations among all indexed series of anatomical traits and **(B)** intra-annual Spearman's correlations in each of the sector's indexed series of anatomical traits at the three study sites: U1—1,200 m a.s.l.; U2—1,600 m a.s.l.; U3—1,950 m a.s.l. Colors represent the correlation coefficient values (r). Only significant correlations (P-value < 0.05) are presented. Weighted summarized values are calculated as the sum of the significant correlation coefficients of the sites and traits, divided by the total number of sites and traits, respectively. E_fW: Early formed wood (0–50% of the ring); L_fW: late formed wood (50–100%), assuming each corresponds to half of each ring. For the anatomical trait abbreviations, see **Figure 2**.

Anatomical trait correlations at the intra-ring level showed different patterns of each trait across tree rings and also differences among sites (**Figure 5B**). In general, anatomical traits from nearby parts of the ring and thus formed at similar times of the growing season were positively correlated. $VA95_{ind}$ showed the strongest correlations between sectors throughout the ring followed by DH_{ind}. DH_{ind} values correlated significantly in 90% or more of all pairs of the L_fW sectors at all sites. $VA95_{ind}$ showed a similar pattern in L_fW except for the last formed sector in U1 trees. In contrast, VA_{ind} and KH_{ind} showed few significant correlations between the different sectors at all sites, with KH_{ind} showing more significant correlations in L_fW sectors at U2.

Climate Correlations and Anatomical Trait Variation in Years With Extreme Climate

As specified before, climate correlation analyses were performed only for VA95 and TRW traits. Other trait chronologies showed moderate (DH), low (RVA, VG, and VD) to very low (VA, KH) robustness (**Table 2**). Significant results included general negative associations of $VA95_{ind}$ sectors with previous summer (June), and current March and summer temperatures (July–August) at U1, and positive and negative associations with the previous summer (July) and winter (December–January) temperatures, respectively, at U3 (**Figure 6A**). Furthermore, positive associations of $VA95_{ind}$ with current summer precipitations (June–July) were observed at U2 and U3, and negative associations with winter precipitation (January–February) at U2 (**Figure 6B**). These correlation patterns were largely different from those of TRW_{ind}, which showed a negative correlation with temperature in the previous winter (December–January) at U1.

Analysis of anatomical traits in years with extreme climate showed scarce differences between years with extreme high and low temperatures and also between them and average years (**Figure 7**). Inter-annual patterns were fairly similar among years with extremely high and normal temperatures, but lower temperature years slightly affected the first and last sectors of $VA95_{std}$ at U2 and U3 sites. No significant differences between normal and extreme summer precipitation years were observed in intra-annual patterns (data not shown). Both the TRW absolute values and TRW_{ind} showed no significant differences between extreme high, low, and normal temperature and precipitation years (**Supplementary Figure 2**).

DISCUSSION

The Anatomical Structure Shows Little Trait Plasticity Apart From Species-Specific Patterns

Different anatomical traits showed different levels of plasticity in response to environmental conditions and land use regime at each site as observed in the previous studies in beech (Fonti and Jansen, 2012; Oladi et al., 2014; Diaconu et al., 2016). The general trend of higher to mid and lower values of all the studied traits (except for VD_{std}) across the tree rings reflects the species-specific wood anatomy of beech, which is characteristic for a diffuse-porous to semi-ring-porous species (Bosshard, 1982; Schweingruber, 2007). The observed wider vessels and the higher vessel grouping in the earlywood are consistent with maximizing hydraulic efficiency in this part of the ring. This fits the higher water availability and lower evaporative demand from the canopy at the beginning compared to the end of the growing season (Sass and Eckstein, 1995; Prislan et al., 2018). Similarly, the increasing trend of VD_{std} toward the end of the growing season, peaking at relative positions 70 and 80% compensates for the hydraulically less efficient smaller, but putatively safer vessels produced in the latewood (lower VA_{std} and $VA95_{std}$).

Apart from these general and mostly species-specific patterns in wood anatomical traits, strongly correlated maximum vessel size and hydraulic diameters across tree-rings with narrow confidence bands (**Figures 3**, **5**) suggests that these beech stands poorly regulate hydraulic responses to changes in water availability throughout the year. The low plasticity of VA95 and DH is likely related to the biophysical constraints associated with tree height (Olson et al., 2014; Carrer et al., 2015). In contrast, the strongly correlated trait group of VA, KH, and RVA showed higher intra-annual plasticity, which has also been observed in previous studies in responses to environmental fluctuations (Oladi et al., 2014; Diaconu et al., 2016). Xylem trait plasticity could be expected considering the wide distribution range of the species, both globally (longitudinally and altitudinally) and locally (elevational band in the Apennines). In fact, beech is known to have high-genetic diversity within populations, resulting in phenotypic plasticity, i.e., short-term acclimation (Bresson et al., 2011; Wortemann et al., 2011; Cocozza et al., 2016). However, the intra-annual plasticity of VA, KH, and RVA could be at least partly related to the less robust data for these traits according to Rbar and EPS statistics (cf. **Table 2**), suggesting the limited number of replicates taken per site ($n = 5$) only allow identifying the strongest relationships.

Plasticity Decreases and Hydraulic Safety Increases Toward the Highest Site

Results supported our first hypothesis (i): trees had less plastic and a hydraulically safer anatomical structure toward higher elevations.

First, the lowest site had a proportionally more efficient, but also hydraulically riskier, anatomical configuration. This was depicted by the significant differences in the maximum values of VA_{std}, $VA95_{std}$, DH_{std}, KH_{std} (higher), and VG_{std} (smaller) at U1 compared with U3 occurring at the beginning of the ring (**Figure 3B**). Second, absolute values of VG were higher with increasing elevation enhancing the hydraulic safety of the individuals. Yet, this must be taken with care as the advantages and disadvantages of vessel grouping in relation to embolism are under debate (Carlquist, 2003; Martinez-Vilalta et al., 2012; Nardini et al., 2012; Scholz et al., 2013). Finally, the high number of correlations among anatomical traits at U3 compared with the other sites also supports the hypothesis of hydraulic limitations of the trees at this site (Oladi et al., 2014). This last result also showed

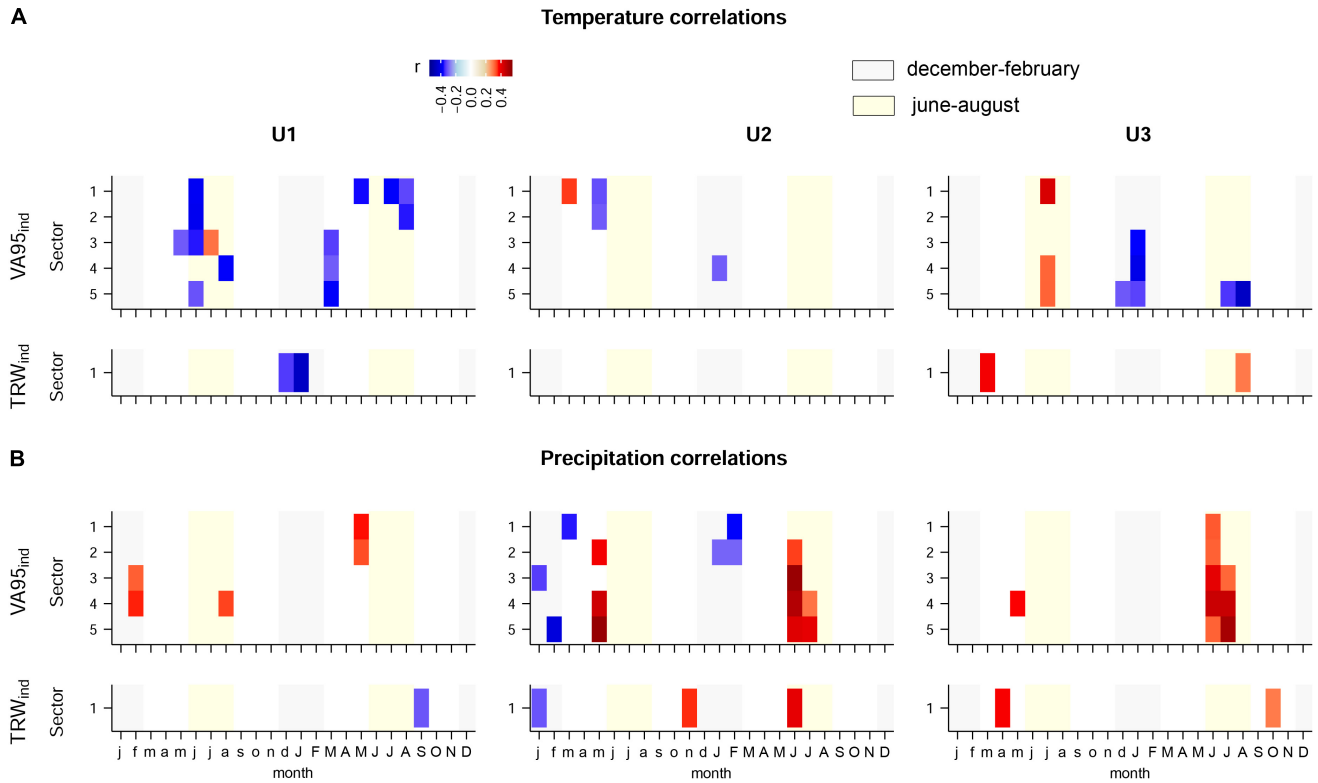

FIGURE 6 | The Spearmans' correlation of the tree-ring sector indexed series of VA95, DH, and TRW with monthly **(A)** temperature and **(B)** precipitation at the three study sites: U1—1,200 m a.s.l.; U2—1,600 m a.s.l.; U3—1,950 m a.s.l. As an annual value, TRW has not been divided into five sectors. Colors represent the correlation coefficient values (r). Only significant correlations (*P*-value < 0.05) are presented. Lower case letters indicate the initials of the previous-year's months, while capital letters indicate the initials of the current year's months. For the anatomical trait abbreviations, see **Figure 2**.

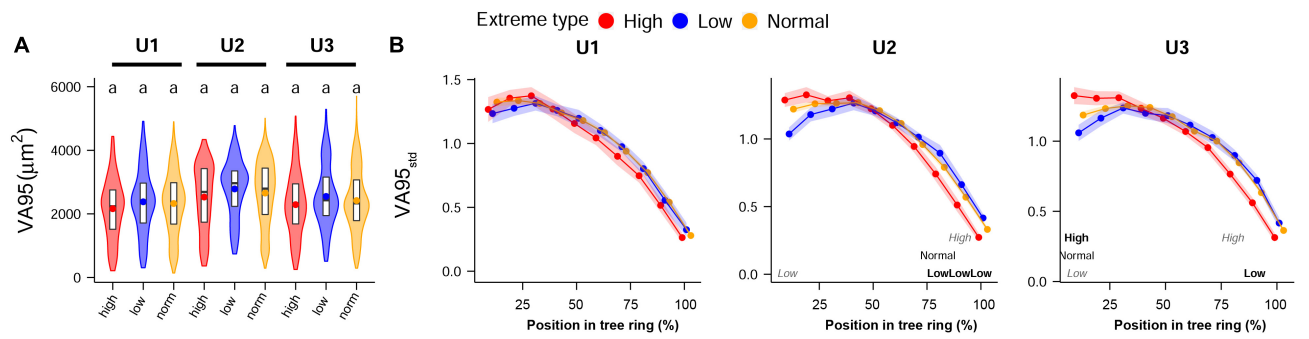

FIGURE 7 | (A) Inter-annual and **(B)** standardized intra-annual values (standardized to the annual mean) of VA95 studied at the 5 years with the highest and lowest temperatures during the dry trimester June–July–August in the time period 1968–2004 at the different study sites: U1—1,200 m a.s.l.; U2—1,600 m a.s.l.; U3—1,950 m a.s.l. Panel **(A)** shows violin plots, with boxplots (1st, 2nd, and 3rd quartiles), and mean values (dots); letters indicate significant differences between sites. Panel **(B)** shows mean values (dots) and 95% CI (shaded area); letters indicate if values are significantly higher (**bold**), lower (*italics gray*), or if they are significantly different at all sites (regular format indicates the middle value). If both the **bold** and *italics gray* are shown, this means that the mid-value was the only one that did not differ significantly. Permutation test of independence, $P < 0.05$. For the anatomical trait abbreviations, **Figure 2**.

how the anatomical structure of U3 trees is constrained to the point that their radial growth correlated with all the studied traits except the most plastic ones (VA and KH), resulting in VA_{ind} being correlated with $VA95_{ind}$.

The less safe and more efficient hydraulic system with decreasing elevation as inferred from anatomy could be related to higher water accessibility due to an earlier start of the growing season at lower elevations (Martínez del Castillo et al., 2016; Prislan et al., 2018) profiting from the more abundant precipitation in this period; the lower freezing-induced embolism probability during milder winters at the lower elevations (Sperry and Sullivan, 1992; Lemoine et al., 1999) and to deeper and more

productive soils (Bouriaud et al., 2004) (observed during the sampling but not quantified).

Increased Competition From Coppicing Cessation Might Lead to a More Conservative Wood Structure

Our results showed some indications to support our second hypothesis regarding the increase in hydraulic safety because of the land use change. After cessation of coppicing, coppices probably sprouted new shoots and kept the already growing stems, leading to the lower mean tree diameters as well as the high density and basal areas observed at U1 (**Table 1**). This might have triggered an increase in competition for water and evaporative demand.

Indeed, the different responses at U2 and U3 compared with U1 might be related to the heavier harvesting pressure at U1. The less plastic trait VA95 showed the highest number of differences between the periods before and after the land use change at U2 and U3 together with DH at U2 (**Figure 4**). Conversely, at U1, VA95 and DH were the only traits without a different intra-annual trend after cessation of coppicing. The increased competition agrees with the more conservative strategy observed at U1 as opposed to the previously observed increase in hydraulic conductance following competition release treatments (Lemoine et al., 2002; Diaconu et al., 2016; Noyer et al., 2017). VA_{ind}, KH_{ind}, and VD_{ind} at U1 turned as well toward a more conservative anatomical configuration after the land use change. However, with the present dataset, it is not possible to investigate in detail the anatomical responses to land use changes, as they are not acute but gradually developing over time and could be confounded with ontogenetic trends. This was the case for the differences observed in absolute values of the anatomical traits between the periods before and after the land use change that went in the same direction as the expected age-related trends.

Intra-Ring Maximum Vessel Size Shows Different Climate Sensitivity but Little Differentiation to Extreme Years

The generally moderate associations of maximum vessel size (VA95) with climate are in line with the previous studies (Giagli et al., 2016; Rosell et al., 2017). However, climate sensitivity changed with elevation, with maximum vessel size being mainly limited by temperature at U1, precipitation at U2, and a mixture of temperature and precipitation at U3. Different sensitivities for the first formed vessels in tree rings (sectors 1–2) might be partly explained by the different drivers and processes involved in the formation of these vessels after cambial reactivation (Marchand et al., 2021). The negative correlation of first-sector VA95 with May temperature and the positive correlation with May precipitation at U1 likely points to reduced turgor because of the water limitation during cell enlargement (Arend and Fromm, 2007). For the later-formed vessels (sectors 3–5), it is difficult to directly link the negative associations with previous March and winter temperatures at U1 and U3, respectively, to tree physiology and cell formation processes. These negative associations probably represent memory effects in either trees or soil conditions (Zweifel et al., 2020; Walthert et al., 2021), as it might be also the case of the positive and negative associations with previous summer and winter temperatures, respectively, at U3. In contrast, the positive correlations of VA95 with summer precipitation at U2 and U3—remarkably the most striking correlation pattern found—is consistent with a reduction in seasonal drought stress and consequently increased turgor that might have triggered the formation of wider vessels (Hsiao, 1973). We cannot rule out the possibility that there are additional relevant relationships with VA95 and even more so with the other anatomical features that were not considered in these analyses if replication had been higher, which would have improved the robustness of the chronologies (EPS and Rbar). Similarly, daily climate records, if available, could strengthen and refine the understanding of the anatomical responses of the studied beech trees to climate.

Results were not conclusive regarding our third hypothesis. Extremely high and low summer temperatures induced only slight intra-annual differences in wood anatomy at U2 and U3, particularly in $VA95_{std}$ values (**Figure 7**). However, in addition to the inclusive definition of extreme years (10 of 37 years), the years with extremely high temperatures were clustered toward the end of the study period and the years with a low temperature toward the beginning. Therefore, as for the land use effects, our results could be confounded with ontogenetic trends. The same applies to the absolute values: differences are probably biased by the unbalanced timing of the considered extreme years throughout the study period. Conversely, extreme precipitation years were more scattered, but there were no differences between high- and low-summer precipitation years.

CONCLUSION

In this study, we assessed the plasticity of different wood anatomical traits of European beech to elevation, coppicing cessation, and climate variability by investigating three beech stands along a 750 m elevational gradient in the Apennines (Italy). The anatomical structure between and within tree rings generally showed limited plasticity apart from species-specific and ontogenetic patterns. Yet, plasticity decreased and the hydraulic safety as inferred from the anatomical configuration increased toward the highest site. After land use change, trees at the most intensively exploited site kept a conservative strategy by maintaining their maximum vessel size in time. Furthermore, intra-ring maximum vessel size showed different climate sensitivity but little differentiation between normal and extreme years.

Our results show that several wood anatomical traits of beech are plastic at different time scales, from seasonal climate fluctuations to changes in stand dynamics as induced by changes in land use to long-term site conditions. The underlying external driver for this plasticity appears to be related to the water supply and water transport capacity in the wood, and also its efficiency and safety. Constraining hydrological conditions limit this plasticity and lead to closer coordination of the

different anatomical traits and an anatomical configuration consistent with increased hydraulic safety. Nevertheless, the considered anatomical traits differed in both the absolute plasticity and immediacy of plasticity, with VA95 and DH being less plastic and VA, KH, RVA, VG, and VD being more plastic. However, it remains a challenge to clearly separate the externally induced medium- to longer-term responses from ontogenetically determined patterns, and insufficient replication could add to this uncertainty. This study, therefore, advocates for more comprehensive studies to further explore and verify the plasticity of wood anatomical traits in European beech, its extent and immediacy in response to short- to long-term environmental fluctuations to support sustainable forest ecosystems.

DATA AVAILABILITY STATEMENT

The raw data supporting the conclusions of this article will be made available by the authors, without undue reservation.

AUTHOR CONTRIBUTIONS

RT, BL, CCo, and CCa designed the study. CCa and CCo collected the samples and performed the field measurements. CCa and GA produced the anatomical data. JM with significant input from GA performed the statistical analysis and wrote the first draft of the manuscript. All authors contributed to manuscript revisions and approved the submitted version of the manuscript.

FUNDING

JM was supported by the fellowship Emilio Gonzalez Esparcia and by the Ramon Areces Foundation (BEVP31A6157).

ACKNOWLEDGMENTS

We thank the Carabinieri Forestali of the city of Pescara, Caramanico Terme, and Palombaro, the management staff of the Majella National Park for their great support during the surveys. We also thank the Labs "Centro Studi dell'Ambiente Alpino" at S. Vito di Cadore and Caterina Palombo for helping in sample preparation. Anne Verstege and Loïc Schneider are acknowledged for support with ring-width and anatomical lab work.

SUPPLEMENTARY MATERIAL

The Supplementary Material for this article can be found online at: https://www.frontiersin.org/articles/10.3389/fpls.2022.855741/full#supplementary-material

REFERENCES

Arend, M., and Fromm, J. (2007). Seasonal change in the drought response of wood cell development in poplar. *Tree Physiol.* 27, 985–992. doi: 10.1093/treephys/27.7.985

Arnic, D., Gricar, J., Jevsenak, J., Bozic, G., von Arx, G., and Prislan, P. (2021). Different wood anatomical and growth responses in European beech (Fagus sylvatica L.) at three forest sites in Slovenia. *Front. Plant Sci.* 12:669229. doi: 10.3389/fpls.2021.669229

Aussenac, G. (2000). Interactions between forest stands and microclimate: ecophysiological aspects and consequences for silviculture. *Ann. For. Sci.* 57, 287–301. doi: 10.1051/forest:2000119

Bittencourt, P. R. L., Pereira, L., and Oliveira, R. S. (2016). On xylem hydraulic efficiencies, wood space-use and the safety-efficiency tradeoff: comment on Gleason et al. (2016) 'Weak tradeoff between xylem safety and xylem-specific hydraulic efficiency across the world's woody plant species'. *New Phytol.* 211, 1152–1155. doi: 10.1111/nph.14044

Bolte, A., Czajkowski, T., Cocozza, C., Tognetti, R., de Miguel, M., Psidova, E., et al. (2016). Desiccation and mortality dynamics in seedlings of different European Beech (Fagus sylvatica L.) populations under extreme drought conditions. *Front. Plant Sci.* 7:751. doi: 10.3389/fpls.2016.00751

Bosela, M., Lukac, M., Castagneri, D., Sedmak, R., Biber, P., Carrer, M., et al. (2018). Contrasting effects of environmental change on the radial growth of co-occurring beech and fir trees across Europe. *Sci. Total Environ.* 615, 1460–1469. doi: 10.1016/j.scitotenv.2017.09.092

Bosshard, H. H. (1982). *Holzkunde: Band 1 Mikroskopie und Makroskopie des Holzes*. Basel: Birkhäuser. doi: 10.1007/978-3-0348-5413-9

Bouriaud, O., Breda, N., Le Moguedec, G., and Nepveu, G. (2004). Modelling variability of wood density in beech as affected by ring age, radial growth and climate. *Trees Struct. Funct.* 18, 264–276. doi: 10.1007/s00468-003-0303-x

Bresson, C. C., Vitasse, Y., Kremer, A., and Delzon, S. (2011). To what extent is altitudinal variation of functional traits driven by genetic adaptation in European oak and beech? *Tree Physiol.* 31, 1164–1174. doi: 10.1093/treephys/tpr084

Brunet, J., Fritz, Ö, and Richnau, G. (2010). Biodiversity in European beech forests - a review with recommendations for sustainable forest management. *Ecol. Bull.* 53, 77–94.

Bunn, A. G. (2008). A dendrochronology program library in R (dplR). *Dendrochronologia.* 26, 115–124. doi: 10.1016/j.dendro.2008.01.002

Calderaro, C., Cocozza, C., Palombo, C., Lasserre, B., Marchetti, M., and Tognetti, R. (2020). Climate–growth relationships at the transition between Fagus sylvatica and Pinus mugo forest communities in a Mediterranean mountain. *Ann. For. Sci.* 77:63. doi: 10.1007/s13595-020-00964-y

Carlquist, S. (2003). *Comparative Wood Anatomy: Systematic, Ecological, and Evolutionary Aspects of Dicotyledon Wood*. Berlin: Springer.

Carlquist, S. (2012). How wood evolves: a new synthesis. *Botany* 90, 901–940. doi: 10.1139/b2012-048

Carrer, M., von Arx, G., Castagneri, D., and Petit, G. (2015). Distilling allometric and environmental information from time series of conduit size: the standardization issue and its relationship to tree hydraulic architecture. *Tree Physiol.* 35, 27–33. doi: 10.1093/treephys/tpu108

Chenlemuge, T., Schuldt, B., Dulamsuren, C., Hertel, D., Leuschner, C., and Hauck, M. (2015). Stem increment and hydraulic architecture of a boreal conifer (Larix sibirica) under contrasting macroclimates. *Trees Struct. Funct.* 29, 623–636. doi: 10.1007/s00468-014-1131-x

Chiesi, M., Maselli, F., Chirici, G., Corona, P., Lombardi, F., Tognetti, R., et al. (2013). Assessing most relevant factors to simulate current annual increments of beech forests in Italy. *Iforest Biogeosci. For.* 7, 115–122. doi: 10.3832/ifor0943-007

Cocozza, C., de Miguel, M., Psidova, E., Ditmarova, L., Marino, S., Maiuro, L., et al. (2016). Variation in ecophysiological traits and drought tolerance of beech (Fagus sylvatica L.) seedlings from different populations. *Front. Plant Sci.* 7:886. doi: 10.3389/fpls.2016.00886

Cook, E., and Kairiukstis, L. (1990). *Methods of Dendrochronology: Applications in the Environmental Sciences, Kluwer Academic Publishers Edn*. Dordrecht: Kluwer Academic Publishers. doi: 10.1007/978-94-015-7879-0

Di Filippo, A., Biondi, F., Cufar, K., de Luis, M., Grabner, M., Maugeri, M., et al. (2007). Bioclimatology of beech (Fagus sylvatica L.) in the Eastern Alps: spatial and altitudinal climatic signals identified through a tree-ring network. *J. Biogeogr.* 34, 1873–1892. doi: 10.1111/j.1365-2699.2007.01747.x

Di Filippo, A., Biondi, F., Maugeri, M., Schirone, B., and Piovesan, G. (2012). Bioclimate and growth history affect beech lifespan in the Italian Alps and Apennines. *Glob. Chang. Biol.* 18, 960–972. doi: 10.1111/j.1365-2486.2011.02617.x

Diaconu, D., Stangler, D. F., Kahle, H. P., and Spiecker, H. (2016). Vessel plasticity of European beech in response to thinning and aspect. *Tree Physiol.* 36, 1260–1271. doi: 10.1093/treephys/tpw053

Eilmann, B., Sterck, F., Wegner, L., de Vries, S. M. G., von Arx, G., Mohren, G. M. J., et al. (2014). Wood structural differences between northern and southern beech provenances growing at a moderate site. *Tree Physiol.* 34, 882–893. doi: 10.1093/treephys/tpu069

Ellenberg, H. (1996). *Vegetation Mitteleuropas mit den Alpen*, 5 Edn. Stuttgart: Ulmer.

Ellenberg, H., and Leuschner, C. (2010). *Vegetation Mitteleuropas mit den Alpen in Ökologischer, Dynamischer und Historischer Sicht: 203 Tabellen*. Stuttgart: Ulmer.

Fonti, P., and Jansen, S. (2012). Xylem plasticity in response to climate. *New Phytol.* 195, 734–736. doi: 10.1111/j.1469-8137.2012.04252.x

Fotelli, M. N., Rennenberg, H., and Gessler, A. (2002). Effects of drought on the competitive interference of an early successional species (Rubus fruticosus) on Fagus sylvatica L. seedlings: N-15 uptake and partitioning, responses of amino acids and other N compounds. *Plant Biol.* 4, 311–320. doi: 10.1055/s-2002-32334

Gessler, A., Keitel, C., Kreuzwieser, J., Matyssek, R., Seiler, W., and Rennenberg, H. (2007). Potential risks for European beech (Fagus sylvatica L.) in a changing climate. *Trees Struct. Funct.* 21, 1–11. doi: 10.1007/s00468-006-0107-x

Giagli, K., Gricar, J., Vavrcik, H., Mensik, L., and Gryc, V. (2016). The effects of drought on wood formation in fagus sylvatica during two contrasting years. *IAWA J.* 37, 332–348. doi: 10.1163/22941932-20160137

Hacke, U. G., and Sperry, J. S. (2001). Functional and ecological xylem anatomy. *Perspect. Plant Ecol. Evol. Syst.* 4, 97–115. doi: 10.1078/1433-8319-00017

Hacke, U. G., Spicer, R., Schreiber, S. G., and Plavcova, L. (2017). An ecophysiological and developmental perspective on variation in vessel diameter. *Plant Cell Environ.* 40, 831–845. doi: 10.1111/pce.12777

Hahn, K., and Fanta, J. (2001). *Contemporary Beech Forest Management in Europe: Working Report 1*. København: University of Copenhagen.

Harris, I., Jones, P. D., Osborn, T. J., and Lister, D. H. (2014). Updated high-resolution grids of monthly climatic observations - the CRU TS3.10 Dataset. *Int. J. Climatol.* 34, 623–642. doi: 10.1002/joc.3711

Hoeber, S., Leuschner, C., Kohler, L., Arias-Aguilar, D., and Schuldt, B. (2014). The importance of hydraulic conductivity and wood density to growth performance in eight tree species from a tropical semi-dry climate. *For. Ecol. Manage.* 330, 126–136. doi: 10.1016/j.foreco.2014.06.039

Hothorn, T., Hornik, K., van de Wiel, M. A., and Zeileis, A. (2008). Implementing a class of permutation tests: the coin package. *J. Stat. Softw.* 28, 1–23. doi: 10.18637/jss.v028.i08

Hsiao, T. C. (1973). Plant responses to water stress. *Ann. Rev. Plant Physiol. Plant Mol. Biol.* 24, 519–570. doi: 10.1146/annurev.pp.24.060173.002511

Jetschke, G., van der Maaten, E., and van der Maaten-Theunissen, M. (2019). Towards the extremes: a critical analysis of pointer year detection methods. *Dendrochronologia* 53, 55–62. doi: 10.1016/j.dendro.2018.11.004

Kahle, H. (2006). "Impact of the drought in 2003 on intra- and inter-annual stem radial growth of beech and spruce along an altitudinal gradient in the Black Forest, Germany," in *TRACE-Tree Rings in Archaeology, Climatology and Ecology, Vol.4: Proceedings of the Dendrosymposium 2005: Reihe Umwelt*, Vol. 61, eds I. Heinrich, H. Gaertner, M. Monbaron, and G. H. Schleser (Fribourg: Forschungszentrums Jülich), 151–163.

Klesse, S. (2021). Critical note on the application of the "two-third" spline. *Dendrochronologia* 65:125786. doi: 10.1016/j.dendro.2020.125786

Kotowska, M. M., Hertel, D., Abou Rafab, Y., Barus, H., and Schuldt, B. (2015). Patterns in hydraulic architecture from roots to branches in six tropical tree species from cacao agroforestry and their relation to wood density and stem growth. *Front. Plant Sci.* 6:191. doi: 10.3389/fpls.2015.00191

Lemoine, D., Granier, A., and Cochard, H. (1999). Mechanism of freeze-induced embolism in Fagus sylvatica L. *Trees Struct. Funct.* 13, 206–210. doi: 10.1007/PL00009751

Lemoine, D., Jacquemin, S., and Granier, A. (2002). Beech (Fagus sylvatica L.) branches show acclimation of xylem anatomy and hydraulic properties to increased light after thinning. *Ann. For. Sci.* 59, 761–766. doi: 10.1051/forest:2002062

Linares, J. C., and Camarero, J. J. (2012). From pattern to process: linking intrinsic water-use efficiency to drought-induced forest decline. *Glob. Chang. Biol.* 18, 1000–1015. doi: 10.1111/j.1365-2486.2011.02566.x

Lourenço, J. Jr., Enquist, B. J., von Arx, G., Oliveira, J., Morino, K., Thomaz, L., et al. (2022). Hydraulic tradeoffs underlie local variation in tropical forest functional diversity and sensitivity to drought. *New. Phytol.* 234, 50–63. doi: 10.1111/nph.17944

Mangiafico, S. (2020). *rcompanion: Functions to Support Extension Education Program Evaluation. R Package Version 2, 27*.

Marchand, L. J., Dox, I., Gricar, J., Prislan, P., Van den Bulcke, J., Fonti, P., et al. (2021). Timing of spring xylogenesis in temperate deciduous tree species relates to tree growth characteristics and previous autumn phenology. *Tree Physiol.* 41, 1161–1170. doi: 10.1093/treephys/tpaa171

Martínez del Castillo, E., Longares, L. A., Gricar, J., Prislan, P., Gil-Pelegrin, E., Cufar, K., et al. (2016). Living on the edge: contrasted wood-formation dynamics in fagus sylvatica and pinus sylvestris under Mediterranean conditions. *Front. Plant Sci.* 7:370. doi: 10.3389/fpls.2016.00370

Martinez-Vilalta, J., Mencuccini, M., Alvarez, X., Camacho, J., Loepfe, L., and Pinol, J. (2012). Spatial distribution and packing of xylem conduits. *Am. J. Bot.* 99, 1189–1196. doi: 10.3732/ajb.1100384

Nardini, A., Dimasi, F., Klepsch, M., and Jansen, S. (2012). Ion-mediated enhancement of xylem hydraulic conductivity in four Acer species: relationships with ecological and anatomical features. *Tree Physiol.* 32, 1434–1441. doi: 10.1093/treephys/tps107

Nocentini, S. (2009). Structure and management of beech (Fagus sylvatica L.) forests in Italy. *Iforest Biogeosci. For.* 2, 105–113. doi: 10.3832/ifor0499-002

Noyer, E., Lachenbruch, B., Dlouha, J., Collet, C., Ruelle, J., Ningre, F., et al. (2017). Xylem traits in European beech (Fagus sylvatica L.) display a large plasticity in response to canopy release. *Ann. For. Sci.* 74:46. doi: 10.1007/s13595-017-0634-1

Oladi, R., Brauning, A., and Pourtahmasi, K. (2014). "Plastic" and "static" behavior of vessel-anatomical features in Oriental beech (Fagus orientalis Lipsky) in view of xylem hydraulic conductivity. *Trees Struct. Funct.* 28, 493–502. doi: 10.1007/s00468-013-0966-x

Olson, M. E., Anfodillo, T., Rosell, J. A., Petit, G., Crivellaro, A., Isnard, S., et al. (2014). Universal hydraulics of the flowering plants: vessel diameter scales with stem length across angiosperm lineages, habits and climates. *Ecol. Lett.* 17, 988–997. doi: 10.1111/ele.12302

Peuke, A. D., Schraml, C., Hartung, W., and Rennenberg, H. (2002). Identification of drought-sensitive beech ecotypes by physiological parameters. *New Phytol.* 154, 373–387. doi: 10.1046/j.1469-8137.2002.00400.x

Pinheiro, J., Bates, D., DebRoy, D., Sarkar, D., and R Core Team (2020). *{nlme}: Linear and Nonlinear Mixed Effects Models. R Package Version 3.1-155*.

Piovesan, G., Biondi, F., Di Filippo, A., Alessandrini, A., and Maugeri, M. (2008). Drought-driven growth reduction in old beech (Fagus sylvatica L.) forests of the central Apennines, Italy. *Glob. Chang. Biol.* 14, 1265–1281. doi: 10.1111/j.1365-2486.2008.01570.x

Prislan, P., Cufar, K., De Luis, M., and Gricar, J. (2018). Precipitation is not limiting for xylem formation dynamics and vessel development in European beech from two temperate forest sites. *Tree Physiol.* 38, 186–197. doi: 10.1093/treephys/tpx167

Prislan, P., Gricar, J., de Luis, M., Smith, K. T., and Cufar, K. (2013). Phenological variation in xylem and phloem formation in Fagus sylvatica from two contrasting sites. *Agric. For. Meteorol.* 180, 142–151. doi: 10.1016/j.agrformet.2013.06.001

R Core Team (2019). *R: A Language and Environment for Statistical Computing*. Vienna: R Foundation for Statistical Computing.

Rosell, J. A., Olson, M. E., and Anfodillo, T. (2017). Scaling of xylem vessel diameter with plant size: causes, predictions, and outstanding questions. *Curr. For. Rep.* 3, 46–59. doi: 10.1007/s40725-017-0049-0

Sabate, S., Gracia, C. A., and Sanchez, A. (2002). Likely effects of climate change on growth of Quercus ilex, Pinus halepensis, Pinus pinaster, Pinus sylvestris and Fagus sylvatica forests in the Mediterranean region. *For. Ecol. Manage.* 162, 23–37. doi: 10.1016/S0378-1127(02)00048-8

Salomon, R., Rodriguez-Calcerrada, J., Gonzalez-Doncel, I., Gil, L., and Valbuena-Carabana, M. (2017). On the general failure of coppice conversion into high forest in Quercus pyrenaica stands: a genetic and physiological approach. *Folia Geobot.* 52, 101–112. doi: 10.1007/s12224-016-9257-9

Salomon, R., Rodriguez-Calcerrada, J., Zafra, E., Morales-Molino, C., Rodriguez-Garcia, A., Gonzalez-Doncel, I., et al. (2016). Unearthing the roots of degradation of Quercus pyrenaica coppices: a root-to-shoot imbalance caused by historical management? *For. Ecol. Manage.* 363, 200–211. doi: 10.1016/j.foreco.2015.12.040

Sass, U., and Eckstein, D. (1995). The variability of vessel size in beech (Fagus Sylvatica L) and its ecophysiological interpretation. *Trees Struct. Funct.* 9, 247–252. doi: 10.1007/BF00202014

Scarascia-Mugnozza, G., Oswald, H., Piussi, P., and Radoglou, K. (2000). Forests of the Mediterranean region: gaps in knowledge and research needs. *For. Ecol. Manage.* 132, 97–109. doi: 10.1016/S0378-1127(00)00383-2

Scholz, A., Rabaey, D., Stein, A., Cochard, H., Smets, E., and Jansen, S. (2013). The evolution and function of vessel and pit characters with respect to cavitation resistance across 10 Prunus species. *Tree Physiol.* 33, 684–694. doi: 10.1093/treephys/tpt050

Schuldt, B., Buras, A., Arend, M., Vitasse, Y., Beierkuhnlein, C., Damm, A., et al. (2020). A first assessment of the impact of the extreme 2018 summer drought on Central European forests. *Basic Appl. Ecol.* 45, 86–103. doi: 10.1016/j.baae.2020.04.003

Schweingruber, F. H. (2007). *Wood Structure and Environment*. Berlin: Springer, 279.

Sperry, J. S., and Sullivan, J. E. M. (1992). Xylem embolism in response to freeze-thaw cycles and water stress in ring-porous, diffuse-porous, and conifer species. *Plant Physiol.* 100, 605–613. doi: 10.1104/pp.100.2.605

Tognetti, R., Lasserre, B., Di Febbraro, M., and Marchetti, M. (2019). Modeling regional drought-stress indices for beech forests in Mediterranean mountains based on tree-ring data. *Agric. For. Meteorol.* 265, 110–120. doi: 10.1016/j.agrformet.2018.11.015

Tognetti, R., Lombardi, F., Lasserre, B., Cherubini, P., and Marchetti, M. (2014). Tree-ring stable isotopes reveal twentieth-century increases in water-use efficiency of Fagus sylvatica and Nothofagus spp. in Italian and Chilean Mountains. *PLoS One* 9:e113136. doi: 10.1371/journal.pone.0113136

Tyree, M. T., and Ewers, F. W. (1991). The hydraulic architecture of trees and other woody-plants. *New Phytol.* 119, 345–360. doi: 10.1111/j.1469-8137.1991.tb00035.x

Tyree, M. T., and Zimmermann, M. H. (2002). *Xylem Structure and the Ascent of Sap*. Berlin: Springer, 283. doi: 10.1007/978-3-662-04931-0

Unrau, A., Becker, G., Spinelli, R., Lazdina, D., Magagnotti, N., Nicolescu, V. N., et al. (2018). *Coppice Forests in Europe*. Freiburg: Albert Ludwig University of Freiburg.

van der Werf, G. W., Sass-Klaassen, U. G. W., and Mohren, G. M. J. (2007). The impact of the 2003 summer drought on the intra-annual growth pattern of beech (Fagus sylvatica L.) and oak (Quercus robur L.) on a dry site in the Netherlands. *Dendrochronologia.* 25, 103–112. doi: 10.1016/j.dendro.2007.03.004

von Arx, G., and Carrer, M. (2014). ROXAS - A new tool to build centuries-long tracheid-lumen chronologies in conifers. *Dendrochronologia* 32, 290–293. doi: 10.1016/j.dendro.2013.12.001

von Arx, G., Archer, S. R., and Hughes, M. K. (2012). Long-term functional plasticity in plant hydraulic architecture in response to supplemental moisture. *Ann. Bot.* 109, 1091–1100. doi: 10.1093/aob/mcs030

von Arx, G., Crivellaro, A., Prendin, A. L., Cufar, K., and Carrer, M. (2016). Quantitative wood anatomy-practical guidelines. *Front. Plant Sci.* 7:781. doi: 10.3389/fpls.2016.00781

von Arx, G., Kueffer, C., and Fonti, P. (2013). Quantifying plasticity in vessel grouping - added value from the image analysis tool ROXAS. *IAWA J.* 34, 433–445. doi: 10.1163/22941932-00000035

Walthert, L., Ganthaler, A., Mayr, S., Saurer, M., Waldner, P., Walser, M., et al. (2021). From the comfort zone to crown dieback: sequence of physiological stress thresholds in mature European beech trees across progressive drought. *Sci. Total Environ.* 753:141792. doi: 10.1016/j.scitotenv.2020.141792

Wickham, H. (2009). *ggplot2: Elegant Graphics for Data Analysis*. Berlin: Springer. doi: 10.1007/978-0-387-98141-3

Wigley, T. M. L., Briffa, K. R., and Jones, P. D. (1984). On the average value of correlated time series, with applications in dendroclimatology and hydrometeorology. *J. Clim. Appl. Meteorol.* 23, 201–213. doi: 10.1175/1520-0450(1984)023<0201:OTAVOC>2.0.CO;2

Wortemann, R., Herbette, S., Barigah, T. S., Fumanal, B., Alia, R., Ducousso, A., et al. (2011). Genotypic variability and phenotypic plasticity of cavitation resistance in Fagus sylvatica L. across Europe. *Tree Physiol.* 31, 1175–1182. doi: 10.1093/treephys/tpr101

Zellweger, F., De Frenne, P., Lenoir, J., Vangansbeke, P., Verheyen, K., Bernhardt-Romermann, M., et al. (2020). Forest microclimate dynamics drive plant responses to warming. *Science* 368, 772–775. doi: 10.1126/science.aba6880

Zimmermann, J., Hauck, M., Dulamsuren, C., and Leuschner, C. (2015). Climate warming-related growth decline affects Fagus sylvatica, but not other broad-leaved tree species in central European mixed forests. *Ecosystems* 18, 560–572. doi: 10.1007/s10021-015-9849-x

Zweifel, R., Etzold, S., Sterck, F., Gessler, A., Anfodillo, T., Mencuccini, M., et al. (2020). Determinants of legacy effects in pine trees - implications from an irrigation-stop experiment. *New Phytol.* 227, 1081–1096.

Conflict of Interest: The authors declare that the research was conducted in the absence of any commercial or financial relationships that could be construed as a potential conflict of interest.

frontiers | Frontiers in Plant Science

ORIGINAL RESEARCH
published: 29 April 2022
doi: 10.3389/fpls.2022.795941

Effects of Provenance, Growing Site, and Growth on *Quercus robur* Wood Anatomy and Density in a 12-Year-Old Provenance Trial

Peter Hietz[1], Kanin Rungwattana[1,2], Susanne Scheffknecht[1] and Jan-Peter George[3,4]*

[1] Department of Integrative Biology and Biodiversity Research, Institute of Botany, University of Natural Resources and Life Sciences, Vienna, Austria, [2] Department of Botany, Faculty of Science, Kasetsart University, Bangkok, Thailand, [3] Department of Forest Genetics, Federal Research and Training Centre for Forests, Natural Hazards and Landscape, Vienna, Austria, [4] Faculty of Science and Technology, University of Tartu, Tartu, Estonia

OPEN ACCESS

Edited by:
Georg von Arx,
Swiss Federal Institute for Forest, Snow and Landscape Research (WSL), Switzerland

Reviewed by:
Stefan Klesse,
Swiss Federal Institute for Forest, Snow and Landscape Research (WSL), Switzerland
Jan Tumajer,
University of Greifswald, Germany

***Correspondence:**
Peter Hietz
peter.hietz@boku.ac.at

Specialty section:
This article was submitted to Functional Plant Ecology, a section of the journal Frontiers in Plant Science

Received: 15 October 2021
Accepted: 22 March 2022
Published: 29 April 2022

Citation:
Hietz P, Rungwattana K, Scheffknecht S and George J-P (2022) Effects of Provenance, Growing Site, and Growth on Quercus robur Wood Anatomy and Density in a 12-Year-Old Provenance Trial. Front. Plant Sci. 13:795941. doi: 10.3389/fpls.2022.795941

Vessels are responsible for an efficient and safe water transport in angiosperm xylem. Whereas large vessels efficiently conduct the bulk of water, small vessels might be important under drought stress or after winter when large vessels are embolized. Wood anatomy can adjust to the environment by plastic adaptation, but is also modified by genetic selection, which can be driven by climate or other factors. To distinguish between plastic and genetic components on wood anatomy, we used a *Quercus robur* trial where trees from ten Central European provenances were planted in three locations in Austria along a rainfall gradient. Because wood anatomy also adjusts to tree size and in ring-porous species, the vessel size depends on the amount of latewood and thereby ring width, we included tree size and ring width in the analysis. We found that the trees' provenance had a significant effect on average vessel area (VA), theoretical specific hydraulic conductivity (Ks), and the vessel fraction (VF), but correlations with annual rainfall of provenances were at best weak. The trial site had a strong effect on growth (ring width, RW), which increased from the driest to the wettest site and wood density (WD), which increased from wet to dry sites. Significant site x provenance interactions were seen only for WD. Surprisingly, the drier site had higher VA, higher VF, and higher Ks. This, however, is mainly a result of greater RW and thus a greater proportion of latewood in the wetter forest. The average size of vessels > 70 μm diameter increased with rainfall. We argue that Ks, which is measured per cross-sectional area, is not an ideal parameter to compare the capacity of ring-porous trees to supply leaves with water. Small vessels (<70 μm) on average contributed only 1.4% to Ks, and we found no evidence that their number or size was adaptive to aridity. RW and tree size had strong effect on all vessel parameters, likely *via* the greater proportion of latewood in wide rings. This should be accounted for when searching for wood anatomical adaptations to the environment.

Keywords: provenance trial, *Quercus robur*, wood anatomical traits, climate effect, vessel size distribution

INTRODUCTION

Wood is responsible for the mechanical stability of trees, for water transport, and for storage and production of metabolites (Hacke and Sperry, 2001; Chave et al., 2009; Morris et al., 2016). In angiosperms, these functions are mainly mediated by fibers, vessels, and living axial and radial parenchyma, respectively. To ensure that a sufficient amount of water is supplied to the transpiring leaves, vessels need to transport the water efficiently. This requires a sufficiently high hydraulic conductance, which is mainly achieved by large vessels and to a lesser degree by vessel density (Tyree and Zimmermann, 2002). At the same time, water transport under high tension needs to avoid the formation of gas emboli and the consequent blockage of the water transport pathway (Tyree and Sperry, 1989). While the anatomical basis for efficient water transport is mainly wide vessel lumina but also the resistance of the cell walls to water passage (Sperry et al., 2005), embolism resistance is mainly a function of the fine structure of the cell walls and particularly the pit membranes connecting adjacent vessels (Delzon et al., 2010; Lens et al., 2011). Although frequently proposed, at least at the inter-specific level, the trade-off between efficiency and safety of plant water transport is quite weak as shown by a global review of data (Gleason et al., 2015). According to the air-seeding hypothesis (Tyree and Sperry, 1989) of embolism formation under drought stress, which is the model best supported by experimental evidence, vessels will embolize when the pressure difference between a gas-filled and a water-filled element is high enough to suck gas through the largest pore in the pit membrane. As the size of these pores is quite variable, the larger vessels with more pit membranes will likely have a larger maximum pore size and thus cavitate at a higher water potential (rare pit hypothesis, Christman et al., 2009, 2012). Therefore, within one species or stem, larger vessels tend to embolize earlier (Jacobsen et al., 2019; Lemaire et al., 2021) and wood with smaller vessels should be more cavitation resistant.

Emboli can are also be formed by freeze-thaw events (Mayr and Améglio, 2016). Gas is hardly soluble in ice and forms bubbles when water freezes. Upon thawing, these bubbles may either dissolve in water, or coalesce and expand, resulting in emboli. The formation of freezing-induced emboli is more likely if water potential is low, which expands the bubbles, and when vessels are large, in which case many bubbles are released that can coalesce into larger ones that will not easily dissolve. As a consequence, species with larger conduit diameters will become more easily embolized following freezing under moderate drought stress. Experiments confirmed predictions that cavitations will occur in vessels with a diameter greater than c. 44 μm under a moderate xylem tension of 0.5 MPa (Davis et al., 1999). Thus, ring-porous trees that have their earlywood macropores embolized after winter and cannot reverse the emboli need to produce new wood before water can be transported to the new leaves (Hacke and Sauter, 1996).

Tree ring research and dendroclimatology mostly rely on ring width, often separating early- and latewood (Schweingruber, 2007). Wood anatomical parameters may yield additional information on past climates or the impact of climate as cell size and numbers might respond more flexibly to variation in temperature and water supply. For instance, conifer ray parenchyma was shown to carry a rainfall signal, although the correlation among trees and the signal-to-noise ratio of the parenchyma was much lower than for ring width (Olano et al., 2013).

More commonly than parenchyma, vessel size and density are measured to support tree ring research (Fonti et al., 2010; Souto-Herrero et al., 2017) and to study hydraulic adaptations of trees (Hietz et al., 2017; Gouveia Fontes et al., 2020). Large vessels of macroporous and ring-porous temperate trees are attractive to study because they are relatively easy to measure in an automated way (Fonti et al., 2009) and they also account for the bulk of water transport capacity. Thus, large vessels (defined as $> 10{,}000\ \mu m^2$) were found to provide an additional signal for spring precipitation in *Quercus petraea* and *Q. pubescens* in Switzerland (Fonti and García-González, 2008). Another study, using a vessel size threshold of $>2{,}500\ \mu m^2$, found that vessel size was related to the previous year wet season in *Quercus boissieri* but to the current wet season in in *Q. ithaburensis* (Castagneri et al., 2017).

It is important to note, however, that short-term adjustments to drought or the effects of drought periods on wood formation are not necessarily the same as growing in arid regions. While inter-annual variation in wood structure is the basis of dendroclimatology, it does not provide a perfect prediction of the effect of long-term changes in climate or of how a genotype would fare in a different environment. Other studies therefore looked at vessel size in trees growing in different environments or originating from different regions and growing in the same environment to identify phenotypic (plastic) and genetic adaptations. For instance, a provenance trial of rubber trees (*Hevea brasiliensis*) found that vessel density and vessel lumen fraction (the proportion of the cross-sectional area covered by vessel lumina) were related to the amount of rainfall in the dry season from the region in Brazil where the genotypes were collected, but vessel size was not (Rungwattana et al., 2018). While that study tested for genetic adaptations, variation observed between trees growing in different environments may result from genetic and/or phenotypic variation. Thus, the significant correlation of *Fagus sylvatica* vessel size with mean annual precipitation at five sites (Schuldt et al., 2016) may have resulted from genetic or phenotypic effects or both.

If large vessels are responsible for the bulk of hydraulic conductance, particularly in ring-porous species such as *Quercus* with very large differences in vessel size, this raises the question what small vessels are for. With a trade-off between efficiency and vulnerability at the level of individual vessels, micropores could provide for a minimum conductance when large vessels have become embolized. If this is indeed a relevant function of micropores, we would expect to see a higher proportion of small vessels in trees adapted to lower water availability. However, with macropores mainly in earlywood and micropores mainly in latewood, the mean vessel size and the vessel size distribution will also depend on the relative areas of early- and latewood and thus on ring width. Therefore, growth rates, which are strongly affected by factors such as water supply, may blur possible

adaptive changes in vessel sizes unless the effects of growth rate or ring width are accounted for.

We here used a *Quercus robur* trial with trees from ten provenances from central Europe planted at three sites in Austria. A previous analysis focusing on growth found strong local adaptation in growth so that trees grow best in climates similar to those the seeds were collected from George et al. (2020). In that study, we found that wood anatomical parameters were more controlled by provenance than site, but there was no clear correlation with climate at the provenance location. However, that study did not explore vessel size variation and the relationship with tree size and growth. Having manually marked large as well as small vessels, we here test to what extent vessel size and vessel size distribution are controlled by genetics and environment. We ask how much small vessels likely contribute to water transport and if small vessels and vessel size distribution reflect genetic and plastic adaptations and tree size. If wood anatomical variation can be explained by variations of tree size and growth rates alone, this would question the common interpretation as evidence adaptive significance.

MATERIALS AND METHODS

Quercus robur seedlings of 20 provenances from Austria, Czech Republic, Croatia, and Slovenia were planted at three trial sites in Austria (**Table 1**) in 2006. Trees were planted as 1-year-old seedlings with a distance of 1 m × 2 m on flat terrain. We selected ten provenances that differ mainly in rainfall and less in temperature (**Table 1**) because the purpose of our study was to look for the effects of aridity. Similarly, trial sites differed mainly in rainfall with mean annual precipitation for the three trial sites (MAPs, 641, 890, and 1,005 mm, respectively), similar to the precipitation gradient, the provenances were collected from (MAPp). By contrast, mean annual temperature varied less among provenances (MATp) and very little among trial sites (MATs). MAT and MAP for provenances and testing sites were derived from the EURO-CORDEX climate dataset (Jacob et al., 2014). For each provenance and site, 110 trees were established with 5 half-siblings from each of 22 mother trees planted in a randomized block design with each provenance replicated three times per site and with each mother tree represented five times in each cell [see George et al. (2020) for details]. We randomly selected trees from nine different mother trees from each of the ten provenances at each site (90 trees per site). Trees originating from the same mother trees (half-siblings) were replicated among, but not within sites.

TABLE 1 | Provenances in central Europe and trial sites in Austria for a *Quercus robur* study.

	Code	Country	Latitude (°N)	Longitude (°E)	MAT (°C)	MAP (mm/year)
Provenance						
Geinberg	1	AT	48.277	13.307	8.7	1066
Linz	2	AT	48.326	14.294	9.2	841
Braunsberger Wald	6	AT	48.473	16.333	9.1	638
Rainfeld	8	AT	48.042	15.732	7.4	785
Luising	12	AT	47.023	16.477	9.7	696
Klagenfurt	14	AT	46.630	14.350	8.0	988
Hluboka	17	CZ	49.090	14.444	7.4	764
Kutina	18	HR	45.433	16.683	10.9	915
Murska suma	19	SLO	46.498	16.511	10.1	810
Velika Gorica	21	HR	45.674	16.161	10.5	920
Trial sites						
Weyerburg	Dry	AT	48.557	16.171	8.8	641
Wels	Interm.	AT	48.185	13.989	8.5	890
Weistrach	Wet	AT	48.053	14.563	8.4	1005

In winter 2017–18, wood samples were collected at breast height, taking care to avoid irregular growth, from nine trees per provenance and site using a 5.15-mm diameter increment borer. Samples covering at least the last 3 years were sealed in plastic straws in the field and measured for wood density (WD) in the laboratory within 30 h.

Wood density of each sample was calculated as dry weight (100°C)/fresh volume, with volume calculated from the diameter (5.15 mm) and the length of the sample, the inner end of which was trimmed with a sharp blade, the outer end being the cambium. We prefer this method of measuring the volume to the water displacement method because with the latter, the volume can be affected by variable swelling of wood after cores are extracted (Schüller et al., 2013). We made 30-μm transverse sections covering the width of the core and the last three growth rings with a rotary microtome (Leica, Wetzlar, Germany), stained with safranin and astrablue, and embedded in Euparal (Carl Roth, Karlsruhe, Germany). Digital images (example in **Figure 1**) with pixel size of 1.157 μm were taken with a DM5500B microscope (Leica, Wetzlar, Germany). The outline of the three outer growth rings (representing years 2015–2017) and all vessels were marked manually in Adobe Photoshop CS6 (Adobe Systems, San José, USA), using the flood-fill feature of Photoshop to mark vessels. Marking vessels manually is more time-consuming than automated vessel detection based on the cell size and shape (e.g., Von Arx and Dietz, 2005), but we found this more reliable to distinguish small vessels from parenchyma. The marked vessels and the growth ring outlines were then measured automatically with ImageJ,[1] so that all vessels were allocated to the precise year. Ring width was measured as the distance between ring boundaries along the rays. We calculated mean vessel area (VA, mm^2), vessel density (VD, vessels mm^{-2}), vessel lumen fraction (VF, the sum of vessel lumina per cross-sectional area), the coefficient of variation of vessel size (Vcv), and the mean area macropores (VAmp, defined as vessels with diameters > 70 μm). Since large vessels are more efficient in water transport while small vessels may be more resistant against emboli (Jacobsen et al., 2019), vessel size variation would indicate how these two demands shape vessel sizes.

Data Analysis

We calculated the theoretical specific hydraulic conductivity (Ks), based on the Hagen–Poiseuille law

[1] imagej.nih.gov/ij

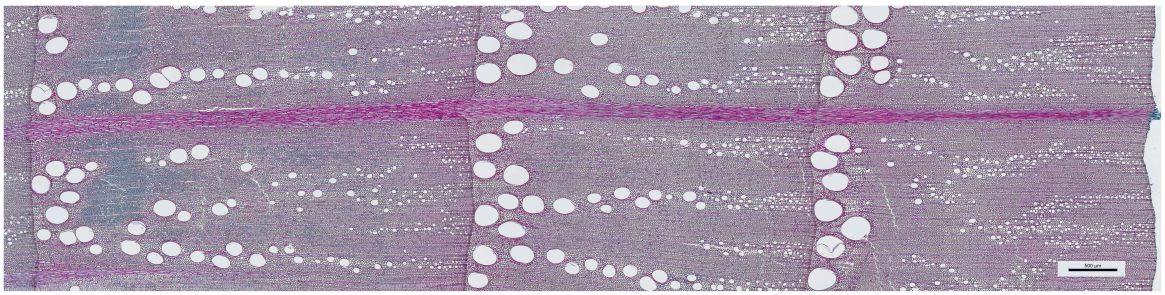

FIGURE 1 | *Quercus robur* wood (the example is from a tree from provenance Geinberg growing at site Wels) showing growth rings for 2015–2017. The scale bar measures 500 μm.

(Tyree and Zimmermann, 2002) as $Ks = (\pi \rho w/128 \eta) \times VD \times Dh^4$, where ρw is the density of water (998.2 kg/m^3 at 20°C), η the viscosity of water (1.002×10^{-3} Pa s at 20°C), VD vessel density (m^{-2}), and $Dh = (\Sigma\ D^4/n)^{1/4}$, where D is the average of minor and major axes of the diameter of each individual vessels and n the number of measured vessels. All anatomical parameters were calculated per sample and per annual ring for each sample, and these sample or annual ring-wise data were used for statistical analyses.

Vessel size distribution showed a bi-modal distribution with the lowest density for vessels with 70 μm diameter, which held true for all provenances and sites (**Figure 2**). We thus defined vessels < 70 μm as micropores and vessels > 70 μm as macropores and calculated the fraction of vessel area occupied by macropores (p_{macro}) and the proportion of Ks contributed by micropores (Ks_{micro}). While large vessels are concentrated in earlywood and small vessels in latewood in most ring-porous trees such as *Q. robur*, this is not always the case and we therefore do not attempt to classify early- and latewood.

We then calculated pairwise correlations between all wood traits. To assess the coordination among wood traits and the dominant trait axes, we calculated a principal component analysis (PCA, using R libraries prcomp for calculation and factoextra for visualization) of traits and provenance climate with trait values per sample scaled to mean = 0 and unit variance.

Trees widen conduits to adjust to increasing path length (Anfodillo et al., 2006), so tree height might be a better predictor of conduit size than diameter. Since height was measured only in 1 year and correlates strongly with diameter at breast height (DBH, **Supplementary Figure 1**), we use DBH as a measure of tree size. We calculated linear models to test whether wood anatomical traits were controlled by provenance, site, provenance × site interactions, or tree size of the form

$$trait_{ijk} \sim provenance_j \times site_k + DBH_{ijk} + \varepsilon_{ijk} \quad (1)$$

where "$trait_{ijk}$" is the trait value per tree i (i.e., covering all years analyzed) from provenance j at site k and ε is the error term. Since wood anatomy frequently changes as trees grow or from pith to cambium in wood cores (Lachenbruch et al., 2011; Rungwattana and Hietz, 2018) and trees had grown at different rates, DBH was included in the model, so that potential differences in wood anatomy among sites or provenances would be independent of trees having grown at different rates. While this tests for the effect of provenance, it does not test whether the provenance effect is caused by differences in MAPp, and we therefore calculated a similar model with MAPp instead of provenance with models of the form

$$trait_{ijk} \sim MAPp_j \times site_k + DBH_{ijk} + \varepsilon_{ijk} \quad (2)$$

where $MAPp_j$ is the MAP at provenance j. To test whether diameter increment or precipitation in any year affect wood traits, we calculated mixed effect models (R library lme4, Bates and Sarkar, 2020) with site, provenance, DBH, ring width, and precipitation (prec) during the growth year at the three sites as fixed and treeID and year nested in site as random variables. Models were thus of the form:

$$trait_{ijky} \sim provenance_j \times site_k + prec_{ky} + ring\,width_{ijky} + DBH_{ijky} + (1|treeID_{ijk}) + (1|site_k/year_y) + \varepsilon_{ijky} \quad (3)$$

where "$trait_{ijky}$" is the value per tree i from provenance j at site k and annual growth ring y, $prec_{ky}$ is the precipitation at site k in the year y, and ring width and DBH are also per year y. For the annual model, DBH for 2016 was estimated as DBH − 2 × ring width of 2017 and DBH_{2015} likewise by subtracting growth of 2016 and 2017. TreeID was treated as a random variable because there were three measurements per tree, and precipitation to avoid pseudo-replication of precipitation, for which data could only be included for three sites and 3 years. While ring width and DBH were correlated, the correlation was not very high (r^2 = 0.27) and the variance inflation factor for ring width and DBH is <2, so the collinearity is not a problem for the model, and we can distinguish the effects of tree size and ring width. Precipitation for 2015, 2016, and 2017 was the total rainfall from October of the previous to September of the current year. Precipitation for the three trial sites was obtained from the closest weather station by the Zentralanstalt für Meteorologie und Geodynamik.[2]

VA, VD, VF, Ks, p_{macro}, and Ks_{micro} were log-transformed for statistical analyses to improve normality of the distribution based

[2]www.zamg.ac.at

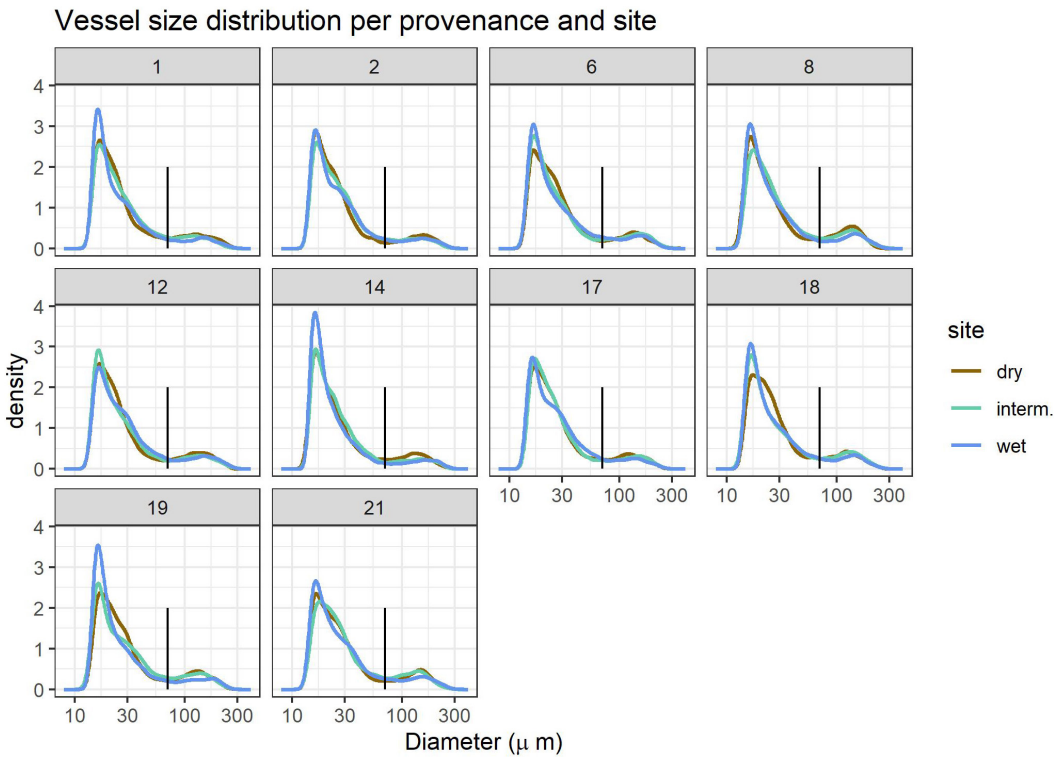

FIGURE 2 | Vessel size distribution per provenance 1–21 (panels) and site (line colors). The vertical black line indicates the 70 μm size cutoff used to define small and large vessels. Kernel density estimates are relative units. Site details are shown in **Table 1**.

on the qqnorm plots. All statistical analyses were calculated with R 4.0.2 (R Core Team, 2020).

RESULTS

Vessel size distribution followed a similar pattern in all samples, but trees grown at the wettest site (WL) often had a higher proportion of very small (<20 μm) vessels (**Figure 2**). Growth and thus DBH and ring width were highest at the wet and lowest at the dry site (**Table 2**).

Mean vessel size (VA) was positively correlated with VF, Ks, and the proportion of large vessels and negatively with VD, Ks_{micro}, vessel size variation (Vcv), and DBH, but was not related to macropores size (VAmp, **Figure 3**). Ks is strongly controlled by VAmp and less by VA and VD, which is explained by the fact that Ks scales to the square of VA and the contribution of micropores (Ks_{micro}) is low. The proportion of Ks contributed by small vessels was small, on average 2% and never more than 10%. Ks_{micro} scaled negatively with Ks calculated form all vessels and with VA and VAmp. Relationships with WD were weak and significantly negative for VAmp, VD, Ks, and Vcv. While the VAmp, Ks, and Vcv increased with tree size, the average vessel size, the proportion of large vessels and WD decreased with DBH. Correlations between wood traits were similar among sites, though correlations between anatomical traits and WD were significantly only for the intermediate and wet, but not the dry site (**Supplementary Figure 2**).

VA, VF, WD, Ks, and p_{macro} decreased from the driest to the wettest site, while VAmp increased from the driest to the wettest site (**Table 2**). All vessel traits were explained to a larger extent by provenance (4.6–12.1% of the variance explained, Model 1) than by site (0.1–6.9%, **Table 3**). This contrasts with WD, which was explained strongly by site (30.7% explained) and was the only trait with significant provenance × site interactions. While overall WD is significantly negatively correlated with tree size, this is entirely due to a site effect and within site WD did not depend on tree size: Trees at the drier site were smaller and had higher WD. Within any site, WD and DBH were not correlated ($p > 0.05$, **Figure 4A**), but WD was related to VF at two sites (**Figure 4B**).

When the model included site and provenance, tree size did not affect VA, VD, and VF, but had a strong effect on maximum vessel size and consequently on Ks, Vcv, the proportion of macropores and Ks_{micro} (7.7–23.9% explained, **Table 3**). Model 2 with MAPp instead of provenance (**Supplementary Table 1**) shows that only a small part of the provenance effect can be explained by the differences in rainfall. Including DBH and site, MAPp was only marginally significantly related to VA, VF, and Vcv, and for none of these explained more than 1.5% of the variation.

When wood anatomy was analyzed year-wise with ring width and tree size included in the model (Model 3),

TABLE 2 | Mean (SD) of wood anatomical parameters, wood density and tree size per site and provenance.

Trait	VA	maxVA	Vcv	VD	VF	Ks	p.macro	Ks.micro	WD	DBH
Unit	μm^2	μm^2		mm^{-1}		$kg\ m^{-1}\ MPa^{-1}\ s^{-1}$	%	%	$g\ cm^{-3}$	cm
Site										
Dry	2734 (794)	15453 (3154)	2.31 (0.40)	46.6 (9.7)	0.124 (0.031)	96 (40)	84.2 (5.7)	1.3 (1.0)	0.61 (0.05)	4.50 (1.05)
Interm.	2579 (617)	15753 (3351)	2.38 (0.43)	47.7 (12.4)	0.119 (0.029)	94 (39)	82.5 (4.5)	1.5 (0.7)	0.57 (0.02)	4.96 (1.24)
Wet	2498 (771)	16981 (3128)	2.60 (0.51)	47.1 (13.9)	0.110 (0.021)	93 (33)	81.3 (5.3)	1.4 (0.7)	0.56 (0.02)	6.68 (1.55)
Provenance										
1	2454 (610)	15921 (3208)	2.53 (0.44)	45.3 (7.3)	0.109 (0.023)	89 (36)	81.7 (4.8)	1.5 (0.7)	0.56 (0.02)	5.56 (1.48)
2	2367 (498)	17097 (3261)	2.62 (0.44)	49.7 (11.1)	0.115 (0.021)	95 (29)	81.3 (4.4)	1.4 (0.8)	0.58 (0.03)	5.99 (1.67)
6	2743 (754)	16276 (2579)	2.42 (0.48)	48.9 (16.7)	0.126 (0.034)	106 (48)	83.4 (5.6)	1.2 (0.6)	0.58 (0.04)	5.24 (1.37)
8	2820 (885)	15182 (2451)	2.25 (0.46)	41.4 (12.1)	0.110 (0.024)	81 (23)	84.5 (5.7)	1.2 (0.6)	0.58 (0.03)	4.85 (1.45)
12	2882 (949)	16699 (3557)	2.40 (0.51)	48.0 (13.2)	0.130 (0.027)	111 (39)	84.3 (4.6)	1.1 (0.5)	0.58 (0.05)	5.89 (1.73)
14	2475 (781)	17619 (3878)	2.65 (0.51)	51.0 (14.9)	0.120 (0.032)	104 (41)	82.5 (5.8)	1.2 (0.7)	0.59 (0.06)	5.74 (1.74)
17	2292 (584)	15511 (2848)	2.49 (0.32)	46.0 (8.9)	0.102 (0.018)	77 (26)	80.1 (5.7)	1.7 (1.2)	0.57 (0.03)	5.24 (1.29)
18	2457 (624)	14866 (3483)	2.34 (0.46)	46.1 (9.3)	0.110 (0.024)	79 (28)	81.4 (5.5)	1.8 (1.2)	0.58 (0.04)	5.04 (1.41)
19	2788 (835)	15384 (2814)	2.29 (0.44)	48.1 (14.0)	0.126 (0.027)	96 (32)	83.7 (5.0)	1.4 (0.8)	0.59 (0.07)	5.11 (1.45)
21	2760 (505)	16068 (3725)	2.29 (0.42)	46.9 (9.2)	0.130 (0.032)	105 (49)	83.7 (4.6)	1.4 (0.8)	0.57 (0.04)	5.18 (2.05)

VA, mean vessel area; VAmp, mean area of macropores (vessels with diameter > 70 μm); VD, vessel density per cross-sectional area; VF, vessel lumen fraction; Ks, theoretical hydraulic conductivity; p_{macro}, fraction of vessel area occupied by vessels with diameter > 70 μm; Ks_{micro}, proportion of hydraulic conductivity contributed by vessels < 70 μm diameter; Vcv, coefficient of variation of vessel area; WD, wood density; DBH, diameter at breast height.

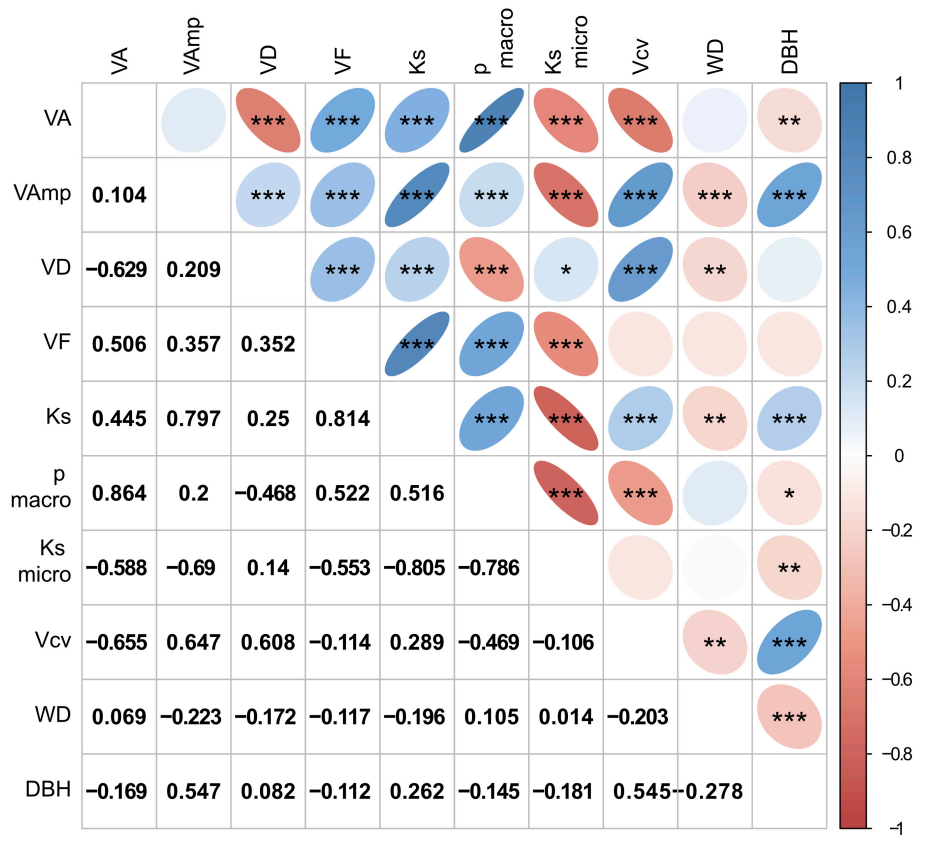

FIGURE 3 | Correlation matrix of wood traits and tree size (DBH). Size and color intensity indicate strength of positive or negative correlations, blue for positive and red for negative correlations. Trait abbreviations as in **Table 2**. Significances in the upper triangle are indicated as $^*p < 0.05$, $^{**}p < 0.01$, $^{***}p < 0.001$, the lower triangle shows *r*-values.

TABLE 3 | Significance of provenance, site, tree size (DBH), and provenance × site interactions on wood traits.

	p-values				Variance explained (%)				
	Prov.	Site	DBH	Prov. × Site	Prov.	Site	DBH	Prov. × Site	Residual
VA	0.014	0.075	0.122	0.874	7.7	1.9	0.9	4.1	85.5
VAmp	0.004	4.8E-04	1.4E-18	0.796	6.5	4.1	23.9	3.3	62.2
VD	0.197	0.891	0.211	0.681	4.6	0.1	0.6	5.5	89.2
VF	4.5E-05	0.007	0.636	0.117	12.1	3.2	0.1	8.2	76.4
Ks	0.001	0.911	2.0E-06	0.436	9.4	0.1	7.7	5.9	76.9
p.macro	6.5E-04	2.0E-05	9.9E-10	0.718	8.8	6.5	11.7	4.1	68.9
Ks.micro	0.019	0.013	1.6E-06	0.350	6.6	2.8	7.8	6.4	76.5
Vcv	3.2E-04	3.7E-06	2.9E-15	0.803	8.5	6.9	18.7	3.3	62.6
WD	0.136	8.5E-23	0.208	5.0E-05	3.3	30.7	0.4	13.2	52.5

Trait abbreviations as in ***Table 2****. Shading from light to dark yellow indicates increasing significance.*

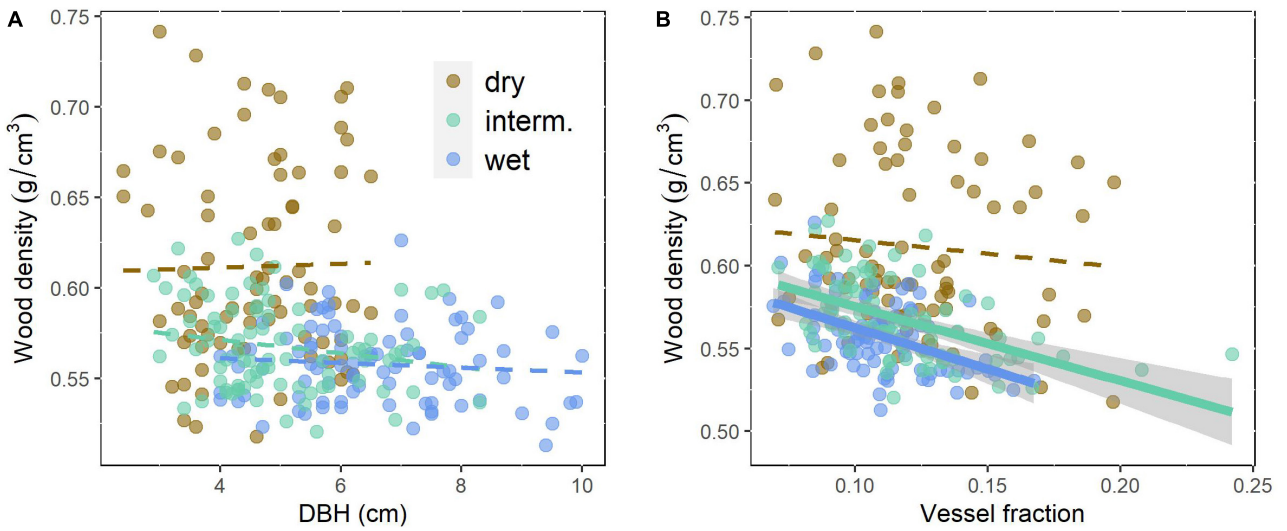

FIGURE 4 | Wood density related to **(A)** tree size (DBH) as a measure of growth rate of the even-aged trees and **(B)** vessel fraction of *Quercus robur* at three trial sites differing in rainfall. Continuous lines indicate significant ($p < 0.05$) correlations, broken lines non-significant relationships. Site details are shown in **Table 1**.

provenance still had significant effects on VD and VF and a marginally significant ($p < 0.1$) effect on p_{macro} and Ks_{micro}, but site effects were no longer significant and VF was the only parameter related to October–September precipitation (**Table 4a**). Ring width had a much stronger effect on nearly all wood traits, except for VAmp (**Table 4b**). Therefore, the site and to a large extent also the provenance effect in **Table 3** are largely the result of differences in ring widths.

In the PCA Ks, Ks_{micro}, p_{macro}, VA, and VF scale along the first axis, which explains 35.1% of the variation, whereas VAmp, VD, WD, and DBH scale mainly along the second axis (21.1%) (**Figure 5**). MAPp and MATp had a very weak loading on the first two principal components. Trial sites separated poorly in the PCA (**Figure 5A**), as did provenances (**Figure 5B**).

Mean VA, VD, Ks, and particularly VF significantly declined with ring width (**Figures 6A,C–E**). Macropore size and Ks_{micro} were not related to ring width at all (**Figures 6B,F**) and the relationship between p_{macro} and ring width weak (**Figure 6F**).

DISCUSSION

The effect of the environment on wood traits can be studied in various ways. Common garden experiments search for a genetic component in the variation by keeping the environmental variation constant. If this variation is related to a clinal gradient of their original locations, this trait variation may point to (but is not proof of) a potential genetic adaptation to a specific environmental factor. Experiments that expose different genotypes or provenances to different environments in a fully crossed design serve to quantitatively distinguish genetic from environmental effects. These experimental approaches are quite different from tree ring studies where inter- (and sometimes intra-) annual variations in climate are related to anatomical variation within individuals. This is ideal for dendroclimatology but does not study genetic adaptation (unless comparing different genotypes). It is also difficult to distinguish ontogenetic adaptations to short-term variations in the environment and direct or indirect effects of tree growth.

TABLE 4 | (a) Significance of provenance, site, tree size (DBH), ring width, and precipitation (Prec is the precipitation from October of the previous year to September in the year the wood was produced) on vessel traits. Shading from light to dark yellow indicates increasing significance. For metric variables, the estimate and standard error (SE) of the estimate are also shown. **(b)** Shows the variance explained (%). Trait abbreviations as in **Table 2**.

(a)	Prov.	Site	Site × Prov.	RW			DBH			Precip.		
				p	Est	SE	*p*	Est	SE	*p*	Est	SE
VA	0.026	0.238	0.931	5.0E-15	−0.084	1E-03	0.968	−0.001	0.010	0.071	0.0147	4E-04
VAmp	0.568	0.827	0.632	1.1E-05	−5E-04	−6E-06	5E-19	0.001	1E-04	0.402	0.0002	6E-06
VD	0.439	0.666	0.612	6.8E-06	−0.040	−5E-04	1.4E-04	0.054	0.009	0.291	0.0141	4E-04
VF	0.009	0.397	0.167	5.9E-57	−0.126	5E-04	6.0E-06	0.047	0.007	0.016	0.0103	2E-04
Ks	0.245	0.843	0.491	3.4E-30	−0.154	3E-04	3.0E-12	0.139	0.013	0.619	0.0192	5E-04
p.macro	0.079	0.219	0.809	2.1E-07	−0.015	3E-04	0.63790681	0.002	0.003	0.084	0.0039	1E-04
Ks.micro	0.099	0.482	0.537	9.6E-07	0.096	−4E-04	2.0E-06	−0.131	0.019	0.561	0.0270	7E-04

(b)	Prov.	Site	Site × Prov.	RW	DBH	Prec.	Residual
VA	4.1	0.8	2.1	13.5	0.0	1.1	80.5
VAmp	1.1	0.1	2.2	2.8	13.3	0.1	82.6
VD	1.6	0.2	2.8	3.7	2.7	0.3	91.6
VF	2.2	0.3	2.4	30.0	2.1	1.2	64.2
Ks	1.3	0.0	1.9	15.8	5.9	0.0	77.0
p.macro	5.1	1.1	4.1	8.9	0.1	1.5	83.4
Ks.micro	3.0	0.3	3.4	5.0	4.8	0.1	86.8

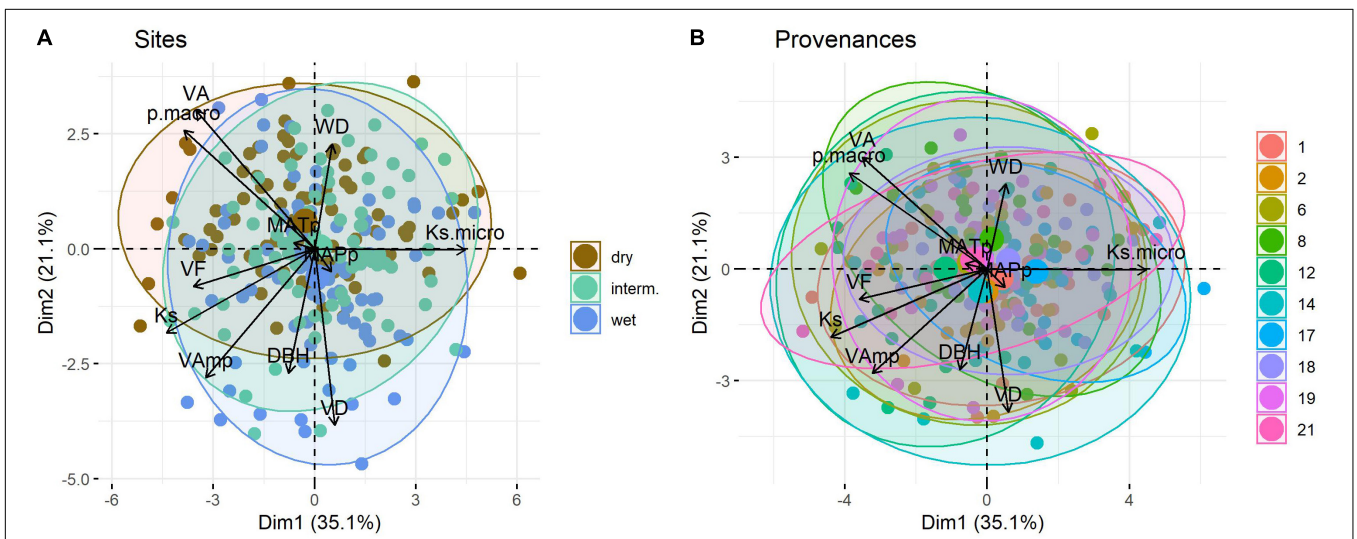

FIGURE 5 | Principal component analysis of wood traits of *Quercus robur* grown at three trial sites in Austria **(A)** and originating from ten provenances **(B)**. Large symbols represent the mean position of trees per trial site or provenance along PC1 and PC2. Ellipse defines the region that contains 95% of all samples per group. Provenances are detailed in **Table 1**, trait abbreviations as in **Table 2**.

Our dataset is from a fully crossed trial with ten provenance and three trial sites (**Table 1**). Trees were 12 years old, so the wood is juvenile wood and wood in older trees might respond differently. Although several *Quercus* provenance trials are conducted (Gea-Izquierdo et al., 2012; Torres-Ruiz et al., 2019; Bert et al., 2020) and macropore size variation of *Quercus* has been studied in several tree ring analyses (e.g., Fonti and García-González, 2008; Martínez-Sancho et al., 2017), we are not aware of comparable studies in neither mature nor juvenile oak. With only 3 years of annual growth rings, our study is not suited to study short-term environmental effects. However, we use ring width as a control variable to test to which extent variation in wood anatomy may be a passive effect of variation in growth, which is important to understand and discuss any adaptive significance of anatomical variation. This may be particularly relevant in ring-porous *Quercus* where earlywood and latewood differ substantially in anatomy and the proportion of latewood mostly increases with ring width (Vavrčík and Gryc, 2012). The selection of provenances and trial sites for this study was designed to test for the effect of water supply on *Quercus* anatomy, and we had therefore chosen sites with a substantial rainfall gradient, but with a small temperature gradient.

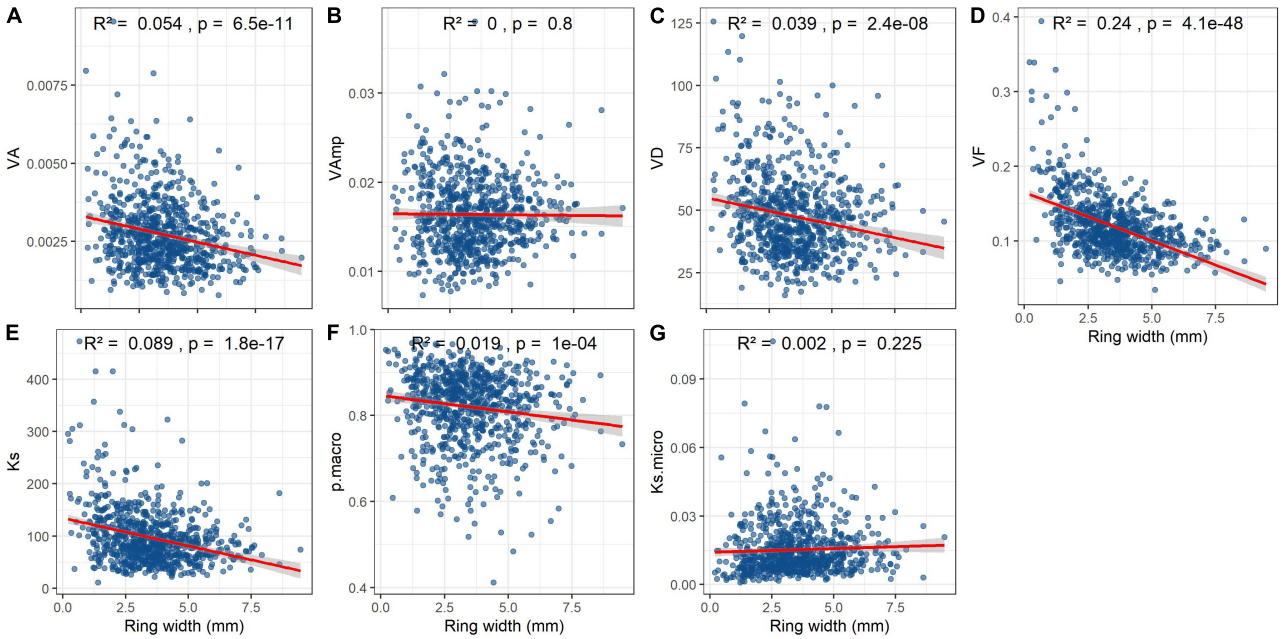

FIGURE 6 | Effect of annual ring width on vessel parameters and hydraulic conductivity in *Quercus robur* wood. Trait abbreviations as in **Table 2**. Note that Ks is the theoretical hydraulic conductivity per cross-sectional area, whereas Ks_{micro} is the proportion of Ks that is contributed by vessels <70 μm. R^2 and *p*-values are from linear regressions.

Overall, vessel traits were strongly correlated (**Figure 3**). This is to be expected given the strong correlation between VD and VA commonly observed across (Zanne et al., 2010) but also within species (Rungwattana and Hietz, 2018) and the fact that the other anatomical traits are in one way or another derived from VA and VD. WD, while correlating significantly with several anatomical parameters never explained more than 5% (for VAmp) of their variation.

Wood Density Variation

The control of the intra-specific variation in WD, which is of substantial practical importance for the timber industry, has been extensively studied (Zobel and van Buijtenen, 1989). WD variation is relatively well-understood and studies have shown a significant inheritance (Zobel and Jett, 1995). By contrast, we found the site effect (explaining 30.7% of the variation) much higher than the provenance effect, with significant site × provenance interaction (**Table 3**). Ring-porous trees including *Quercus robur* and *Q. petraea* (Zhang et al., 1993) tend to have higher WD when they are growing fast. In these trees, the thickness of earlywood, with large vessels and low density, is less variable, when growth rates are high more latewood with small vessels and high WD is added (Saranpää, 2003). This was not reported in all studies and site conditions may or may not additionally affect WD (Zobel and van Buijtenen, 1989 and many older studies cited therein). If WD was controlled by the early wood or late wood ratio and late wood had higher WD, WD should scale positively with growth rates. Surprisingly, we found WD to be negatively correlated with tree size, but this was entirely a site effect with trees at the drier site being smaller and having higher WD. Within any of the three sites, there was no correlation (**Figure 4A**). WD will be affected by vessel lumen fraction because lumina, unless filled with extractives, effectively have a density of 0. VF did explain a substantial part of the variation in WD in the intermediate and wet sites (**Figure 4B**), but not in the dry site and does not explain the difference in WD between sites. In many tree species, WD increases or less commonly decreases with tree size (Hietz et al., 2013), the latter has been observed in *Quercus* (Zhang et al., 1993). Other studies suggest that some size-related changes in wood characteristics may actually be controlled by cambial age rather than tree size (Lachenbruch et al., 2011). None of this can explain the variation between sites observed as all trees were of the same age and WD was higher in the dry site independent of tree size (**Figure 4A**). Most studies that looked into the anatomical basis of WD variation found that this is mostly achieved by the variation in fibers and particularly fiber wall thickness (Martínez-Cabrera et al., 2009; Ziemińska et al., 2014). High WD and fibers are clearly important for the mechanical strength of wood, and across species, WD explains c. 80% of the variation in various measures of mechanical strength (Niklas and Spatz, 2010). However, there is no obvious explanation as to why trees in drier sites would need to be mechanically stronger.

Alternatively, WD may be related to drought tolerance, whether in some way affecting cavitation resistance or otherwise. Some studies found a moderately significant link between WD and cavitation resistance (Awad et al., 2010; Fichot et al., 2010; Guet et al., 2015) within species. Many studies have also reported higher WD in dry regions, although across species aridity explains only a small part in the variation of WD

(Ibanez et al., 2017). Lacking an alternative explanation for the variation of WD, our study lends cautious support to the idea that high WD is an adaptation to drought. However, we note that this variation is explained by plastic and not by genetic adaptation, which means that selecting drought-tolerant individuals or provenances based on the WD from the provenance site is not a workable strategy.

Wood Anatomical Variation

The control of WD contrasts with wood anatomical parameters, which were primarily under provenance (i.e., genetic) control with less site effects and none for Ks (**Tables 3**, **4**). Interestingly, tree size, which has been shown to affect wood anatomical parameters, had no significant effect on mean VA, VD, and VF, but does affect macropores and consequently Ks and parameters related to vessel size variation (**Table 3**). The importance of tree size on wood structure is well-known, and more recent studies are including this effect in studies that try to understand the adaptive value of wood anatomy (Hietz et al., 2017; Rosell et al., 2017). Accounting for tree size, we found significant site and/or provenance effects on most measures. However, studying the annual resolution and including ring width and tree size, site effects completely disappear and provenance effects are weaker. This suggests that site and to a large extent provenance effects mainly result from the effects on growth and thus ring width. Except for VAmp, also the tree size effect is largely the result of variations in ring width (**Table 4** and **Figure 6**), likely through the variation in the proportions of earlywood and latewood. Ring-porous trees such as *Quercus robur* show strong differences in wood anatomy between early- and latewood, the proportion of which is affected by ring width. We expect that the dominant effect of ring width or growth rates seen here will be less in diffuse-porous species and perhaps absent in tropical trees that have less annual variation in wood structure.

When tree size and ring width are included, only VF was significantly related to rainfall (**Table 4**). Since this analysis relates wood parameters to rainfall at the trial sites in the year the wood was produced plus rain since the previous October, we are here testing for plastic adaptations. We are aware that this analysis is less than ideal as there are only 9 years (3 years at three trial sites) to test, for which reason we refrain from testing for effects of rainfall in individual months or seasonal climate variation as is common in dendroclimatological studies.

Average VA and Ks (though not VAmp) were greater in trees growing in the drier sites. This appears surprising given that these trees are smaller and thus need to supply fewer leaves and may have less water available to transport. Similarly, Pérez-de-Lis et al. (2018) found larger vessels in *Q. robur* and *Q. pyrenaica* from drier regions and speculate about the potential benefit of high hydraulic conductivity in trees from seasonal climates. However, using Ks here is misleading. In oaks as in other ring-porous trees, only the outermost ring(s) typically conduct water (Poyatos et al., 2007). The capacity of a stem to transport water is the hydraulic conductivity (Ks) times the conductive area. Therefore, if the same number of outer rings contributes to water transport, the potential conductance should be approximately proportional to conductivity x ring width. Average ring width was greater in the wet (4.3 mm) than in intermediate (3.3) and dry (2.8) site, thus the hydraulic conductance of the whole stem is likely greater in the wetter site and speculations about the advantage of high conductivity in dry sites are unfounded. Similarly, the larger mean vessel areas at the dry site can be explained by the fact that the thinner annual growth rings had proportionally less latewood and thus a greater proportion of macropores (**Table 2**).

Various hydraulic traits including xylem vulnerability to cavitation, leaf turgor loss point, and osmotic potential (Pfautsch et al., 2016; Li et al., 2018; Kunert et al., 2021) have been shown to correlate with indices of aridity across species, sampled at their natural environment or a common garden. Within species, the trait variation is generally smaller and their climatic range is more limited, so finding significant trends is more challenging. Indeed, there are few studies, at least for hardwoods, directly addressing adaptations of intra-species variation in wood anatomy. Hajek et al. (2016) found vessel diameter (but not VD) of *Fagus sylvatica* grown in a common garden and originating from ten locations across Europe significantly related to the forest aridity index at their place of origin. However, in their dataset, the correlation with mean annual temperature was almost as high and no attempt was made to distinguish between adaptations to temperature vs. aridity. Another study found that the xylem was more resistant to cavitation in Mediterranean compared to Central European *Quercus* species, but there was no difference between provenances within *Q. robur* (Lobo et al., 2018). In this study, we only tested for clines related to MAPp because there were only ten provenances. We did not try to correlate a host of different aridity measures with a limited dataset, which is likely to produce spurious correlations, but we are aware that MAP may not be the best measure of aridity.

The overall pattern of vessel size variation was remarkably constant across sites and provenances and showed a peak for small vessels with a maximum density at c. 20 μm diameter and a much smaller peak for vessels > 70 μm diameter (**Figure 2**). Like other anatomical parameters, vessel size variation, the fraction occupied by large vessels and the proportion of hydraulic conductivity contributed by small vessels was controlled largely by tree size, ring width and provenance, and only to a minor extent by site. While most vessel parameters except for VAmp were related to ring width (**Figure 6** and **Table 4**), the effect was very small for p_{macro} and Ks_{micro}. Vessels < 70 μm diameter in most cases contributed <3% to total Ks. Although Ks_{micro} showed a significant effect of provenance, it was not related to the climate at the provenance location (**Table 4**). Small vessels contribute less to Ks but might still be relevant when large vessels are embolized, and wood needs to transport a minimum of water to leaves with strongly reduced stomatal conductance as a consequence of drought. However, we found no evidence that the contribution of small pores would increase by plastic or genetic adaptation to aridity in *Q. robur*.

According to the most accepted model, xylem emboli arise under drought stress when the pressure gradient across the cell wall permits gas to pass through the pit membranes. Emboli can also form when after freeze-thaw events minute gas bubbles coalesce and expand and water tension is high enough. In the latter case, the vulnerability is directly related to vessel size (large

vessels thawing yield more and larger gas bubbles), whereas in the first case, vulnerability is related to the fine structure of the cell walls and only indirectly to vessel size (rare pith hypothesis). Indeed, experimental studies found a stronger link between vessel size and loss of conductivity following freezing (Davis et al., 1999) than between vessel size and drought-induced cavitation (Jacobsen et al., 2019). A global analysis of woody plants found small vessels to be an important adaptation to cold environments (Zanne et al., 2014). This suggests that it would be worthwhile to investigate intra-specific variation in vessel size also in relationship with minimum temperature and not mainly focus on adaptations to drought. That said, unless there is clearer evidence for a climate signal carried by small vessel, the substantially greater effort to measure these may not justify the additional time that would be needed for the studies in dendroclimatology.

Other provenance studies found particularly phenology under strong genetic control and more so than leaf traits or WD. A stronger genetic control for leaf than for wood traits was also shown in a previous paper on the *Q. robur* provenance trial (George et al., 2020). This study found the genetic control of WD (i.e., the provenance effect) among the lowest of all wood traits measured (**Table 3**). This is important for tree breeding programs that seek to select genotypes better adapted to a warmer climate with higher water deficit. However, we also caution against quick recommendations based on the individual traits and correlations with climate. First, while drought resistance (at least xylem vulnerability, which is only one component of drought resistance) has been shown to correlate and to some extent is functionally related with wood traits (see Section "Introduction"), these relationships are often quite weak. Second, while anatomical traits may be under strong genetic control and the result of evolutionary selection, the relationship to climate is often weak. Third, the provenance trials that have looked at wood traits other than WD mostly include temperature as well as aridity clines (the latter often weaker) in the climate of origin, which makes it difficult to distinguish between adaptations to temperature or aridity. Finally, wood traits represent only part of the complex adaptations to drought. Adjustments in roots, leaves, phenology, or other components can be equally or more important (e.g., Rungwattana et al., 2018). A study on 22 North American tree species found that, while WD was positively related to cavitation resistance, species with high WD actually suffered more under drought whereas species with low WD suffered less as these relied on various strategies of drought avoidance (Hoffmann et al., 2011). Similarly, deciduous trees in tropical dry forests follow quite different strategies (high hydraulic conductivity, low WD, high water storage, and high xylem vulnerability) to survive under similar conditions as evergreen trees (Méndez-Alonzo et al., 2012). The ultimate measure for the trees' adaptations to and suitability for a given environment should be growth and mortality. In the *Q. robur*, provenance trial trees grew better if transferred to a climate similar to their provenance (George et al., 2020). This effect was also stronger for temperature than for precipitation. More complex datasets and provenance trials should try to disentangle effects of and adaptations to variation in water availability as well as temperature but need to account for tree size or growth rates to avoid a biased interpretation of trait adaptations.

DATA AVAILABILITY STATEMENT

The raw data supporting the conclusions of this article will be made available by the authors, without undue reservation.

AUTHOR CONTRIBUTIONS

PH conceived the idea, analyzed the data, and wrote the manuscript. KR and SS sampled wood and analyzed wood samples. J-PG sampled wood and provided access to and additional information on the provenance trial. All authors contributed to the article and approved the submitted version.

FUNDING

KR was supported a grant from the Austrian Federal Ministry of Science, Research, and Economy (BMWFW) within the framework of the ASEA UNINET.

ACKNOWLEDGMENTS

We appreciate support by the Bundesforschungszentrum Wald and in particular Lambert Weiszenbacher for managing the reforestation trial. The two reviewers provided helpful comments that improved the manuscript.

SUPPLEMENTARY MATERIAL

The Supplementary Material for this article can be found online at: https://www.frontiersin.org/articles/10.3389/fpls.2022.795941/full#supplementary-material

REFERENCES

Anfodillo, T., Carraro, V., Carrer, M., Fior, C., and Rossi, S. (2006). Convergent tapering of xylem conduits in different woody species. *New Phytol.* 169, 279–290. doi: 10.1111/j.1469-8137.2005.01587.x

Awad, H., Barigah, T., Badel, E., Cochard, H., and Herbette, S. (2010). Poplar vulnerability to xylem cavitation acclimates to drier soil conditions. *Physiol. Plant.* 139, 280–288. doi: 10.1111/j.1399-3054.2010.01367.x

Bates, D., and Sarkar, D. (2020). *Lme4: Linear Mixed-Effects Models Using S4 Classes*. R Package Version 1.1-23.

Bert, D., Lebourgeois, F., Ponton, S., Musch, B., and Ducousso, A. (2020). Which oak provenances for the 22nd century in Western Europe? Dendroclimatology in common gardens. *PLoS One* 15:e0234583. doi: 10.1371/journal.pone.0234583

Castagneri, D., Regev, L., Boaretto, E., and Carrer, M. (2017). Xylem anatomical traits reveal different strategies of two Mediterranean oaks to cope with drought

and warming. *Environ. Exp. Bot.* 133, 128–138. doi: 10.1016/j.envexpbot.2016.10.009

Chave, J., Coomes, D., Jansen, S., Lewis, S. L., Swenson, N. G., and Zanne, A. E. (2009). Towards a worldwide wood economics spectrum. *Ecol. Lett.* 12, 351–366. doi: 10.1111/j.1461-0248.2009.01285.x

Christman, M. A., Sperry, J. S., and Adler, F. R. (2009). Testing the 'rare pit' hypothesis for xylem cavitation resistance in three species of Acer. *New Phytol.* 182, 664–674. doi: 10.1111/j.1469-8137.2009.02776.x

Christman, M. A., Sperry, J. S., and Smith, D. D. (2012). Rare pits, large vessels and extreme vulnerability to cavitation in a ring-porous tree species. *New Phytol.* 193, 713–720. doi: 10.1111/j.1469-8137.2011.03984.x

Davis, S. D., Sperry, J. S., and Hacke, U. G. (1999). The relationship between xylem conduit diameter and cavitation caused by freezing. *Am. J. Bot.* 86, 1367–1372. doi: 10.2307/2656919

Delzon, S., Douthe, C., Sala, A., and Cochard, H. (2010). Mechanism of water-stress induced cavitation in conifers: bordered pit structure and function support the hypothesis of seal capillary-seeding. *Plant Cell Environ.* 33, 2101–2111. doi: 10.1111/j.1365-3040.2010.02208.x

Fichot, R., Barigah, T. S., Chamaillard, S., Le Thiec, D., Laurans, F., Cochard, H., et al. (2010). Common trade-offs between xylem resistance to cavitation and other physiological traits do not hold among unrelated *Populus deltoides* × *Populus nigra* hybrids. *Plant Cell Environ.* 33, 1553–1568. doi: 10.1111/j.1365-3040.2010.02164.x

Fonti, P., and García-González, I. (2008). Earlywood vessel size of oak as a potential proxy for spring precipitation in mesic sites. *J. Biogeogr.* 35, 2249–2257. doi: 10.1111/j.1365-2699.2008.01961.x

Fonti, P., Treydte, K., Osenstetter, S., Frank, D., and Esper, J. (2009). Frequency-dependent signals in multi-centennial oak vessel data. *Palaeogeogr. Palaeoclimatol. Palaeoecol.* 275, 92–99. doi: 10.1016/j.palaeo.2009.02.021

Fonti, P., von Arx, G., García-González, I., Eilmann, B., Sass-Klaassen, U., Gärtner, H., et al. (2010). Studying global change through investigation of the plastic responses of xylem anatomy in tree rings. *New Phytol.* 185, 42–53. doi: 10.1111/j.1469-8137.2009.03030.x

Gea-Izquierdo, G., Fonti, P., Cherubini, P., Martín-Benito, D., Chaar, H., and Cañellas, I. (2012). Xylem hydraulic adjustment and growth response of Quercus canariensis Willd. to climatic variability. *Tree Physiol.* 32, 401–413. doi: 10.1093/treephys/tps026

George, J.-P., Theroux-Rancourt, G., Rungwattana, K., Scheffknecht, S., Momirovic, N., Neuhauser, L., et al. (2020). Assessing adaptive and plastic responses in growth and functional traits in a 10-year old common garden experiment with pedunculate oak (*Quercus robur* L.) suggests that directional selection can drive climatic adaptation. *Evol. Appl.* 13, 2422–2438. doi: 10.1111/eva.13034

Gleason, S. M., Westoby, M., Jansen, S., Choat, B., Hacke, U. G., Pratt, R. B., et al. (2015). Weak tradeoff between xylem safety and xylem-specific hydraulic efficiency across the world's woody plant species. *New Phytol.* 209, 123–136. doi: 10.1111/nph.13646

Gouveia Fontes, C., Fine, P. V. A., Wittmann, F., Bittencourt, P. R. L., Fernandez Piedade, M. T., Higuchi, N., et al. (2020). Convergent evolution of tree hydraulic traits in Amazonian habitats: implications for community assemblage and vulnerability to drought. *New Phytol.* 228, 106–120. doi: 10.1111/nph.16675

Guet, J., Fichot, R., Lédée, C., Laurans, F., Cochard, H., Delzon, S., et al. (2015). Stem xylem resistance to cavitation is related to xylem structure but not to growth and water-use efficiency at the within-population level in *Populus nigra L. J. Exp. Bot.* 66, 4643–4652. doi: 10.1093/jxb/erv232

Hacke, U. G., and Sperry, J. S. (2001). Functional and ecological xylem anatomy. *Perspect. Plant Ecol. Evol. Syst.* 4, 97–115.

Hacke, U., and Sauter, J. J. (1996). Xylem dysfunction during winter and recovery of hydraulic conductivity in diffuse-porous and ring-porous trees. *Oecologia* 105, 435–439. doi: 10.1007/BF00330005

Hajek, P., Kurjak, D., von Wühlisch, G., Delzon, S., and Schuldt, B. (2016). Intraspecific variation in wood anatomical, hydraulic, and foliar traits in ten European beech provenances differing in growth yield. *Front. Plant Sci.* 7:791. doi: 10.3389/fpls.2016.00791

Hietz, P., Rosner, S., Hietz-Seifert, U., and Wright, S. J. (2017). Wood traits related to size and life history of trees in a Panamanian rainforest. *New Phytol.* 213, 170–180. doi: 10.1111/nph.14123

Hietz, P., Valencia, R., and Wright, S. J. (2013). Strong radial variation in wood density follows a uniform pattern in two neotropical rain forests. *Funct. Ecol.* 27, 684–692. doi: 10.1111/1365-2435.12085

Hoffmann, W. A., Marchin, R. M., Abit, P., and Lau, O. L. (2011). Hydraulic failure and tree dieback are associated with high wood density in a temperate forest under extreme drought. *Glob. Change Biol.* 17, 2731–2742. doi: 10.1111/j.1365-2486.2011.02401.x

Ibanez, T., Chave, J., Barrabé, L., Elodie, B., Boutreux, T., Trueba, S., et al. (2017). Community variation in wood density along a bioclimatic gradient on a hyper-diverse tropical island. *J. Veg. Sci.* 28, 19–33. doi: 10.1111/jvs.12456

Jacob, D., Petersen, J., Eggert, B., Alias, A., Christensen, O. B., Bouwer, L. M., et al. (2014). EURO-CORDEX: new high-resolution climate change projections for European impact research. *Reg. Environ. Change* 14, 563–578.

Jacobsen, A. L., Brandon Pratt, R., Venturas, M. D., Hacke, U. G., and Lens, F. (2019). Large volume vessels are vulnerable to water-stress-induced embolism in stems of poplar. *IAWA J.* 40:4. doi: 10.1163/22941932-40190233

Kunert, N., Zailaa, J., Herrmann, V., Muller-Landau, H. C., Wright, S. J., Pérez, R., et al. (2021). Leaf turgor loss point shapes local and regional distributions of evergreen but not deciduous tropical trees. *New Phytol.* 230, 485–496. doi: 10.1111/nph.17187

Lachenbruch, B., Moore, J. R., and Evans, R. (2011). "Radial variation in wood structure and function in woody plants, and hypotheses for its occurrence," in *Size- and Age-Related Changes In Tree Structure And Function*, eds F. C. C. Meinzer, B. Lachenbruch, and T. E. E. Dawson (Dordrecht: Springer Netherlands), 121–164. doi: 10.1007/978-94-007-1242-3_5

Lemaire, C., Quilichini, Y., Brunel-Michac, N., Santini, J., Berti, L., Cartailler, J., et al. (2021). Plasticity of the xylem vulnerability to embolism in Populus *tremula x alba* relies on pit quantity properties rather than on pit structure. *Tree Physiol.* 41, 1384–1399. doi: 10.1093/treephys/tpab018

Lens, F., Sperry, J. S., Christman, M. A., Choat, B., Rabaey, D., and Jansen, S. (2011). Testing hypotheses that link wood anatomy to cavitation resistance and hydraulic conductivity in the genus Acer. *New Phytol.* 190, 709–723. doi: 10.1111/j.1469-8137.2010.03518.x

Li, X., Blackman, C. J., Choat, B., Duursma, R. A., Rymer, P. D., Medlyn, B. E., et al. (2018). Tree hydraulic traits are coordinated and strongly linked to climate-of-origin across a rainfall gradient. *Plant Cell Environ.* 41, 646–660. doi: 10.1111/pce.13129

Lobo, A., Torres-Ruiz, J. M., Burlett, R., Lemaire, C., Parise, C., Francioni, C., et al. (2018). Assessing inter- and intraspecific variability of xylem vulnerability to embolism in oaks. *For. Ecol. Manag.* 424, 53–61. doi: 10.1016/j.foreco.2018.04.031

Martínez-Cabrera, H. I., Jones, C. S., Espino, S., and Schenk, H. J. (2009). Wood anatomy and wood density in shrubs: responses to varying aridity along transcontinental transects. *Am. J. Bot.* 96, 1388–1398. doi: 10.3732/ajb.0800237

Martínez-Sancho, E., Dorado-Liñán, I., Heinrich, I., Helle, G., and Menzel, A. (2017). Xylem adjustment of sessile oak at its southern distribution limits. *Tree Physiol.* 37, 903–914. doi: 10.1093/treephys/tpx036

Mayr, S., and Améglio, T. (2016). "Freezing stress in tree xylem," in *Progress in Botany 77*, eds U. Lüttge, M. F. Cánovas, and R. Matyssek (Cham: Springer International Publishing), 381–414. doi: 10.1007/978-3-319-25688-7_13

Méndez-Alonzo, R., Paz, H., Zuluaga, R. C., Rosell, J. A., and Olson, M. E. (2012). Coordinated evolution of leaf and stem economics in tropical dry forest trees. *Ecology* 93, 2397–2406. doi: 10.1890/11-1213.1

Morris, H., Plavcová, L., Cvecko, P., Fichtler, E., Gillingham, M. A. F., Martínez-Cabrera, H. I., et al. (2016). A global analysis of parenchyma tissue fractions in secondary xylem of seed plants. *New Phytol.* 209, 1553–1565. doi: 10.1111/nph.13737

Niklas, K. J., and Spatz, H.-C. (2010). Worldwide correlations of mechanical properties and green wood density. *Am. J. Bot.* 97, 1587–1594. doi: 10.3732/ajb.1000150

Olano, J. M., Arzac, A., García-Cervigón, A. I., von Arx, G., and Rozas, V. (2013). New star on the stage: amount of ray parenchyma in tree rings shows a link to climate. *New Phytol.* 198, 486–495. doi: 10.1111/nph.12113

Pérez-de-Lis, G., Rozas, V., Vázquez-Ruiz, R. A., and García-González, I. (2018). Do ring-porous oaks prioritize earlywood vessel efficiency over safety? Environmental effects on vessel diameter and tyloses formation. *Agric. For. Meteorol.* 248, 205–214. doi: 10.1016/j.agrformet.2017.09.022

Pfautsch, S., Harbusch, M., Wesolowski, A., Smith, R., Macfarlane, C., Tjoelker, M. G., et al. (2016). Climate determines vascular traits in the ecologically diverse genus *Eucalyptus*. *Ecol. Lett.* 19, 240–248. doi: 10.1111/ele.12559

Poyatos, R., Cermák, J., and Llorens, P. (2007). Variation in the radial patterns of sap flux density in pubescent oak (*Quercus pubescens*) and its implications for tree and stand transpiration measurements. *Tree Physiol.* 27, 537–548. doi: 10.1093/treephys/27.4.537

R Core Team (2020). *R: A Language And Environment For Statistical Computing*. R Foundation for Statistical Computing. Vienna, Austria.

Rosell, J. A., Olson, M. E., and Anfodillo, T. (2017). Scaling of xylem vessel diameter with plant size: causes, predictions, and outstanding questions. *Curr. For. Rep.* 3, 46–59. doi: 10.1007/s40725-017-0049-0

Rungwattana, K., and Hietz, P. (2018). Radial variation of wood functional traits reflect size-related adaptations of tree mechanics and hydraulics. *Funct. Ecol.* 32, 260–272. doi: 10.1111/1365-2435.12970

Rungwattana, K., Kasemsap, P., Phumichai, T., Kanpanon, N., Rattanawong, R., and Hietz, P. (2018). Trait evolution in tropical rubber (Hevea brasiliensis) trees is related to dry season intensity. *Funct. Ecol.* 32, 2638–2651. doi: 10.1111/1365-2435.13203

Saranpää, P. (2003). "Wood density and growth," in *Wood Quality And Its Biological Basis*, eds J. R. Barnett and G. Jeronimidis (Oxford: Blackwell Publishing), 87–117.

Schuldt, B., Knutzen, F., Delzon, S., Jansen, S., Müller-Haubold, H., Burlett, R., et al. (2016). How adaptable is the hydraulic system of European beech in the face of climate change-related precipitation reduction? *New Phytol.* 210, 443–458. doi: 10.1111/nph.13798

Schüller, E., Martínez-Ramos, M., and Hietz, P. (2013). Radial gradients in wood specific gravity, water and gas content in trees of a Mexican tropical rain forest. *Biotropica* 45, 280–287. doi: 10.1111/btp.12016

Schweingruber, F. H. (2007). *Wood Structure And Environment*. Berlin: Springer.

Souto-Herrero, M., Rozas, V., and García-González, I. (2017). A 481-year chronology of oak earlywood vessels as an age-independent climatic proxy in NW Iberia. *Glob.Planet. Change* 155, 20–28. doi: 10.1016/j.gloplacha.2017.06.003

Sperry, J. S., Hacke, U. G., and Wheeler, J. K. (2005). Comparative analysis of end wall resistivity in xylem conduits. *Plant Cell Environ.* 28, 456–465. doi: 10.1111/j.1365-3040.2005.01287.x

Torres-Ruiz, J. M., Kremer, A., Carins Murphy, M. R., Brodribb, T., Lamarque, L. J., Truffaut, L., et al. (2019). Genetic differentiation in functional traits among European sessile oak populations. *Tree Physiol.* 39, 1736–1749. doi: 10.1093/treephys/tpz090

Tyree, M. T., and Sperry, J. S. (1989). Vulnerability of xylem to cavitation and embolism. *Ann. Rev. Plant Physiol. Plant Mol. Biol.* 40, 19–38. doi: 10.1146/annurev.pp.40.060189.000315

Tyree, M. T., and Zimmermann, M. H. (2002). *Xylem Structure And The Ascent Of Sap*. Berlin: Springer.

Vavrčík, H., and Gryc, V. (2012). Analysis of the annual ring structure and wood density relations in English oak and sessile oak. *Wood Res.* 57, 573–580.

Von Arx, G., and Dietz, H. (2005). Automated image analysis of annual rings in the roots of perennial forbs. Int. *J. Plant Sci.* 166, 723–732. doi: 10.1086/431230

Zanne, A. E., Tank, D. C., Cornwell, W. K., Eastman, J. M., Smith, S. A., FitzJohn, R. G., et al. (2014). Three keys to the radiation of angiosperms into freezing environments. *Nature* 506, 89–92. doi: 10.1038/nature12872

Zanne, A. E., Westoby, M., Falster, D. S., Ackerly, D. D., Loarie, S. R., Arnold, S. E. J., et al. (2010). Angiosperm wood structure: global patterns in vessel anatomy and their relation to wood density and potential conductivity. *Am. J. Bot.* 97, 207–215. doi: 10.3732/ajb.0900178

Zhang, S.-Y., Owoundi, R. E., Nepveu, G., Mothe, F., and Dhôte, J.-F. (1993). Modelling wood density in European oak (*Quercus petraea and Quercus robur*) and simulating the silvicultural influence. *Can. J. For. Res.* 23, 2587–2593. doi: 10.1139/x93-320

Ziemińska, K., Butler, D. W., Gleason, S. M., Wright, I. J., and Westoby, M. (2014). Fibre wall and lumen fractions drive wood density variation across 24 Australian angiosperms. *AoB Plants* 5:plt046.

Zobel, B. J., and Jett, J. B. (1995). "The genetics of wood density," in *Genetics of Wood Production*, eds B. J. Zobel and J. B. Jett (Berlin: Springer), 98–125. doi: 10.1007/978-3-642-79514-5_5

Zobel, B. J., and van Buijtenen, J. P. (1989). *Wood Variation: Its Causes And Control*. Berlin: Springer.

Conflict of Interest: The authors declare that the research was conducted in the absence of any commercial or financial relationships that could be construed as a potential conflict of interest.

Publisher's Note: All claims expressed in this article are solely those of the authors and do not necessarily represent those of their affiliated organizations, or those of the publisher, the editors and the reviewers. Any product that may be evaluated in this article, or claim that may be made by its manufacturer, is not guaranteed or endorsed by the publisher.

frontiers | Frontiers in Plant Science

ORIGINAL RESEARCH
published: 09 June 2022
doi: 10.3389/fpls.2022.855003

Contrasting Climate Sensitivity of *Pinus cembra* Tree-Ring Traits in the Carpathians

Marian-Ionuț Știrbu[1], Cătălin-Constantin Roibu[1], Marco Carrer[2], Andrei Mursa[1], Lucrezia Unterholzner[2] and Angela Luisa Prendin[2,3]**

[1]Forest Biometrics Laboratory, Faculty of Forestry, 'Stefan cel Mare' University of Suceava, Suceava, Romania, [2]Department of Land Environment Agriculture and Forestry, University of Padova, Legnaro, Italy, [3]Department of Biology, Aarhus University, Aarhus, Denmark

High-elevation ecosystems are one of the most sensitive to climate change. The analysis of growth and xylem structure of trees from marginal populations, especially the ones growing at the treeline, could provide early-warning signs to better understand species-specific responses to future climate conditions. In this study, we combined classical dendrochronology with wood density and anatomical measurements to investigate the climate sensitivity of *Pinus cembra* L., a typical European high-elevation tree species distributed in isolated patches in the Carpathians. Samples were collected from the Retezat Mountains, South-Western Romania. We analyzed ring width (TRW), maximum density (MXD), xylem anatomical traits [cell number per ring (CNo), cell density (CD), conduit area (CA), and cell wall thickness (CWT)] time series, split into ring sectors and assessed the relationships with monthly and daily climate records over the last century (1901–2015). The analysis showed a strong dependency of TRW on CNo and MXD on CWT. Summer temperature positively correlated with MXD and CWT [monthly correlation (*r*) were 0.65 and 0.48 respectively] from the early to late wood but not TRW ($r = 0.22$). CA positively correlated with water availability ($r = 0.37$) and negatively correlated with temperature ($r = -0.39$). This study improves our general understanding of the climate–growth relationships of a European high-elevation tree species and the results could be considered for forecasting population dynamics on projected changes in climate.

Keywords: dendroanatomy, functional traits, inter–intra-annual climate–structure relationships, stone pine, treeline, climatic divergence

OPEN ACCESS

Edited by:
Dario Martin-Benito, Centro de Investigación Forestal (INIA), Spain

Reviewed by:
Irina P. Panyushkina, University of Arizona, United States
Jan Tumajer, University of Greifswald, Germany

****Correspondence:***
Cătălin-Constantin Roibu
catalinroibu@usm.ro
Angela Luisa Prendin
angelaluisa.prendin@bio.au.dk

Specialty section:
This article was submitted to Functional Plant Ecology, a section of the journal Frontiers in Plant Science

Received: *14 January 2022*
Accepted: *22 April 2022*
Published: *09 June 2022*

Citation:
Știrbu M-I, Roibu C-C, Carrer M, Mursa A, Unterholzner L and Prendin AL (2022) Contrasting Climate Sensitivity of Pinus cembra Tree-Ring Traits in the Carpathians. Front. Plant Sci. 13:855003. doi: 10.3389/fpls.2022.855003

INTRODUCTION

Temperatures have increased rapidly worldwide during the last decades (IPCC, 2021) along with variation in seasonal precipitation and evaporation regimes (Konapala et al., 2020). This climate change is observed and predicted to deeply affect the structure and functioning of different forest ecosystems (Dawes et al., 2013; Büntgen et al., 2015). Among the different ecosystems, the high altitude ones, generally identified as temperature-limited environments, are experiencing warming at a faster rate than the global average (Körner, 2012; Pepin et al., 2015). Therefore, high-elevation forests are expected to be very sensitive terrestrial regions,

where the effects of climate change are most likely to be observed (Harsch et al., 2009; Körner, 2012; Dawes et al., 2015). Further, the frequency, duration, and severity of the extreme climatic events are expected to increase in the future with additional consequences on the productivity, function, and distribution of forests worldwide. Recently, a trend of shifting vegetation belts toward higher altitudes and latitudes has occurred at the global scale (Körner, 1998; Harsch et al., 2009), together with an increase in productivity and photosynthetic activities (Grace et al., 2002; Carlson et al., 2017; Cazzolla Gatti et al., 2019). These changes have been mainly attributed to the effects of increasing anthropogenic greenhouse gas emissions on global temperatures (Cannone et al., 2007; Körner, 2012). Still, it is not clear what the long-term implications of such plant responses are, nor which structural adjustments will primarily allow trees to acclimate to environmental changes. For this reason, marginal populations, such as the ones growing at the elevational edge of a species' distribution, are of particular interest. Compared to populations growing within their optimum (Fritts, 1976), marginal populations allow for investigation of climate–growth relationships and for gaining insight into inter- and intra-specific responses of trees growing at their physiological limits. The improved understanding of these plant responses could allow for forecasting the future dynamics of these populations (Hampe and Petit, 2005).

To have accurate forecasting, we need long-term data sets. Tree-ring data give a long-term, retrospective quantification of annual growth of trees, from different sites and species (Fritts, 1976; Cook and Kairiukstis, 1990), and enables identification of the factors that mainly determine tree growth (D'Arrigo and Jacoby, 1993; Mäkinen et al., 2003; Bouriaud et al., 2005). Additionally, wood density reflects a plant's carbon accumulation in the xylem (Rathgeber, 2017), giving insight to the plant's ecology, including functional physiology, mechanical properties, architecture, and climate responses (Hacke et al., 2001; Chave et al., 2009; Rathgeber, 2017). Tree-ring width and wood density have been the most widely used tree-ring features in dendro-climatological and -ecological studies. They are commonly used environmental proxies, that effectively record the climate signal (e.g., maximum density MXD), and they are also used to calibrate models that predict net primary production (Babst et al., 2014; Klesse et al., 2018). Still, a better understanding of plant responses to ongoing climate change requires insight into the physiological growth responses at a finer resolution (e.g., intra-annual). Therefore, coupling dendrochronology with tree-ring anatomy adds a "time component" to the functional mechanisms and plasticity of xylem formation (Fonti et al., 2010). This aids in identifying how wood anatomical adjustments determine variation in growth and density and can improve the interpretation of how they are connected and climatically controlled (Björklund et al., 2017). Thus, investigating how tree xylem structures and their associated functions change over time and in relation to environmental variability is of high importance to improve the ecophysiological understanding of the process of growth and to infer potential marginal population responses under different climate change scenarios.

Dendroanatomy is an emerging field that specifically focuses on the quantitative assessment of xylem tissues, cells, and derived metrics or traits linked to specific functional roles. This approach is based on the fact that the xylem structural adjustments are permanently recorded and chronologically archived in the structure of tree rings (Fonti et al., 2010), thus allowing retrospective analysis of the structure–function responses of trees to climate variability (Fonti and Jansen, 2012). Therefore, wood anatomical features (e.g., lumen area, related to hydraulic efficiency or cell wall thickness, related to carbon costs), localized at a certain position within yearly dated annual growth rings are linked to the time of their formation and become useful proxies to quantify long-term tree structural–functional responses and growth dynamics at an unprecedented time resolution (Fonti et al., 2010; Pritzkow et al., 2014; Baas et al., 2016; Prendin et al., 2017; Björklund et al., 2020).

The recent methodological progress in sample processing and image analysis allow for, for example, an increasing in the number of automatically measured tracheids of ~10- to 20-fold (Gärtner and Schweingruber, 2013; Von Arx et al., 2016; Prendin et al., 2017). Thanks to this, studies that combined tree-ring proxies at both annual and intra-annual resolution added depth to the inferences and improved our understanding of plant responses to climate and environmental variability (Panyushkina et al., 2003; Ziaco et al., 2014; Lange et al., 2020). Despite such progress, studies evaluating the responses of marginal populations at high elevation are scarce (Carrer et al., 2018).

A limited number of European high-elevation stands are characterized by the presence of the glacial relict stone pine (*Pinus cembra* L.; Caudullo et al., 2017). Isolated populations are growing in the Alps and Carpathians (Blada, 2008; Saulnier et al., 2011; Beloiu and Beierkuhnlein, 2019) as a consequence of climatic fluctuations, such as glacial/interglacial periods, together with species competition and anthropogenic disturbances that occurred in the last millennia (Ali et al., 2005). However, the future dynamics of these isolated populations are still uncertain as they could both expand their range due to the limitation of anthropogenic pressure and increasing temperature (Vittoz et al., 2008) or retreat, due to water limitations and competition with other taxa (Lyu et al., 2019). Despite being very suitable for investigating the climate–growth relationship, as they are rarely affected by biotic disturbances (e.g., defoliators and bark beetle outbreaks) compared to European larch (*Larix decidua* Mill.) or Norway spruce (Baltensweiler, 1993; Carrer et al., 2007; Saulnier et al., 2011), to our knowledge, only a few studies assessed the long-term intra annual climate sensitivity of this typical treeline species at the edge of its distribution (Carrer et al., 2018) and none have investigated it in combination with wood density measurements (that are rarely performed in this species).

In this study, we used a multiproxy approach to investigate the mechanism that regulates xylem growth of *Pinus cembra* L. at high elevation in the Carpathians, Romania. Specifically, we combined the classical dendroecological measurements (TRW, MXD) with dendroanatomical ones (e.g., cell density, cell

number, conduit area, and cell wall thickness) to: (i) gain insight into the anatomical basis of tree-ring width and wood density; (ii) identify the key factors that determine stone pine growth and structural variability at inter- and intra-annual resolution; (iii) and shed light on the mechanism that regulates xylem growth formation of this species at the easternmost margin of its distribution area.

MATERIALS AND METHODS

Study Site and Climate

The study site is represented by a natural timberline (1,700–1,800 m) of stone pine stands, located on the north-facing slope in the Retezat National Park in the South-Western Carpathians (Romania; 45°39′ N, 22°89′ E; **Figure 1**). The soil is shallow and the geological structure complex, mostly composed of crystalline rocks and limestone. The mean annual temperature is 4.6°C with monthly values ranging from −9.7°C in January to 19.7°C in July. Mean multiannual precipitation is 1,066 mm/year, with a peak of 156 mm/month in June (**Figure 1C**). Climate records used in this study were obtained from the CRU TS4.04 (Harris et al., 2020; monthly and self-calibrating Palmer Drought Severity Index (scPDSI), 1901–2015) from the closest grid points to our study region (22.50–23.00°E/45.00–45.50°N) and Rocada dataset (Dumitrescu and Birsan, 2015, daily, 1961-2013) from the closest grid points to our study region (22.80–22.90°E/45.25–45.50°N).

Sample Collection and Processing

One increment core per tree was extracted from 28 dominant, isolated, and undamaged mature stone pine trees in June 2015. The increment cores were collected at breast height following standard procedure (Schweingruber et al., 1990) using a Pressler borer and later stored in paper straws. To perform densitometric measurements, a one-millimeter-thick longitudinal lath of wood was cut from the middle of each core, paying attention to the tracheid orientation. To obtain the MXD time series, the laths were boiled for 48 h in a Soxhlet extractor with 98% ethanol following standard protocol (Wang et al., 2002; Pritzkow et al., 2014). The radiographic images were obtained with an Itrax MultiScanner (Cox Analytical Systems, Gothenburg,

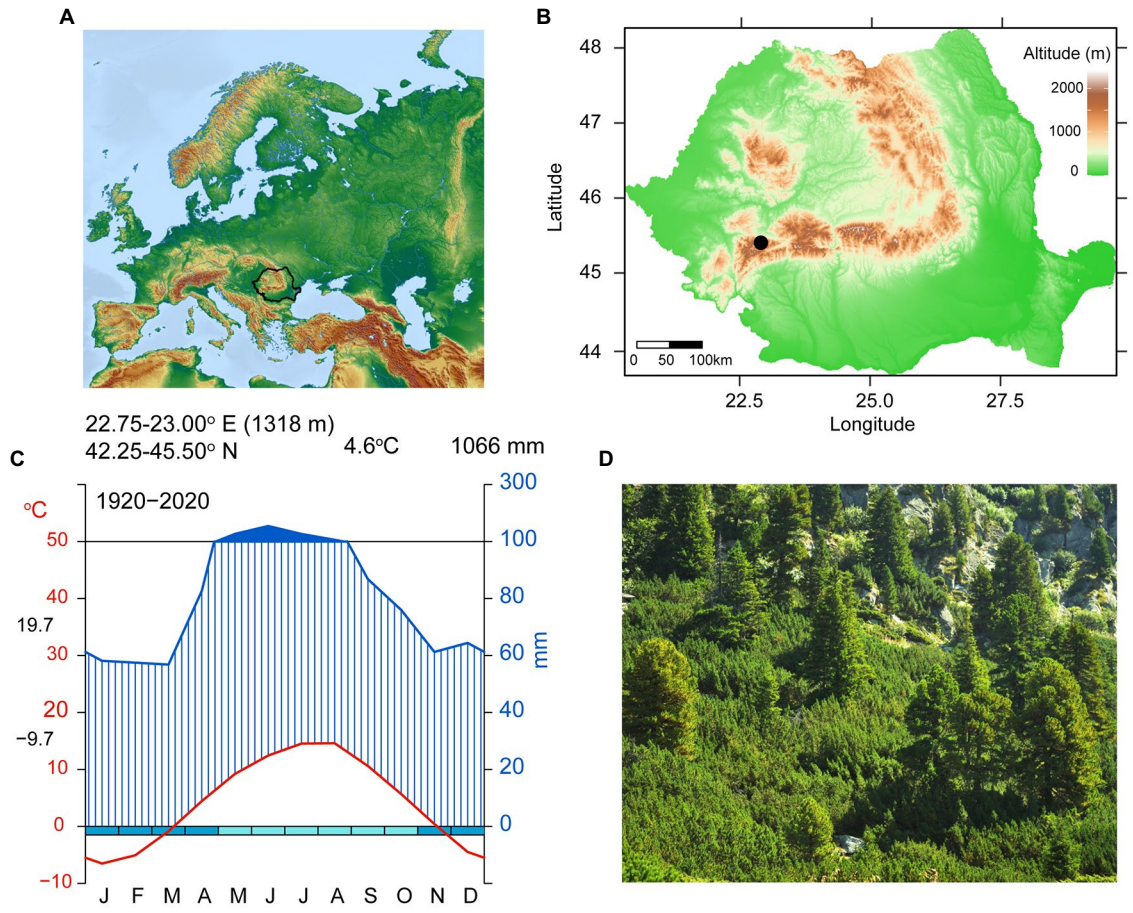

FIGURE 1 | Site location **(A)** Map of Europe—black contour is Romania; **(B)** Map of Romania—black dot shows Retezat National Park location; **(C)** Walter–Lieth Climodiagram showing mean monthly precipitation (blue, mm), mean monthly temperature (red, °C), months in which frost events are likely to occur (light-blue and turquoise boxes) and wet periods (dark-blue filled areas) based on grided data; **(D)** General view of the sampling site.

Sweden) in a climate-controlled medium (50% relative humidity and 20°C) using the following settings for the X-ray tube: voltage to 30 kV, current to 50 mA, and exposure time equal to 50 ms. A 16-bit, grey level, radiographic (X-ray) digital image was obtained for each sample at 1270 dpi resolution. The maximum density (MXD) was measured using WinDENDRO density version software (Regent Instruments, 2018). Tree-ring widths (TRW) were measured to the nearest 0.001 mm on the flat surface of the remaining sides of the cores using the LINTAB system and TSAP 0.53 software (Rinn, 2003). Measurement and dating accuracy were then checked using COFECHA (Holmes, 1983). After TRW and MXD measurements, a subset of nine samples without any visible defects or cross-dating issue were selected for anatomical analysis. These nine laths left after MXD samples preparation were split into 4–5 cm long pieces, and from each one, a thin (10 µm) transversal section was cut using a rotary microtome (Leica, Heidelberg, Germany). The resulted microsections were double-stained with safranin (0.8 g in 100 ml distilled water) and astrablue (0.5 g in 100 ml distilled water +2 ml acetic acid; Gärtner and Schweingruber, 2013), and mounted on permanent slides with Eukitt (BiOptica, Milan, Italy). Anatomical images were captured using the D-sight 2.0 System (Menarini Diagnostics, Florence, Italy) at 100x magnification corresponding to a resolution of 1.99 pixels/µm and were analyzed with ROXAS v3.0.250 (von Arx and Carrer, 2014; Prendin et al., 2017). Anatomical analysis was performed on >40 radial tracheid's rows per ring and a total of 2.5×10^6 tracheids were measured. To increase the temporal resolution without compromising the statistics regarding sample size (i.e., cell number; Castagneri et al., 2017), based on the information of tracheid's positions within each ring, we divided each ring into 10 ring sectors (with the 1st and 10th sectors corresponding, respectively, to the tracheid formed at the beginning and at the end of the growing season (Carrer et al., 2014). We finally obtained a time series for the whole ring and for each decile ring sector of the following anatomical parameters: cell density (CD; as cell number divided by the ring area), cell number (CNo; number of conduit per ring, standardized to a tangential width of 1.5 mm to account for size differences in the images collected, similarly to Castagneri et al. (2015), conduit area (CA), radial and tangential cell wall thickness (rCWT/tCWT), and mean cell wall thickness (CWT).

Statistical Analysis

All TRW, MXD, and anatomical series were standardized to remove the typical age-size trend (**Supplementary Figure 1**; Enquist, 2002; Carrer et al., 2014; Prendin et al., 2018) using a cubic smoothing spline with a 50% frequency cutoff response of 100 years (Cook and Kairiukstis, 1990; Castagneri et al., 2015; Carrer et al., 2018). The residual autocorrelation was removed using an autoregressive model and the mean chronologies were obtained by using bi-weight robust mean (**Supplementary Figure 2**; Fritts, 1976; Cook and Peters, 1997). We calculated the following descriptive statistics for both raw and detrended chronologies: mean sensitivity (MS), an index of the mean relative change between trait values in consecutive years, to assess the high-frequency variations in the chronologies; mean series inter-correlation (Rbar), and the expressed population signal (EPS; Fritts, 1976; Briffa and Jones, 1990) to estimate the level of year-by-year growth variations shared by trees in the same site (**Table 1**).

To investigate the association between TRW, MXD, and xylem traits chronologies, the residual chronologies were grouped employing hierarchical cluster analysis (HCA; Ludwig and Reynolds, 1988) based on Ward's minimum variance criterion (Everitt et al., 2011). Moreover, to verify the grouping consistency at intra-annual resolution, a cluster per ring sector was performed using TRW and MXD and the anatomical parameters time series.

To identify the limiting factors of tree-ring formation, the climate/growth and structural relationships were quantified using bootstrap correlations with the R packages *treeclim* (Zang and Biondi, 2015) and *dendroTools* (Jevšenak and Levanič, 2018). In particular, the analysis tested the correlation between temperature, precipitation and scPDSI, monthly/daily climate records, and TRW, MXD, and xylem traits chronologies. Monthly correlations were computed from June of the previous year to September of the current year whereas, with the daily climate records, we kept the same time span adopted for the monthly climate–growth relationship, but we first averaged the temperature and precipitation series in a 15-day windows, then correlations were computed between June of the previous year to September of the current year shifting the time window at a daily step (Carrer et al., 2017, 2018). Three distinct 40-yr periods (1901–1940, 1941–1080, and 1981–2013) were used in order to identify possible shifts in the climate growth relationship.

RESULTS

Tree-Ring Width Maximum Density and Xylem Traits Chronologies

The mean series length is 225 ± 62 years, with a mean ring width of 1.10 ± 0.6 mm· and a MXD of 0.7 ± 0.1 g·cm^{-3}. The subset of the nine samples included relatively younger individuals (174 ± 60 years), wider annual rings (1.40 ± 0.5 mm), and higher MXD (see **Table 1; Supplementary Figure 2**). The averaged cell density was 1110.2 ± 102.0 cells·mm^{-2}, while the mean conduit area (CA) corresponded to 476.5 ± 58.4 µm^{2}·, and the anatomical parameters related to cell wall thickness, presented similar values, ranging from 3.3 ± 0.1 (rCWT) to 3.1 ± 0.2 µm (tCWT) with a mean of 3.2 ± 0.2 µm (CWT). The strength of the common signal and the quality of the chronologies assessed using Rbar and EPS statistics found that MXD and cell wall thickness traits showed generally higher values compared to TRW, CD, and CA both in the RAW and detrended chronologies (**Table 1**). The mean sensitivity for TRW and CNo was higher (0.18) compared to MXD, CD, CA, and cell wall thickness traits (0.05; **Table 1**). Similar results were obtained when assessing the descriptive statistics of xylem traits chronologies at intra-annual resolution (10 ring sectors; **Supplementary Table 1**). Nevertheless, the signal strength between chronologies increased from first to last ring sectors for all anatomical traits (except for cell density).

TABLE 1 | Main statistical parameters for raw and detrended xylem traits chronologies.

Trait	Number of cores	First year	Last year	MA ± SD	MV ± SD	RAW chronology			Detrended chronology	
						rbar	EPS	MS	*rbar*	EPS
CD	9	1735	2015	174 ± 60	1110.2 ± 102.0	0.20	0.58	0.06	0.13	0.47
CA					476.5 ± 58.4	0.19	0.57	0.10	0.20	0.58
tCWT					3.1 ± 0.2	0.23	0.63	0.05	0.32	0.72
rCWT					3.3 ± 0.1	0.24	0.64	0.05	0.31	0.72
CWT					3.2 ± 0.2	0.25	0.66	0.05	0.33	0.73
CNo					1711 ± 700	0.13	0.46	0.18	0.14	0.47
MXD		1735	2014	180 ± 55	0.9 ± 0.1	0.23	0.63	0.09	0.33	0.74
TRW					1.4 ± 0.5	0.17	0.54	0.18	0.19	0.58
MXD all	28	1,684	2015	225 ± 62	0.7 ± 0.1	0.27	0.87	0.09	0.30	0.89
TRW all		1,684	2015		1.1 ± 0.6	0.18	0.81	0.18	0.24	0.86

CD, Conduit density (number·mm^{-2}); CA, Conduit area (μm); tCWT, Tangential cell wall thickness (μm); rCWT, Radial cell wall thickness (μm); CWT, mean Cell wall thickness (μm); CNo, Conduit number (number of conduit measured in the analyzed ring area); MXD, Maximum wood density (g·cm^{-3}); TRW, Tree-ring width (mm); MXD all and TRW all—Maximum wood density and tree-ring width of all the 28 cores; cores—number of cores; MA, mean age; MV, mean values for each parameter; SD, standard deviation; rbar, inter-series correlation; EPS, expressed population signal; MS, mean sensitivity.

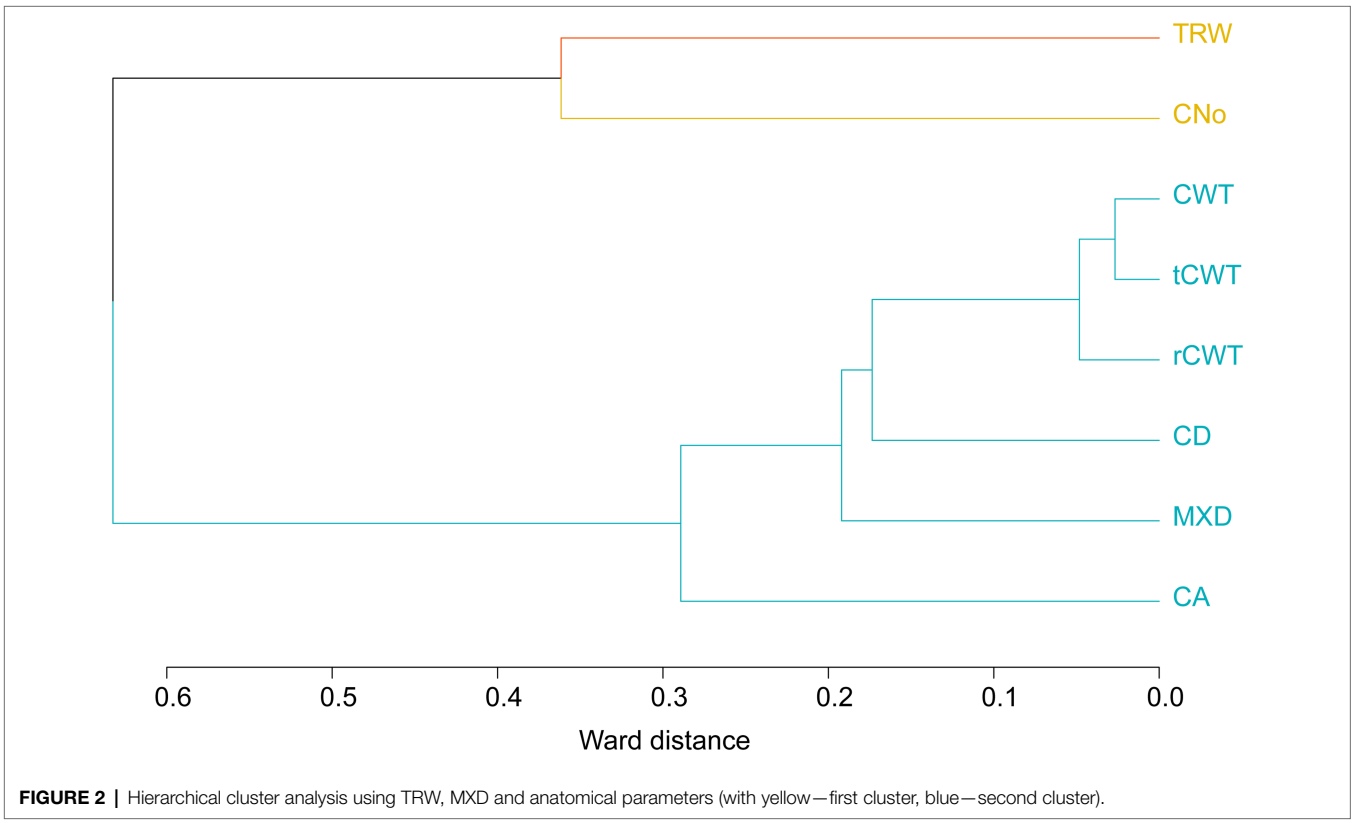

FIGURE 2 | Hierarchical cluster analysis using TRW, MXD and anatomical parameters (with yellow—first cluster, blue—second cluster).

Relationships Between Tree-Ring, Maximum Density, and Anatomical Traits

The hierarchical cluster analysis showed a strong relationship between CA, MXD, CD, and CWT. TRW and CNo were more independent in comparison with other variables (**Figure 2** and **Table 1**). Cell wall thickness chronologies (rCWT, tCWT, and CWT) formed two relatively closed (<0.1) clusters referring to the Ward distance followed by CD, MXD (<0.02), and finally CA (<0.3), while TRW and CNo formed the furthest away (>0.3) cluster on the axis (**Figure 2**). The HCA analysis based on intra-annual resolution chronologies (10 ring sectors) showed similar results compared to the HCA based on chronologies at annual resolution (see **Supplementary Figure 3**). Due to the comparable statistical parameters and similar associations between the rCWT, tCWT, and CWT chronologies, further analysis focus on the CWT chronologies only.

Relationships With Climate

Correlations computed with monthly climate records highlight TRW and CNo as the least sensitive parameters with very similar

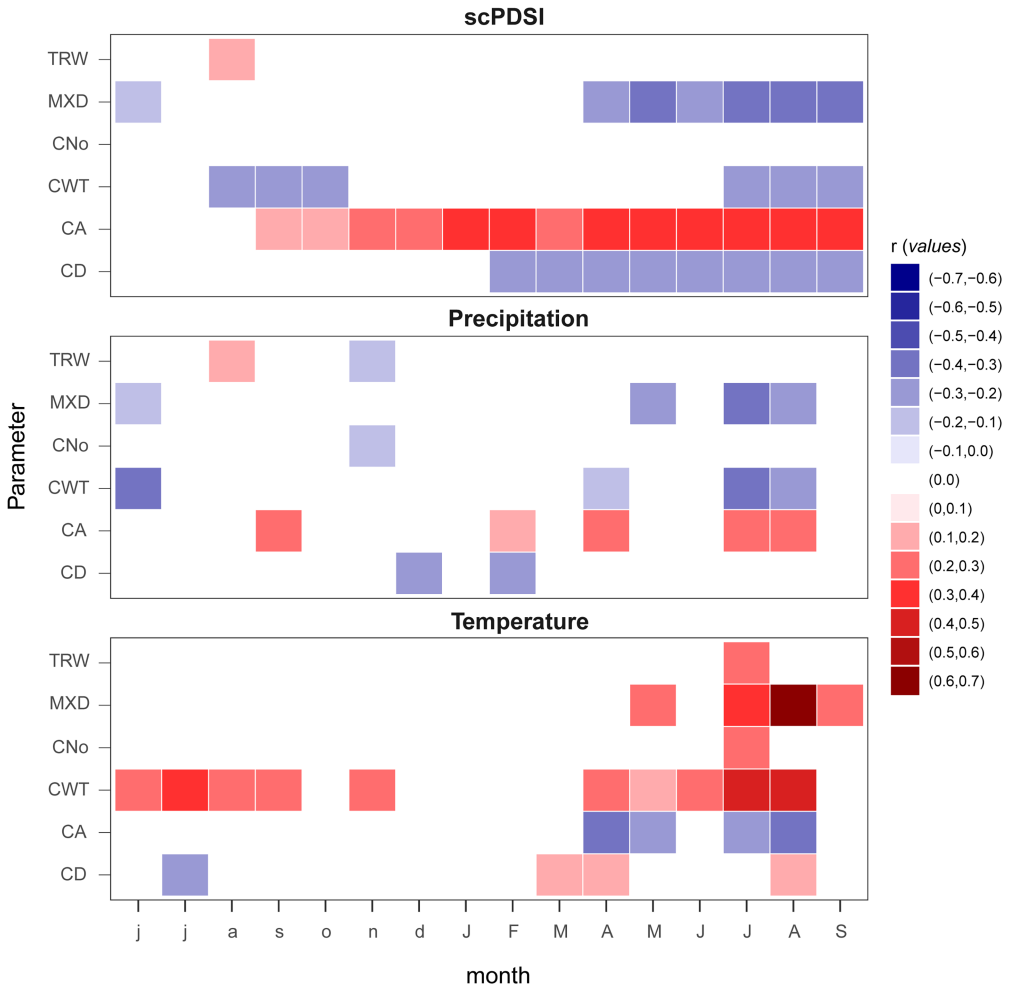

FIGURE 3 | Climate growth relationships computed between monthly climatic parameters (mean temperature, accumulation of precipitation, and scPDSI; from 1901 to 2015) and TRW, MXD, and anatomical parameters (CA, CNo, CD, and CWT). Lower case letters show the previous year and capitalized the current year.

cluster associations, while, the temperature is the main factor, positively influencing xylem density (MXD and CWT). High precipitation amount (June previous and current year summer) and high self-calibrating Palmer Drought Severity Index (scPDSI) values seemed to negatively affect MXD and CWT (**Figure 3**).

The higher resolution of the 15-day running correlations showed more detailed information (**Figures 4A,B**). CD showed the least significant correlations with temperature, randomly scattered, mostly during the summer to autumn months. CA showed a negative correlation with temperature starting from the third ring sector from mid-June to the end of August in the last ring sectors. CA is also negatively correlated with the temperatures of April. CWT showed an overall stronger correlation value with respect to CA, with a positively significant response at the beginning of the growing season (April–May period) in all ring sectors. During the growing season the correlation shifts from sectors 1 to 6 in the early June–July period, to sectors 4 to 10 in late June–late August, with a peak for the 10th ring sector in August ($r = 0.63$). Additionally, when splitting the last century into three equal periods (see **Supplementary Figure 4**), a clear weakening of the climatic signal emerged in all tree-ring parameters. In addition, the climate signal overturned in almost all the climate–growth and structural relationships, shifting from being positive in the first period to negative in the last one. MXD was one exception, with consistent positive and negative relationships throughout all the periods, despite experiencing a weakening of its climatic signal (especially for temperature) through time. Another exception was CA showing strong correlation with the increase of drought limitation in the most recent periods, while in the early period there was a non-significant relationship between CA and scPDSI.

Similarly, to the monthly analysis, the correlations between precipitation and xylem traits chronologies resulted in scattered points and were significant for a relatively short time window, indicating that precipitation plays a minor role here. Still, late spring precipitation showed the stronger signal in the first half of the ring sectors for CD (positive) and CA (negative). CWT shows a positive response to precipitation with higher correlations in the first six ring sectors for a very limited time window in mid-May. Negative correlations of CWT to daily

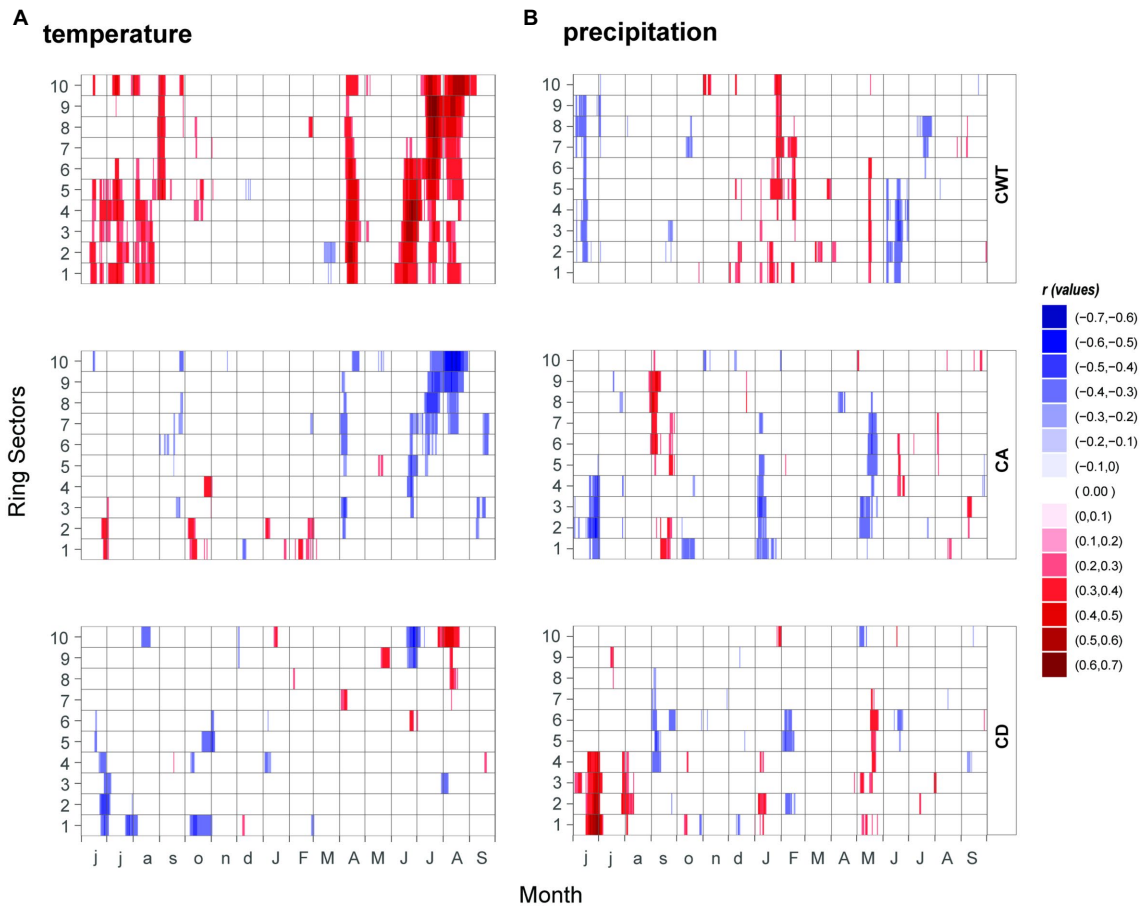

FIGURE 4 | Relationships between **(A)** temperature, **(B)** precipitation and xylem anatomical traits (CA, CD and CWT) from 1961 to 2013. Correlation coefficients were assessed at 15-day windows, represented by sliding daily steps from previous June to current September and coded according to the color key on the right.

precipitation are also found in June (from the 1st to the 5th sector) and July (from the 6th to the 8th sector).

DISCUSSION

Trees continuously increase in size during ontogeny by accumulating xylem biomass and adjusting their xylem structure to achieve an optimal balance between competing needs mostly related to water transport and mechanical support (Sauter, 1986). These xylem adjustments must also take into account all the external environmental factors and their variability with climate likely being the major one, always and pervasively present. In the ongoing climate change context, it is fundamental to deal with processes often operating at decadal and longer time scales, especially when studying long-living organisms, such as trees. The retrospective analysis of tree rings provides useful insight into long-term wood formation dynamics and related relationships with climate (Fritts, 1976), and into the role of trees and forests in the terrestrial carbon cycle (Babst et al., 2013). Within this framework, the analysis of xylem anatomical parameters, in parallel with tree-ring width and wood density, might allow insight to not just yearly and longer time scales but also at an intra-annual resolution (Fonti et al., 2010; Seo et al., 2011; Pritzkow et al., 2014). This study, by combining classical dendrochronology (ring width and maximum density) with quantitative wood anatomy (anatomical parameters related to water transport and cell enlargement (CA), mechanical support and wall thickening (CWT) and CD) allows us to better understand tree-ring structure of stone pine's and assess the sensitivity to climate variability, shedding light on the mechanism that regulates xylem growth formation.

The HCA analysis indicated CNo as the main determinant for the TRW (Vaganov et al., 2006), confirming that wider tree rings were mostly formed by a higher number of cells, rather than larger cells (Vaganov et al., 2006; Björklund et al., 2017; Carrer et al., 2017, 2018). The CWT and MXD resulted in highly similar associations at both annual and intra-annual resolution (**Figure 2** and **Supplementary Figure 3**), showing the strong dependency of cell wall material in determining the MXD, especially in the last ring sectors (Wang et al., 2002; Cuny et al., 2014; Pritzkow et al., 2014; Björklund et al., 2017, 2020). Furthermore, MXD and CWT chronologies showed a strong common signal compared to tree-ring width, CNo, CA, and

CD. This confirms its high potential as high-resolution paleoclimate proxy (Büntgen et al., 2005; Björklund et al., 2019, 2020; Nagavciuc et al., 2019). The descriptive statistics of TRW and xylem traits chronologies from stone pine are consistent with previous studies (Briffa et al., 2001; Vaganov et al., 2006; Carrer et al., 2018).

Despite being at high elevation, where summer temperature is expected to be the most important limiting factor (Büntgen et al., 2006; Popa and Kern, 2009; Popa and Bouriaud, 2013; Nagavciuc et al., 2019; Ionita et al., 2020), in this site TRW and CNo seemed minimally influenced by temperature. The lack of climatic signal could be explained at different levels: (i) cambial activity and the maximum growth rate are more influenced by the photoperiod and are unconstrained by concurrent climate conditions (Rossi et al., 2006); (ii) this unexpected result could be a consequence of the Atlantic and Mediterranean climatic influences on the study site on the site (ANM, 2008) that could buffer the role of temperature as a growth-limiting factor; or (iii) a weakening of the climatic signal in the TRW has also been observed in recent decades (D'Arrigo et al., 2008; Carrer et al., 2017; Camarero et al., 2021). In this study, the negative correlations between CA and temperature could be related to the cell wall thickening process. Higher temperatures can induce the formation of cells with narrower lumen thanks to the positive stimulus on cell wall thickening but with the side effect of reducing lumen area (CA negatively associated with temperature) from earlywood to latewood, causing a denser wood and higher MXD (Cuny et al., 2014). Indeed, cell dimension could be considered the main factor of wall thickness and density changes along a ring, as cell wall thickening proceeds inside the cell whose dimension have already been fixed before the starting of the thickening process (Cuny et al., 2014; Björklund et al., 2017; Carrer et al., 2017). Temperature is generally positively associated with CWT and wood density with the resistance to cavitation (Rosner, 2013; e.g., a freeze–thaw induced embolism that can occur at high elevation). Similarly, it seems that hydraulic safety is prioritized over efficiency under droughts as CA was positively associated with scPDSI. This suggests potential xylem modification under drought scenarios (Campelo et al., 2010) since the shallow soils often associated with such treeline stands have low water holding capacity (Anfodillo et al., 1998; Oberhuber, 2004; Mayr, 2007). Therefore, we can infer that the improved growing condition, mostly related to warming in the last decades, is playing a key role in influencing the xylogenesis process and cell morphology (Schweingruber, 1996; Körner, 1998; Gruber et al., 2009).

The uphill treeline shift observed in many sites worldwide could be related to this relaxation of the limiting conditions at high elevation (Körner, 1998, 2012; Harsch et al., 2009). This significant modifications recorded at high-elevation over time implies that older trees are now growing in less constrained conditions and brings potential implication for the climatic signal encoded in the tree-ring parameters (Drew et al., 2013; see **Supplementary Figure 4**). Previous studies found similar contrasting results between tree-ring parameters. For example, temperature and TRW were not related, especially where trees are growing in their optimum (Poussart and Schrag, 2005; Gagen et al., 2006; Drew et al., 2013), while a strong correlation with summer temperature of MXD and CWT have been observed in similar areas (Büntgen et al., 2010; Diego Galván et al., 2015; Björklund et al., 2017). On the contrary, the negative relationship between MXD and CWT chronologies with precipitation could reflect the inverse relationship between precipitation and temperature, especially in mountain regions (Rebetez, 1996).

In this study, CWT was highly influenced by previous-year summer temperature (Frank and Esper, 2005; Babst et al., 2013), whereas CA mainly reflected the previous autumn–winter water availability conditions (Castagneri et al., 2015). Thus, the xylem structure encoded information also related to previous-year climate condition. These outcomes stressed the key role, not just of the current environmental conditions, but also of the lag effects which are usually overlooked in many investigations (Carrer et al., 2010; Babst et al., 2012). The higher detailed analysis at intra-monthly resolution computed with the daily climatic data shows significant positive correlations between temperature and CWT and a negative correlation with CA within almost all ring sectors between April and May. This probably reflects the effect of late spring temperatures on the timing of cambial activity onset and growing season duration (Carrer et al., 2017), and possibly the availability of resources stored before the wood formation (Björklund et al., 2017). Also, higher spring temperatures trigger the release of growth hormones (i.e., auxin and gibberellin; Aloni, 2015), implying an earlier onset of cambial activity (Olano et al., 2013; Carrer et al., 2017; Castagneri et al., 2017) which translates into more intense carbon assimilation (Wolf et al., 2012; Castagneri et al., 2017; Nagavciuc et al., 2020) and finally in thicker cell walls.

Different tracheids, based on their position within the ring can distinctly record different climatic time windows as shown through the increasing significant correlations between CWT and temperature from the beginning of June in the first ring sector until the start of September in the last one (Castagneri et al., 2017; Carrer et al., 2018). CWT and MXD correlations with temperature are very similar, especially when considering the last CWT ring sectors. Therefore, we suggest using CWT in dendroclimatological investigations as it represents a parameter less influenced by laboratory-dependent measuring techniques (Wang et al., 2002; Björklund et al., 2019).

CONCLUSION

The combination of classical dendrochronology with quantitative wood anatomy (dendroanatomy), is a powerful tool that provides high-resolution information on structure–function tree responses over the last century. The analysis of intra-annual variation of anatomical traits, together with daily temperature and precipitation records allowed us to assemble xylem traits chronologies that maximize climatic responses compared to the classical approach, which considers just monthly climatic values and yearly resolution tree-ring data. Hence, this study contributes to the general understanding of the climate–growth and xylem structure relationship of this species on different time scales. With this, we highlighted the strong role of temperature in influencing the "carbon-sink" capacity of stone pine and gained insights into such high-elevation marginal populations under future climate scenarios.

DATA AVAILABILITY STATEMENT

Data associated with this article are deposited in the Dryad Digital Repository https://doi.org/10.5061/dryad.tqjq2bw28.

AUTHOR CONTRIBUTIONS

C-CR and MC initiated the collaboration project. M-IS, C-CR, and AM defined the sampling design. C-CR and AM collected samples and performed fieldwork activities. C-CR, MC, and AP designed the work. AM was responsible with the MXD sample preparation and data acquisition. M-IS carried out the dendrochronological investigations in terms of data acquisition and analyses with the help of C-CR, MC, and AP. AP was responsible for the ring sector analysis. M-IS interpreted the data results with the help of C-CR, MC, LU, and AP. C-CR processed the data and prepared all the figures with inputs from all co-authors. M-IS, MC, and AP drafted the first version of the manuscript with the help of C-CR and LU. M-IS and AP wrote the paper with input from all co-authors. The final version of the manuscript was read and approved by all the co-authors.

FUNDING

C-CR was partially funded by Ministry of Research, Innovation and Digitalization within Program 1 - Development of national research and development system, Subprogram 1.2 - Institutional Performance - RDI excellence funding projects, under contract no. 10PFE/2021; C-CR and AM were partially supported by EEA Financial Mechanism 2009–2014 under the project CLIMFOR contract no. 18SEE/2014; C-CR, AM, and M-IS were partially supported by the EU cross-border project "Promote deadwood for resilient forests in the Romanian-Ukrainian cross border region" (RESFOR), no. 2SOFT/1.2/13; M-IS was partially supported by an ERASMUS+ internship in 01.03–01.06.2019 period. AP was supported by the 2017 BIRD Project of TeSAF Department University of Padova, and by Marie Sklodowska-Curie Individual Fellowship (IF) under contract number 895233.

SUPPLEMENTARY MATERIAL

The Supplementary Material for this article can be found online at: https://www.frontiersin.org/articles/10.3389/fpls.2022.855003/full#supplementary-material

REFERENCES

Ali, A. A., Carcaillet, C., Talon, B., Roiron, P., and Terral, J. F. (2005). *Pinus cembra* L. (arolla pine), a common tree in the inner French Alps since the early Holocene and above the present tree line: a synthesis based on charcoal data from soils and travertines. *J. Biogeogr.* 32, 1659–1669. doi: 10.1111/j.1365-2699.2005.01308.x

Aloni, R. (2015). Ecophysiological implications of vascular differentiation and plant evolution. *Trees Struct. Funct.* 29, 1–16. doi: 10.1007/s00468-014-1070-6

Anfodillo, T., Carrer, M., Rento, S., and Urbinati, C. (1998). Long and short term growth dynamics of Picea abies (L.) Karst, Larix decidua Mill., *Pinus cembra* (l.) and climatic factors: first results of an integrated study at the timberline in eastern Italian Alps*. *Écologie* 29, 253–259.

ANM (2008). *Clima României*. eds. I. Sandu, V. I. Pescaru and I. Poiană (Bucureşti (in Romanian): Editura Academiei Române).

Baas, P., Beeckman, H., Čufar, K., and De Micco, V. (2016). Functional traits in wood anatomy. *IAWA J.* 37, 124–126. doi: 10.1163/22941932-20160139

Babst, F., Bouriaud, O., Papale, D., Gielen, B., Janssens, I. A., Nikinmaa, E., et al. (2014). Above-ground woody carbon sequestration measured from tree rings is coherent with net ecosystem productivity at five eddy-covariance sites. *New Phytol.* 201, 1289–1303. doi: 10.1111/nph.12589

Babst, F., Carrer, M., Poulter, B., Urbinati, C., Neuwirth, B., and Frank, D. (2012). 500 years of regional forest growth variability and links to climatic extreme events in Europe. *Environ. Res. Lett.* 7, 45705–45716. doi: 10.1088/1748-9326/7/4/045705

Babst, F., Poulter, B., Trouet, V., Tan, K., Neuwirth, B., Wilson, R., et al. (2013). Site- and species-specific responses of forest growth to climate across the European continent. *Glob. Ecol. Biogeogr.* 22, 706–717. doi: 10.1111/geb.12023

Baltensweiler, W. (1993). Why the larch bud-moth cycle collapsed in the subalpine larch-cembran pine forests in the year 1990 for the first time since 1850. *Oecologia* 94, 62–66. doi: 10.1007/BF00317302

Beloiu, M., and Beierkuhnlein, C. (2019). Differences in the spatial structure of two *Pinus cembra* L. populations in the Carpathian Mountains. *Forests* 10, 1–16. doi: 10.3390/f10040326

Björklund, J., Seftigen, K., Fonti, P., Nievergelt, D., and von Arx, G. (2020). Dendroclimatic potential of dendroanatomy in temperature-sensitive Pinus sylvestris. *Dendrochronologia* 60:125673. doi: 10.1016/j.dendro.2020.125673

Björklund, J., Seftigen, K., Schweingruber, F., Fonti, P., von Arx, G., Bryukhanova, M. V., et al. (2017). Cell size and wall dimensions drive distinct variability of earlywood and latewood density in northern hemisphere conifers. *New Phytol.* 216, 728–740. doi: 10.1111/nph.14639

Björklund, J., von Arx, G., Nievergelt, D., Wilson, R., Van den Bulcke, J., Günther, B., et al. (2019). Scientific merits and analytical challenges of tree-ring densitometry. *Rev. Geophys.* 57, 1224–1264. doi: 10.1029/2019RG000642

Blada, I. (2008). *Pinus cembra* distribution in the Romanian Carpathians. *Ann. For. Res.* 51, 115–132. doi: 10.15287/afr.2008.149

Bouriaud, O., Leban, J. M., Bert, D., and Deleuze, C. (2005). Intra-annual variations in climate influence growth and wood density of Norway spruce. *Tree Physiol.* 25, 651–660. doi: 10.1093/treephys/25.6.651

Briffa, K. R., and Jones, D. (1990). "Basic chronology statistics and assessment," in *Methods of Dendrochronology*. eds. E. R. Cook and L. Kairiukstis (Dordrecht: Kluwer Academic Publishers), 137–153.

Briffa, K. R., Osborn, T. J., Schweingruber, F. H., Harris, I. C., Jones, P. D., Shiyatov, S. G., et al. (2001). Low-frequency temperature variations from a northern tree ring density network. *J. Geophys. Res. Atmos.* 106, 2929–2941. doi: 10.1029/2000JD900617

Büntgen, U., Esper, J., Frank, D. C., Nicolussi, K., Schmidhalter, M., Frank, C. D., et al. (2005). A 1052-year tree-ring proxy for alpine summer temperatures. *Clim. Dyn.* 25, 141–153. doi: 10.1007/s00382-005-0028-1

Büntgen, U., Frank, D. C., Nievergelt, D., and Esper, J. (2006). Summer temperature variations in the European Alps, A.D. 755-2004. *J. Clim.* 19, 5606–5623. doi: 10.1175/JCLI3917.1

Büntgen, U., Frank, D., Trouet, V., and Esper, J. (2010). Diverse climate sensitivity of Mediterranean tree-ring width and density. *Trees Struct. Funct.* 24, 261–273. doi: 10.1007/s00468-009-0396-y

Büntgen, U., Hellmann, L., Tegel, W., Normand, S., Myers-Smith, I., Kirdyanov, A. V., et al. (2015). Temperature-induced recruitment pulses of Arctic dwarf shrub communities. *J. Ecol.* 103, 489–501. doi: 10.1111/1365-2745.12361

Camarero, J. J., Gazol, A., Sánchez-Salguero, R., Fajardo, A., McIntire, E. J. B., Gutiérrez, E., et al. (2021). Global fading of the temperature–growth coupling at alpine and polar treelines. *Glob. Chang. Biol.* 27, 1879–1889. doi: 10.1111/gcb.15530

Campelo, F., Nabais, C., Gutiérrez, E., Freitas, H., and García-González, I. (2010). Vessel features of Quercus ilex L. growing under Mediterranean

climate have a better climatic signal than tree-ring width. *Trees Struct. Funct.* 24, 463–470. doi: 10.1007/s00468-010-0414-0

Cannone, N., Sgorbati, S., and Guglielmin, M. (2007). Unexpected impacts of climate change on alpine vegetation. *Front. Ecol. Environ.* 5, 360–364. doi: 10.1890/1540-9295(2007)5[360:UIOCCO]2.0.CO;2

Carlson, B. Z., Corona, M. C., Dentant, C., Bonet, R., Thuiller, W., and Choler, P. (2017). Observed long-term greening of alpine vegetation – a case study in the French Alps. *Environ. Res. Lett.* 12:114006. doi: 10.1088/1748-9326/aa84bd

Carrer, M., Castagneri, D., Prendin, A. L., Petit, G., and von Arx, G. (2017). Retrospective analysis of wood anatomical traits reveals a recent extension in tree cambial activity in two high-elevation conifers. *Front. Plant Sci.* 8:737. doi: 10.3389/fpls.2017.00737

Carrer, M., Nola, P., Eduard, J. L., Motta, R., and Urbinati, C. (2007). Regional variability of climate–growth relationships in *Pinus cembra* high elevation forests in the Alps. *J. Ecol.* 95, 1072–1083. doi: 10.1111/j.1365-2745.2007.01281.x

Carrer, M., Nola, P., Motta, R., and Urbinati, C. (2010). Contrasting tree-ring growth to climate responses of Abies alba toward the southern limit of its distribution area. *Oikos* 119, 1515–1525. doi: 10.1111/j.1600-0706.2010.18293.x

Carrer, M., Unterholzner, L., and Castagneri, D. (2018). Wood anatomical traits highlight complex temperature influence on *Pinus cembra* at high elevation in the Eastern Alps. *Int. J. Biometeorol.* 62, 1745–1753. doi: 10.1007/s00484-018-1577-4

Carrer, M., von Arx, G., Castagneri, D., and Petit, G. (2014). Distilling allometric and environmental information from time series of conduit size: the standardization issue and its relationship to tree hydraulic architecture. *Tree Physiol.* 35, 27–33. doi: 10.1093/treephys/tpu108

Castagneri, D., Fonti, P., Von Arx, G., and Carrer, M. (2017). How does climate influence xylem morphogenesis over the growing season? Insights from long-term intra-ring anatomy in Picea abies. *Ann. Bot.* 119, 1011–1020. doi: 10.1093/aob/mcw274

Castagneri, D., Petit, G., and Carrer, M. (2015). Divergent climate response on hydraulic-related xylem anatomical traits of Picea abies along a 900-m altitudinal gradient. *Tree Physiol.* 35, 1378–1387. doi: 10.1093/treephys/tpv085

Caudullo, G., Welk, E., and San-Miguel-Ayanz, J. (2017). Chorological maps for the main European woody species. *Data Br.* 12, 662–666. doi: 10.1016/j.dib.2017.05.007

Cazzolla Gatti, R., Callaghan, T., Velichevskaya, A., Dudko, A., Fabbio, L., Battipaglia, G., et al. (2019). Accelerating upward treeline shift in the Altai Mountains under last-century climate change. *Sci. Rep.* 9, 7678–7613. doi: 10.1038/s41598-019-44188-1

Chave, J., Coomes, D., Jansen, S., Lewis, S. L., Swenson, N. G., and Zanne, A. E. (2009). Towards a worldwide wood economics spectrum. *Ecol. Lett.* 12, 351–366. doi: 10.1111/j.1461-0248.2009.01285.x

Cook, E. R., and Kairiukstis, L. A. (1990). Methods of dendrochronology: applications in the environmental sciences. *Kluwer* 23:120. doi: 10.2307/1551446

Cook, E. R., and Peters, K. (1997). Calculating unbiased tree-ring indices for the study of climatic and environmental change. *The Holocene* 7, 361–370. doi: 10.1177/095968369700700314

Cuny, H. E., Rathgeber, C. B. K., Frank, D., Fonti, P., and Fournier, M. (2014). Kinetics of tracheid development explain conifer tree-ring structure. *New Phytol.* 203, 1231–1241. doi: 10.1111/nph.12871

D'Arrigo, R. D., and Jacoby, G. C. (1993). Secular trends in high northern latitude temperature reconstructions based on tree rings. *Clim. Chang.* 25, 163–177. doi: 10.1007/BF01661204

D'Arrigo, R., Wilson, R., Liepert, B., and Cherubini, P. (2008). On the "divergence problem" in northern forests: a review of the tree-ring evidence and possible causes. *Glob. Planet. Change* 60, 289–305. doi: 10.1016/j.gloplacha.2007.03.004

Dawes, M. A., Hagedorn, F., Handa, I. T., Streit, K., Ekblad, A., Rixen, C., et al. (2013). An alpine treeline in a carbon dioxide-rich world: synthesis of a nine-year free-air carbon dioxide enrichment study. *Oecologia* 171, 623–637. doi: 10.1007/s00442-012-2576-5

Dawes, M. A., Philipson, C. D., Fonti, P., Bebi, P., Hättenschwiler, S., Hagedorn, F., et al. (2015). Soil warming and CO_2 enrichment induce biomass shifts in alpine tree line vegetation. *Glob. Chang. Biol.* 21, 2005–2021. doi: 10.1111/gcb.12819

Diego Galván, J., Büntgen, U., Ginzler, C., Grudd, H., Gutiérrez, E., Labuhn, I., et al. (2015). Drought-induced weakening of growth–temperature associations in high-elevation Iberian pines. *Glob. Planet. Change* 124, 95–106. doi: 10.1016/J.GLOPLACHA.2014.11.011

Drew, D. M., Allen, K., Downes, G. M., Evans, R., Battaglia, M., and Baker, P. (2013). Wood properties in a long-lived conifer reveal strong climate signals where ring-width series do not. *Tree Physiol.* 33, 37–47. doi: 10.1093/treephys/tps111

Dumitrescu, A., and Birsan, M.-V. V. (2015). ROCADA: a gridded daily climatic dataset over Romania (1961–2013) for nine meteorological variables. *Nat. Hazards* 78, 1045–1063. doi: 10.1007/s11069-015-1757-z

Enquist, B. J. (2002). Universal scaling in tree and vascular plant allometry: toward a general quantitative theory linking plant form and function from cells to ecosystems. *Tree Physiol.* 22, 1045–1064. doi: 10.1093/treephys/22.15-16.1045

Everitt, B. S., Landau, S., Leese, M., and Stahl, D. (2011). *Cluster Analysis*. Hoboken, NJ: John Wiley & Sons, Ltd.

Fonti, P., and Jansen, S. (2012). Xylem plasticity in response to climate. *New Phytol.* 195, 734–736. doi: 10.1111/J.1469-8137.2012.04252.X

Fonti, P., Von Arx, G., García-González, I., Eilmann, B., Sass-Klaassen, U., Gärtner, H., et al. (2010). Studying global change through investigation of the plastic responses of xylem anatomy in tree rings. *New Phytol.* 185, 42–53. doi: 10.1111/j.1469-8137.2009.03030.x

Frank, D., and Esper, J. (2005). Characterization and climate response patterns of a high-elevation, multi-species tree-ring network in the European Alps. *Dendrochronologia* 22, 107–121. doi: 10.1016/j.dendro.2005.02.004

Fritts, H. C. (1976). *Tree Rings and Climate*. London: Academic Press.

Gagen, M., McCarroll, D., and Edouard, J. L. (2006). Combining ring width, density and stable carbon isotope proxies to enhance the climate signal in tree-rings: an example from the southern French Alps. *Clim. Chang.* 78, 363–379. doi: 10.1007/s10584-006-9097-3

Gärtner, H., and Schweingruber, F. (2013). *Microscopic Preparation Techniques for Plant Stem Analysis*. Verlag Dr. Kessel, Remagen-Oberwinter.

Grace, J., Berninger, F., and Nagy, L. (2002). Impacts of climate change on the tree line. *Ann. Bot.* 90, 537–544. doi: 10.1093/aob/mcf222

Gruber, A., Baumgartner, D., Zimmermann, J., and Oberhuber, W. (2009). Temporal dynamic of wood formation in *Pinus cembra* along the alpine treeline ecotone and the effect of climate variables. *Trees Struct. Funct.* 23, 623–635. doi: 10.1007/s00468-008-0307-7

Hacke, U. G., Sperry, J. S., Pockman, W. T., Davis, S. D., and McCulloh, K. A. (2001). Trends in wood density and structure are linked to prevention of xylem implosion by negative pressure. *Oecologia* 126, 457–461. doi: 10.1007/S004420100628

Hampe, A., and Petit, R. (2005). Conserving biodiversity under climate change: the rear edge matters. *Ecol. Lett.* 8, 461–467. doi: 10.1111/j.1461-0248.2005.00739.x

Harris, I., Osborn, T. J., Jones, P., and Lister, D. (2020). Version 4 of the CRU TS monthly high-resolution gridded multivariate climate dataset. *Sci. Data* 7, 109–118. doi: 10.1038/s41597-020-0453-3

Harsch, M. A., Hulme, P. E., McGlone, M. S., and Duncan, R. P. (2009). Are treelines advancing? A global meta-analysis of treeline response to climate warming. *Ecol. Lett.* 12, 1040–1049. doi: 10.1111/j.1461-0248.2009.01355.x

Holmes, R. L. (1983). Computer-assisted quality control in tree-ring dating and measurement. *Tree-Ring Bull.* 43, 69–75.

Ionita, M., Nagavciuc, V., and Guan, B. (2020). Rivers in the sky, flooding on the ground: the role of atmospheric rivers in inland flooding in Central Europe. *Hydrol. Earth Syst. Sci.* 24, 5125–5147. doi: 10.5194/hess-2020-149

IPCC (2021). *Climate Change 2021: The Physical Science Basis. Contribution of Working Group I to the Sixth Assessment Report of the Intergovernmental Panel on Climate Change*. Geneva: IPCC.

Jevšenak, J., and Levanič, T. (2018). dendroTools: R package for studying linear and nonlinear responses between tree-rings and daily environmental data. *Dendrochronologia* 48, 32–39. doi: 10.1016/j.dendro.2018.01.005

Klesse, S., Babst, F., Lienert, S., Spahni, R., Joos, F., Bouriaud, O., et al. (2018). A combined tree ring and vegetation model assessment of European forest growth sensitivity to interannual climate variability. *Global Biogeochem. Cycles* 32, 1226–1240. doi: 10.1029/2017GB005856

Konapala, G., Mishra, A. K., Wada, Y., and Mann, M. E. (2020). Climate change will affect global water availability through compounding changes in seasonal precipitation and evaporation. *Nat. Commun.* 11, 1–10. doi: 10.1038/s41467-020-16757-w

Körner, C. (1998). A re-assessment of high elevation treeline positions and their explanation. *Oecologia* 115, 445–459. doi: 10.1007/S004420050540

Körner, C. (2012). *Alpine Treelines: Functional Ecology of the Global High Elevation Tree Limits*. Basel: Springer.

Lange, J., Carrer, M., Pisaric, M. F. J., Porter, T. J., Seo, J. W., Trouillier, M., et al. (2020). Moisture-driven shift in the climate sensitivity of white spruce xylem anatomical traits is coupled to large-scale oscillation patterns across northern treeline in Northwest North America. *Glob. Chang. Biol.* 26, 1842–1856. doi: 10.1111/gcb.14947

Ludwig, J. A., and Reynolds, J. F. (1988). *Statistical Ecology*. New York, USA: Wiley.

Lyu, L., Zhang, Q. B., Pellatt, M. G., Büntgen, U., Li, M. H., and Cherubini, P. (2019). Drought limitation on tree growth at the northern Hemisphere's highest tree line. *Dendrochronologia* 53, 40–47. doi: 10.1016/j.dendro.2018.11.006

Mäkinen, H., Nöjd, P., and Saranpää, P. (2003). Seasonal changes in stem radius and production of new tracheids in Norway spruce. *Tree Physiol.* 23, 959–968. doi: 10.1093/treephys/23.14.959

Mayr, S. (2007). "Limits in water relations," in *Trees at Their Upper Limit*. eds. G. Wieser, and M. Tausz (Dordrecht: Springer), 145–162.

Nagavciuc, V., Kern, Z., Ionita, M., Hartl, C., Konter, O., Esper, J., et al. (2020). Climate signals in carbon and oxygen isotope ratios of *Pinus cembra* tree-ring cellulose from the Călimani Mountains. *Romania. Int. J. Climatol.* 40, 2539–2556. doi: 10.1002/joc.6349

Nagavciuc, V., Roibu, C.-C., Ionita, M., Mursa, A., Cotos, M.-G., and Popa, I. (2019). Different climate response of three tree ring proxies of Pinus sylvestris from the eastern Carpathians, Romania. *Dendrochronologia* 54, 56–63. doi: 10.1016/j.dendro.2019.02.007

Oberhuber, W. (2004). Influence of climate on radial growth of *Pinus cembra* within the alpine timberline ecotone. *Tree Physiol.* 24, 291–301. doi: 10.1093/treephys/24.3.291

Olano, J. M., Almería, I., Eugenio, M., and von Arx, G. (2013). Under pressure: how a Mediterranean high-mountain forb coordinates growth and hydraulic xylem anatomy in response to temperature and water constraints. *Funct. Ecol.* 27, 1295–1303. doi: 10.1111/1365-2435.12144

Panyushkina, I. P., Hughes, M. K., Vaganov, E. A., and Munro, M. A. R. (2003). Summer temperature in northeastern Siberia since 1642 reconstructed from tracheid dimensions and cell numbers of Larix cajanderi. *Can. J. For. Res.* 33, 1905–1914. doi: 10.1139/x03-109

Pepin, N., Bradley, R. S., Diaz, H. F., Baraer, M., Caceres, E. B., Forsythe, N., et al. (2015). Elevation-dependent warming in mountain regions of the world. *Nat. Clim. Chang.* 5, 424–430. doi: 10.1038/nclimate2563

Popa, I., and Bouriaud, O. (2013). Reconstruction of summer temperatures in eastern Carpathian Mountains (Rodna Mts, Romania) back to AD 1460 from tree-rings. *Int. J. Climatol.* 34, 871–880. doi: 10.1002/joc.3730

Popa, I., and Kern, Z. (2009). Long-term summer temperature reconstruction inferred from tree-ring records from the eastern Carpathians. *Clim. Dyn.* 32, 1107–1117. doi: 10.1007/s00382-008-0439-x

Poussart, P. F., and Schrag, D. P. (2005). Seasonally resolved stable isotope chronologies from northern Thailand deciduous trees. *Earth Planet. Sci. Lett.* 235, 752–765. doi: 10.1016/j.epsl.2005.05.012

Prendin, A. L., Petit, G., Carrer, M., Fonti, P., Björklund, J., and Von Arx, G. (2017). New research perspectives from a novel approach to quantify tracheid wall thickness. *Tree Physiol.* 37, 976–983. doi: 10.1093/treephys/tpx037

Prendin, A. L., Petit, G., Fonti, P., Rixen, C., Dawes, M. A., and von Arx, G. (2018). Axial xylem architecture of Larix decidua exposed to CO2 enrichment and soil warming at the tree line. *Funct. Ecol.* 32, 273–287. doi: 10.1111/1365-2435.12986

Pritzkow, C., Heinrich, I., Grudd, H., and Helle, G. (2014). Relationship between wood anatomy, tree-ring widths and wood density of Pinus sylvestris L. and climate at high latitudes in northern Sweden. *Dendrochronologia* 32, 295–302. doi: 10.1016/j.dendro.2014.07.003

Rathgeber, C. B. K. (2017). Conifer tree-ring density inter-annual variability – anatomical, physiological and environmental determinants. *New Phytol.* 216, 621–625. doi: 10.1111/nph.14763

Rebetez, M. (1996). Seasonal relationship between temperature, precipitation and snow cover in a mountainous region. *Theor. Appl. Climatol.* 54, 99–106. doi: 10.1007/BF00865152

Regent Instruments (2018). WinDENDRO, an image analysis system for annual tree-rings analysis. Available at: https://www.regentinstruments.com/assets/windendro_about.html (Accessed February 15, 2021).

Rinn, F. (2003). *TSAP-Win User Reference*. Heidelberg: Rinntech.

Rosner, S. (2013). Hydraulic and biomechanical optimization in Norway spruce trunkwood – a review. *IAWA J.* 34, 365–390. doi: 10.1163/22941932-00000031

Rossi, S., Deslauriers, A., Anfodillo, T., Morin, H., Saracino, A., Motta, R., et al. (2006). Conifers in cold environments synchronize maximum growth rate of tree-ring formation with day length. *New Phytol.* 170, 301–310. doi: 10.1111/j.1469-8137.2006.01660.x

Saulnier, M., Edouard, J. L., Corona, C., and Guibal, F. (2011). Climate/growth relationships in a *Pinus cembra* high-elevation network in the southern French Alps. *Ann. For. Sci.* 68, 189–200. doi: 10.1007/s13595-011-0020-3

Sauter, J. J. (1986). "Xylem: structure and function," in *Progress in Botany* (New York: John Wiley & Sons, Ltd), 388–405.

Schweingruber, F. (1996). *Tree Rings and Environment*. Birmensdorf: Swiss Federal Intitute of Forest, Snow and Landscape Research WSL/FNP.

Schweingruber, F. H., Eckstein, D., and Serre-Bachet, F. (1990). Identification, presentation and interpretation of event years and pointer years in dendrochronology. *Dendrochronologia* 8, 9–38.

Seo, J. W., Eckstein, D., Jalkanen, R., and Schmitt, U. (2011). Climatic control of intra- and inter-annual wood-formation dynamics of scots pine in northern Finland. *Environ. Exp. Bot.* 72, 422–431. doi: 10.1016/j.envexpbot.2011.01.003

Vaganov, E., Hughes, M., and Shashkin, A. (2006). Growth dynamics of conifer tree rings. doi: 10.1007/3-540-31298-6

Vittoz, P., Rulence, B., Largey, T., and Freléchoux, F. (2008). Effects of climate and land-use change on the establishment and growth of cembran pine (*Pinus cembra* L.) over the altitudinal treeline ecotone in the central Swiss Alps. Arctic. *Antarct. Alp. Res.* 40, 225–232. doi: 10.1657/1523-0430(06-010)[VITTOZ]2.0.CO;2

von Arx, G., and Carrer, M. (2014). Roxas -A new tool to build centuries-long tracheid-lumen chronologies in conifers. *Dendrochronologia* 32, 290–293. doi: 10.1016/j.dendro.2013.12.001

Von Arx, G., Crivellaro, A., Prendin, A. L., Čufar, K., and Carrer, M. (2016). Quantitative wood anatomy—practical guidelines. *Front. Plant Sci.* 7:781. doi: 10.3389/fpls.2016.00781

Wang, L., Payette, S., and Bégin, Y. (2002). Relationships between anatomical and densitometric characteristics of black spruce and summer temperature at tree line in northern Quebec. *Can. J. For. Res.* 32, 477–486. doi: 10.1139/x01-208

Wolf, S., Hématy, K., and Höfte, H. (2012). Growth control and cell wall signaling in plants. *Annu. Rev. Plant Biol.* 63, 381–407. doi: 10.1146/annurev-arplant-042811-105449

Zang, C., and Biondi, F. (2015). Treeclim: an R package for the numerical calibration of proxy-climate relationships. *Ecography* 38, 431–436. doi: 10.1111/ecog.01335

Ziaco, E., Biondi, F., Rossi, S., and Deslauriers, A. (2014). Climatic influences on wood anatomy and tree-ring features of Great Basin conifers at a new mountain observatory. *Appl. Plant Sci.* 2:1400054. doi: 10.3732/APPS.1400054

Conflict of Interest: The authors declare that the research was conducted in the absence of any commercial or financial relationships that could be construed as a potential conflict of interest.

Publisher's Note: All claims expressed in this article are solely those of the authors and do not necessarily represent those of their affiliated organizations, or those of the publisher, the editors and the reviewers. Any product that may be evaluated in this article, or claim that may be made by its manufacturer, is not guaranteed or endorsed by the publisher.

Advantages of publishing in Frontiers

OPEN ACCESS
Articles are free to read for greatest visibility and readership

FAST PUBLICATION
Around 90 days from submission to decision

HIGH QUALITY PEER-REVIEW
Rigorous, collaborative, and constructive peer-review

TRANSPARENT PEER-REVIEW
Editors and reviewers acknowledged by name on published articles

Frontiers
Avenue du Tribunal-Fédéral 34
1005 Lausanne | Switzerland

Visit us: www.frontiersin.org
Contact us: frontiersin.org/about/contact

REPRODUCIBILITY OF RESEARCH
Support open data and methods to enhance research reproducibility

DIGITAL PUBLISHING
Articles designed for optimal readership across devices

FOLLOW US
@frontiersin

IMPACT METRICS
Advanced article metrics track visibility across digital media

EXTENSIVE PROMOTION
Marketing and promotion of impactful research

LOOP RESEARCH NETWORK
Our network increases your article's readership